

The Eurasia Proceedings of Science, Technology, Engineering & Mathematics

EPSTEM

VOLUME 24 ICONTECH CONFERENCE

ISSN: 2602-3199

ISBN: 978-625-6959-25-5

ICONTECH 2023: 3rd International Conference on Technology (IConTech)

November 16 - 19, 2023

Antalya, Turkey

Edited by: Prof.Dr. Sabri KOCER - Necmettin Erbakan University, Turkey

ICONTECH 2023 NOVEMBER**Volume 24, Pages 1-300 (November 2023)****The Eurasia Proceedings of Science, Technology, Engineering & Mathematics (EPSTEM)****e-ISSN: 2602-3199****©2023 Published by the ISRES Publishing****Address:** Istanbul C. Cengaver S. No 2 Karatay/Konya/TURKEY**Website:** www.isres.org**Contact:** isrespublishing@gmail.com**Conference:** ICONTECH2023: : 3rd International Conference on Technology (ICONTECH)**Conference website:** <https://www.2023.icontechno.net>**Dates:** November 16 – 19, 2023**Location:** Antalya, Turkey**Edited by:** Prof. Dr. Sabri Kocer**About Editor**

Prof Dr. Sabri Kocer

Engineering Faculty, Department of Computer Engineering,

Division of Computer Software, Necmettin Erbakan University, Turkey

Email: skocer@erbakan.edu.tr**Language Editor(s)**

Assoc. Prof. Dr. Kagan Buyukkarci

Department of English Language Education, Suleyman Demirel University, Turkey

Email: kaganbuyukkarci@sdu.edu.tr**CONFERENCE PRESIDENT**

Prof Dr. Sabri Kocer

SCIENTIFIC BOARD

Agata Mesjasz-Lech - Czestochowa University of Technology, Poland

Bahar Tercan - Institute for Systems Biology, USA

Besnik Hajdari - University "isa Boletini" Mitrovica, Kosovo

Bogdan PATRUT - Alexandru Ioan Cuza Universitesi , Romania

Dariusz Jacek Jakóbczak - Technical University of Koszalin, Poland

Ebba Ossiannilsson - Swedish Association for Distance Education, Swedish

Eleonora Guseinoviene - Klaipeda University, Lithuania

Gabriel DELGADO-TORAL - Universidad Nacional Autónoma de México, Mexico

Isti HIDAYAH - Semarang State University, Indonesia

Jose Manuel Lopez Guede - University of Basque Country, Spain

Katarzyna Szymczyk - Czestochowa University of Technology, Poland

Marija STANIĆ - University of Kragujevac, Serbia
M. Hanefi CALP - Karadeniz Technical University, Turkey
Mohamed Ahmed - Mansoura University, Egypt
Nicu BIZON - Pitesti University, Romania
Ossi AUTIO - University of Helsinki, Finland
Pandian VASANT - Teknology Petronas University, Romania
Rajnalkar LAXMAN - Gulbarga University, India
Tunde Anifowose-Kelani, Siegener Sabithos College of Health Science & Technology, Nigeria
Utku KÖSE - Süleyman Demirel University, Turkey
Yiyang Chen - Soochow University (CN), China
Zairi Ismael Rizman - MARA University of Technology, Malaysia
Zipporah Pewat DUGURYIL - Federal College of Education, Nigeria

ORGANIZING COMMITTEE

Agata Mesjasz-Lech - Czestochowa University of Technology, Poland
Hakan YUKSEL - Isparta University of Applied Sciences, Turkey
Mohammad SARWAR - Scialert, Dubai, United Arab Emirates
M. Hanefi CALP - Karadeniz Technical University, Turkey
Mustafa Özhan KALAC - Manisa Celal Bayar University, Turkey
Resul BUTUNER - Adil Karaağac Vocational and Technical Anatolian High School, Turkey
Robert Beloiu - University of Pitesti, Romania
Ozgur DUNDAR - Necmettin Erbakan University, Turkey
Selahattin ALAN - Selcuk University, Turkey
Yusuf UZUN - Necmettin Erbakan University, Turkey
Zairi Ismael Rizman - MARA University of Technology, Malaysia

Editorial Policies

ISRES Publishing follows the steps below in the proceedings book publishing process.

In the first stage, the papers sent to the conferences organized by ISRES are subject to editorial oversight. In the second stage, the papers that pass the first step are reviewed by at least two international field experts in the conference committee in terms of suitability for the content and subject area. In the third stage, it is reviewed by at least one member of the organizing committee for the suitability of references. In the fourth step, the language editor reviews the language for clarity.

Review Process

Abstracts and full-text reports uploaded to the conference system undergo a review procedure. Authors will be notified of the application results in three weeks. Submitted abstracts will be evaluated on the basis of abstracts/proposals. The conference system allows you to submit the full text if your abstract is accepted. Please upload the abstract of your article to the conference system and wait for the results of the evaluation. If your abstract is accepted, you can upload your full text. Your full text will then be sent to at least two reviewers for review. The conference has a double-blind peer-review process. Any paper submitted for the conference is reviewed by at least two international reviewers with expertise in the relevant subject area. Based on the reviewers' comments, papers are accepted, rejected or accepted with revision. If the comments are not addressed well in the improved paper,

then the paper is sent back to the authors to make further revisions. The accepted papers are formatted by the conference for publication in the proceedings.

Aims & Scope

In the past, accessing information was tiring both financially and morally, but today, thanks to technology, it is easier and faster to access information. With this feature, technology not only makes daily life easier, but also accelerates the developments in science. Therefore, the focus of the conference is to share the studies on the developments in technology and the applications of technology in fields such as science and engineering by the participants. Studies in the fields of technology are accepted to the conference.

The aim of the conference is to bring together researchers and administrators from different countries, and to discuss theoretical and practical issues in the field of technology. At the same time, being aware of the applications of technology in different fields (such as engineering) is among the objectives of the conference.

Articles: 1-37

CONTENTS

AI-Powered Game Design: Experts Employing ChatGPT in the Game Design Process / Pages: 1-9
Michael LANKES, Andreas STOCKL

Quality Issue Classification by Using Dedicated Data Analysis Software Created in Python Language / Pages: 10-20
Elena RADUCAN, Mihaita ARHIP

Exploring Social Engineering Attacks Using Spear Phishing in a University / Pages: 21-28
Trust Tshepo MAPOKA, Keneilwe ZUVA, Gaedupe KUKUMARA, Tebogo SEIPONE, Tranos ZUVA

The Effect of Antenna Spacing on Active S-Parameters in Planar Array Antennas / Pages: 29-36
Emirhan AYDIN, Ramiz ERDEM AYKAC

The Role of Internet of Things, Machine Learning, Artificial Neural Networks and Industry 5.0 in Business Research: Trends and Future Insights / Pages: 37-48
Zeynep BAYSAL, Hamide OZYUREK, Ali OZARSLAN, Serdar CELIK

Implementation of Industry 4.0 in Ship Repair Industry: Challenges and Opportunities / Pages: 49-54
Yordan DENEV

Detecting Litter in Street Sweepers Using Deep Learning / Pages: 55-62
Suheda GOKBUDAK, Emir Enes TAS, Onur OZER, Veysel TILEGI

Origin of Raw Materials of Ancient Glass (B.C.) from Kythnos Island, Greece / Pages: 63-70

Petros KARALIS, Elissavet DOTSIKA, Alexandros MAZARAKIS-AINIAN, Evaggelia KOLOFOTIA, Foteini RIZOU, Anastasia Electra POUTOUKI, Panagiotis Leandros POUTOUKIS, Anastasios DROSOU, Dimitrios TZOVARAS

Artificial Intelligence Technology to Predict the Financial Crisis in Business Companies / Pages: 71-82

Mohamed Ahmed HAMADA, Khaled M. K. ALHYASAT

S/MIME Certificate Test Suite / Pages: 83-88

Yagmur FIDANER, Aysun COSKUN, Tamer ERGUN

Investigation of Damping Energy in Trusses / Pages: 89-95

Victor RIZOV

Enhancing Call Center Efficiency: Data Driven Workload Prediction and Workforce Optimization / Pages: 96-100

Muhammet Ali KADIOGLU, Bilal ALATAS

PV Supplied Electrochemical Production of Hydrogen Peroxide: A Green Pathway for Fenton Based Advanced Oxidation Processes / Pages: 101-109

Kaouther KERBOUA

User-Defined Autogenerated Fuzzy Solvers for Embedded Applications / Pages: 110-118

Alexei Evgenievich VASSILIEV, Ye Min HTET, Htut SHINE, Ant-on Victorovich VEGNER

Provenance Study of Gypsum Black Crusts / Pages: 119-125

Petros KARALIS, Elissavet DOTSIKA, Dafni KYROPOULOU, Alexandros MAZARAKIS-AINIAN, Evaggelia KOLOFOTIA, Iakovos RAPTIS, Anastasios DROSOU, Dimitrios TZOVARAS, Anastasia Electra POUTOUKI, Giorgos DIAMANTOPOULOS, Panagiotis Leandros POUTOUKIS

A Research on Determining the Degree of Risk by Using ResNet / Pages: 119-125

Serap TEPE, Serkan ETI

Energy Management of the Hybrid Electric Wheel Loader / Pages: 135-140

Mustafa KARAHAN

Performance Assessment of Sustainable Machining Techniques / Pages: 141-148

Vamsi Krishna PASAM, Kartheek GAMIDI, Banoth SRINU, Lingaraju DUMPALA

Industry 5.0 and National Development Plans / Pages: 149-157

Beste ALPASLAN, Serdar CELIK

The Effect of HFMI Treatment on Stress Concentration for S355J2C+N Steel with Fillet Weld Joint / Pages: 158-164

Mehmet Can KATMER, Sami Gokberk BICER

The Prototype of Reactor for Carbon Capture in Molten Salts / Pages: 165-170

Stanisław PIETRZYK, Piotr PALIMĄKA

Isotopic Geochemistry Applied on Marble Samples of Kythnos Island in Greece / Pages: 171-176
Petros KARALIS, Elissavet DOTSIKA, Alexandros MAZARAKIS-AINIAN, Evaggelia KOLOFOTIA, Iakovos RAPTIS, Anastasia Electra POUTOUKI, Anastasios DROSOU, Brunella RACO, Panagiotis Leandros POUTOUKIS, Dafni KYROPOULOU, Dimitrios TZOVARAS

Utilizing Flink and Kafka Technologies for Real-Time Data Processing: A Case Study / Pages: 177-183
Alper BOZKURT, Furkan EKICI, Hatice YETISKUL

Student-Company Assignment: Simulation Approach / Pages: 184-189
Serdar CELIK, Beste ALPASLAN

Smart Cart Application for E-Commerce Websites: A Case Study / Pages: 190-195
Tahir Enes ADAK, Mehmet S. AKTAS

Torsional Fatigue and Static Torsion Strength and Test Validations of Composite Tube Hybrid Drive Shafts / Pages: 196-203
Onur OZBEK, Serdar Kaan HORTOUGLU, Sedat TARAKCI, Efe ISIK

Experimental Investigation on Thermal Properties of Al2024 Alloy by Friction Stir Welding / Pages: 204-210
Lingaraju DUMPALA, Shaik Ghouse MOHIDDIN, P. Vamsi KRISHNA, U. RAJYALAKSHMI

Quenching: An Improvement Factor of HSS Twist Drill Tool-Life When Machining C22 Steel / Pages: 211-218
Nacer MOKAS, Sabiha TEKILI, Youcef KHADRI

The Effects of the Use of DRx Antenna Structure on the Rx Performance of Smartphones / Pages: 219-224
Emirhan AYDIN, Ramiz Erdem AYKAC, Tekin AKPOLAT

Reduction of Shipping Greenhouse Emission by Alternative Fuels Used / Pages: 225-234
Yordan DENEV

Indeterminate Continuously Inhomogeneous Beam under End Rotation: A Longitudinal Fracture Study / Pages: 235-242
Victor RIZOV

A Numerical Study of the Efficiency of the Sono Galvano-Fenton Process as a Tertiary Treatment Technique for the Wastewater Reuse in Agriculture / Pages: 243-256
Kaouther KERBOUA

User-Selected Sets of Algorithmic Implementation of Fuzzy Processing Subsystem for Embedded Intelligent Control Systems / Pages: 257-262
Alexei Evgenievich VASSILIEV, Htut SHINE, Ye Min HTET, Viktoriia Alexeevna KARPENKO

Using Oxygen and Carbon Isotopic Signatures in order to Infer Dietary Information in Bones from Kythnos Island, Greece / Pages: 263-270
Giorgos DIAMANTOPOULOS, Petros KARALIS, Elissavet DOTSIKA, Alexandros MAZARAKIS-AINIAN, Evaggelia KOLOFOTIA, Stavroula SAMARTZIDOU-ORKOPOULOU, Katerina TRANTALIDOU, Eleanna

PREVEDOROU, Panagiotis Leandros POUTOUKIS, Vasileios MPLETSOS Anastasios DROSOU, Anastasia Electra POUTOUKI, Dimitrios TZOVARAS

Design and Development of Mobile Payment Platform Software Supported by Analytical Capabilities for Payment Systems / Pages: 271-278

Pinar CELDIRME-KAYGUSUZ, Unal ASIL, Semih KOKCU

Integration of STM32 Microcontroller with Arm Cortex Architecture into the 8-Bit Measurement Circuit Customized for Real-Time Data Acquisition on Propeller Shaft to Increase Data Speed and Accuracy / Pages: 279-286

Oguzhan ALDEMIR, Sedat TARAKCI, Serhan OZDEMIR, Efe ISIK

Numerical Simulation on Microwave Melting of Hastelloy C-276 / Pages: 287-300

Kadapa Vijaya Bhaskar REDDY, K. V. Hari SHANKAR, Venkatesh GUDIPADU

The Eurasia Proceedings of Science, Technology, Engineering & Mathematics (EPSTEM), 2023

Volume 24, Pages 1-9

IConTech 2023: International Conference on Technology

AI-Powered Game Design: Experts Employing ChatGPT in the Game Design Process

Michael Lankes

University of Applied Sciences Upper Austria

Andreas Stockl

University of Applied Sciences Upper Austria

Abstract: In today's rapidly evolving gaming industry, there's an increasing need for tools that can aid game designers in creating intricate games within tight schedules. One promising solution lies in artificial intelligence (AI)-assisted game design tools. This research delves into the potential of ChatGPT, an advanced AI language model, in assisting game design experts with specific tasks related to game development. By conducting detailed interviews, we obtained invaluable feedback from experts about their experiences interacting with the model, focusing on the quality and outcomes of those interactions. Our findings not only shed light on the advantages of utilizing AI-driven tools in game design but also highlight the challenges that designers encounter when integrating these tools into their workflow. This study enriches the expanding literature on AI-assisted game design, giving a more profound insight into AI's capabilities and potential in supporting game designers. Our results will be particularly enlightening for game designers, AI enthusiasts, and all those keen on understanding the symbiosis of AI and game design.

Keywords: Artificial intelligence, ChatGPT, Game design

Introduction

Artificial Intelligence (AI) can potentially transform various industries, including the game industry (e.g., Machado et al., 2018; Kreminski et al., 2019; Zhao et al., 2020). Game development is a dynamic and fast-paced environment, where game designers are often challenged to create complex games in a limited amount of time. AI-assisted game design tools have the potential to help game designers overcome these challenges and develop games faster and with greater efficiency (e.g., Araujo et al., 2020; Conroy et al., 2011). With advancements in AI technology, there is an increasing interest in exploring how AI can assist game designers in creating games. AI-assisted game design tools offer several benefits to game designers. These tools can automate repetitive tasks, allowing game designers to focus on more creative aspects. Besides, AI-assisted tools can give game designers new ideas and suggestions for game design elements, such as characters, settings, and storylines. In addition, these tools can help game designers iterate on their designs faster and more effectively, allowing them to make rapid progress on their projects. However, while the technology offers many benefits, it is crucial to understand how well they support game designers in carrying out specific tasks. Knowing how these tools compare to traditional game design methods regarding their effectiveness and efficiency is also essential.

In this study, we explored the use of ChatGPT (OpenAI, 2022), a state-of-the-art AI language model, in supporting game designers in carrying out various game design tasks. The experts were then asked in an interview to provide feedback on their experience using the tool and to evaluate its effectiveness in supporting them in carrying out the tasks. The results of this study provide valuable insights into the use of AI-assisted game design tools and the challenges that game designers face when using these tools. Our findings contribute to the growing body of research on AI-assisted game design and offer a deeper understanding of how AI can

- This is an Open Access article distributed under the terms of the Creative Commons Attribution-Noncommercial 4.0 Unported License, permitting all non-commercial use, distribution, and reproduction in any medium, provided the original work is properly cited.

- Selection and peer-review under responsibility of the Organizing Committee of the Conference

© 2023 Published by ISRES Publishing: www.isres.org

support game designers in creating games. Furthermore, our results can inform the development of new AI-assisted game design tools that better meet the needs of game designers.

Related Work

The use of AI in game development is a rapidly growing field of research, with numerous studies exploring the potential of AI to support game developers in various aspects, such as game content generation, level design, and game design (Elton Pym, 2020; Riedl & Zook, 2013; Yannakakis, 2012; Politowski & Guéhéneuc, 2021). Game content generation is one area where AI-assisted tools have shown significant promise (Liebana et al., 2019; Togelius et al., 2011, Summerville et al., 2018). Tools, such as AI Dungeon (2019), use AI to generate game content based on player inputs, such as story, dialogue, descriptions, or characters. AI-powered platforms, such as GPT-3, have also been used to generate game content (Sobieszek & Price, 2022; Vartinen et al., 2022; Shakeri et al., 2021). These tools have the potential to free up game developers' time and creativity by taking care of repetitive or time-consuming tasks, enabling them to focus on other aspects of game development (Delarosa et al., 2021, Larsson et al., 2022; Charity et al., 2020; Li & Xing, 2021; Zagal & Tomuru, 2013; Busurkina et al., 2020; Eberhard et al., 2018; Cho et al., 2020). By enabling faster iteration, these tools have increased game design efficiency and creativity. Additionally, they provide valuable resources to game designers, such as assisting them in obtaining feedback from players through game reviews, which could be utilized to improve the overall game design or specific features.

Apart from getting AI-supported feedback, AIs could support game designers regarding game systems and the design and tuning of individual game mechanics. For instance, Machado et al. (2019) evaluate a recommender system for assisting game designers at a junior level that provides recommendations based on frequent itemset data mining algorithms. AI algorithms have also been used to generate game mechanics and rules, such as in the AI Dungeon game engine (2019). These algorithms can create unique and engaging game mechanics that may not have been possible with traditional design methods (Roohi et al., 2020; Paraschos & Koulouriotis, 2023; Horn et al., 2017; Partlan et al., 2021). AI approaches also offer opportunities to support the ideation process for a game design (Treanor et al., 2015). After Kim and Maher (2023), co-creative AI systems in design allow users to collaborate with an AI partner on open-ended creative tasks in the design process that enhance design creativity by inspiring the exploration of novel design solutions in the initial idea generation. Zhu and Luo (2022) propose a generative approach to design ideation that utilizes the fine-tuning mechanism of GPT to leverage knowledge understanding and domain synthesis. Although showing intriguing results, the output may vary in quality. The authors note that the AI system should not be seen as a designer on its own but as an assistant supporting the ideation phase and brainstorming with human designers to boost their creativity. However, the current approaches only investigate design in a general sense. The integration of AI systems that support the creation of innovative ideas and game design concepts has yet to be explored.

In summary, the study of AI-assisted game design is a crucial area of research, as it can revolutionize how games are designed and developed. This study contributes to this research by exploring ChatGPT, a state-of-the-art language model developed by OpenAI (2022), in supporting game design experts in carrying out various game design tasks, including mechanics and game goals.

Approach

The previous section discussed the various ways in which AI can support game design processes. One particular tool, the popular chatbot ChatGPT, has become popular over the last months and has been employed in various domains. Using a tool such as ChatGPT in the context of game design appears to be an interesting field of investigation. By allowing designers to discuss problem areas with the chatbot in a context-sensitive manner, designers can receive interactive feedback on topics such as game mechanics, initial design ideas, and functions of game systems. While the use of AI systems like ChatGPT can be positive, it's important to acknowledge potential negative effects or areas for improvement, such as the possibility of the system providing insufficient or unusable solutions that could negatively impact the game production process. Our work explores the potential of the exchange between game designers and ChatGPT. Specifically, the paper investigates whether current AI chatbots can effectively support designers in specific design tasks, focusing on the professional perspective of game designers who face these challenges daily. To achieve this, the study will guide designers in interacting with ChatGPT and exploring the system's limitations, using frameworks in the form of tasks. The results of these interactions will be discussed in expert interviews. The upcoming sections will describe the essential elements of the study in greater detail. First, the paper will list the tasks that the designers processed and that

served as the basis for the expert interviews. In the subsequent section, the study's procedures will be described in greater detail, along with more information about the participating experts. Finally, the technical description of the analyses will be presented. By providing a comprehensive overview of the study, this paper aims to shed more light on the potential of AI chatbots like ChatGPT to support game design processes.

Task Design

The tasks are based on the results of a previous study, where game designers were asked about the possible applications of AI and game design. During the study, several scenarios or situations were suggested by the experts, which proved to be helpful for the construction of the tasks of the current study. Based on the experts' suggestions, ten tasks were defined. These were sent out to three experts participating in the survey before the start of this study of this paper. The experts were asked to select three of the ten tasks using Google Forms that were most interesting to them. The tasks that received the most votes were selected for this study. The tasks are listed below:

- **Task 1:** You want to design a serious game for older people (70+) to train their memory playfully. Find out what kind of games and mechanics suit this target group. In addition, clarify the length of interaction and the frequency of interaction (frequency of play, repetitions). The question of whether the game should be designed for single or multiplayer should also be considered.
- **Task 2:** You aim to create a tutorial for an action-adventure game (e.g., Uncharted series, Tomb Raider). You want to find out how to build the tutorial so that the players can grasp essential points (objectives, controls, mechanics) in as short a time as possible, and the tutorial is integrated into the game story.
- **Task 3:** You are considering integrating a time limit (countdown) into your turn-based strategy game, so the opponent does not have to wait too long. Find out which games include time limits, whether players rate time limits well in this context, and how such a limit can be integrated (e.g., the timer only becomes visible after a specific time).

Participants & Procedure

We recruited three game designers from the indie game industry to evaluate our approach (two male and one female). Expert 1 (E1) currently deals primarily with system design, while Expert 2 (E2) deals with various topics in game design (e.g., character controls, balancing, pacing). Expert 3 (E3) can already look back on several years of experience in the field of game design, especially in the area of turn-based strategy. All experts were interviewed individually in a remote scenario. The experts received the tasks via mail one week before the interview. In the mail, we asked them to read through the tasks carefully and solve them before the interview date. As an indication of the time required, 20 to 30 minutes per task was given. In addition to the instructions, a link to ChatGPT was also provided. After the experts had completed all tasks and sent the ChatGPT conversation history, an interview appointment was scheduled to discuss the results. After the interviews for the three tasks were completed, the game design experts could provide their views on the potential for AI in their field of activity by discussing the following questions:

- How valuable is using AI tools, such as ChatGPT, in your professional work as a game designer?
- Will you use ChatGPT or a similar tool for your activities?
- How do you see future applications of services like ChatGPT in your career?
- What risks do you see for your field of activity in the context of AI?

After these questions were discussed in detail, the interview ended. All interviews were recorded with the experts' consent and lasted about 60 to 70 minutes.

Results

This section deals with the experts' perceptions of the individual tasks. The qualitative content analysis procedure by Mayring (2004) was utilized to evaluate the survey's open questions and semi-structured interview notes. For this purpose, the choice fell on the inductive category formation approach to obtain the categories for this evaluation method. The questions listed in section *Participants and Procedure* were employed, which shall provide insights into the potential of ChatGPT to support experts in solving game design tasks. In addition, the experts describe their assessments of the implications of using AI in general in their field of activity.

For the evaluation, we used video recordings of the interviews with the game designers. The individual interviews are between 32 and 38 minutes, resulting in a total of about 108 minutes of material. For evaluation, it was necessary to have the content in text form. Therefore, as a first step, it was required to transcribe the recordings. Since manual transcription means a very high expenditure, a machine procedure was used. The method can also be scaled to more extensive data volumes. A recent paper (Radford et al., 2022) presented a new method, including open-source software, that produces a shallow error rate comparable to human transcription. The model “OpenAI Whisper” is a robust multilingual speech recognizer consisting of a neural network according to the Transformer architecture (Vaswani et al., 2017) trained on 680,000 hours of audio. We used the “large” version, which promises the most accurate results but requires powerful hardware with GPU support to obtain usable transcription times. We ended up with text files with an average length of 12,522 characters. In the following, we report our findings separately for the different tasks.

Task Design General Impression

When reviewing the interview data, it became apparent that each expert had something positive to say about using AI in game design. For instance, E1 explains that AI tools help him save time and energy by helping him gather and structure information (E1: “I don't have to do some research because ChatGPT already provides patterns. I pick two approaches out of eight and can work with them because they fit my concrete problem very well, and it saves time.”). E02 mentions that AI could be used in many areas, including groundwork, tossing ideas back and forth, localization, defining keyframes, text production, and balancing. He and his team want to try out the ChatGPT tool to see how they can tie it into the production process. E2 considers the strengths of AI in areas where the designer defines the essential points. The AI closes the gaps (E2: “...if you as a designer define the key points, the most important points, if you transfer it to animation, the keyframes, and the system interpolates in between, so to speak, or how can you imagine that? Exactly, so I think that will help me a lot, especially when it comes to writing designs, that just much faster and much easier and more pleasant for me to communicate to people”). Like E2, E3 believes tools like ChatGPT can be valuable for generating ideas and serve as a starting point.

However, not only positive things were mentioned. The risks of AI in the game design field and for game development, in general, were also discussed: For instance, E01 emphasizes that it is essential to be aware that third parties can control AI systems, so one should only rely on them a little. Furthermore, E01 states that AI systems need to be critiqued, as one would do with input from another designer (E1: “For me, the program is a design colleague, an assistant that reminds you of things, that maybe sometimes even corrects you if there's a mistake if you've remembered it wrong or whatever, so it's an assistance system that has contextual knowledge. But colleagues can also make errors”). E3 also mentions that there are also risks, such as the danger that AI-based programs could replace jobs and entail legal issues (E3: “I think that's just about the biggest problem I see with it in professional use. This probably has nothing to do with the tool itself but simply that the terms of use are too unclear.”). E3 also sees the need for humans to be able to control AI and judge artistic representation. Besides, E3 is open to using such tools in his work and thinks it's great that such technologies are being researched (E3: “We've already joked with the design team that we'll somehow generate some story with it and then move away from that. So yes, I think these basic ideas and suggestions are really interesting that you can probably get from them.”).

Task Design Task 1: Game Design for Elderly People

When evaluating ChatGPT concerning Task 1, the experts had several points of criticism. Although the chatbot supported them in the task, they saw the potential for improvement on several levels. For instance, E03 noted that she had to dig deeper into specific areas to get the correct and satisfying answer (E3: “The text is then simply iterated, i.e., you ask for something, and ChatGPT then actually just tries to put somehow what has already been said into another form. That was a little bit of strange.”). E2 noted that ChatGPT could not provide expert knowledge, but the system did assist him in completing the tasks (E2: “I wouldn't call it expert knowledge. ChatGPT has not played any games. It is purely based on text. To be an expert, you must have played the games, at least in my opinion.”). E02 also envisioned a research project combining image generators with text adventures to see what emerges.

Another interesting observation was that E1 had not expected that he would get the ultimate answer for the target audience (E1: “Some of the input didn't fit - honestly, that's what I assumed. You must think for yourself just as much as if you get feedback from someone. That's why it was mixed in terms of my impression of how

helpful it was.”). E1 also had the impression that the AI was careful regarding its formulations and did not try to present the ultimate solution.

However, E1 saw this aspect as something positive by mentioning: “This is also the case when we analyze and discuss concepts internally and compare new concepts with old concepts because we are aware that just because something has worked in the past does not mean it will work the same way for the new concept.” Besides, E1 thought he had to look critically at the results and see if they fit his use case. In general, the experts also identified some positive aspects: E2 found completing the requirements fun and answered the game design questions with three suggestions provided by the chatbot. Besides, E03 mentioned that the ChatGPT could give the details in some cases when needed. E03 also noted that he received surprising responses concerning game design suggestions, including a progression system that she had not expected.

Task Design Task 2: Tutorial for Action-Adventure Game

As with task 1, there were several positive and negative points. According to E1, ChatGPT helped him complete the task by providing him with several solution strategies. E01 picked out specific points to obtain more information on the given task. However, E1 noted that it is not easy to come up with a solution in design work within the given task (E1: “I didn't expect in advance that I would now get the ultimate answer as to the ideal result for this target group. And that was not the case. And I think that has to do with the fact that our work is primarily creative.”). Besides, he notes that ChatGPT needs to be careful about suggestions because not everything that works in the provided examples will apply to Task 2 (E2: “That's also the case when we analyze and discuss any concepts internally and compare new concepts with old ones because it's just conscious. Just because it worked now in the past doesn't mean that it will work the same for the new concept.”). E2 also mentioned some positive aspects by stating that the ChatGPT helped him solve the task by providing him with a checklist to cover the basics. E2 noted that he was surprised at how much knowledge the system provided and that he might try it for his next game. The expert also said that he would have found it interesting if he could have seen a game to get more concrete suggestions for the tutorial (E2: “It would have been interesting if I had seen a game, an adventure game. If I could somehow feed the game or the rules of the game and if he could then give me more specific suggestions for the tutorial. That would be interesting. But I don't know if that wouldn't eat up too much time and effort as opposed to just doing it myself.”). E3 was rather negative about the outcome of task 2. She felt ChatGPT did not help her complete the task because it needed to be more specific and address the requirements of the task (E3: “I think that that was a bit too general for me; probably a relatively good starting point, but where you would then have to do further research yourself and would then have to consider how something like that could look.”). Furthermore, the expert got some results that confused him (E3: “You ask I want a tutorial that integrates well with the story, and then ChatGPT suggests that you should make the tutorial so that it integrates with the story.”) In general, she felt that the knowledge gained was limited in this form.

Task Design Task 3: Timers in Games

In this task, the experts were relatively positive about the results obtained with ChatGPT. According to E1, ChatGPT was helpful and provided suggestions based on specific examples. Like E1, E2 felt that ChatGPT assisted with this task and would even go so far as to say that he would now do the actual design and continue working on it. He explained that ChatGPT saves a lot of research and writing time (E2: “The program saves tedious work. Yes, or it's also very effective for brainstorming because I've talked to ChatGPT, for example, where I somehow designed a city planning game just for fun.”). However, E2 remarks that designers still must follow up and correct certain things because ChatGPT doesn't know everything and sometimes makes mistakes (E2: “But now I have noticed that you can't believe everything the program says. Sometimes there is an error in it, or it just does not know everything. You always have to check and correct now and then.”). Besides, E2 was surprised that ChatGPT told him something he didn't already know (E2: “It also surprised me because, for example, the mechanics of Advanced Wars, which ChatGPT listed, I didn't know at all, or the game in general.”). Overall, the E2 was delighted with the outcome and felt it was a time saver. As in the previous task, the experts identified several negative aspects: E1 notes that the tool was agnostic and did not provide an ultimate solution to the problem (E1: “Because the AI then gave a concrete example of a game in which this and that was good. And when I then ask about it, the AI suddenly becomes very cautious again and says, yes, of course, you can't say that unequivocally. ChatGPT then tried to justify itself. That also sounds so funny.”). E1 was surprised by the level of detail and specificity in the tool's responses but noted that it was cautious in its suggestions and did not make any definitive claims. The conversation touches on the limitations of the tool's

suggestions and the speaker's uncertainty about adopting the tool's recommendations in a professional setting. E3 mentions that ChatGPT provided a good overview in completing the task, but there were problems in the implementation. The expert thinks it did not go deep enough to understand how to integrate timers into a game to avoid discouraging players (E3: "There are also players who are really put off by timers. So, where it goes in the direction of the game with a timer, they would not play it. ChatGPT indicated some players might feel pressured by a timer. It can be problematic that people don't want that. That's where the program could have gone more in-depth."). Overall, E3 feels the information was rather superficial, and there could have been more concrete game situations to understand how to use timers effectively.

Discussion

One of the critiques expressed by the experts was that the exchange lacked depth in terms of content, and they wanted more detailed information on specific issues. The experts suggested that some of the recommendations made by ChatGPT could have been more precise and provided more profound insights into particular topic areas. In addition, the program was hesitant to commit fully to specific proposals, even when prompted by one of the experts to provide more detailed answers. This led one of the experts to infer that ChatGPT may have intentionally imposed restrictions in certain areas.

Despite these criticisms, there were also positive aspects of the exchange that surprised the experts. For instance, the program encouraged experimentation when one of the experts used ChatGPT for game design, which provided a basis for the expert's work. The experts agreed that the program was a good foundation for further design work and could positively impact the development of game design ideas. However, none of the experts provided a purely positive evaluation of the results, and E3 summarized the situation by noting that ChatGPT tended to focus more on the positive rather than the negative aspects of the responses.

In conclusion, there were both positive and negative aspects to the interaction. The experts' criticism of the lack of depth in content and ChatGPT's tendency to repeat certain statements may have limited the effectiveness of the exchange. However, the experts noted the program's encouragement of experimentation and ability to provide a good foundation for further design work. Therefore, it can be concluded that the exchange was a mixed success with strengths and weaknesses that should be considered in future interactions.

ChatGPT as a Fellow Game Designer

During the implementation phase, it was observed that the experts began attributing human-like qualities or behaviors to the program, which is not uncommon in the field of interactions with AIs (Reeves & Nass, 1996). This phenomenon was evidenced in several instances. For instance, E1 expressed that he sometimes felt that the chatbot was cautious about providing specific recommendations for fear of being proven wrong. He explained that he found it somewhat eerie that he was beginning to think of the program as a person. As he continued to work through the tasks, he started to view ChatGPT as a work colleague, a game designer who assisted him with specific problems. E1 even mentioned that he communicated with the program in a way that was similar to how he interacted with other work colleagues. This interaction aspect stood out to E1 and was revisited several times during the interview.

E2 also exhibited a similar tendency to attribute human qualities to the program. While he frequently referred to the chatbot as a design tool, he also called it an AI designer and assigned anthropomorphic pronouns such as "he" to the program. E2 also used adjectives such as "smart" to describe the program, a characteristic often associated with humans. E3 also had a comparable impression when she remarked during the interview that she was eager to experiment with the new chat designer. This further supports the idea that the experts viewed the program as a human-like entity.

This tendency to anthropomorphize the program has been studied in the field of human-AI interaction and is a well-documented phenomenon (Salles et al., 2020; Li et al., 2021; Sung et al., 2021; Troshani et al., 2021). Anthropomorphism refers to the attribution of human-like characteristics to non-human entities. It is often observed in interactions with AIs, where users may unconsciously assign human traits to the program. This may be since humans have a natural inclination to perceive and interpret things in anthropomorphic terms. This phenomenon can be advantageous in human-AI interactions as it helps to establish a more natural and engaging connection with the program. However, it can also have negative consequences, such as unrealistic expectations of the AI's capabilities or a distorted perception of its limitations.

The Future of AI-Powered Game Design

The experts who participated in the study were optimistic about future use cases of AI technologies in the game development industry. They believed that AI technologies would revolutionize the industry by providing innovative and efficient solutions to many of the challenges game designers face. One area where AI could be beneficial is the conceptual phase of game development. AI technologies could help designers by filling in the content gaps in their initial ideas, allowing them to focus on the critical aspects of the game. Additionally, AI could simplify the time-consuming process of formulating and updating game design documents, freeing designers to focus on other parts of the development process. The experts also noted that AI could be useful in researching specific target groups or game mechanics, allowing designers better to understand the needs and preferences of their intended audience. AI could also be used to compile game reviews of existing games, providing designers with valuable insights and recommendations for new designs. Another area where AI could be highly beneficial is in defining and balancing complex game systems, such as strategy games. By allowing the designer to define the framework and letting AI handle the time-consuming details, designers could save significant amounts of time and effort. AI could also present complex and large amounts of data efficiently and in an easily understandable way, facilitating design decisions and speeding up the development process. In sum, the experts saw many potential future applications for AI technologies in game development. They believe these technologies will play a significant role in transforming the industry in the coming years.

Limitations

The discussion of the interviews and analysis conducted in the study provides valuable insights into the intersection of game design and AI. However, it is essential to acknowledge that the study has some limitations that must be considered. One of the main limitations is that the study only focuses on a limited set of tasks, as the experts processed only three tasks to manage the workload of game designers. These tasks primarily deal with conceptual aspects or relatively clearly defined topics. Future studies should consider including other elements, such as game development's production and post-production phases. This would allow for a more comprehensive understanding of how AI can support game design, including relevant topics like balancing game systems and interpreting playtests. Moreover, it is worth noting that there are overlapping topics between different departments involved in game development, such as game design, programming, and game art. Exploring how these various departments can work together to achieve a specific goal, such as realizing a particular game mechanic, would provide valuable insights into the game development process. Another significant limitation is the rapidly evolving nature of AI research, which can make technology quickly become obsolete or improved. As the study uses ChatGPT to enrich work processes in game design, it is crucial to recognize its limitations. The experts identified some weaknesses in ChatGPT, such as more content depth in recommendations to extract concrete action instructions. However, the game designers believe that these issues will be addressed in the future, and AI will radically change the game development process.

Conclusions

In conclusion, this paper explored the potential of the exchange between game designers and ChatGPT, investigating whether current AI chatbots can effectively support designers in specific design tasks. While ChatGPT and the experts held different views on the exchange quality, several positive aspects were mentioned. The experts noted the program's encouragement of experimentation and its ability to provide a good foundation for further design work. However, the experts criticized ChatGPT's tendency to repeat certain statements and the lack of depth in content. It was also quite interesting that the experts also tended to anthropomorphize the program, attributing human-like qualities to it. In sum, the experts believe that AI technologies have the potential to revolutionize the game development industry, particularly in the conceptual phase of game development. The results so far encourage us to look even deeper into the topic. Thus, we plan to include other game design tasks in future studies that deal with production processes over a more extended period. The players' involvement in the game design process, which an AI moderates, proves to be an exciting field of research.

Scientific Ethics Declaration

The authors declare that the scientific ethical and legal responsibility of this article published in EPSTEM journal belongs to the authors.

Acknowledgements or Notes

* This article was presented as an oral presentation at the International Conference on Technology (www.icontechno.net) held in Antalya/Turkey on November 16-19, 2023.

References

- AI Dungeon. (2019). Home. Retrieved from <https://play.aidungeon.io/main/home>
- Araújo, W., & Aranha, E. (2020). Collaborative artificial intelligence for supporting the development of games. *Proceedings of the Brazilian Symposium on Computer Games (SBGames)*, 1116–1119.
- Busurkina, I., Karpenko, V., Tulubenskaya, E., & Bulygin, D. (2020). Game experience evaluation. A study of game reviews on the Steam platform. In D. A. Alexandrov, A. V. Boukhanovsky, A. V. Chugunov, Y. Kabanov, O. Koltsova, & I. Musabirov (Eds.), *Digital Transformation and Global Society* (pp. 117–127). Cham: Springer International Publishing.
- Charity, M., Khalifa, A., & Togelius, J. (2020). Baba is y'all: Collaborative mixed-initiative level design. *2020 IEEE Conference on Games (CoG)*, 542–549.
- Cho, H., Bossaller, J. S., Adkins, D., & Lee, J. H. (2020). Human versus machine: Analyzing video game user reviews for plot and narrative. *Proceedings of the Association for Information Science and Technology*, 57(1).
- Conroy, D., Wyeth, P., & Johnson, D. (2011). Modeling player-like behavior for game AI design. *Proceedings of the 8th International Conference on Advances in Computer Entertainment Technology*. Lisbon, Portugal.
- Delarosa, O., Dong, H., Ruan, M., Khalifa, A., & Togelius, J. (2021). Mixed-initiative level design with RL brush. In J. Romero, T. Martins, & N. Rodríguez Fernández (Eds.), *Artificial Intelligence in Music, Sound, Art and Design* (pp. 412–426). Cham: Springer International Publishing.
- Eberhard, L., Kasper, P., Koncar, P., & Gutl, C. (2018). Investigating helpfulness of video game reviews on the Steam platform. *2018 Fifth International Conference on Social Networks Analysis, Management and Security (SNAMS)*, 43–50.
- Elton Pym, A. (2020). Principles for AI co-creative game design assistants. *Artificial Intelligence and Interactive Digital Entertainment Conference*.
- Hendrikx, M., Meijer, S., Van Der Velden, J., & Iosup, A. (2013). Procedural content generation forgames: A survey. *ACM Trans. Multimedia Comput. Commun. Applications*, 9(1).
- Horn, B., Hoover, A. K., Folajimi, Y., Barnes, J., Hartevel, C., & Smith, G. (2017). AI-assisted analysis of Player Strategy across Level Progressions in a Puzzle Game. *Proceedings of the 12th International Conference on the Foundations of Digital Games*. Hyannis, Massachusetts.
- Kim, J., & Maher, M. L. (2023). The effect of AI-based inspiration on human design ideation. *International Journal of Design Creativity and Innovation*, 1–18.
- Kreminski, M., Acharya, D., Junius, N., Oliver, E., Compton, K., Dickinson, M., ... Wardrip Fruin, N. (2019). Cozy mystery construction kit: Prototyping toward an AI-assisted collaborative storytelling mystery game. *Proceedings of the 14th International Conference on the Foundations of Digital Games*. San Luis Obispo, California, USA.
- Larsson, T., Font, J., & Alvarez, A. (2022). Towards AI as a Creative Colleague in Game Level Design. *Proceedings of the AAAI Conference on Artificial Intelligence and Interactive Digital Entertainment*, 18(1), 137–145.
- Li, X., & Sung, Y. (2021). Anthropomorphism brings us closer: The mediating role of psychological distance in User–AI assistant interactions. *Computers in Human Behavior*, 118, 106680.
- Li, M., & Suh, A. (2021). Machinelike or humanlike? A literature review of anthropomorphism in AI-enabled technology. *Proceedings of the 54th Hawaii International Conference on System Sciences*, 4053–4062.
- Li, X., Zhang, Z., & Stefanidis, K. (2021). A data-driven approach for video game playability analysis based on player's reviews. *Information*, 12(3).
- Machado, T., Gopstein, D., Nealen, A., Nov, O., & Togelius, J. (2018). AI-assisted game debugging with Cicero. *2018 IEEE Congress on Evolutionary Computation (CEC)*, 1–8.
- Machado, T., Gopstein, D., Wang, A., Nov, O., Nealen, A., & Togelius, J. (2019). Evaluation of a recommender system for assisting novice game designers. *Proceedings of the Fifteenth AAAI Conference on Artificial Intelligence and Interactive Digital Entertainment*. Atlanta, Georgia: AAAI Press.
- Mayring, P., & Others. (2004). Qualitative content analysis. *A Companion to Qualitative Research*, 1(2), 159–176.
- OpenAI. (2022). Chat. Retrieved from <https://chat.openai.com/>

- Paraschos, P. D., & Koulouriotis, D. E. (2023). Game difficulty adaptation and experience personalization: a literature review. *International Journal of Human-Computer Interaction*, 39(1), 1–22.
- Partlan, N., Kleinman, E., Howe, J., Ahmad, S., Marsella, S., & Seif El-Nasr, M. (2021). Design-driven requirements for computationally co-creative game AI design tools. *Proceedings of the 16th International Conference on the Foundations of Digital Games*. Montreal, QC, Canada.
- Perez-Liebana, D., Liu, J., Khalifa, A., Gaina, R. D., Togelius, J., & Lucas, S. M. (2019). General video game AI: A multitask framework for evaluating agents, games, and content generation algorithms. *IEEE Transactions on Games*, 11(3), 195–214.
- Politowski, C., Petrillo, F., & Guéhéneuc, Y.-G. (2021). A survey of video game testing. *2021 IEEE/ACM International Conference on Automation of Software Test (AST)*, 90–99.
- Radford, A., Kim, J. W., Xu, T., Brockman, G., McLeavey, C., & Sutskever, I. (2022). *Robust speech recognition via large-scale weak supervision*. <https://cdn.openai.com/papers/whisper.pdf>
- Reeves, B., & Nass, C. (1996). *The media equation: How people treat computers, television, and new media like real people and places*. Retrieved from <https://books.google.at/books?id>
- Riedl, M. O., & Zook, A. (2013). AI for game production. *2013 IEEE Conference on Computational Intelligence in Games (CIG)*, 1–8.
- Roohi, S., Relas, A., Takatalo, J., Heiskanen, H., & Hämäläinen, P. (2020). Predicting game difficulty and churn without players. *Proceedings of the Annual Symposium on Computer-Human Interaction in Play*, 585–593. Virtual Event, Canada.
- Salles, A., Evers, K., & Farisco, M. (2020). Anthropomorphism in AI. *AJOB Neuroscience*, 11(2), 88–95.
- Shakeri, H., Neustaedter, C., & DiPaola, S. (2021). SAGA: Collaborative storytelling with GPT-3. *Companion Publication of the 2021 Conference on Computer Supported Cooperative Work and Social Computing*, 163–166. Virtual Event, USA.
- Sobieszek, A., & Price, T. (2022). Playing games with ais: The limits of GPT-3 and similar large language models. *Minds and Machines*, 32(2), 341–364.
- Summerville, A., Snodgrass, S., Guzdial, M., Holmgård, C., Hoover, A. K., Isaksen, A., ... Togelius, J. (2018). Procedural content generation via machine learning. *IEEE Transactions on Games*, 10(3), 257–270.
- Togelius, J., Kastbjerg, E., Schedl, D., & Yannakakis, G. N. (2011). What is procedural content generation? Mario on the borderline. *Proceedings of the 2nd International Workshop on Procedural Content Generation in Games*. Bordeaux, France.
- Treanor, M., Zook, A., Eladhari, M. P., Togelius, J., Smith, G., Cook, M., ... Smith, A. (2015). AI-based game design patterns. In *Proceedings of the 10th International Conference on the Foundations of Digital Games 2015 (FDG 2015)*. Retrieved from <http://www.fdg2015.org>
- Troshani, I., Hill, S. R., Sherman, C., & Arthur, D. (2021). Do we trust in AI? *Role of Anthropomorphism and Intelligence*. *Journal of Computer Information Systems*, 61(5), 481–491.
- Vaswani, A., Shazeer, N., Parmar, N., Uszkoreit, J., Jones, L., Gomez, A.N., Kaiser, L. & Polosukhin, I. (2017) Attention is all you need. *Advances in neural information processing systems*, 30 (2017).
- Värtinen, S., Hämäläinen, P., & Guckelsberger, C. (2022). Generating role-playing game quests with GPT language models. *IEEE Transactions on Games*, 1–12.
- Yannakakis, G. N. (2012). Game AI revisited. *Proceedings of the 9th Conference on Computing Frontiers*, 285–292. Cagliari, Italy.
- Zagal, J. P., & Tomuro, N. (2013). Cultural differences in game appreciation: A study of player game reviews. *FDG*, 86–93.
- Zhao, Y., Borovikov, I., de Mesentier Silva, F., Beirami, A., Rupert, J., Somers, C., ... Zaman, K. (2020). Winning is not everything: Enhancing game development with intelligent agents. *IEEE Transactions on Games*, 12(2), 199–212.
- Zhu, Q., & Luo, J. (2023). Generative design ideation: A natural language generation approach. In J. S. Gero (Ed.), *Design Computing and Cognition '22* (pp. 39–50). Cham: Springer International Publishing.

Author Information

Michael Lankes

University of Applied Sciences Upper Austria
Softwarepark 11, 4232 Hagenberg, Austria

Andreas Stockl

University of Applied Sciences Upper Austria
Softwarepark 11, 4232 Hagenberg, Austria
Contact e-mail: Andreas.stoeckl@fh-hagenberg.at

To cite this article:

Lankes, M. & Stoeckl, A. (2023). AI-powered game design: Experts employing ChatGPT in the game design process. *The Eurasia Proceedings of Science, Technology, Engineering & Mathematics (EPSTEM)*, 24, 1-9.

The Eurasia Proceedings of Science, Technology, Engineering & Mathematics (EPSTEM), 2023

Volume 24, Pages 10-20

IConTech 2023: International Conference on Technology

Quality Issue Classification by Using Dedicated Data Analysis Software Created in Phyton Language

Elena Raducan

“Dunarea de Jos” University of Galati

Mihaita Arhip

Liberty Steel Galati

Abstract: Quality issues enroll as one of the most important aspects which needs to be avoided in a factory. When a product has quality issues always the economic losses for the company are experienced. The paper approaches manufacturing steel sector and presents the methodology used to classify the quality issues detected to coils in hot strip mill (HSM) factory. The algorithm was developed in python software language and tested on data sets from the plant site. The method used proves the efficacy of the algorithm through the quality issues classification identified on HSM. Also, the HSM represents one of the most important components from a steel factory. Any kind of issues that may occur on HSM production line has direct impact on finished products, which may conduct to big economic losses to the company. In this paper, a method for coils issues classification is described. The dedicated software was created in phyton language and after months of tests was installed to the operators computers for a quick quality issues identification.

Keywords: Telescopicity, Hot strip mill, Coils, Data analysis, Algorithms, Distance lasers sensor

Introduction

Metallurgical plants contain mixed and quite complex processes that extended along the flow of production lines to the finished product. All these processes have a great impact on final quality of the products in higher or lower ratios. In a hot strip mill, slabs are heated and passed through a series of rough stands, are transformed in a plate with proper thickness and width. The finishing train – a tandem with 7 stands – transform this plate in a continuous strip. After exit of finishing train, the strip passes through the run-out table where is cooled at a proper temperature to be coiled (Figure 1). Coils are the most efficient manner to storage, manipulate and deliver strips, without needs to cut or fold.

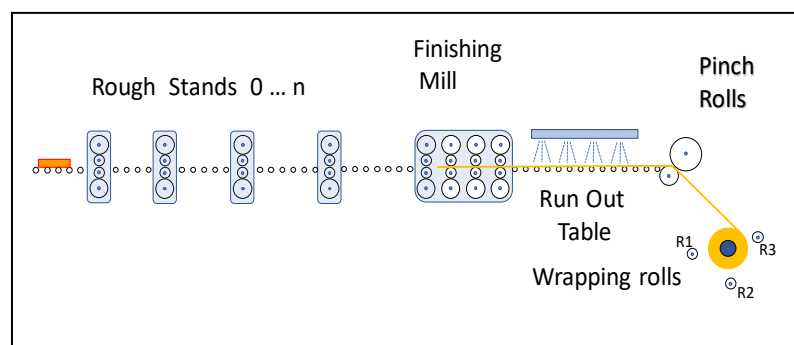


Figure 1. Hot strip mill layout.

- This is an Open Access article distributed under the terms of the Creative Commons Attribution-Noncommercial 4.0 Unported License, permitting all non-commercial use, distribution, and reproduction in any medium, provided the original work is properly cited.

- Selection and peer-review under responsibility of the Organizing Committee of the Conference

© 2023 Published by ISRES Publishing: www.isres.org

In a hot strip mill, the coiling process is totally different from other lines, where the first layers are performed at low speed with or without help of a belt wrapper. Here the coiler is a special device which consists of a mandrel and a few wrappers rolls and with the aid of two pinch rolls is capable to “catch” and roll the strip head at very high speed.

Quality Issue That May Occur in Hot Strip Mill

The European Standard EN 10051 for coils results from hot strip mills contains information to be supplied by the purchaser at the time of enquiry and order and tolerances for the main characteristics (European Standard EN 10051, 1991): thickness, length, width, flatness, out of squareness and edge camber. All these quality issues may occur in different stages of manufacturing process. Hot strip mill has a great impact on final product and the continuous adjustment is needed to be performed. To achieve the tolerances for the main features, the laminating and coiling processes must be very well performed by high-speed modern controllers, the mill maintenance must be excellent, the mechanical and hydraulic parts must be in good conditions.

A supplementary requirement for coil is in general asked by the customers, regarding the coil shape. The coil aspect at hot strip mill exit not only indicates the ability of manufacturer to manage the process. A coil with uneven laps can provoke supplementary defects when transporting by bending of out triggered edges or in the further manipulating of coils – in pickling, skin pass, galvanizing lines or cold strip mills.

Telescopeness

The misalignment of coil wraps is called telescopeness (Ostroverhov, et al., 1992) . Even if the telescopeness is not an issue described in European standard for coils, the winding quality is more and more important for clients, which introduce in contracts special requirements in this direction, because of further problems that can appear. Most coil deliverers define their own internal standards regarding the telescopeness. So, in company’s products catalogues, we can meet values like 50mm, 60mm or, in worst case 70 mm for this feature. An example of the telescopeness quality issue can be seen in Figure 2, here below.

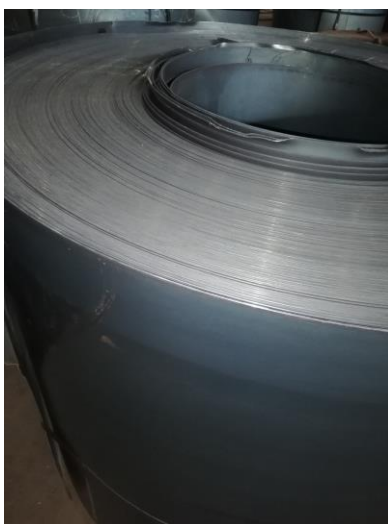


Figure 2. Example of telescopeness quality issue

The customers and the manufacturer are interested by the telescopeness issue and the cause that produce this need to be investigated, because can appear in different locations on the coil and has different causes. Generally, the coil defects depend on the process variables. At the coiling beginning, the first laps are performed with a low tension in the strip. The expansion of the mandrel and the disturbance in strip tension can provoke a misalignment of the first laps – the so called internal telescopeness. In the middle of the process, an incorrect tension in strip between finishing mill and mandrel, can also generate an alternate coiling. At the end of the process, after the tail of strip leaves the finishing mill, the uncontrolled movement of the strip on running table can generate the so called external telescopeness.

Similar study was presented in different science papers, and the methods applied to measure the distance with the laser sensor were different. For example, in Tonnon et al. (1998, pp. 801-808) and in Degner et al. (1999, pp. 87-89), motorized laser distance sensor was used to trace a half of coil profile, directly on the mandrel or near the mandrel.

Another publication, Lima Junior et al. (2007, pp. 7-11), propose a hydraulic device to correct the telescopeness of coil, for horizontal and vertical position. For online correction, (Popovich et al., 1994), a device with two variable frequency drives and two linear induction motors corrects the aluminum strip position by manipulating the tension across the strip and the same problem is solved by applying two different forces on the upper pinch roll shaft (Zhang & Ren Lianeli, 2018). In literature we can find the description of an offline simulator, (Choi & Lee, 2009, pp. 53-61), and the influence of temperature is studied to reduce the coiling telescope.

Installation Description

The coils are transported by a chain conveyor to the expedition sector. Over the chain, a distance laser sensor, using triangulation method is placed in a protective case (Figure 3). The distance between the hot coil and laser sensor must be enough to avoid the sensor damage, even in case of conveyor stoppage.

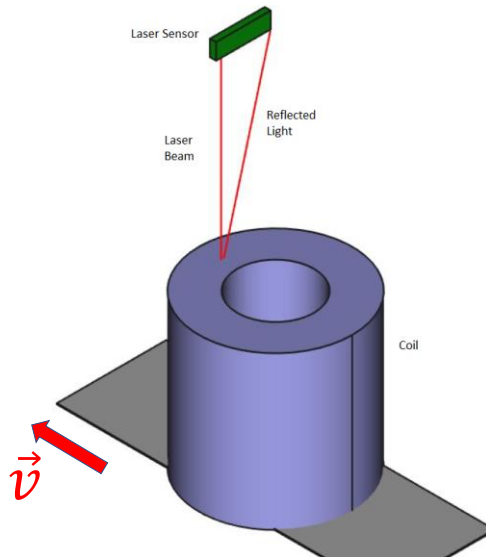


Figure 3. Principle of coil telescopeness measuring.

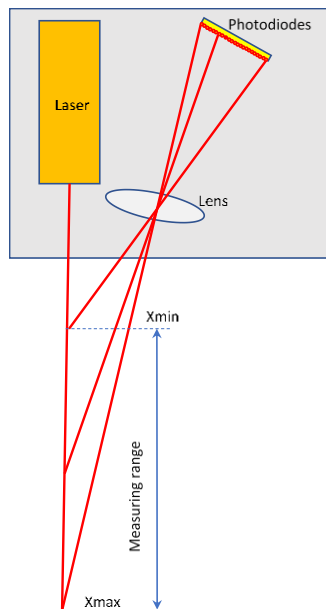


Figure 4. Triangulation principle.

The triangulation method was used because of the advantage of continuous energy radiated. In this method, a laser beam is projected on the side of coil and created a spot on the wraps and the reflected light is analyzed by a receiver placed at a known distance from the laser. The light passes the receiver window and is concentrated on a photodetector with 2000 cell arranged in line with a lens. Knowing the angle of received light, the distance can be measured with a precision 1/2000 of the measuring range. With the help of DSP (Digital Signal Processor) the resolution can be improved to 1/32000 of measuring range. The principle is sketched in Figure 4 where Xmin and Xmax represents the minimum and maximum distance of the laser sensor.

In Figure 5, a simplified diagram of quality classification system is presented. Laser sensor (LIMAB, PreciCura) includes an electronic part capable to filter itself the signals and to deliver a proportional signal with the distance to the obstacle. The laser sensor is used at maximum sample speed (2 kHz) provided by the internal synchronizing bloc (Sinc In.). The Detector CCD is the light sensor with 2000 photodiodes. With the COG (Center of Gravity) bloc, the distance is measured with an improved precision, up to 1/32000 of measuring range. The results are divided and filtered (not in this case because we have our own algorithm to process the signals) and delivered to some interfaces. The interface is RS232 with a baud rate 38400 bit/s. The serial interface baud rate and data format for information about distance (6 bytes) permit to transmit the distance in samples in less than 2 ms. With help of an IOT (Internet of Things) device, data in serial format are transferred through Enterprise Ethernet Network to a server. For every coil, a .csv (Comma Separated Variable) file is generated containing the successive results of measuring. There are hundreds of files every day.

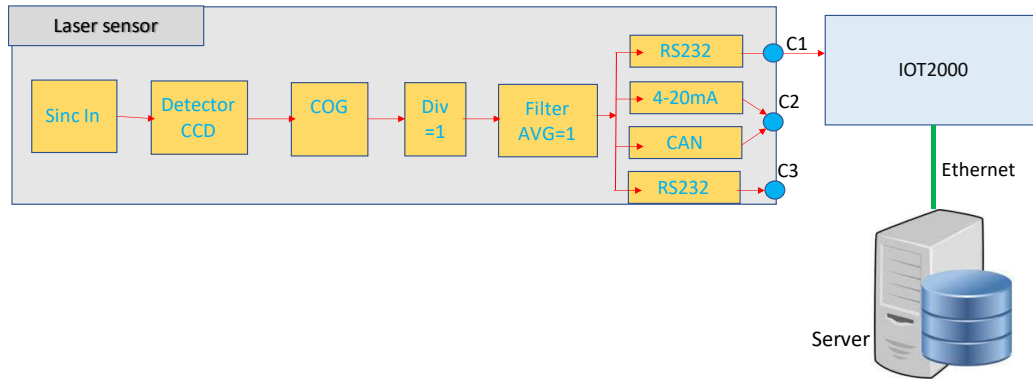


Figure 5. Quality classification system simplified diagram.

The sampling time must be small enough to avoid missing wraps. For continuous - time signals of finite bandwidth, the Shannon-Nyquist theorem (Shanon, 1998) establish a sufficient condition for the sample period to capture the entire information contained in it. The formulation of the theorem is:

“If a function $x(t)$ contains no frequencies higher than B hertz, it is completely determined by giving its ordinates at a series of points spaced $1/2B$ seconds apart” (Shanon, 1998).

In other words, the sampling must accomplish the Nyquist criteria (Nyquist, 1928, p. 617):

$$T = 1 / 2B \quad (1)$$

where:

- T – the sample time or sampling period
- the bandwidth of the signal – there are not frequencies higher in the continuous time signal

In our case, for the smallest thickness of the strip with at least 2 samples for every wrap, we can reconstruct “the envelope” of the coil.

The criteria become:

$$T = b_{min} / 2v \quad (2)$$

where:

- T – the sample time required for DSP

- b_{min} – minimum strip thickness
- v – the chain conveyor speed (constant)

By replacing variables in (2) with mill characteristics, T is equal to 4.3ms. The installation, that means the laser sensor, the IOT system and the server must be able to process the samples in this time or faster.

Methodology Used for Classification

For daily reports, the .csv files are opened one by one, and the workflow of the algorithm is indicated in Figure 6, here below.

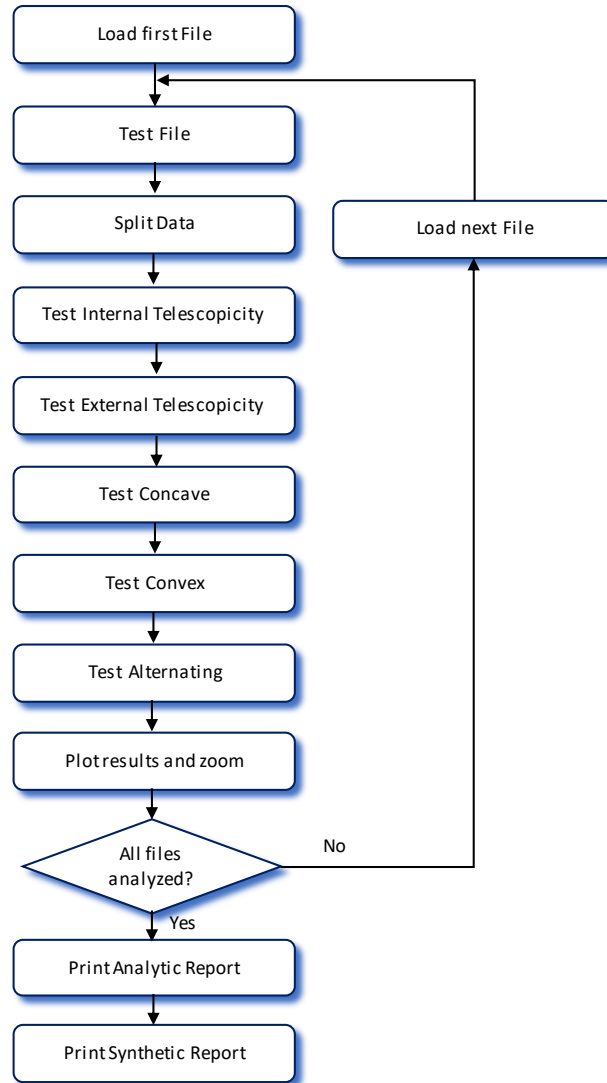
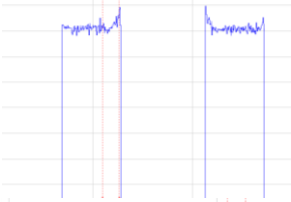

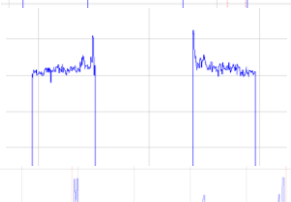

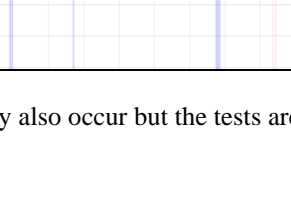


Figure 6. The classification algorithm workflow.

First, the opened file is tested if data are ok. That means the number of rows must be equal with the declared value in the first row of the file, the measured distance must be in the width range of the mill products, the calculated hole diameter must be equal with the mandrel diameter, the coil must be symmetric, etc. If the chain conveyor is stopped when the coil is passing under the laser beam, this test will generate an alarm. In the next step, the recorded data are split in six groups to test for internal telescopeness, external telescopeness, for concave and convex test, alternating test.

Examples of telescopeness issues, observed with the actual PDA (Process Data Acquisition) system before implementation of the algorithm in server are shown in the Table 1.

Table 1. Telescopeness issues -data visualization in actual PDA system	
PDA image	Type of quality issues
	Internal telescopeness
	External telescopeness
	Convex telescopeness
	Concave telescopeness
	Alternate wrapping

Mixed telescopeness issue may also occur but the tests are more complex to identify all of them.

Results and Reports

For an easy interpretation, data are plotted. Three graphs are plotted for every coil – an overall graph, a zoom graph, and a graph with sample times. At the same time, a row in a file with test results is recorded. After all files are tested, two reports are printed in pdf format, classification, and analytic reports.

In the classification report, for every coil, that means for every file, a row with test results is added. In Figure 7, a facsimile from a daily report, with coils with indexes from 196-202 is shown. We can observe that data are not OK for coil with index 200, the coils with indexes 198 and 200 have internal telescopicity (TI) marked with yellow filled circle (Test TI – deviation between 30 mm and 60 mm), coils with indexes 198, 199 and 202 are marked with yellow filled circle for external telescopicity (TE) (Test TE – between 30 mm and 60 mm) while all the other tests are marked with green filled circle (between 0 and 30 mm).






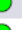





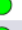





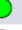
























CLASSIFICATION REPORT: DD-MM-YY							
OK Data	Width	Test TI	Test TE	Test Convex	Test Concave	Test Alternating	INDEX
	1304.17						196
	1207.34						197
	1206.62						198
	1204.93						199
	1210.66						200
	1210.29						201
	1210.92						202

Figure 7. The classification report – facsimile.

In the analytic report, one page for every coil is added. At page 197 we find all the information about the coil with index 196 marked with green circles at all tests. Green circles mean deviation between 0 and 30 mm. We can observe a value for telescopeness equal to 29 mm and a standard deviation equal to 2.84 mm. Knowing the chain conveyor speed and measuring the passing time, also the approximate coil diameter is calculated. This value is also checked in algorithm to accomplish the mill feature.



Figure 8. The analytic report – facsimile from page 197.

An example of external telescopeness identification (yellow class) is shown in Figure 9, below, where, the telescopeness has the value 52.80 mm and the standard deviation is 4.33 mm.

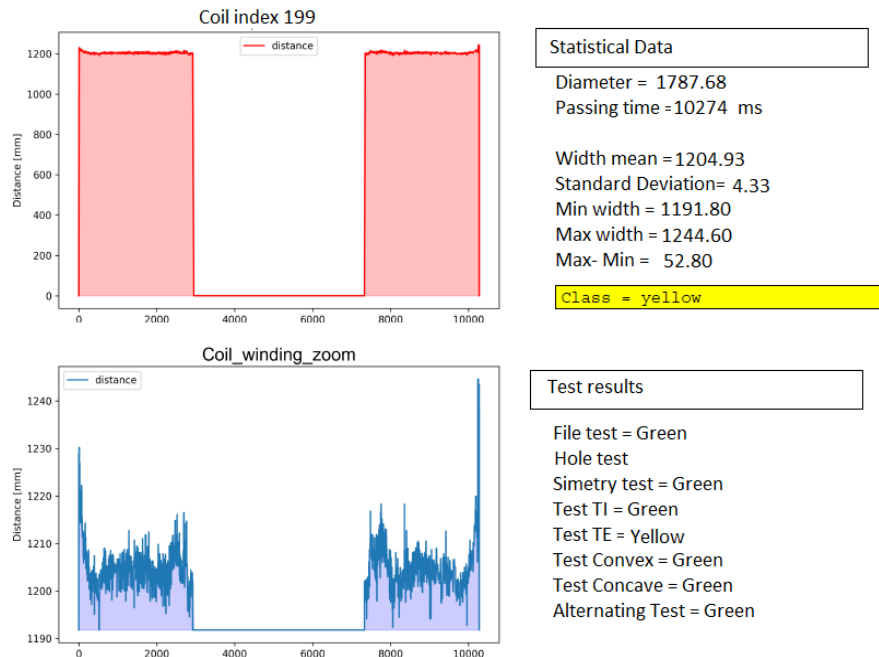


Figure 9. The analytic report – facsimile from page 200.

For index 200, as shown in Figure 7 (extraction from the classification report), in analytical report at page 201, the cause for the red circle was identified – the coil was stopped under the laser beam. An example of a

combination of internal and external telescopeness identification (yellow class – both) is shown in Figure 11 and the overall telescopeness has the value of 40.50 mm and the standard deviation is of 3.86 mm.

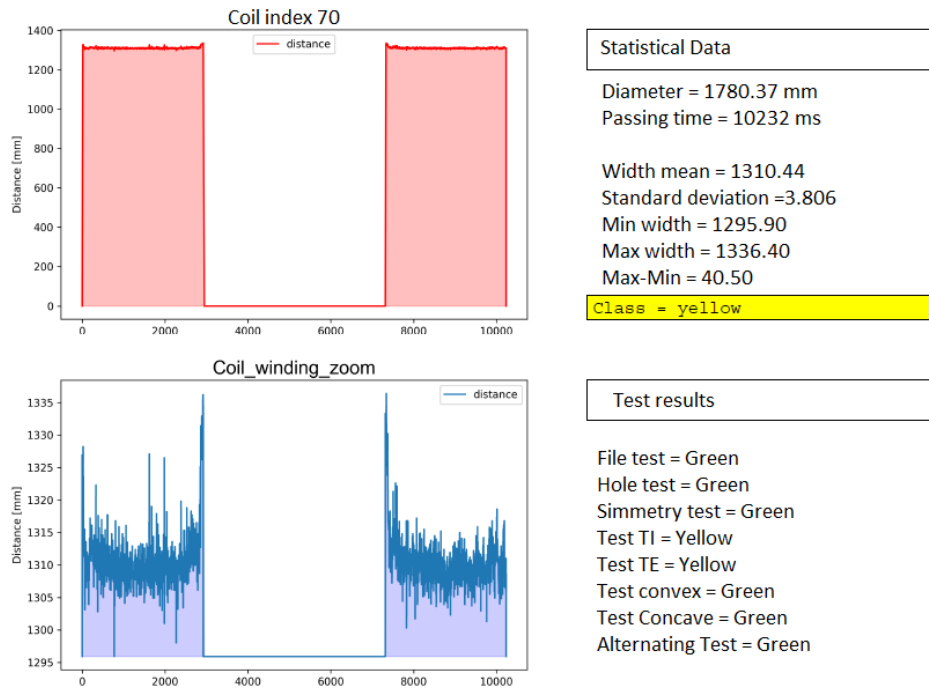


Figure 10. The analytic report – facsimile from page 71.

A bad coil with a combination of three issues - internal telescopeness – red class, external telescopeness – yellow class, and concave issue – yellow class is shown in Figure 12. The overall telescopeness has the value 103.30 mm and the standard deviation is 10.646 mm. But the coil is easy to repair. The internal telescopeness can be easy decrease to yellow class by applying a force with a special device and the coil can be delivered further.



Figure 11. The analytic report – facsimile from page 65.

Another analysis, made for each coil is about the data quality. In the same analytical report, for every coil is generated a graph about the sensor performances. Due to harsh conditions and because the reflected light from

moving strip edges has a very unregulated pattern, the laser can vary the sample time to achieve stability of a certain measurement. In next figure the mean for sample time is 2.15 ms and represent a good value in order to analyze the coil.

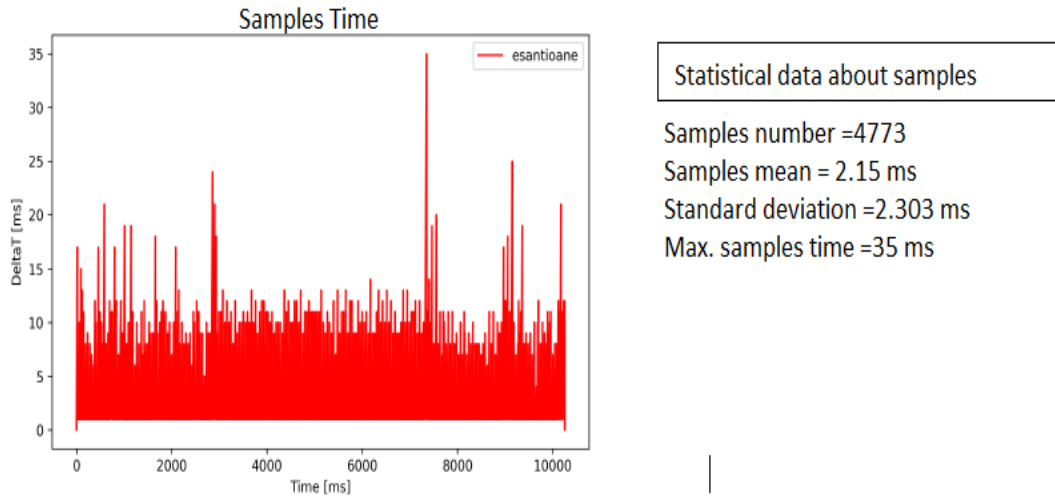


Figure 12. The analytic report – facsimile about sample time.

An automatic schedule service is folding the files and generates the two reports at the end of the day.

The Online Interface

An on-line interface was also developed to be used by operators to analyze the quality of coiling process, and to signalize to engineers any issue. In this way, small adjustment can be made from coil to coil. In Figure 14, here below, can be seen a photo with the interface.



Figure 13. The on-line operator interface.

The same results of tests presented in the „Results and reports” are displayed for the last coil immediately it passed under the laser beam (the left part of the monitor). In the right-upper part part of the monitor, a notebook

with 3 pages shows the results of laser measurement, without and with zoom and the statistical about samples. In the right-lower part of the monitor, the results for the last 9 coils are shown.

Conclusions

A more and more important issue in hot strip mills is the coiling quality or telescopeness. In this paper, a method and an algorithm for coils classification was described. A distance sensor using laser triangulation was used to measure the position of every lap of coil, during the passing of coils under the sensor. For every coil, a data file was created and send to the server. An algorithm, implemented in Python programming language classified the coils and delivers online reports and daily analytic and classification reports. This system is exploited today and together with process parameters recorded by data acquisition system (like torque from mandrel, pinch rolls, wrapper rolls, strip temperature, steel grades, etc.) is very useful in improving coiling quality.

The on-line interface detects anomalies immediately and permits to make small adjustments from coil to coil. The classification reports are very useful to identify at a glance the coils with problems and in the analytic reports at indicated pages a lot of details about the coil can be found. The environment is harsh, the strip edges are not the best reflectors for laser beam so some signal missing can appear, but the results are encouragers.

Scientific Ethics Declaration

The author declares that the scientific ethical and legal responsibility of this article published in EPSTEM journal belongs to the author.

Acknowledgement

* This article was presented as an oral presentation at the International Conference on Technology (www.icontechno.net) held in Antalya/Turkey on November 16-19, 2023.

* This paper and the research behind it would not have been possible without the support of Liberty Galati Company. We would also like to show our gratitude to the workers teams from Liberty Galati Hot Strip Mill plant for support offered during this research.

References

- Choi, Y. J., & Lee, M. C. (2009). A downcoiler simulator for high performance coiling in hot strip mill lines. *International Journal of Precision Engineering and Manufacturing*, 10(2), 53-61.
- Degner, M., Mentrup, H. C., Messner, K. L., U. Muller, U., & Thiemann, G. (1999). Measuring the end-face profile of hot-rolled coils. *Stahl und Eisen*, 119(10), 87-89.
- European Standard EN 10051 .(1991). Continuously hot-rolled uncoated plate, sheet and strip of non-alloy and alloy steels – tolerances on dimensions and shape. <https://genorma.com/en/project/show/cen:proj:19766>
- LIMAB® .(n.d.). Manual precicura SR, MR, LR distance measuring sensor. Retrieved from <https://www.limab.com>
- Lima Junior, S. O., Riberio, J. W. L., Barros, J. A. G., Franca, R. A., Fraipont, M., & Zorzanelli, L. R. (2007). Implantacao de dispositivo de correcao de telescopicidade em bobinas a quente no LTQ da arcelormittal tubarao. *Technologia em Metalurgia a Materials*, 3(3), 7-11.
- Nyquist, H. (1928). *Certain topics in telegraph transmission theory*, 47, 617-644. AIEE Trans.
- Ostroverhov, N., Popovich, N., Pyzhov, V., & Minhao, Z. (1992). Digital linear electrical drive for metal strip coil telescopeness control. *IEEE International Symposium on Industrial Electronics*, 2.
- Popovich, N., Pyzhov, V., & Ostroverhov, N .(1994). *Linear induction motors drive for Coil telescopeness control. IECON'94*, 1.
- Shanon, C. E. (1998). *Communication in the presence of noise* (2nd ed.). IEEE.

- Tonnon, E., C. Moretto, C., Francois, P., Conti, M.D., & Wadoux, P. M. (1998). Developpement d'un nouveau systeme de mesure de la qualite du bobinage au train a bandes. *La Revue de Metallurgie*, 95(6), 801-808.
- Zhang, D., & Ren Lianeli, R. (2018). Research on strip head telescope control of hot strip coiling based on Orowan uniform compression theory. *5th International Conference on Information Science and Control Engineering(ICISCE)*, 968-973.

Author Information

Elena Raducan

University "Dunarea de Jos" from Galati
Str. Domneasca, No.47
Galati, Romania
Contact e-mail: elena.raducan@ugal.ro

Mihaita Arhip

Liberty Galati
Str. Smirdan, No.1
Galati, Romania

To cite this article:

Raducan, E., & Arhip, M. (2023). Quality issue classification by using dedicated data analysis software created in python language. *The Eurasia Proceedings of Science, Technology, Engineering & Mathematics (EPSTEM)*, 24, 10-20.

The Eurasia Proceedings of Science, Technology, Engineering & Mathematics (EPSTEM), 2023

Volume 24, Pages 21-28

IConTech 2023: International Conference on Technology

Exploring Social Engineering Attacks Using Spear Phishing in a University

Trust Tshepo Mapoka
University of Botswana

Keneilwe Zuva
University of Botswana

Gaedupe Kylian Kukumara
University of Botswana

Tebogo Seipone
University of Botswana

Tranos Zuva
Vaal University of Technology

Abstract: A thorough investigation of social engineering attacks was performed on the lab environment. Numerous users can be easily attacked through the use of illegitimate emails that may come from trusted users. Organizations often try to implement security measures but they remain susceptible to these attacks. The purpose of this study was to show that university students are at risk of being attacked. The deployment of a dedicated lab environment and the susceptibility of the network to countless social engineering attacks were completely assessed in a controlled lab environment. The targeted audience, students, showed that they were more vulnerable. The findings of these investigations revealed that the network is vulnerable to social engineering attacks, specifically spear phishing attempts. Recommendations were made that included that universities should invest in educating students, staff members, and the faculty at large about certain threats and how to avoid falling prey to them.

Keywords: Cyber vigilant, Deployment, Spear phishing, Vulnerability

Introduction

The continuous use of the internet by the current generation, especially university students, has placed them at huge risk of being prone to social engineering attacks even if they are not aware (Hatfield, 2018). Social engineering is, in most cases, described as the art of convincing individuals to reveal sensitive information in order to perform certain malicious tasks. In most cases, it is often described with the theory of gaining something in exchange for a loss to someone (Helminem, 2021). The best security measures and practices do not guarantee that a certain organization is safeguarded against these attempts. The majority of students and staff members are mostly affected by Spear Phishing attempts. Spear Phishing is the attack on certain users under the pretense of a candid individual that is mostly trusted through the use of any electronic medium. This attack is directed to specific individuals. Vast information regarding users is first collected; for example, all emails about targeted users will be known. Spear phishing attempts are the most triumphant, as information about users has already been studied (Chilisa & Preece, 2005).

This paper is arranged as follows: Section 1 specifies the introduction; Section II unravels the problem statement; section III shows the main aim of this research paper; Section IV shows the related studies in the form of a literature review. Section V shows the methodological approaches, and Section VI outputs the results and findings of the study. The last section shows conclusions and future recommendations.

Problem Statement

Social engineering attacks have the potential to seriously jeopardize the confidentiality, integrity, and availability of most university's computing resources (Bongiovanni, 2019). Despite the potential harm that social engineering attacks can inflict, the various social engineering techniques and the efficacy of the current security measures in preventing or reducing them are not fully understood. In order to uncover potential flaws and provide practical solutions to protect against these threats, a systematic evaluation of some university network vulnerability to social engineering attacks is explored.

Aim of Study

- To identify potential weaknesses in the network's security controls.
- To explore effective countermeasures to protect against social engineering attacks.

Literature Review

The social engineering attacks on university computer networks are a growing concern, and their effects cannot be magnified. These attacks have been used to gain unauthorized access to delicate data and even compromise network security (Omoyiola, 2020). Human behavior plays a crucial role in this type of attack, as people can easily succumb to social engineering attacks due to their lack of awareness of this type of attack (Eltahir & Ahmed, 2023). It is the onus of Universities to educate students and staff members about the repercussions of these attacks and their impact at large. Firewalls and antivirus applications are ways that universities can try to mitigate against this type of attack; however, the human factor must not be neglected in addressing these cybersecurity breaches. According to the University of Botswana Computer Science important, as it outlines and provides backing for efforts aimed at improving information security practices across various units in the department (Annamalai et al., 2021). Access controls and monitoring systems are technology control measures that can Department, there is a great need to execute comprehensive training programs that may help raise awareness about cybersecurity complications (Harris, 2019).

Communication in an organization is salient as it helps employees understand how crucial information security is. Support from management is also be implemented before issues get out of hand (Alzahrani & Alfouzan, 2022). Cybercriminals use various tactics to gain unauthorized access to sensitive information in the University Of Botswana Computer science networks. The review conducted on this study shows that attackers often use baiting tactics such as leaving an infected USB around or sending malicious emails with links to targeted users. Pretexting and creating false identities may also be used to manipulate users into divulging certain information (Salahdine & Kaabouch, 2019). Accomplished social engineers often use tailgating tactics, which involve following the victim through secured areas without permission and gaining access to secured places in order to loot data. This attack can lead to loss of clients, reputation, and even financial losses, which may affect organizations (Mberekı & Doss, 2021). Most university students are still unaware that password guessing is still one of the key components of their data that is easily exposed. Most social networking sites are built with basic settings that do not prioritize data acceptance mandates, making them prone to attacks (Kikerpill & Siibak, 2021). The same university is prone to vulnerabilities because of where students' data is stored. Hackers often find ways to access the students' data when attacking them (Xiangyu et al., 2017). They can also be disguised as technical staff by asking users their passwords while masquerading as the help center team (Ryck et al., 2013). There has been an increased number of publications since 2010 due to curiosity about the research topic; therefore, awareness about cyber-attack risks has been raised, making Universities around to be keen-eyed. There has been various review studies on social engineering attacks. The selected few are described below.

According to Kharrazi (2018), his article titled "Social Engineering Attacks and Countermeasures: Review" highlighted the significance of social engineering attacks. This study has a limited focus on specific social engineering tactics and countermeasures. The "The Psychology of Social Engineering" article by Hadnag (2010) emphasizes the role of human behavior in social engineering attacks, but it did not focus specifically on the role

of human factors in successful social engineering attacks. Yet in another by D'Angelo (2019) titled "Social Engineering Attacks: A Survey", a survey investigated the prevalence of social engineering attacks in organizations and identified the most common tactics used. Its limitation was that its general overview, lacked in depth analysis of specific tactics. Finally, Ross (2020) compared the effectiveness of different social engineering techniques and identified the most successful ones in the article "Social Engineering Techniques: An Analysis and Comparison" but used a limited sample size and his findings lacked real-world application.

Methodology

A lab environment was set up, deployed, and configured as shown in Figure 1 below.

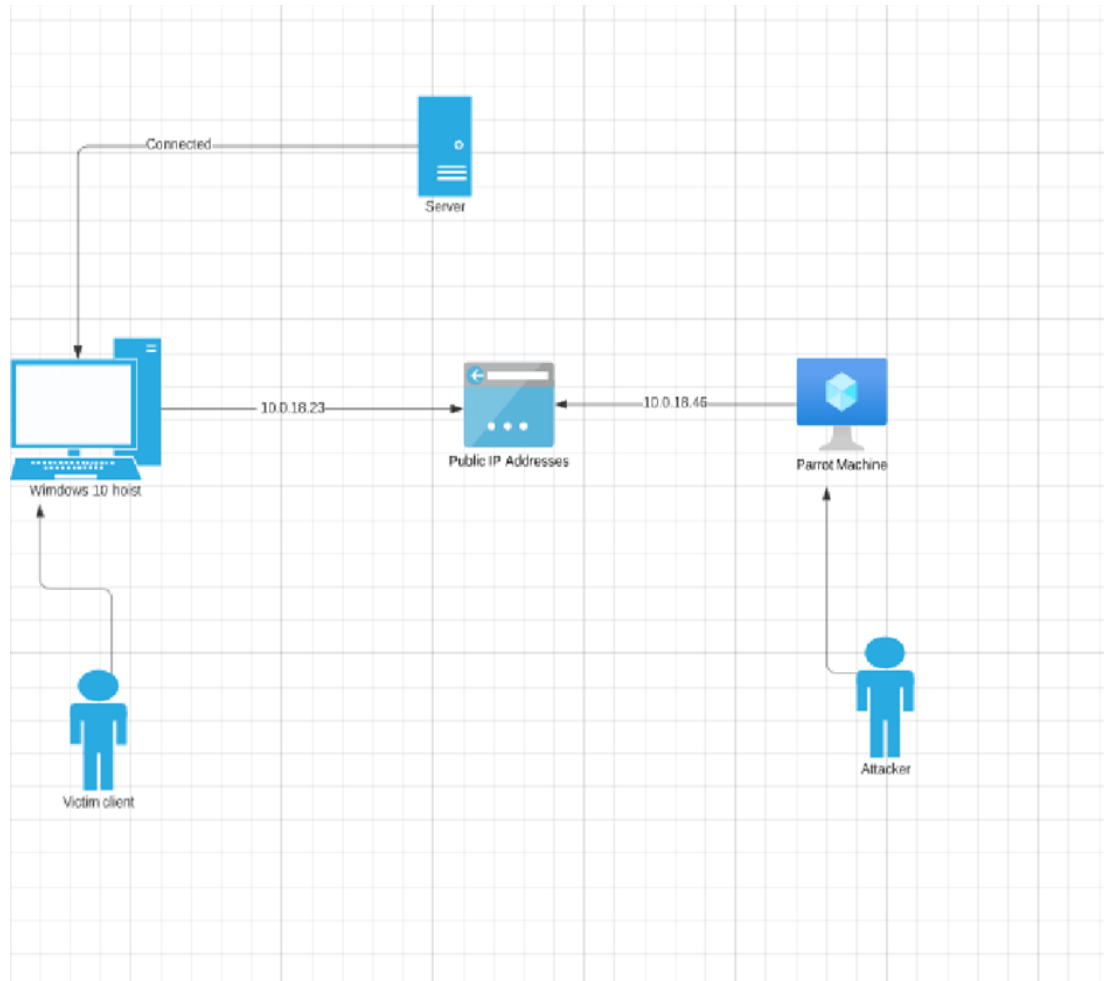


Figure 1. High level diagram showing how the attack was made

For the hardware components, lab environment was set up using Parrot Security Machine and a lab of thirty one (31) networked Windows 10 machines. The Parrot Security Machine served as the attacker machine, where the Social Engineer Toolkit was used to perform credential sniffing and cloned websites. The Windows 10 machines were used to serve as the victim machines, where the sniffing and cloned websites by the attacker machines was executed. As a control, lectures continued to take place within the lab in a controlled environment without the knowledge of the students or the lecturer. Three classes went in, therefore 90 students were subjected to the experiment.

The software components included Social Engineer Toolkit and Simple Mail Transfer Protocol (SMTP). The Simple Mail Transfer Protocol (SMTP) protocol was used to send an email to the victim machines. The new email will flash to lure the students to click on the link. The web browser on the victim machines was used to open a malicious website, which was used to steal sensitive information such as passwords. Both the Windows 10 machines and the Parrot OS machine had IP addresses assigned to their network interfaces. They had the same subnet to enable easier communication.

Social Engineering Toolkit

The Social Engineer Toolkit is an open-source penetration testing platform made to mimic social engineering assaults. It is often used to craft spear phishing emails. The Social Engineer Toolkit's main objective is to mimic actual social engineering attacks in order to assess an organization's security posture (Segovia et al., 2017). It allows security experts to evaluate how well their defenses work against social engineering strategies including phishing, pretexting, and impersonation. Using SET, testers may assess how vulnerable different employees are to these kinds of attacks, spot potential security holes, and create plans to improve security awareness.



Figure 2. Social Engineer toolkit

Experiments

A Demonstration Using the Social Engineer Toolkit on a Protected Lab Environment

Figure 3 shows how after logging into the parrot machine, the parrot (MATE) terminal was launched.

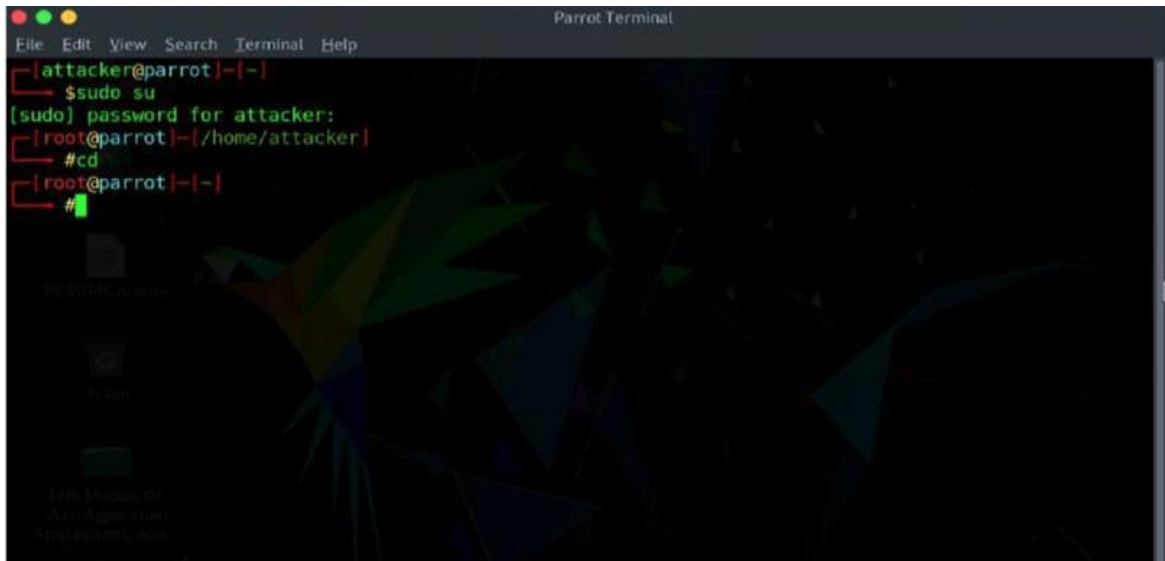
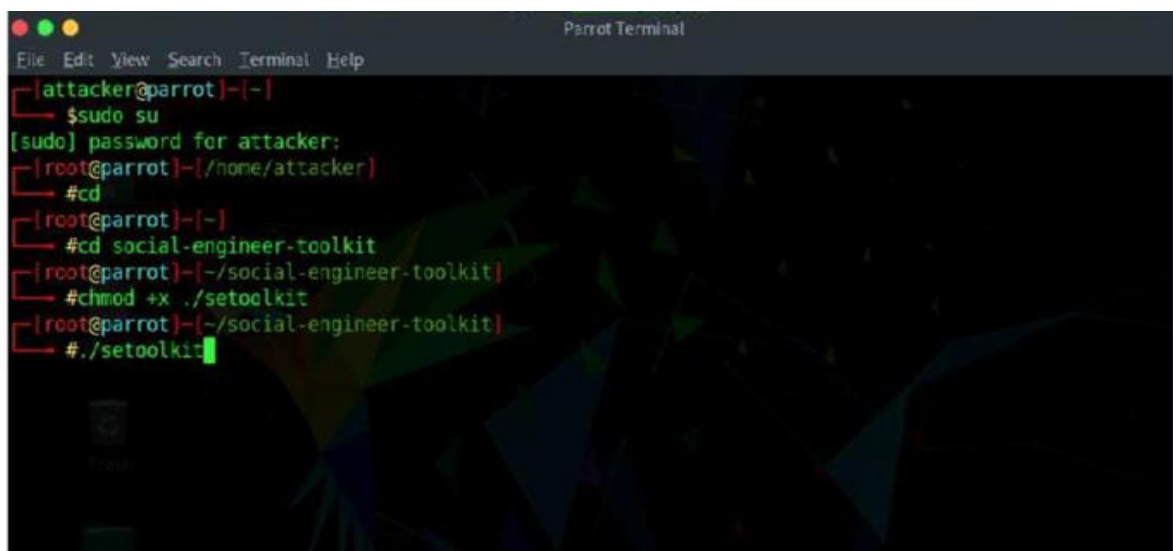


Figure 3. Launching parrot (MATE) terminal

To run the programs as a root user, sudo su command was used. To change to the root folder and navigate the SEtoolkit, the user may type cd social-engineer-toolkit. Then type chmod+x./setoolkit to execute the script and launch the social engineer toolkit as shown in Figure 4 below.



```

[attacker@parrot]-[~]
$ sudo su
[sudo] password for attacker:
[root@parrot]-[/home/attacker]
# cd
[root@parrot]-[~]
# cd social-engineer-toolkit
[root@parrot]-[/social-engineer-toolkit]
# chmod +x ./setoolkit
[root@parrot]-[/social-engineer-toolkit]
# ./setoolkit
  
```

Figure 4. Generating malicious code using the Social Engineering toolkit

The social engineer toolkit was selected, then navigated to the credential harvester attacker. The IP address of the local machine was entered. In the case of the above scenario, it was 10.0.18.46 and then the URL to clone was entered. Then an email (see Figure 5) was sent to the victim machines, attaching both the URL link after the successful cloning of the website. Email flashed that made the students to quickly go to their emails and some students fell for the trap.



Figure 5. Malicious email

After email was sent, the victims fell for the trick and clicked the link they received and were prompted to enter their details on what looks like a real web page.

Lab Parameters

500 simulated spear phishing attempts were run in the lab environment

Results and Findings

The success rate of spear phishing attacks against students was examined. According to the findings. Data was gathered and examined on how quickly phishing emails were responded to. Students took an average of 2 hours to click on a phishing link, 60% of the recipients clicked on the phishing emails' dangerous links. 40% of these individuals went on to enter private data on the phony websites, including usernames and passwords. The screenshots on Figure 6 below shows the details that were captured from the cloned website. This was the well laid out results after students clicked on the link sent via an email.


```

View Search Terminal Help
le: http://www.thisisafakesite.com
back> Enter the url to clone:https://moithuti-webl.ub.ac.bw/login/index.php
ing the website: https://moithuti-webl.ub.ac.bw/login/index.php
could take a little bit...

way to use this attack is if username and password form fields are available. Regardless, this captures all POSTs on
e.
ocial-Engineer Toolkit Credential Harvester Attack
ntial Harvester is running on port 80
mation will be displayed to you as it arrives below:
5 - - [20/Apr/2023 21:09:42] "GET / HTTP/1.1" 200 -
T A HIT! Printing the output:
USERNAME FIELD FOUND: logintoken=gz68zdAJnhXLeJj85v51eMUb1Qcj9wFR
USERNAME FIELD FOUND: username=261902568
PASSWORD FIELD FOUND: password=dupskukumara.com
YOU'RE FINISHED, HIT CONTROL-C TO GENERATE A REPORT.

5 - - [20/Apr/2023 21:10:04] "POST /index.html HTTP/1.1" 302 -
5 - - [20/Apr/2023 21:11:27] "GET / HTTP/1.1" 200 -
T A HIT! Printing the output:
USERNAME FIELD FOUND: logintoken=gz68zdAJnhXLeJj85v51eMUb1Qcj9wFR
USERNAME FIELD FOUND: username=261904495
PASSWORD FIELD FOUND: password=Madikwe
YOU'RE FINISHED, HIT CONTROL-C TO GENERATE A REPORT.

5 - - [20/Apr/2023 21:11:43] "POST /index.html HTTP/1.1" 302 -
5 - - [20/Apr/2023 21:13:31] "GET / HTTP/1.1" 200 -
T A HIT! Printing the output:
USERNAME FIELD FOUND: logintoken=gz68zdAJnhXLeJj85v51eMUb1Qcj9wFR
USERNAME FIELD FOUND: username=26190196
PASSWORD FIELD FOUND: password=grasshoppers
YOU'RE FINISHED, HIT CONTROL-C TO GENERATE A REPORT.

```

Figure 6. URL cloned and details captured

After certain details of students were captured, their student portals accounts were accessed, and certain details were exposed, as further clarified by the details following. Withdrawing student assignment, deleting of some files and many other malicious activities could be carried out easily.

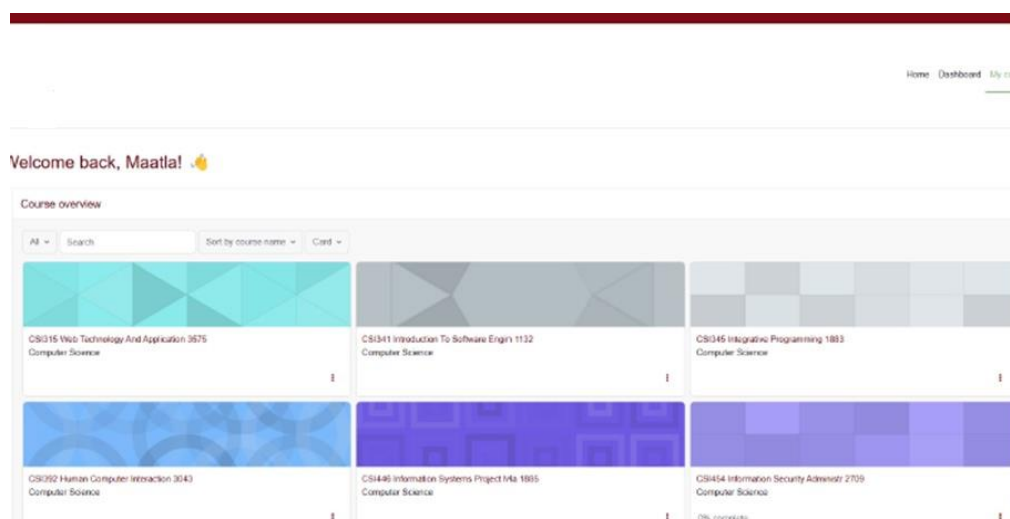


Figure 7. Student data in moodle

Conclusion

The results show that students do not use complex passwords and are easily tricked into clicking any link available. Some are just simple passwords with no complicated characters. This network was configured, tested, and final conclusions were drawn from the results obtained. Thus, the network was vulnerable to phishing attacks on their websites.

Future Recommendations

Most universities should invest in educating students, staff members, and the faculty at large about certain threats and how to avoid falling prey to them. Implementation of multi-factor authentication (MFA) systems, which may include facial recognition and fingerprint recognition, when accessing their websites at the university should be utilized. Implementing a phishing detection system specifically for the university is necessary, as it appears that human factors are the leading contributors to these attacks.

Limitations of Research

While the research has yielded valuable insights into social engineering attacks, particularly spear phishing attempts within university networks, it is essential to acknowledge certain limitations inherent in the study. These limitations, however, do not diminish the practical implications of the findings or their potential to contribute to enhanced security practices.

Lab Environment Constraints: The study was conducted within a controlled lab environment, which, by its nature, may not fully replicate the complexities of real-world university networks. While this controlled setting ensured the safety and privacy of the participants, it may not encompass all the intricacies of dynamic network behaviors.

Sample Size: We acknowledge that the study's sample size was limited due to resource constraints and the need for volunteer participants. As such, the findings may not be entirely representative of the entire university community.

Despite these limitations, the research holds significant practical implications for improving security within university networks:

Tailored Security Awareness Programs: The findings underscore the importance of targeted security awareness programs within academic institutions. By recognizing the specific vulnerabilities of students and staff to spear phishing attacks, universities can develop tailored training modules that empower users to identify and respond to such threats effectively.

User Behavior Analysis: The insights gained into user behavior when faced with spear phishing emails can inform the design of security controls. Universities can adapt their security measures to align with the typical responses of their users, enhancing the overall security posture.

Recommendations for Defense: The research provides actionable recommendations for strengthening network defenses against social engineering attacks. These recommendations encompass both technical measures, such as email filtering and authentication protocols, and non-technical strategies, such as user education and multi factor authentication implementation.

Building Cyber Vigilance: Beyond the technical aspects, these studies emphasize the role of user awareness and vigilance. By acknowledging the human element in cybersecurity, universities can cultivate a culture of cyber vigilance among students and staff, reducing the overall risk of social engineering attacks.

Scientific Ethics Declaration

The authors declare that the scientific ethical and legal responsibility of this article published in EPSTEM journal belongs to the authors.

Acknowledgements or Notes

* This article was presented as an oral presentation at the International Conference on Technology (www.icontechno.net) held in Antalya/Turkey on November 16-19, 2023.

References

- Alzahrani, N.M., & Alfouzan, F.A. (2022). Augmented reality (AR) and cyber-security for smart cities a systematic literature review. *Sensors*, 22(7), 2792.
- Annamalai, A., Poonia, R. C., & Shanmugasundaram, S. (2021). A broach study on issues in social engineering attacks on social networking sites. *International Journal of Mechanical Engineering*, 6(2), 105.
- Bongiovanni, I. (2019). The least secure places in the universe? A systematic literature review on information security management in higher education. *Computers & Security*, 86(1), 350-357.
- Chilisa, B., & Preece, J. (Eds.). (2005). African perspectives on adult learning: Research methods for adult educators in Africa. *Adult Education Quarterly*, 59(1), 84-86.

- De Ryck, N. P., Nikiforakis, L., & Desmet, J. W., (2013). Tabshots: Client-side detection of tabnabbing attacks. In *Proceedings of the 8th ACM SIGSAC Symposium on Information, Computer and Communications Security*. Hangzhou, China.
- Eltahir, M.E., & Ahmed, O.S. (2023). Cybersecurity awareness in African higher education institutions: A case study of Sudan. *Inf. Sci. Lett*, 12(1).
- Harris, J.K. (2019). *Statistics with R: solving problems using real-world data*. SAGE Publications
- Hatfield, J. M. (2018). Social engineering in cybersecurity: The evolution of a concept. *Computers and Security*, 73, 102-113.
- Helminen, N. (2021). *Social Engineering: Introduction to social engineering through real-life hacking attempts*. JAMK University of Applied Sciences. Retrieved from <https://www.theseus.fi/handle/10024/503239>
- Kalnins, R., Purins, J., & Alksnis, G. (2017). Security evaluation of wireless network access points. *Applied Computer Systems*, 21(1), 38–45.
- Kikerpill, K., & Siibak, A., (2021). Maze phishing: The COVID-19 pandemic as credible social context for social engineering attacks. *Trames: A Journal of the Humanities and Social Sciences*, 25(4), 371-393.
- Krombholz, K., Hobel, H., Huber, M., & Weippl, E. (2015). Advanced social engineering attacks. *Journal of Information Security and Applications*, 22, 113-122.
- Mbereki, K., & Doss, S. (2021). Investigating the Level of Awareness on Information Security amongst Users at Botho University. *International Journal of Innovative Research in Applied Sciences and Engineering (IJIRASE)*, 4(9), 905-912.
- Omoiyola, B.O. (2020). *Exploring strategies for enforcing cybersecurity policies*. Walden University.
- Riquarts, K., (1987). Technology education: Science-technology-society. *Science and Technology Education and the Quality of Life*, 2.
- Salahdine, F., & Kaabouch, N., (2019). Social engineering attacks: A survey. *Future internet*, 11(4), 89.
- SCRIBD. (2011, Jun 9). The official social engineering framework- computer based social engineering tools- social engineering toolkit. Retrieved from <http://www.socialengineer.org>
- Segovia, F., Torres, L., Rosillo, M., Tapia, E., Albarado, F., & D. Saltos, D. (2017). Social engineering as an attack vector for ransomware. In *Proceedings of the Conference on Electrical Engineering and Information Communication Technology*, 1-6. Pucon, Chile.
- Trusted Sec. (2013). Social-engineer toolkit. Retrieved from: <https://www.trustedsec.com/downloads/socialengineer-toolkit/>, last accessed 03/12/2013.
- Wyld, D. C., & Nagamali, D. (2021). Computer science and information technology. *2nd International Conference on Soft Computing, Artificial Intelligence and Machine Learning (SAIM 2011)* (p.146). Toronto, Canada.
- Xiangyu, L., Qiuyang, I., & Chandel, S. (2017). Social engineering and insider threats. In *Proceedings of the International Conference on Cyber-Enabled Distributed Computing and Knowledge Discovery*, 25-34. Nanjing, China.

Author Information

Trust Tshepo Mapoka

University of Botswana
Botswana, South Africa
Contact e-mail: mapokat@ub.ac.bw

Keneilwe Zuva

University of Botswana
Botswana, South Africa

Gaedupe Kukumara

University of Botswana
Botswana, South Africa

Tebogo Seipone

University of Botswana
Botswana, South Africa

Tranos Zuva

Vaal University of Technology
Vanderbijlpark, South Africa

To cite this article:

Mapoka, T.T., Zuva K., Kukumara G.K., Seipone T., & Zuva, T. (2023). Exploring social engineering attacks using spear phishing in a university. *The Eurasia Proceedings of Science, Technology, Engineering & Mathematics (EPSTEM)*, 24, 21-28.

The Eurasia Proceedings of Science, Technology, Engineering & Mathematics (EPSTEM), 2023

Volume 24, Pages 29-36

IConTech 2023: International Conference on Technology

The Effect of Antenna Spacing on Active S-Parameters in Planar Array Antennas

Emirhan Aydin

Samsung Electronics Turkey

Ramiz Erdem Aykac

Samsung Electronics Turkey

Abstract: In wireless communication systems, an RF signal generated by a transmitter is sent into free space and eventually picked up by a receiver. An antenna radiation pattern can be defined as the directional function that characterizes the relative power distribution radiated by an antenna. It is more advantageous to restrict the direction in which signals are sent or received. This requires a steerable antenna. This is referred to as antenna directivity. Directivity refers to the ability of an antenna to transmit or receive signals over a narrow range of horizontal directions. In other words, the physical orientation of the antenna gives it a highly directional response or directivity curve. A directional antenna eliminates interference from other signals received in all directions other than the direction of the desired signal. Directional antennas provide great efficiency of power transmission because the transmitter power can be focused into a narrow beam directed toward the station of interest. The combination of two or more antennas used together is known as an antenna array. Although an array need not contain identical radiating elements, most arrays prefer identical elements such as dipoles, horn antennas or parabolic dish antennas. Antenna arrays provide high directivity, narrow beams, low side apertures, steerable beams and shaped antenna patterns starting from very simple antenna elements. In this study, a series of simulations are performed by varying the inter-antenna distances and the effects of the inter-antenna distance on the S-parameters of planar antenna arrays are investigated at 3GHz center frequency, which will be mostly available for 5G NR applications in the future.

Keywords: Planar antenna array, Antenna gain, Antenna directivity, S-parameters, Millimeter-wave antenna

Introduction

In wireless communication systems, an RF signal generated by a transmitter is sent into free space and eventually picked up by a receiver. An antenna can be defined as a transducer that converts a guided wave into an electromagnetic wave propagating on a transmission line. Antennas are made in a variety of shapes and sizes and are frequently used in radio and television broadcasting and reception, radio-wave communication systems, cell phones, radar systems and anti-collision car sensors, among many other applications.

The radiation and impedance characteristics of an antenna are governed by its shape, size and material properties. The dimensions of an antenna are usually defined in terms of the wavelength (λ) of the transmitted or received wave. The length of the antenna depends on the center operating frequency. Antennas have the most effective radiation pattern when their length is directly related to the wavelength of the transmitted signal. Most antennas are defined by a length in terms of a wavelength.

An antenna radiation pattern can be defined as the directional function that characterizes the relative power distribution radiated by an antenna. A direction independent antenna is a hypothetical antenna that radiates the

- This is an Open Access article distributed under the terms of the Creative Commons Attribution-Noncommercial 4.0 Unported License, permitting all non-commercial use, distribution, and reproduction in any medium, provided the original work is properly cited.

- Selection and peer-review under responsibility of the Organizing Committee of the Conference

© 2023 Published by ISRES Publishing: www.isres.org

same in all directions and is often used as a reference radiation pattern when describing the radiation characteristics of real antennas. In many types of communication systems, it is desirable to use antennas with omnidirectional characteristics, i.e. antennas that can send messages in any direction and receive them in any direction. In others, it is more advantageous to restrict the direction in which signals are sent or received. This requires a steerable antenna. This is referred to as antenna directivity.

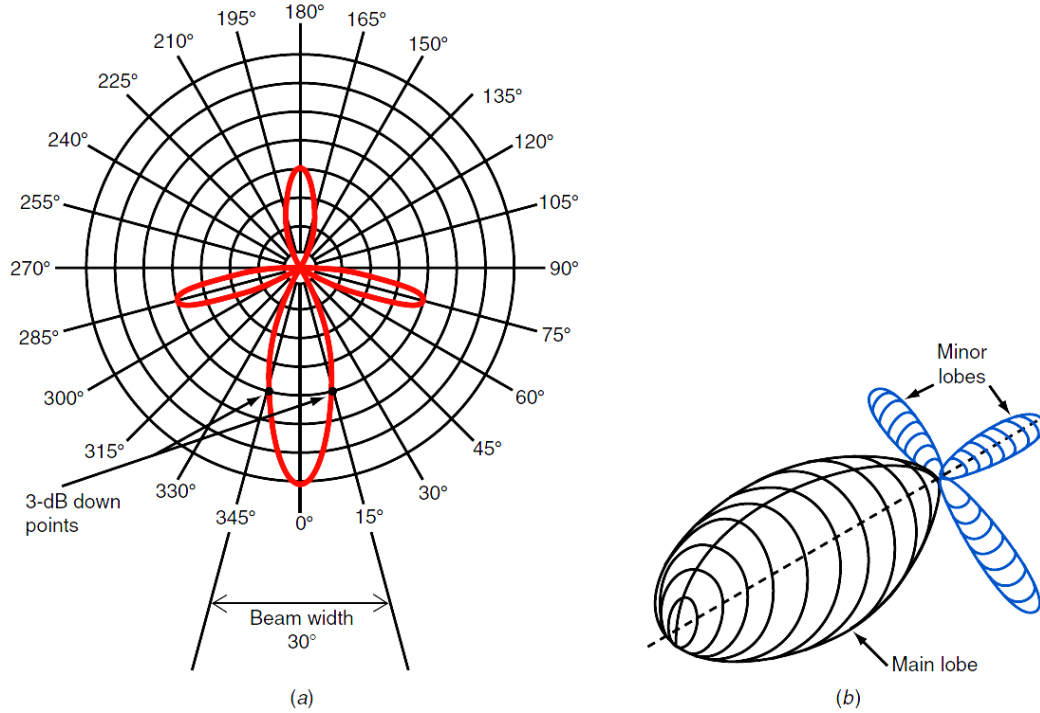


Figure 1. (a) Horizontal radiation pattern. (b) Three-dimensional radiation pattern.

Directivity refers to the ability of an antenna to transmit or receive signals over a narrow range of horizontal directions. In other words, the physical orientation of the antenna gives it a highly directional response or directivity curve. A directional antenna eliminates interference from other signals received in all directions other than the direction of the desired signal. Directional antennas provide great efficiency of power transmission because the transmitter power can be focused into a narrow beam directed toward the station of interest (R. S. Elliott, 1963). Antennas can be designed to be unidirectional; unidirectional antennas send or receive signals in one direction only. A three-dimensional version of the horizontal radiation pattern shown in (Figure 1 (a)) is given in (Figure (b)) (Principles of Electronic Communication Systems, 2014; Aksimsek, 2021)

Figure 1 shows the directivity pattern of a highly directional antenna. The larger loop represents the main response curve for the antenna. Maximum radiation or reception is in the direction of 0°. The three smaller patterns or loops going off in different directions from the main larger pattern are called minor lobes. When using a highly directional antenna, all the transmitted power is focused in one direction. Because the power is concentrated in a small beam, the effect is as if the antenna amplifies the transmitted signal. The directivity causes the antenna to show gain, a form of amplification, because it focuses the power (Tai, 1964). Since an antenna can focus energy in a single direction, the amount of power radiated is significantly higher than the power output of the transmitter. The power gain of an antenna can be expressed as the ratio of the power transmitted P_{trans} to the input power of the antenna P_{in} and expressed in decibels (Principles of Electronic Communication Systems, 2014).

$$dB = 10 \log \frac{P_{trans}}{P_{in}} \quad (1)$$

To create an antenna with directivity and gain, two or more antenna elements are combined to form an array. In this paper, we aimed to design an antenna array with different distance between them to see distance effect on active S-parameters and radiation pattern.

Antenna Arrays

The combination of two or more antennas used together is known as an antenna array. Although an array need not contain identical radiating elements, most arrays prefer identical elements such as dipoles, horn antennas or parabolic dish antennas. Antenna arrays provide high directivity, narrow beams, low side apertures, steerable beams and shaped antenna patterns starting from very simple antenna elements. Antenna arrays are used to direct radiated power to a desired angular sector. The number, geometrical arrangement and relative amplitude and phase of the array elements depend on the angular pattern to be achieved. Once an array has been designed to focus in a particular direction, changing the relative phases of the array elements (called steering or scanning) to steer it in another direction makes the solution of the problem a simpler matter.

The most basic characteristic of an array is that the relative displacement of the antenna elements relative to each other provides relative phase shifts in the radiation vectors (Cheng, 1971). This can then be added constructively in some directions or destructively in others. This is a direct consequence of the translational phase shift property of Fourier transforms. Collinear antennas usually consist of two or more half-wave dipoles mounted end to end (Figure 2). With this configuration, the individual antenna signals combine, producing a more focused beam (Principles of Electronic Communication Systems, 2014; Yang et al.,2016).

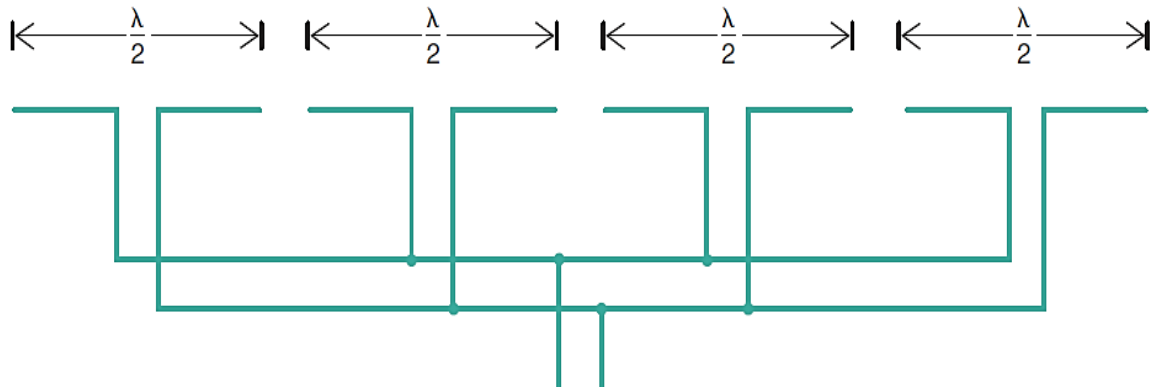


Figure 2. Collinear antenna array

Antenna arrays are generally used for the following purposes:

- To increase the overall directivity of the antenna at the operating frequency
- To achieve maximum radiation in the desired directions and a low side lobe level due to this radiation
- Optimizing the SNR value of the communication system for the desired ranges
- Blocking radiation to unwanted areas

The radiation pattern of an antenna array:

- Depending on the types of antennas
- Distance between antennas used in the array
- Phase difference between the antennas used in the array
- Feed amplitudes of the antennas used in the array
- How the antennas are arranged in the array in question

varies depending on the parameters of the array. In this study, the effect of the distance between the antennas in the array on the directivity and active S-parameters of the array will be investigated.

Method

Design Preparation

In order to investigate the effect of the distance between the antennas on the antenna radiation pattern, three different use cases were simulated. By this way, we planned to have an observation on the radiation pattern. Within the scope of the study, each array structure was implemented using the CST Studio Suite program for the following 3 different cases.

Distance Based Use Cases

Within the scope of this study, we simulated below cases:

- A planar antenna array consisting of 5 antennas spaced $\lambda/2$ apart in the X-axis and 6 antennas spaced $\lambda/3$ apart in the Y-axis
- A planar antenna array consisting of 5 antennas spaced at a distance of $\lambda/2$ in the X-axis and 6 antennas spaced at a distance of $\lambda/2$ in the Y-axis
- A planar antenna array consisting of 5 antennas spaced at a distance of $\lambda/2$ in the X-axis and 6 antennas spaced at a distance of $2\lambda/3$ in the Y-axis

Design Results for a Planar Antenna Array Consisting of 5 Antennas Placed at a Distance of $\lambda/2$ in the X-axis and 6 Antennas Placed at a Distance of $\lambda/3$ in the Y-axis (Case-I)

For the 3 GHz operating frequency, the wavelength value to be used was calculated as $\lambda = 102.5$ mm using the equation $\lambda = c/f$, taking into account the impedance matching margin of 4.5%. Since the effect of distance on the array will be analyzed in this study, all antennas are fed with the same feed amplitude and no phase difference is defined between the antennas. The distance between the antennas placed on the X and Y axes were calculated as $\lambda/2 = 51.25$ mm for the X axis and $\lambda/3 = 34.17$ mm for the Y axis, shown in Figure 3.

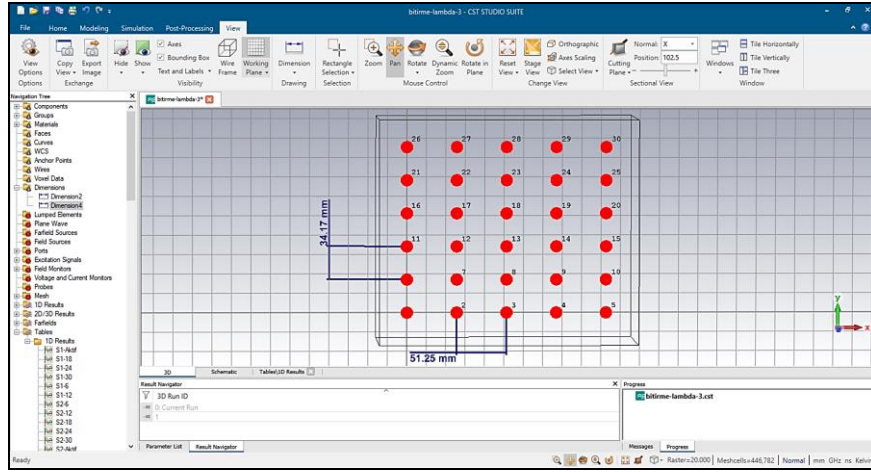


Figure 3. Antenna array design for case-I

Since the array in question is a planar structure, there is a symmetry. Therefore, it will be sufficient to take into account one of the elements with the same radiation in the calculations. In the following simulations, calculations will be made only for one of the symmetric array elements as shown in Table 1.

Table 1. Symmetric antenna matrix

Located antenna elements on antenna array	
1	30
2	29
3	28
4	27
5	26
6	25
7	24
8	23
9	22
10	21
11	20
12	19
13	18
14	17
15	16

The results of the active S-parameters obtained for the planar antenna array we have designed are shown in (Figure 4). It was observed that this design has a directivity of approximately -7.36 dB at the operating frequency. In the Figure 5, we can see the overall radiation pattern of the simulation was obtained. Based on this pattern, it is observed that the maximum radiation gain is low and therefore no effective directionality can be achieved.

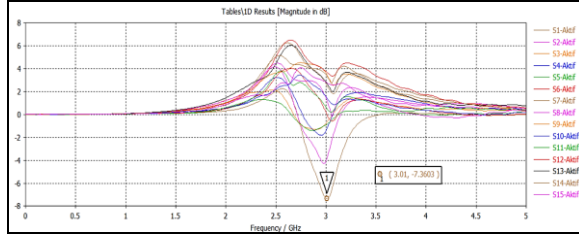


Figure 4. Active S-parameter result for case-I

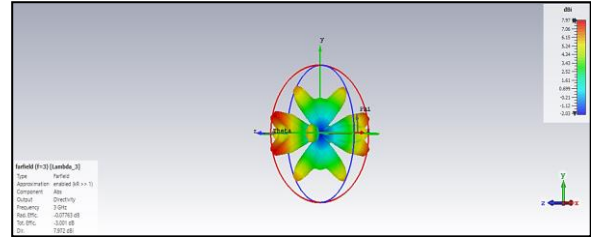


Figure 5. 3D radiation pattern for case-I

Design Results for a Planar Antenna Array Consisting of 5 Antennas Placed at a Distance of $\lambda/2$ in the X-axis and 6 Antennas Placed at a Distance of $\lambda/2$ in the Y-axis (Case-II)

For 3 GHz operating frequency, the wavelength value to be used was calculated as $\lambda = 102.5$ mm using the equation $\lambda = c/f$, taking into account the impedance matching margin of 4.5%. The distance between the antennas placed on the X and Y axes were calculated as $\lambda/2 = 51.25$ mm for the X axis and $\lambda/2 = 51.25$ mm for the Y axis, shown in Figure 6.

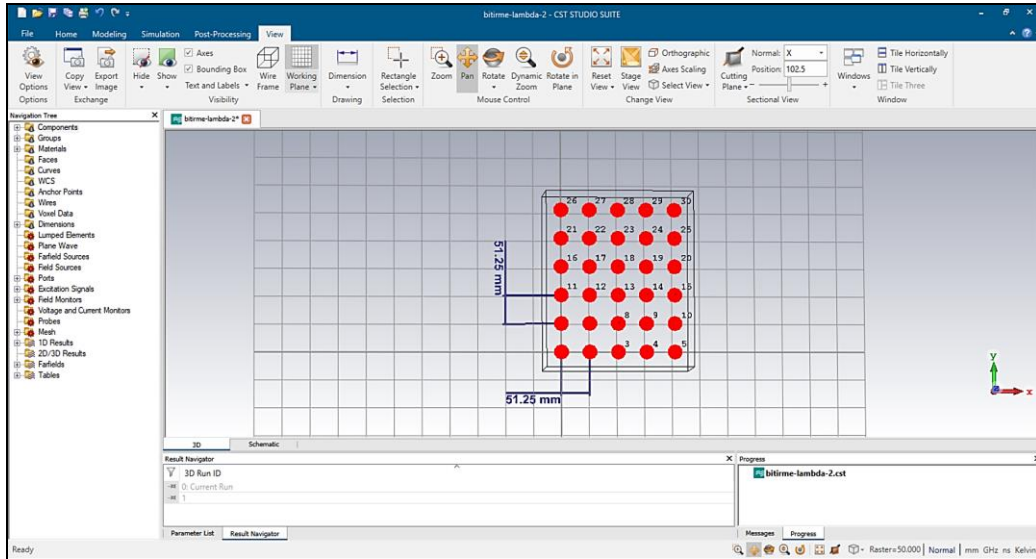


Figure 6. Antenna array design for case-II

The active S-parameters obtained for a planar antenna array consisting of 5 antennas spaced $\lambda/2$ apart in the X-axis and 6 antennas spaced $\lambda/2$ apart in the Y-axis were shown in (Figure 7). The design has directivity of approximately -8.97 dB at the operating frequency. Compared to Case-I, the gain and directivity of the designed antenna array were increased due to same distance between the antennas, as shown in Figure 8.

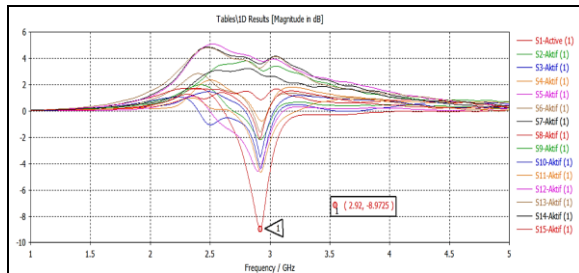


Figure 7. Active S-parameter result for case-II

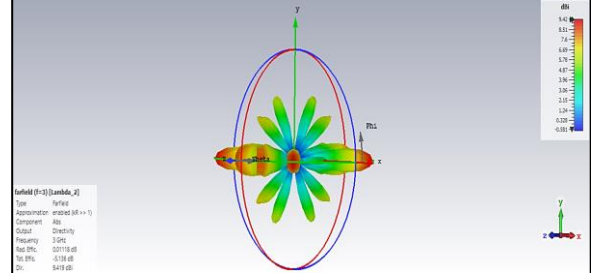


Figure 8. 3D radiation pattern for case-II

Design Results for a Planar Antenna Array Consisting of 5 Antennas Placed at a Distance of $\lambda/2$ in the X-axis and 6 Antennas Placed at a Distance of $2\lambda/3$ in the Y-axis (Case-III)

For 3 GHz operating frequency, the wavelength value to be used was calculated as $\lambda = 102.5$ mm using the equation $\lambda = c/f$, taking into account the impedance matching margin of 4.5%. The distance between the antennas placed on the X and Y axes were calculated as $\lambda/2 = 51.25$ mm for the X axis and $2\lambda/3 = 68.33$ mm for the Y axis, shown in Figure 9.

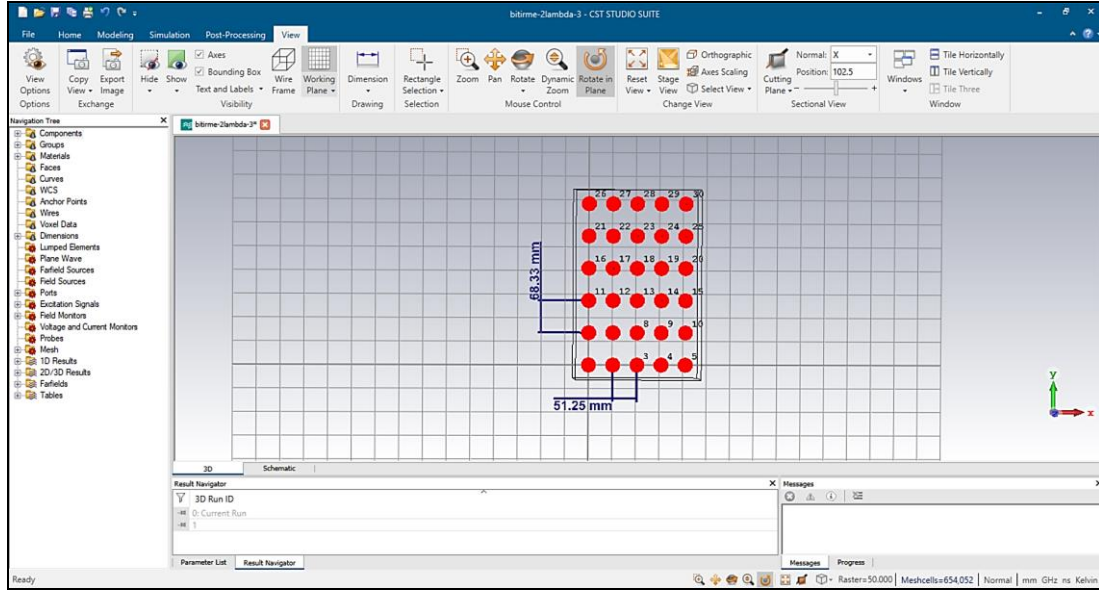


Figure 9. Antenna array design for case-III

The active S-parameters obtained for a planar antenna array consisting of 5 antennas spaced $\lambda/2$ apart in the X-axis and 6 antennas spaced $2\lambda/3$ apart in the Y-axis were shown in (Figure 9). The design has a directivity of approximately -7.90 dB at the operating frequency (Figure 10). Compared to Case-II, the gain and directivity of the designed antenna array were decreased due to the different distance between the antennas. In the Figure 11, we can see the overall radiation pattern of the simulation was obtained. Based on this pattern, it is observed that the maximum radiation gain is low and therefore no effective directionality can be achieved.

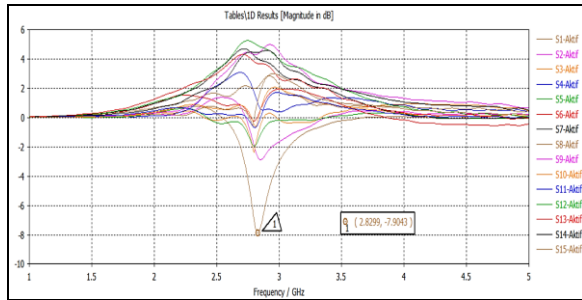


Figure 10. Active S-parameter result for case-III

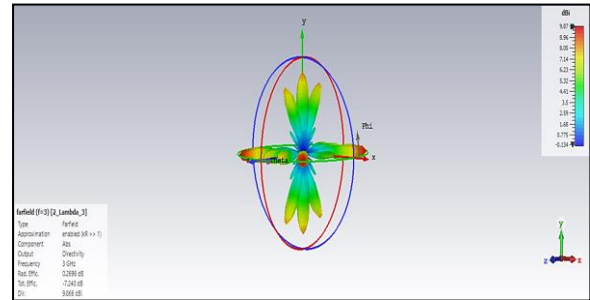


Figure 11. 3D radiation pattern for case-III

Results and Discussion

The simulation results obtained are summarized in Table 2 below. As a result of this work, we observed that:

- The best results are obtained for the planar antenna array designed using half-wave dipole antennas
- The distance between the antenna elements needs to be same for both x-axis and y-axis to reach maximum directivity for $\lambda/2$ dipole antennas, as shown in Figure 12 with green plot, also can be seen on Table 2
- The antenna gains increased based on the distance, it is very important for antenna performance, the higher gain means the more directional antenna-narrower beam-width
- The 3D radiation pattern could not effectively provide directionality as the effect

Table 2. Result matrix

Dx-distance	Dy-distance	Gain (dB)
$\lambda/2$	$\lambda/3$	-7.36
$\lambda/2$	$\lambda/2$	-8.97
$\lambda/2$	$2\lambda/3$	-7.9

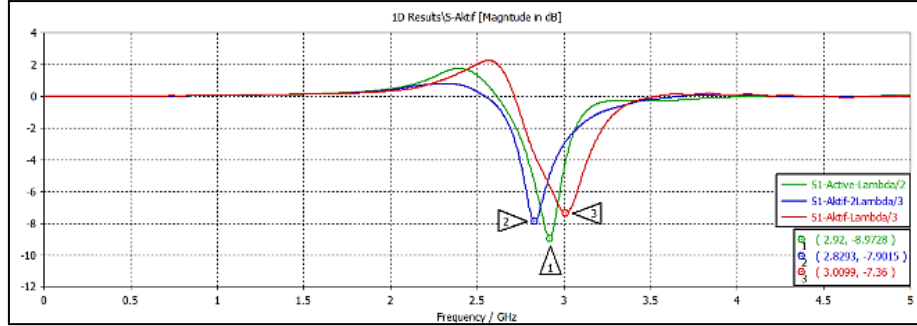


Figure 12. Compare active S-parameter results

Conclusion

This study has shown that the distances between antennas to be used in high performance antenna designs depend on the wavelength of the antennas to be used. Correct antenna distance selection for high frequency antennas will have a direct impact on the gain of the system to be designed. The use of antenna arrays is expected to increase with 5G NR technology. As a result of the meaningful data and outputs provided, this study is intended to be a reference for future studies.

Scientific Ethics Declaration

The authors declare that the scientific ethical and legal responsibility of this article published in EPSTEM journal belongs to the authors.

Acknowledgements or Notes

* This article was presented as an oral presentation at the International Conference on Technology (www.icontech.net) held in Antalya/Turkey on November 16-19, 2023.

References

- Aksimsek, S. (2021). Development of a millimeter wave eight-element phased array antenna for 5G mobile communications. *European Journal of Science and Technology*, 29, 323-326.
- Cheng, D. K. (1971). Optimization techniques for antenna arrays. *Proc. IEEE*, 59, 1664- 1674.
- Elliott, R. S. (1963a). Beamwidth and directivity of large scanning arrays. *Microwave Journal*, 63.
- Elliott, R. S. (1964b). Beamwidth and directivity of large scanning arrays. *Microwave Journal*, 74.
- Frenzel, L. E. (1994). *Principles of electronic communication systems* (4th ed. pp.526-530).
- Lima de Paula, I., Lemey S., Bosman, D., Brande, Q., Caytan, O., Lambrecht, J., Cauwe, M., Torfs, G., & Rogier, H. (2021). Cost-effective high-performance air-filled SIW antenna array for the global 5G 26 GHz and 28 GHz bands. *IEEE Antennas and Wireless Propagation Letters*, 20(2), 194-198.
- Ozpinar, H., Aksimsek, S., & Tokan, N. T. (2020). A novel compact, broadband, high gain millimeter-wave antenna for 5G beam steering applications. *IEEE Transactions on Vehicular Technology*, 69(3), 2389-2397.
- Park, J., Ko, J., Kwon, H., Kang, B., Park B., & Kim, D., (2016). A tilted combined beam antenna for 5G communications using a 28-GHz band. *IEEE Antennas and Wireless Propagation Letters*, 15, 1685-1688.

- Tai, C. T. (1964). The optimum directivity of uniformly spaced broadside arrays of dipoles. *IEEE Trans. Antennas Propagat*, 12(4), 447-454.
- Yang, Q., Ban, Y., Kang, K., Sim, C., & Wu, G. (2016). SIW, multibeam array for 5G mobile devices. *IEEE Access*, 4, 2788-2796.

Author Information

Emirhan Aydın

Samsung Electronics Turkey
Cerkezkoy, Tekirdag, Turkey
Contact e-mail: e.aydin@samsung.com

Ramiz Erdem Aykac

Samsung Electronics Turkey
Cerkezkoy, Tekirdag, Turkey

To cite this article:

Aydın, E., & Aykac, R. E. (2023). The effect of antenna spacing on active S-parameters in planar array antennas. *The Eurasia Proceedings of Science, Technology, Engineering & Mathematics (EPSTEM)*, 24, 29-36.

The Eurasia Proceedings of Science, Technology, Engineering & Mathematics (EPSTEM), 2023

Volume 24, Pages 37-48

IConTech 2023: International Conference on Technology

The Role of Internet of Things, Machine Learning, Artificial Neural Networks and Industry 5.0 in Business Research: Trends and Future Insights

Zeynep Baysal

OSTIM Technical University

Hamide Ozyurek

OSTIM Technical University

Ali Ozarslan

OSTIM Technical University

Serdar Celik

OSTIM Technical University

Abstract: The globalization of the business world, the rapid advancement of the Internet, and the increased flexibility of information flow have led to rapid digitalization. In this context, this study aims to better understand the trends and developments in the field of business research on the topics of the Internet of Things (IoT), machine learning, artificial neural networks, and Industry 5.0. Study types, keywords, authors, author collaborations, citations, and countries were analyzed for articles published on the above-mentioned topics in the Web of Science (WoS) database between 2007-2023 (limited to September 27th, 2023). Within the scope of the study, 545 articles were identified in the WoS database and for the purposes of the research, this database was limited to the open access articles published in English, under the Business category and indexed in Social Sciences Citation Index (SSCI), Science Citation Index (SCI), and Emerging Sources Citation Index (ESCI). A bibliometric analysis was conducted by employing the VOSviewer tool to analyze network visualization of keywords and layered and density visualizations of subject areas. Results of the analysis demonstrate that studies in this field have continued to increase since 2018. The top five most frequently used keywords with the highest connection power are machine learning, Internet of Things, artificial intelligence, big data, and natural language processing, respectively. This research has revealed that the journals with the highest number of articles in this field and the highest number of citations were Technological Forecasting and Societal Change, Journal of Business Research, Electronic Markets, and Marketing Science. In terms of the number of articles and citations by country in these fields, England, the USA, Germany, Italy, and Australia ranked the highest. This research provides information on latest technologies, identifies gaps and research opportunities in the field, and contributes to shaping future research paths in the field.

Keywords: Internet of things, Machine learning, Neural networks, Industry 5.0

Introduction

Nowadays, the rapidly changing world of technology and industry is shaped by a variety of important concepts. These concepts are at the center of scientific research as well as technological advances. Terms such as the internet of things (IoT), machine learning, artificial neural networks and Industry 5.0 are important topics that drive innovation and revolutionize different sectors (Chander et al., 2022).

- This is an Open Access article distributed under the terms of the Creative Commons Attribution-Noncommercial 4.0 Unported License, permitting all non-commercial use, distribution, and reproduction in any medium, provided the original work is properly cited.

- Selection and peer-review under responsibility of the Organizing Committee of the Conference

© 2023 Published by ISRES Publishing: www.isres.org

IoT is a technology and concept that enables physical objects to communicate with each other and with people over the internet. These objects can include all kinds of devices, sensors, household appliances and industrial equipment. IoT allows these objects to collect, process and share their data. This data can be used for many different purposes, such as making better decisions, improving efficiency, ensuring security and developing new services.

Machine learning is a branch of artificial intelligence that enables computers to recognize patterns and predict future events by analyzing data. Algorithms learn by processing large amounts of data and draw conclusions from that data. Machine learning is used in many application areas such as classification, regression, clustering, natural language processing and prediction.

Artificial neural networks are a model of artificial intelligence that mimics the functioning of the human brain. These networks consist of many connected nodes and layers. Each node performs complex calculations by processing inputs and passing the results to other nodes. Deep learning is based on neural networks, which are very successful on large and complex datasets. It is used in applications such as image recognition, natural language processing and autonomous vehicles.

Industry 5.0 is considered a new era in the manufacturing industry. It is characterized by the fact that industrial production involves smart factories where people work collaboratively. Industry 5.0 represents an approach in which humans and robots work collaboratively, the use of data analytics and artificial intelligence increases, and production processes become more flexible and customizable. This aims to increase productivity as well as develop more sustainable and competitive production methods.

Bibliometric analysis is an important method used to study various aspects of academic research, scientific publications and the scientific world (Donthu et al., 2021). These analyses are used to track scientific developments, understand interdisciplinary relationships, and assess the evolution of specific topics or fields. Bibliometric analysis measures and compares various data points using scientific metrics and statistical methods.

In this study, four important technology and industry concepts, IoT, Machine Learning, Artificial Neural Networks and Industry 5.0 are discussed from a bibliometric perspective. While addressing these four key topics, we explain the definition and importance of each of them and emphasize that these concepts have become the focus of scientific research in recent years. Assessing the development and impact of these topics in the literature will provide a scientific perspective to trace this transformation.

Literature Review

Internet of Things

The term Internet of Things (IoT) was first used by a British technologist named Kevin Ashton. Ashton coined the term in 1999. Kevin Ashton had a vision of connecting the physical world of things to the internet and ensuring them to have interaction with each other. Ashton's work, and the term itself, has subsequently led to IoT becoming a concept with a wide range of applications. From smart homes to healthcare, transportation to industrial automation, IoT is used in many different fields and has become a fundamental component of the modern digital world (Madakam et al., 2015).

In IoT, connected devices collect information, exchange operational details and perform specified activities (Sahni et al. 2017). The IoT involves web-enabled smart devices that compile, transmit and act on the data they receive through integrated systems, including processors, sensors and communication hardware (Medhat et al., 2019). IoT devices make the sensor data they collect visible through the use of an IoT sink or other edge device. These devices occasionally interact with other connected devices and take action based on the data they exchange. While humans can contact with devices to understand, manage or retrieve data, devices perform most of the work without human involvement (Wei et al. 2019). IoT is also capable of machine learning, commonly known as artificial intelligence, which can lead to more utilized and dynamic data processes (Piccialli et al., 2019).

Previous bibliometric studies on IoT have been analyzed in relation to concepts or fields such as marketing (Miskiewicz, 2020), supply chain management and logistics (Rejeb et al., 2020), food safety (Bouzemrak et al.,

2019), blockchain (Kamran et al., 2020), agriculture (Rejeb et al., 2022) and tourism (Suneel et al., 2022). In general, it has been observed that interest in IoT has increased rapidly, especially since 2010.

Machine Learning

Machine learning, recognized as a pivotal discipline within the field of artificial intelligence, empowers computer systems to acquire knowledge through the analysis of data. Its fundamental objective is to equip these systems with the capability to forecast future events by discerning patterns inherent in data. The potency of machine learning in handling copious datasets endows it with a broad spectrum of applications, spanning across diverse sectors such as business, science, healthcare, finance, and numerous others.

Machine learning can be categorized into two principal domains: supervised and unsupervised learning. Supervised learning entails the training of models using labeled data, whereas unsupervised learning is instrumental in extracting patterns and relationships from unlabeled data. Furthermore, advanced methodologies like deep learning have attained remarkable success, particularly in tasks demanding higher complexity.

Machine learning is poised to continue its transformative impact on the realms of science and industry, providing valuable tools for diverse applications including data mining, recommendation systems, automation, and the anticipation of future trends (Freeman et al., 2019). This technology harnesses algorithms to elucidate patterns and relationships embedded within datasets, making it indispensable for decision-making processes across various domains. Its significance is exemplified in applications encompassing natural language processing, robotics, image analysis, object recognition, and notably, the healthcare sector, where machine learning plays a pivotal role (Tzanakou et al., 2017). The overarching objective of machine learning is to facilitate automatic inference from data without human intervention (Dietterich, 1990).

Artificial Neural Networks (ANNs)

ANNs, often referred to simply as neural networks, represent a class of machine learning algorithms inspired by the structural and functional principles of the human brain. These networks are composed of interconnected computational units termed neurons, which collaboratively process and analyze data. ANNs' rising prominence in recent years is attributed to their capacity for continuous learning and improvement, rendering them particularly suited for tasks characterized by extensive data volumes.

The architecture of a neural network is often likened to that of the human brain. Analogous to the brain's neural networks, artificial neural networks consist of layers of interconnected neurons. The input layer serves to receive information from the external environment, while the output layer delivers the final result. Hidden layers situated in between execute the requisite computations to transform the input into the desired output. Each neuron within a neural network receives input from neurons in the preceding layer and applies a mathematical function, referred to as the activation function, to this input to generate an output. Subsequently, this output is propagated to the following layer of neurons until it reaches the output layer. The activation function is pivotal in determining the neuron's output based on its input.

The connections between neurons in a neural network are represented by numerical values known as weights, which specify the strength of the connection between two neurons. Over the course of training, these weights are iteratively adjusted to minimize the disparity between the output generated by the neural network and the desired output.

One of the most compelling attributes of ANNs is their ability to learn from extensive datasets. By fine-tuning the neuron weights, neural networks are capable of recognizing patterns and correlations in data, thus enabling precise predictions and classifications. This makes ANNs exceptionally valuable in applications such as image and speech recognition, natural language processing, and financial forecasting.

Several distinct types of ANNs exist, each characterized by its unique architecture and application. Feed-forward neural networks, the most elementary type, feature data flow from the input layer to the output layer without feedback loops. Convolutional neural networks, frequently employed in image recognition, involve multiple layers of convolution and pooling operations. Recurrent neural networks, on the other hand, are tailored for processing sequential data, including time series data and text.

Industry 5.0

The advent of intelligent manufacturing systems, as catalyzed by Industry 4.0, has underscored the pivotal role of human capabilities. Industry 5.0 seeks to build upon this foundational premise, placing its emphasis on a human-centric, sustainable, and adaptable approach to the realm of production. At its core, Industry 5.0 is dedicated to the amplification of productivity and efficiency, achieved through the synergistic utilization of human, robotic, and artificial intelligence technologies. Concurrently, it endeavors to rekindle awareness of societal sensitivities that were at times marginalized during the Industry 4.0 era. The essential competencies inherent in Industry 5.0 orbit the nurturing of inventive products and cutting-edge technologies. This conceptual framework has risen to paramount importance for both individual enterprises and the broader national economies, fortifying their competitive prowess (Balog & Demirova, 2021). In a more expansive context, Industry 5.0 embodies a concept that has matured to harness human ingenuity in harmonious coaction with potent, intelligent, and precision-driven machinery (Maddikunta et al., 2022).

Methodology

In the literature, there is no study in which the trends and development of research on the Internet of Things, machine learning, artificial neural networks and industry 5.0 are evaluated together with bibliometric analysis. In this context, in this study, the types of studies, keywords, authors, author collaborations, author collaborations, citations, and countries related to the research conducted in these fields were analyzed using bibliometric analysis method. Software programs such as VOSviewer, CiteSpace, RStudio's bibliometrics package, BibExcel, Gephi and Histcite are frequently used for bibliometric analysis, which is a statistical method used to reveal the publication trends of research in a healthier way (Rashmi & Kataria, 2021). In this study, VOSviewer (1.6.19) (Van Eck & Waltman, 2010) was used to visualize the clusters and interdisciplinary mapping of the field so that researchers from different disciplines can easily understand the findings obtained.

Data Selection and Data Collection

Studies on the Internet of Things, machine learning, artificial neural networks and industry 5.0 between 2007-2023 (limited to 27.09.2023) in the Web of Science (WoS) database were evaluated. Within the scope of the study, 545 articles identified in the WoS database, which is among the most comprehensive databases in terms of articles in multidisciplinary fields, scanned in SSCI, SCI and ESCI, covering business categories, open access and published in English, open access, were evaluated.

Search Criteria

Firstly, articles published in WoS indexed journals with the keywords "Internet of Things" "Machine Learning" "Artificial Neural Network" and "Industry 5.0" in their titles and/or abstracts were searched in Web of Science Categories business. 545 English articles in SSCI, SCI (SCI-E) and ESCI, which are considered as the most prestigious indexes, were recorded to be included in the analysis.

Results and Discussion

Number of Publications by Year

The total number of studies in the WoS database with the keywords "Internet of Things" "Machine Learning" "Artificial Neural Network" and "Industry 5.0" is 545 as shown in Table 1 and Figure 1. It is seen that the first study record belongs to 2007. It can be stated that the studies on the field have continued to increase since 2016.

Keyword Analysis

Figure 2 shows all subject areas related to the keywords Internet of Things, machine learning, artificial neural networks and industry 5.0. In the bibliometric analysis with VOSviewer, 3 different mapping visualizations were analyzed: network visualization Figure 2, layered visualization Figure 3 and density visualization Figure 4.

Table 1. Distribution of studies by years

Year	Frequency	Percentage %
2007	1	0,0018
2010	1	0,0018
2012	3	0,0055
2013	3	0,0055
2014	4	0,0073
2015	7	0,0128
2016	11	0,0202
2017	20	0,0367
2018	34	0,0624
2019	43	0,0789
2020	80	0,1468
2021	116	0,2128
2022	128	0,2349
2023	94	0,1725
Total	545	1,0000

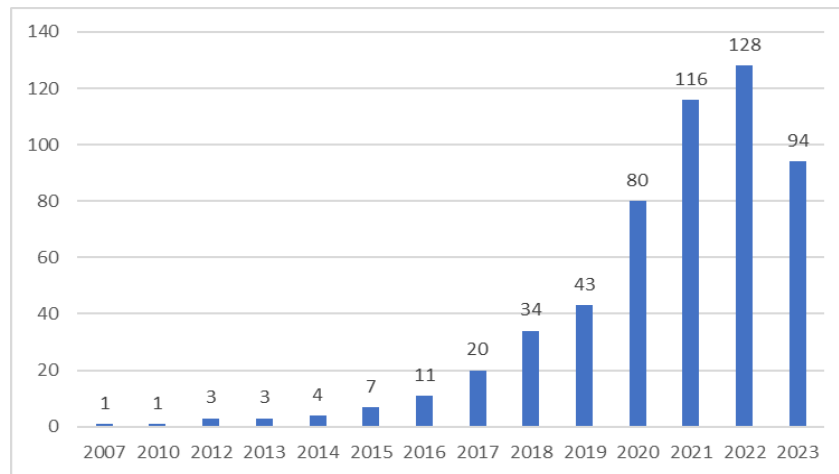


Figure 1. Number of studies by year

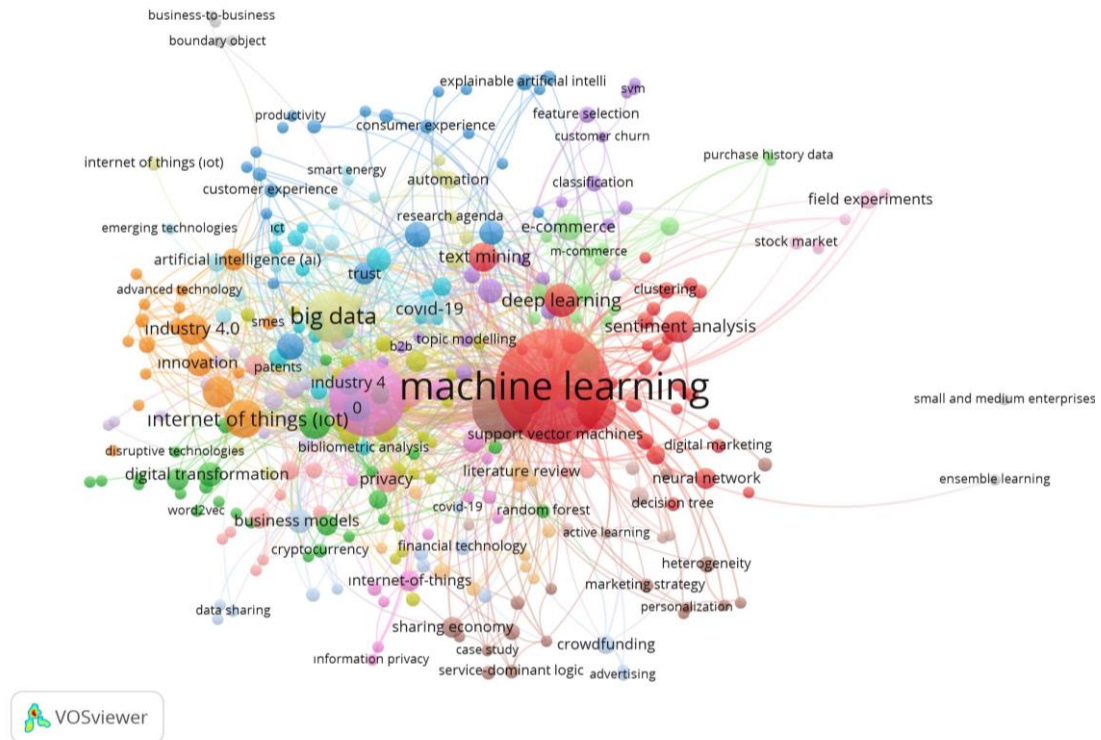


Figure 2. Network visualization map of keywords

Keywords used 2 times or more in 545 articles scanned in the WoS database were analyzed. According to these criteria; 314 keywords were reached from 2108 keywords; 21 clusters were evaluated as 1693 links and total link strength was 2144. Figure 2 shows that the most frequently used keywords in the 21 clusters are machine learning (178), internet of things (80), artificial intelligence (50), big data (38), natural language processing (21). Figure 3 indicates that machine learning and internet of things clusters are more frequently analyzed in recent years when compared to industry 4.0 and big data.

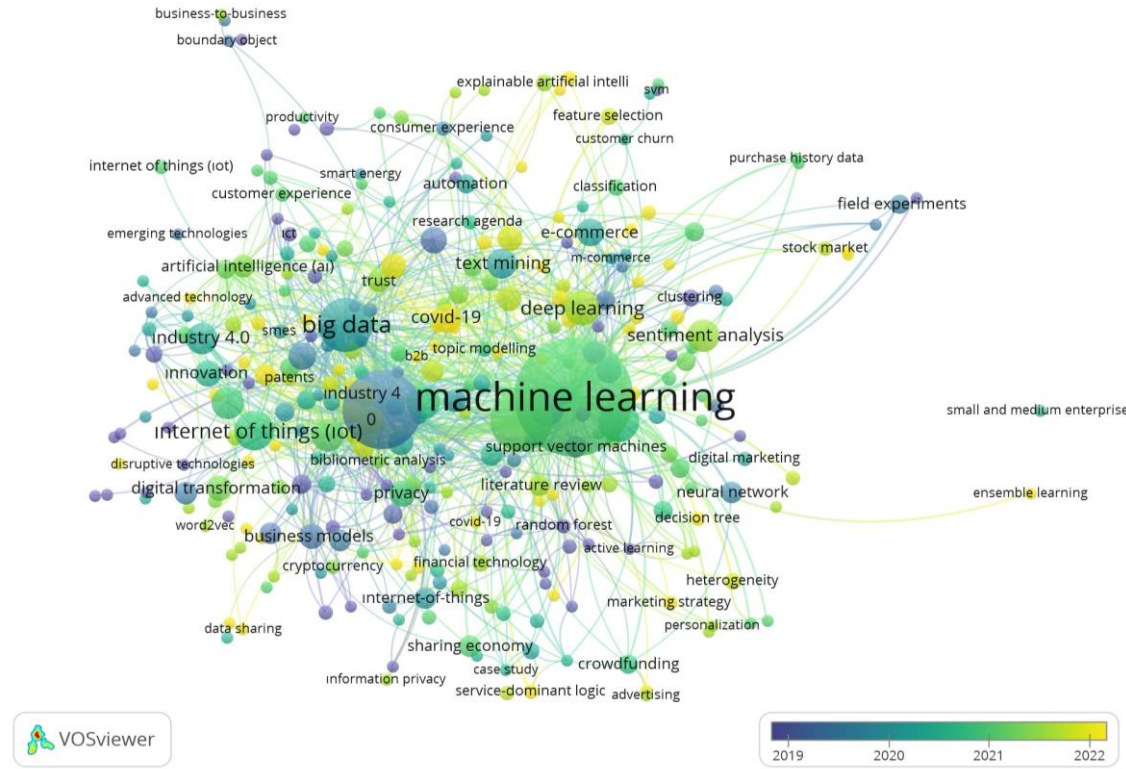


Figure 3. Layered visualization of keywords

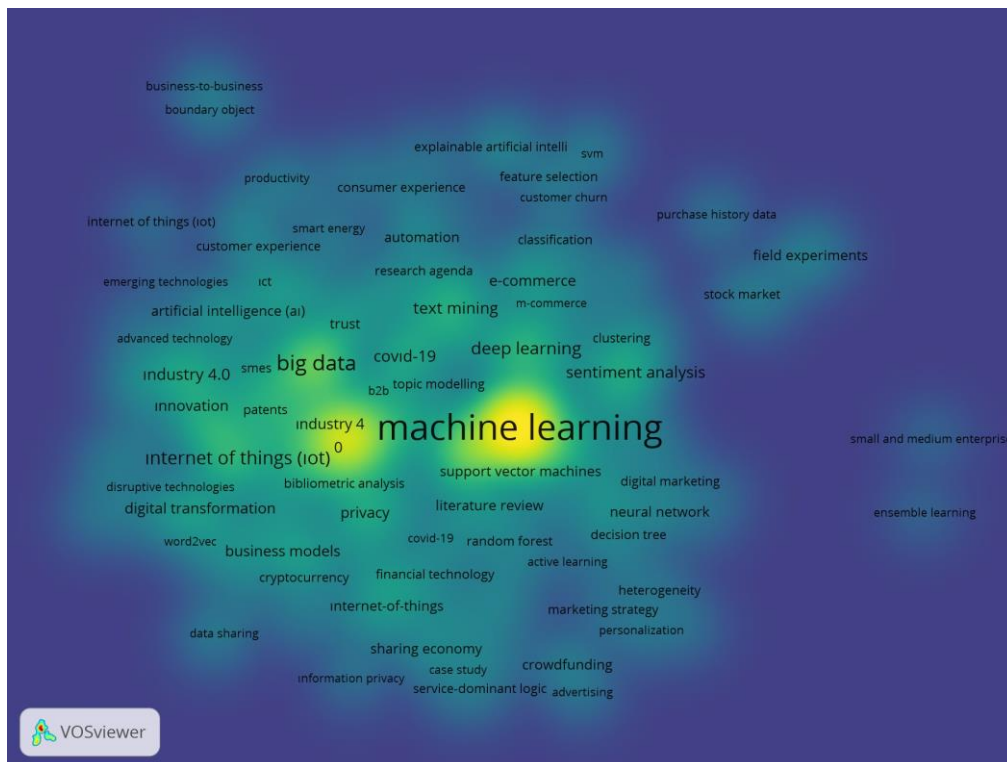


Figure 4. Density visualization map of keywords

According to Figure 4, the keywords with the highest linking power are machine learning (395), internet of things (188), artificial intelligence (151), big data (135), natural language processing (70). Clusters that are interconnected with each other constitute the connection foci of related clusters. While the proximity of the elements to each other expresses the strength of the relationship, the distance means that there is not enough relationship or similarity. There is no relationship between elements consisting of keywords that are not connected to each other by link strength (Dogan et al., 2021).

Co-Author Analysis

Within the scope of the co-author analysis, 1355 out of 1644 authors were evaluated, provided that the author has at least 1 article and at least 1 citation (Figure 5). In this context, the co-authors with the highest total link strength are Dwivedi and Yogesh (22); Rana and Nripendra (p.17); Hauser and John (15).

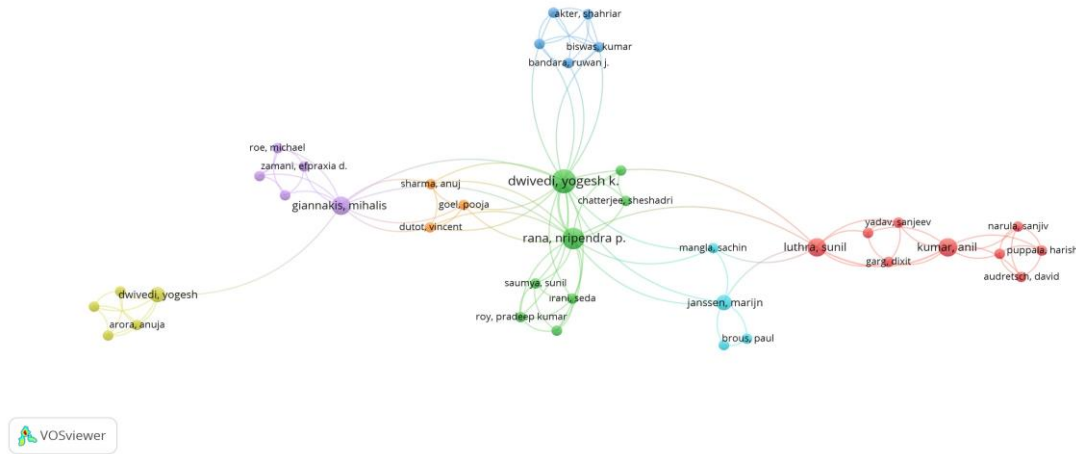


Figure 5. Co-author analysis map

Author Citation Analysis

When the author citation analysis was evaluated with at least 1 study and at least 2 citations, 568 authors were evaluated. In this context; Gretzel, Ulrike 672 is seen as the most cited author (Figure 6).

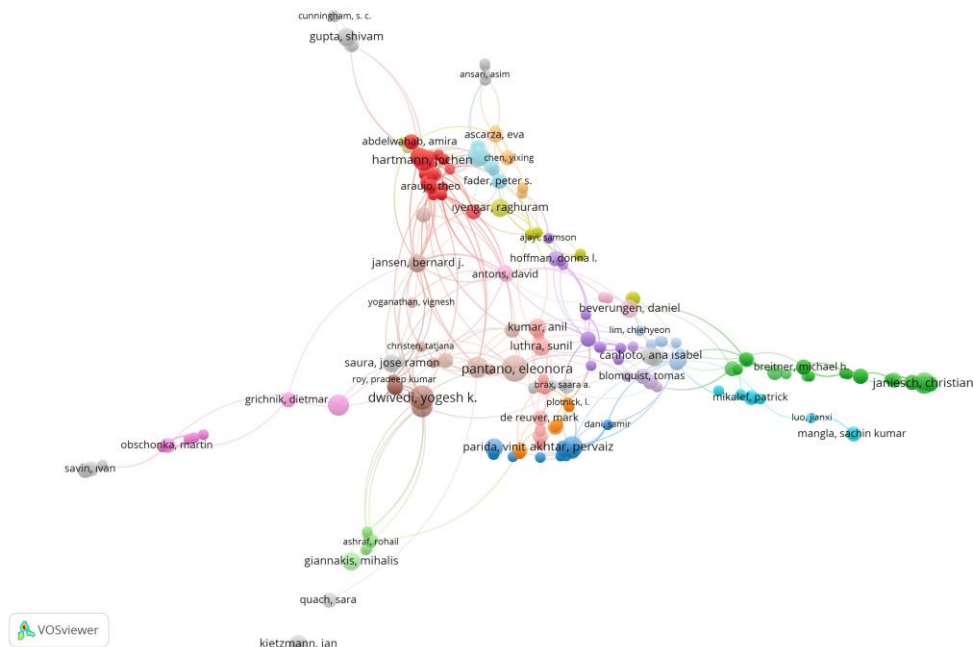


Figure 6. Author citation analysis map

Source Citation Analysis

Regarding the source citation analysis, 69 out of 133 sources were evaluated when limited to at least 2 studies and at least 2 citations (Table 2). Source citation analysis map is shown in Figure 7.

Table 2. Journals in which the Articles are Mostly Published, Number of Articles and Citations

No	Article	F	Citation
1	Technological Forecasting and Social Change	62	2105
2	Journal of Business Research	37	1544
3	Electronic Markets	30	1473
4	Marketing Science	14	776
5	Long Range Planning	2	646
6	Business Horizons	8	517
7	Journal of Retailing and Consumer Services	7	450
8	IEEE Transactions on Engineering Management	24	410
9	Journal of Consumer Research	3	331
10	Journal of Marketing Management	5	285

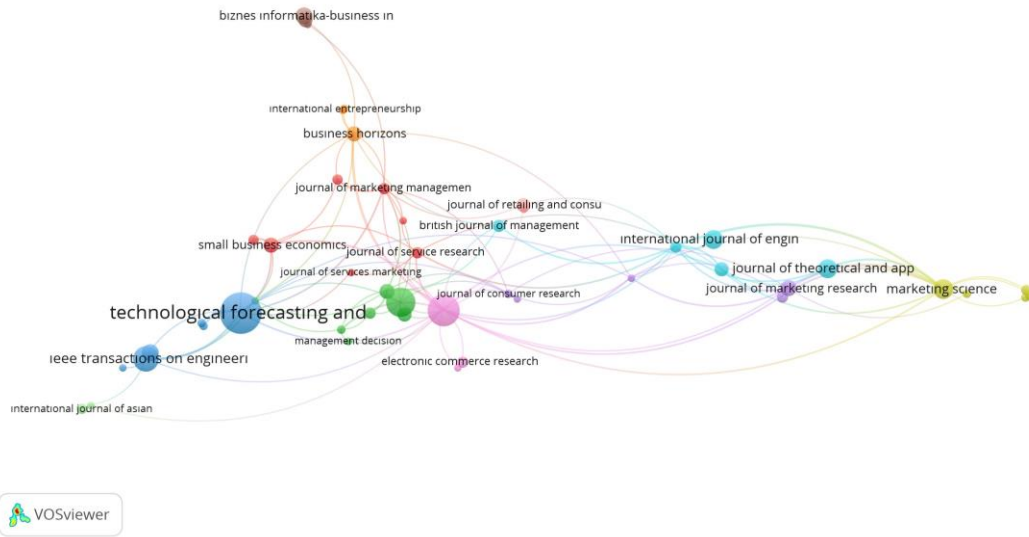


Figure 7. Source Citation Analysis Map

Table 3. Number of studies and citations by country

No	Country	Documents	Citations	Total Link Strength
1	England	117	3927	230
2	USA	105	3834	214
3	Germany	66	2579	147
4	Italy	48	1913	96
5	Australia	31	1311	83
6	India	42	1027	77
7	Peoples R China	42	851	61
8	Netherlands	35	844	103
9	South Korea	16	837	29
10	Finland	28	801	71
11	France	27	792	77
12	Sweden	14	659	25
13	Scotland	7	657	12
14	Wales	9	619	37
15	Austria	11	492	33
16	Norway	8	377	11
17	Spain	24	364	27
18	Canada	21	357	32
19	Cyprus	2	350	10
20	Taiwan	11	332	29

Country Citation Analysis

Regarding the number of country studies and citations, it was analyzed as at least 1 study and at least 1 citation. As a result of the analysis, 51 out of 74 countries that meet the specified criteria were evaluated in this category. The top 20 countries, number of articles and citations are shown in Table 3. The ranking is based on the number of citations.

When the number of country studies and citations are evaluated; the top countries are England, USA, Germany, Italy, Australia, India, Peoples r China, Netherlands, South Korea, Finland (Figure 8).

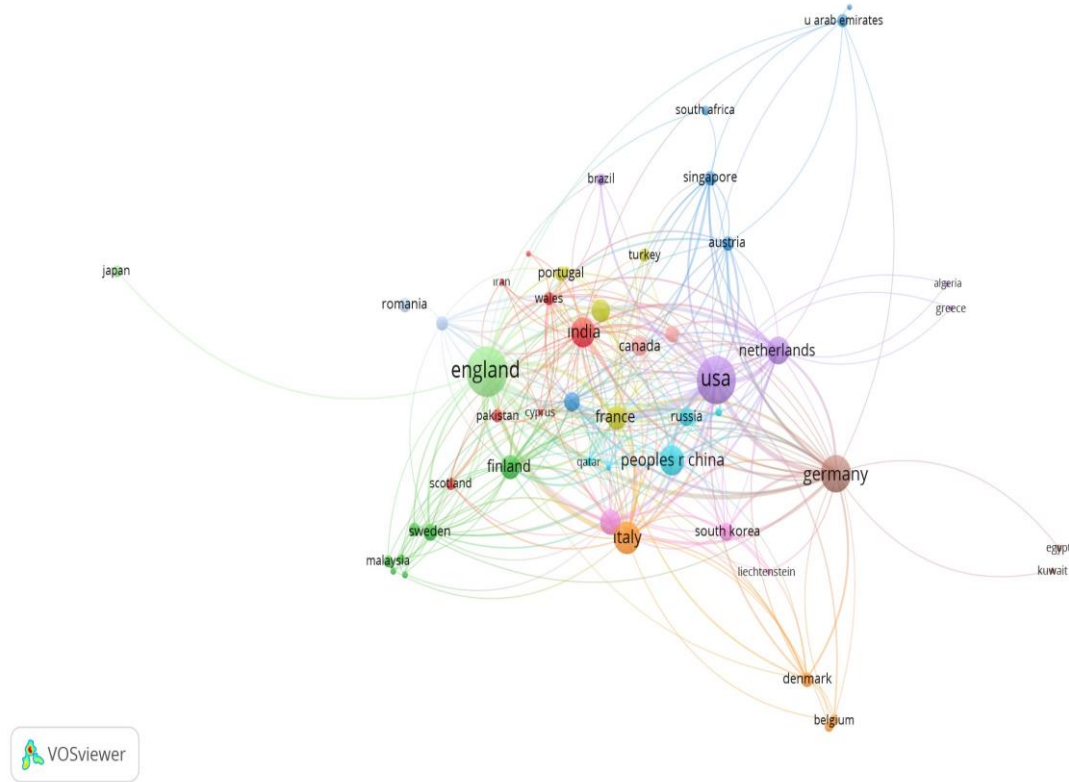


Figure 8. Visualization of studies by country

Institution Citation Analysis

Regarding the number of institutional citations, 176 out of 877 organizations were evaluated when the institution was limited to at least 2 studies and at least 2 citations. The top 10 institutions are as follows; York Univ, Rutgers State Univ, Southwestern Univ Finance & Econ, Swinburne Univ Technol, Univ Southern Calif, Osnabruck Univ, Shanghai Lixin Univ Accounting & Finance, Univ Manchester, Rmit Univ, Charles Sturt University (Table 4). Figure 9 shows the institution citation analysis map.

Table 4. Number of articles, citations and total link strength by institutions

No	Organization	Documents	Citations	Total Link Strength
1	Univ Queensland	4	694	16
2	Virginia Polytech Inst & State Univ	2	679	9
3	Swansea Univ	9	619	34
4	Friedrich Alexander Univ Erlangen Nurnberg	2	478	8
5	Univ Turin	2	443	7
6	Univ Hamburg	5	407	49
7	New York Univ	4	401	21
8	George Washington Univ	2	390	14
9	Lulea Univ Technol	4	362	7
10	Univ Vaasa	6	362	19

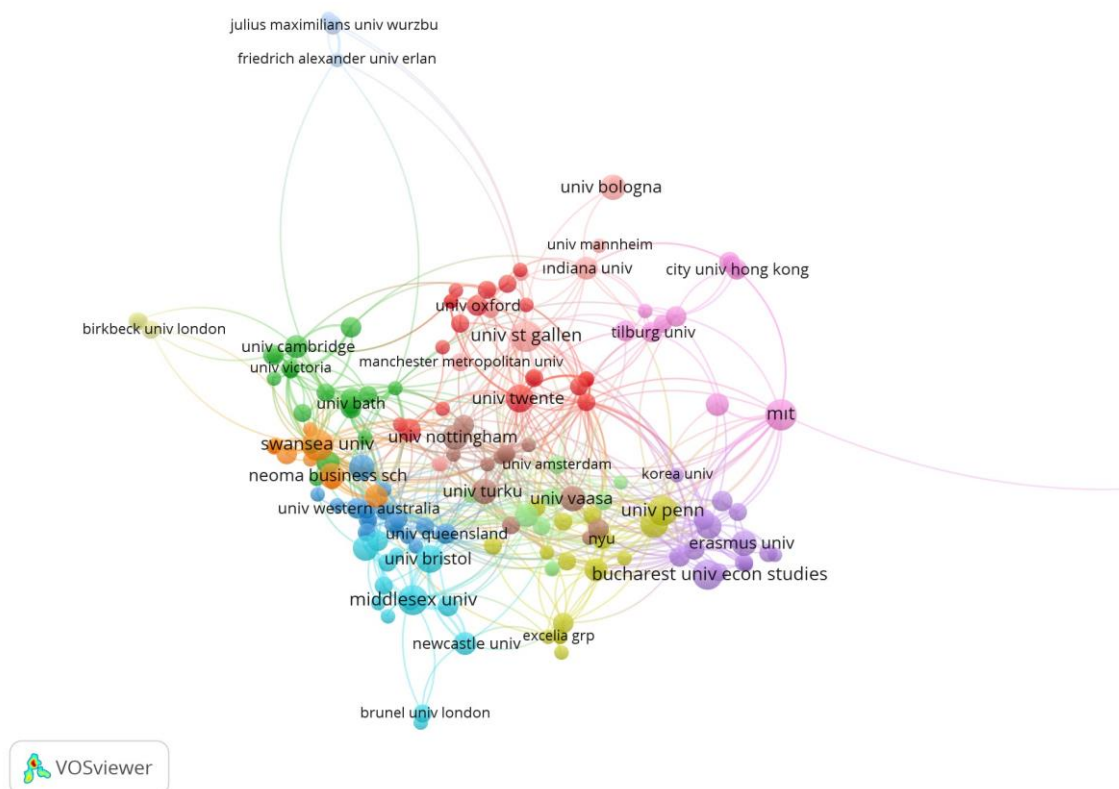


Figure 9. Institution citation analysis map

As analyses demonstrate, the concepts of Internet of Things (IoT), Machine Learning, Artificial Neural Networks and Industry 5.0 has been studied by various researchers in a broad range of countries, publishing their works in a variety of journals. The main purpose of these analyses is to provide future researchers with inspiration to produce their own research and guide them in this endeavor.

Conclusion

In conclusion, the convergence of Internet of Things (IoT), Machine Learning, Artificial Neural Networks, and the emergence of Industry 5.0 is ushering in a new era of possibilities in business research. These technologies have already transformed the way we collect, analyze, and utilize data, offering businesses unprecedented insights and efficiencies. As we move forward, it is essential for researchers, businesses, and professionals to stay at the forefront of these trends and adapt to the ever-evolving landscape. The integration of IoT devices with ML and ANNs is enhancing our ability to process vast amounts of data, extract meaningful patterns, and make real-time decisions. This synergy empowers businesses to optimize their operations, enhance customer experiences, and drive innovation. The advent of Industry 5.0, which emphasizes human-technology collaboration and the reintegration of physical and digital worlds, will further revolutionize industries and open up new avenues for research.

In this study, a bibliometric analysis was conducted to provide insight into the prevalence of the concepts of Internet of Things (IoT), Machine Learning, Artificial Neural Networks, and Industry 5.0 in the field of business research. A total of 545 articles were identified in the WoS database and for the purposes of the research, study types, keywords, authors, author collaborations, citations, and countries of articles published on these topics in the Web of Science (WoS) database between 2007-2023 (limited to September 27th, 2023) were analyzed based on the criteria that the articles were open access, in English, categorized under “business” and indexed in Social Sciences Citation Index (SSCI), Science Citation Index (SCI), and Emerging Sources Citation Index (ESCI). A bibliometric analysis was conducted by employing the VOSviewer tool and the results of the analysis demonstrated that studies in this field have continued to increase since 2018. The top five most frequently used keywords with the highest connection power were machine learning, Internet of Things, artificial intelligence, big data, and natural language processing, respectively. The journals with the highest number of articles and citations were Technological Forecasting and Societal Change, Journal of Business Research, Electronic Markets, and Marketing Science. In terms of the number of articles and citations by country in these fields,

England, the USA, Germany, Italy, and Australia ranked the highest. This research provides information on latest technologies, identifies gaps and research opportunities in the field, and contributes to shaping future research paths in the field.

The future of business research lies in harnessing the transformative power of IoT, Machine Learning, Artificial Neural Networks, and Industry 5.0. By embracing these trends, businesses can gain competitive advantage, foster innovation, and contribute to the ongoing evolution of their own industries. As the digital and physical realms become more interconnected, researchers and businesses will play a pivotal role in shaping the way people work, produce, and interact in the years to come. Therefore, staying informed, adaptable, and ethically responsible in this technological journey will be key to unlocking the full potential of these cutting-edge tools in business research.

Recommendations

Authors of this study recommend future business researchers in the fields of IoT, Machine Learning, Artificial Neural Networks, and Industry 5.0 to examine the analyses and acquire guidance and insight into the topics they may focus on in their own studies and also find journals, countries and other authors that may be interested in their work.

Scientific Ethics Declaration

The authors declare that the scientific ethical and legal responsibility of this article published in EPSTEM journal belongs to the authors.

Acknowledgements or Notes

* This article was presented as an oral presentation at the International Conference on Technology (www.icontech.net) held in Antalya/Turkey on November 16-19, 2023.

References

- Balog, M., & Demirova, S. (2021). Human capital development in the context of the fourth industrial revolution. *IOP Conference Series: Earth and Environmental Science*. IOP Publishing.
- Maddikunta, P., Pham, Q.V., B, P., Deepa, N., Dev, K., Gadekallu, T., . . . Liyanage, M. (2022). Industry 5.0: A survey on enabling technologies and potential applications. *Journal of Industrial Information Integration*, 26(2), 100257.
- Freeman, I., Haigler, A., Schmeelk, S., Ellrodt, L., & Fields, T. (2019). What are they researching? Examining industry-based doctoral dissertation research through the lens of machine learning. *Proceedings 17th IEEE International Conference on Machine Learning and Applications, ICMLA 2018*, 1338–1340.
- Tzanakou, E. M. (Ed.). (2017). *Supervised and unsupervised pattern recognition: Feature extraction and computational intelligence*. CRC Press.
- Dietterich, T. G. (1990). Machine learning. *Annual Review of Computer Science*, 4(1), 255-306.
- Bouzembrak, Y., Kluche, M., Gavai, A., & Marvin, H. J. (2019). Internet of things in food safety: Literature review and a bibliometric analysis. *Trends in Food Science & Technology*, 94, 54-64.
- Chander, B., Pal, S., De, D., Buyya, R. (2022). Artificial intelligence-based internet of things for industry 5.0. In S. Pal D. De & R. Buyya (Eds.), *Artificial intelligence-based internet of things systems internet of things* (pp. 3-45). Springer: Cham.
- Donthu, N., Kumar, S., Mukherjee, D., Pandey, N. and Lim, W. M. (2021). How to conduct a bibliometric analysis: An overview and guidelines? *Journal of Business Research*, 133, 285-296.
- Kamran, M., Khan, H. U., Nisar, W., Farooq, M., & Rehman, S. U. (2020). Blockchain and internet of things: A bibliometric study. *Computers & Electrical Engineering*, 81, 106525.
- Madakam, S., Ramaswamy, R., & Tripathi, S. (2015). Internet of things (IoT): A literature review. *Journal of Computer and Communications*, 3, 164-173.

- Medhat, G. M., Aneiba, A., Basurra, S., Batty, O., Elmisery, A. M., Kovalchuk, Y., & Rehman, M. H. U. (2019). Internet of things and data mining: from applications to techniques and systems. *Wiley Interdiscip Rev Data Min Knowl Disc*, 9(3), 21.
- Miskiewicz, R. (2020). Internet of things in marketing: Bibliometric analysis. *Marketing and Management of Innovations*, 3, 371-381.
- Piccialli, F., Cuomo, S., di Cola, V. S. and Casolla, G. (2019). A machine learning approach for IoT cultural data. *Journal of Ambient Intelligence Humanized Computing*, 10(1), 1–12.
- Rashmi, K., & Kataria, A. (2021). Work–life balance: A systematic literature review and bibliometric analysis. *International Journal of Sociology and Social Policy*, 42(11-12), 1028-1065.
- Rejeb, A., Rejeb, K., Abdollahi, A., Al-Turjman, F., & Treiblmaier, H. (2022). The interplay between the internet of things and agriculture: A bibliometric analysis and research agenda. *Internet of Things*, 19, 100580.
- Rejeb, A., Simske, S., Rejeb, K., Treiblmaier, H., & Zailani, S. (2020). Internet of things research in supply chain management and logistics: A bibliometric analysis. *Internet of Things*, 12, 100318.
- Sahni, Y., Cao, J., Zhang, S., & Yang, L. (2017) Edge mesh: a new paradigm to enable distributed intelligence in internet of things. *IEEE Access*, 5, 16441–16458.
- Suneel, K., Saini, A., Kumar, S., & Kumar, V. (2022). Bibliometric analysis on Internet of things (IoT) and tourism industry: a study based on Scopus database. *South Asian Journal of Tourism and Hospitality*, 2(1), 76-95.
- Van Eck, N., & Waltman, L. (2010). Software survey: VOSviewer, a computer program for bibliometric mapping. *Scientometrics*, 84(2), 523-538.
- Wei, Z., Jia, Y., Yao, Y., Zhu, L., Guan, L., Mao, Y., Liu, P. and Zhang, Y. (2019). Discovering and understanding the security hazards in the interactions between IoT devices, mobile apps, and clouds on smart home platforms. In *28th {USENIX} security symposium ({USENIX} security*, 19, 1133–1150.

Author Information

Zeynep Baysal

OSTIM Technical University
Ankara, Turkey

Contact e-mail: zeynep.baysal@ostimteknik.edu.tr

Hamide Ozyurek

OSTIM Technical University
Ankara, Turkey

Ali Ozarslan

OSTIM Technical University
Ankara, Turkey

Serdar Celik

OSTIM Technical University
Ankara, Turkey

To cite this article:

Baysal, Z., Ozyurek, H., Ozarslan, A., & Celik, S. (2023). The role of internet of things, machine learning, artificial neural networks and industry 5.0 in business research: Trends and future insights. *The Eurasia Proceedings of Science, Technology, Engineering & Mathematics (EPSTEM)*, 24, 37-48.

The Eurasia Proceedings of Science, Technology, Engineering & Mathematics (EPSTEM), 2023

Volume 24, Pages 49-54

IconTech 2023: International Conference on Technology

Implementation of Industry 4.0 in Ship Repair Industry: Challenges and Opportunities

Yordan Denev

Technical University of Varna

Abstract: : In recent years, the concept of Industry 4.0 has found its way into the industry, particularly heavy machinery manufacturing. This article explores Industry 4.0 in the context of ship repair, which is part of the heavy industry in the Republic of Bulgaria. The characteristic of the ship repair industry is presented by comparing it with that of shipbuilding. The two industries are similar, but despite that, they have differences. The challenges and opportunities in its implementation in the ship repair process are presented and analyzed. Particular attention is paid to ship repair enterprises of the small and medium-sized (SME) type, which are quite numerous in the Republic of Bulgaria. For them, the adaptation and transition to Industry 4.0 are more challenging. There are identified benefits and opportunities for improving energy efficiency in enterprises, especially small and medium-sized ones, enhancing the working environment, reducing waste generation in the production process, and maintaining competitiveness at a relatively high level.

Keywords: Industry 4.0, Ship repair, Challenges, Opportunities, Energy efficiency

Introduction

At the core of the concept of Industry 4.0 lies the implementation of intelligent digital technologies in manufacturing and industry. Industry 4.0 is the fourth stage in the development of techniques and technologies in the industrialization of the world. Its impact is observed in all areas of heavy machinery manufacturing, particularly in shipbuilding and ship repair. Building on the concept of Industry 4.0, the concept of Shipbuilding 4.0 has been introduced, which aligns with the principles of Industry 4.0. Following this logic and considering that shipbuilding and ship repair are closely connected in terms of production capabilities and equipment, it is appropriate to introduce the concept of Ship repair 4.0.

An analysis of the current level of development of Industry 4.0 in the context of shipbuilding has been conducted in (Stanic, 2018). Various publications have been summarized, different topics have been analyzed, and levels of production aspects within the industry have been examined. By harnessing the technologies of Industry 4.0, conditions are created for reducing production and operational costs, leading to improvements in manufacturing.

Digitization is one of the directions in industrial development. A branch of digitization is digital twins, which are entering many branches of the industry. A concept for developing a digital twin of the ship design and construction process is presented in (Iwankowicz, 2023). The concept developed in this way has been tested through a shipbuilding process, and practical aspects of its implementation have been highlighted. The development of a digital twin for a shipbuilding enterprise based on statistical and empirical data with the aim of improving competitiveness is presented in (Kunkera, 2022). Digital twins also contribute to environmental protection and workplace safety, making them increasingly applicable in manufacturing.

After the emergence and integration of the Internet of Things, which is a part of Industry 4.0, things in various industries began to change. This led to the maritime industry's interest, resulting in the creation of the Internet of

- This is an Open Access article distributed under the terms of the Creative Commons Attribution-Noncommercial 4.0 Unported License, permitting all non-commercial use, distribution, and reproduction in any medium, provided the original work is properly cited.

- Selection and peer-review under responsibility of the Organizing Committee of the Conference

© 2023 Published by ISRES Publishing: www.isres.org

Ships, which, to some extent, refers to a network of interconnected objects related to ship repair or shipbuilding yards. Through this Internet of Ships technology, the information generated by it can be managed throughout the entire lifecycle of the ship (Sokolov, 2018).

Augmented reality is one of the new technologies that can be useful in shipbuilding and ship repair production. Its use enables operators to receive more and clearer information about the stages of the production process. Potential augmented reality solutions with future applications in ship construction and repair are presented and analyzed in (Fernandez, 2023). The authors have introduced hardware, software, and technological solutions tailored to this industry with their developments.

Ship Repair Industry Overview

The ship repair industry is more dynamic compared to shipbuilding. In shipbuilding, the process takes a long time. Depending on the type of ship, its construction can take anywhere from 6 months to 3 years, while in ship repair, the duration of repairs in modern production, regardless of the type of ship, is around 20 calendar days. The ship repair market is a market characterized by sinusoidal growth and decline. Growth has been observed since 2020, and it is expected to reach approximately 6% by 2028, which corresponds to an increase in profitability (Mark Wide, 2023). The distribution of the market share among the major global regions involved in ship repair, as well as the expected increase in activities across various areas of the ship hull, is presented in the Figure.1.

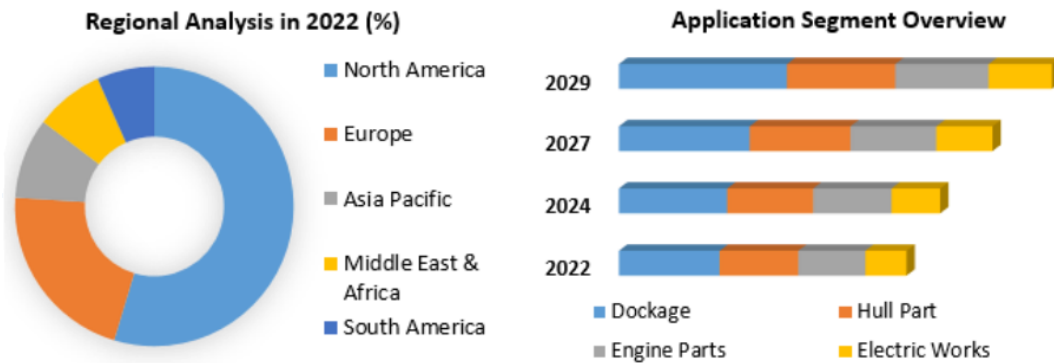


Figure 1. Distribution of ship repair market in major ship repair regions (Ship repair and maintenance, 2023)



Figure 2. Ship repair map in Europe (Trusteddocks, 2023)

From Figure 1, it can be seen that the region with the largest percentage share in ship repair is North America, followed by Europe and Asia. Regarding the different activities related to the ship, the largest share belongs to

ship docking. This is associated with sandblasting and painting of the ship's hull, as well as inspections and repairs of the underwater part. The other three activities, hull repair, machinery, and electrical activities, are almost evenly distributed among themselves. The data indicate that there is an increase in each of these activities by 2029, which will also lead to higher industry profitability. In Europe are located about 150 ship repair yards, Figure 2. Each of these plants is characterized by an index called the ship repair index. It is individual for each plant, but overall for Europe, as of today, it is lower by about 26% compared to the same period in 2022. The types of ships most frequently resorting to repairs are presented in Figure 3.

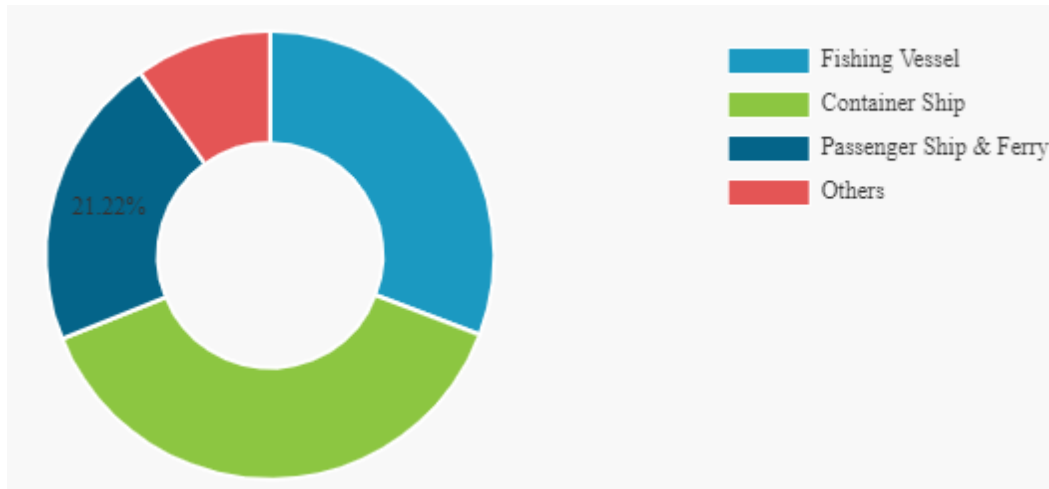


Figure 3. Ship types most involved in ship repair (Fortune Business, 2023)

It can be seen that the largest percentage share is held by container ships, followed by fishing and passenger ships. Considering the requirements and equipment of these groups of ships, it becomes clear that Industry 4.0 is highly pronounced in them, posing challenges to ship repair plants during dry-docking and class repairs of these ships.

Challenges in Implementation of Industry 4.0 in Ship Repair

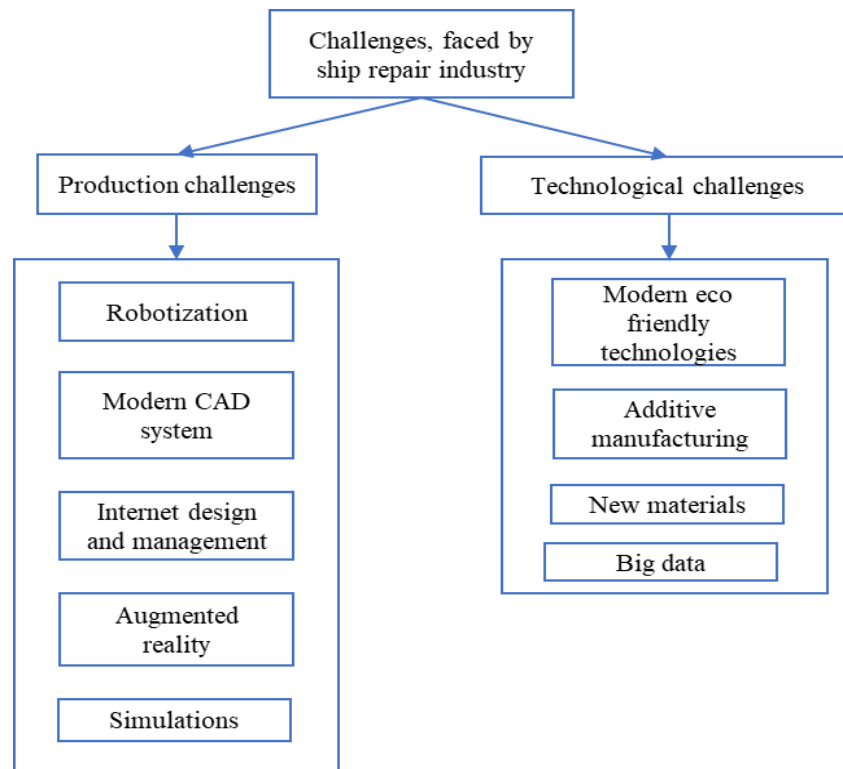


Figure 4. Challenges faced by ship repair industry

The challenges facing ship repair after the entry of Industry 4.0 can be broadly divided into two groups, as presented in Figure 4. The aspects presented in Figure 4 are referred to as challenges because their implementation in the real industry would be costly for the plants, and not all of them would have the capability to adopt these technologies.

The challenges facing the ship repair industry manifest in both production and technological aspects. Each group includes representatives directly corresponding to the impact of modern technologies entering the industry. The use of robots and augmented reality poses challenges to SMEs, as well as to those primarily engaged in ship repair. Significant capital investments are required for their implementation in production, and these investments need to have a return on investment over a certain period of time. Analyzing the current global situation, Europe, and Bulgaria, along with the war in Ukraine and the consequences of COVID-19, the adoption of such industrializations is not very favorable, as there is a ban on the entry of ships flying the Russian flag into our waters, and these are the main clients of many ship repair yards in Bulgaria. This challenge could be addressed through targeted funding from the EU. Challenges such as simulations and internet management are not as directly related to financial investments. They are more oriented as activities that are beneficial to have in the plant for easier production flow and scheduling planning.

The group of technological challenges relates to modern technological aspects that have an impact on the productivity and competitiveness of ship repair enterprises. The use of eco-friendly technologies and additive manufacturing gives a modern look to the plants. Some of these challenges can be easily overcome, as there are European projects and framework agreements for this purpose.

The introduction of new materials in shipbuilding that have an impact on ship repair would be challenging. Examples of such materials include carbon fiber, honeycomb panels, and others. These types of materials require specific processing technology, which also demands specific skills from the personnel. However, with additional training, the desired results can be achieved.

Opportunities in Implementation of Industry 4.0 in Ship Repair

The opportunities resulting from the implementation of Industry 4.0 in ship repair are expressed in two directions: economic and environmental, as shown in Figure 4. They are the result of fully or partially overcome challenge.

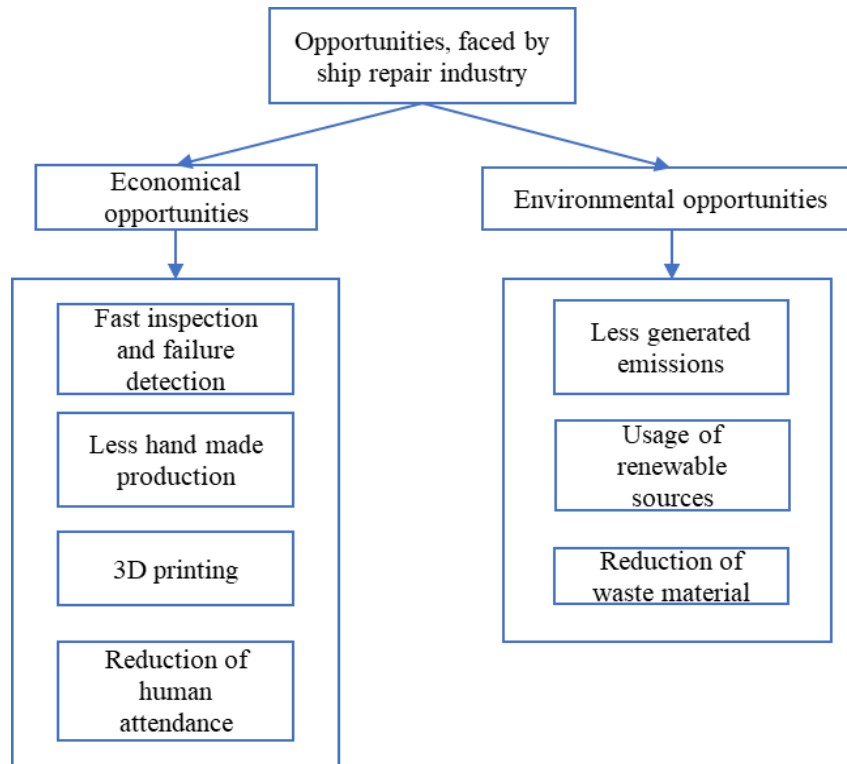


Figure 5. Opportunities in ship repair industry after Industry 4.0 implementation

The rapid inspection and identification of damages resulting from augmented reality and robotics contribute to faster and more accurate planning of work teams in the plant, as well as a reduction in manual labor. The benefit of implementing 3D printing as part of the production process is particularly significant. It can largely replace the long lead times for the delivery of a particular machine, mechanism, or system component. The greatest benefit of the adoption of Industry 4.0 is the reduction of human labor, but not completely, to a certain extent, in order to optimize the process, as there are activities that cannot be performed without human intervention, such as repairing the main engine, diesel generator, etc.

Lately, there is an increasing emphasis on environmental conservation. This applies not only to transportation, which is a small part of the pollutants but also to the industry. The use of renewable energy sources and alternative fuels leads to a reduction in harmful emissions. High-tech CAD systems in production and proper process planning lead to a reduction in technological waste. All these presented possibilities and their gradual implementation lead factories towards so-called Green Manufacturing, which undoubtedly aligns with environmental conservation policies.

Conclusion

The article examines the challenges and opportunities facing the ship repair industry following the introduction of Industry 4.0. The current situation in the global and European ship repair market is presented and analyzed. Special attention is given to the most commonly repaired types of ships, with the largest number being container ships, followed by fishing vessels and passenger ships.

Starting from the current situation in ship repair, the challenges that shipyards face after the widespread adoption of Industry 4.0 are presented and analyzed. These challenges are examined and presented on two levels, production leads to opportunities that reflect the different groups of challenges. The opportunities are presented in two directions, economic and ecological. Both groups of opportunities aim to improve the competitiveness of ship repair yards and respond to national, international, and global measures to combat greenhouse gases.

Scientific Ethics Declaration

The author declares that the scientific ethical and legal responsibility of this article published in EPSTEM journal belongs to the author.

Acknowledgements or Notes

* This article was presented as an oral presentation at the International Conference on Technology (www.icontechno.net) held in Antalya/Turkey on November 16-19, 2023.

References

- Fernandez, C., Tiago, M., & Fraga Lamas, P. (2023). *Augmented and mixed reality for shipbuilding* (pp. 643-667) Springer Handbook.
- Iwankowicz, R., & Radosław, R. (2023). Digital twin of shipbuilding process in shipyard 4.0. *Sustainability* 15 (12).
- Kunkera, Z., Opetuk, T., Hadzic, N., & Tosanovic, N. (2022). Using digital twin in a shipbuilding project. *Applied Sciences (Switzerland)*, 12 (24)
- Stanic, V., Hadjina, M., Fafandjel, N., & Matulja, T. (2018). Toward shipbuilding 4.0—an industry 4.0 changing the face of the shipbuilding industry. *Brodogradnja*, 69(3), 111–128.
- Sokolov, S., Antonova, A., Knysh, T., & Li, I. (2022). Automation of ship building and ship repairing using internet of ships technology, *E3S Web Conferences*, 363(1), 6.
- Mark Wide Research Inspiring Growth. (2023, October 12). Ship repair and maintenance services market. Retrieved from <https://markwideresearch.com/ship-repair-and-maintenance-services-market/>
- Maximize Market Research (2023, October 16). Ship repair and maintenance services market: Global industry analysis and forecast (2023-2029). Retrieved from <https://www.maximizemarketresearch.com/>

Fortune Business Insight. (2023, October 18). Retrieved from form <https://www.fortunebusinessinsights.com/ship-repair-and-maintenance-services-market-105801>
Trusteddocks. (2023, October 21). Ship repair statistics. Retrieved from <https://www.trusteddocks.com/ship-repair-statistics>

Author Information

Yordan Denev

Technical University of Varna

Varna, Bulgaria

Contact e-mail: y.denev@tu-varna.bg

To cite this article:

Denev, Y. (2023). Implementation of industry 4.0 in ship repair industry: Challenges and opportunities. *The Eurasia Proceedings of Science, Technology, Engineering & Mathematics (EPSTEM)*, 24, 49-54.

The Eurasia Proceedings of Science, Technology, Engineering & Mathematics (EPSTEM), 2023

Volume 24, Pages 55-62

IConTech 2023: International Conference on Technology

Detecting Litter in Street Sweepers Using Deep Learning

Suheda Gokbudak

Koluman Automotive Industry

Emir Enes Tas

Koluman Automotive Industry

Onur Ozer

Koluman Automotive Industry

Veysel Tilegi

Koluman Automotive Industry

Abstract: Street sweeping vehicles are essential equipment in our daily lives designed to clean streets and roads. With numerous mechanical components, they play a significant role in collecting all types of waste and contributing to environmental cleanliness. These vehicles typically consist of rotating brushes, collecting belts, and components involving water or air currents. Among these parts, brushes and vacuums are the most energy-consuming elements in street sweepers. Moreover, they are often operated in full power mode due to semi-automatic control systems, leaving the remaining control to the driver. However, this practice results in energy wastage and noise pollution. The aim of this study is to adjust vacuum suction in street sweepers according to the size of waste using image processing and deep learning techniques, thus achieving energy conservation. In this research, the YOLOv7 model and OpenCV are employed to train artificial intelligence for waste detection in street sweepers and accordingly regulate vacuum suction.

Keywords: Waste detection, Artificial intelligence, OpenCV, YOLOv7, Street sweeper.

Introduction

Road sweepers are typically vehicles used by city and municipal cleaning teams. These vehicles are designed to sweep and collect garbage in areas such as streets, roads, and sidewalks (Min et al., 2019). Road sweepers have a vacuum nozzle located at the lower part of the vehicle's center, and side brushes push the garbage toward the vacuum nozzle, allowing the garbage to be collected. However, when there is a large piece of debris, it needs to be manually adjusted for removal. In other words, the suction power of the vacuum needs to be adjusted according to the size of the debris. The constant adjustment of vacuum suction is the responsibility of the driver, which can distract the driver's attention while operating the vehicle. If these machines are constantly operated at full power, it leads to energy waste and noise pollution.

To address these issues, artificial intelligence and image processing can be used. The necessary equipment for such a system includes a camera, a PC board, and a GPU. The images captured by the camera are processed using artificial intelligence to detect the size of the garbage and adjust the vacuum suction accordingly. In this study, the YOLOv7 model, the latest version of the YOLO system, is used for real-time object detection and dimensioning. Training is conducted to teach the AI system to recognize garbage and adjust the vacuum suction, making the system autonomous. This not only leads to energy savings but also prevents the vacuum from operating at full power, reducing energy waste and noise pollution (Uzun & Karaca, 2022).

- This is an Open Access article distributed under the terms of the Creative Commons Attribution-Noncommercial 4.0 Unported License, permitting all non-commercial use, distribution, and reproduction in any medium, provided the original work is properly cited.

- Selection and peer-review under responsibility of the Organizing Committee of the Conference

© 2023 Published by ISRES Publishing: www.isres.org

Related Studies

In the present day, there are various methods for waste detection, and studies related to waste detection using YOLOv7 have also been conducted. Uzun and Karaca (2022) conducted a study on deep learning-based waste detection for autonomous waste collection vehicles. In this study, 500 images of paper cups and 250 images of other types of waste were classified using deep learning algorithms, and a new dataset was proposed. To classify paper cups, pre-trained networks such as SqueezeNet, VGG-19, and GoogleNet were used, and it was concluded that SqueezeNet achieved the highest classification accuracy at 97.77%.

Donati et al. (2020) carried out a study on waste detection using deep learning to achieve energy savings in street sweepers. In this study, a known and simple neural network called U-Net was used for semantic segmentation. The U-Net architecture was modified and improved to work with less training data and provide more precise segmentation. Such networks are primarily used in defense and biomedical fields. The left side of the model represents the encoder, where the model learns what the image contains, and the right side represents the decoder, where the model learns where the image is located. These studies demonstrate the effective utilization of artificial intelligence and deep learning techniques in waste detection and waste management.

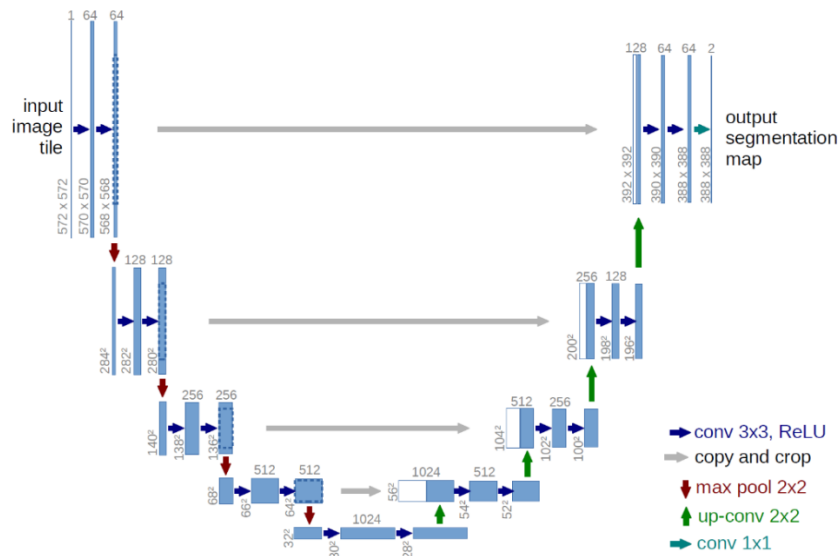


Figure 1. U-Net architecture

Normally, the U-Net architecture is not real-time. However, a downsized version of U-Net, known as U-Net 2020, is capable of pixel-wise segmentation of a 1-megapixel image on a mobile GPU in less than one second, making it suitable for real-time use. Furthermore, the study selected the DALSA Genie Nano C1920 camera model with a resolution of 1920x1200 for image processing. For the computer used to process the images, an Nvidia Jetson TX2 was chosen. In the experimental study conducted, a dataset comprising approximately 400 images and 80 test images was used, and the system demonstrated a sensitivity of 94%.

TABLE I
TRACKING RESULTS ON THE MOT16 CHALLENGE. WE COMPARE THE
TRACKING PERFORMANCE OF YOLOv7-DEEPSORT AND
YOLOv5(S/M/L)-DEEPSORT.

Model	YOLOv5s	YOLOv5m	YOLOv5l	YOLOv7
MOTA	39.60	39.01	40.77	40.82
MOTP	80.85	81.87	81.96	82.01
IDF1	52.39	51.56	52.43	53.65
IDs	432	432	547	514
ML	39.65%	33.27%	31.92%	32.11%
MT	15.45%	17.41%	20.70%	20.12%
FP	5375	7612	7853	7940
FN	60882	59297	56990	57434

Figure 2. Experimental results Yang (2022)

In the article by Yang. (2022), it was observed that incorporating DeepSort into the YOLOv7 method has resulted in more successful multi-object tracking in target tracking. This was achieved by conducting comparisons with YOLOv5 and its derivatives, leading to the obtained results.

Min et al. (2019) employed the Faster R-CNN model to classify waste types. This novel approach for object detection is built upon the Fast R-CNN method, with the addition of a Region Proposal Network (RPN) responsible for generating region proposals

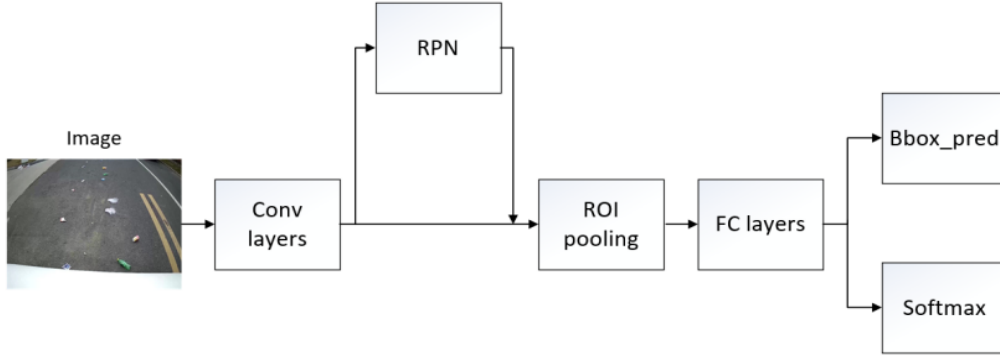


Figure 3. Faster-RCNN flow chart

In the article by Zheng et al. (2022), a segmentation model for waste detection in road sweepers is described. The model utilizes an encoder-decoder structure similar to SegNet. In this approach, feature extraction is applied to input images by the convolutional blocks in the encoder part. Simultaneously, pixel-wise segmentation is generated by gradually recovering the spatial dimensions of feature maps in the decoder part. In addition to the convolutional blocks, the model adopts two modules in the decoder structure, namely, FPG and SG, along with down-sampling and up-sampling blocks.

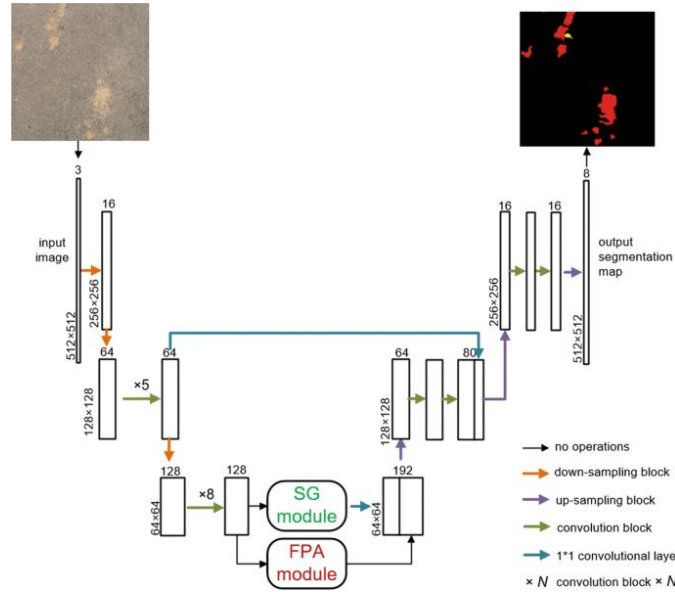


Figure 4. Overall framework of the proposed method

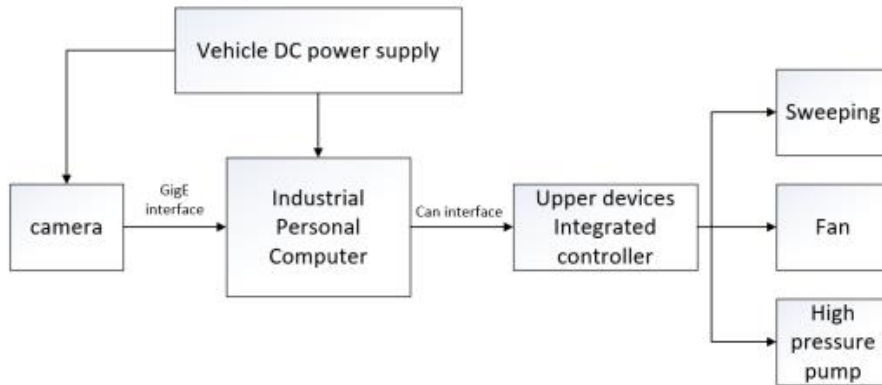


Figure 5. The power control system of intelligent road sweeper operation

In the article by Min et al. (2019c), a power control system is proposed for road sweeper operation, and the design of its fundamental technologies is addressed. Visual recognition and detection algorithms have been developed to recognize essential features such as waste type and quantity. An intelligent power control system is created by integrating an industrial computer, Nuvo-5095GC, a vehicle DC power supply, and a cleaning device controller. The camera is connected to the industrial computer via a GigE interface. The vehicle's DC power supply provides power to both the vehicle's industrial computer and the camera. The in-vehicle industrial computer is connected to the integrated controller through a CAN interface. The cleaning unit's integrated controller is connected to the sweeping disk, fan, and high-pressure water pump via a digital I/O interface.

Applied Methods

YOLO (You Only Look Once)

YOLO, which stands for "You Only Look Once," is a widely used algorithm in object tracking. The YOLO algorithm was introduced by Joseph Redmon (2015). (Nasrullah & Diker, 2021). It is an extremely fast object detection algorithm known for its capabilities in object recognition and detection. The YOLO model can process an image of 416x416 pixels in just 22 milliseconds, making it an ideal algorithm for real-time applications due to its speed. Furthermore, YOLO can detect a large number of objects and classes simultaneously, making it a highly versatile approach for object classification and detection. When evaluated in terms of accuracy and speed, it is much faster than the Single Shot Detection (SSD) method and provides similar accuracy (Ozel et al., 2021). Additionally, YOLO's network architecture is more effective than other methods and is easily scalable, allowing for a balance between speed and accuracy by adjusting the model's size. Its most superior feature compared to other algorithms is that it does not require retraining for artificial intelligence.

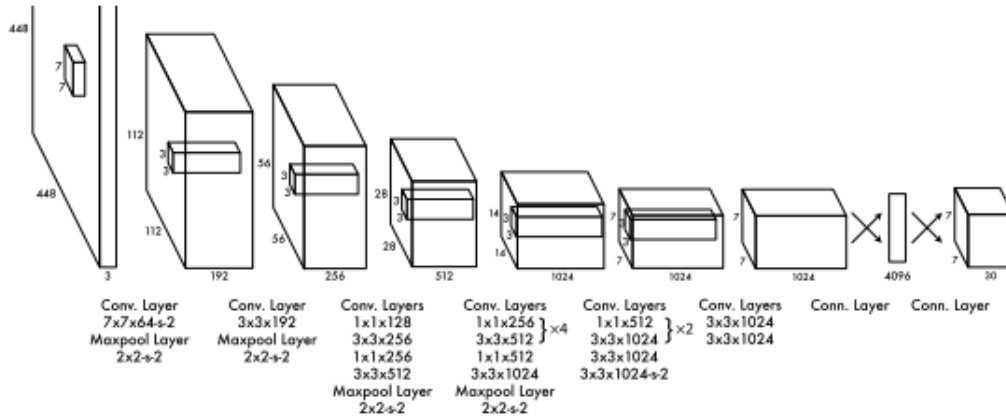


Figure 6. YOLO architecture

Equation (1) provides the mathematical model of the YOLO algorithm.

$$\begin{aligned}
 & \lambda_{\text{coord}} \sum_{i=0}^{S^2} \sum_{j=0}^B \mathbb{1}_{ij}^{\text{obj}} \left[(x_i - \hat{x}_i)^2 + (y_i - \hat{y}_i)^2 \right] \\
 & + \lambda_{\text{coord}} \sum_{i=0}^{S^2} \sum_{j=0}^B \mathbb{1}_{ij}^{\text{obj}} \left[(\sqrt{w_i} - \sqrt{\hat{w}_i})^2 + (\sqrt{h_i} - \sqrt{\hat{h}_i})^2 \right] \\
 & + \sum_{i=0}^{S^2} \sum_{j=0}^B \mathbb{1}_{ij}^{\text{obj}} (C_i - \hat{C}_i)^2 \\
 & + \lambda_{\text{noobj}} \sum_{i=0}^{S^2} \sum_{j=0}^B \mathbb{1}_{ij}^{\text{noobj}} (C_i - \hat{C}_i)^2 \\
 & + \sum_{i=0}^{S^2} \mathbb{1}_i^{\text{obj}} \sum_{c \in \text{classes}} (p_i(c) - \hat{p}_i(c))^2
 \end{aligned} \tag{1}$$

YOLO uses certain terms to determine the bounding box of detected objects:

Bx: x-coordinate of the center point of the object.
By: y-coordinate of the center point of the object.
Bw: Width of the object.
Bh: Height of the object.
c: Represents the class of the object.

The score resulting from the calculation of Equation (1) indicates whether an object is detected within a valid region.

YOLOv7

YOLOv7 (You Only Look Once version 7) is a prominent algorithm that stands out as a fast and accurate real-time object detection model for computer vision tasks. This model was introduced as an official research paper published by Wang, et al. (2022) (Wang, 2023). Furthermore, the source code of YOLOv7 has been released as open-source software and is available for free under the GPL-3.0 license. This allows developers and researchers to use YOLOv7 in their own projects, providing them with the opportunity to enhance and contribute to the YOLOv7 name and their personal expertise (Yang, 2022).

Data Set

For training purposes, a dataset was prepared using existing datasets and Google Images. This dataset was organized in such a way that each waste group, such as biological waste, metal, plastic, and paper, had separate files. This was done with the aim of ensuring more accurate inferences. After creating the dataset, the data labeling process needs to be carried out. The performance of a deep learning model depends on how well the data is labeled. After the data labeling process, the resulting TXT files are added to the dataset.



Figure 6. Images from the prepared data set

Data augmentation is a technique employed to artificially increase the number of training examples (Shorten et al., 2021). This is commonly carried out on the existing input dataset either before or during the training process. Essentially, it involves applying transformations to the original data without altering the original images to generate new images that may be different but belong to the same classes as the original data. This is a fundamental step in addressing scalability issues, particularly in fully supervised datasets. The original dataset is utilized to create additional variations and construct a larger training dataset by automatically rotating, zooming, and flipping the images with random parameters (Perez, 2017).

Real-Time Vehicle Control

After the completion of dataset preparation, labeling, and data augmentation processes, the final stage is to ensure that the sweeper vacuums work effectively with the model. This is achieved by being able to control the actuators of the sweeper via CanBus. The sweeper vehicle in consideration has a vacuum on the left and right sides, each equipped with brushes that can collect debris when lifted.

In this design, one critical aspect is the y-coordinates of the debris (the distance of debris from the vehicle). The reason for its significance is that it directly affects the delay before activating the vacuum based on this distance. Assuming the vehicle moves in a straight line, if we frame the debris at a y-coordinate between d_{near} and d_{far} at

time t_0 , the brushes and vacuums should operate at time $t_1 = \frac{v_{\text{avg}}}{y}$

Here, v_{avg} represents the average vehicle speed. However, this situation can be risky when the vehicle speed is high (Donati et al., 2020).

System Design

Camera

The camera system constitutes one of the most critical components of the system. The camera to be used should have certain features, including low power consumption, adequate resolution (for accurate debris detection), fast and high-bandwidth data communication with the computer, and resistance to vibration and electromagnetic fields. To find a camera that possesses these features, it is necessary to conduct product research on cameras designed for industrial applications. The DALSA Genie Nano C1920 (@1920×1200) camera could be a suitable choice for this system, but there are many options available as well.



Figure 7. DALSA genie nano C1920 (@1920×1200)

Computer Selection

In computer selection, another essential feature to consider is low power consumption. Additionally, having a fast GPU, a CanBus interface, and resistance to vibrations are critical factors in the selection process. Based on these features, the Nvidia Jetson TX2 model has been chosen.

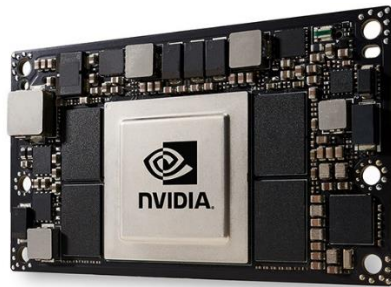


Figure 8. Nvidia Jetson TX2

Software

In this system, the YOLOv7 algorithm, commonly used in image processing, has been employed. The operational flowchart of the intelligent control system is provided in Figure 1.1 below. Furthermore, artificial intelligence training has been carried out using a dataset to achieve the automation of debris detection.

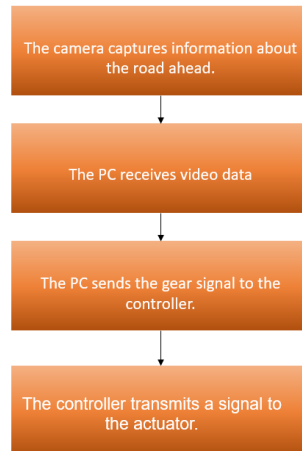


Figure 9. Intelligent control process

Conclusion

The developed system aims to achieve autonomous debris detection in road sweepers through image processing and artificial intelligence, while maintaining cost-effectiveness. Although it remains theoretical at this stage, accuracy will be substantiated through the necessary experiments in the future.

Scientific Ethics Declaration

The authors declare that the scientific ethical and legal responsibility of this article published in EPSTEM. journal belongs to the authors.

Acknowledgements or Notes

* This article was presented as an oral presentation at the International Conference on Technology (www.icontechno.net) held in Antalya/Turkey on November 16-19, 2023.

References

- Donati, L. L., Fontanini, T., Tagliaferri, F., & Prati, A. (2020). An energy saving road sweeper using deep vision for garbage detection. *Applied Sciences*, 10(22), 8146.
- Min, H., Zhu, X., Yan, B., & Yu, Y. (2019). Research on Visual Algorithm of road garbage based on intelligent control of road sweeper. *Journal of Physics*, 1302(3)
- Nasrullah, M., & Diker, A. (2021). Derin öğrenme ve YOLO algoritmaları ile nesne tespiti ve serit belirleme. 2nd International Conference on Intelligent Transportation Systems. Balıkesir, Turkey.
- Ozel, M. A., Baysal, S. S., & Sahin, M. E. (2021). Derin öğrenme algoritması (YOLO) ile dinamik test suresince suspansiyon parçalarında catlak tespiti. *European Journal of Science and Technology*, 26(1-5).
- Perez, L. (2017, December 13). The effectiveness of data augmentation in image classification using deep learning. Retrieved from <https://arxiv.org/abs/1712.04621>
- Shorten, C., & Khoshgoftaar, T. M. (2019). A survey on image data augmentation for deep learning. *Journal of Big Data*, 6(1).
- Shorten, C., Khoshgoftaar, T. M., & Furht, B. (2021). Text data augmentation for deep learning. *Journal of Big Data*, 8(1), 101.

- Uzun, S., & Karaca, D. (2022). Deep learning based garbage detection for autonomous garbage collection vehicles. *European Journal of Science and Technology*, 32, 1194-1198.
- Wang, C. (2023). YOLOV7: Trainable bag-of-freebies sets new state-of-the-art for real-time object detectors. *Computer Vision Foundation*, 1-12.
- Yang, F. (2022). Video object tracking based on YOLOv7 and DeepSORT.
- Zheng, C., Cao, D., & Hu, C. (2022). A similarity-guided segmentation model for garbage detection under road scene. *Frontiers of Optoelectronics*, 15(1), 22.

Author Information

Suheda Gokbudak

Koluman Automotive Industry
Mersin, Turkey
Contact e-mail: suheda.gokbudak@koluman.com

Emir Enes Tas

Koluman Automotive Industry
Mersin, Turkey

Onur Ozer

Koluman Automotive Industry
Mersin, Turkey

Veysel Tilegi

Koluman Automotive Industry
Mersin, Turkey

To cite this article:

Gokbudak, S., Tas, E.E., Ozer, O., & Tilegi, V. (2023). Detecting litter in street sweepers using deep learning. *The Eurasia Proceedings of Science, Technology, Engineering & Mathematics (EPSTEM)*, 24, 55-62.

The Eurasia Proceedings of Science, Technology, Engineering & Mathematics (EPSTEM), 2023

Volume 24, Pages 63-70

IConTech 2023: International Conference on Technology

Origin of Raw Materials of Ancient Glass (B.C.) from Kythnos Island, Greece

Petros Karalis

National Centre for Scientific Research (N.C.S.R.)

Elissavet Dotsika

National Centre for Scientific Research (N.C.S.R.).

Alexandros Mazarakis- Ainian

University of Thessaly

Evaggelia Kolofotia

University of Thessaly

Foteini Rizou

Centre for Research and Technology Hellas

Anastasia Electra Poutouki

University of Pavia

Panagiotis Leandros Poutoukis

University of Patras

Anastasios Drosou

Centre for Research and Technology Hellas

Dimitrios Tzovaras

Centre for Research and Technology Hellas

Abstract: Glass samples (B.C.) from the ancient town of Kythnos in the Cyclades were selected and analyzed for their oxygen isotopic and chemical compositions. Results show that the majority of glass samples are produced using natron as flux, suggesting that raw materials probably came from Wadi Natron and the Levantine area. The majority of the analyzed samples from Kythnos have a homogeneous oxygen isotopic composition, which is equal or very close to the mean value of “B.C.” glass, as deduced from a set of isotopic measurements on glass from Europe dated from the 8th to the 4th centuries B.C., showing a relatively narrow range of $\delta^{18}\text{O}$ values. Similar results were also obtained from Ancient Pydna in Northern Greece.

Keywords: Oxygen isotopes, Compositional analysis, Ancient glass, Kythnos

Introduction

Natron was the dominant type of glass from the 10th century BC until almost the 9th century AD. For all these centuries the natron they used mainly came from the natural natron deposits found in the evaporating lakes of Wadi Natron (Beni Salama, Bir Hooker and Zakikin the oases of the Western Desert of Egypt) (Nenna, et al.,

- This is an Open Access article distributed under the terms of the Creative Commons Attribution-Noncommercial 4.0 Unported License, permitting all non-commercial use, distribution, and reproduction in any medium, provided the original work is properly cited.

- Selection and peer-review under responsibility of the Organizing Committee of the Conference

© 2023 Published by ISRES Publishing: www.isres.org

2005). During different times, glass was produced by a silica sand source mixed with a soda-rich mineral matter (i.e. natron) acting as the flux and a lime-source was added as shells or limestone sand components (Henderson, 1985). Other potential facilities for glass production from the 6th to the 9th century AD were found at Apollonia (Tal, et al., 2004), at Bet Eli'ezer (Gorin-Rosen & Hadera, 1995; Gorin-Rosen, 2000; Freestone, et al., 2000) and at Bet She'arim (Brill, 1967; Freestone, 2005; Gorin-Rosen, 1999). In Greek area, the main natron source that has been known and proven in international literature since 2003, is Lake Pikrolimni in Macedonia (Dotsika et al., 2004(a), 2004(b), 2008(a), 2008(b), 2009, 2014, 2015, 2018; Ignatiadou et al., 2003).

Archaeological Information

Kythnos belongs to the complex of northwestern Cyclades, located between Kea and Serifos. It is an island with a long history and special archaeological interest. The most important site of the historical era was Vryokastro, the ancient capital of Kythnos. The fortified polis is situated on the northwest coast of the island and has been continuously inhabited from the beginning of the first millennium B.C. until the 6th – 7th century A.D (Fig 1). The remains of the ancient city occupy an area of approximately 28,5 hectares, including the small islet of Vryokastraki, which was connected to the shore in antiquity by a narrow isthmus.

During the systematic investigations that have been in progress since 1990 (survey and subsequent excavations) several ancient structures, such as temples, public buildings, houses, port facilities, burial monuments, etc., and numerous finds from a wide range of materials and possibly of different origins, have been brought to light. These discoveries have provided valuable insights into the urban planning of the city and the sociopolitical and economic development of the ancient community. The determination of the origin and construction technology of the movable finds will be crucial to understanding and interpreting the production and circulation of artifacts on the island, as well as the role of Kythnos in the trade network of these objects in the wider Aegean area.

For this reason, samples were selected from the Archaic sanctuary dedicated to Artemis and Apollo (Mazarakis Ainian, 2017, 2019), dating from the 6th to 5th century BC. They encompass 8 fragments of vessels such as amforiskoi (perfume bottles) from translucent turquoise blue, deep blue to yellow color glass, pendants and beads of glass paste (for instance triangular and rock-cut pendant types) (Fig 2.).



Figure 1. Aerial photograph of Vryokastro

During the excavation, a wide range of glass vessels and glass beads were discovered, dating back to the 5th to 6th century BC. The purpose of the current study is to investigate the composition of the glass and the origin of the material during this time period. The study's primary objective was to expand the archaeometric database of B.C. aged glass discovered in Greece. Additionally, we aimed to compare the chemical composition of these glass samples with other Greek glass samples based on similar external features and functions.

Henderson, J., Evans, J., Sloane, H., Leng, M., & Doherty, C.(2005). The use of oxygen, strontium and lead isotopes to provenance ancient glasses in the Middle East. *Journal of Archaeological Science*, 32(5), 665–673.



Figure 2. Glass samples

Materials and Methods

Colorful and colorless samples of ancient glass objects, with Roman ages, were selected and characterized. The collection represents different typologies of glass objects, such as vases, flasks, incense holders, plates, lamps, and bottles. These artifacts show a variety of colors (yellow, green, blue, purple, honey, to opaque) caused by the addition of various colors and opacifying agents. Elemental analysis is usually applied to determine the raw materials of glass-made artifacts. Compositional variations in major and trace elements are an indication of the use of different raw material mixtures or different manufacturing procedures. The relation between certain elements detected in glass and the original mineral resources offers the potential to use them as indicators of glass origin (Degryse & Shortland, 2009).

Chemical analysis was performed by Scanning Electron Microscopy (SEM) with Energy – Dispersive X-ray microanalysis (EDX). Energy Dispersive X-Ray Spectroscopy (EDS or EDX) is calculating element concentrations based on energy measurement of X-Rays. The X-Rays are produced after an electron beam from SEM strikes the given point or area. Electrons from inner shells are released and outer shell electrons cover their positions. The X-Ray has a specific energy that is equal to the energy difference between the two shells and is characteristic of each element. The spectrum is taken at the same time for all energies. All the peaks are being evaluated and those that have a value above the detection limit are presented in the results. The detection limit is not strictly dictated, it depends on the area or the element, commonly is somewhere between 0.1-0.2% but it could be more or less than these values. Samples were measured through a Jeol JEE-4X, with an attached Rontec EDX microanalysis system equipped with a windowless Si (Li) detector, using acceleration voltage 15 kV and 20 kV. Before the measurement small parts of each glass were mounted in epoxy resin blocks, then polished with a 1 μm diamond paste and, last, to ensure conductivity, samples were coated with a thick carbon layer. Conductivity is necessary for observation, photography, and analysis in a SEM-EDS. Standardization for the EDS analysis is achieved by a daily Co analysis. The EDS spectrum is taken at the same time for all elements. And the same peaks (K, L, or M) are placed linearly. Each peak has on its right the next heavier element's same peak and on its left the previous lighter element's same peak ($K\alpha$, $L\beta$, whatever). By analyzing Co we have a standard point for our spectra and all other peaks are positioned accordingly. For each glass sample, we measured 5 different areas/angles and we present the mean value as a result.

The isotopic analyses took place in the Stable Isotope Unit of the Institute of Materials Science (NCSR Demokritos) on a Thermo Delta V Plus IRMS. $^{18}\text{O}/^{16}\text{O}$ ratio was determined and expressed as $\delta^{18}\text{O}$ relative to the international VSMOW standard. Isotopic results are reported in the usual delta terminology versus the VSMOW isotopic standard, delta being defined as follows:

$$\delta = [(R_{\text{sample}} - R_{\text{standard}}) / R_{\text{standard}}] * 1000$$

where R is the ratio between the heavy and the light isotope, in this case $^{18}\text{O}/^{16}\text{O}$.

Chemical Analysis

34 colorful and colorless samples of ancient glass objects were selected and characterized, with ages ranging from the origin of the first millennium B.C. From the data, it appears that the chemical analyses of almost all the samples are quite homogenous and the major element compositions of all samples are consistent with typical natron glasses produced between 8th and 4th c. BC (Shortland & Schroeder, 2009; Arletti et al., 2010; Arletti et al., 2012; Panighello et al., 2012). In Fig. 3, the levels of K_2O and MgO show that almost all the glass samples analyzed, regardless of the typology (vessels, beads) and site of provenance, were produced starting from a sodic inorganic source of alkalis, as confirmed by the high levels of Na_2O found in the chemical analyses. In fact, the glasses show K_2O and MgO contents below 1.5 wt% and high levels of Na_2O , between 17.3 and 20.1 wt%, confirming that the analyzed glass samples were made on a soda-lime-silicate basis and produced using mineral natron as a source alkaline flux (Fig. 3). This hypothesis is also consistent with the low levels of SO_3 , Cl , and P_2O_5 in these glasses (Shortland et al., 2007). The values of SO_3 , Cl and P_2O_5 , ranging between 0.1 and 0.3% wt., 0.8 - 1.45% wt. and 0.02 and 0.1 wt% respectively, show which is typical of glasses made with natron as a fluxing agent. In fact, natron is a relatively pure mineral source of soda containing low levels of magnesium and potash, indicating that all measured soda lime silicate glasses were produced in the Roman glassmaking tradition using natron as a flux.

In the same image, Fig 3., data of glasses from Pydna and Methoni are given. Compared to the B.C period (8th - 4th BC) natron glasses (which utilize a pure soda alkali as a flux) from Greece (Blomme et al., 2017; Karalis, 2023), these glasses present similar compositions (Figs 3 and 4). All the glasses are colored by either or both Co and Cu metals.

Also, the majority of the glass present also lime contents that are similar to the glass artefacts of the first millennium AD, (e.g. Silvestri et al., 2017; Foster & Jackson, 2009; Conte et al., 2014; Freestone, 1994; Foy et al., 2003; Karalis, 2023). The samples show very similar ratios of the two components, CaO and Al_2O_3 , indicating the use of same silica sources (Fig 4).

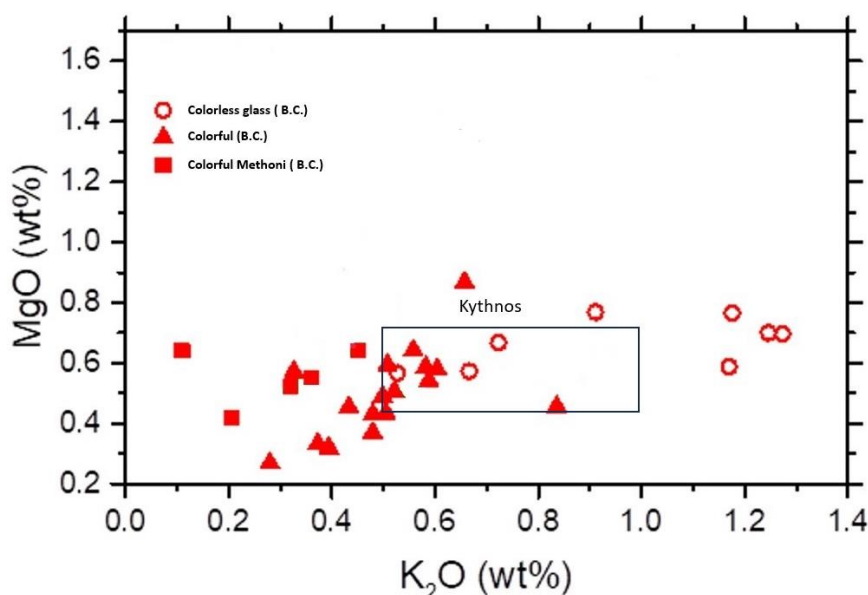


Figure 3. Elemental analysis of glass, K_2O vs MgO

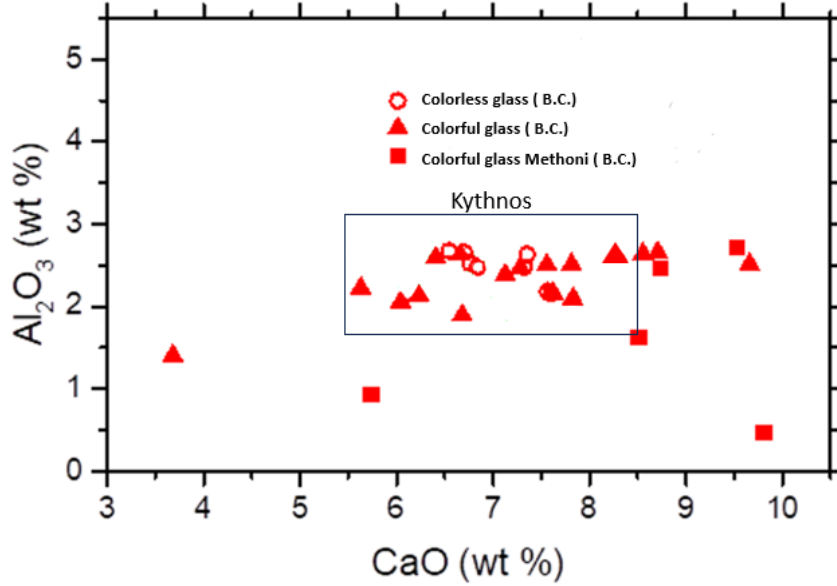


Figure 4. Depicts the Al_2O_3 (lower than 3%) and CaO (lower than 6%) contents of the analyzed glass, further emphasizing the chemical homogeneity of the sample sets.

The plot of Al_2O_3 versus CaO (Fig. 4) further shows the chemical homogeneity of the glass group. Therefore, based on soda ash, alumina and lime content, the glass samples were produced with soda ash and calcareous sand as a source of alkaline flux and vitrifying component respectively. Finally, based on the soda, alumina, and lime contents, the Kythnos glass samples were produced with natron and calcareous sand, as the source of alkali flux and vitrifying components respectively. Colored and colorless natron glass (BC) samples were analyzed for $\delta^{18}\text{O}$. The colored glass samples show fairly homogeneous $\delta^{18}\text{O}$ values, ranging from 15‰ (VSMOW) to 16.6‰, with an average value of 15.3‰, which is equal or very close to the mean value of “Roman” glass, as deduced from a set of isotopic measurements on glass from Europe, which show a relatively narrow range of $\delta^{18}\text{O}$ (from about 15.4‰ to 16.0‰) (Fig. 5). These Roman glasses were produced with Syro-Palestinian coast sand as raw material and Wadi natron as flux.

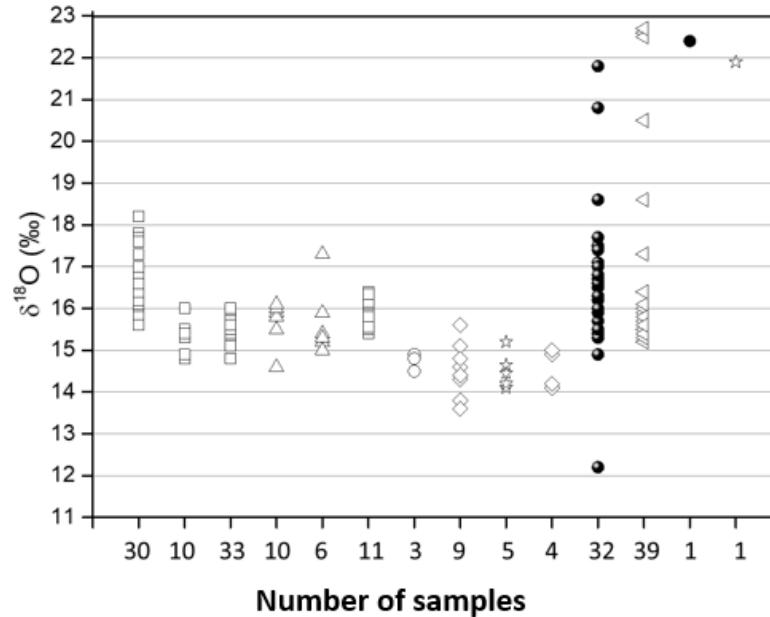


Figure 5. Comparisons among $\delta^{18}\text{O}$ (VSMOW) values of natron glass samples, [open symbols: Doman glass (\square) (Silvestri et al., 2010; Brill et al., 1999) - 4th AD. (\circ)(Brill et al., 1999; Dotsika et al., 2018) – 4th to 6th AD (\star) (Leslie et al., 2006) – 6th to 9th AD (\diamond) (Leslie et al., 2006; Henderson et al., 2005) – 1st to 6th AD- (\triangleleft) (Silvestri et al., 2017) – (\bullet) (1st to 4th AD, Silvestri et al., 2017; Dotsika et al., 2018; Karalis, 2023). (\triangle) (present work)].

Conclusions

The possible origin of 6th to 5th century BC glass artifacts recovered at Kythnos island was discussed from chemical and isotopic data. All glass samples could be classified as natron glass, made from a mixture of silica sand, and natron. The assemblage exhibits similar chemical characteristics with contemporary artifacts from archaeological sites on the Italian peninsula, and on the Ancient Pydna, Greece (Shortland & Schroeder, 2009; Arletti et al., 2010; Arletti et al., 2012; Panighello et al., 2012; Blomme et al., 2017; Karalis, 2023), suggesting that raw materials probably came from Wadi Natron and the Levantine area.

Recommendations

In the continuation of this study, the residual stress effect together with the geometry effect can be evaluated. This experiment would be more appropriate because HFMI does not only perform geometry improving. The relationship between residual stress and geometry can be direct or inverse. A test bench for residual stress measurement will make the results more realistic and consistent. In addition, outputs in terms of life can be obtained with a fatigue test bench.

Scientific Ethics Declaration

The authors declare that the scientific ethical and legal responsibility of this article published in EPSTEM journal belongs to the authors.

Acknowledgments

This research has been co-financed by the European Regional Development Fund of the European Union and Greek national funds through the Operational Program Competitiveness, Entrepreneurship and Innovation, under the call RESEARCH – CREATE – INNOVATE (project code: T1EDK-12500)

References

- Arletti, R., Ferrari, D., & Vezzalini, G. (2012). Pre-Roman glass from Mozia (Sicily-Italy): The first archaeometrical data. *Journal of Archaeological Science*, 39(11), 3396–3401.
- Arletti, R., Maiorano, C., Ferrari, D., Vezzalini, G., & Quartieri, S. (2010). The first archaeometric data on polychrome Iron Age glass from sites located in northern Italy. *Journal of Archaeological Science*, 37(4), 703–712.
- Blomme, A., Degryse, P., Dotsika, E., Ignatiadou, D., Longinelli, A., & Silvestri, A. (2017). Provenance of polychrome and colorless 8th–4th century BC glass from Pieria, Greece: A Chemical and isotopic approach. *Journal of Archaeological Science*, 78, 134–146.
- Brill, R. H. (1999). *Chemical analyses of early glasses* (Volume 1) [Catalogue]. Corning Museum of Glass.
- Brill, R. H., & Wampler, J. M. (1967). Isotope studies of ancient lead. *American Journal of Archaeology*, 71(1), 63–77.
- Conte, S., Chinni, T., Arletti, R., & Vandini, M. (2014). Butrint (Albania) between eastern and western Mediterranean glass production: EMPA and LA-ICP-MS of late antique and early medieval finds. *Journal of Archaeological Science*, 49(1), 6–20.
- Degryse, P., & Shortland, A. J. (2009). Trace elements in provenancing raw materials for Roman glass production. *Geologica Belgica*, 12(3), 135–143.
- Dotsika, E., Filly A., Maniatis J., Poutoukis D., & Tzavidopoulos, E. (2004). Hydrochemistry, Isotope contents and Origin of water at Pikrolimni Lake (Greece). *UNESCO: Isotopes in the Hydrological Cycle and Environment*, 89-90. Paris.
- Dotsika, E., & Ignatiadov, D. (2015). Pikrolimni Lake as a Natron source in glassmaking technology, *International Workshop on virtual archaeology: Museums y cultural tourism*. Delphi. Greece.
- Dotsika, E., Maniatis, Y., & Ignatiadov, D. (2008). A Natron source for glass making in Greece: Preliminary results. *BAR International Series*, 1746, 359–362.
- Dotsika, E., Maniatis, Y., Tzavidopoulos, E., Poutoukis, D., & Albanakis, K. (2004). Hydrochemical condition of the Pikrolimni Lake (Kilkis, Greece). *Bull. Geol. Soc. Greece*, 192–195.

- Dotsika, E., Tsoukala, E., Chantzi, P., Karalis, P., & Heliadis, E. (2014). Palaeoenvironmental information from isotopic fingerprints of the Early Villafranchian Mammot borsoni from Milia (Grevena, Macedonia, Greece). *Scientific Annals, School of Geology, & Aristotle University of Thessaloniki. Greece VIth international special*, 102 p. 10.
- Dotsika, E., Tzavidopoulos, I., Poutoukis, D., Maniatis, Y., Albanakis, K., & Psomiadis, D. (2008). Geochemistry of Picrolimni Lake for the evidence of natron precipitation. *37th International Symposium of Archaeometry*. Siena, Italy
- Dotsika, E., Poutoukis, D., Tzavidopoulos, I., Maniatis, Y., Ignatiadou, D., & Raco, B. (2009). A natron source at Pikrolimni Lake in Greece? Geochemical evidence. *Journal of Geochemical Exploration*, 103(2–3), 133–143.
- Dotsika, E., Ignatiadou, D., Longinelli, A., Poutoukis, D., & Diamantopoulos, G. (2018). The fingerprint of Greek raw materials in the composition of ancient glasses with “unexpected” isotopic compositions. *Journal of Archaeological Science: Reports*, 22, 559–567.
- Foster, H. E., & Jackson, C. M. (2009). The composition of “naturally coloured” Late Roman vessel glass from Britain and the implication for models of glass production and supply. *Journal of Archaeological Science*, 36(2), 189–204.
- Foy, D., Picon, M., Vichy, M., & Thirion Merle, V. (2003). Caractérisation des verres de la fin de l’Antiquité en Méditerranée occidentale: l’émergence de nouveaux courants commerciaux. In D. Foy & M.-D. Nenna (Eds.), *Échanges et commerce du verre dans le monde antique. Actes du colloque de l’AIHV, Aix-en-Provence et Marseille, juin 2001* (pp.41-85). Monographies instrumentum 24.
- Freestone, I. C. (1994). Chemical analysis of “raw” glass fragments. In H. R. Hurts (Ed.), *Excavations at Carthage, 1, the circular harbour, North Side* (p.290). Oxford University Press.
- Freestone, I. C., & Gorin-Rosen, Y. (1999). The great glass slab at Bet She’ Arim, Israel: An early Islamic glassmaking experiment? *Journal of Glass Studies*, 41, 105–116.
- Freestone, I. C., Wolf, S., & Thirlwall, M. (2005). The production of HIMT glass: Elemental and isotopic evidence. *Annales. 16e Congrès de l’association Internationale pour l’histoire de Verre* (pp. 153-157). London.
- Gorin Rosen, Y. (1995). Hadera, Bet Eli’ezer. *Excavations and Surveys in Israel*, 13, 42–43.
- Gorin Rosen, Y. (2000). The ancient glass industry in Israel: Summary of the finds and new discoveries. *La Route du verre. Maison de l’Orient et de la Méditerranée*, 33, 49–63.
- Henderson, J. (1985). The raw materials of early glass production. *Oxford Journal of Archaeology*, 4(3), 267–291.
- Henderson, J., Evans, J. A., Sloane, H. J., Leng, M. J., & Doherty, C. (2005). The use of oxygen, strontium and lead isotopes to provenance ancient glasses in the Middle East. *Journal of Archaeological Science*, 32(5), 665–673.
- Ignatiadou, D., Dotsika, E., Kouras, A., & Maniatis, Y. (2003). Nitrum Chalestricum: The natron of Macedonia. In H. Cool (Ed.), *Annales du 16 Congress del/Association Intern. Pour l’Histoire du Verre-London* (pp. 64–67).
- Karalis, P. (2023). *Isotopic traceability of raw materials of ancient glass*. (Doctoral dissertation). National and Kapodistrian University of Athens.
- Leslie, K. A., Freestone, I. C., Lowry, D., & Thirlwall, M. (2006). The provenance and technology of Near Eastern glass: Oxygen isotopes by laser fluorination as a complement to strontium. *Archaeometry*, 48(2), 253–270.
- Nenna, M. D., Picon, M., Thirion-Merle, V., & Vichy, M. (2005). Ateliers primaires du Wadi Natrun: Nouvelles découvertes. In I. Lazar (Ed.), *Annales du 16e Congrès de l’Association Internationale pour l’Histoire du Verre* (pp. 59–63). AIHV.
- Mazarakis Ainian, A. (2017). Νεότερα για τα ιερά της αρχαίας πόλης της Κύθνου. In V. Vlachou & A. Gadolou (Eds.), *ΤΕΡΨΙΣ. Studies in Mediterranean archaeology in honour of nota Kourou* (pp. 303–315). Brussels.
- Mazarakis Ainian, A. (2019). *The sanctuaries of Ancient Kythnos*. Rennes, France.
- Panighello, S., Orsega, E. F., van Elteren, J. T., & Šelih, V. S. (2012). Analysis of polychrome Iron Age glass vessels from Mediterranean I, II and III groups by LA-ICP-MS. *Journal of Archaeological Science*, 39(9), 2945–2955.
- Shortland, A. J., & Schroeder, H. (2009). Analysis of first millennium BC glass vessels and beads from the Pichvnari necropolis, Georgia*. *Archaeometry*, 51(6), 947–965.
- Shortland, A. J., Rogers, N., & Eremin, K. (2007). Trace element discriminants between Egyptian and Mesopotamian late Bronze Age glasses. *Journal of Archaeological Science*, 34(5), 781–789.
- Silvestri, A., Longinelli, A., & Molin, G. (2010). “ $\delta^{18}\text{O}$ measurements of archaeological glass (Roman to Modern age) and raw materials: possible interpretation. *Journal of Archaeological Science*, 37(3), 549–560.

- Silvestri, A., Dotsika, E., Longinelli, A., Selmo, E., & Doukata-Demertzi, S. (2017). Chemical and oxygen isotopic composition of Roman and late antique glass from Northern Greece. *Journal of Chemistry*, 2017(2), 1–14.
- Tal, O., Jackson Tal, R. E., & Freestone, I. C. (2004). New evidence of the production of raw glass at late Byzantine Apollonia-Arsuf. Israel. *Journal of Glass Studies*, 46, 51–66.

Author Information

Petros Karalis

Stable Isotope and Radiocarbon Unit, Institute of Nanoscience and Nanotechnology, National Centre for Scientific Research (N.C.S.R.) “Demokritos”, 15341 Attiki, Greece

Elissavet Dotsika

Stable Isotope and Radiocarbon Unit, Institute of Nanoscience and Nanotechnology, National Centre for Scientific Research (N.C.S.R.) “Demokritos”, 15341 Attiki, Greece
Contacting e-mail: e.dotsika@inn.demokritos.gr

Alexandros Mazarakis- Ainian

Department of History, Archaeology and Social Anthropology, University of Thessaly, 38221 Volos, Greece

Evaggelia Kolofotia

Department of History, Archaeology and Social Anthropology, University of Thessaly, 38221, Volos, Greece

Foteini Rizou

Information Technologies Institute, Centre for Research and Technology Hellas, 57001, Thessaloniki, Greece

Anastasia Electra Poutouki

Department of Pharmaceutical Sciences
University of Pavia, 27100
Pavia, Italy

Panagiotis Leandros Poutoukis

Department of Physics, University of Patras, 26504 Patra, Greece

Anastasios Drosou

Information Technologies Institute, Centre for Research and Technology Hellas, 57001
Thessaloniki, Greece

Dimitrios Tzouvaras

Information Technologies Institute, Centre for Research and Technology Hellas, 57001
Thessaloniki, Greece

To cite this article:

Karalis, P., Dotsika E., Mazarakis-Ainian, A., Kolofotia, E., Rizou, F., Poutouki, A.E., Poutoukis, P.L., Drosou, A., & Tzouvaras, D. (2023). Origin of raw materials of ancient glass (B.C.) from Kythnos Island, Greece. *The Eurasia Proceedings of Science, Technology, Engineering & Mathematics (EPSTEM)*, 24, 63-70.

The Eurasia Proceedings of Science, Technology, Engineering & Mathematics (EPSTEM), 2023

Volume 24, Pages 71-82

IconTech 2023: International Conference on Technology

Artificial Intelligence Technology to Predict the Financial Crisis in Business Companies

Mohamed Ahmed Hamada
Abu Dhabi University

Khaled M. K. Alhyasat
Abu Dhabi University

Abstract: It is difficult to imagine a business in the modern world of digitization that does not use technology and artificial intelligence in some capacity. Business transformation brought a severe time of trouble for small and medium-sized enterprises all over the world. Throughout our study, we have based analysis on factual information that highlights the critical function that the Information Technology (IT) industry plays in maintaining corporate relevance and encouraging customer involvement. Our investigation goes beyond merely highlighting the value of using big data to analyze financial crises in a predictive manner. It also emphasizes the proactive incorporation of artificial intelligence (AI) into corporate operations as a preventive step to avoid them. Our study includes the examination of viewpoints from people who were actively involved in their careers before lockdown procedures were implemented and incorporated into our research the opinions of people who work for small and medium-sized businesses and government agencies. Based on the literature that already exists on the critical role that Artificial Intelligence (AI) plays in protecting companies from disasters, we looked closely at a particular case study. The case study's conclusions highlight how important corporate automation is. In this article, we provide case studies of well-known, globally renowned companies that demonstrate how they skillfully employ new technology to maintain their competitive position. These model organizations include both internationally recognized companies like Google and Facebook and local organizations like Sberbank. In conclusion, our research adopted an artificial intelligence framework that can help business organizations to predict problems and financial crises.

Keywords: Artificial intelligence, Information technology, Digitization, Financial crises, Developing models

Introduction

The term Artificial intelligence appeared at the same time as the development of digital machines in the 1940s. Artificial intelligence is the property of intelligent systems to perform creative functions that are traditionally considered the prerogative of a human; science and technology of creating intelligent machines, especially intelligent computer programs. Early AI research in the 1950s included topics like problem-solving and it paved the way for the opportunities of computers nowadays: smart searches, decision-making, data analysis, visualization of information, and so on. Hollywood films always demonstrate to us human-like robots that can take over the world in the future, but the reality with automatized computers promises to be more fascinating and easier.

AI is applied in various fields, beginning with a win in World War II by Alan M. Turing's Enigma machine and ending with Smart Assistance like Siri or self-driving cars. If earlier computers could make decisions based on people's experiences, now they can use the warehouses of databases and rapidly increase as an individual. Sometimes, huge machines with many wires were considered a huge step for humanity, but now we use AI in

everyday life and the development of IT does not stop there. Both established economies and emerging economies have been impacted by the crisis (Saleh, 2023).

As companies implement AI into their business processes, the capabilities of technology continue to grow. Therefore, if executives want to keep their business relevant, they must maintain a good relationship between their employees and digital technologies. AI can Boost Financial transformation with digital technology for crisis management (Dafri & Al-Qaruty, 2023). Furthermore, AI in business can be applied in various industries and perform different functions:

- **Automation of operational processes:** It is mainly used in the back office to control the interactions of internal processes: CRM system, storage and creation of a database, payroll, and payment to suppliers, control of time shifts, and so on.
- **Analysis:** This function is more related to crisis prediction in companies. Data visualization, analysis of customer choice, analysis of supply and demand in the market, targeted marketing - all this work was taken over by computers.
- **Interaction:** These AI functions are capable of expanding and improving the services that businesses provide and the companies that implement these technologies always have advantages over the competition. The main ones are chatbots for 24/7 customer support and suggestions based on their previous orders robots, which can serve you in a restaurant.

Unfortunately, the situation with COVID-19 has been disastrous for many companies. We were able to see a real crisis situation in the business companies in the whole world. Those companies that didn't underestimate the importance of using digital technology suffered from the most losses, they hoped for a quick end to the pandemic. At the same time, some executors realized that the world is changing forever and the only solution to hold on in a crisis moment is to introduce AI and automatize most of their processes. Particularly interesting that many companies are still cutting their budgets for IT instead of expanding their functions and services because in the future it can help to save more time and money. In this research, we will investigate how AI can help predict a crisis in companies and explain cases where it helped to increase the profit of companies even during the lockdown.

Literature Review

The study of the possibilities of AI began with its first use. We have many resources, articles, and books that are used in this research. A huge amount of information and research was written. In 2023, James and Menzies offered novel mathematical approaches and examined the similarities in market dynamics and the ensuing implications for equity investors between different financial market crises. In order to achieve the best possible systematic risk reduction, they first examine the strength of collective dynamics during various market crises and contrast appropriate portfolio diversification strategies based on the distinct number of sectors and stocks (James & Menzies, 2023). Tolo in 2020, introduced a predicting systemic artificial model for financial crises based on neural networks, He demonstrated that the Long-Short Term Memory (RNN-LSTM) and the Gated Recurrent Unit (RNN-GRU) neural nets may be utilized to greatly enhance such predictions (Tolo, 2020).

Zhailybayevich and Hamada introduced the application of extremely efficient neural network technologies as one possible resolution to the problem of financial crises. In this study, eleven input criteria were used to create a mathematical neural network model that predicted bank bankruptcy (Zhailybayevich & Hamada, 2023). About the role of Artificial Intelligence in a crisis and its onset in the modern world nowadays, this topic is more relevant than ever. All works describe algorithms and prevention methods differently. Most of the current work on predicting a business crisis points to the importance of big data analytics. Not only private companies need to calculate algorithms for the behavior of their business, but government agencies must monitor and analyze the financial conditions of all sectors of the economy based on all information (Kakavand, et al, 2017). Big data and its analytic capabilities in real-time interpretation of events bring value to management (Akter & Wamba, 2016).

Wu and others investigated the risks involved into artificial intelligence applications specially the business intelligence they defined a crisis or disaster as "a triggering event that is so important that it challenges the existing structure, routine, or survival of the organization." In corporate finance, data science is widely used to assist

management in tasks such as fraud detection and credit risk assessment (Wu et al., 2014). The first step to analyzing and predicting a company crash is collecting network data. For large organizations, the main data issues are scale (volume), streaming (speed), shapes (variety), and uncertainty (fidelity) (Ezerins et al., 2022). Media, web analytics and media have been effective marketing tools for increasing brand awareness, loyalty, engagement, sales, impact on customer satisfaction, and business-to-business (B2B) and business-to-customer (B2C) communication. Interactions (Agnihotri et al., 2016; Järvinen & Taiminen, 2016).

The interaction of businesses with digital solutions, statistics show that not all entrepreneurs appreciated the importance of automation before the onset of the pandemic. “It is difficult to conduct a constant analysis of activities, sources of income and expenses to make quick management decisions without using information technology. At the same time, in times of crisis, a significant factor for maintaining the sustainable development of an organization is the prompt adoption of balanced management decisions. The main goal of introducing AI into the processes of companies doesn’t imply a complete replacement of people and their labor, but the optimization of the processes of integration of human and technology. Zhang in 2022, constructed the quantitative warn-supporting system of enterprise financial crisis in the enterprise’s internal and external environments, case reasoning artificial intelligence technology (CRAIT) is introduced into the intelligent warn-supporting system based on expert knowledge and experience (Zhang, 2022).

Research Methodologies

In general terms, AI can support three important business needs: automate business processes, obtain information through data analytics, and interact with customers and employees. So, a survey was conducted in which about 30 people took part. The crisis situation was taken into account both for companies and for all people - Covid-19. How life has changed before and after the human pandemic and how artificial intelligence has affected this situation.

By 2030, automation will displace about a third of all workers in the United States, predicted back in 2017 by McKinsey experts (Mindell & Reynolds, 2023). It is now clear that this and, probably, the next pandemics will only accelerate this process. And the Spot robot is one example. Among his tasks is to reduce the number of patrolmen, because this reduces the risk of infection. The reliance on robots becomes even more attractive. The isolation regime led to the temporary closure of non-vital factories and offices in many countries, those employees who could have switched to a remote mode of work. But even in developed countries, the number of those who can fully work remotely is only about 27%. In this research significant questions were covered in the survey:

1. What industry are you currently working in?
2. In which industry did you work before the crises?
3. Did you have the opportunity to work online? And which programs did you use to work online?
4. Do you think these programs helped you keep your job?

Special attention should be paid to programs used. According to survey, most of the people who passed it were able to work online and used various types of platforms, in general around 78% have ability to work online this can support the using of AI techniques as shown in Figure1.

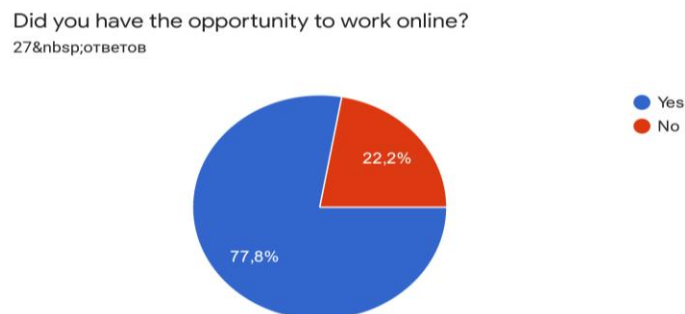


Figure 1. Opportunity to work online

Figure 2 explains the percentage of used platforms such as zoom, skype, Microsoft Teams were used mostly.

If yes, what programs did you use to work online?

27 ответов



Figure 2. Programs to use in order to work online

Regarding the importance of artificial intelligence to support and boost the companies' duties, figure 3 shows the results that the artificial intelligence is a significant part of companies that were developed.

Do you think these programs helped you keep your job?

26 ответов

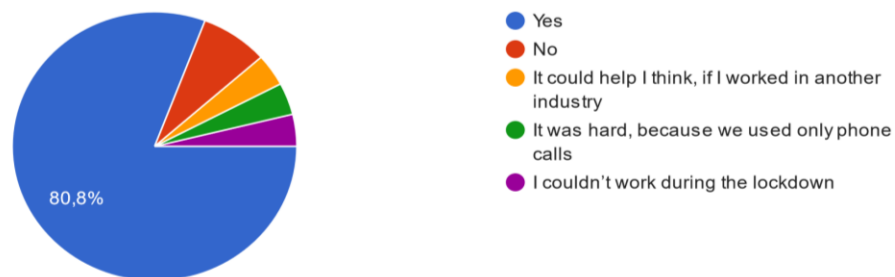


Figure 3. AI can keep work opportunity.

Figure 4 represent the answers of participants about job changes within crises for the different work sector as the following:

- 1) most of the participants keep working since Covid-19;
- 2) the biggest amount were able to use online platforms, which means that artificial intelligence is being developed in companies;
- 3) people could save the same job as before the pandemic.

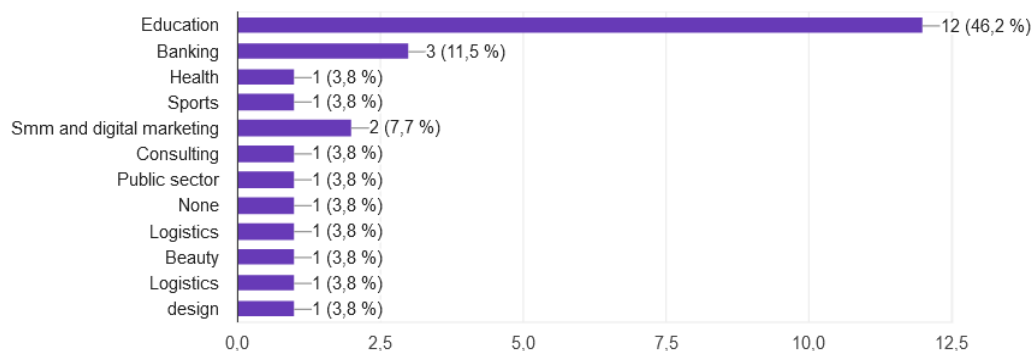


Figure 4. Industries in which people still working through the crises.

Companies, large and small, are expanding the use of robots in the context of social distancing to reduce the number of staff who need to come to work. Robots are also used to perform functions that employees cannot perform from home. For example, now robots are used to measure temperature in humans, as well as to distribute hand sanitizers. Also, artificial intelligence systems are now being created that can replace teachers, fitness instructors and financial consultants. Artificial intelligence applications and large technology companies are expanding. For example, Facebook and Google use it to moderate inappropriate posts, because human moderators working from home may not check everything.

For many enterprises, improving the work of the company, financial planning processes (including financial planning and analysis, sales planning and operational planning, integrated business planning and forecasting) is one of the highest priorities. Automation, better integration between systems, and more efficient processes seem to be an ongoing effort. Therefore, the development of artificial intelligence is growing rapidly (Aydin & Cavdar, 2015). Also, in this research we will demonstrate the suitable framework for applying artificial intelligence models and concepts in predicting the financial crises in business companies to mitigate the risks and failures in the market.

Research Framework Design

Nowadays the most appropriate method to get the direction of the current economic situation looks like a bet on the digital economy and new achievements in the field of creating artificial intelligence. Optimization in this case can be carried out by more advanced methods: by reforming the structure of the labor market with the use of various high-tech solutions for automating intellectual and physical work. Thus, to make up for the decline in the share of the working-age population in the Kazakhstan through the robotization of production, including employees of "intellectual labor".

First of all, the progress of algorithms that can emulate information processing methods and can reproduce a "virtual employee". Already, the improvement of machine learning technologies, as well as voice and face recognition, is leading to the fact that robots are beginning to replace people even in professions that require interaction with customers.

Digital technologies like artificial intelligence models have primarily permeated organizational activities, cutting costs and times associated with producing and delivering goods and services. However, the process of designing those goods and services has mainly remained labor-intensive (Verganti et al., 2020). By 2020, 2 million jobs will be added to the global labor market, but about 7.1 million will disappear, according to The Future of Jobs study published by the World Economic Forum (WEF) in early 2017. According to a Bank of America report last year, in 10 years robots will perform 45% of manufacturing tasks in the United States. Now this figure is 10%. Most researchers consider jobs that involve a high degree of creativity, analytical thinking, or interpersonal communication to be the most stable (Sun & Scanlon, 2019).

The financial sector in central Asia is adapting to new technologies faster than other industries. The underwriting profession is a thing of the past, and the decision-making operation is almost completely automated. The use of such services in risk management allows banks and insurance companies to further reduce losses by 12-15%, even when using advanced risk analysis systems from world market leaders (Gertseva, 2020). Machine learning of all kinds can radically change the global economy and increase income inequality. In particular, it makes no economic sense to move production facilities to regions with cheap labor (Jain et al., 2018).

First of all, low-skilled and low-paid employees suffer from labor automation, the import of which to developed countries is becoming less and less justified, taking into account technological progress and the increase in the volume of the digital economy. The fear of unemployment following increasing automation is justified in emerging economies, but in the case of central Asia is not talking about replacing people with technology, but about filling the lack of human capital. The coming transformation of the labor market does not mean the dismissal of people, but an adjustment in specialization and the emergence of demand for other types of work (Soni et al., 2019; Bhosale et al., 2020).

High technologies, in particular solutions in the field of artificial intelligence, are one of the few sectors of the central Asia economy that is currently actively growing. Our products have always been and remain competitive in

the global market, which allows us to count on a significant share in this segment. According to Tractical trading, the segment of artificial intelligence solutions in the world will grow to \$59.75 billion by 2025 (Agrawal et al., 2019; Korobeynikova, et al., 2021).

Construction the Intelligence Framework

In fact, to develop an intelligence framework that depicts the interaction between financial forecasting and artificial intelligence (AI) technology has become an important requirement, especially when it comes to anticipating and handling financial crises. significant contributions that shed light on how AI can improve financial models' predictive skills and have ramifications for both foreseeing and mitigating crises. This framework should include the following phases and contents as explained in Figure 5:

Here are key components included in AI research model that designed for predicting financial crises:

Data Collection and Preprocessing

- * Financial Indicators: collect relevant financial data like stock prices, interest rates, inflation rates, GDP growth, and other macroeconomic indicators.
- * Market Sentiment Data: contains the sentiment analysis from news articles, social media, and other textual sources to gather investor sentiment.
- * Historical Data: use historical financial data to identify patterns and trends that may precede financial crises.

Feature Selection and Engineering

- * Identify Relevant Features: pick up the features that have been historically indicative of financial crises, such as volatility, liquidity, and credit risk.
- * Create New Features: develop new features that may enhance the model's ability to capture complex relationships in the data.

Machine Learning Algorithms

- * Supervised Learning Algorithms: build machine learning algorithms such as decision trees, random forests, support vector machines, and neural networks for predictive modeling.
- * Unsupervised Learning Algorithms: Consider clustering techniques or anomaly detection methods to identify abnormal patterns in the data.

Integral Methods

- * Combine Models: employ the integral methods like bagging or boosting to combine multiple models and improve overall prediction accuracy.
- * Stacking Models: Stack multiple models together to leverage the strengths of different algorithms.

Time Series Analysis

- * Temporal Patterns: develop time series analysis to capture temporal dependencies in the financial data.
- * Autoregressive Models: Utilize autoregressive integrated moving average (ARIMA) or other time series models to account for sequential dependencies.

Deep Learning Models

- * Neural Networks: investigate the use of neural networks, especially deep learning architectures, to capture intricate patterns in large and complex financial datasets.
- * Long Short-Term Memory (LSTM): Employ LSTM networks for their ability to capture long-term dependencies in sequential data.

Model Validation and Evaluation

- * Cross-Validation: Implement cross-validation techniques to assess the model's performance on different subsets of the data.
- * Metrics: Use appropriate evaluation metrics such as accuracy, precision, recall, F1 score, or area under the receiver operating characteristic curve (AUC-ROC).

Interpretability and Explainability

- * Feature Importance Analysis: Conduct feature importance analysis to understand the variables contributing most to predictions.
- * Explainable AI (XAI): Utilize XAI techniques to make the model's decision-making process interpretable.

Risk Management Strategies

- * Portfolio Optimization: Integrate portfolio optimization strategies that consider the predicted risks when allocating assets.
- * Dynamic Hedging Strategies: Develop strategies for dynamically adjusting portfolios based on changing risk conditions.

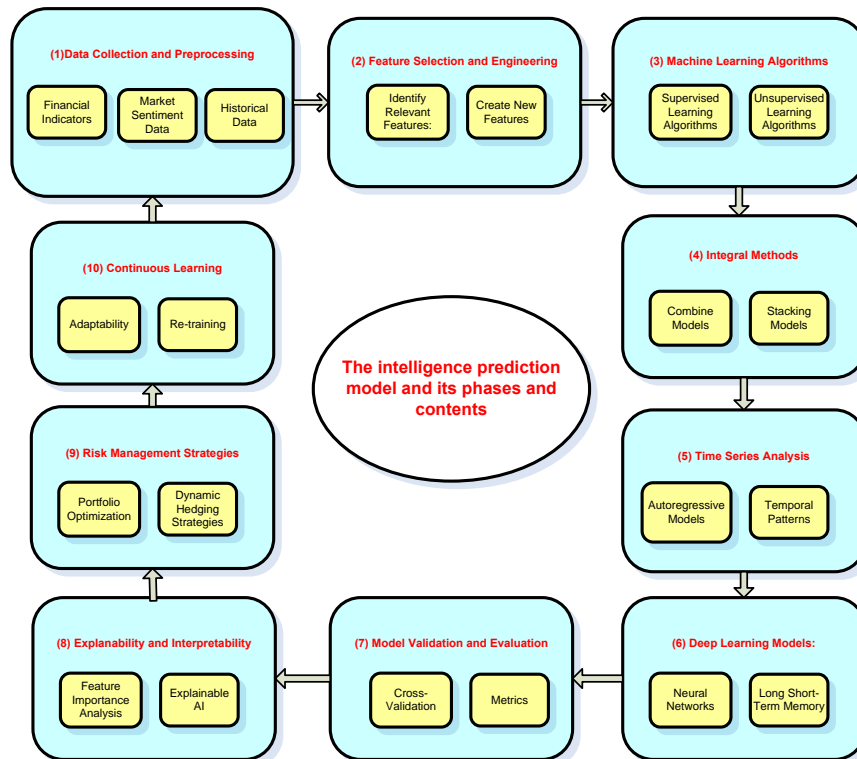


Figure 5. The contents of the intelligence framework and its ten phases

Continuous Learning

* Adaptability: Design the model to adapt to evolving market conditions and incorporate new information as it becomes available.

* Re-training: Implement regular re-training of the model to ensure it remains relevant and effective over time.

Research Results and Analysis

Information technology pattern is possible to train qualified IT personnel through joint efforts of the state and major technology companies. However, the problem of lack of qualified specialists can be solved not only through education, but also with the help of the same artificial intelligence that can automate routine tasks of programmers, freeing up the potential to solve complex technological issues, create more advanced artificial intelligence, products with higher added value. A whole technological spiral, which the sooner you start to unwind, the faster you will reach a new stage of progress. Also using virtual assistants is one of the AI tools that will eventually be more widely implemented in business processes and everyday life of a modern person. According to Facebook statistics, more than 10 thousand companies are developing chatbots. Actually, adopting the suggested artificial intelligence (AI) model to predict financial crises in business organizations has a number of possible advantages. It's crucial to remember that the model's efficacy is dependent on several variables, such as the quality of the data, the resilience of the model, and the volatility of the financial markets. Here are a few anticipated findings and outcomes:

Early Alert Signals

By spotting trends and abnormalities in financial data, the AI model can offer early warning signs of impending financial catastrophes. Businesses are able to take preventative action before the situation gets worse because to this early detection.

Risk Reduction

Businesses can pinpoint specific risk areas in their operations and portfolios by using AI forecasts. This gives them the ability to put specific risk reduction plans into action, such diversifying assets, modifying financial policies, or modifying investment portfolios.

Making Strategic Decisions

The AI model can help with strategic decision-making by offering perceptions into future changes in the economy and market dynamics. Businesses are able to optimize resource allocation and operational plans by modifying their business strategy in response to anticipated financial conditions.

Improved Distribution of Resources

Businesses are able to maximize the allocation of resources, such as capital expenditures, staffing levels, and financial investments, when they possess excellent forecasting capabilities. This guarantees that resources are allocated more effectively in advance of recessions.

Better Financial Organization

Businesses might improve their financial planning procedures by utilizing AI forecasts. Organizations may create more robust financial plans that take uncertainties and future crises into account by integrating AI insights into forecasting and budgeting processes.

Confidence among Customers and Stakeholders

Gaining the ability to anticipate and manage financial crises can boost stakeholder and customer confidence. Fostering trust and showcasing the company's dedication to prudent financial management can be achieved by open and honest communication regarding preventive steps implemented based on AI predictions.

Regulatory Compliance

AI algorithms that predict financial crises can help businesses stay in line with financial regulations. Legal problems and regulatory fines can be avoided by proactive risk management that complies with regulations.

Mitigate the Money and Investment Losses

Businesses can lessen the effect of crises on their financial performance by recognizing and resolving possible financial risks early on. This entails reducing investment losses, preventing liquidity issues, and safeguarding the company's overall financial stability.

A Competitive Advantage

Businesses may obtain a competitive edge if they successfully incorporate AI for financial crisis prediction. A company can stand out from rivals by projecting an image of resilience and forward-thinkingness through its improved ability to handle economic uncertainty.

Ongoing Learning and Adjustment

AI models can be created with ongoing learning and adaptability in mind. The model continues to be applicable and useful in offering continuous insights into future financial crises as it learns from real-time data and adapts to shifting market conditions. Another area of application of artificial intelligence algorithms is predictive analytics. AI-algorithmic technologies can operation huge amounts of data, identify patterns, and perform predictive functions. Promising areas of application of artificial intelligence are those processes in which human actions are tracked and repeated. Some companies' examples are shown in Table 1.

Table 1. Prospects for using artificial intelligence in digital companies

No.	Company name	Project name	Areas of application of artificial intelligence
1	Google	Google Health	Diagnostics of health status, plotting a route to the nearest hospital, reminder of medication intake time, assessment of progress in fitness classes
		Medical Brain	Analysis of the patient's condition, determination of prospects for the further course of the disease, prediction of the probability of an unfavorable outcome
2	Sberbank of Russia	The Sberbank Online app	Analysis of preferences of 50 million users by 1000 parameters and personalized formation of a package of services and information, making transfers and payments, maintaining spending statistics Provision of all loans (starting from 2021) based on the client's biometric data, study of credit history, income, expenses Conducting a preliminary interview with candidates for mass vacancies
3	Facebook	Online App	Correction of the eye image in the photo of a blinked customer

It should be noted that the progress of AI and Big Data is closely linked. Machine learning requires huge amounts of data. The ability to correctly select raw data for the neural network training operation is one of the specific competencies of specialized specialists, but not the only one. The AI training operation also needs to be monitored and adjusted. For example, if incorrect or questionable results are obtained because of neural networks, it is necessary to change the source data sets and "retrain" the system. The learning operation can also not always be fully automated. For most tasks, along with "machine learning", "expert" training is also required, during which a person manually indicates to the artificial intelligence system which solutions for this problem are correct and which are not. Furthermore, the answers of participants of this research study supported the importance and the crucial benefits of this developed intelligence model as the following:

In figure 6, 82% of participants confirmed to the importance of applying this model to mitigate and prevent the financial crises,

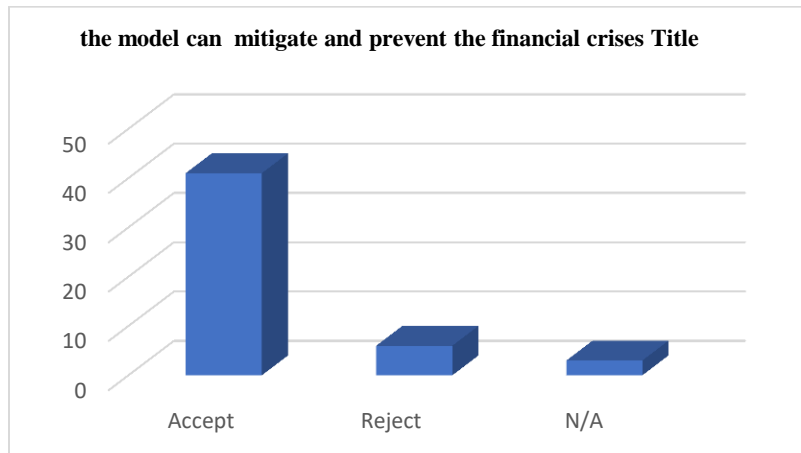


Figure 6. The importance of applying this model to mitigate and prevent financial crises

Regarding the main benefits that business companies can attain through applying this model are shown in Figure 7.

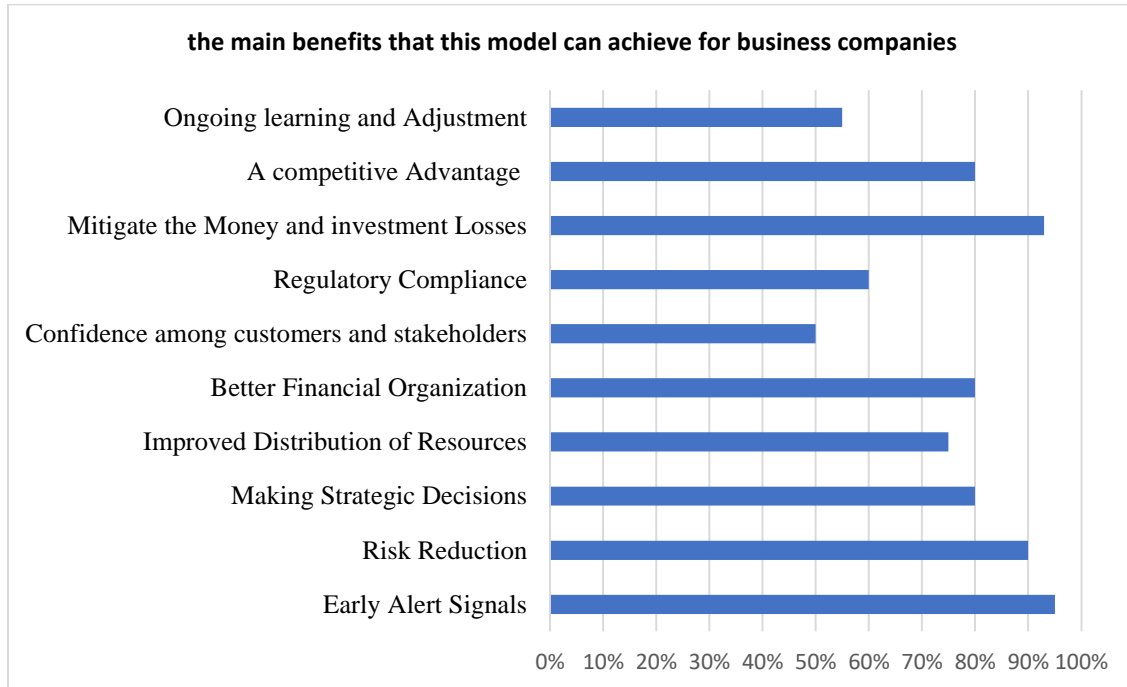


Figure 7. The main benefits that this model can achieve for business companies.

Research Conclusions

There is more interest about the research of the benefits of using artificial intelligence in business and predicting the financial crisis. The majority argues for the need to automate processes and data analysis for analytics. Many companies do not really trust the transition to new technologies, but this is what can help them stay competitive. Some of them believe that investing in process automation requires a lot of money, but this will help to build the right steps to avoid a crisis and bankruptcy of the company. In this paper, we have mentioned an example based on the statistics of the Yandex company. It tells how important it is to switch all your attention and budget on time to the development of a convenient and automated work format.

Many entrepreneurs mistakenly assume that there is no need to implement AI, since they have enough human resources to support the business, but this is a big misconception. Automation does not entail a reduction in employees, it entails an increase in work efficiency. Yes, big data analysis does all the analytical work on its own, but there are always people who know the basic principles of analytics through Data analysis. IT specialists are divided into many different directions and now this professional area is considered one of the most stable and in high demand.

Also, artificial intelligence systems are now being created and can replace teachers, fitness instructors and financial consultants. Artificial intelligence applications and large technology companies are expanding. For example, Facebook and Google use it to moderate inappropriate posts, because human moderators working from home may not check everything. Of course, companies cannot predict any events 100%, but the sooner companies start using statistical data and cloud solutions, the more accurate the probability of crisis situations will be.

This research introduced an intelligence model to help business companies to mitigate the risks of financial crises, this model based on artificial intelligence algorithms and components like neural network, time series and artificial intelligence.

Scientific Ethics Declaration

The authors declare that the scientific ethical and legal responsibility of this article published in EPSTEM journal belongs to the authors.

Acknowledgements or Notes

* This article was presented as an oral presentation at the International Conference on Technology (www.icontechno.net) held in Antalya/Turkey on November 16-19, 2023.

References

- Agnihotri, R., Dingus, R., Hu, M. Y., & Krush, M. T. (2016). Social media: Influencing customer satisfaction in B2B sales. *Industrial Marketing Management*, 53, 172-180.
- Agrawal, A., Gans, J., & Goldfarb, A. (Eds.). (2019). *The economics of artificial intelligence: an agenda*. University of Chicago Press
- Akter, S., & Wamba, S. F. (2016). Big data analytics in E-commerce: a systematic review and agenda for future research. *Electronic Markets*, 26, 173-194.
- Aydin, A. D., & Cavdar, S. C. (2015). Prediction of financial crisis with artificial neural network: an empirical analysis on Turkey. *International Journal of Financial Research*, 6(4), 36.
- Bhosale, S. S., Salunkhe, A. G., & Sutar, S. S. (2020). Artificial intelligence and its application in different areas. *International Journal of Advance and Innovative Research*, 7(1).
- Dafri, W., & Al-Qaruty, R. (2023). Challenges and opportunities to enhance digital financial transformation in crisis management. *Social Sciences & Humanities Open*, 8(1).

- Ezerins, M. E., Ludwig, T. D., O'Neil, T., Foreman, A. M., & Acikgoz, Y. (2022). Advancing safety analytics: A diagnostic framework for assessing system readiness within occupational safety and health. *Safety Science*, 146.
- Gertseva, Y. V. (2020). Operational management of production: the problem of selecting a system in the market environment. *Вестник молодых учёных и специалистов Самарского Университета*, 2(17), 82-87
- Jain, M., Kumar, P., Kota, R., & Patel, S. N. (2018). Evaluating and informing the design of chatbots. In *Proceedings of the 2018 Designing Interactive Systems Conference*, 895-906.
- James, N., & Menzies, M. (2023). An exploration of the mathematical structure and behavioural biases of 21st century financial crises. *Physica A: Statistical Mechanics and its Applications*, 630.
- Järvinen, J., & Taiminen, H. (2016). Harnessing marketing automation for B2B content marketing. *Industrial Marketing Management*, 54, 164-175.
- Kakavand, H., Kost De Sevres, N., & Chilton, B. (2017). *The blockchain revolution: An analysis of regulation and technology related to distributed ledger technologies*. Luther Systems. Retrieved from <https://deliverypdf.ssrn.com/delivery.php>
- Korobeynikova, O. M., Korobeynikov, D. A., Popova, L. V., Chekrygina, T. A., & Shemet, E. S. (2021, March). Artificial intelligence for digitalization of management accounting of agricultural organizations. In *IOP Conference Series: Earth and Environmental Science*, 699(1).
- Mindell, D. A., & Reynolds, E. (2023). *The work of the future: building better jobs in an age of intelligent machines*. MIT Press.
- Saleh, E. A. (2023). The effects of economic and financial crises on FDI: A literature review. *Journal of Business Research*, 161.
- Soni, N., Sharma, E. K., Singh, N., & Kapoor, A. (2019). Impact of artificial intelligence on businesses: from research, innovation, market deployment to future shifts in business models. Retrieved from *arXiv preprint arXiv:1905.02092*
- Sun, A. Y., & Scanlon, B. R. (2019). How can Big Data and machine learning benefit environment and water management: a survey of methods, applications, and future directions. *Environmental Research Letters*, 14(7).
- Tolo, E. (2020). Predicting systemic financial crises with recurrent neural networks. *Journal of Financial Stability*, 49.
- Verganti, R., Vendraminelli, L., & Iansiti, M. (2020). Innovation and design in the age of artificial intelligence. *Journal of Product Innovation Management*, 37(3), 212-227.
- Wu, D. D., Chen, S. H., & Olson, D. L. (2014). Business intelligence in risk management: Some recent progresses. *Information Sciences*, 256, 1-7.
- Zhailbayevich, Z. K., & Hamada, M. A. (2023). Development of a predictive intellectual model for predicting the financial crisis in banks. In *2023 2nd International Conference on Applied Artificial Intelligence and Computing (ICAAIC)* (pp. 661-665). IEEE.
- Zhang, A. (2022). Research on enterprise financial crisis based on case reasoning artificial intelligence technology. In *2022 International Conference on Computation, Big-Data and Engineering (ICCBDE)* (pp. 199-201). IEEE.

Author Information

Mohamed Ahmed Hamada

Abu Dhabi University
Abu Dhabi, United Arab Emirates

Khaled M. K. Alhyasat

Abu Dhabi University
Abu Dhabi, United Arab Emirates
Contact e-mail: khaled.alhyasat@adu.ac.ae

To cite this article:

Hamada, M. A., & Alhyasat, K.M.K (2023). Artificial intelligence technology to predict the financial crisis in business companies. *The Eurasia Proceedings of Science, Technology, Engineering & Mathematics (EPSTEM)*, 24, 71-82.

The Eurasia Proceedings of Science, Technology, Engineering & Mathematics (EPSTEM), 2023

Volume 24, Pages 83-88

IConTech 2023: International Conference on Technology

S/MIME Certificate Test Suite

Yagmur Fidaner
Gazi University

Aysun Coskun
Gazi University

Tamer Ergun
Cloudpeer

Abstract: In today's world, email usage has become a necessity. Emails, with a large user base, serve various functions not only for personal purposes but also for facilitating communication between teams in the business world and acting as a point of contact for organizations with their customers. Emails that have infiltrated our lives are also at the center of data breaches, leaks, and malicious attacks. To ensure email security, it is possible to send digitally signed and encrypted emails using the public key infrastructure-based S/MIME certificates. The existing standards for S/MIME certificates were deemed insufficient, and in 2023, for the first time, the Certificate Authority/Browser (CA/B) Forum, consisting of Certificate Authorities (CA) and application software providers and recognized as an international authority, published the S/MIME Baseline Requirements (BR) document. While compliance with the Baseline Requirements document published by the CA/B Forum ensures reliability through conformity checks for SSL certificates used in web security, this audit was considered insufficient. To monitor and audit SSL certificates, the Certificate Transparency project was introduced, aiming to provide an open structure to safeguard the certificate issuance process. However, in reliable S/MIME certificates, the control mechanism is limited to BR audits. The study establishes a comprehensive S/MIME certificate public key infrastructure that allows analyzing email applications; behaviors in the face of certificates that do not comply with the BR during the certificate validation phase. Additionally, the study aims to develop a user application that enables end-users to test the security and compliance of certificates with the BR.

Keywords: S/mime, Email, Public key infrastructure, Certificate, Security

Introduction

Secure/Multipurpose Internet Mail Extensions (S/MIME) is a protocol that ensures secure sending and receiving of electronic messages (Schaad, 2019). S/MIME employs digital signatures for authentication, non-repudiation and message integrity, while encryption ensures data confidentiality. These capabilities are derived from public key infrastructure (Schaad et al., 2019). Using certificates in X.509 format (ITU, 2019), cryptographic key pairs are digitally associated with email addresses. Certification Authorities (CAs) are responsible for certificate generation, issuance, revocation, and management. The CA/B Forum, a voluntary international organization comprising certificate authorities, email service providers, web browser providers, and third-party application software vendors, has been established (CA/ Browser Forum, 2023). In 2020, the CA/B Forum formed a working group to define rules for the production of reliable S/MIME certificates, leading to the publication of the Baseline Requirements (BR) in 2023. CAs must comply with BR to produce internationally recognized trustworthy S/MIME certificates (CA/Browser Forum, 2023).

- This is an Open Access article distributed under the terms of the Creative Commons Attribution-Noncommercial 4.0 Unported License, permitting all non-commercial use, distribution, and reproduction in any medium, provided the original work is properly cited.

- Selection and peer-review under responsibility of the Organizing Committee of the Conference

© 2023 Published by ISRES Publishing: www.isres.org

The Certificate Transparency (CT) project, initially developed for SSL certificates, aims to maintain the integrity of the certificate issuance process by providing an open framework for monitoring and auditing SSL certificates (Laurie et al., 2021). A study revealed 907,000 SSL certificates were issued without compliance to the CA/B Forum's Baseline Requirements, using data from CT logs (Scheitle & Gasser, 2018). Despite the expectation that CAs produce certificates following a specific template, the number of SSL certificates in use that do not align with public key infrastructure and BR requirements is significant. Literature suggests the creation of a test suite to evaluate web browsers' behavior towards certificates not conforming to the SSL Baseline Requirements (Simsek et al., 2022). The Baseline Requirements document considered in the study is specific to SSL certificates, and the test suite was tailored to SSL certificates.

Unlike SSL certificates, there is no third-party framework for monitoring and auditing generated S/MIME certificates; the control mechanism is limited to the certifying authorities and email applications. It is crucial not only for CAs to produce certificates using appropriate templates but also for email applications to authenticate the utilized certificate properly. A study in 2009 focused on the user interfaces of applications supporting S/MIME structure, resulting in a product emphasizing these interfaces (Levi & Guder, 2009). Additionally, research has been conducted on plugins verifying digital signatures in S/MIME and OpenPGP-supported applications (Poddebniak, 2018; Muller, 2019). These studies include attacks on various aspects, one of which is the Cryptographic Message Syntax (CMS) attack utilizing the Encrypted Message Syntax (CMS) standard developed by IETF for cryptographic protection and digital signing and encryption processes (Housley, 2009). Vulnerabilities in handling various CMS structures and secure certificate chain establishment in S/MIME applications were identified and exploited for attack purposes. Our product will preemptively identify and mitigate these vulnerabilities in S/MIME applications' CMS structures.

This study will analyze email application certificate verification mechanisms, referencing the Baseline Requirements document, which encompasses RFC 5280 and X.509 standards and additional requirements. An S/MIME certificate test public key infrastructure, the S/MIME Test Suite, has been established. The S/MIME Test Suite consists of PKI components, each representing a scenario with a single BR requirement violation. This enables the analysis of email application behavior concerning the specific violation.

Method

In the study, a certificate hierarchy has been established to be used in the conducted tests. Within the certificate hierarchy, root certificates, sub-root certificates, and end-user certificates have been generated in the X.509 ASN.1 structure. Certificate Revocation Lists (CRLs) have been utilized to ensure the revocation status checks of the generated certificates. An example certificate hierarchy model is illustrated below:

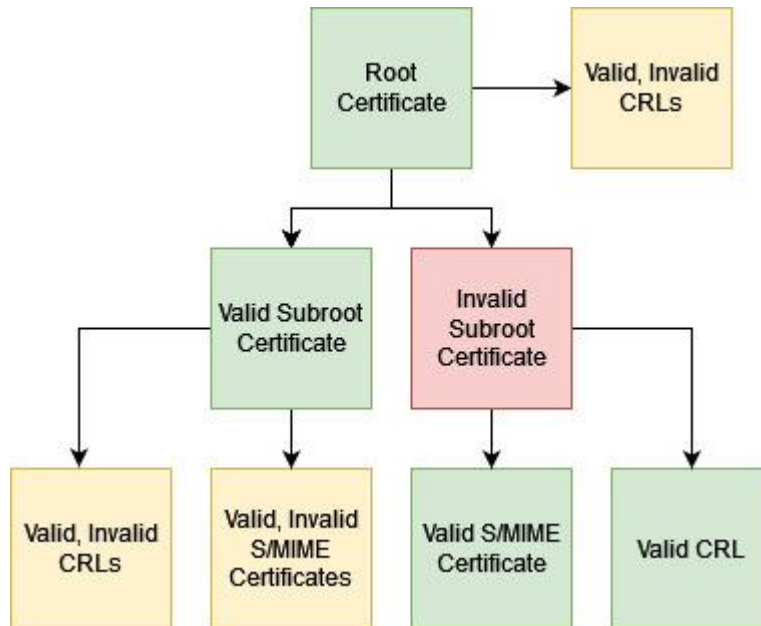


Figure 1. S/MIME certificate hierarchy model

The certificate hierarchy progresses from a valid root certificate that complies with BR requirements. Scenarios will be tested using different sub-root and end-user certificates generated by this root. Signing and encryption operations on emails will be performed using both invalid and valid S/MIME certificates. The behaviors of email applications in response to these scenarios will be analyzed.

Certificate Validation and Scenario Generation

Requirements related to the validation of S/MIME certificate profiles in BR have been shared, which should not be overlooked during the certificate verification phase. Based on BR 1.0.0 version, the following requirements have been identified and added to the test scenarios for verification.

Certificate Version Control

X.509 certificates in Version 1 and Version 2 formats were found lacking in certain aspects, necessitating additional information within the certificates. Therefore, the Version 3 certificate format, which includes Version 2, was introduced (Cooper, et al., 2008). BR-compliant certificates must be in X.509 format and Version 3, as specified in BR Section 7.1.1 (Yee, 2013). To ensure compliance, Version 2 S/MIME certificates were generated.

Certificate Algorithm and Key Control

According to BR Section 6.1.5, certificates must be signed starting from root certificates using RSA and ECDSA key pairs. RSA key pairs should be at least 2048 bits in size. For ECDSA, NIST P-256, NIST P-384, NIST P-521 elliptic curves, and *curve25519* and *curve448* elliptic curve algorithms in EdDSA are accepted. BR Section 7.1.3 provides detailed object identifiers (OIDs) for algorithms. Certificates with algorithms and OIDs not specified in the accepted algorithms were generated to conduct the checks.

Certificate Validity Period Control

Certificates generated must have a maximum validity period of 825 days for Strict and Multipurpose certificates and 1185 days for Legacy certificates, as per BR Section 6.3.2. Certificates exceeding the allowed validity period were generated for verification.

Certificate Content and Extension Checks

BR Section 7.1.2 specifies the required format for certificate content and extensions, termed as the application of RFC 6818. RFC 6818 updates RFC 5280, presenting profiles for X.509 public key infrastructure certificates and CRLs. Certificates not adhering to these specifications were generated for analysis.

Basic Constraints Extension Control

Certificates in a certificate chain can generate other certificates. This extension specifies if a certificate is a CA certificate or an end-entity certificate and how deep a certification path may exist. According to BR, root and sub-root certificates must have this extension, with the CA bit set. For end-user certificates, even if this extension exists, the CA bit must not be set. Certificates were generated both without this extension and with this extension set but the CA bit unset for sub-root certificates.

Key Usage Extension Control

This extension indicates the purposes for which the public key can be used. It includes flags for *digitalSignature*, *dataEncipherment*, *keyEncipherment* and *nonRepudiation*. According to BR, root and sub-root certificates must have this extension with the *keyCertSign* and *cRLSign* bits set. Certificates were generated without this extension or with bits set outside those specified in BR.

Extended Key Usage (EKU) Extension Control

For sub-root and end-user certificates other than cross-certificates, this extension must be present and must contain the *id-kp-emailProtection* value. It must not contain *id-kp-codeSigning*, *id-kp-serverAuth*, *id-kp-timeStamping*, or *anyExtendedKeyUsage* values. Certificates were generated both without this extension and with this extension containing undesirable values.

Subject Alternative Name Extension Control

End-user certificates must include this extension. All email addresses found in the subject field must also be in this extension. Certificates were generated that did not comply with this requirement.

Certificate Policies Extension Control

End-user certificates must have policy identifiers as defined in BR Section 7.1.6.1, based on certificate type and usage. Certificates were generated without these specified policy identifiers.

CRL Distribution Points Extension Control

Sub-root and end-user certificates must have this extension, containing at least one URI address of a CA CRL service. Certificates without this extension or with incorrect URI addresses were generated.

Certificate Revocation Checks

Certificates generated using the public key infrastructure can be revoked for specific reasons before their validity period expires. BR-compliant certificates' revocation reasons and periods are detailed in BR Section 4.9.1. Certificate status checks can be done online and offline. CRLs carry information about revoked certificates, generated by the CA, and are published offline after being signed. OCSP allows online certificate revocation checks. In OCSP usage, the certificate status is checked instantly, providing a reliable response to end-users (Santesson et al., 2013). After discussions among authorities in CA/B Forum, OCSP usage is optional in BR (2022-09-29 Minutes of the CA/Browser Forum Teleconference, 2022). This change aims to prevent a potential scenario where OCSP usage might allow a CA to track when and where an S/MIME protected message is opened by the recipient (Digicert, 2023). Additionally, for sub-root and end-user certificates, CRL usage is mandatory for certificate status checks.

CRL Validity Period Control

CRLs for end-users should be updated at least every 7 days, with the difference between *nextUpdate* and *thisUpdate* fields within the CRL not exceeding 10 days, as per BR Section 4.9.7. For sub-root certificates, CRLs should be renewed every 12 months under normal circumstances and within 24 hours if a sub-root certificate is revoked. The difference between *nextUpdate* and *thisUpdate* fields within the CRL should not exceed 12 months. Certificates not meeting these conditions were generated to ensure compliance.

Results and Discussion

As a result, considering BR requirements and potential vulnerabilities, a comprehensive test suite has been designed. The test suite infrastructure consists of 1 root, 4 sub-roots, 8 CRLs, and 19 end-user certificates. Detailed information about the generated certificates for this suite is provided in Table 1.

Conclusion

As a result, emails are frequently used and distributed in nature. The behavior of email applications in the face of non-compliant certificates with BR requirements is crucial for secure email communication.

Table 1. Generated end -user certificates for S/MIME test suite

Certificate name	Certificate information	Expected validation result
SMIME_1	Valid certificate	VALID
SMIME_2	The version information of the certificate is not valid (Version 2)	NOT VALID
SMIME_3	Certificate has expired	NOT VALID
SMIME_4	Certificate has been revoked in CRL	NOT VALID
SMIME_5	Certificate has expired CRL	NOT VALID
SMIME_6	Certificate has incorrect URI address for CRL	NOT VALID
SMIME_7	Certificate has invalid signing algorithm	NOT VALID
SMIME_8	Certificate has no ECU extension	NOT VALID
SMIME_9	Certificate has invalid ECU extension (has no id-kp-emailProtection)	NOT VALID
SMIME_10	Certificate has no SAN extension	NOT VALID
SMIME_11	Certificate has invalid SAN extension	NOT VALID
SMIME_12	Certificate has invalid Key Usage extension (digitalSignature bit not set)	NOT VALID
SMIME_13	Certificate has invalid Basic Constraints extension	NOT VALID
SMIME_14	Certificate has no specified policy identifier	NOT VALID
SMIME_15	Certificate has invalid digital signature	NOT VALID
SMIME_16	The signature of the sub-root certificate is invalid	NOT VALID
SMIME_17	Sub-root certificate has expired	NOT VALID
SMIME_18	Sub-root certificate has been revoked in CRL	NOT VALID
SMIME_19	Root certificate is not trusted	NOT VALID

In this study, potential scenarios have been derived based on BR, and a comprehensive test suite has been designed. In the follow-up study, using the test S/MIME certificates generated in this research, email signing and encryption operations will be conducted to analyze existing email client applications from a security perspective. Additionally, the study aims to develop a user application that allows end users to test the security and compliance of certificates, ensuring compatibility with BR.

Scientific Ethics Declaration

The authors declare that the scientific ethical and legal responsibility of this article published in EPSTEM journal belongs to the authors.

Acknowledgements or Notes

* This article was presented as an oral presentation at the International Conference on Technology (www.icontech.no) held in Antalya/Turkey on November 16-19, 2023.

References

- CA/ Browser Forum. (2022, September 29). Minutes of the CA/Browser Forum teleconference. Retrieved from <https://cabforum.org/2022/09/29/2022-09-29-minutes-of-the-ca-browser-forum-teleconference/>
- CA/ Browser Forum. (2023, August 7). CA/ Browser Forum. Retrieved, from <https://cabforum.org/>
- CA/Browser Forum. (2023). *Baseline requirements for the issuance and management of publicly trusted S/MIME certificates*. Retrieved from <https://cabforum.org/wp-content/uploads/CA-Browser-Forum-SMIMEBR-1.0.0.pdf>
- Cooper, D., Santesson, S., Farrell, S., Boeyen, S., Housley, R., & Polk, W. (2008). Internet X.509 public key infrastructure certificate and certificate revocation list (CRL) profile, RFC:5280. *Network Working Group*, 1-151.
- Digicert. (2023, July 8). CA/Browser forum adopts first baseline requirements for S/MIME certificates. Retrieved from <https://www.digicert.com/blog/ca-browser-forum-adopts-s-mime-baseline-requirements>
- Housley, R. (2009). Cryptographic message syntax (CMS) RFC:5652. *Network Working Group*.
- ITU. (2019). X.509: Information technology - open systems interconnection - the directory: Public-key and attribute certificate frameworks.

- Laurie, B., Messeri, E., & Stradling, R. (2021). Certificate transparency version 2.0 RFC:9162. 1-53. *Internet Engineering Task Force (IETF)*.
- Levi, A., & Guder, C. (2009). Understanding the limitations of S/MIME digital signatures for e-mails: A GUI based approach. *Computers & Security*, 105-120.
- Muller, J. (2019). {"Johnny"}, you are {"fired!"}—Spoofing {OpenPGP} and {S/MIME} signatures in emails. *28th USENIX Security Symposium (USENIX Security 19)*.
- Poddebniak, D. (2018). Efail: Breaking {S/MIME} and {OpenPGP} email encryption using exfiltration channels. *27th USENIX Security Symposium*.
- Santesson, S., Myers, M., Ankney, R., & Malpani, A. (2013). X.509 internet public key infrastructure online certificate status protocol - OCSP RFC:6960. *Internet Engineering Task Force (IETF)*.
- Schaad, J. (2019). Secure/multipurpose internet mail extensions (S/MIME) version 4.0 message specification.
- Schaad, J., Cellars, A., & Ramsdell, B. (2019). Secure/multipurpose internet mail extensions (S/MIME) version 4.0 RFC:8550. *Internet Engineering Task Force (IETF)*.
- Scheitle, Q., & Gasser, O. (2018). The rise of certificate transparency and its implications on the internet ecosystem. *IMC '18: Proceedings of the Internet Measurement Conference*.
- Simsek, M. M., Ergun, T., & Temucin, H. (2022). SSL test suite: SSL certificate test public key infrastructure. *30th Signal Processing and Communications Applications Conference (SIU)*.
- Yee, P. (2013). Updates to the internet X.509 public key infrastructure certificate and certificate revocation list (CRL) profile. *Internet Engineering Task Force (IETF)*.

Author Information

Yagmur Fidaner

Gazi University
Ankara, Turkey
Contact e-mail: yagmur.fidaner@gazi.edu.tr

Aysun Coskun

Gazi University
Ankara, Turkey

Tamer Ergun

Cloudpeer
İstanbul, Turkey

To cite this article:

Fidaner, Y., Coskun, A., & Ergun, T. (2023). S/MIME certificate test suite. *The Eurasia Proceedings of Science, Technology, Engineering & Mathematics (EPSTEM)*, 24, 83-88.

The Eurasia Proceedings of Science, Technology, Engineering & Mathematics (EPSTEM), 2023

Volume 24, Pages 89-95

IConTech 2023: International Conference on Technology

Investigation of Damping Energy in Trusses

Victor Rizov

University of Architecture

Abstract: Trusses are important load-bearing constructions. They are widely applied in various areas of contemporary engineering. Considering the elastic-plastic behaviour of trusses is an important step in developing the methods for analysing the mechanics of these constructions. A specific problem that appears when trusses of elastic-plastic behaviour are subjected to cyclic external loads is the damping energy. In the present paper, a general treatment of the damping problem in trusses with elastic-plastic behaviour is presented. The trusses investigated may have arbitrary geometry and external loading. First, damping in static determinate trusses is considered. A general methodology for deriving the damping energy is developed. Determination of the damping energy in statically indeterminate trusses with arbitrary number and location of the supports is also considered. The general treatment of the damping energy problem is applied to a particular static determinate truss configuration loaded by one external cyclic force. Then the damping energy in a statically indeterminate truss that has the same geometry and loading as that of the statically determinate one is analyzed. A parametric study of the damping energy is performed.

Keywords: Truss, Damping energy, Statically indeterminate structure, General treatment, Parametric investigation

Introduction

Truss constructions representing systems of rectilinear uniform bars rigidly connected at their ends are well known for their high efficiency for a long time (Huang, 1967; Aleksandrov & Potapov, 1990; Blake, 1985; Varvak, 1997). Trusses are frequently used especially for supporting heavy loads in various structural applications in civil engineering, mechanical engineering, and road and railway infrastructure (Aleksandrov & Potapov, 1990; Koltunov et al., 1983). Ensuring of safety and reliability of the truss constructions requires development and application of methods for analysis which take into account as much as possible aspects of their mechanical behaviour under various kinds of external loading (Collins, 1984; Lukash, 1997; Rabotnov, 1992; Zubchaninov, 1990). For instance, there is a variety of problems associated with analysing of truss constructions built-up by using engineering materials with elastic-plastic mechanical behaviour. When such trusses are subjected to cyclic external loadings, damping energy takes place. Thus, analyzing of damping energy in truss constructions is an up-to-date problem that needs special attention.

The present theoretical paper deals with the damping energy problem in trusses with elastic-plastic behaviour under cyclic loading (it should be mentioned that the damping energy analyses in the technical literature are concerned mainly with elastic-plastic beam structures (Collins, 1984; Dowling, 2007; Rizov, 2021). General treatment of the damping energy problem in trusses is presented here. Determination of the damping energy in statically determinate truss constructions of general configuration under arbitrary cyclic load is considered first. The problem of damping energy analysis in statically indeterminate trusses is also treated on general level. Practical applications of the general treatment are given. The damping energy in a particular statically determinate truss configuration is determined. Damping analysis is done also for a statically indeterminate truss having the same geometry and loading as the statically determinate one. Parametric investigation of the damping energy is carried-out to evaluate the influence of various parameters.

- This is an Open Access article distributed under the terms of the Creative Commons Attribution-Noncommercial 4.0 Unported License, permitting all non-commercial use, distribution, and reproduction in any medium, provided the original work is properly cited.

- Selection and peer-review under responsibility of the Organizing Committee of the Conference

© 2023 Published by ISRES Publishing: www.isres.org

Damping Energy Studying

First, the problem of damping energy in statically determinate trusses with elastic-plastic behaviour under cyclic loading will be treated. We assume that the truss under consideration has an arbitrary number of bars. Besides, the bars have individual material properties, length and cross-section. The configuration of the truss is arbitrary. The truss is under cyclic external forces, F_{ai} , about zero mean. All external forces are applied at the joints of the truss. By considering the equilibrium of the joints, the forces, N_{ai} , in the bars of the truss can be written as

$$N_{ai} = \sum_{j=1}^{j=n} \alpha_{ij} F_{aj}, \quad (1)$$

where

$$i = 1, 2, \dots, p. \quad (2)$$

In the above formulas, n is the number of external forces, p is the number of bars. The stresses, σ_{ai} , in the bars are

$$\sigma_{ai} = \frac{N_{ai}}{A_i}, \quad (3)$$

where A_i is the area of the bar cross-section. After calculation of the stresses in the bars, the damping energy, ΔU , in the truss is found as

$$\Delta U = \sum_{i=1}^{i=p} \Delta u_i l_i A_i, \quad (4)$$

where Δu_i is the unit damping energy, l_i is the length of the i -th bar, p is the number of bars. The problem of damping energy in statically indeterminate trusses with elastic-plastic behaviour is treated too. In this case, the forces in the bars of a truss can be expressed as

$$N_{ai} = \sum_{j=1}^{j=n} \alpha_{ij} F_{aj} + \sum_{k=1}^{k=m} \alpha_{ik} X_k, \quad (5)$$

where

$$i = 1, 2, \dots, p. \quad (6)$$

In formula (5), X_k is the k -th hyperstatic unknown, m is the degree of the static indeterminacy of the truss under consideration. In addition to the static equilibrium equations of the truss, m equations can be written by using the theorem of Castigliano to resolve the static indeterminacy. The theorem Castigliano is written as

$$\frac{\partial U^*}{\partial X_k} = 0, \quad (7)$$

where

$$k = 1, 2, \dots, m, \quad (8)$$

In formula (7), U^* is the complementary strain energy (it should be specified here that the complementary strain energy is used since the truss has elastic-plastic behaviour). Formula (9) is applied to derive the complementary strain energy, i.e.

$$U^* = \sum_{i=1}^{i=p} u_{0i}^* l_i A_i , \quad (9)$$

where u_{0i}^* is the unit complementary strain energy. The latter is defined by

$$u_{0i}^* = \sigma_{ai} \varepsilon_{ai} - \int_0^{\varepsilon_{ai}} \sigma_{ai} d\varepsilon_{ai} , \quad (10)$$

where ε_{ai} is the amplitude of the strain. It should be noted that stresses, σ_{ai} , which is involved in (10) is a continuous function of the amplitude of the strain representing the constitutive law, i.e.

$$\sigma_{ai} = \sigma_{ai}(\varepsilon_{ai}) . \quad (11)$$

The equations written by applying (7) can be solved together with the static equilibrium equations by using the MatLab. After determination of forces in the bars, the stresses can be obtained by using dependence (3). Then the damping energy is calculated by (4).

Numerical Results

The general treatment of the damping energy problem in trusses with elastic-plastic behaviour presented in section 2 of this paper is applied here by using the following constitutive law (Dowling, 2007):

$$\varepsilon_{ai} = \frac{\sigma_{ai}}{E_i} + \left(\frac{\sigma_{ai}}{H_i} \right)^{\frac{1}{q_i}} , \quad (12)$$

where E_i is the modulus of elasticity, H_i , and q_i are material properties. The unit damping energies is given by Dowling (2007)

$$\Delta u_i = \frac{4(1 - q_i) \sigma_{ai}^{1 + \frac{1}{q_i}}}{(1 + q_i) (H_i)^{\frac{1}{q_i}}} . \quad (13)$$

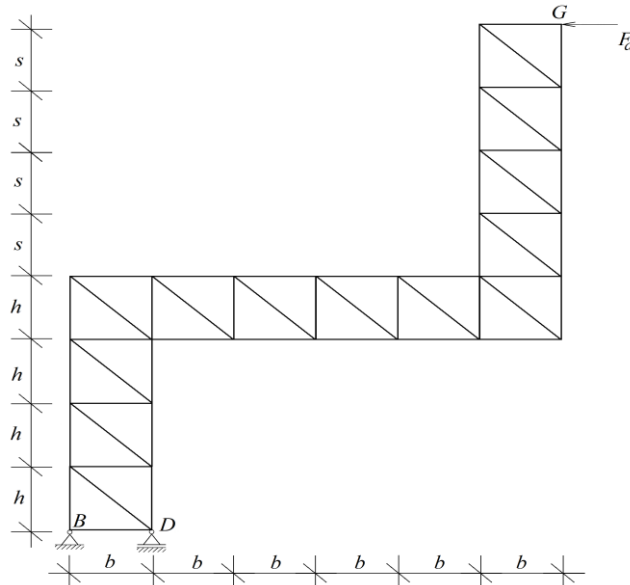


Figure 1. Statically determinate truss.

First, the damping energy in the statically determinate truss configuration shown in Fig. 1 is analyzed.

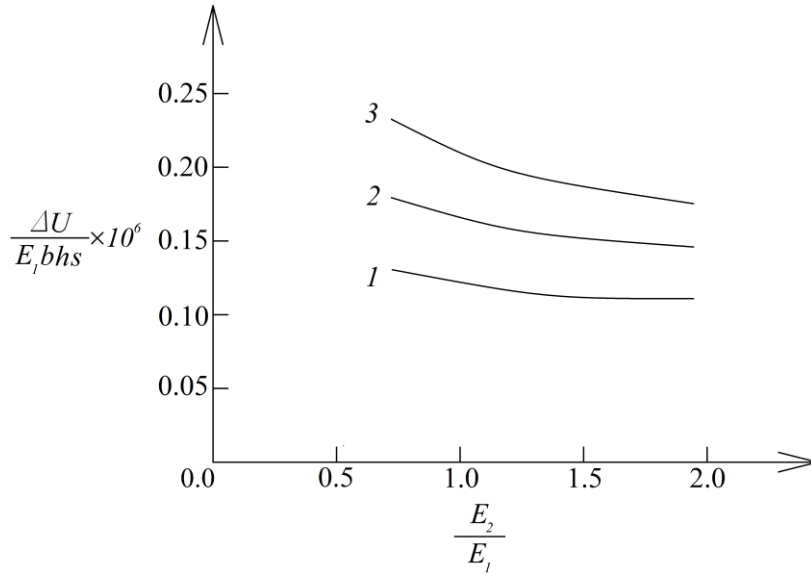


Figure 2. Change of damping energy with varying of E_2 / E_1 ratio (curve 1 – at $F_a = 2$ N, curve 2 – at $F_a = 3$ N and curve 3 – at $F_a = 4$ N).

The truss is restrained in points, B and D , as illustrated in Fig. 1. The external loading on the truss consists of a cyclic horizontal force, F_a , applied in point, G . It is assumed that $h = 3$ m, $s = 5$ m, $b = 2$ m and $F_a = 3$ N. A parametric investigation of the damping energy is carried-out.

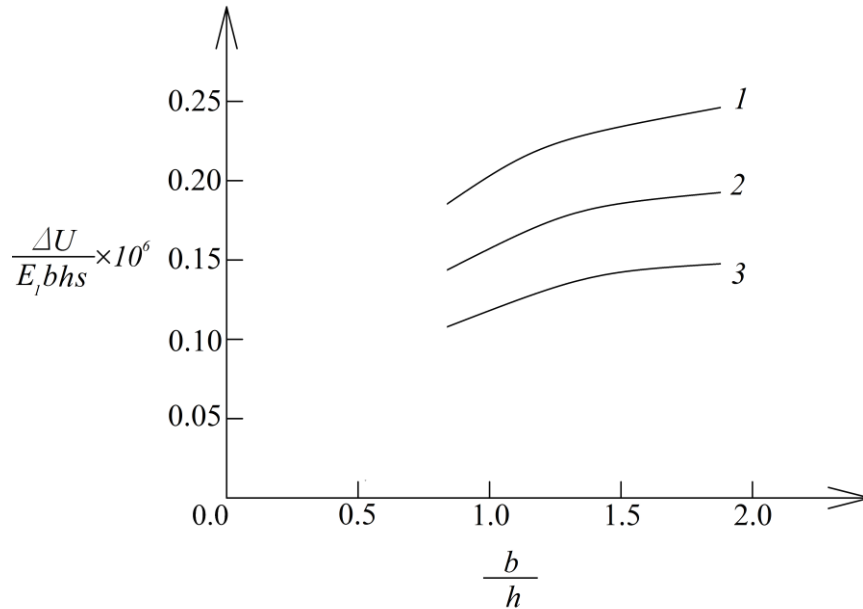


Figure 3. Change of damping energy with varying of b / h ratio (curve 1 – at $H_2 / H_1 = 0.5$, curve 2 – at $H_2 / H_1 = 1.0$ and curve 3 – at $H_2 / H_1 = 2.0$).

The purpose of the investigation is to study the dependence of the damping energy on various parameters of the truss geometry, properties and loading conditions. These dependences are presented in form of graphs in Fig. 2 and Fig. 3. The change of the damping energy with increasing of E_2 / E_1 ratio at three values of F_a is shown in Fig. 2.

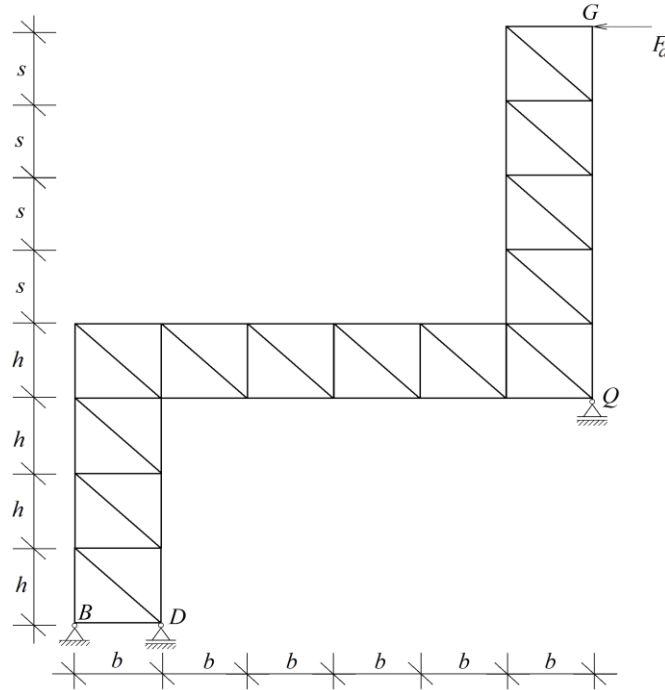


Figure 4. Statically indeterminate truss.

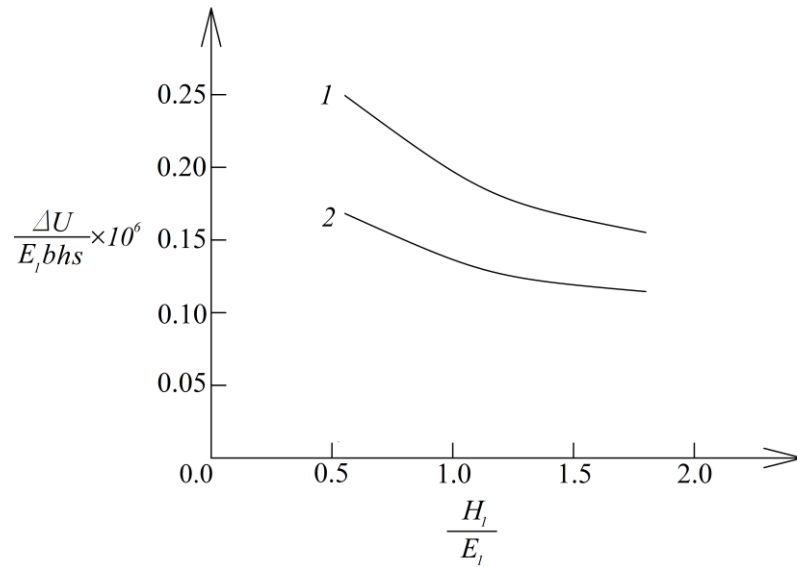


Figure 5. Change of damping energy with varying of H_1 / E_1 ratio (curve 1 – in statically determinate truss and curve 2 – in statically indeterminate truss).

It can be observed in Fig. 2 that the damping energy continuously reduces with increase of E_2 / E_1 ratio. As expected, growth of F_a cause a rise of the damping energy in the truss (Fig. 2). Figure 3 illustrates the dependence of the damping energy in the truss on b/h and H_2 / H_1 ratios. As can be seen, increase of b/h ratio generates growth of the damping energy (Fig. 3). However, increase of H_2 / H_1 ratio generates a substantial reduction of the damping energy as shown in Fig. 3. The damping energy in a truss with one degree of static indeterminacy is also studied. This truss is shown in Fig. 4. The geometry and the loading conditions of this truss are the same as these of the statically determinate truss depicted in Fig. 1. The static indeterminacy of the truss in Fig. 4 is due the roller introduced in point, Q , (actually, this the only difference between truss configurations in Fig. 1 and Fig. 4).

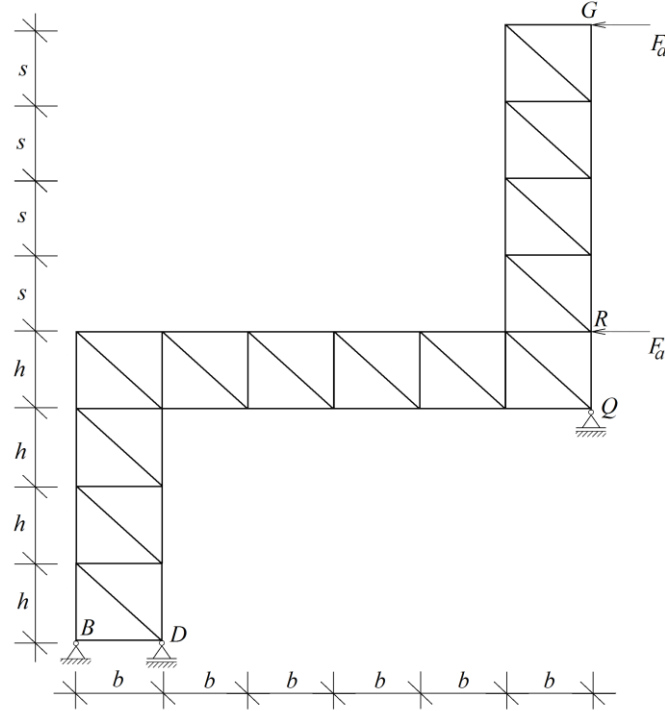


Figure 6. Statically indeterminate truss loaded by two forces.

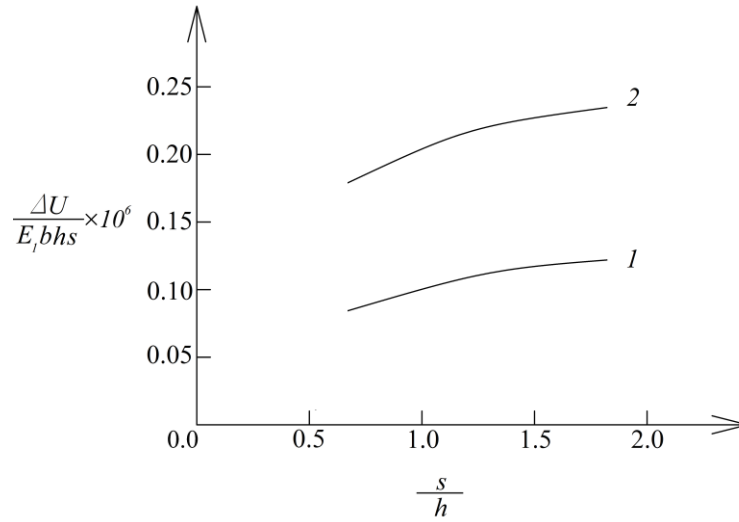


Figure 7. Change of damping energy with varying of s/h ratio (curve 1 – in truss loaded by one force and curve 2 – in truss loaded by two forces).

The change of the damping energy in the statically indeterminate truss with growth of H_1/E_1 ratio is presented in Fig. 5. It can be seen in Fig. 5 that growth of H_1/E_1 ratio induces reduction of the damping energy. The change of the damping energy with growth of H_1/E_1 ratio is shown in Fig. 5 also for the statically determinate truss. The inspection of curves in Fig. 5 indicates that the damping energy in the static indeterminate truss is lower than that in the determinate one. Finally, a damping energy analysis is performed also for the case of a statically indeterminate truss that is loaded by two horizontal forces of value, F_a , applied in points, G and R , as shown in Fig. 6. For this case, the effect of s/h ratio on the damping energy is evaluated. The results are depicted in Fig. 7. As can be seen, rise of s/h ratio generates growth of the damping energy (Fig. 7). The effect of s/h ratio on the damping energy is evaluated also for the statically indeterminate truss loaded only by one horizontal force applied in point, G , and the corresponding curve is depicted in Fig. 7. It can be observed that loading by two forces leads to increase of the damping energy (Fig. 7).

Conclusion

General treatment of the damping energy problem in trusses with elastic-plastic behaviour is presented. The analysis performed indicates that:

- the damping energy reduces with increase of E_2 / E_1 ratio;
- growth of F_a cause a rise of the damping energy;
- increase of b/h and s/h ratios generate growth of the damping energy;
- increase of H_2 / H_1 and H_1 / E_1 ratios generate a substantial reduction of the damping energy;
- the damping energy in the static indeterminate truss is lower than that in the determinate one.

Recommendations

The general treatment of the damping energy problem developed in this paper can be recommended for application in analyses of trusses under cycling loading.

Scientific Ethics Declaration

The author declares that the scientific ethical and legal responsibility of this article published in EPSTEM Journal belongs to the author.

Acknowledgements or Notes

* This article was presented as an oral presentation at the International Conference on Technology (www.icontech.net) held in Antalya/Turkey on November 16-19, 2023.

References

- Aleksandrov, A. V., & Potapov, V. D. (1990). *Theory of elasticity and plasticity*. Vishaya shkola, Moscow.
- Blake, A. (1985). *Handbook of mechanics, materials, and structures*. John Wiley & Sons.
- Collins, J. A. (1984). *Failure of materials in mechanical design*. Mir
- Dowling, N. (2007). *Mechanical behavior of materials*. Pearson.
- Huang, T. C. (1967). *Engineering mechanics*. Addison-Wesley Publishing Company.
- Koltunov, M. A., Kravchuk, A. S., & Maiboroda, V. P. (1983). *Applied solid mechanics*. Vishaya shkola, Moscow.
- Lukash, P. (1997). *Fundamentals of non-linear structural mechanics*. Science.
- Rabotnov, Y. N. (1992). *Resistance of materials*. Science.
- Rizov, V. I. (2021). On the analysis of damping in elastic-plastic inhomogeneous beams. *Materials Science Forum*, 1046, 59-64.
- Varvak, P. (1997). *Strength of materials*. Science.
- Zubchaninov, V. G. (1990). *Theory of elasticity and plasticity*. Vishaya shkola, Moscow.

Author Information

Victor Rizov

University of Architecture

Bulgaria, Sofia

Contact e-mail: V_RIZOV_FHE@UACG.BG

To cite this article:

Rizov, V. (2023). Investigation of damping energy in trusses. *The Eurasia Proceedings of Science, Technology, Engineering & Mathematics (EPSTEM)*, 24, 89-95.

The Eurasia Proceedings of Science, Technology, Engineering & Mathematics (EPSTEM), 2023

Volume 24, Pages 96-100

IConTech 2023: International Conference on Technology

Enhancing Call Center Efficiency: Data Driven Workload Prediction and Workforce Optimization

Muhammet Ali Kadioglu
Dogus Teknoloji R&D Center
Istanbul Technical University

Bilal Alatas
Firat University

Abstract: Organizations can improve customer service quality, reduce wait times, and enhance overall operational efficiency by aligning staffing levels with predicted workload volume. Decision makers in the call centers gain valuable insights and practical guidance from the integration of workload forecasting and workforce optimization. Businesses can effectively utilize their personnel and resources by accurate workload forecasting and workforce optimization. Faster and more profitable services can be provided at customer contact points. It also increases employee satisfaction and enhances the organization's competitive advantage. A tailored solution is essential because every issue has its distinct dynamics. The two-layered pipeline known as "Predict and Optimize" is created by combining ML approaches for forecasting and mathematical programming techniques for optimization. The method offers a comprehensive solution for call center managers seeking to improve resource allocation and boost operational performance. In this study, we have tried to predict future workload levels by training a LSTM model and used integer programming techniques to optimize the allocation of available staff resources according to the forecasted workload. The workforce optimization model generates minimum staffing requirements by considering call center-specific various constraints.

Keywords: Predict and optimize, Time series, Integer programming

Introduction

Workload forecasting and workforce planning are critical for optimizing the operational efficiency of call centers. They are the two main parts of the proposed "Predict and Optimize" approach for call center operations. The effectiveness of the prediction layer can be quantitatively evaluated by comparing the forecasted and actual call volumes. The staffing levels suggested by the optimization model can be used to make predictions as valuable insights. A customized framework for managing data driven projects can greatly enhance innovations within organizations (Kadioglu & Takci, 2022). By operationalizing data science models, organizations can achieve exceptional AI outcomes. Researchers' interest has grown as a result of call centers' expanding role in operations management within the services industry. Most articles in this field focus on large call centers with several hundred connected agents. Chevalier and Schrieck, similar to us, deviate from this trend by focusing specifically on small-size call centers. These call centers may operate in business-to-business (B2B) companies or be part of small-scale business-to-consumer (B2C).

Planning in call centers leverage numerical analysis of queueing models, mathematical modeling, and decision-making based on economic and technical performance measures for improved outcomes (Stolletz, 2003). Workforce management typically begins with the Erlang formula or one of its generalizations (Kooole, 2004). Nag and Helal present a comparative analysis of the Erlang A and Erlang C models for inbound calls. Prior to

this study, research was conducted in a different call center operating within a B2C. Forecasting for incoming and outgoing calls was made using machine learning (ML) models and planning was completed using Erlang C.

Hybrid solutions offer an adaptable approach to planning processes, allowing for better solutions. An approach can be created by a combination of methods and compatibility between the chosen methods is crucial to ensure seamless integration and cohesive functioning. By adapting and integrating these methods, it is possible to construct a high-performance pipeline that effectively utilizes the strengths of each approach. This enables the development of a robust and efficient solution for complex planning problems. The combination of Long Short-Term Memory (LSTM) based workload forecasting, and workforce optimization can provide call center managers with a data-driven approach to make informed decisions, optimize resource allocation, and improve operational performance. An integer program is typically used to solve the problem of choosing staff shifts that meet the requirements (Ertogral & Bamuqabel, 2008). Using real-world call center data, we evaluate the proposed approach and show how well it performs in terms of accurately forecasting workload and allocating the workforce. Operation Research (OR) and Machine Learning (ML) approaches are needed to overcome the limitations of existing methods. Linear programming offers a structured and mathematical foundation for optimization, while deep learning models can extract insights from data and make predictions. Organizations can achieve effective workforce management and better decision-making by combining these approaches.

Literature Review & Model Design

Workload Prediction

The time series prediction techniques can be classified as statistical approaches, ML approaches, and Deep Learning (DL) approaches. The statistical approaches employ the linear prediction structure, and they are widespread forms of predicting workload for stable datasets. In our first research for call center operations, we applied this approach to produce a quick win solution. On the other hand, we need to remember that many datasets are unstable. AutoML can be a substantial starting point in data science projects (Kadioglu, 2022). As well, ML approaches are widely used for workload prediction. So, we have improved our previous solution using ML algorithms. Finally, DL approaches are also applied for workload prediction in recent years. This study uses LSTM as a deep-learning method for workload prediction. According to Gao et al. (2020), they show LSTM can achieve higher accuracy than the Autoregressive method, artificial neural network (ANN), and autoregressive integrated moving average (ARIMA) in load prediction.

Additional information like holidays, promotional activities, and other special events may improve model predictions. These events and occasions often introduce variations and outliers in the data that can significantly influence patterns, trends, and behavior. (Albrecht et al., 2021) By incorporating holiday and event information into the analysis, models can provide more accurate predictions, identify outliers, and capture the nuances of customer behavior during these special periods. This additional context can improve decision-making for call centers.

Workforce Planning

To accurately estimate Customer Service Agent (CSA) requirements based on forecasted incoming call volumes, various mathematical and statistical methods can be employed. Among these, queuing theory, particularly the M/M/c model, also provides valuable insights by modeling the incoming call process. The Erlang C formula stands as a traditional choice, considering factors such as average call duration and time between calls to determine optimal staffing. Kanthanathan et al. (2020) used the Erlang C queuing theory and the forecasted incoming call rate per day to estimate the required number of CSAs per day.

More complex systems may opt for simulations, running numerous iterations to identify a range of outcomes and thus better predict staffing needs. Further granularity can be achieved through workload distribution, breaking down predictions by day and hour to accommodate fluctuating call volumes. Optimization algorithms can also be a highly effective approach for determining the optimal staffing levels in a call center based on projected call volumes. Optimization involves making the best (most profitable or least costly) use of resources under a set of constraints. While each method carries its assumptions and limitations, selecting or combining them based on specific call center attributes can facilitate efficient staffing, minimizing customer wait times and idle agent periods.

In the context of a call center, the objective might be to minimize the total staffing cost or to minimize the customer waiting time, subject to constraints such as the forecasted call volumes, the service rate of the CSAs, and the minimum and maximum number of agents available at any given time. An optimization model for a call center could have variables representing the number of agents working in each time slot, and constraints ensuring that the number of agents working at any time is enough to handle the projected call volume during that period. One of the advantages of using LP for this kind of problem is its flexibility. Optimization models can be easily adjusted to account for different types of shift patterns, different service level requirements, and other operational constraints. In addition, there are many efficient algorithms available for solving optimization problems, so solutions can often be obtained quickly even for large-scale problems.

Practical Implementation

Different forecasting methods can be used to predict the number of calls for short time intervals, such as mean values, exponential smoothing, ARIMA-models, and neural networks (Stolletz, 2003). In this study, we propose a comprehensive approach that combines time series forecasting with optimization techniques for call centers. The workload forecasting component utilizes LSTM, a powerful deep learning model, to capture the temporal patterns and dependencies in historical call volume data. LSTM model has become widely used in the field of DL. This neural network model is particularly well-suited for handling time-series data. By incorporating forget gates and input gates, the model effectively reduces the impact of pathological data, ensuring robust performance and high accuracy in prediction tasks. The LSTM model can efficiently identify long-term dependencies and patterns in sequential data due to its ability to selectively retain or discard information at various time steps.

When investigating prediction methods, two approaches have been identified. The first method, referred to as the "0-gap" prediction method, involves making predictions without any time gap between the input and output. This means that the prediction can be completed prior to the actual occurrence, but it leaves limited time for scheduling tasks before the actual workload appears. To address this limitation, an alternative technique known as the "m-gap" prediction method has been proposed. In the m-gap prediction method, a time window gap of m is introduced between the last time point of the input data and the output time point. This approach allows for workload forecasting to be performed a certain time before the predicted time point, thereby providing much time for task scheduling based on the predicted workload. Gao et al. (2020) presented the m-gap prediction method specifically for workload prediction, emphasizing the importance of leaving sufficient time for task scheduling based on the predicted workload.

Workload Prediction

The dataset used for experimentation was preprocessed. Any missing values were filled with zeros. Min-Max scaling technique was applied to normalize the data. The LSTM model was implemented using the Keras library, following a sequential architecture. It comprised three LSTM layers, each followed by a dropout layer to prevent overfitting. The number of LSTM units in each layer was set to 512, 512, and 256, respectively. The final layer of the model was a dense layer with a number of units corresponding to the prediction period, activated by the Rectified Linear Unit (ReLU) function.

Prior to training the model, the dataset was divided into training and testing sets. For the training set, input sequences (X_{train}) were created by selecting the previous n_{steps} values of all features, while the target variables (y_{train}) for the subsequent period time steps. Similarly, the testing set was constructed. The LSTM model was trained using the Adam optimizer with a custom learning rate of 0.001, optimizing the mean squared error (MSE) loss function. The training process was conducted for a total of 10 epochs, with a batch size of 64. Once the model was trained, it was evaluated using the testing data, and the loss value was computed and reported. Finally, the model was employed to generate predictions for the upcoming week using the testing data (X_{test}), with the predicted values stored in the prediction's variable.

Workforce Planning

Determining the number and types of agents who will be handling calls and their work schedules is one of the main optimization challenges that must be overcome to manage call centers. This task must adhere to restrictions on acceptable schedules and service quality (Buist et al., 2008). In our case, there is a single group of

agents that can serve all inbound calls. The call center operates dialogue management, roadside assistance, operational services. We present the staffing problem for a single-skill call center. The objective is to minimize operating costs. The objective function represents the total number of agents required. When the assignments' time slots are defined, the day is divided into hourly periods. Our model can easily handle additional constraints as needed.

In the second phase, the LSTM model's predictions for the number of inbound calls and AHT have been integrated into an optimization framework. The predictions for inbound calls and AHT have been assigned as inputs in the optimization model. This framework, implemented using the Pyomo library, aimed to determine the minimum number of agents required to handle the projected workload. Decision variables are defined to represent the number of agents assigned to each hour and day. The objective function is to minimize the total number of assigned agents.

A constraint was formulated by comparing the predicted call volume with the maximum call load an agent could handle within a given hour. Additionally, a constraint was imposed to ensure that at least one agent was assigned to each hour, guaranteeing the presence of an agent to handle the workload. The optimization problem was solved using the GLPK solver, which searched for the optimal solution that minimized the total number of assigned agents while satisfying the constraints. Upon successful optimization, the minimum agent requirements were determined for each hour and day. These results provided valuable insights into resource allocation, facilitating effective scheduling and management decisions within the call center.

Findings & Conclusion

While our approach demonstrates significant improvements in both forecasting accuracy and operational efficiency, the complexity of LSTM models and the need for sufficient historical data may limit its application in smaller or newer call centers. Further research could explore methods for streamlining the LSTM training process or for incorporating other types of data into the workload forecasting model. On the other hand, Pot et al. (2008) addressed the staffing issue in multiskilling call centers, focusing on the labor allocation process. Buist et al. (2008) discussed the problems of optimizing staffing and scheduling in large multiskilling call centers. Their key contribution lies in developing a staffing method that enables the creation of schedules in multiskilling call centers, ensuring a reasonable alignment between projected workload and available labor capacity. Additional constraints to the optimization model can be incorporated.

The obtained MSE and MAE values suggest that the LSTM model performed reasonably well in capturing the underlying patterns and trends in the time series data, yielding predictions that were relatively close to the true values. Upon evaluating the LSTM model's performance on the testing data, we computed the Mean Squared Error (MSE) and Mean Absolute Error (MAE) metrics to assess the accuracy of the predictions. The MSE value was found to be 96.4373, indicating the average squared difference between the predicted and actual values. MAE value, on the other hand, was 6.6996, representing the average absolute difference between the predicted and actual values.

The LSTM model was also executed to predict the AHT, and the evaluation metrics for this specific prediction task were computed. MSE was found to be 312.3277, indicating the average squared difference between the predicted and actual AHT values. Additionally, the Mean Absolute Error (MAE) was determined as 13.9535, representing the average absolute difference between the predicted and actual AHT values. These evaluation metrics shed light on the performance of the LSTM model in predicting the AHT. The integration of the LSTM model predictions into the optimization framework provides informed staffing decisions. By incorporating the forecasted call volume and AHT, the model optimized agent assignments to ensure that service levels were met while minimizing operating costs.

Scientific Ethics Declaration

The authors declare that the scientific ethical and legal responsibility of this article published in EPSTEM journal belongs to the authors.

Acknowledgements or Notes

* This article was presented as an oral presentation at the International Conference on Technology (www.icontechno.net) held in Antalya/Turkey on November 16-19, 2023.

References

- Albrecht, T., Rausch, T. M., & Derra, N. D. (2021). Call me maybe: Methods and practical implementation of artificial intelligence in call center arrivals' forecasting. *Journal of Business Research*, 123, 267-278.
- Buist, E., Chan, W., & L'Ecuyer, P. (2008). Speeding up call center simulation and optimization by Markov chain uniformization. *2008 Winter Simulation Conference*.
- Chevalier, P., & Van den Schrieck, J. C. (2008). Optimizing the staffing and routing of small-size hierarchical call centers. *Production and Operations Management*, 17(3), 306–319.
- Ertogral, K., & Bamuqabel, B. (2008). Developing staff schedules for a bilingual telecommunication call center with flexible workers. *Computers & Industrial Engineering*, 54(1), 118–127.
- Gao, J., Wang, H., & Shen, H. (2020). Machine learning based workload prediction in cloud computing. *2020 29th International Conference on Computer Communications and Networks (ICCCN)*.
- Kadioglu, M. A. (2022). End-to-end AutoML implementation framework. *The Eurasia Proceedings of Science Technology Engineering and Mathematics*, 19, 35-40.
- Kadioglu, M. A., & Takci, H. (2022). *A data science project management methodology: From development to production* (p.2). Proceedings Book.
- Kanthanathan, C., Carty, G., Raja, M. A., & Ryan, C. (2020). Recurrent neural network based automated workload forecasting in a contact center. In *2020 3rd International Conference on Intelligent Sustainable Systems (ICISS)* (pp. 1423-1428). IEEE.
- Koole, G. (2004). Performance analysis and optimization in customer contact centers. *First International Conference on the Quantitative Evaluation of Systems, 2004. QEST 2004*.
- Nag, K., & Helal, M. (2017). Evaluating erlang C and erlang A models for staff optimization: A case study in an airline call center. In *2017 IEEE International Conference on Industrial Engineering and Engineering Management (IEEM)*.
- Pot, A., Bhulai, S., & Koole, G. (2008). A simple staffing method for multiskill call centers. *Manufacturing & Service Operations Management*, 10(3), 421-428.
- Stolletz, R. (2003). *Performance analysis and optimization of inbound call centers*. Springer Science & Business Media.
- Ta, T., l'Ecuyer, P., & Bastin, F. (2016). Staffing optimization with chance constraints for emergency call centers. In *MOSIM 2016-11th International Conference on Modeling, Optimization and Simulation*.

Author Information

Muhammet Ali Kadioglu

Dogus Teknoloji R&D Center

Istanbul Technical University

Istanbul, Turkey

Contact e-mail: kadioglumuhammetali@gmail.com

Bilal Alatas

Firat University

Elazig, Turkey

To cite this article:

Kadioglu, M.A. & Alatas, B. (2023). Enhancing call center efficiency: Data driven workload prediction and workforce optimization. *The Eurasia Proceedings of Science, Technology, Engineering & Mathematics (EPSTEM)*, 24, 96-100.

The Eurasia Proceedings of Science, Technology, Engineering & Mathematics (EPSTEM), 2023

Volume 24, Pages 101-109

IConTech 2023: International Conference on Technology

PV Supplied Electrochemical Production of Hydrogen Peroxide: A Green Pathway for Fenton Based Advanced Oxidation Processes

Kaouthar Kerboua

National Higher School of Technology and Engineering

Abstract: Hydrogen peroxide is the common reagent of the Fenton Based advanced oxidation processes, it is generally added in stoichiometric yields to the Fenton catalyst (Ferrous or ferric ions) to produce hydroxyl radicals. In the present study, a green technique for the in-situ production of hydrogen peroxide is examined numerically, using modelling and simulation, based on PV supplied electrochemical process and carbon-based electrodes. The PV supply model is based on Maximum Power Point Tracking using ET-Solar M53640 panel, while the modelling of the performance of the electrochemical cell is based on an electrical equivalent schema of activation, ohmic, and concentration resistances. Two production pathways of hydrogen peroxide under acidic conditions are considered, namely the reduction of O_2 and the oxidation of H_2O . The performed simulations under 3 scenarios of solar radiation (low, middle and high) demonstrated that 300 W/m^2 of incident global radiation results in 0.35 A of feeding current, against 0.88 A under 600 W/m^2 and 1.41 A under 900 W/m^2 . Simulations for hydrogen peroxide production under the three scenarios have been compared based on the O_2 reduction pathway, which is proved to be more performant, especially with the lower H_2O_2 cathodic decomposition.

Keywords: Simulation, PV supply, Fenton, Hydrogen peroxide, Model, Production.

Introduction

Advanced oxidation processes AOPs are nowadays recognized as the key solution for the tertiary treatment of wastewater, aiming at eliminating the recalcitrant pollutant from liquid effluents. The integration of AOPs as tertiary treatment techniques in the autonomous stations of onsite treatment of wastewater for irrigation is expected to be the future solution for providing safe and sufficient quantities of water to smallholding farmers adapted to all the type of cultures, particularly in lockdown areas. The efficiency of AOPs is related to the non-selective and highly reactive $\bullet OH$ radicals (Haag, 1992), which are chemical species of great interest in terms of degradation of organic pollutants and recalcitrant contaminants in aqueous solutions (Madhavan et al., 2010; Pawar & Gawande, 2015). Fenton-based techniques are ones of the most important classes of AOPs which use the decomposition of hydrogen peroxide in the presence of ferrous ions to produce hydroxyl radicals, while $Fe(II)$ oxidizes to $Fe(III)$. However, these processes require a stoichiometric amount of hydrogen peroxide and the catalyst, $Fe(II)$ (Andreozzi et al., 2000). $Fe(III)$ is expected to regenerate $Fe(II)$ through the reaction with hydrogen peroxide. However, this reaction is known to be very slow, owing to the formation of intermediate non-radical species such as $Fe(HO_2)^{2+}$. Consequently, the Fenton process needs high amounts of Fenton's reagent to generate a high enough quantity of $HO\bullet$.

The present paper suggests a solar based technique for the in-situ production of hydrogen peroxide, in parallel to the in-situ production of Fenton's catalyst using the Galvano-Fenton technique. The integrated process is composed of an electrochemical cell supplied by a PV solar panel, and of carbon-based cathode and nickel anode, and a galvanic cell made of iron waste based anode and copper cathode. The process is modelled numerically from the solar supply to the chemical kinetics of Fenton's reaction initiated by the in situ produced

hydrogen peroxide and ferrous ions. The simulations are performed considering three scenarios of global solar radiation, namely 300, 600 and 900 W/m²

Method

Configuration of the Process and Numerical Model

The modelled process is a combination of a PV supplied electrochemical cell for hydrogen peroxide production in acidic conditions, and a Galvanic cell for the spontaneous production of ferrous iron, as described in Fig.1. The electrochemical cell is designed using carbon based cathode and nickel anode, while the galvanic cell couples a sacrificial anode made of iron waste and a cathode of copper. Both cells are immersed within an acidic electrolyte that consists of an aqueous solution of sulfuric acid at pH 3. This pH allows the formation of ferrous ions according to the Pourbaix diagram, and favors the cathodic reduction of oxygen in the presence of hydrogen ions. Both reactions are shown respectively in Eqs.1 and 2.



In order to ensure a sufficient yield of oxygen at the cathode of the electrochemical cell, pure oxygen is continuously pumped into the electrolyte, the electrolyte is then permanently saturated with oxygen, whose concentration is described by the below Eq.3 (Tromans, 1998).

$$\begin{aligned} c_{\text{O}_2} & \\ = P_{\text{O}_2} &\left(\frac{0.046 T^2 + 203.357 T \ln \left(\frac{T}{298} \right) - (299.378 + 0.092T)(T - 298) - 20.591 \times 10^3}{8.3144 T} \right) \end{aligned} \quad (3)$$

The parallel cathodic reactions of decomposition of the formed hydrogen peroxide, that may occur at the cathode, and described in Eqs.4 and 5 (Lim & Hoffmann, 2019), are limited by the carbon based material used as a cathode in the electrochemical cell.



The possible reactions of formation or decomposition of hydrogen peroxide at the anode of the electrochemical cell are considered as very limited in acidic conditions, thus, the only pathway considered in the present paper in the cathodic one described earlier.

The electrochemical cell is energetically supplied by a continuous current provided by a PV solar panel ET-Solar M53640 connected to a maximum power point tracker MPPT. The current I produced from the PV generator can be given by the Eq.6 (Villalva et al., 2009).

$$I = I_{pv} - I_d - I_{sh} \quad (6)$$

Where I_{pv} is the light-generated current of the PV cell I_d and I_{sh} are the current of the diode and current crossing shunt resistance, respectively (Rahim et al. 2015; Villalva, Gazoli, and Filho 2009). These parameters can be expressed through Eqs. 7, 8 and 9 (Rahim et al. 2015; Villalva et al., 2009):

$$I_{pv} = \frac{(I_{pv0} + K_I \Delta T)G}{G_0} \quad (7)$$

$$I_d = I_0 \left(\exp \left(\frac{R_s I + V}{V_t a} \right) - 1 \right) \quad (8)$$

$$I_{sh} = \frac{V + R_s I}{R_p} \quad (9)$$

I_0 and ΔT are the diode saturation current and the variation in temperature at real and standard conditions that are given according Eqs. 10 and 11 (Villalva et al., 2009):

$$I_0 = \frac{I_{sc,n} + K_I \Delta T}{\exp\left(\frac{V_{ocn} + K_V \Delta T}{aV_t}\right) - 1} \quad (10)$$

$$\Delta T = T_p - T_n \quad (11)$$

Where V_{ocn} , K_I and K_V are the nominal open circuit voltage, current and voltage coefficient %/°C respectively. $I_{sc,n}$ is the nominal short circuit current and V_{tn} presents the thermal voltage at standard temperature and is given by Mohamed et al. (2016) in function of Boltzmann constant K_B , the charge of the electron q and the temperature at standard conditions T_n , as indicated in Eq.12.

$$V_{tn} = \frac{K_B T_n}{q} \quad (12)$$

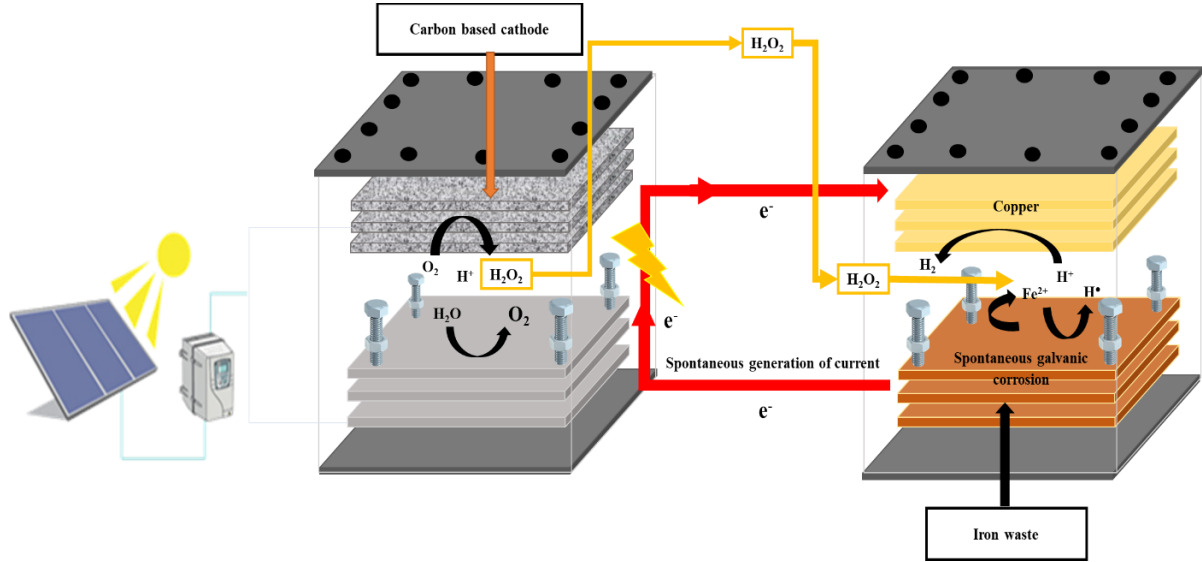


Figure 1. Galvanic cell for the spontaneous production of ferrous iron

Table 1. Specifications of the PV supplied electro-Galvano-Fenton process

	Parameter	Specification
Galvanic cell	Electrodes form	rectangular smooth plates
	Anode surface	12 cm ²
	Cathode surface	12 cm ²
	Anode material	Iron waste
	Cathode material	Copper
Electrolyte	Electrodes disposition	In parallel
	Electrolyte nature	Acidified water (H ₂ SO ₄)
	Electrolyte volume	300 mL
	pH	3
	Electrical connection	External wire
Electrochemical cell	Ionic displacement	Aided by a magnetic stirring
	Initial concentration of hydrogen peroxide	0
	Cathode material	Carbon-based
	Anode material	Nickel
	Electrodes disposition	Parallel

In the Galvanic cell, the spontaneous corrosion of iron occurs under the effect of the higher redox potential of the couple (Cu²⁺/Cu) constituting the cathode. The process is simulated considering a corrosion current of 300 μ A, determined experimentally using a zero ammeter placed between both electrodes of the galvanic cell described in Table.1. The polarization curves have been also plotted using a galvanostat-potentiostat connected to the same cell, the corrosion current has been confirmed by this method as well, through the intersection of both Tafel's lines.

The current value is equivalent to a current density of 25 $\mu\text{A}/\text{cm}^2$ reported to the active surface of the anode of 12 cm^2 . The Galvano-Fenton system is modeled by combining electrochemical reactions taking place at the anode and the cathode with chemical reactions related to the Fenton mechanism occurring in the bulk liquid volume. Table. 2 describes the whole evolution of the reactions occurring at the electrodes and in the electrolyte.

Table 2. Electrochemical and chemical scheme of the possible reactions occurring at the electrodes and in the electrolyte by the integrated electrochemical and galvanic cells; k_i is the absolute reaction constant of the i^{th} reaction. Adapted from electrolyte by the Sono-Galvano Fenton-based processes. k_j is the absolute reaction constant of the j^{th} reaction. Adapted from Bray (1931) and Kopřivanac & Lonč (2006) and De Laat & Le 2006 and Machulek et al. (2009).

	i	i^{th} Reaction	k_i	Unit of k_i
Anode GC	1	$\text{Fe} \rightarrow \text{Fe}^{2+} + 2e^-$	-	-
Cathode GC	2	$2\text{H}^+ + 2e^- \rightarrow \text{H}_2$	-	-
Anode EC	3	$\text{O}_2 + 2\text{H}^+ + 2e^- \rightarrow \text{H}_2\text{O}_2$	-	-
	4	$\text{Fe}^{2+} + \text{H}_2\text{O}_2 \rightarrow \text{Fe}^{3+} + \text{OH}^- + \text{HO}^\bullet$	6.3×10^{-2}	$\text{mol}^{-1} \cdot \text{m}^3 \cdot \text{s}^{-1}$
	5	$\text{Fe}^{3+} + \text{H}_2\text{O}_2 \rightarrow \text{Fe}(\text{HO}_2)^{2+} + \text{H}^+$	3.1×10^4	$\text{mol}^{-1} \cdot \text{m}^3 \cdot \text{s}^{-1}$
	6	$\text{Fe}(\text{HO}_2)^{2+} + \text{H}^+ \rightarrow \text{Fe}^{3+} + \text{H}_2\text{O}_2$	1.0×10^7	$\text{mol}^{-1} \cdot \text{m}^3 \cdot \text{s}^{-1}$
	7	$\text{Fe}(\text{HO}_2)^{2+} \rightarrow \text{Fe}^{2+} + \text{HO}_2^\bullet$	2.3×10^{-3}	s^{-1}
	8	$\text{H}_2\text{O}_2 + \text{HO}^\bullet \rightarrow \text{HO}_2^\bullet + \text{H}_2\text{O}$	3.3×10^4	$\text{mol}^{-1} \cdot \text{m}^3 \cdot \text{s}^{-1}$
	9	$\text{HO}_2^\bullet \rightarrow \text{O}_2^{\bullet-} + \text{H}^+$	1.58×10^5	s^{-1}
	10	$\text{O}_2^{\bullet-} + \text{H}^+ \rightarrow \text{HO}_2^\bullet$	1.0×10^7	$\text{mol}^{-1} \cdot \text{m}^3 \cdot \text{s}^{-1}$
	11	$\text{Fe}^{2+} + \text{HO}^\bullet \rightarrow \text{Fe}^{3+} + \text{OH}^-$	3.2×10^5	$\text{mol}^{-1} \cdot \text{m}^3 \cdot \text{s}^{-1}$
	12	$\text{HO}_2^\bullet + \text{Fe}^{2+} + \text{H}_2\text{O} \rightarrow \text{Fe}^{3+} + \text{H}_2\text{O}_2 + \text{OH}^-$	1.2×10^3	$\text{mol}^{-1} \cdot \text{m}^3 \cdot \text{s}^{-1}$
	13	$\text{HO}_2^\bullet + \text{Fe}^{3+} \rightarrow \text{Fe}^{2+} + \text{H}^+ + \text{O}_2$	3.6×10^2	$\text{mol}^{-1} \cdot \text{m}^3 \cdot \text{s}^{-1}$
	14	$\text{O}_2^{\bullet-} + \text{Fe}^{2+} + 2\text{H}_2\text{O} \rightarrow \text{Fe}^{3+} + \text{H}_2\text{O}_2 + 2\text{OH}^-$	1.0×10^4	$\text{mol}^{-1} \cdot \text{m}^3 \cdot \text{s}^{-1}$
	15	$\text{O}_2^{\bullet-} + \text{Fe}^{3+} \rightarrow \text{Fe}^{2+} + \text{O}_2$	5.0×10^4	$\text{mol}^{-1} \cdot \text{m}^3 \cdot \text{s}^{-1}$
	16	$\text{HO}^\bullet + \text{HO}^\bullet \rightarrow \text{H}_2\text{O}_2$	5.2×10^6	$\text{mol}^{-1} \cdot \text{m}^3 \cdot \text{s}^{-1}$
	17	$\text{HO}_2^\bullet + \text{HO}_2^\bullet \rightarrow \text{H}_2\text{O}_2 + \text{O}_2$	8.3×10^2	$\text{mol}^{-1} \cdot \text{m}^3 \cdot \text{s}^{-1}$
	18	$\text{O}_2^{\bullet-} + \text{H}^+ \rightarrow \text{HO}_2^\bullet$	1.0×10^7	$\text{mol}^{-1} \cdot \text{m}^3 \cdot \text{s}^{-1}$
	19	$\text{HO}^\bullet + \text{HO}_2^\bullet \rightarrow \text{O}_2 + \text{H}_2\text{O}$	7.1×10^6	$\text{mol}^{-1} \cdot \text{m}^3 \cdot \text{s}^{-1}$
	20	$\text{HO}^\bullet + \text{O}_2^{\bullet-} \rightarrow \text{O}_2 + \text{OH}^-$	1.01×10^7	$\text{mol}^{-1} \cdot \text{m}^3 \cdot \text{s}^{-1}$
Electrolyte	21	$\text{HO}_2^\bullet + \text{O}_2^{\bullet-} + \text{H}_2\text{O} \rightarrow \text{H}_2\text{O}_2 + \text{O}_2 + \text{OH}^-$	9.7×10^4	$\text{mol}^{-1} \cdot \text{m}^3 \cdot \text{s}^{-1}$
	22	$\text{HO}_2^\bullet + \text{H}_2\text{O}_2 \rightarrow \text{O}_2 + \text{HO}^\bullet + \text{H}_2\text{O}$	5.0×10^{-4}	$\text{mol}^{-1} \cdot \text{m}^3 \cdot \text{s}^{-1}$
	23	$\text{O}_2^{\bullet-} + \text{H}_2\text{O}_2 \rightarrow \text{O}_2 + \text{HO}^\bullet + \text{OH}^-$	1.3×10^{-4}	$\text{mol}^{-1} \cdot \text{m}^3 \cdot \text{s}^{-1}$
	24	$\text{Fe}^{2+} + \text{SO}_4^{2-} \rightarrow \text{FeSO}_4$	2.29×10^8	$\text{mol}^{-1} \cdot \text{m}^3 \cdot \text{s}^{-1}$
	25	$\text{SO}_4^{2-} + \text{HO}^\bullet \rightarrow \text{SO}_4^{\bullet-} + \text{OH}^-$	1.4×10^4	$\text{mol}^{-1} \cdot \text{m}^3 \cdot \text{s}^{-1}$
	26	$\text{HSO}_4^- + \text{HO}^\bullet \rightarrow \text{SO}_4^{\bullet-} + \text{H}_2\text{O}$	3.5×10^2	$\text{mol}^{-1} \cdot \text{m}^3 \cdot \text{s}^{-1}$
	27	$\text{SO}_4^{\bullet-} + \text{H}_2\text{O} \rightarrow \text{H}^+ + \text{SO}_4^{2-} + \text{HO}^\bullet$	3.0×10^5	s^{-1}
	28	$\text{SO}_4^{\bullet-} + \text{OH}^- \rightarrow \text{SO}_4^{2-} + \text{HO}^\bullet$	1.4×10^4	$\text{mol}^{-1} \cdot \text{m}^3 \cdot \text{s}^{-1}$
	29	$\text{SO}_4^{\bullet-} + \text{H}_2\text{O}_2 \rightarrow \text{SO}_4^{2-} + \text{H}^+ + \text{HO}_2^\bullet$	1.2×10^4	$\text{mol}^{-1} \cdot \text{m}^3 \cdot \text{s}^{-1}$
	30	$\text{SO}_4^{\bullet-} + \text{HO}_2^\bullet \rightarrow \text{SO}_4^{2-} + \text{H}^+ + \text{O}_2$	3.5×10^6	$\text{mol}^{-1} \cdot \text{m}^3 \cdot \text{s}^{-1}$
	31	$\text{SO}_4^{\bullet-} + \text{Fe}^{2+} \rightarrow \text{Fe}^{3+} + \text{SO}_4^{2-}$	3.0×10^5	$\text{mol}^{-1} \cdot \text{m}^3 \cdot \text{s}^{-1}$
	32	$\text{FeSO}_4 \rightarrow \text{Fe}^{2+} + \text{SO}_4^{2-}$	1.0×10^{10}	s^{-1}
	33	$\text{Fe}^{3+} + \text{H}_2\text{O} \rightarrow \text{FeOH}^{2+} + \text{H}^+$	2.9×10^7	s^{-1}
	34	$\text{FeOH}^{2+} + \text{H}^+ \rightarrow \text{Fe}^{3+} + \text{H}_2\text{O}$	1.0×10^7	$\text{mol}^{-1} \cdot \text{m}^3 \cdot \text{s}^{-1}$
	35	$\text{FeOH}^{2+} + \text{H}_2\text{O}_2 \rightarrow \text{Fe}(\text{OH})\text{HO}_2^+ + \text{H}^+$	2.0×10^3	$\text{mol}^{-1} \cdot \text{m}^3 \cdot \text{s}^{-1}$
	36	$\text{Fe}(\text{OH})\text{HO}_2^+ + \text{H}^+ \rightarrow \text{FeOH}^{2+} + \text{H}_2\text{O}_2$	1.0×10^7	$\text{mol}^{-1} \cdot \text{m}^3 \cdot \text{s}^{-1}$
	37	$\text{Fe}(\text{OH})\text{HO}_2^+ \rightarrow \text{Fe}^{2+} + \text{HO}_2^\bullet + \text{OH}^-$	2.3×10^{-3}	s^{-1}

Iron constitutes the sacrificial electrode in the galvanic cell, Fe oxidizes to Fe^{2+} ($E^0 = -0.44$ V vs. SHE) according to Equation 1, in Table.2. While at the cathode, the most probable reaction concerns the reduction of H^+ to form H_2 ($E^0 = 0$ V vs. SHE) according to Eq.2 in Table.2, owing to the acidity of the medium. This has been proven in a previous work conducted by our research group (Gasmi et al., 2020). The kinetics related to all of the electrochemical reactions are governed by Faraday's law (Ahmad, 2006), given in Eq.13, and describe the evolution of the C_k concentration of the species involved in the electrochemical reactions in a function of time.

$$\frac{dC_k}{dt} = \pm \frac{i_{\text{corr}}}{nFV} \quad (13)$$

n represents the valence number; it equals 2 for reaction 1 and 1 for reaction 2. F is Faraday's number, which equals 96,490 C/mol. i_{corr} represents the corrosion current, while V constitutes the volume of the electrolyte.

The chemical kinetic equations describing the evolution of the chemical mechanism occurring in the electrolyte are set based on the kinetics constant reported in previous table. Each reaction can be schematized according to Eq.14

$$\sum_{k=1}^K v'_{ki} X_k \rightarrow \sum_{k=1}^K v''_{ki} X_k \quad (14)$$

v'_{ki} is the stoichiometric coefficient related to the k th species X_k within the i th chemical reaction. The kinetics rate related to the i^{th} reaction is expressed as reported in Eq.15.

$$r_i = k_i \prod_{k=1}^K [C_k]^{\theta'_{ki}} \quad (15)$$

k_i is the kinetic constant related to the i^{th} reaction occurring in the electrolyte as reported in Table 2 and is determined at the operating temperature of 25 °C in the present study. The kinetics of apparition and the disappearance of a species X_k in the electrolyte is governed by Eq.16 for species involved in the electrochemical reactions:

$$\frac{d[X_k]}{dt} = \pm \frac{1}{nV} \frac{i_{corr}}{F} + \sum_{i=1}^N (v''_{ki} - v'_{ki}) k_i \prod_{j=1}^K [X_j]^{\theta'_{ji}} \quad (16)$$

While Eq.17 is applicable to species that are only implicated in the electrolytic reactions (Davis and Davis 2003).

$$\frac{d[X_k]}{dt} = \sum_{i=1}^N (v''_{ki} - v'_{ki}) k_i \prod_{j=1}^K [X_j]^{\theta'_{ji}} \quad (17)$$

The system of non-linear differential equations is resolved using the fourth-order Runge–Kutta algorithm with the function Ode 23s on Matlab with a fixed step of 1 s. The simulation is performed over 1500 s.

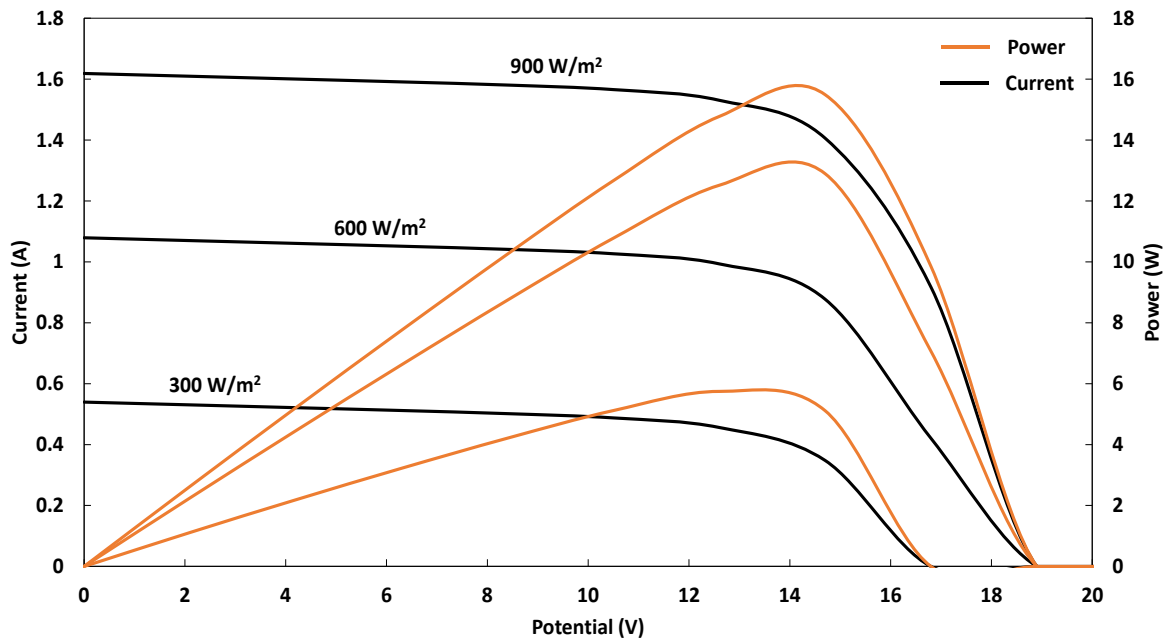


Figure 2. Simulated polarization curves of the ET-Solar M53640 panel

Results and Discussion

Performance of the PV Supply

The polarization curves of the studied solar panel have been simulated under three assumptions if incident global solar radiation, namely 300, 600 and 900 W/m². The highest values of deliverable power have been identified on the curves of the power vs. potential shown in Fig.2, they vary from 4.11 to 15.49 W when the solar radiation is increased from 300 to 900 W/m². The corresponding values of delivered current are then deduced from the curves of current vs. potential reported in the same figure, these values represent the feeding current of the electrochemical cell delivered by the MPPT regulator. The feeding current equals 0.35 A under 300 W/m², 0.88 A under 600 W/m² and finally 1.41 A under 900 W/m². These values are used in the model simulating the performance of the integrated process under the three studied situations.

Kinetics of Hydrogen Peroxide

The electrochemical in situ production of hydrogen peroxide is simulated according to the previous results and kinetics of hydrogen peroxide is reported in Fig.3 under the three scenarios of incident global solar radiation. As expected, the figure shows that the highest solar radiation leads to the highest production of hydrogen peroxide. A fraction of the produced hydrogen peroxide decomposes in the presence of ferrous ion, also produced in situ through the galvanic corrosion occurring in the integrated galvanic cell, Fig.3 depicts the evolution of the concentration of hydrogen peroxide as the result of the simultaneous in situ production and consumption in the Fenton reaction. After 1500 s, we can observe that the concentration of hydrogen peroxide attains 36.08 mol/m³ under the highest solar radiation, i.e., 900 W/m². It equals 22.15 mol/m³ under 600 W/m² and 8.69 mol/m³ under 300 W/m². The availability of hydrogen peroxide in the solution reveals that the electrochemical technique produces in excess the Fenton's reagent, which is not actually in stoichiometric yields with the produced Fenton catalyst, suggesting to create parallel galvanic cells in order to augment the molar yield of ferrous ions and consume rapidly the produced hydrogen peroxide. This will be verified later in the section related to ferrous and ferric ions.

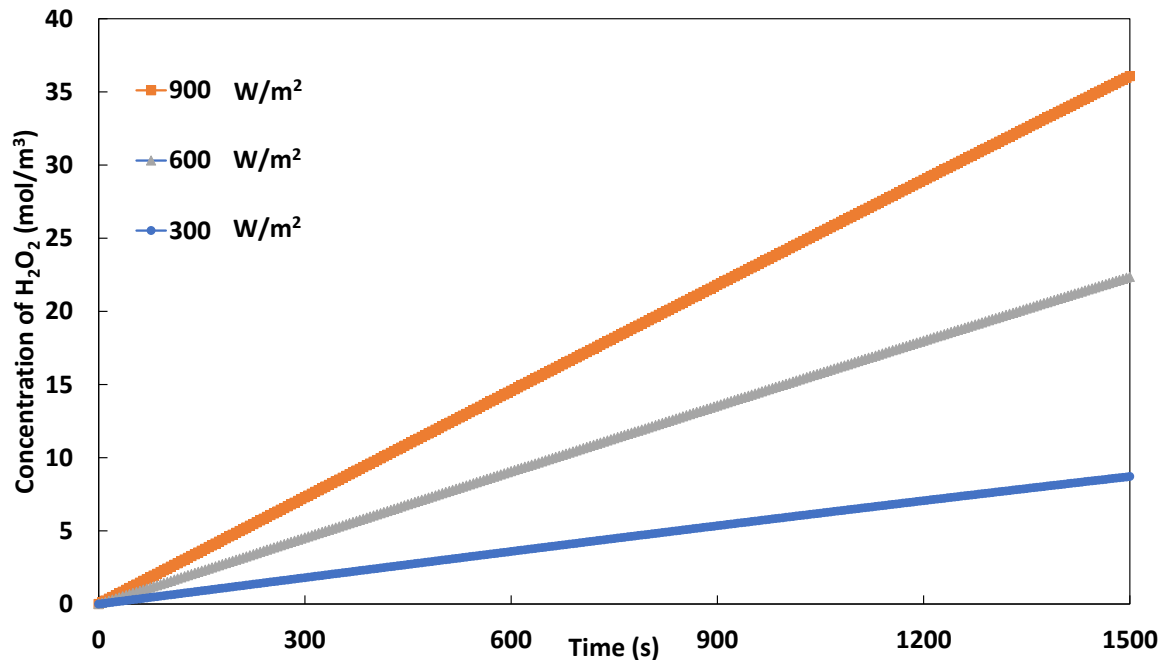


Figure 3. Evolutions of H₂O₂ concentration as a function of time under the different solar radiations

Kinetics of Ferrous and Ferric Ions

The simulated concentrations of ferrous and ferric ions are reported as function of time in Fig.4, according to the mechanism described in Table.2. interestingly, the highest solar radiation leads to the lowest concentrations of ferrous ions, revealing an important reactivity when hydrogen peroxide is available in higher molar yields. This

is verified with both other scenarios. However, the concentration of ferric ions does not follow the same trend, the values are almost the same with the three scenarios. This observation is probably explained by the slow regeneration of ferrous ions from ferric ions.

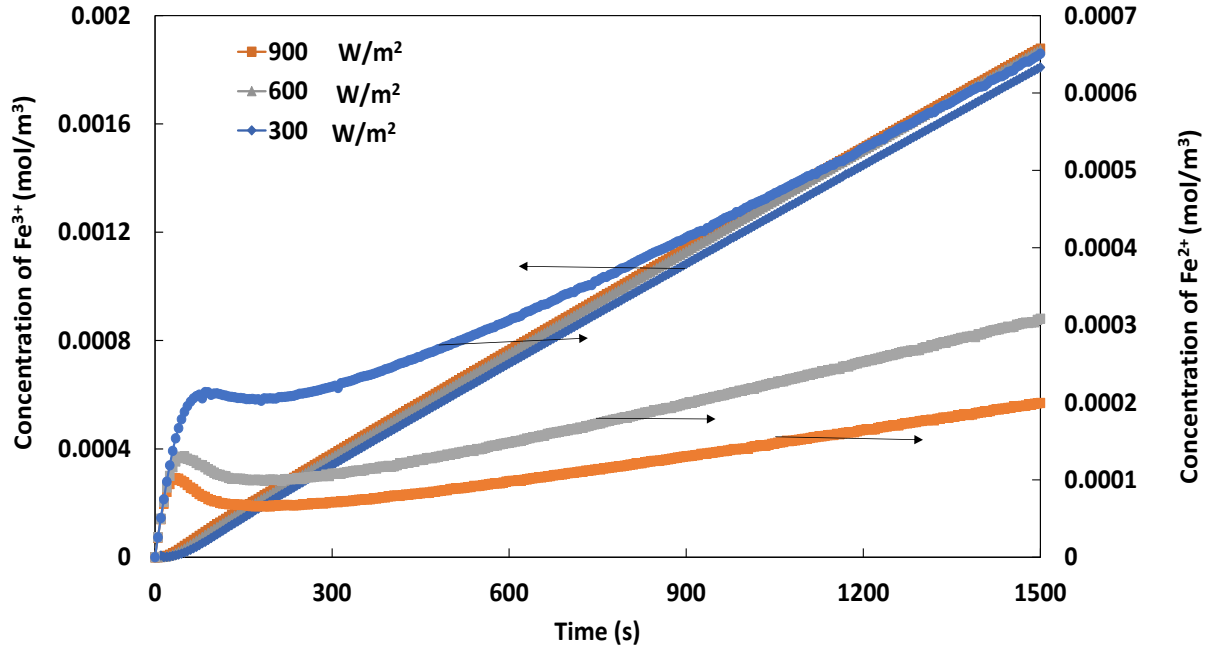


Figure 4. Evolution of the concentrations of ferric and ferrous ions as function of time under the different solar radiations.

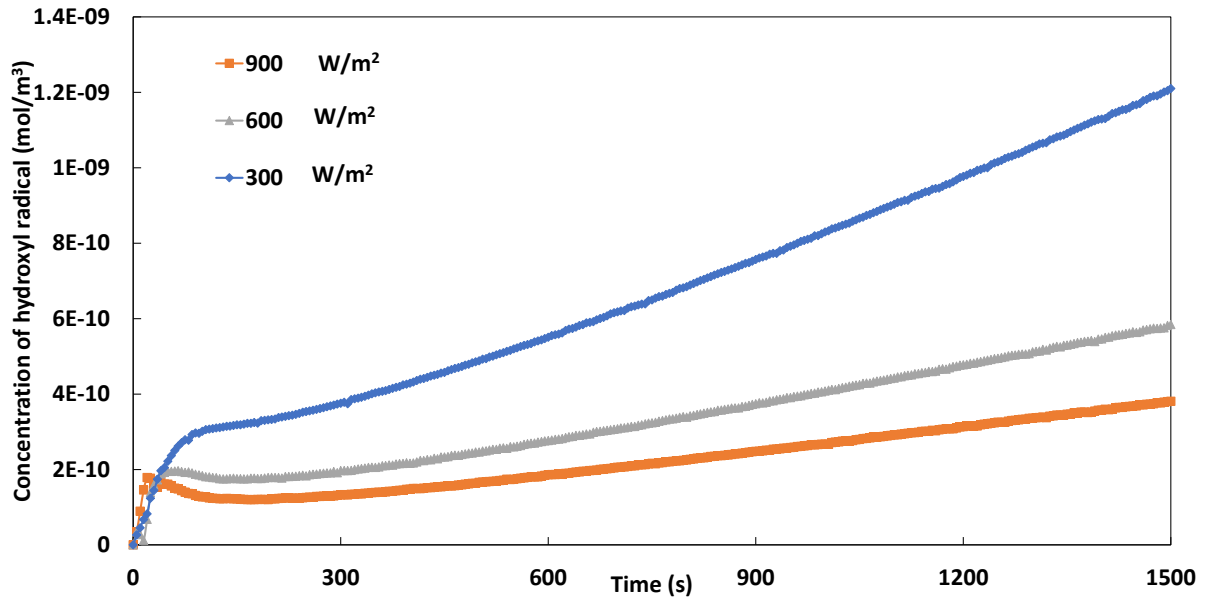


Figure 5. Evolution of the concentration of hydroxyl radical as a function of time under the different solar radiations

Production of Hydroxyl Radical

Fig. 5 reports the evolution of the concentration of hydroxyl radicals available in the electrolyte under the three scenarios of solar radiation. It is shown that the highest yield is observed under the lowest solar radiation, which confirms the unbalanced availability of hydrogen peroxide and ferrous ions leading to a rapid consumption of the catalyst and hence a braking in the instantaneous production of HO^\bullet . The lifetime of hydroxyl radicals being short, its rapid recombination leads to the emergence of hydrogen peroxide again in the medium, explain the higher concentrations observed under lower solar radiation, where the excess of hydrogen peroxide is

relatively reduced. This result confirms the need for parallel galvanic cells offering higher molar yields of ferrous ions, playing the role of catalyst in the decomposition of hydrogen peroxide, and making more efficient the proposed design of advanced oxidation process.

Conclusion

The PV supply of the electrochemical cell has been studied using modelling and simulation and the polarization curves revealed that under 300, 600 and 900 W/m² of incident global solar radiation, the selected panel delivers 0.35, 0.88 and 1.41 A, respectively, according to the MPPT regulation. These current feed the designed electrochemical cell, to initiate the reduction of oxygen to hydrogen peroxide on a carbon based cathode, based on the assumption of a continuous pumping of oxygen making the electrolyte permanently saturated. The simulations of the concentrations of hydrogen peroxide over time reveal that the electrochemical cell performs by far higher than the designed galvanic cell, suggesting to put several galvanic cells in parallel in order to reach stoichiometric yields of Fenton's reagent and catalyst.

The trends retrieved with ferrous and ferric ions were interestingly unexpected. The highest solar radiation leads to the lowest concentrations of ferrous ions, revealing an important reactivity when hydrogen peroxide is available in higher molar yields. However, the concentration of ferric ions does not follow the same trend, the values are almost the same with the three scenarios, which is probably explained by the slow regeneration of ferrous ions from ferric ions. Similar trends were retrieved with hydroxyl radicals, which confirms the need for parallel galvanic cells offering higher molar yields of ferrous ions, playing the role of catalyst in the decomposition of hydrogen peroxide, and making more efficient the proposed design of advanced oxidation process.

Scientific Ethics Declaration

The author declares that the scientific ethical and legal responsibility of this article published in EPSTEM journal belongs to the author.

Acknowledgements or Notes

* This article was presented as an oral presentation at the International Conference on Technology (www.icontechno.net) conference held in Antalya/Turkey on November 16-19, 2023.

* This work was financially supported by the National Direction for Research and Technological Development DGRSDT, Algeria, in the frame of the "PISE" project entitled "GreEnAREA", supported by the mixed team of research "PVA" and affiliated to the National Higher School of Technology and Engineering.

References

- Ahmad, Z. (2006). Corrosion kinetics. In B. T. Zaki (Ed.), *Principles of corrosion engineering and corrosion control* Ahmad (pp.57-119). Oxford: Butterworth-Heinemann.
- Andreozzi, R., Antonio D Apuzzo, D. A., & Raffaele Marotta, R. (2000). A kinetic model for the degradation of benzothiazole by Fe³⁺ -photo-assisted fenton process in a completely mixed batch reactor. *Journal of Hazardous Materials*, 80, 241–257.
- Artusi, R., Verderio, P., & Marubini, E. (2002). Bravais-Pearson and Spearman correlation coefficients: Meaning, test of hypothesis and confidence interval. *International Journal of Biological Markers*, 17(2), 148–151.
- Bray, W.C. (1931). The mechanism of reactions in aqueous solution examples involving equilibria and steady states. *Chemical Reviews*, 1, 161–77.
- Davis, M. E., Robert, J., & Davis, R. J. (2003). The basics of reaction kinetics for chemical reaction engineering *Fundamentals of Chemical Reaction Engineering* (pp.1-52). New York, NY: McGraw Hill. Retrieved from <http://resolver.caltech.edu>.
- De Laat, J., & Le, T.G. (2006). Effects of chloride ions on the iron(III)-catalyzed decomposition of hydrogen peroxide and on the efficiency of the fenton-like oxidation process. *Applied Catalysis B*:

- Environmental*, 66(1–2), 137–146.
- Gasmi, I. (2020). Kinetic pathways of iron electrode transformations in galvano-fenton process: A mechanistic investigation of in-situ catalyst formation and regeneration. *Journal of the Taiwan Institute of Chemical Engineers*, 116, 81–91.
- Haag, W. R. (1992). Rate constants for reaction of hydroxyl radicals with several drinking water contaminants. *Environmental Science and Technology*, 26(5), 1005–1013.
- Koprivanac, N., & Lonč, A. (2006). Photo-assisted fenton type processes for the degradation of phenol : A kinetic study. *Journal of Hazardous Materials*, 136(3), 632–644.
- Jonghun, L., & Hoffmann, M.R. (2019). Substrate oxidation enhances the electrochemical production of hydrogen peroxide. *Chemical Engineering Journal*, 374, 958–64.
- Machulek, A., de Moraes, J. E.F., & Okano, L.T.(2009). Photolysis of ferric ions in the presence of sulfate or chloride ions : Implications for the photo-fenton process.” *Photochemical & Photobiological Sciences*, 8, 985–991.
- Madhavan, J., Grieser, F., & Ashokkumar, M. (2010). Combined advanced oxidation processes for the synergistic degradation of ibuprofen in aqueous environments. *Journal of Hazardous Materials*, 178(1–3), 202–208.
- Mohamed, B., Ali, B., Belasri, A., & Bouariou, A.(2016). Study of hydrogen production by solar energy as tool of storing and utilization renewable energy for the desert areas. *International Journal of Hydrogen Energy*, 41(45), 20788–20806.
- Pawar, V., & Gawande, S. (2015). An overview of the Fenton process for industrial wastewater. *IOSR Journal of Mechanical and Civil Engineering (IOSR-JMCE)*, 127–136.
- Rahim, A. H., A. R., Tijani, A. S., Fadhillah, M., & Hanapi, S. (2015). Optimization of direct coupling solar PV panel and advanced alkaline electrolyzer system. *Energy, Procedia*, 79, 204–211.
- Tromans, D. (1998). Temperature and pressure dependent solubility of oxygen in water: A thermodynamic analysis. *Hydrometallurgy*, 48(3), 327–342.
- Villalva, M. G., Gazoli, J. R., & Filho, E. R.. (2009). Comprehensive approach to modeling and simulation of photovoltaic arrays. *IEEE Transactions on Power Electronics*, 24(5), 1198–1208.

Author Information

Kaouthar Kerboua

Department of Process and Energy Engineering.
National Higher School of Technology and Engineering,
23005, Annaba, Algeria
Contact e-mail: k.kerboua@ensti-annaba.dz

To cite this article:

Kerboua, K. (2023). PV supplied electrochemical production of hydrogen peroxide: Green pathway for Fenton based advanced oxidation processes. *The Eurasia Proceedings of Science, Technology, Engineering & Mathematics (EPSTEM)*, 24, 101-109.

The Eurasia Proceedings of Science, Technology, Engineering & Mathematics (EPSTEM), 2023

Volume 24, Pages 110-118

IConTech 2023: International Conference on Technology

User-Defined Autogenerated Fuzzy Solvers for Embedded Applications

Alexei Evgenievich Vassiliev

Saint Petersburg State Marine Technical University

Ye Min Htet

Saint Petersburg State Marine Technical University

Htut Shine

Saint Petersburg State Marine Technical University

Anton Victorovich Vegner

Saint Petersburg State Marine Technical University

Abstract: A characteristic modern trend in control systems is the use of artificial intelligence methods (including fuzzy methods) in embedded applications. The presence of limitations in the resources of such systems leads to the need to choose the best combination of fuzzifier, inference system, and defuzzifier, which requires appropriate tools. In this paper, based on the principles of fuzzy logic and fuzzy sets, we propose an integrated development environment (IDE) that generates assembly codes for microcontrollers, which will be used as fuzzy controllers in embedded applications. The user of this IDE will have the option to choose the desired fuzzifier, inference system, and defuzzifier based on the established indicators of accuracy, speed, and the amount of required memory. Our interest is to improve the efficiency of developing systems with fuzzy data processing by creating specialized integrated development environments. An example of the practical implementation of such a tool is given in this article.

Keywords: Fuzzy controller, Intelligent control system, On-board microcontroller, Embedded application.

Introduction

Decision-making systems based on the methods of fuzzy computing theory are widely used in control systems, including embedded control systems (Piegat, 2013). The fuzzy computing paradigm is based on the concepts of the intensity of manifestation of sets of properties of objects (processes) and the degree of validity of statements operating with these sets. When designing a fuzzy solver, the developer specifies sets of values ("memberships") of input signals X, sets of values ("memberships") of output signals Y, as well as the statements ("decision rules") of the form "If (Set of X) Then (Set of Y)". The fuzzy solver consists of three subsystems: the fuzzification subsystem - "fuzzifier" (for each input signal, by its instantaneous value, forms the intensities of its correspondence to each of the given input memberships), the inference subsystem - "solver" (for each rule, according to the values of instantaneous intensity of its input memberships forms the intensity of manifestation of the output memberships), and the defuzzification subsystem - "defuzzifier" (it calculates the resulting value of each output signal from the intensity of output memberships).

Component Models of Fuzzy Solvers and Methods of Their Implementation

- This is an Open Access article distributed under the terms of the Creative Commons Attribution-Noncommercial 4.0 Unported License, permitting all non-commercial use, distribution, and reproduction in any medium, provided the original work is properly cited.

- Selection and peer-review under responsibility of the Organizing Committee of the Conference

© 2023 Published by ISRES Publishing: www.isres.org

First of all, it should be noted that the mathematical apparatus of the theory of fuzzy sets is quite diverse: there are various ways of defining membership functions (singleton, linear, nonlinear), various methods of processing complex conditions, various types of logical operations (Ramot et al., 2003; Vassiliev, 2018; Van Leekwijck & Kerre, 1999; Šaletić et al., 2002). The listed elements of the mathematical apparatus have different degrees of complexity, require different amounts of resources for their implementation, and at the same time provide a different degree of adequacy of the fuzzy models being formed. Estimates of the "quality to resource capacity" ratios are known for some implementations of fuzzy systems, however, the theory of formal synthesis of optimal fuzzy solvers is still in its infancy (Ghosh & Dubey, 2013; Kim et al., 2000). Based on the principle of information processing stages in fuzzy solvers, we will give a brief overview of common ways to describe the three subsystems listed above that are part of a fuzzy solver.

Fuzzification Subsystem

Membership functions of input variables can be described by piecewise linear or non-linear functions (Fig. 2).

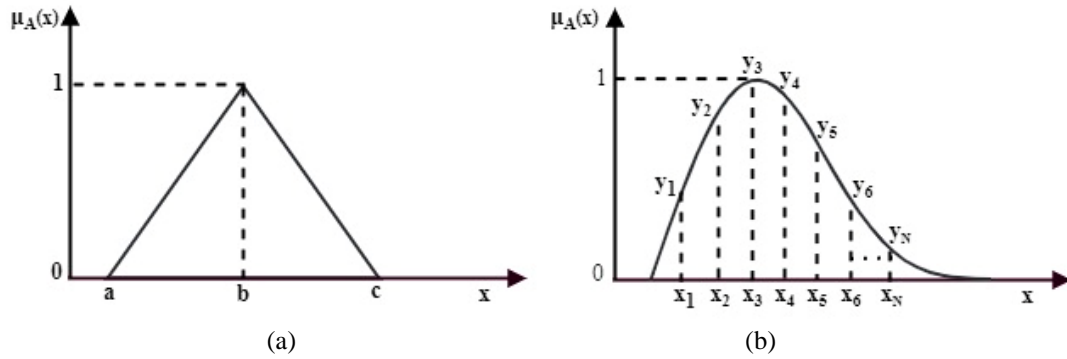


Figure 1. Membership functions of input variables: (a) piecewise linear and (b) nonlinear

The first type of description makes it possible to efficiently use the memory of a fuzzy solver, since three points are enough to store information about a piecewise linear term, however, to determine the degree of membership of the input variable (Fig. 1(a)), it is necessary to perform calculations according to triangular membership function formula (1).

$$\mu_A(x) = \begin{cases} 0, & \text{if } x \leq a \\ \frac{x-a}{b-a}, & \text{if } a \leq x \leq b \\ \frac{c-x}{c-b}, & \text{if } b \leq x \leq c \\ 0, & \text{if } x \geq c \end{cases} \quad (1)$$

In addition, in the case of fuzzification of piecewise linear description, the results of fuzzy calculations will be approximate values. The second type of description allows one to describe an arbitrary form of a membership function (2) with the highest possible accuracy, but requires either memory costs for point-by-point storage of the scan of the membership function (in this case, the maximum fuzzification rate is ensured), or the calculation of an externally specified function that analytically describes the form of the membership function (in this case, additional time for calculations and memory is consumed to store and execute code of the function).

$$\mu_A(x) = \{(y_1, x_1), (y_2, x_2), (y_3, x_3), \dots, (y_N, x_N)\} \quad (2)$$

Inference Subsystem

The "If" parts of the rules can operate on several input variables, and the conditions for these variables to correspond to their membership functions can be combined by various logical expressions. So, for example, if the particular conditions of a certain rule are combined by the "OR" operation, the degree of membership of the entire rule is determined by the greatest degree of membership among these particular conditions, and if by the "AND" operation, then the least. In addition, particular conditions can be hierarchically grouped among themselves utilizing logical operations (Fig. 2). A variety of such operations provides an increase in the degree

of flexibility of the description, but increases the amount of memory required to store the rule base; in addition, when the description of the rule becomes more complicated, the time of its processing in the fuzzy solver increases.

1	IF (X1 is mf1) AND (X2 is mf1)	THEN (Y1 is mf1)
2	IF (X2 is mf1) AND (X1 is mf2 OR X3 is mf3)	THEN (Y2 is mf2) AND (Y3 is mf3)
.		
.		
N	IF (X1 is mf3 AND X2 is mf2) OR (X3 is mf3 AND X4 is mf4)	THEN (Y3 is mf2) AND (Y4 is mf3)

Figure 2. Example of rule base for a fuzzy solver

Defuzzification Subsystem

Defuzzification is a procedure or process of finding the crisp (non-fuzzy) value for each of the output linguistic variables of the set (Driankov et al., 1993). The procedure that extracts crisp output value from a fuzzy output set is called defuzzification (Grum, 2008). Currently, there are a significant number of defuzzification methods, as noted in Van Leekwijck & Kerre (1999). Among them, the simplest way to perform the defuzzification procedure is to choose the corresponding number of a maximum output membership function. Variants of this method are FOM (first of maximum), MOM (middle of maximum), and LOM (last of maximum) which are called maxima methods. However, regardless of their computational simplification, they generally ignore the rules that are triggered below the maximum level of the membership, and hence, this makes their results less accurate (Mamdani et al., 1984). As such, the center of gravity (COG) and the weighted average method (WAM) have been mostly used to come up with crisp controller outputs. These methods give more accurate results than maxima methods, but their computability is much more complex.

Let us illustrate with an example of a fuzzy approximation function to see clearly how the results will be obtained according to the defuzzification methods they used. Here we will use the cross-section method for the fuzzy solver to approximate the function (Vassiliev, 2018). Let's consider the application of the cross-section method in the example of solving the problem of fuzzy approximation of the nonlinear function below.

$$F(x_1, x_2) = 128 + \left[\cos \left[\frac{(x_1 - 127.5) \cdot \pi}{128} \right] + \sin \left[\frac{(x_2 - 127.5) \cdot \pi}{128} \right] \right] \cdot 32 \quad (3)$$

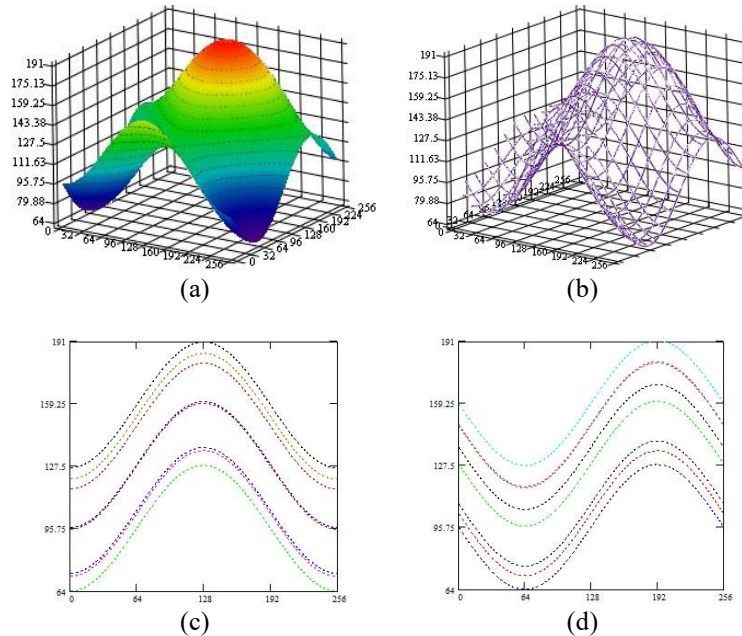


Figure 3. The approximated surface (a, b), and the projections of its sections on the plane x1-z (c) and on the plane x2-z (d)

Analysis of a given functional dependence (in some cases, for example, when conducting heuristic analysis, it is convenient to use a graphical representation of the dependence, rather than its mathematical notation) allows us to conclude that the desired graph is a cosine wave function (the argument of which is the variable x_1) experiencing a vertical shift (the intensity of this shift depends according to the sinusoidal law on the variable x_2) — see Figure 3.

According to the cross-section method, sections of the original function are constructed parallel to the planes that limit the space of its permissible values (in this case 0 to 256). Each new shape of the section is described by a pair of membership functions (direct and inverse; in general, the membership functions of these inputs will be nonlinear. In this way, we get a pair of membership functions for each input: membership functions ‘cos’ and ‘not_cos’ for input variable x_1 and membership functions ‘sin’ and ‘not_sin’ for input variable x_2 (Fig. 4).

In our case, the value of the cosine function decreases to a minimum value as it approaches the center of the first half-period and increases to a maximum value as it approaches the center of the second half-period (passing through the median value at the edges and in the center of the interval on which it is defined).

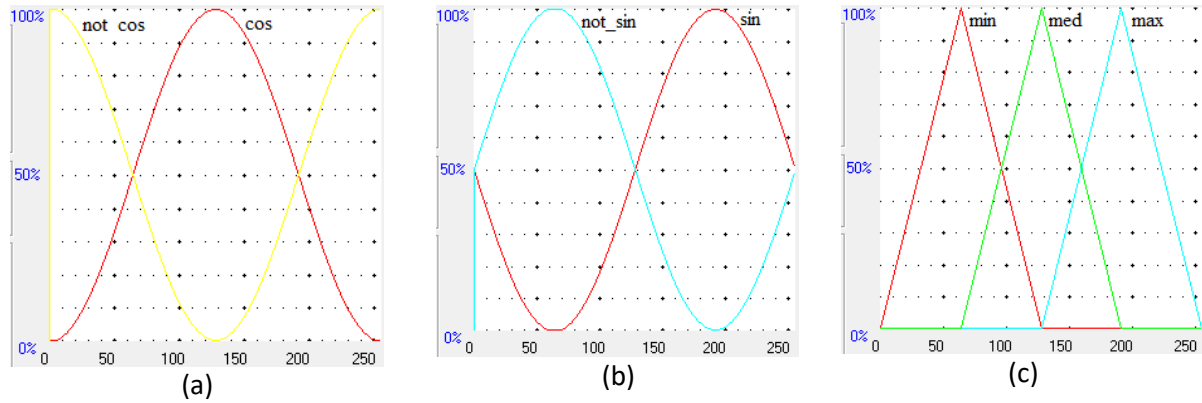


Figure 4. Membership functions of (a) input variable x_1 , (b) input variable x_2 , and (c) output variable y

So, the output value varies from minimum to maximum according to the sinusoidal law (depending on the measure of proximity of the current value of the variable x_1 to the edges and the center of its interval), but in two different ranges (depending on the measure of proximity of the current value of the variable x_2). This allows us to set the membership functions of the output variable and link them by rules with functions describing changes in input variables.

1	IF (x_1 is cos) AND (x_2 is sin)	THEN (y is max)
2	IF (x_1 is cos) AND (x_2 is not_sin)	THEN (y is med)
3	IF (x_1 is not_cos) AND (x_2 is sin)	THEN (y is med)
4	IF (x_1 is not_cos) AND (x_2 is not_sin)	THEN (y is min)

Figure 5. Rule base for fuzzy approximation

After setting all membership functions and the inference rules, we then implement and debug this fuzzy inference system into assembly codes, load them into the microcontroller, and then, test and record their operational characteristics by using different defuzzification methods. Here we use an x51-compatible 8-bit microcontroller with 12 MHz crystal oscillator. Table 1 shows approximation errors of the results from the MATLAB fuzzy toolbox and microcontroller. By comparing the approximation errors of our fuzzy solver to MATLAB, it can be seen that the microcontroller (fuzzy solver) executes reliable and exact output values for the fuzzy approximation function.

And then let us compare some options for the user of fuzzy solver. Table 2 shows various results for various defuzzification methods (each of them possesses the same input-output membership functions and inference rules) and clearly, we can see that each method has different accuracies, different execution times, and different memory sizes.

As we can see in Table 2, the maxima methods have very less computational time due to their simplicity of method of choosing crisp output values. However, approximation errors of these methods are significantly high

compared to the COG method. This is because they ignore rules that are triggered below the maximum level of membership function and hence, these methods are discontinuous because an arbitrarily small change in the input values of the fuzzy system can cause the output value to switch to another, more plausible result (Saade & Diab, 2004). This process can be seen in Figure 6 as their approximated surfaces are mostly discontinuous and suddenly change very roughly at certain points.

Table 1. Comparison of approximation errors with the ideal function

Defuzzification Methods	MATLAB			Microcontroller		
	Minimum Error	Maximum Error	Approximation Error (%)	Minimum Error	Maximum Error	Approximation Error (%)
FOM ($\min(x_m)$)	-32.06	62.647	24.472 %	-29.86	63.547	24.823 %
LOM ($\max(x_m)$)	-60.9	31.492	23.789 %	-61.827	32.419	24.152 %
MOM ($\frac{\sum x_i \in M(x_i)}{ M }$)	-44.81	44.537	17.504 %	-43.86	45.292	17.692 %
COG ($\frac{\sum (\mu(x_i) \cdot x_i)}{\sum \mu_i}$)	-9.382	11.9	4.648 %	-9.598	11.9	4.648 %

Table 2. Experimental results of fuzzy solver

Defuzzification Methods	Code Size	Execution Time	Total Machine Cycles	Approximation Error (%)
FOM ($\min(x_m)$)	2262 bytes	1.7 ms/cycle	1700	24.823 %
LOM ($\max(x_m)$)	2283 bytes	2 ms/cycle	2000	24.152 %
MOM ($\frac{\sum x_i \in M(x_i)}{ M }$)	2366 bytes	3.7 ms/cycle	3700	17.692 %
COG ($\frac{\sum (\mu(x_i) \cdot x_i)}{\sum \mu_i}$)	2678 bytes	2.7 ms/cycle	2700	4.648 %
Modified WAM $\frac{\sum (\prod_{i \in 1:M} \mu_k) Y_{max_i}}{\sum (\prod_{i \in 1:M} \mu_k)}$	2598 bytes	4.2 ms/cycle	4200	0.976 %

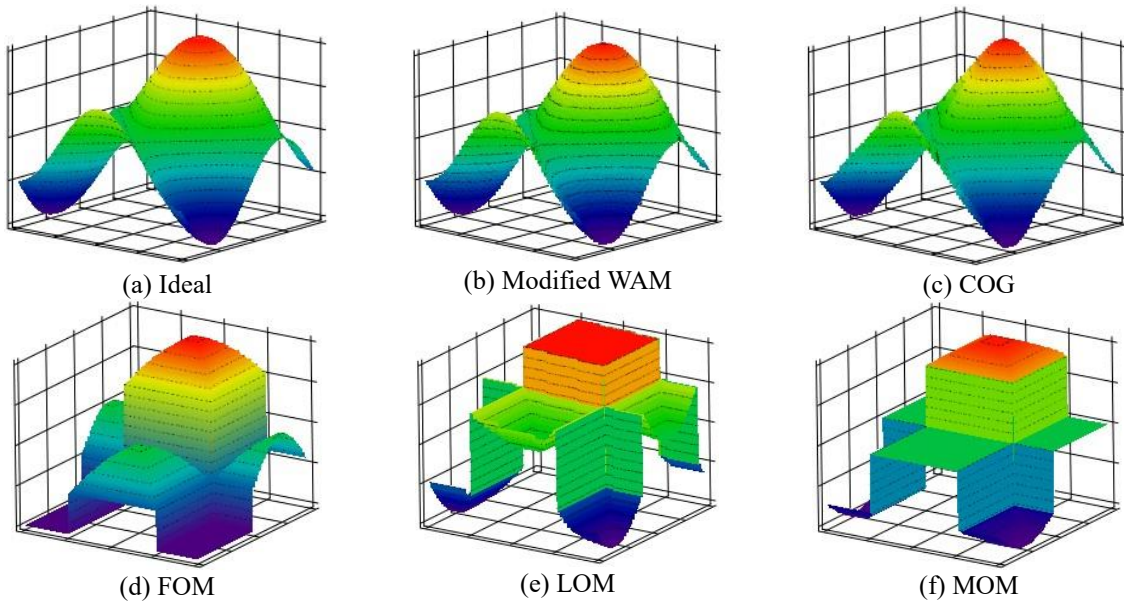


Figure 6. Comparison of surfaces of the fuzzy approximated function

COG method takes into account all the rules, but it does not allow control actions in the extreme limits of the range of output signal. This is because the Center of Gravity (COG) defuzzification method evaluates the area

under the scaled membership functions only within the range of the output linguistic variable, the resulting crisp output values cannot cover the full range (Talon & Curt, 2017). As shown in Figure 6, the approximated surface of the COG method is very similar to the ideal one, since it gives continuous action, but the edges slightly differ which makes the approximation error 4.648 %. But, compared to maxima methods, COG has good accuracy and not much execution time.

MOM and COG are the most famous and frequently used defuzzification methods, but still, we see that they have some approximation errors compared to the ideal function, and, suppose the user is not satisfied with these errors and wants to increase the quality of accuracy. Then we consider the new defuzzification method. Vassiliev et al. (2023) proposed this method and this is a modified method of weighted average of maximums. According to this method, the weight of the next rule will be determined not by the minimum degree of validity of the conditions that make up the “IF” part, but by the product of all their values. Hence, software implementation of this method becomes more complex and it takes most execution time compared to others, but it increases the accuracy significantly which is 0.976 % approximation error. Another feature of this method is that it can only be used for symmetrical and singleton membership functions but not asymmetrical memberships. Again, the centroid method can be used for both symmetrical and asymmetrical membership functions, but not singletons. So, depending on the type of membership functions we choose to use, we need to choose a suitable defuzzification method accordingly.

Again, the code sizes of each method are not significantly different because the code size only depends on the algorithm of each method and, in this case, we use the same fuzzification method and the same inference rules. So, the code sizes of each method differ only by their defuzzification method. As mentioned above, here, input membership functions are nonlinear and are defined as values in look-up tables of assembly language programs. Since we use 256 values for one membership function, a single membership will take 256 bytes of memory. So, if we need a lot of membership functions and have some limits for the memory size of the microcontroller we chose, to implement the membership functions as piecewise linear will be the option for users.

Thus, since there is no single optimal combination of options for implementing the stages of fuzzy information processing, and the theory of synthesis of optimal fuzzy solvers (which could analytically substantiate the variant of such a combination for each specific task) is in the process of becoming, to expand the possibilities of developing fuzzy solvers and achieve suboptimal indicators of their quality, tools are needed that provide the developer with the opportunity to choose the method of implementing information processing for each stage of the fuzzy solver, and the combined use of these implementations.

Therefore, an urgent task is to develop methods and tools for the automated generation of fuzzy solvers with combinations of options for fuzzification, inference, and defuzzification subsystems specified by the developer, which guarantee the operability of the fuzzy solver and the adequacy of the a priori assessment of its performance characteristics.

Structure of the Instrumental System

Let's consider the variant of the structurally functional organization of the automated synthesis system for the software implementation of fuzzy solvers (Fig. 7) and the stages and steps of its application. The first stage (steps 1–4) ensures the formation and replenishment of libraries of ready-made software solutions for fuzzifiers, solvers, and defuzzifiers. The idea of each new prototype of a fuzzy computer component is developed and analyzed in the simulation environment (stage 1), then it is implemented and debugged in the form of program code for the microcontroller (step 2), loaded into the microcontroller (step 3) to test and record the values of real operational characteristics - accuracy, speed, and memory costs, after which it replenishes the corresponding library of software implementations (step 4).

The second stage (steps 5–7) provides automated generation of a software implementation of a fuzzy solver that meets the specified requirements for a specific control system. From the total set of requirements, those related to the fuzzy decision-making system are determined (step 5), from the triad of libraries of ready-made solutions of fuzzifiers, solvers, and defuzzifiers, solutions that satisfy the given constraints are selected, aggregated into a fuzzy solver and analyzed as a whole (step 6), after which they are combined with other software components to obtain the resulting software part of the control device (step 7).

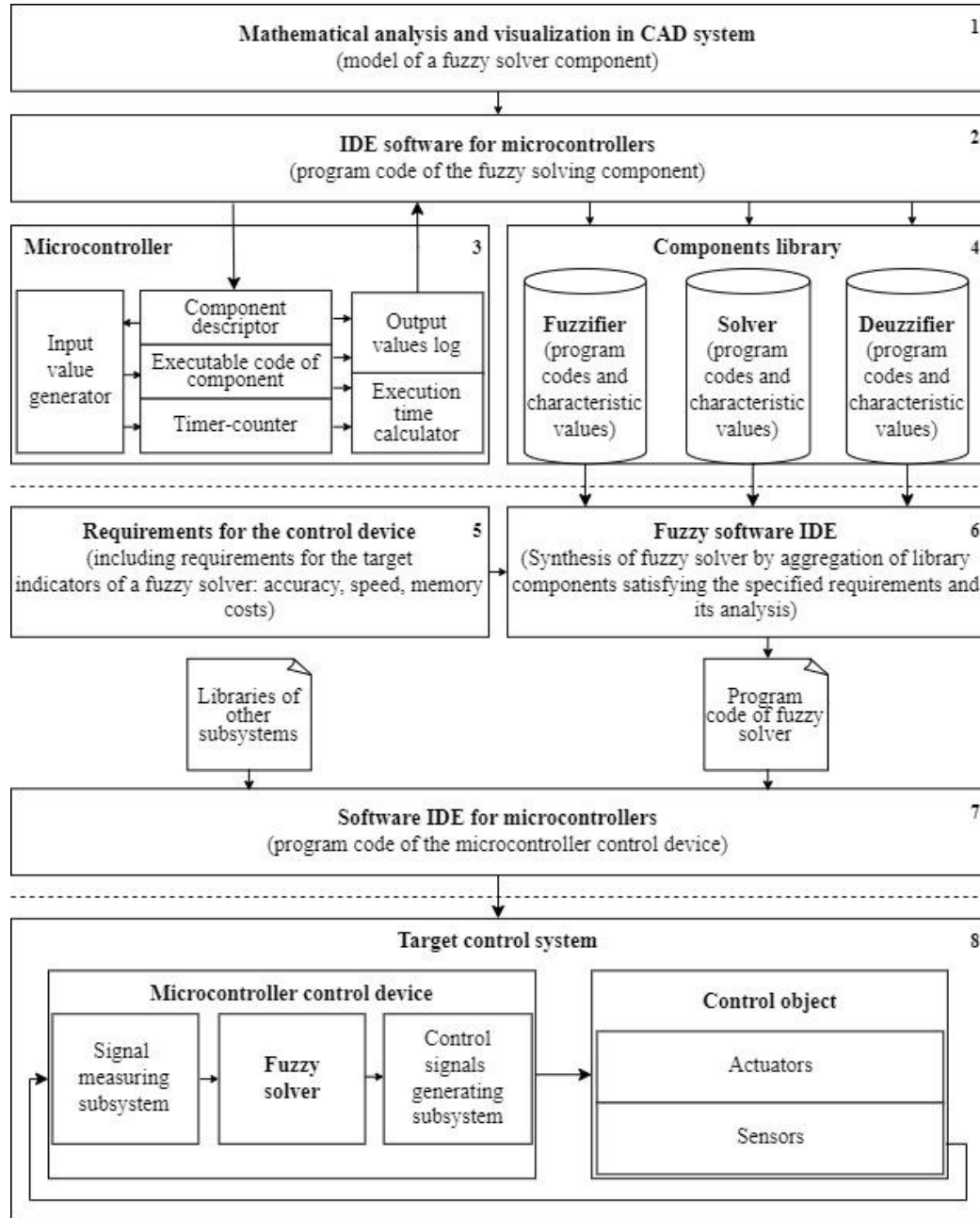


Figure 7. The process of designing control systems with auto-generated fuzzy solver

Third stage (stage 8) - the target microcontroller device with a fuzzy computer is put into operation, which serves as a source of new ideas for improving fuzzy computers.

A Variant of Implementation of the Instrumental System

For experimental purposes, the authors of the article have developed and continue to improve a prototype of an instrumental system for the automated generation of software implementations of fuzzy solvers with established performance characteristics – FuzzyWizard-51 (Fig. 8). The user of the system - the developer of fuzzy solvers - can declare libraries of ready-made solutions and perform the necessary manipulations with them (add, exclude, and modify program modules and their descriptions), make the necessary settings for the tool environment, and at the stage of generating the program code of the target fuzzy solver - set the required restrictions on the execution time, the amount of code and data for each of the three types of modules, and select them according to the selected criteria. After analyzing the found library modules that satisfy the constraints of interest to the developer, the automatic assembly of the program code of the resulting fuzzy solver is carried out.

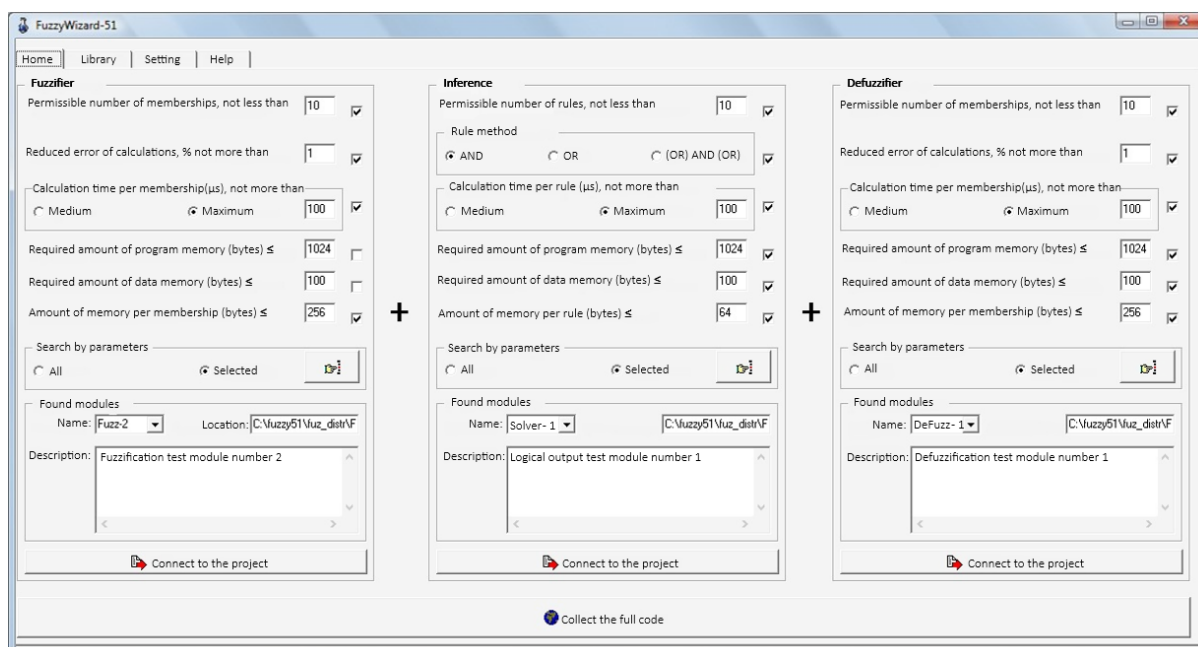


Figure 8. Appearance of the main window of Fuzzy Wizard-51

Conclusion

Thus, the methods and means of automating the design of fuzzy solvers with specified performance characteristics proposed by the authors contribute to the expansion of the methodological and technological base of instrumental support for intelligent decision-making and control systems based on applications of fuzzy set theory.

Scientific Ethics Declaration

The authors declare that the scientific ethical and legal responsibility of this article published in EPSTEM journal belongs to authors.

Acknowledgements or Notes

* This article was presented as an oral presentation at the International Conference on Technology (www.icontechno.net) held in Antalya/Turkey on November 16-19, 2023.

References

- Driankov, D., Hellendoorn, H., & Reinfrank, M. (1993). *An introduction to fuzzy control*. Springer eBooks.
- Ghosh, S., & Dubey, S. K. (2013). Comparative analysis of K-Means and fuzzy C-Means algorithms. *International Journal of Advanced Computer Science and Applications*, 4(4).
- Grum, J. (2008). Book review: Fuzzy controller design, theory and applications by Z. Kovacic and S. Bogdan. *International Journal of Microstructure and Materials Properties*, 3(2-3), 465.
- Kim, Y. H., Ahn, S. C., & Kwon, W. H. (2000). Computational complexity of general fuzzy logic control and its simplification for a loop controller. *Fuzzy Sets and Systems*, 111(2), 215–224.
- Mamdani, E. H., Efstathiou, H., & Sugiyama, K. (1984). Developments in fuzzy logic control. *23rd Conf. On Decision and Control*, 7(1), 1-13.
- Piegat, A. (2013). *Fuzzy modeling and control*. Physica.
- Ramot, D., Friedman, M., Langholz, G., & Kandel, A. (2003). Complex fuzzy logic. *IEEE Transactions on Fuzzy Systems*, 11(4), 450–461.

- Saade, J. J., & Diab, H. (2004). Defuzzification methods and new techniques for fuzzy controllers. *Iranian Journal of Electrical and Computer Engineering*, 3(2), 161–174.
- Šaletić, D. Z., Saletic, Velasevic, D., & Mastorakis, N. E. (2002). Analysis of basic defuzzification techniques. Retrieved from <https://www.researchgate.net/publication>
- Talon, A., & Curt, C. (2017). Selection of appropriate defuzzification methods: Application to the assessment of dam performance. *Expert Systems with Applications*, 70, 160–174.
- Van Leekwijck, W., & Kerre, E. (1999). Defuzzification: Criteria and classification. *Fuzzy Sets and Systems*, 108(2), 159–178.
- Vasiliev A.E. (2018). *Embedded automation and computer technology systems* (p.590). Microcontrollers. – M.: Hotline-Telecom.
- Vassiliev, A.E, Vegner, A. V., Golubeva, D. E., Dotsenko, A. S., & Карпенко, B. A. (2023). Increasing the quality indicators of the functioning of fuzzy solvers at the defuzzification stage. *Journal of Communications Technology and Electronics*, 68(7), 810–818.

Author Information

Alexei Evgenievich Vassiliev

Saint Petersburg State Marine Technical University
Saint Petersburg, Russia
Contact e-mail: avasil@smtu.ru

Ye Min Htet

Saint Petersburg State Marine Technical University
Saint Petersburg, Russia

Htut Shine

Saint Petersburg State Marine Technical University
Saint Petersburg, Russia

Anton Victorovich Vegner

Saint Petersburg State Marine Technical University
Saint Petersburg, Russia

To cite this article:

Vassiliev, A.E, Htet, Y.M., Shine, H. ,& Vegner, A. V (2023). User-defined autogenerated fuzzy solvers for embedded applications. *The Eurasia Proceedings of Science, Technology, Engineering & Mathematics (EPSTEM)*, 24, 110-118.

The Eurasia Proceedings of Science, Technology, Engineering & Mathematics (EPSTEM), 2023

Volume 24, Pages 119-125

IConTech 2023: International Conference on Technology

Provenance Study of Gypsum Black Crusts

Petros Karalis

National Centre for Scientific Research (N.C.S.R.)

Elissavet Dotsika

National Centre for Scientific Research (N.C.S.R.).

Dafni Kyropoulou

National Centre for Scientific Research (N.C.S.R.)

Alexandros Mazarakis - Ainian

University of Thessaly

Evaggelia Kolofotia

University of Thessaly

Iakovos Raptis

Centre for Research and Technology Hellas

Anastasios Drosou

Centre for Research and Technology Hellas

Dimitrios Tzovaras

Centre for Research and Technology Hellas

Anastasia Electra Poutouki

University of Pavia

Giorgos Diamantopoulos

National Centre for Scientific Research (N.C.S.R.)

Panagiotis Leandros Poutoukis

University of Patras

Abstract: CaSO_4 black crusts are the major cause of the deterioration of cultural heritage monuments. Gypsum black crusts are formed on marble or other carbonate rocks as a result of the reaction of atmospheric sulfur with the calcium of the stone causing erosion of its surface. Samples of CaSO_4 crusts were collected by scraping off about 1 g of the layer of decayed carbonate rocks. A total of 18 samples from the archaeological site of Vryokastro at Kythnos island in Greece, were collected. These salts may have originated from different natural and anthropogenic sources. Understanding this deterioration process is crucial for the restoration/conservation of cultural heritage monuments. The natural sources include biological sources, construction materials, rainwater, marine spray, and pyrite oxidation within the rock substrate. Anthropogenic sources include pollution from fossil fuels. The oxygen and sulfur isotopes can help to discriminate the S-origin of black crusts. The isotopic analysis was conducted in the Stable Isotope Unit of the Institute of Nanoscience and Nanotechnology (NCSR Demokritos). For S isotope analyses, sulfate minerals were dissolved in deionized water and subsequently precipitated as BaSO_4 . Sulfur isotopic compositions were measured after the conversion

- This is an Open Access article distributed under the terms of the Creative Commons Attribution-Noncommercial 4.0 Unported License, permitting all non-commercial use, distribution, and reproduction in any medium, provided the original work is properly cited.

- Selection and peer-review under responsibility of the Organizing Committee of the Conference

© 2023 Published by ISRES Publishing: www.isres.org

of BaSO₄ to SO₂ using an elemental analyzer (Flash EA device) coupled with an isotope ratio mass spectrometer.

Keywords: Sulfur isotopes, Oxygen isotopes, Gypsum crust, Monument degradation

Introduction

Environmental degradation of historic mortars is a main threat to the safe preservation of historic monuments (Yates, 2003; Sabbioni, 2001; Zappia, 1994). Climatic and environmental conditions are often very severe for construction materials, namely in the presence of high humidity or in direct contact with water. Agents of decay such as sulfate attack, acid attack, leaching action, salts attack, damage due to frost and fire, poor mixing and choice of constituents and many more can cause extensive cracks and total disintegration of historic constructions (Sabbioni 1998; Grossi & Brimblecombe, 2007). The sources of mortar decay could be physical-related to physical variations of water inside masonry (evaporation, capillary flow, ice formation, etc.) or chemical (formation of expansive products such as ettringite and thaumasite).

Sulfate salts crystallizing on the surface of building stones are one of the most important factors of monument degradation. The natural sources of these salts include biological sources (Hanoso, 2006), construction materials (Vallet 2006; Schleicher 2010; Kloppmann et al., 2011), rainwater, marine spray (Kloppmann et al., 2011), and pyrite oxidation within the rock substrate (Kramar, 2011). Anthropogenic sources include pollution from fossil fuels (Kramar, 2011). The microstructure, the mineralogical and chemical composition of historic mortars have been examined to some extent using traditional techniques of instrumental analysis and microscopy, but the literature is dispersed and there is no generally accepted or preferred protocol for their investigation [Dotsika et al., 2009]. Recently it has been shown that the stable isotopes of carbon and oxygen offer considerable potential in the investigation of lime mortar and plaster but relatively little work has been conducted so far (Dotsika et al., 2018).

The oxygen and sulfur isotopes can help to discriminate the S-origin of black crusts (Vallet, 2006; Schleicher, 2010; Kloppmann et al., 2011; Kramar, 2011; Schwigstillova, 2009). Black crusts have $\delta^{34}\text{S}$ and $\delta^{18}\text{O}$ values around 0 ‰ vs. CDT and +11 ‰ vs. SMOW respectively, which is typical for atmospheric sulfates (air pollution). Marine sulfate ranges around 20-21 ‰ vs. CDT and around +9,5 ‰ vs. SMOW for $\delta^{34}\text{S}$ and $\delta^{18}\text{O}$ respectively. The data from Kythnos Island (Greece) show clear isotopic contrasts between black crusts, which can be considered as representative of a predominantly atmospheric origin [urban air present value between 0‰ and +20‰ (Newman et al., 1991), and marine sulfate (marine aerosol present value around 20‰), (Siedel & Klemm, 2000). These potential end-members of sulfate contamination have distinct and well-defined isotopic signatures.

Archaeological Informations

An island with a long history and particular archaeological importance is Kythnos, which is situated between Kea and Serifos. The ancient city of "Vryokastro", on the island's northwest shore, was a fortified polis that was continually inhabited from the first millennium B.C. to the sixth or seventh century A.D (Figure 1). The remains of the ancient city occupy an area of approximately 28,5 hectares, including the small islet of Vryokastraki, which was connected to the shore in antiquity by a narrow isthmus. During the systematic investigations that have been in progress since 1990 (survey and subsequent excavations) numerous finds and several ancient structures, such as temples, public buildings, houses, port facilities, burial monuments, etc., have been brought to light. These discoveries have provided valuable insights into the urban planning of the city and the sociopolitical and economic development of the ancient community.

Regarding the construction of the buildings, the island's ground is composed of various types of crystalline slates (metamorphic rock) with intervening marble horizons. Slate and limestone appear to have been used extensively for the buildings of the ancient city, and the discovery of marble fragments of architectural elements from the sanctuaries of the Upper Town confirms its parallel use. Several samples of marble were chosen in order to identify the marble's provenance. A selection of numerous stones, coquina rocks, slates, and mortars that were structural components of the buildings and belonged to structures of various chronological periods was made during the field inspection of the intramural sanctuaries located on the Middle Plateau.



Figure 1. Aerial photograph of Vryokastro



Figure 2 . Sanctuary dedicated to Artemis and Apollo

More specifically, the chosen specimens were procured from the Upper Town precinct, housing the Late Classical sanctuary of **Asklepios**, Aphrodite, and the Samothracian Gods (Mazarakis - Ainian, 2017, 2019), as well as from the Archaic sanctuary dedicated to **Artemis and Apollo** (Mazarakis - Ainian 2017, 2019) (Figure 2.). Furthermore, samples were taken from a public building of the Hellenistic period identified as the Hellenistic Prytaneion of the Kythnians and from the Sanctuary of Demeter and Core on the Acropolis Hill (Mazarakis – Ainian, 2019).

Sampling

To gather crust samples, approximately 1 gram of decayed carbonate rocks was scraped off. A total of 18 samples were collected from the Vryokastro archaeological site on Kythnos island in Greece. Comparative samples were also taken from four historic constructions - Hellenistic, Late Roman, Byzantine, and Ottoman - located in Anaktoroupoli, Marmarion tower in Kavala, Fortification walls in Drama (n=4), and Funerary monuments in Makrygialos (n=4) in North Greece. Additionally, a sample was collected from an area in Athens that is heavily affected by atmospheric pollution.

Methods

The isotopic analysis was conducted in the Stable Isotope Unit of Institute of Nanoscience and Nanotechnology (NCSR Demokritos). For S isotope analyses, sulfate minerals were dissolved in deionized water and subsequently precipitated as BaSO₄. Sulfur isotopic compositions were measured after conversion of BaSO₄ to SO₂ using an elemental analyzer (Flash EA device) coupled with an isotope ratio mass spectrometer. Sulfur isotope measurements were performed with an analytical error of better than $\pm 0.3\%$ and results reported in delta notation ($\delta^{34}\text{S}$) as ‰ deviation relative to the Cañon Diablo Troilite (CDT) standard. Oxygen isotope measurement results were performed with an analytical error of better than $\pm 0.3\%$ and are expressed in delta notation ($\delta^{18}\text{O}$) as ‰ deviation relative to Vienna Standard Mean Ocean Water (V-SMOW), according to:

$$\delta = [(R_{\text{sample}} - R_{\text{standard}}) / R_{\text{standard}}] \times 1000 \quad (1)$$

where R is the ratio between the heavy and the light isotope, in this case $^{18}\text{O}/^{16}\text{O}$ or $^{34}\text{S}/^{32}\text{S}$. The reported values are the mean of two or more consistent measurements of each sample.

Results and Discussion

In table 1 and Fig.4 we present the isotopic values of oxygen ($\delta^{18}\text{O}$) and sulfur ($\delta^{34}\text{S}$) of black crusts from the five sampled areas. The shaded areas are the mean isotopic values of black crust samples from different sampled monument of France (Kloppmann et al., 2011) and Italy (Longinelli & Bartelloni, 1978) as gathered from the literature. Chemically, all analyzed black crusts are dominated by Ca and SO₄, (up to 85 wt). Both sulfur and oxygen isotope ratios of all analyzed black crusts (Fig. 4) from Kythnos show $\delta^{34}\text{S}$ values from -2 to $+8\%$ and $\delta^{18}\text{O}$ from $+6$ to $+12\%$, and these values stay within the ranges of black crusts observed in literature (Table 1, Fig.4).

Table 1. $\delta^{34}\text{S}$ and $\delta^{18}\text{O}$ for black crusts

Material	Location	Sites	$\delta^{34}\text{S}$	$\delta^{18}\text{O}$
black crusts	Greece	Anaktoroupoli, Kavala	4.7	3.5
black crusts	Greece	Marmarion tower, Kavala	7.5	5.4
black crusts	Greece	Fortification walls, Drama	2.1	3.2
black crusts	Greece	Funerary monuments, Makrygialos	2.2	4.7
black crusts	Greece	Athens	-1.2	11.9
black crusts	France	Bourges, Chenonceau, Versailles, Marseille, Chartes	-1.4 to 7.4	6.3 to 12.4
black crusts	Italy	San Marco, Venice	4 to 6	7 to 9
black crusts	Greece	Kythnos 1	-2 to 2	8 to 12
black crusts	Greece	Kythnos 2	7 to 8	6 to 12

There are, though, significant differences between the two study sites. Whereas all $\delta^{18}\text{O}$ values for Kythnos 1 and 2 are close to $9\text{--}10\% \pm 2\%$, $\delta^{34}\text{S}$ values are different, Kythnos 1 being situated around $0 \pm 2\%$, while Kythnos 2 are closer to $+7\text{--}8\%$. The oxygen in sulphates comes from various sources such as air (with a delta value of $+23\%$ for gaseous O₂), water (with delta values ranging from -11 to -5% (Dotsika et al., 2010; Dotsika et al., 2018b), and diesel combustion residues (with a delta value of 24.5% according to (Rivas et al., 2014)). The contribution of each source depends on the reaction mechanism used, whether it is hydrolysis-oxidation or oxidation-hydrolysis, as noted by Holt et al. studies in (Holt et al., 1981a, 1981b). So, the differences in the $\delta^{18}\text{O}$ of the black crusts could be derived as a result from two Oxygen sources: low $\delta^{18}\text{O}$ values of rain water (variable negative values) and high $\delta^{18}\text{O}$ values of sulfates contained in dusts. Therefore, the differences in the value of $\delta^{18}\text{O}$ in black crusts may reflect slight climatic differences, a different signature of rainfall, and/or variable participation of ‘polluted’ sulfates. In our case, the continental effect (isotopic gradient of Greece is around $-0.2\%/100$ km (Dotsika et al., 2010) should not affect the O isotope signal given the very small spatial rain distribution of Kythnos Island. These values, Kythnos 1, are very similar to Bourges and Versailles (Kloppman et al., 2011), that are attributed to the isotopic difference of local meteoric conditions. This is not our case due to the small dimension of the Island and also the samples coming from the same area. The $\delta^{34}\text{S}$ values of Kythnos 1 vary within a very limited range around $0 \pm 2\%$ ‰ vs. CDT. These values are typical of atmospheric sulfates ($\delta^{34}\text{S}$ and $\delta^{18}\text{O}$ values range around 0 ‰ vs. CDT and around $+11$ ‰ vs. SMOW respectively). Newman et al. (Newman et al., 1991), suggests that this participation surpasses the other sources.

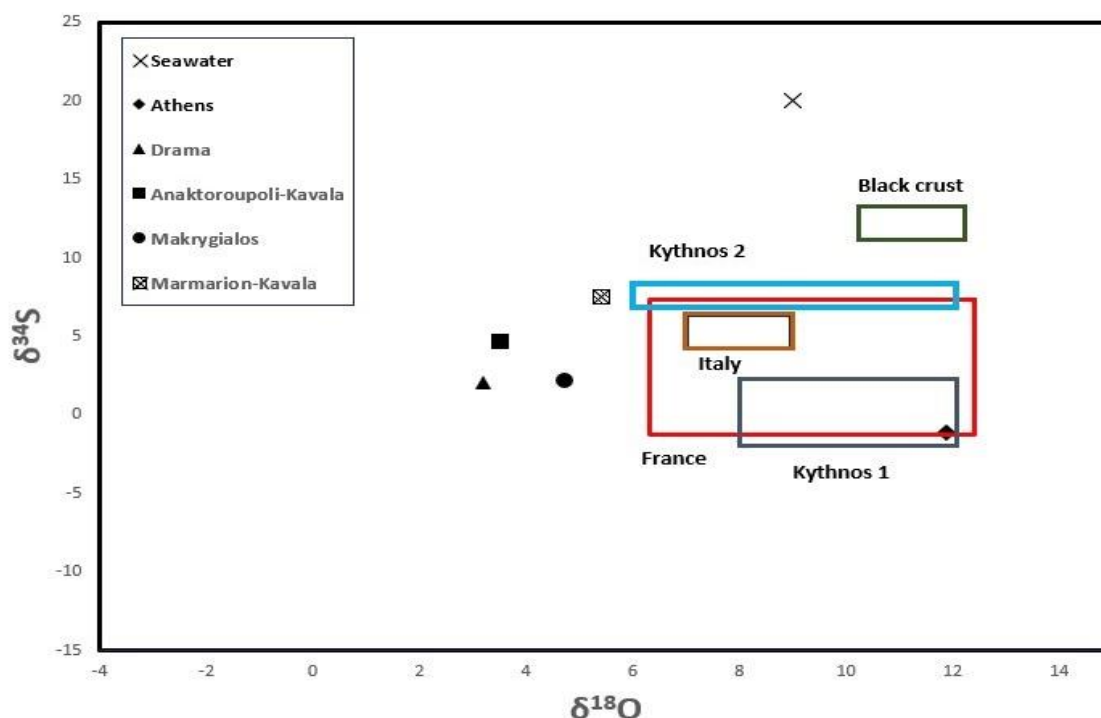


Figure 3. $\delta^{18}\text{O}$ vs $\delta^{34}\text{S}$ for black crusts

The black crusts of Kythnos 2 are significantly enriched in $\delta^{34}\text{S}$ by 7‰ with respect to Kythnos 1 isotopic values. This enrichment in heavy sulfur probably reflects a sea spray contribution (Siedel & Klemm, 2000). Similar values show also the black crust from San Marco Cathedral, Venice (Longinelli & Bartelloni, 1978). Probably the difference between the two sites is attributed to the orientation of the buildings, which receive winds from different directions, charged with more or less sea droplets. The competitive role of the sulfates of different origins was revealed (marine versus pollution).

Conclusions

In this preliminary study it is evident that the stable isotope analysis of the ^{34}S and ^{18}O can successfully discriminate the origin of the black crust on the deteriorated surface of the Kythnos monuments. The competitive role of the sulfates of different origin was revealed (marine versus pollution). In general, the isotopic values appear to be a useful tool to diagnose mortar degradation and determine the different sources of decay.

Scientific Ethics Declaration

The authors declare that the scientific ethical and legal responsibility of this article published in EPSTEM journal belongs to the authors.

Acknowledgments or Notes

* This article was presented as an oral presentation at the International Conference on Technology (www.icontechno.net) held in Antalya/Turkey on November 16-19, 2023.

*This research has been co-financed by the European Regional Development Fund of the European Union and Greek national funds through the Operational Program Competitiveness, Entrepreneurship and Innovation, under the call RESEARCH – CREATE – INNOVATE (project code: T1EDK-12500)

References

- Dotsika, E., Kyropoulou, D., Christaras, V., & Diamantopoulos, G. (2018). $\delta^{13}\text{C}$ and $\delta^{18}\text{O}$ stable isotope analysis applied to detect technological variations and weathering processes of ancient lime and hydraulic mortars. *Geosciences*, 8(9), 339.
- Dotsika, E., Psomiadis, D., Poutoukis, D., Raco, B., & Gamaletsos, P. N. (2009). Isotopic analysis for degradation diagnosis of calcite matrix in mortar and plaster. *Analytical and Bioanalytical Chemistry*, 395, 2227–2234.
- Dotsika, E., Lykoudis, S., & Poutoukis, D. (2010). Spatial distribution of the isotopic composition of precipitation and spring water in Greece. *Global and Planetary Change*, 71(3–4), 141–149.
- Dotsika, E., Diamantopoulos, G., Lykoudis, S., Poutoukis, D., & Kranioti, E. (2018). Isotopic composition of spring water in Greece: Spring waters isoscapes. *Geosciences*, 8(7), 238.
- Grossi, C.M., & Brimblecombe, P. (2007). *Effect on long-term changes in air pollution and climate on the decay and blackening of European stone building, building stone decay: from diagnosis to conservation*. Prikkry, I. R., & Simith, B. J. (Eds.), (pp.117-130). London, UK: Geological Society Special Publication.
- Holt, B. D., Cunningham, P. T., & Kumar, R. (1981a). Oxygen isotopy of atmospheric sulfates. *Environmental Science and Technology*, 15(7), 804–808.
- Holt, B. D., Kumar, R., & Cunningham, P. T. (1981b). Oxygen-18 study of the aqueous-phase oxidation of sulfur dioxide. *Atmospheric Environment*, 15(4), 557–566.
- Hosono, T., Uchida, E., Suda, C., Ueno, A., & Nakagawa, T. (2006). Salt weathering of sandstone at the Angkor monuments, Cambodia: Identification of the origins of salts using sulfur and strontium isotopes. *Journal of Archaeological Science*, 33(11), 1541–1551.
- Kloppmann, W., Bromblet, P., Vallet, J. M., Verges Belmin, V., Rolland, O., Guerrot, C., & Gosselin, C. (2011). Building materials as intrinsic sources of sulphate: A hidden face of salt weathering of historical monuments investigated through multi-isotope tracing (B, O, S). *Science of the Total Environment*, 409(9), 1658–1669.
- Kramar, S., Mirtic, B., Knoller, K., & Rogan Smuc, N. (2011). Weathering of the black limestone of historical monuments (Ljubljana, Slovenia): Oxygen and sulfur isotope composition of sulfate salts. *Applied Geochemistry*, 26(9–10), 1632–1638.
- Longinelli, A., & Bartelloni, M. (1978). Atmospheric pollution in Venice, Italy, as indicated by isotope analyses. *Water, Air, and Soil Pollution*, 10, 335–341.
- Mazarakis Ainian, A. (2017). Νεότερα για τα ιερά της αρχαίας πόλης της Κύθνου. In V. Vlachou & A. Gadolou (Eds.), *ΤΕΡΨΙΣ. Studies in Mediterranean archaeology in honour of nota Kourou* (pp. 303–315). Brussels.
- Mazarakis Ainian, A. (2019). *The sanctuaries of Ancient Kythnos*. Rennes: France.
- Newman, L., Krouse, H., & Grinenko, V. (1991). Sulphur isotope variations in the atmosphere. In H. R. Krouse & V. A. Grinenko (Eds.), *Stable isotopes in the Assessment of natural and anthropogenic sulphur in the Environment* (pp. 133–142). John Wiley & Sons Ltd. Publisher.
- Rivas, T., Pozo, S., & Paz, M. (2014). Sulphur and oxygen isotope analysis to identify sources of sulphur in gypsum-rich black crusts developed on granites. *Science of the Total Environment*, 482–483, 137–147.
- Sabbioni, C., Zappia, G., Riontino, C., Blanco Varela, M.T., Aguilera J, Puertas, F. et al. (2001). Atmospheric deterioration of ancient and modern hydraulic mortars. *Atmospheric Environment*, 35, 539–48.
- Sabbioni, C., Zappia, G., Ghedini, N., Gobbi, G., & Favoni, O. (1998). Black crusts on ancient mortars. *Atmospheric Environment*, 32(1998), 215–223.
- Schleicher, N., & Recio Hernandez, C. R. (2010). Source identification of sulphate forming salts on sandstones from monuments in Salamanca, Spain a stable isotope approach. *Environmental Science and Pollution Research International*, 17(3), 770–778.
- Schweigstilova, J., Prikkryl, R., & Novotna, M. (2009). Isotopic composition of salt efflorescence from the sandstone castellated rocks of the Bohemian Cretaceous Basin (Czech Republic). *Environmental Geology*, 58(1), 217–225.
- Siedel, H., & Klemm, W. (2000). Evaluation of the environmental influence on sulphate salt formation at monuments in Dresden (Germany) by sulfur isotope measurements. In V. Fassina (Ed.), *Proceedings of the 9th International Congress on Deterioration and Conservation of Stone*. (pp. 401–409). Elsevier.
- Vallet, J. M., Gosselin, C., Bromblet, P., Rolland, O., Verges Belmin, V., & Kloppmann, W. (2006). Origin of salts in stone monument degradation using sulphur and oxygen isotopes: First results of the Bourges cathedral (France). *Journal of Geochemical Exploration*, 88(1–3), 358–362.
- Yates, T. (2003), Mechanisms of air pollution damage to brick concrete and mortar. In: P. Brimblecombe (Ed.), *Air pollution reviews: the effects of air pollution on the built environment* (pp. 107–132). London, UK: Imperial College Press.

Zappia, G., Sabbioni, C., Pauri, M.G., & Gobbi, G. (1994), Mortar damage to airborne sulfur compounds in a simulation chamber. *Material Structures*, 27, 469–73.

Author Information

Petros Karalis

National Centre for Scientific Research (N.C.S.R.)
Attiki, Greece

Elissavet Dotsika

National Centre for Scientific Research (N.C.S.R.)
Attiki, Greece
Email: e.dotsika@inn.demokritos.gr

Dafni Kyropoulou

National Centre for Scientific Research (N.C.S.R.)
Attiki, Greece

Alexandros Mazarakis - Ainian

University of Thessaly
Volos, Greece

Evaggelia Kolofotia

University of Thessaly
Volos, Greece

Iakovos Raptis

Centre for Research and Technology Hellas
Thessaloniki, Greece

Anastasios Drosou

Centre for Research Technology Hellas
Thessaloniki, Greece

Dimitrios Tzovaras

Centre for Research and Technology Hellas,
Thessaloniki, Greece

Anastasia Electra Poutouki

University of Pavia
Pavia, Italy

Giorgos Diamantopoulos

National Centre for Scientific Research (N.C.S.R.)
Attiki, Greece

Panagiotis-Leandros Poutoukis

University of Patras
Pavia, Italy

To cite this article:

Karalis, P., Dotsika, E., Kyropoulou, D., Mazarakis Ainian, A., Kolofotia, E., Raptis, I., Drosou, A., Tzovaras, D., Poutouki, A.E. Diamantopoulos, G., & Poutoukis, P.L. (2023). Provenance study of gypsum black crusts. *The Eurasia Proceedings of Science, Technology, Engineering & Mathematics (EPSTEM)*, 24, 119-125.

The Eurasia Proceedings of Science, Technology, Engineering & Mathematics (EPSTEM), 2023

Volume 24, Pages 126-134

IConTech 2023: International Conference on Technology

A Research on Determining the Degree of Risk by Using ResNet

Serap Tepe

The University of Health Sciences

Serkan Eti

Istanbul Medipol University

Abstract: Risk analysis, considered one of the most crucial building blocks of occupational safety with a multidisciplinary approach, is an area that requires quick solutions with proactive methods, has high operational costs, and a low error tolerance level. Utilizing image classification and enabling learning is the main goal of this study to achieve objective outcomes in risk analysis, reduce costs, increase efficiency, and ensure standardization. For the proposed paper, 325 labeled images were collected from the field, standardized to a resolution of 224x224, and a separate file was created for each category after labeling. Python's TensorFlow Keras libraries were used, and the model employed was a semi-learned ResNet model. While 501,765 parameters were learned, 23,587,712 parameters were trained from the data. The total parameter count was 24,089,477. Categorical cross-entropy was used as the loss function, Adam optimization algorithm was preferred for parameter optimization, and the Accuracy Rate metric was used to evaluate the model's quality. The learning success of the model reached 58% in 100 steps, and the maximum accuracy rate observed was determined to be 67%. Traditional risk analysis methods rely on statistical analysis of historical data to obtain results, while machine learning-based approaches allow for the evaluation of complex and multidimensional data. Machine learning-based image classification methods assist in effectively performing risk analysis in situations involving visual information. These techniques make valuable contributions to identifying and managing potential risks in different sectors. As research and applications in this field continue to grow in the future, the role of image classification in risk analysis will gain even more importance.

Keywords: Image processing, Image classification, Risk analysis, ResNet, Occupational safety

Introduction

Image processing is the process of obtaining and analyzing information from digital images using various algorithms and techniques through computers (Gonzalez & Woods, 2008). In this field, properties of images such as color, brightness, and contrast can be modified, edges and corners can be detected, objects can be recognized, and the quality of images can be enhanced. The fundamental purpose of image processing is to render acquired information more meaningful for application in various contexts (Pratt, 2007). The essential components of image processing consist of analog-to-digital converters that transform images into digital format, algorithms that process images, and digital-to-analog converters that transform processed images into visual or numerical outputs (Sonka et al., 2014). These procedural steps are executed using diverse algorithms and methodologies employed in various applications (Jain, 1989).

Image processing plays a significant role in fields such as medicine, security, agriculture, automotive, robotics, entertainment, and many more. Within medical imaging, it aids in the detection and monitoring of diseases by providing support for diagnosis and treatment processes, while in security systems, it contributes to the recognition of individuals and objects through technologies like facial recognition and object detection. Image classification is an increasingly significant field within artificial intelligence and image processing. This process

- This is an Open Access article distributed under the terms of the Creative Commons Attribution-Noncommercial 4.0 Unported License, permitting all non-commercial use, distribution, and reproduction in any medium, provided the original work is properly cited.

- Selection and peer-review under responsibility of the Organizing Committee of the Conference

© 2023 Published by ISRES Publishing: www.isres.org

involves assigning a given image to specific categories or classes (Krizhevsky et al., 2012). Classification is commonly accomplished using deep learning and machine learning techniques. At its core, image classification encompasses the computer's understanding of images and its ability to identify objects, patterns, or features similar to the human eye (Simonyan & Zisserman, 2014). Presently, deep learning models, particularly Convolutional Neural Networks (CNNs), have achieved substantial success in this domain. Thanks to their multi-layered architectures, these models learn features hierarchically from images, thereby enhancing accuracy and performance (He et al., 2016).

Risk is a concept stemming from the combination of probability and severity. Probability encompasses situations that have a likelihood of occurrence, while severity refers to the effects that will emerge based on the outcomes of these situations. Risk essentially constitutes a fusion of the infinite possibilities of probabilities and the traces left when any of these possibilities materialize. From this perspective, risk is thought to possess a complex structure with both pre- and post-components.

In the pre-component stage, which is referred to as the "before" phase, managing probabilities and taking proactive measures are necessary. This phase involves activities aimed at controlling the potential risks of events, places, individuals, and situations. The post-component stage, labeled as the "after" phase, includes activities required to minimize the damage resulting from realized risks and to navigate through them with the least possible loss.

Risk is commonly perceived as a threat; however, it is actually also associated with opportunities. Risk analysis constitutes a set of methods used to identify, mitigate, and reduce hazards to an acceptable level, and each risk analysis holds importance in terms of recognizing available or assessable opportunities. Therefore, through accurate definition and effective management processes facilitated by risk analyses, the transformation of risks into opportunities is plausible. Risk analysis processes can enhance working environments, elevate individual awareness, and unearth possibilities for intervention. By precisely identifying and efficiently managing risks, not only can the current state be maintained, but there is also a chance to elevate it to a superior level.

In this study, the aim is to achieve real-time detection of risk analyses, a crucial field in occupational safety, through the assistance of image classification, with the objective of eliminating subjectivity in classification. The motivation behind the study lies in the prevention of negative or inadequate situations arising from subjective assessments in risk analysis within occupational safety. It strives to enable swift and effective decision-making through instant detection, prompt intervention, proactive approaches, increased efficiency, and reduced operational costs. In this context, the subsequent sections of the study are organized as follows.

The second section of the study provides a literature review, delving into the topics of image processing, image classification, and risk analysis. The third section succinctly summarizes the methodology of the study. The fourth section presents the findings, and the following sections discuss the acquired findings, culminating in the evaluation of the results.

Literature Review

In parallel with scientific and technological advancements, computer technology has been applied to various fields, offering numerous conveniences (Fradi et al., 2022). One of these areas is the widely acclaimed field of image processing (Sotvoldiev et al., 2020). Image processing involves the manipulation of image data using various algorithms or mathematical methods in a computer environment. Fundamentally, it revolves around capturing digital images, digitizing them into the desired format, conducting analyses, and ultimately transforming the image into desired parameters to obtain the final output (Soyhan et al., 2021; Venkatakrishnan & Kalyani, 2016; Zhang, 2022). To process images digitally, the first step is to create and transfer data libraries into a digital environment. Once these data libraries are established, the images are processed, and the procedure is carried out (Sin & Kadioglu, 2019).

Image processing methods enable rapid and efficient error detection processes, allowing for comprehensive product differentiation and classification within very short timeframes. Additionally, image processing methods minimize issues such as human exposure to risky environments in terms of health and safety. The advancing computer control systems, automatic machine systems, and cameras contribute to faster, safer, and more accurate operations (Ak & Dereli, 2021; Boyacıgil, 2022). Due to its capability to significantly enhance performance and efficiency, image processing technology finds extensive applications across various domains like military, medical, and industrial sectors (Feng, 2022). In this context, image processing technology is

widely used in areas such as identifying the origin of a chemical through microplate reading tests, automatic counting of items on a factory conveyor belt, detecting cracks in metal welding, cancer detection, remote sensing, and robotic navigation to avoid collisions (Venkatakrishnan & Kalyani, 2016).

There are various techniques used for automatically analyzing images, and the combination of these techniques with image processing technology leads to the emergence of diverse application areas. These techniques encompass 2D and 3D object recognition, image segmentation, motion detection, video surveillance, optical flow, medical scanning analysis, 3D pose estimation, and automatic license plate recognition (Venkatakrishnan & Kalyani, 2016). Image processing is utilized for real-time detection and monitoring of field objects to establish security conditions (Kim et al., 2014). Object recognition, in particular, is a widely employed image processing technology. YOLO algorithms are commonly used for object detection purposes, as indicated by the literature.

In the context of Occupational Health and Safety (OHS), image processing technologies predominantly focus on Personal Protective Equipment (PPE). Basaran and Cagil (2022) utilized the YOLOv4 algorithm in their study for detecting OHS measures. They designed a system that employs object detection algorithms to monitor the use of protective eyewear. This system facilitates easy monitoring of protective measures in areas where OHS measures are mandatory. Images of eyewear taken through cameras were identified using image processing and deep learning techniques.

Bo et al. (2019) employed the YOLOv3 model for object detection to determine whether construction workers were wearing helmets on construction sites. Torres et al. (2021) developed two different deep learning-based approaches to detect the usage of PPE by workers. Similarly, a real-time object recognition model was developed using data collected from construction sites to detect the use of PPE by workers (Moohialdin et al., 2021). A framework was designed to detect PPE usage in construction workers based on visuals, enabling real-time understanding of whether construction workers adhere to safety rules (Delhi et al., 2020).

Onal and Dandil (2021) employed the YOLOv4 deep learning algorithm to detect whether workers in industrial production facilities were using appropriate equipment correctly within their working environments. These studies collectively showcase the utilization of image processing and deep learning techniques for enhancing safety measures, monitoring PPE usage, and ensuring compliance with safety regulations across various industries. In their study, Lee and Lee (2023) have developed a CCTV-based security management application using image recognition models. A deep learning-based object recognition model was created by collecting data from images of construction site workers. In the three models they created: firstly, the aim was to check whether construction workers are present at the construction sites and to identify unauthorized entries into the work area; in the second model, the goal was to detect workers' postures to identify falls, predict hazardous situations in advance, and thereby intervene in case of an accident as quickly as possible; the third model was used to determine whether employees are wearing their PPEs (Personal Protective Equipment) such as helmets.

Ahn et al. (2023), on the other hand, designed a visual monitoring system named SafeFac to detect human activities near assembly lines in a factory, aiming to prevent injuries to workers due to accidents. This system utilizes a deep learning model based on YOLOv3 and supports multiple camera input streams to detect abnormal behaviors occurring near machinery. Although most of the modern factory operations are automated, unexpected accidents are still possible. In a similar vein, Yu et al. (2017) developed an image-based method to detect unsafe behaviors of construction workers in real-time. On the other hand, with the support of artificial intelligence, image processing technology has given rise to various applications in the field of Occupational Health and Safety (OHS) as highlighted by Turker et al. (2023). Through AI applications, it is expected that risks present in workplaces can be analyzed, proactive preventive measures can be identified, accident data can be analyzed, and work-related accidents and occupational diseases can be prevented (Fu et al., 2020).

Current camera images can be processed using AI algorithms to enable data analysis and real-time video content analysis. Smart manufacturing and intelligent security systems allow for the monitoring of risky activities that could lead to injuries, and through data obtained from wearable devices, swift actions can be taken in case of potential accidents (Shiklo, 2018). The intelligent security system developed by Erkan et al. (2015) processes images captured by cameras and activates an alarm and sends an email to the relevant unit in case of a threat. The system can be controlled remotely, and during the scanning process, information about the object's height and width can be accessed. Balakreshnan et al. (2020) combined Microsoft Azure image technology with AI to develop a system that determines whether protective goggles are worn in a factory setting. The combination of Unmanned Aerial Vehicles (UAVs), also known as drones, and image processing methods makes it inevitable

for UAVs to enter various domains of our lives (Sin and Kadioglu, 2019). For instance, through UAVs, engineering of risk assessment and management procedures becomes possible (Salvini et al., 2017).

In their study, Rossi et al. (2016) designed a UAV capable of detecting gas leaks. The UAV system, equipped with a gas measurement sensor and a 4G communication module, slows down its speed during autonomous flight when gas concentration increases, transmitting coordinate and gas measurement information to the control system through the 4G communication module. Asad et al. (2017) created a system capable of detecting concentrations of CO, CO₂, and H₂S gases using gas sensors, thermal cameras, and Cyber-Physical Systems (CPS) data. The data was integrated using a point density algorithm in the ArcGIS Pro computer software.

Image classification is a machine learning technique aimed at categorizing images into specific classes (Liu et al., 2016). Image classification involves predicting a label for an input image based on its visual content (Rajalingappaa et al., 2015). The objective is to assign a class label to an input image based on predefined categories. This learning approach falls within the realm of supervised learning (Yao & Fei-Fei, 2010), where a model is trained on a labeled dataset. The quality of such a model is evaluated on a separate test dataset. The architecture and training process of the model play a crucial role in achieving high accuracy in image classification tasks (Krizhevsky et al., 2012). This technique finds diverse applications across various domains.

Image classification is employed in e-commerce to categorize product images, organize search results, and determine product categories. In medical image analysis, it is utilized for classifying medical images like X-rays and MRIs to aid in disease diagnosis. In content filtering, image classification serves to filter and protect against inappropriate content. Additionally, image classification is used for driverless vehicles to classify traffic signs and road images, enabling vehicles to navigate and comprehend their surroundings. Within the realm of visual media, it facilitates the classification and tagging of photographs and videos (Goodfellow et al., 2016; Minaee et al., 2020; Ren et al., 2015; He et al., 2016; Redmon et al., 2016). These applications underscore the significance and wide-ranging utility of image classification. Irrespective of the method, the ultimate goal of all developed image processing and classification techniques is to minimize hazards and risks in the working environment within the Occupational Health and Safety (OHS) domain, and to enhance the efficiency and speed of monitoring processes. Through these developed systems, the aim is to mitigate the impact on workers and the workspace in the event of an accident, and thus reduce the potential workload and losses that might arise in such scenarios.

Method

The Convolutional Neural Network (CNN) is a widely used deep learning algorithm in image classification tasks. CNNs are a type of deep neural network and are commonly employed in computer vision tasks, particularly in image classification. They are designed to process grid-structured data with interactive pixels such as images, videos, and audio signals. CNNs are tailored to handle grid-structured data with interactive pixels like images. In a CNN, the first layer serves as the input layer and helps extract local features from the image. Subsequent layers are built to construct higher-level, more abstract features. The final layer is designed to extract class scores and make predictions as the outcome.

A distinctive feature of CNNs is the use of convolutional layers that apply filters to input data. The pooling layer aims to subsample the output of the convolutional layer and reduce its dimensions. This allows the model to detect significant features and learn unique representations of the data, enabling CNNs to be effective in image classification tasks. In CNNs, an input image undergoes several layers of convolutional and pooling operations, with each layer learning more complex features. The convolutional layer applies filters to the input image, which are used to extract local features. These filters are learned during the training process and capture relevant patterns in the image. Subsequently, the pooling layer reduces the spatial dimensions of the output from the convolutional layer. This makes the model computationally efficient and prevents overfitting by preventing the memorization of training data. In other words, it prevents excessive learning. After several layers of convolutional and pooling operations, the final layer of the CNN generates a probability distribution over defined class. The class with the highest probability is selected as the final prediction.

The utilization of convolutional layers and pooling operations makes CNNs particularly effective for image classification tasks. The convolutional layer enables the model to learn local features like edges and textures, and more complex features are learned in subsequent layers. The pooling layer further enhances the model's unique response to small translations and changes in the input image, making it more resilient to variations in the data.

Residual Network (ResNet) is a type of neural network used in deep learning. It was developed by Microsoft Research in 2015 to improve the structure of very deep neural networks. ResNet addresses the vanishing gradient problem in earlier layers of deep networks, preventing overfitting and structural loss. ResNet uses a function called a skip connection or shortcut connection. This function combines the input of a layer with its output, preventing overfitting. The skip connection also facilitates the updating of data and preserves features from previous layers. Due to its ability to prevent overfitting and enhance the structure of deep networks, ResNet is widely used in various visual applications like image classification, object recognition, and face recognition. ResNet has produced top results in numerous image classification benchmarks and has played a pioneering role in deep learning research.

In the mentioned study, the aim was to classify images obtained for occupational safety according to their risk levels. Towards this goal, the ResNet algorithm was implemented using Python for training the model. To achieve this objective, a total of 325 images captured at different times from the field were utilized for training the established model. These images were labeled through expert assessment. The labeling process involved the use of 5 categories. The first category represents images with the lowest level of risk, while the fifth category includes images of the most hazardous areas. The distribution of categories in the training dataset is provided in Table 1 and Figure 1.

Table 1. The distribution of categories

The number of images in Category 1	45
The number of images in Category 2	49
The number of images in Category 3	79
The number of images in Category 4	68
The number of images in Category 5	84

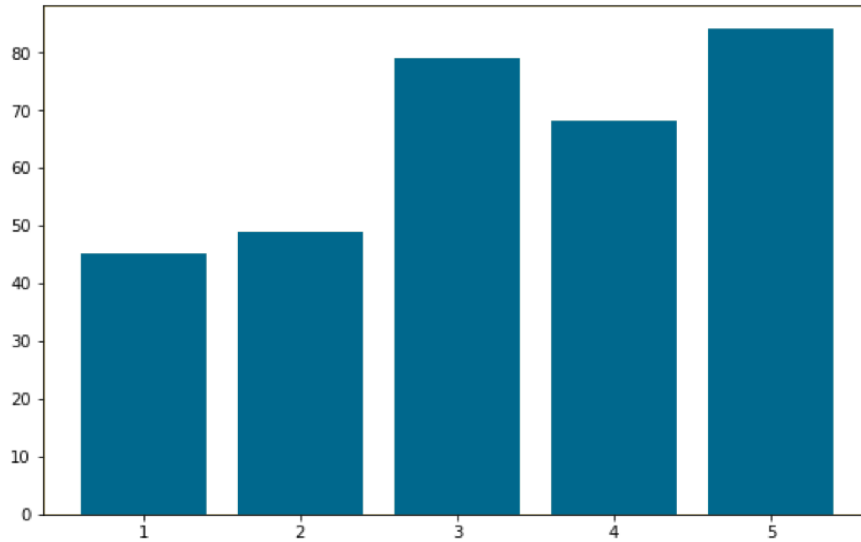


Figure 1. The distribution of categories

Findings

In the proposed study, after labeling, all images were standardized and resized to a resolution of 224x224. A file was created for each category. The TensorFlow Keras library in Python was utilized for this purpose. Upon examining the model, a pretrained ResNet model was employed. While 501,765 parameters were learned, the model was trained to learn 23,587,712 parameters from the data. The total number of parameters is 24,089,477. The categorical cross-entropy loss function was used, and the Adam optimization algorithm was chosen for parameter optimization. The Accuracy Rate metric was utilized to assess the quality of the model. Throughout the learning process of the model, with 100 epochs and a batch size of 16, the variation of the loss value and accuracy value is depicted in Figure 2 and Figure 3.

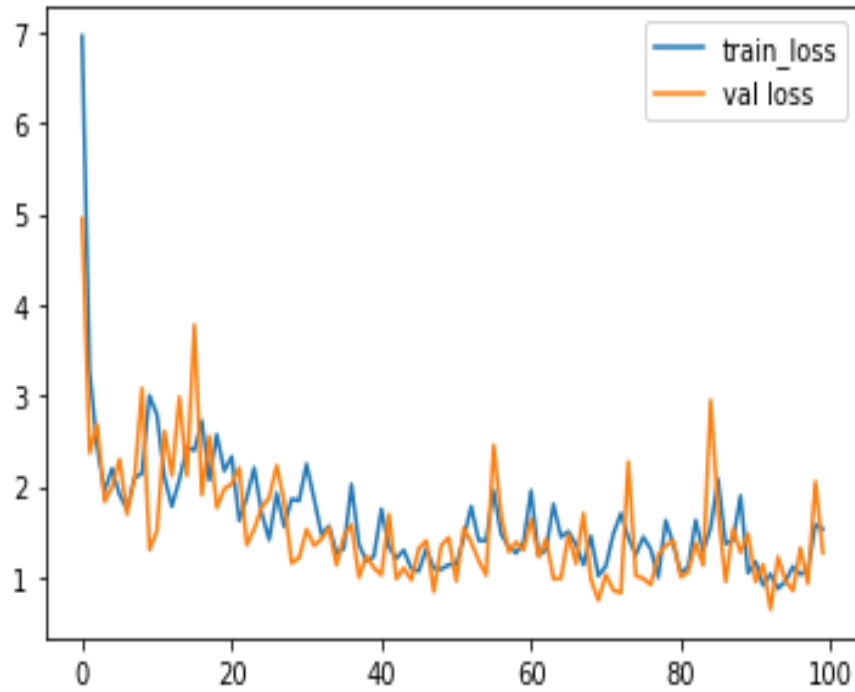


Figure 2. Loss value

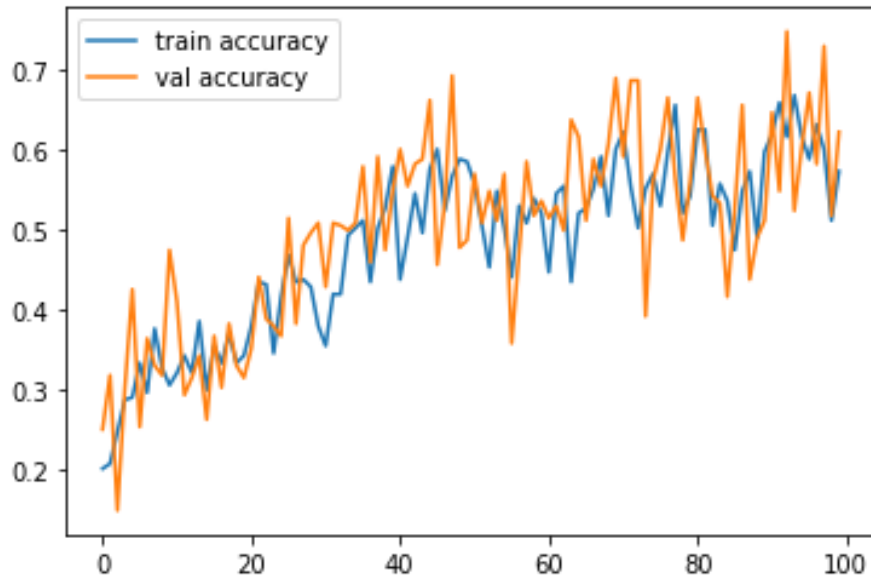


Figure 3. The rate of change of the accuracy value

The learning success of the model reaches 58% accuracy in 100 steps, with its peak value being 67% accuracy. In other words, the accuracy of correctly labeling a given image is observed to be around 60%. This rate, which could be considered high for a five-category model, can be further improved with more data to enhance its learning.

Results and Discussion

Risk analysis in occupational safety is a crucial process aimed at identifying, assessing, and preventing potential hazards in workplaces. In this process, risk analysis is used to identify potential hazards in workplaces and evaluate the risks these hazards may pose, making it an effective method as well as a legal requirement. In risk analysis, accurate and rapid analysis of data holds critical importance in obtaining accurate results.

In this context, image classification methods play a significant role in occupational safety risk analysis. Image classification relies on analyzing visual data to detect hazardous situations, potential risks, and security breaches in workplaces. Occupational safety experts can utilize images obtained from security cameras to identify hazardous situations and anticipate potential risks, contributing to proactive safety measures.

Image classification methods, powered by deep learning and artificial intelligence algorithms, can operate with high accuracy and sensitivity. This technology aids in swiftly detecting hazardous situations and can mitigate risks arising from human errors. Moreover, it enables occupational safety experts to redirect their time and efforts towards other vital tasks. As a result, image classification techniques have the potential to revolutionize occupational safety risk analysis by enhancing hazard detection, reducing human-related risks, and optimizing the allocation of expertise and resources.

In this study, for the purpose of conducting risk analysis, a model was established according to the objective. To train the model, 325 images taken at different times from the field were used. These images were labeled through expert evaluations. The labeling involved 5 categories, where the first category represents images with the lowest risk and the fifth category contains images from the most high-risk areas. The model's learning success reached 58% accuracy in 100 steps, with the maximum value observed being 67% accuracy. In other words, the accuracy of correctly labeling a given image is seen to be in the range of 60%. While this rate can be considered high for a five-category model, it can be further strengthened with the assistance of more data.

In conclusion, image classification techniques are a significant tool that enhances the effectiveness of occupational safety risk analysis. They allow for a better understanding of potential hazards and reinforce security measures in workplaces. The integration of innovative technologies into occupational safety practices plays a vital role in preserving the health and safety of workers. Occupational safety is a multidisciplinary field with various stakeholders, and one of the most critical areas of focus is conducting risk analyses. Conventional methods involve risk analyses conducted by occupational safety experts of varying experience levels. Due to differences in experience, age, gender, years of work, and field specialization, disparities can arise in risk assessments, often leading to flawed or inadequate analyses. The study's starting point addresses the prevention of negative or insufficient situations resulting from person-dependent evaluations during risk analysis in occupational safety. The aim is to achieve rapid and effective decision-making through instant detections, swift interventions, proactive approaches, increased efficiency, and reduced operational costs. The method utilized in this study yields accurate results, with a success rate of up to 60% in correctly labeling images, aligning with these objectives. In future studies, it is anticipated that the method's enhancement, expansion of application areas, and diversification of work environments will lead to even more successful outcomes.

Scientific Ethics Declaration

The authors declare that the scientific ethical and legal responsibility of this article published in EPSTEM journal belongs to the authors.

Acknowledgements or Notes

* This article was presented as an oral presentation at the International Conference on Technology (www.icontechno.net) held in Antalya/Turkey on November 16-19, 2023.

References

- Ahn, J., Park, J. Lee, S.S., Lee, K., Do, H. & Ko, J. (2023). Safefac: Video-based smart safety monitoring for preventing industrial work accidents. *Expert Systems with Applications*, 215.
- Ak, Y. & Dereli, S. (2021). Bir otomasyon hattında parça secim ve ayırıştırma işlemlerinde kullanılan çoklu robotlar için goruntu isleme temelli gorev ataması yapan sistem onerisi. *ISITES2021*, 82-90. Sakarya, Turkey.
- Asad, M., Aidaros, O.A., Beg, R., Dhahri, M. A., Neyadi, S. A., & Hussein, M. (2017). Development of autonomous drone for gas sensing application. *2017 International Conference on Electrical and Computing Technologies and Applications (ICECTA)*, 1-6.
- Balakreshnan, B., Richards, G., Nanda, G., Mao, H., Athinarayanan, R., & Zaccaria, J. (2020). PPE compliance detection using artificial intelligence in learning factories. *Procedia Manuf.*, 45, 277–282.

- Basaran, G., & Cagil, G. (2022). Koruyucu gozluk kullanımının goruntu isleme yontemiyle tespit edilmesi. *El-Cezeri*, 9(1), 86-95.
- Bo, Y., Huan, Q., Huan, X., Rong, Z., Hongbin, L., Kebin, M., ... & Lei, Z. (2019). Helmet detection under the power construction scene based on image analysis. In *2019 IEEE 7th international conference on computer science and network technology (ICCSNT)*, 67-71. Dalian, China.
- Boyacıgil, M.F. (2022). *Goruntu isleme teknikleriyle bir endustriyel kalite kontrol uygulaması*. (Master's dissertation). Necmettin Erbakan University, Konya.
- Delhi, V.S.K., Sankarlal, R., & Thomas, A. (2020). Detection of personal protective equipment (PPE) compliance on construction site using computer vision based deep learning techniques. *Front. Built Environment*, 6, 136.
- Erkan, E., Ozcalik, H.R. & Yilmaz, S. (2015). Goruntu isleme teknikleri kullanılarak insan hareketlerini algılayan akıllı guvenlik sistemi tasarımı. *Journal of Engineering and Science*, 3(1), 1-6.
- Feng, L. (2022). Application analysis of artificial intelligence algorithms in image processing. *Mathematical Problems in Engineering*, 10.
- Fradi, M. Zahzah, E. H. & Machhout, M. (2022). Real-time application based CNN architecture for automatic USCT bone image segmentation. *Biomedical Signal Processing and Control*, 71.
- Fu, G., Xie, X., Jia, Q., Li, Z., Chen, S., & Ge, Y. (2020). The development history of accident causation models in the past 100 years: 24Model, a more modern accident causation model. *Process Safety and Environmental Protection*, 134, 47-82.
- Gonzalez, R. C., & Woods, R. E. (2008). *Digital image processing*. Pearson Education.
- Goodfellow, I., Bengio, Y., & Courville, A. (2016). *Deep learning* (Vol. 1). MIT Press.
- He, K., Zhang, X., Ren, S., & Sun, J. (2016). Deep residual learning for image recognition. In *Proceedings of the IEEE conference on computer vision and pattern recognition (CVPR)* (pp. 770-778).
- Jain, A. K. (1989). *Fundamentals of digital image processing*. Prentice Hall.
- Kim, H., Elhamim, B., Jeong, H., Kim, C., & Kim, H. (2014). On-site safety management using image processing and fuzzy inference. *International Conference on Computing in Civil and Building Engineering*, 1013-1020.
- Krizhevsky, A., Sutskever, I., & Hinton, G. E. (2012). ImageNet classification with deep convolutional neural networks. In *Advances in Neural Information Processing Systems (NIPS)*, 1097-1105.
- Lee, J. & Lee, S. (2023). Construction site safety management: A computer vision and deep learning approach. *Sensors*, 23(2), 944.
- Liu, W., Anguelov, D., Erhan, D., Szegedy, C., Reed, S., Fu, C. Y., & Berg, A. C. (2016). SSD: Single shot multibox detector. In *European Conference on Computer Vision* (pp. 21-37). Springer.
- Minaee, S., Boykov, Y., Porikli, F., & Plaza, A. J. (2020). Image segmentation using deep learning: A survey. *IEEE Transactions on Pattern Analysis and Machine Intelligence*.
- Moohialdin, A., Lamari, F., Marc, M., & Trigunarsyah, B. (2021). A real-time computer vision system for workers PPE and posture detection in actual construction site environment, *EASEC16* (pp.2169-218). Springer: Singapore.
- Onal, O., & Dandil, E. (2021). Object detection for safe working environments using YOLOv4 deep learning model. *Avrupa Bilim ve Teknoloji Dergisi*, 26, 343-351.
- Pratt, W. K. (2007). *Digital image processing*. John Wiley & Sons.
- Rajalingappaa, M., Niblack, W., Stober, J., & Nguyen, T. (2015). A deep learning based approach for automatic fetal facial feature detection and recognition. In *International Workshop on Machine Learning in Medical Imaging* (pp. 62-70). Springer.
- Redmon, J., Divvala, S., Girshick, R., & Farhadi, A. (2016). You only look once: Unified, real-time object detection. In *Proceedings of the IEEE conference on computer vision and pattern recognition* (pp. 779-788).
- Ren, S., He, K., Girshick, R., & Sun, J. (2015). Faster R-CNN: Towards real-time object detection with region proposal networks. In *Advances in Neural Information Processing Systems (NIPS 2015)*, 91-99.
- Rossi, M. & Brunelli, D. (2016). Autonomous gas detection and mapping with unmanned aerial vehicles. *IEEE Transactions on Instrumentation and Measurement*, 65(4), 1-11.
- Salvini, R., Mastrorocco, G., Esposito, G., Bartolo, S., Coggan, J. & Vanneschi, C. (2017). Use of a remotely piloted aircraft system for hazard assessment in a rocky mining area Lucca, Italy. *National Hazards and Earth System Sciences*, 18, 287-302.
- Shiklo, B. (2018, December 25). IoT in manufacturing: The ultimate guide. *ScienceSoft*. Retrieved from <https://www.scnsoft.com>
- Simonyan, K., & Zisserman, A. (2014). Very deep convolutional networks for large-scale image recognition. *ICLR 2015*.
- Sonka, M., Hlavac, V., & Boyle, R. (2014). *Image processing, analysis, and machine vision*. Cengage Learning Inc.

- Sotvoldiev, D., Muhamediyeva, T. & Juraev, Z. (2020). Deep learning neural networks in fuzzy modeling,” *Journal of Physics: Conference Series*, 144(1).
- Soyhan, I., Gurel, S. & Tekin, S. A. (2021). Yapay zeka tabanlı görüntü işleme tekniklerinin insansız hava araçları üzerinde uygulamaları. *European Journal of Science and Technology*, 24, 469-473.
- Sin, B., & Kadioglu, I. (2019). İnsansız hava aracı (IHA) ve görüntü işleme teknikleri kullanılarak yabancı ot tespiti yapılması. *Turkish Journal of Weed Science*, 22(2), 211-217.
- Tepe, S. (2023). *Sağlık sektöründe iş sağlığı ve güvenliği*. Akademisyen yayınevi.
- Torres, P., Davys, A., Silva, T., Silva, L. J. S., Kuramoto, A., Itagyba, B., ... Lopes, H. (2021). A robust real-time component for personal protective equipment detection in an industrial setting (pp.693-700). *International Conference on Enterprise Information Systems, Online Streaming -ICEIS 2021*.
- Turker, O., Toprak, O., Erarslan, B.A., Asilcioglu, E., Yılmaz, Y.,..... Engin, N. (2023). *Görüntü işleme teknolojileri. Tasarımda fotoğraf kullanımı* (1st ed., pp.193-213). Erzurum: Atatürk Üniversitesi Açık ve Uzaktan Öğretim Fakültesi Yayını.
- Venkatakrishna, S., & Kalyani, C. (2016). Basic of image processing technologies. *International Journal of World Research*, 1(34).
- Yao, B., & Fei Fei, L. (2010). *Grouplet: A structured image representation for recognizing human and object interactions. Computer vision—ECCV 2010* (pp. 339-352). Berlin, Heidelberg: Springer.
- Yu, Y., Guo, H., Ding, Q., Li, H., & Skitmore, M. (2017). An experimental study of real-time identification of construction workers' unsafe behaviors, *Autom. Constr*, 82, 193–206,.
- Zhang, X. (2022). Application of artificial intelligence recognition technology in digital image processing. *Wireless Communications and Mobile Computing*, 10.

Author Information

Serap Tepe

The University of Health Sciences
Department of Occupational Health and Safety,
Istanbul, Turkey
Contact e-mail: serap.tepe@sbu.edu.tr

Serkan Eti

Istanbul Medipol University
Department of Computer Programming, Medipol University
Istanbul, Turkey

To cite this article:

Tepe, S., & Eti, S. (2023). A research on determining the degree of risk by using ResNet. *The Eurasia Proceedings of Science, Technology, Engineering & Mathematics (EPSTEM)*, 24, 126-134.

The Eurasia Proceedings of Science, Technology, Engineering & Mathematics (EPSTEM), 2023

Volume 24, Pages 135-140

IconTech 2023: International Conference on Technology

Energy Management of the Hybrid Electric Wheel Loader

Mustafa Karahan

HIDROMEK Research and Development Center

Abstract: In recent years, the design and development of battery or hybrid electric vehicles that work with high efficiency instead of conventional vehicles with internal combustion engines have been very popular, and a lot of vehicle and machine manufacturers are focusing on these kinds of projects and research. In developed countries, electric construction machines are already in use in urban areas. Electric or hybrid vehicles have not only less or zero carbon emission but also less noise emission. In this study, the energy management system of a hybrid electric wheel loader is described. The algorithm of the energy storage system is designed with energy recuperation. In this vehicle, supercapacitors are used to store energy and recuperation. There is no electric battery except 24 V of the local engine batteries. The pros and cons of supercapacitors are mentioned by comparing them to lithium batteries. Power and energy calculations of the supercapacitors are described. This study also provides a valuable approach to fully electric construction machinery. The energy management of a vehicle is quite significant to have better efficiency and less fuel consumption for hybrid electric vehicles. In vehicles with conventional internal combustion engines, some amount of energy is converted to heat energy to slow down or stop the vehicles by the brake system. In this study, some of the energy, called regenerative brake energy, is stored in supercapacitors to use later in the systems.

Keywords: Energy management, Electrification, Hybrid electric construction machinery, Supercapacitors

Introduction

Hybrid Electric Wheel Loader

Hybrid electric driveline is one of the ways to increase the efficiency of vehicles and reduce fuel consumption and carbon emissions. This study is based on a real electrification development project of the wheel loader. The vehicle which is described in this study, the primary energy provider is the generator driven by the engine.

In conventional wheel loaders with internal combustion engines, the energy coming from flywheels of engines is transmitted to drivelines by torque converters, which have 70% efficiency. This means the other 30% is wasted as heat energy and released into the atmosphere. Due to the vehicles' operation conditions, connecting engines to the driveline is not a safe and proper solution. This system does not need a torque converter between the energy source electric motors and the driveline. The electric motors are able to drive the powertrain directly.

The diesel engine drives the generator to provide energy to the system. The separate electric motor drives the implementation and fan pumps. Although the primary energy source is the generator, the supercapacitors store the regenerative brake energy and provide high instantaneous energy demand, which is very common for wheel loader operational conditions. Thus, it is possible to run the diesel engine in a highly efficient range.

Driving separately the electric motors of the powertrain and hydraulic systems improves the overall efficiency. Besides these, avoiding engine speed fluctuation contributes to efficiency. The main focus of this electrification project is increasing energy efficiency and reducing fuel consumption and exhaust gas emissions. The overall layout is shown in Figure 3.

- This is an Open Access article distributed under the terms of the Creative Commons Attribution-Noncommercial 4.0 Unported License, permitting all non-commercial use, distribution, and reproduction in any medium, provided the original work is properly cited.

- Selection and peer-review under responsibility of the Organizing Committee of the Conference

© 2023 Published by ISRES Publishing: www.isres.org

Parallel Hybrid Topology

In parallel hybrid vehicles, the engine drives the generator as well as the drive train and hydraulic system. This means the engine is mechanically connected to both the generator and energy consumers. For wheel loader implementations, this solution is a less efficient, however cost-effective solution. Parallel hybrid topology is shown in Figure 1.

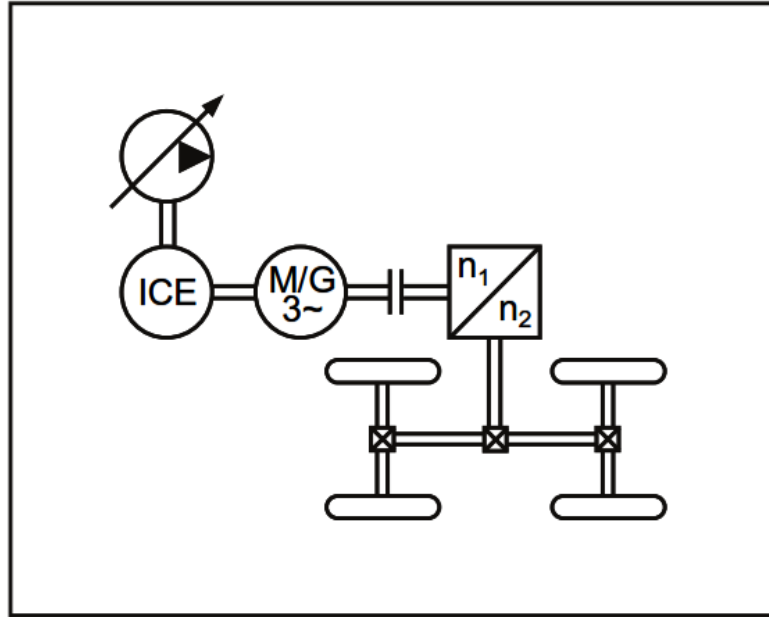


Figure 1. Parallel hybrid topology

Serial Hybrid Topology

There is no direct mechanical connection to the drivetrain, implement, and steering hydraulic pumps. Especially for construction equipment such as wheel loaders, serial hybrid topology brings advantages such as higher efficiency, less fuel consumption, and carbon/noise emissions. Parallel hybrid topology is shown in Figure 2. In this study, a serial hybrid topology has been used to develop the overall vehicle layout.

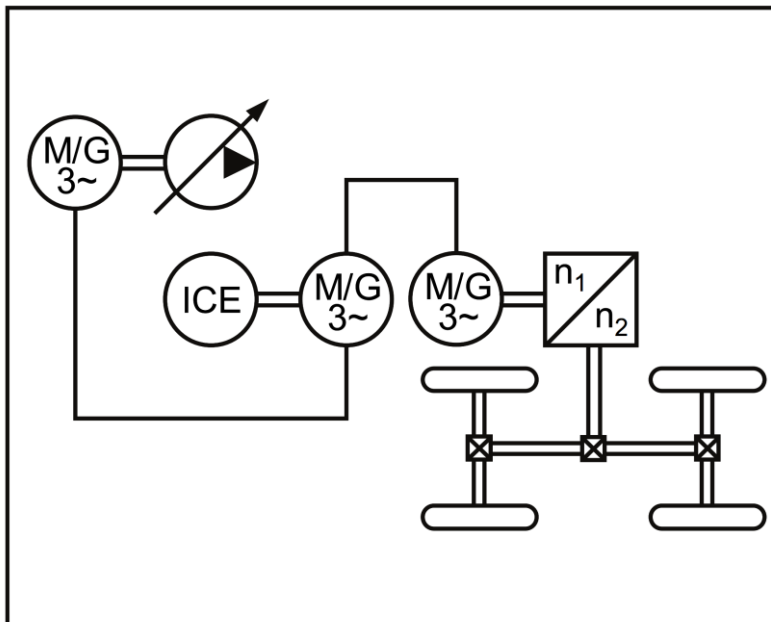


Figure 2. Serial hybrid topology

Electronic Brake System

In conventional vehicles, a hydromechanical brake system is used to slow down or stop vehicles. The hydromechanical brake system consists of a mechanical pedal and a hydraulic system. It doesn't have any electronic control equipment. An electronic brake system can manage vehicle brake systems through electronic signals and software. New-generation electric vehicles need this kind of electronic controls to improve efficiency. The electronic brake system provides sufficient and efficient management to the regenerative brake system. Meanwhile, not only in electric vehicles but also in autonomous vehicles, the system plays a crucial role.

The electronic brake system consists of a hydraulic pump providing the hydraulic power, an electronic pedal that detects the brake signals from the operator, an electronic control unit that includes the software according to the algorithm, a proportional electronic dual brake valve, accumulators, and accumulator charge valve which stores some of the hydraulic energy.

Energy Management and System Algorithm

Energy management plays a very significant role in electric vehicles or construction machines to improve efficiency, reduce energy consumption, and increase range or duty period. With recent technologies, energy management is carried out by sophisticated algorithms and software. Only by improving the software of electric vehicles, not changing the hardware or equipment, overall efficiency can be improved highly.

One innovative way of this study is developing an algorithm to run vehicle energy efficiently. The algorithm determines the conditions when regenerative brake energy is obtained and when the supercapacitors are charged. By means of the electronic brake system, regenerative brake energy is managed successfully and efficiently. The regenerative energy is based on running the traction motors as a generator to obtain energy from the brake system instead of converting the heat energy. The system works through detecting the brake signal. The energy management system detects the charge level of the energy storage package of supercapacitors and decides whether the package needs to be charged or not. For safety reasons and emergency conditions, the system must know the signal status and determine the charging strategy.

Supercapacitors can be charged by the generator to the defined level to meet the vehicle's short-time peak power demands so that the engine can work at a highly efficient torque and speed range. Due to the limited energy storage capacity of the supercapacitors, after they are charged to 100%, the main energy provider generator runs as a motor to meet the engine's parasitic losses and the energy demand of auxiliary equipment such as air conditioning and cabin electricity. Running the primary energy source generator as a motor is considered state-of-the-art. The working algorithm of the energy management system is shown in the Figure 4.

Energy and Power Calculation of Supercapacitors

Supercapacitors are called with their capacitance Farad. In engineering, energy and power units are used for comparison. (1) and (2) formulas describe the calculation of energy and power calculation of supercapacitors.

C : Capacitance [F]
ESR : Equivalent series resistance [$m\Omega$]
V : Voltage [Volt]
E : Energy [Wh]
 P_{max} : Maximum power [kW]

$$E = 0.5 * C * V^2 \quad (1)$$

$$P = V^2 / 4 * ERS \quad (2)$$

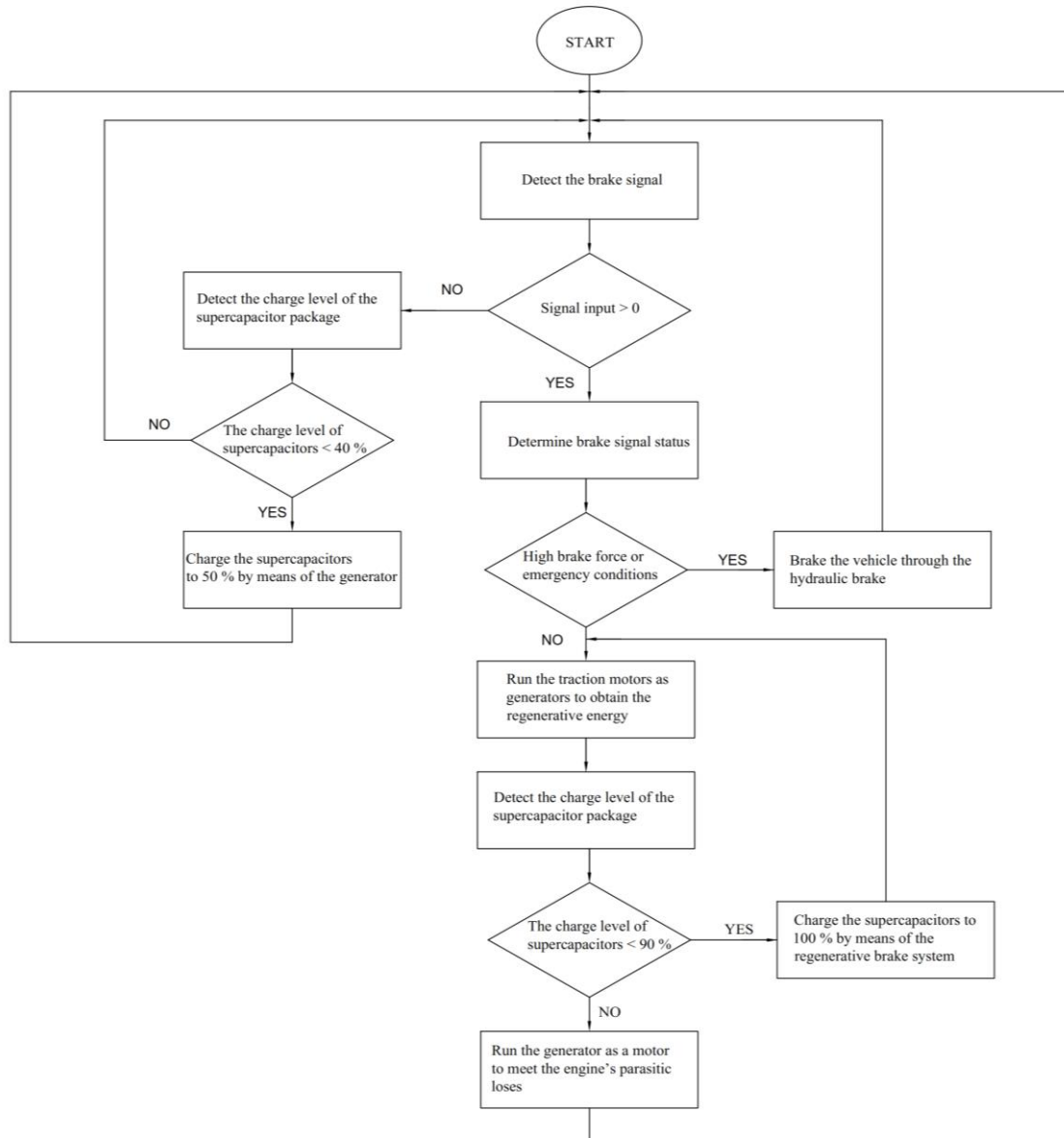


Figure 4. Working algorithm of the energy management system

Table 1. Comparison between supercapacitors and lithium batteries

	Supercapacitors	Lithium Batteries
Operating Temperature, °C	-40 / +70 (85)	-20 / +40
Cycle Life	> 1.000.000	3.000 – 10.000
Calendar Life, Year	5 - 20	3 - 10
Energy Density, Wh/L	1-10	250-650
Power Density, W/L	1.000- 10.000	850-3.000
Efficiency, %	> 98	80-90
Charge Rate, C/x	> 1.500	< 40
Discharge Time	Seconds or Minutes	Hours
Voltage Output	Variable	Constant
Self-Discharge	High	Low

Pros and Cons of Supercapacitors

Supercapacitors have become prominent with their high efficiency, long service life, extensive operating temperature range, short charging time, high instantaneous power, and current capabilities. On the other hand,

compared to lithium-ion batteries, their disadvantages are low energy density, changing voltage output, and high self-discharge. The comparison is shown in the Table 1.

Conclusions and Recommendations

Why conventional wheel loaders with internal combustion engines are energy inefficient, and their reasons are explained. The working algorithm of the hybrid electric wheel loader has been created. Supercapacitors have high power density. However, their energy storage amount is relatively low. With several aspects, supercapacitors and batteries are compared. In this study, the working strategy of the regenerative brake system is described, and the charging strategy of the supercapacitors is defined. In which cases, the traction motors run as generators, and the generator runs as a motor are defined.

For on-road and off-road vehicles, it is recommended to use supercapacitors and batteries together. Significantly, the regenerative braking system can cause stresses and thermal runaway on lithium batteries and can reduce their lifetime. Thus, the better approach for the regenerative braking system is using supercapacitors to store the regenerative energy. Supercapacitors are capable of charging and discharging continuously with a high-power rate without thermal runaway.

Scientific Ethics Declaration

The author declares that the scientific ethical and legal responsibility of this article published in EPSTEM journal belongs to the author.

Acknowledgements or Notes

* This article was presented as an oral presentation at the International Conference on Technology (www.icontech.net) held in Antalya/Turkey on November 16-19, 2023.

References

- Corbett, F. (n.d.). *Supercapacitors as long-life solution in battery powered applications*. Retrieved from <https://www.tti-europe.com/content/supercapacitors-in-battery-powered-applications.pdf>
- Eaton Electronics Division. (2022). *The major differences between supercapacitors and batteries*. Retrieved from <https://www.eaton.com/content/dam/eaton/products/electronic-white-paper-elx1150-en.pdf>
- Eaton Electronics Division. (n.d.). *Supercapacitors versus batteries*. Retrieved from <https://www.eaton.com>
- Filla, R. (2009). Hybrid power systems for construction machinery: aspects of system design and operability of wheel loaders. In: *ASME International Mechanical Engineering Congress and Exposition*, 611-620.
- Sleppy, J. (2021, April, 15). Batteries vs supercapacitors? The answer is both Retrieved from <https://www.capacitehenergy.com>

Author Information

Mustafa Karahan

HIDROMEK, Research and Development Center
Ahi Evran OSB mh. Osmanlı cd. No:1
06935 Sincan – Ankara / TURKEY
Contact e-mail: mustafa.karahan@hidromek.com.tr

To cite this article:

Karahan, M. (2023). Energy management of the hybrid electric wheel loader. *The Eurasia Proceedings of Science, Technology, Engineering & Mathematics (EPSTEM)*, 24, 135-140.

The Eurasia Proceedings of Science, Technology, Engineering & Mathematics (EPSTEM), 2023

Volume 24, Pages 141-148

IConTech 2023: International Conference on Technology

Performance Assessment of Sustainable Machining Techniques

Vamsi Krishna Pasam

National Institute of Technology Warangal

Kartheek Gamidi

National Institute of Technology Warangal

Banoth Srinu

National Institute of Technology Warangal

Lingaraju Dumpala

JNTU Kakinada

Abstract: One of the often used strategies in the machining process is to lower the cutting temperature and enhance the tool life with the application of cutting fluids. The application of conventional cutting fluids is wide spread and commonly found in industries. In spite of their advantages, the application of these conventional cutting fluids is not financially feasible because of their high disposal costs, non eco-friendly and also damages the operator's health. In this context, alternative techniques to cutting fluids that can be more sustainable is the need of the hour. This work focuses on a comprehensive experimental investigation of such alternative techniques, including MQL (Minimum Quantity Lubrication) using vegetable oil-based hybrid nano fluids which are more environmentally friendly, and machining processes that are assisted by ultrasonic vibration without the use of cutting fluid. The study also highlights the advantages of these processes over machining using conventional cutting fluids and provides insights in to the available alternate techniques in terms of their machining performance. These approaches can be a better alternative option for reducing cutting forces, cutting temperatures, and tool wear while improving surface finish.

Keywords: MQL, Vegetable oils, Nano fluids, Hybrid nano fluids, Ultrasonic machining

Introduction

The standard technique for improving surface quality of workpiece and productivity is through lubrication and cooling by employing cutting fluids. By decreasing friction between contacting surfaces, lubrication reduces heat generation, and provides cooling action that lowers the cutting temperature by dispersing heat. (HMT & Production Technology, 2001) Most of the industries were utilizing lubricants for lubricating their machines. Among the constituents of lubricant, petroleum remains the primary ingredient with significant percentage (De Silva & Wallbank, 1999). Furthermore, In the machining industries, metal working lubricants are the form of lubricants that boost product efficiency by lubricating and cooling actions. As a result, the consumption of metalworking fluids in the machining industries increased. Despite the numerous advantages they offer, it was discovered that standard cutting fluids have certain drawbacks. Conventional cutting fluids need to be disposed of since they lose their effectiveness and quality over time. Because these fluids are not biodegradable, their disposal causes ecological imbalance. Due of their concern over the environment and sense of responsibility, manufacturing industries have thus started to put an endeavor to clean up the zones that are prone to cutting fluids slurry. Mist production is another issue connected to the application of cutting fluids. Aerosol buildup in the respiratory systems of workers exposed to these conditions, causes chronic pulmonary diseases. According to numerous studies undertaken by academia, exposure to cutting fluids causes chronic skin

- This is an Open Access article distributed under the terms of the Creative Commons Attribution-Noncommercial 4.0 Unported License, permitting all non-commercial use, distribution, and reproduction in any medium, provided the original work is properly cited.

- Selection and peer-review under responsibility of the Organizing Committee of the Conference

© 2023 Published by ISRES Publishing: www.isres.org

conditions including dermatitis in machine tool operators, accounting for over 80% of their work-related medical disorders. (Bennett, 1983).

When used as lubricants during machining, conventional cutting fluids cause a number of technological and environmental issues. Some of these include respiratory and skin issues for the workers, water and soil contamination while disposal, and more significantly, chemically disassociation of cutting fluids causes environmental pollution (Howes et al.1991; Passman & Roosemoore et al. , 2002) reported that gram-positive bacteria produced by the use of artificial and semi-synthetic cutting lubricants is growing, which promotes the spread of diseases to workers exposed to such conditions. According to Korde et al. (1993), over 7–10 lakh operators in the United States alone were exposed to cutting fluids, based on the bio degradation of chlorinated chemicals. The existence of bacteria and fungi, especially in water-soluble cutting solutions, results in the production of toxic microbial byproducts. Zeman et al.(1995) and Sreejith et al. (2000) concluded that standard cutting fluids harm both the operators health and environment. Also, due to increased environmental concern and positive actions for pollution control, manufacturing businesses have been facing a significant barrier to minimize the application of conventional cutting fluids (Tan et al.,2002) . The amount of lubricants used worldwide in manufacturing industries totaled about 38 mmt (million metric tonnes), with an (estimated growth of 1.2% over the next ten years (Kilne& company, 2006). According to Filipovic et al.(2000), using cutting fluids in bulk results in a significant share of the overall manufacturing cost. Installation and maintenance expenses for fluid supply systems, the fundamental cost of purchasing fluid, the price of fluid disposal, and the economics of treating fluid waste are only a few of the costs associated with cutting fluids. The aforementioned expenses are substantial because production facilities use numerous reservoirs that have a storage capacity of thousands of gallons of fluid.

Due to issues with quality, it is occasionally necessary to flush out all of the fluid in the tanks systems to clean the system. (Byrne & Scholta, 1993). Relative to cutting tools, manufacturing facilities spend higher cost on cutting fluids (Sokovic & Mijanovic, 2001; Sanchez et al., 2010). Researchers were urged to do in-depth study on cutting fluid substitutes that could eventually lead to environmental friendliness and sustainable production. To be able to reduce the negative impact on the environment and worker's health, a variety of alternatives to the usual cutting fluids are presented, including solid lubricants, dry machining, Minimum Quantity Lubrication (MQL), cryogenic coolant, vegetable oils, and nanofluid (Padmini et al., 2015).

In view of the reported literature, it can be understood that the conventional cutting fluids in spite of the widespread use in the manufacturing industry, has lot of disadvantages from environmental and human health perspectives. In addition, cost of production also increases due to the high cost incurred in their disposal. This work suggests alternative techniques that can be more advantageous and ecofriendly. The study deals with a consolidated experimental study of the development of environmentally friendly cutting fluids, such as vegetable oils based nanocutting fluids, and cutting fluid-free ultrasonic machining methods.

Alternative Sustainable Techniques

Nano Cutting Fluids Based on Vegetable Oil

One of the alternatives proposed is the employment of nano fluids in place of traditional cutting fluids following a thorough analysis of the application of vegetable oils, solid lubricants, and nanofluids in turning operation utilizing the MQL (minimum quality lubrication) method.

Vegetable oils were used to prepare nanofluid, which is a base fluid with nanoparticle suspensions. Due to their efficient cooling and lubricating qualities, coconut, sesame, and canola oils have been used as base fluids. Nano boric acid (nBA) and nano molybdenum di-sulphide (nMoS₂) suspensions were dispersed in base fluids at different percentages by weight (0.25%, 0.5%, 0.75%, and 1%) to produce various nano fluids.. The viscosity, thermal conductivity(k), and stability of the newly created nanofluid were examined to test whether they are suitable as cutting fluids for AISI 1040 steel. Figure 1 illustrate the experimental setup used to supply nanofluids. The cutting parameters that could be configured on the machine tool utilized for the turning operation are selected based on the literature reviewed. Cutting speeds of 40, 60, and 100 m/min, depth of cut of 0.5 mm and feed rates of 0.14, 0.17, and 0.2 mm/rev were chosen for the turning process.. By using the MQL approach, 10 ml/min of the nanofluid was fed to the machining zone by means of a nozzle. Surface roughness measurements and tool flank wear studies were done offline where as observations of machining conditions, cutting temperatures, and forces were done online. Several factors were looked at in order to determine how well nanofluid improved machining performance.

In contrast to dry machining with similar cutting conditions and 0.25% nano particle inclusion, results from experiments indicated that cutting temperature, cutting force, tool wear, and surface roughness were reduced by 33%, 45.5%, 19% and 46%, respectively due to the presence of nano fluids in the machining zone. CC+nMoS₂ performed better than the evaluated vegetable oil based nanofluids. Additional research found that 0.5% of nMoS₂ displayed greater performance, which is also evident from Figs.2 (a) – (d). This effect is a result of less friction at the tool-work interface and improvement in heat transfer from the cutting zone. ANOVA and Grey Relational Analysis are also used to anticipate the principal cutting force, cutting tool temperatures, surface roughness, and tool wear that are produced by employing nano fluids during machining. The findings indicated that the percentage of nanoparticles followed by the type of base fluid are the major factors. In addition, cutting speed was found to be an important machining parameter. The use of nano particles at low concentration in bio degradable vegetable oils under MQL condition ensures the sustainability of the process.

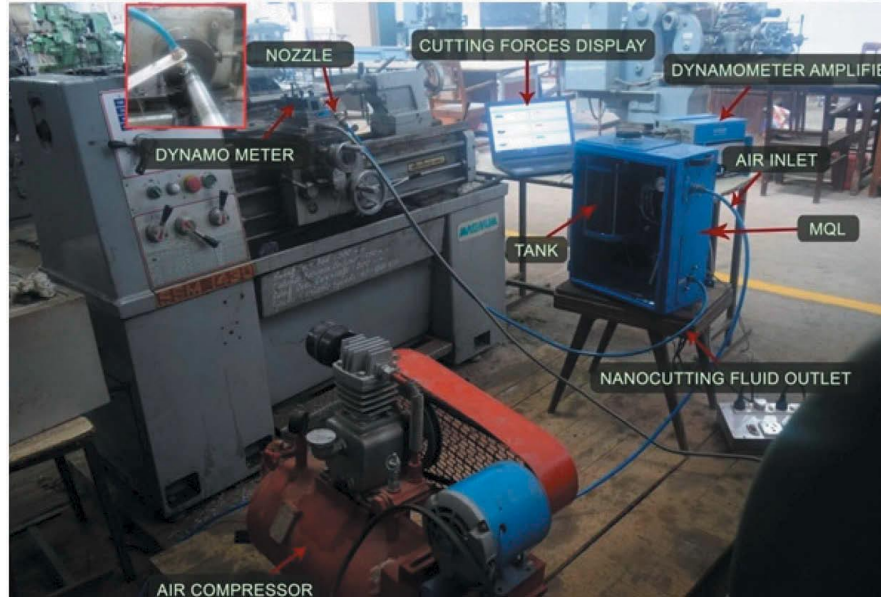


Figure 1. Experimental setup

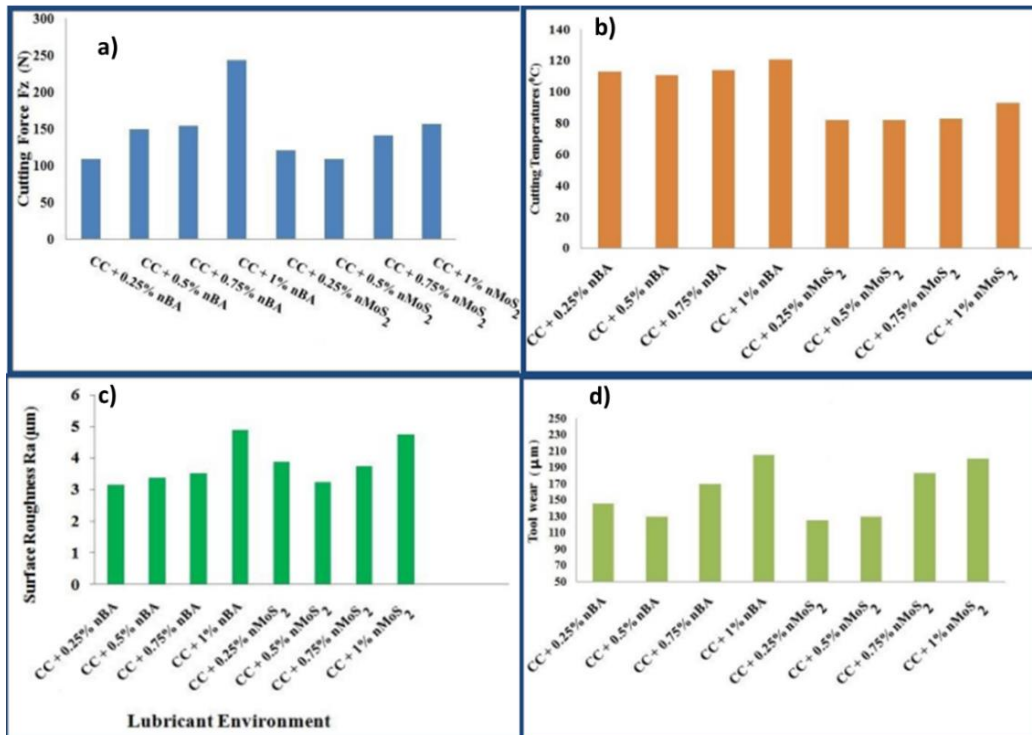


Figure 2. Machining responses with different combinations of nano fluids a) Cutting force b) Cutting temperature c) Surface roughness d) Tool wear

Hybrid Cutting Fluids Made with Vegetable Oil

In-depth investigation was made into the MQL technique's ability to reduced cutting force, cutting temperature, surface roughness, and tool flank wear. As mentioned earlier, dry machining and vegetable oil-based nano fluid (VOBNCF) offer distinct advantages over conventional cutting fluids (CCF). Also, research showed that hybrid nano fluid (HNF) outperformed nanofluid in terms of anti-wear and anti-friction performance. Unfortunately, relatively few studies on the assessment of HNF stability and use of HNFs in machining were reported by researchers.. The improved thermophysical, anti-friction, and anti-wear characteristics of HNCFs serve as the driving force behind this effort, which aims to comprehend the ability of HNCFs when turning AISI 1040 steel. The same experimental set-up used for nanofluids is employed in the investigation of hybrid nanofluids also. Initially, three vegetable oils namely , sesame, neem and mahua oil were used with 1% weight of CNT/BA and CNT/MoS₂ nanoparticles. The distinct HNCFs were prepared using SDS (sodium dodecyl sulphate), TritonX100, and Tween80 as surfactants. Moreover, the weight proportion of nanoparticles in the surfactant composition varied between samples. The preparation of these HNCFs involved the use of hybrid ratios of 1:1, 1:2, and 2:1. Using the sedimentation test and the Zeta potential test, stability was assessed. On the basis of stability, the Taguchi method was used to choose the optimal HNCF composition. In contrast to CNT/BA hybrid nanofluid, it is discovered that the CNT/MoS₂ hybrid nanofluid based on sesame oil is more stable. The best hybrid ratio for improved nanofluid stability is CNT/MoS₂ hybrid nanofluid based on sesame oil with SDS surfactant at 15% concentration of nanoparticles by weight in base oil.

The same stable HNCF was used to assess and compare the machining performance under constant cutting conditions (80 m/min cutting speed; 0.161 mm/rev feed rate; 0.5 mm depth of cut). MQL flow rate for supplying cutting fluid in machining zone is 10 ml/min. By dispersing CNT/MoS₂ nanoparticles in sesame oil at a hybrid ratio of 1:2 in concentrations of 0.5%, 1%, 1.5%, 2%, 2.5%, and 3% (wt.), HNCFs are prepared. Sodium dodecyl sulphate (SDS), was employed as surfactant. The content of SDS was taken as 15% weight of nanoparticles in all concentrations. Stability of prepared HNCFs was evaluated using sedimentation technique.

The optimal concentration of CNT/MoS₂ is shown to have the lowest coefficient of friction and better machining performance in terms of reduced cutting force, cutting temperature, surface roughness, and tool flank wear. Turning experiments were carried out under various cutting conditions to evaluate the effectiveness of HNCFs in the machining of AISI 1040 steel. Analysis of variance (ANOVA) was also carried out while designing experiments utilising the RSM technique. Using hybrid nano cutting fluids, significant reductions in cutting force, cutting temperature, surface roughness, and tool flank wear were found and the same is illustrated in Figs. 3 (a) - (d).

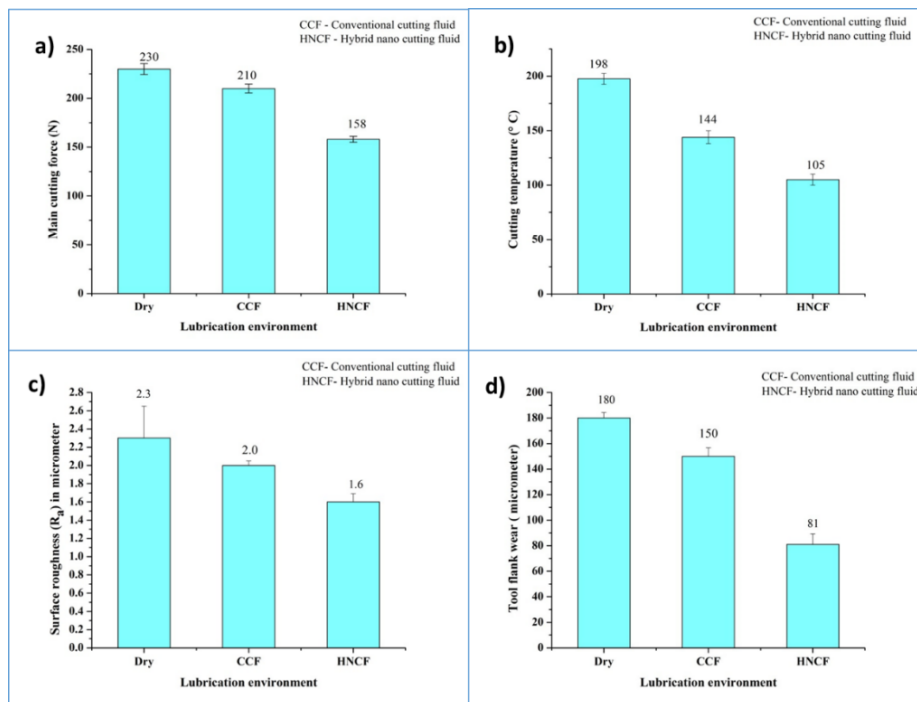


Figure 3. Machining responses with different cutting fluids a) Cutting force b) Cutting temperature c) Surface roughness d) Tool wear

At 2 weight percent of CNT/MoS₂ hybrid nano cutting fluid, in comparison to dry machining and CCF, the thrust force, feed force, and primary cutting force are reduced by 22% and 1.2%, 28.3% and 13.8 %, and 32 % and 27.3 %, respectively. CNT/MoS₂ (1:2) hybrid nano cutting fluid at 3 wt% reduces cutting temperature by 43.4% and 28%, tool flank wear by 81.3% and 75%, compared to dry machining and CCF, respectively. Surface roughness is decreased at 2 wt% of the hybrid CNT/MoS₂ (1:2) nano cutting fluid by 28.5% and 18.3% when compared to dry machining and CCF, respectively. Cutting speed, feed, and depth of cut are significant variables effecting the cutting temperature and cutting force. Cutting speed and feed are more significant than depth of cut when it comes to tool flank wear and surface roughness.

Vibration Assisted Machining

To circumvent the issues with CT, one of the best machining techniques for challenging materials like Ti6Al4V alloy is ultrasonic vibration assisted turning . The UVAT(Ultrasonic Vibration Assisted Turning) setup is shown in Fig. 4. In this technique, the cutting tool is subjected to low amplitude and high frequency vibrations. The intermittent cutting nature due to applied vibrations is the reason for improved machinability of UVAT process. When compared to CT of Ti6Al4V alloy, UVAT method significantly improves surface finish while reducing cutting force and cutting temperature, according to experimental and numerical observations. The surface integrity induced by the machining process may have significant effect on fatigue life of components. The surface integrity refers to the surface characteristics (topography characteristics) and sub surface characteristics (sub layer characteristics). These characteristics may change due to variation of thermomechanical loading during cutting process. Residual stress is one of the important characteristic affected by the variation of thermomechanical loading during cutting process. So, it is crucial to research how machining factors affect residual stresses in Ti6Al4V alloy UVAT. According to numerical and experimental investigations, when machining Ti6Al4V alloy using the UVAT process, compressive residual stresses are produced on the surface of the machined component. The TWCR (tool work contact ratio), which is a function of the cutting speed, frequency, and amplitude employed in the process, significantly effects the performance of UVAT. With lower TWCR, the machining process performs better. Studies indicate that frequency, amplitude, and cutting speed are the three key factors influencing TWCR in the UVAT process. TWCR increased with increasing cutting speed but decreased with increasing frequency and amplitude.

This study assessed UVAT's ability to machine Ti6Al4V alloy in terms of cutting force, cutting temperature, and surface roughness. The trials were conducted using various machining and vibration conditions. According to the observations, cutting force, cutting temperature, and surface roughness were reduced in UVAT than CT. Cutting forces are reduced at lower cutting speeds and they are increased as the cutting speed is increased. This is due to increased TWCR with increase in cutting speed. For both UVAT and CT processes, increasing cutting speed causes the cutting temperature to increase while decreasing surface roughness.



Figure 4. Ultrasonic turning setup

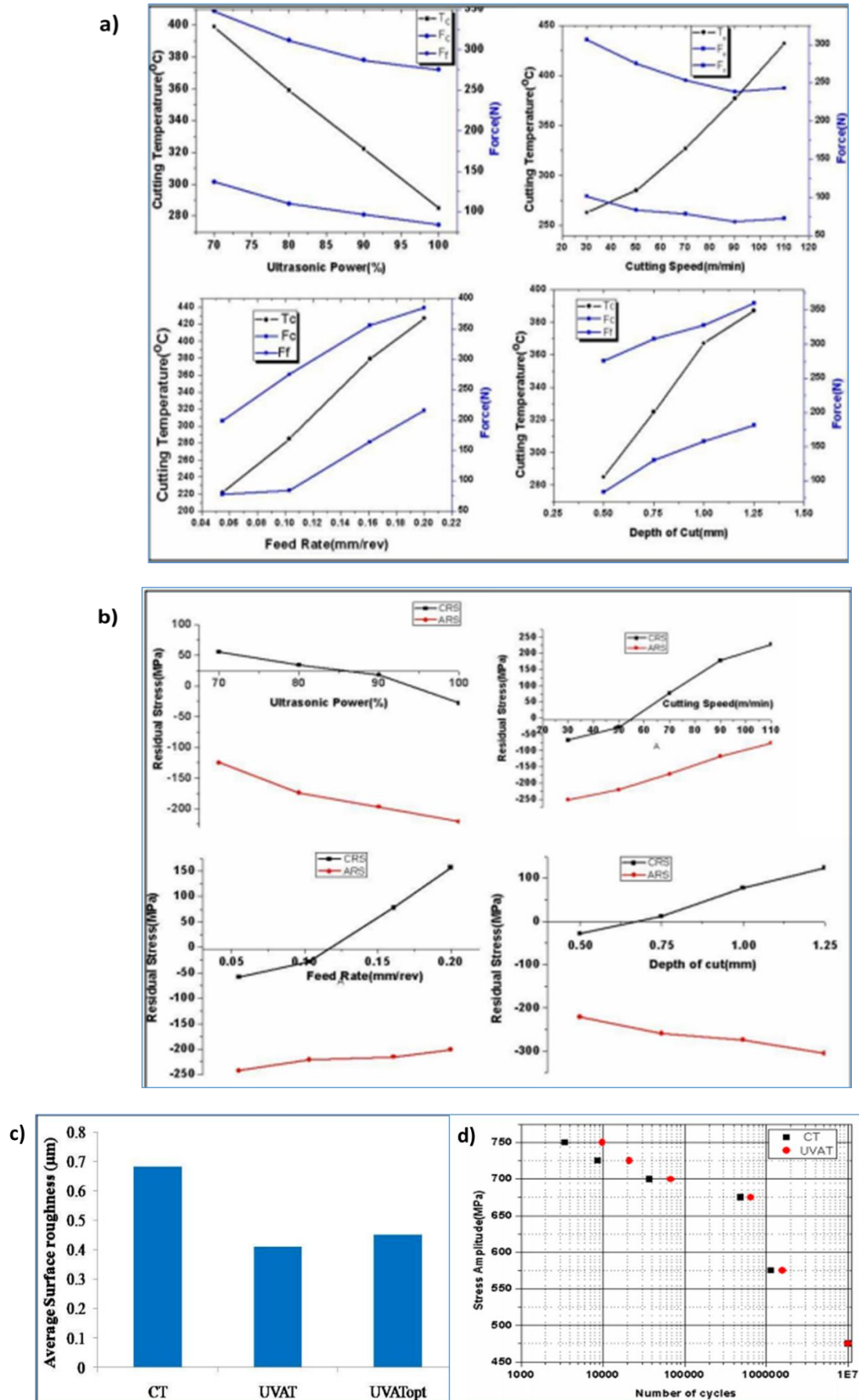


Figure 5. Machining responses in UVAT a) cutting temperature b) residual stress c) surface roughness d) fatigue life

The machining performance in the UVAT process is influenced by both mechanical and thermal loading. However, because to the combined effects of TWCR, adiabatic heat, and aerodynamic lubrication, the influence of mechanical loading dominates at lower values of machining conditions whereas thermal loading dominates at higher values of machining conditions. Because to shorter contact time in the UVAT process compared to CT at higher ultrasonic powers, the maximum and average flank wear of the tool decreases with increase in ultrasonic power. When ultrasonic power is increased from 80% to 90%, the tool life was doubled. Moreover, UVAT generates compressive residual stresses that are intended to improve the component's fatigue life. The responses from the experimental studies were shown in fig. 5 (a) – (c). The variation in fatigue life for specimens machined using UVAT and CT is shown in fig. 5 (d). The Fatigue life of UVAT sample performed is better than the CT in the selected range of machining parameters.

Conclusion

The conclusions form experimental studies conducted on alternate to cutting techniques are as follows:

Nano fluids made from vegetable oil and solid lubricants could lower the cutting force by 45.5%, cutting temperature by 33%, and tool wear by 19% and Surface finish is improved by 46% in comparison with dry machining making the cutting better and sustainable. The performance is influenced by workpiece material, base oil, type of nano particle and percentage of nano particles.

Hybrid nano cutting fluids showed a reduction in cutting forces by 27.3%, cutting temperatures by 28%, tool wear by 75%, and surface finish is enhanced by 18.5% compared to conventional cutting fluids. Hybrid nanofluid performance depends on base oil and type of nano particles used, ratio of nano particles and quantity of nano particles in the base fluid.

UVAT of Ti6Al4V alloy is found to reduce cutting force and temperature by 10 % to 40% and 10% to 30%, respectively, while improving surface finish by 20% to 50% compared to dry cutting. Notably, the procedure uses no cutting fluid, which increases its sustainability. In UVAT cutting speed, vibration frequency and amplitude are the significant parameters on the performance of the process.

Scientific Ethics Declaration

The authors declare that the scientific ethical and legal responsibility of this article published in EPSTEM journal belongs to the authors.

Acknowledgements or Notes

* This article was presented as an oral presentation at the International Conference on Technology (www.icontechno.net) held in Antalya/Turkey on November 16-19, 2023.

References

- Bennett, E. O. (1983). Water based cutting fluids and human health. *Tribol Int*,16(3),133-136.
- Byrne, G., & Scholta, E. (1993). Environmentally clean machining processes- a strategic approach. *Annals of CIRP*, 42(1), 471-474.
- De Silva, M.B., & Wallbank, J. (1999). Cutting temperature: prediction and measurement methods-a review. *Journal of Materials Processing Technology*, 88(1-3), 195-202
- Filipovic, A., Olson, W., Pandit, S., & Sutherland, J. (2000). Modeling of cutting fluid system dynamics. *Proc.2000 Japan – U.S.A. Symposium on Flexible Automation*.
- HMT. (2001). *Production technology* (18th ed.). Tata McGraw Hill Publishers.
- Howes, T.D., Toenshoff, H.K., & Heuer, W. (1991). Environmental aspects of grinding fluids. *Annals of CIRP*, 40(2), 623-629.
- Kline & Company, Inc. (2006). Competitive intelligence for the global lubricants industry 2004–2014. Retrieved from <https://klinegroup.com/>

- Korde, V.M., Phelps, T., J, Bienkowski, P.R., & White, D.C. (1993). Biodegradation of chlorinated aliphatics and aromatic compounds in total-recycle expanded-bed reactors. *Appl. Biochem Biotechnol*, 45(46), 731–740.
- Padmini, R., Vamsi Krishna, P., & Krishna Mohana Rao, G. (2015). Performance assessment of micro and nano solid lubricant suspensions in vegetable oils during machining, *Proc. Inst. Mech. Eng. Part B J. Eng. Manuf.*, 229(12), 2196–2204.
- Passman, F.J., & Roossmore, H.W. (2002). Reassessing the health risks associated with employee exposure of 203 metalworking fluid microbes. *Lubrication Engineering* 58(7), 30-38.
- Sanchez, J.A., Pombo, I., Alberdi, R., Izquierdo, B., Ortega, N., Plaza, S., & Martinez J. (2010). Machining evaluation of a hybrid MQL-CO₂ grinding technology. *Journal of Cleaner Production*, 18(18), 1840-1849.
- Sokovic, M., & Mijanovic, K. (2001). Ecological aspects of the cutting fluids and its influence on quantifiable parameters of the cutting processes. *Journal of Materials Processing Technology*, 109(1-2), 181-189.
- Sreejith, P.S., & Ngoi, B. K. A. (2000). Dry machining: of the future. *Journal of Material Processing Technology*, 101, 287 - 291.
- Tan, X.C., Tan, X.C., Liu, F., Co, H.J., & Zhang, H. (2002). A decision making frame work model of cutting fluid selection for green manufacturing and a case study. *International Journal of Machine Tools and Manufacture*, 129,467- 470.
- Zeman, A., Sprengel, A., Niedermeier, D., & Spath, M. (1995). Biodegradable lubricants-studies on thermo oxidation of metal-working fluids by differential scanningcalorimetry (DSC). *Thermochim Acta*, 268, 9–15.

Author Information

Vamsi Krishna Pasam

National Institute of Technology Warangal
Warangal, India
Contact e-mail: vamsikrishna@nitw.ac.in

Kartheek Gamidi

National Institute of Technology Warangal
Warangal, India

Banoth Srinu

National Institute of Technology Warangal
Warangal, India

Lingaraju Dumpala

JNTU Kakinada,
Andhra Pradesh, India

To cite this article:

Pasam, V. K., Gamidi, K., Srinu, B., & Dumpala, L. (2023). Performance assessment of sustainable machining techniques. *The Eurasia Proceedings of Science, Technology, Engineering & Mathematics (EPSTEM)*, 24, 141-148.

The Eurasia Proceedings of Science, Technology, Engineering & Mathematics (EPSTEM), 2023

Volume 24, Pages 149-157

IconTech 2023: International Conference on Technology

Industry 5.0 and National Development Plans

Beste Alpaslan

OSTIM Technical University

Serdar Celik

OSTIM Technical University

Abstract: The Industrial Revolutions, occurring since the 18th century, have constituted some of the most significant milestones in history, fundamentally altering numerous vital domains such as production, economy, transportation, and healthcare through remarkable inventions. The expeditious evolution of the industry has concurrently instigated revisions in the midterm development strategies of nations. This research endeavors to assess the degree to which the attributes delineated in the academic literature about Industry 5.0 have been assimilated by countries that have established national development plans. Specifically, a bibliometric study was conducted by analyzing 545 articles in the Web of Science Core Collection database using the keyword "Industry 5.0". Eight primary concepts, big data, internet of things, artificial intelligence, blockchain, collaborative robotics, digital twins, edge computing, and 6G, were delineated as overarching categories within which a total of 37 keywords were systematically classified. The presence of these keywords in the national development plans of countries was examined and their alignment with the understanding of Industry 5.0 was evaluated. Document analysis, a qualitative research design, was employed in this research. The MaxQda 2020 software package was used to conduct qualitative analyses and development plans were matched with the identified codes. The concepts related to Industry 5.0 were categorized into eight main codes and sixteen sub-codes within the program. For the purpose of clarity and coherence, a comprehensive array of analytical techniques, encompassing frequency analysis, code cloud visualization, comparative analysis, and relationship analyses, were meticulously employed to explain and graphically illustrate the prominent thematic codes and their interconnectedness. The findings of this research identify countries that prominently integrate the attributes of Industry 5.0 into their development plans, thus offering potential contributions to the refinement of nations developmental strategies.

Keywords: Industry 5.0, Development planning, National planning

Introduction

Production has been carried out by humans throughout history; however, this process has undergone significant transformations due to industrial revolutions since the early 18th century (Ok & Kagitci, 2023). These revolutions include the emergence of steam power and mechanical machines in Industry 1.0, the advent of electric power and assembly line production in Industry 2.0, the rise of electronic and computer technologies in Industry 3.0, and the integration of technologies such as digitalization, the Internet of Things, and artificial intelligence in Industry 4.0. Industrial revolutions have fundamentally altered the way tasks are performed, resulting in a remarkable increase in production efficiency and quality. The acceleration of economic progress and the widespread adoption of these industrial revolutions across various sectors have given rise to numerous business opportunities. The developmental processes initiated with Industry 1.0 and continued through subsequent phases have led to the emergence of the concept of Industry 5.0 we have today. The term "Industry 5.0" was first introduced by Michael in 2015. Industry 5.0 represents a digital transformation of future industrial eras, although the precise form it will take and the specific technologies it will encompass remain uncertain.

- This is an Open Access article distributed under the terms of the Creative Commons Attribution-Noncommercial 4.0 Unported License, permitting all non-commercial use, distribution, and reproduction in any medium, provided the original work is properly cited.

- Selection and peer-review under responsibility of the Organizing Committee of the Conference

© 2023 Published by ISRES Publishing: www.isres.org

Nevertheless, it is anticipated that sustainability, flexibility (Xu et al., 2021), and a human-centered approach will be key principles (Madsen & Berg, 2021).

Industrialization plays a pivotal role in the economic development of nations and significantly influences the economic disparities among different countries. Each country possesses a unique history, resources, and population structure, which in turn shape their distinct economic landscapes. In the present day, most countries have established development plans with the dual objective of fostering economic growth, closing the gap with more developed nations, and enhancing the overall standard of living (Avcı & Ergen, 2022). The advent of industrial revolutions has further reshaped the national development plans of countries, thanks to the technological innovations and economic policies brought about by these revolutions. This study seeks to analyze the degree to which the attributes of the Industry 5.0 concept have been embraced by countries that are implementing national development plans. We will employ qualitative analysis methods to explore this subject.

Key Features of Industry 5.0

The smart production systems approach, which emerged with Industry 4.0, and the human-oriented, sustainable, and flexible production approach aimed at in Industry 5.0, have underscored the importance of human skills once again. The primary objective of Industry 5.0 is to enhance productivity and efficiency through the collaborative use of humans, robots, and artificial intelligence technologies, while also reintroducing significance to social sensitivities that were sometimes overlooked during Industry 4.0. The core competencies of Industry 5.0 revolve around the development of innovative products and technologies, becoming a crucial concept for the competitiveness of both individual and national economies (Balog & Demirova, 2021). In broad terms, Industry 5.0 is a concept that has emerged to harness human creativity in cooperation with powerful, intelligent, and precise machines (Maddikunta et al., 2022).

The fundamental components of Industry 5.0 are expected to exert significant influences on various professions, depending on the societal changes it generates. It has been projected that by 2030, 400-800 million people around the world may face job displacement (McKinsey, 2017). The primary factor behind this risk is the integration of technologies like artificial intelligence into the workplace. In this context, substantial transformations will be necessary in development plans, serving as a cornerstone of economic transformation, to facilitate the inclusion of individuals into new areas of business. The industrial revolutions experienced thus far have had profound effects on economic transformation, with one of the most notable consequences being the alteration and evolution of existing employment opportunities.

National Development Plans

Considering the development plans of nations, there are no obstacles to commencing the Industry 5.0 process in countries where the Industry 4.0 process has not yet begun or is in its early stages. The most influential catalyst for the transformation to Industry 5.0 is expected to be the rise in consciousness and awareness. In this context, it is essential to assess the interest and awareness levels of countries with respect to industrial revolutions. In pursuit of this objective, it is feasible to scrutinize the developments in the literature, which can be viewed as an outcome of Industry 4.0. As the transition to Industry 5.0 unfolds, varying levels of awareness are likely to emerge in both developed and developing countries. Different levels of awareness are anticipated as an expected outcome.

Method

In this section, which aims to provide information about the main features of Industry 5.0, the Web of Science (WoS) Core Collection database was searched using the Vosviewer program. It includes scientific literature in the WoS database from 2010 to the present. The complete citation network, all cited references, and fully indexed and searchable publications were utilized. Bibliometric analysis offers an overview of the research field (Hood & Wilson, 2001). Bibliometric methods help identify structural aspects and trends in the research topic (Rey Martí et al., 2015). The selected analysis period covers the time when the topic was prominent, resulting in the identification of 545 articles. A cluster analysis was conducted using the software developed by Van Eck and Waltman. Networks of co-occurring keywords were created and visualized based on the number of articles. The visualization presents a network of elements shaped according to the density and strength of relationships between keywords, with links indicating the closeness of the relationship between the elements. The circles'

colors and positions are employed to group the elements. It is expected that the clusters and keywords generated by this program will enhance awareness in the development plans of nations.

This section presents the main results of the bibliometric analysis applied to the records available in WoS, aiming to draw attention to the extent to which the features of Industry 5.0 that garnered the most attention in academic literature between 2010 and 2023 have been incorporated into national development plans. A total of 545 articles were selected for screening, and the analysis was conducted in October 2023. A network visualization of the most frequently used keywords in conjunction with Industry 5.0 trends is presented to assess the topic by scholars from 2010 to 2023 (Figure 1).

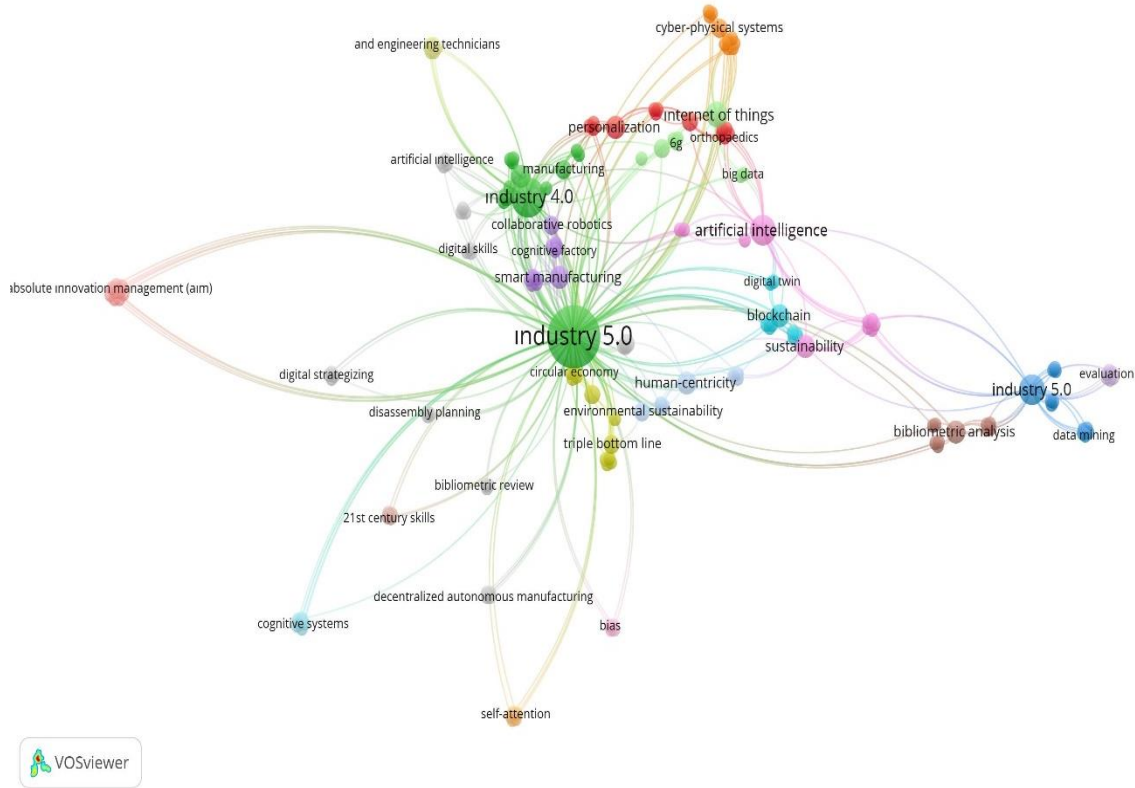


Figure 1. Network visualization of top Industry 5.0 keywords

In the network visualization, items are represented by their labels and, by default, with circles. The size of both the label and the circle of an item is determined by the item's weight. The higher an item's weight, the larger its label and circle. The color of an item is determined by the cluster to which it belongs. The lines between items represent connections. In the visualization, the large circles indicate the most frequently used words, and the lines indicate their associations with other words. Both the thickness of the lines and the size of the circles provide insights into the frequency of usage. Eight clusters related to Industry 5.0 and 37 keywords associated with these clusters were identified. The program used helped identify the clusters based on the most frequently used related keywords. The words within the clusters were grouped according to their most frequent co-occurrence rates. (Table 1.) displays the organized clusters.

Each cluster pertains to a different topic. For example, the first cluster encompasses 6G applications, which represent one of the significant challenges for Industry 5.0. 6G entails a personalized intelligent network that integrates artificial intelligence technologies, transitioning the network from the traditional function-centered model to a user-centric, data-centered, and content-centered one (Chen et al., 2020). The second cluster revolves around topics such as big data analytics. Big data refers to the flow of digital data from various sources in the digital world, including sensors, scanners, numerical modeling, mobile phones, the internet, videos, emails, and social networks (Hsu et al., 2015). The third cluster includes discussions on blockchain technology. Blockchain serves as a ledger that records committed transactions to enable the tracking and security of digital assets in a commercial network (Kumas, 2023). The fourth cluster emphasizes digital twins, which can be described as virtual models created to simulate the behavior of physical systems (Tuegel et al., 2011). These digital twins facilitate the connection of information between the physical reality and its virtual representation. The fifth cluster centers on edge computing, a novel computing model that combines resources close to the user within

network proximity to provide computing, storage, and network services. The sixth cluster encompasses the concept of the Internet of Things, which enables the interconnection between physical devices and virtual worlds. In the seventh cluster, artificial intelligence is the focus, while the eighth cluster pertains to collaborative robotics. These clusters are based on a literature review and the individual opinions and experiences of the authors. Consequently, all eight clusters offer a comprehensive overview of the most emphasized features associated with Industry 5.0. This approach enables a comprehensive perspective on research and theory in the field of Industry 5.0.

Table 1. Keywords related to Industry 5.0

Cluster	Keywords
6G	sensor, robotics
Big Data	data mining, optimization, cloud computing, big data analytics
Blockchain	decentralized learning, decentralized autonomous manufacturing
Digital Twins	digitalization, digital innovation, digital technology, digital product passport, digital transformation, digital strategizing, digital skills, human digital twin, industrial systems, data mining, big data, artificial intelligence, machine learning, smart manufacturing
Edge Computing	network analysis, network automation
Internet of Things	industrial internet of things, sensor, artificial intelligence, big data, cloud computing
Artificial Intelligence	machine learning, smart manufacturing, cobots
Collaborative Robotics	cobots, human-robot collaboration, human-robot interaction, sensor, human machine collaboration

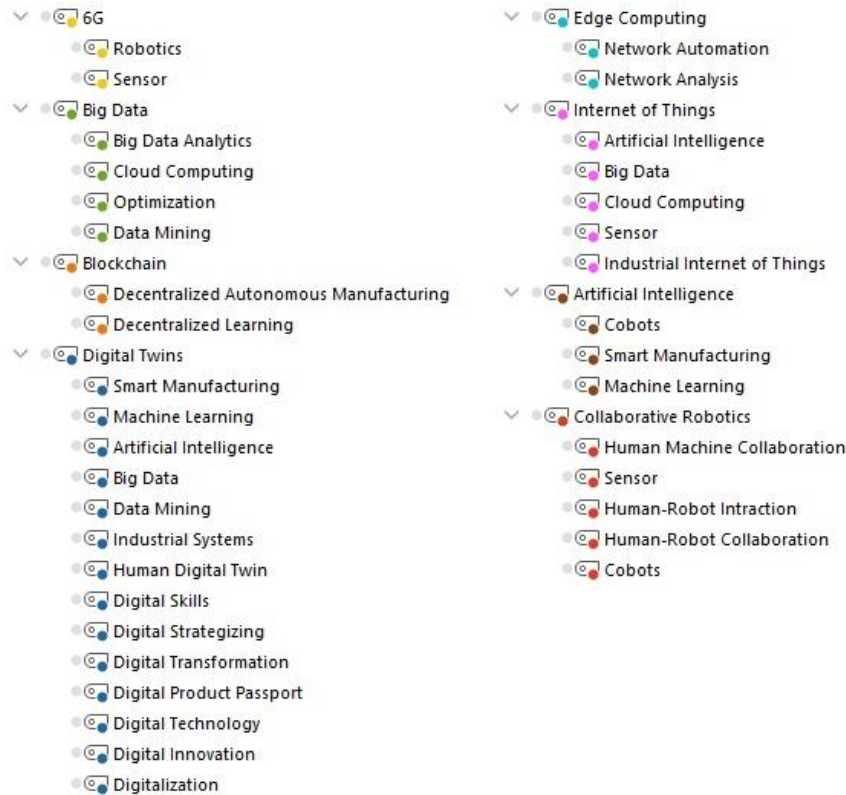


Figure 2. Code list

The analysis of this study is centered around the extent to which nations have incorporated Industry 5.0 features into their development plans. A qualitative research method was chosen as it is a suitable approach for comprehending the nature and structure of the subject matter. Furthermore, qualitative analysis aims to understand and explore both compiled and uncompiled information. In this study, the document analysis method, one of the qualitative analysis techniques, was employed, utilizing information extracted from the national development plans of 92 countries.

The concepts associated with the characteristics of Industry 5.0 within these national development plans were systematically examined. The most recent development plans of each country were considered, and these plans

were accessed from the respective countries' official websites. In the process of data analysis, Industry 5.0 features were coded using the MaxQda 2020 software package. During the data analysis, primary codes were initially identified, and subsequent sub-codes related to the main codes were appended as necessary. While scrutinizing the development plans of each country, identical or closely related expressions were matched with the established codes. The codes and sub-codes pertaining to Industry 5.0 are presented in Figure 2. The frequencies and percentages resulting from this analysis are also displayed.

During the coding process, codes were assigned to paragraphs, sentences, or individual words. In total, there are eight main codes and 37 sub-codes. Once the national development plans were coded, a word cloud and document overview of the Industry 5.0 features were generated. In the subsequent sections of the findings, the codes and the frequencies of the sub-codes are presented in a chart.

Table 2. Countries whose national development plans were analysed

N	Country	Plan timeframe	N	Country	Plan timeframe	N	Country	Plan timeframe
	Africa			Asia			Middle East	
1	Angola	2018-22	33	Bangladesh	2020-25	63	Algeria	2013-30
2	Benin	2018-25	34	Bhutan	2018-23	64	Bahrain	2017-20
3	Botswana	2017-23	35	Brunei	2018-23	65	Egypt	2020-30
4	Burkina Faso	2016-20	36	China	2021-35	66	Lebanon	2016-40
5	Burundi	2018-27	37	India	2012-17	67	Oman	2021-25
6	Chad	2017-21	38	Laos	2021-25	68	Palestine	2021-23
7	Congo	2019-23	39	Malaysia	2021-25	69	Qatar	2018-22
8	Ethiopia	2021-30	40	Myanmar	2018-30	70	Iraq	2018-22
9	Ghana	2022-25	41	Pakistan	2013-18	71	Saudi Arabia	2018-30
10	Guinea	2016-20	42	Papua New Guinea	2008-50	72	Tunisia	2022-25
11	Guinea-Bissau	2020-23	43	Philippine	2023-28		Latin America	
12	Kenya	2018-22	44	Thailand	2023-27	73	Argentina	2023-25
13	Lesotho	2018-23	45	Timor Leste	2011-30	74	Barbados	2013-20
14	Liberia	2018-23	46	Vietnam	2015-35	75	Belize	2010-30
15	Madagascar	2019-23		Europe		76	Bolivia	2021-25
16	Malawi	2017-22	47	Albania	2015-20	77	Chile	2014-18
17	Mali	2019-23	48	Armenia	2014-25	78	Colombia	2018-20
18	Mozambique	2020-24	49	Azerbaijan	2022-26	79	Costa Rica	2023-26
19	Namibia	2017-22	50	Belarus	2018-25	80	Dominica	2020-30
20	Nigeria	2021-25	51	Bosnia	2021-27	81	Ecuador	2023-27
21	Rwanda	2017-24	52	Estonia	2018-20	82	El Salvador	2014-19
22	R. of Congo	2018-22	53	Georgia	2014-20	83	Guatemala	2021-24
23	Sierra Leone	2019-23	54	Kazakhstan	2018-25	84	Haiti	2018-30
24	Somaliland	2023-27	55	Kosovo	2016-21	85	Honduras	2010-38
25	South Africa	2012-30	56	Kyrgyzstan	2018-26	86	Jamaica	2018-21
26	South Sudan	2021-24	57	Lithuania	2011-30	87	Mexico	2019-24
27	Swaziland	2019-22	58	Moldova	2018-30	88	Nicaragua	2019-23
28	Tanzania	2021-26	59	Mongolia	2016-30	89	Panama	2019-24
29	Togo	2018-22	60	Tajikistan	2021-25	90	Peru	2016-21
30	Uganda	2015-20	61	Turkey	2019-23	91	Tobago	2020-30
31	Zambia	2022-26	62	Ukraine	2017-30	92	Venezuela	2020-23
32	Zimbabwe	2021-25						

Results and Discussion

The national development plans of 92 countries were analyzed. Among these countries, 32 are located in Africa, 14 in Asia, 16 in Europe, 10 in the Middle East, and 20 in Latin America. Before delving into the analysis of the Industry 5.0 concept, the 100 most frequently used words in these countries' national development plans were identified and visually presented in a word cloud (Figure 3). Additionally, Table 3 displays the frequency and percentage values for the top 10 words. The word cloud was generated based on the frequency of occurrence within the development plans.



Figure 3. National development plans word cloud

Table 3. Word frequency distributions of development plans

Word	Frequency	Percentage %
Development	45971	1,36
Sector	34192	1,01
National	26773	0,79
Plan	26307	0,78
Economic	24256	0,72
Services	20558	0,61
Strategy	19112	0,56
Public	17128	0,51
Government	16542	0,49
Policy	15079	0,45

The code cloud obtained from the concepts related to Industry 5.0 in the national development plans of 92 countries was also created and shown (Figure 4.).



Figure 4. Industry 5.0 code cloud

In the code cloud representing Industry 5.0 concepts, "digitalization" stood out as the most frequently used concept. "Digital technology" ranked second, "digital transformation" took the third spot, followed by "Internet of Things" in fourth place, and "artificial intelligence" in fifth place. Notably, concepts such as "human digital twin," "cobots," and "human-machine collaboration" were not found within the development plans of the analyzed countries. Table 4 presents the frequency and percentage values associated with the characteristics of the Industry 5.0 concept. The total frequency of the codes in the study amounts to 653. When considering the frequency values of the codes, the top five countries with the highest code frequencies are as follows: "Bangladesh" with 93 frequencies, "Malaysia" with 58 frequencies, "the Philippines" with 52 frequencies, "China" with 44 frequencies, and "Azerbaijan" with 36 frequencies, as depicted in Figure 5.

Table 4. Word frequency distributions of Industry 5.0 features

Word	Frequency	Percentage %
Digitalization	70	10,7
Digital Technology	59	9,0
Digital Transformation	56	8,6
Internet of Things	51	7,8
Artificial Intelligence	50	7,7
Digital Skills	46	7,0
Robotics	40	6,1
Blockchain	33	5,1
Big Data	32	4,9
Cloud Computing	28	4,3



Figure 5. Distribution of Industry 5.0 features by country

Conclusion

Today, the world is under the influence of industrial revolutions, and technological advancements have compelled both developed and developing countries to reassess their policies. Since the introduction of the concept of Industry 4.0 in 2011, significant progress has been made in both theoretical and practical applications. These advancements have triggered a swift reorganization of country policies. Some nations have revised their action plans to maintain their competitive advantages, while others have adjusted their strategies not to miss out on the opportunities brought by this new revolution. To cope with the challenges of high labor, raw material, and logistics costs, developed countries have shifted towards technology-oriented production. They have harnessed smart production technologies to reduce manufacturing costs and preserve their economic competitiveness derived from a production-based economy. In this context, this study aims to underscore the significance of national development plans in countries and explore their relationship with the features of the Industry 5.0 concept. Qualitative analysis was conducted by aligning the national development plans of countries with codes using the MaxQda 2020 software package. Within the program, features related to the

concept of Industry 5.0 were categorized into eight main codes and 37 sub-codes. Frequency analysis and code cloud analysis were performed to visually represent the codes. Upon analyzing the collected data, the countries that most prominently featured the Industry 5.0 concept were identified. The research findings revealed that out of a total of 3,384,467 words in national development plans, the word "digitalization" held a predominant position concerning the features of the Industry 5.0 concept. The emphasis on digitalization in these national development plans holds significant implications across various dimensions, including cultural, economic, communication, and international competition among nations. It is worth noting that this study is limited to the latest national development plans of the countries and may be extended by examining similar policy documents where countries outline their strategic objectives. In conclusion, this research aims to determine which countries worldwide have incorporated the features of the Industry 5.0 concept and to what extent. The findings are expected to provide valuable insights for the national development plans of countries in the future.

Recommendations

In future studies, it is advisable to consider the sustainable development plans of nations.

Scientific Ethics Declaration

The authors declare that the scientific ethical and legal responsibility of this article published in EPSTEM journal belongs to the authors.

Acknowledgements or Notes

* This article was presented as an oral presentation at the International Conference on Technology (www.icontechno.net) held in Antalya/Turkey on November 16-19, 2023.

References

- Avcı, T., & Ergen, E. (2022). Researching development plans with multi-criteria decision-making methods. *Pamukkale University Journal of Business Research*, 9(1), 90-106.
- Balog, M., & Demirova, S. (2021). Human capital development in the context of the fourth industrial revolution. *IOP Conference Series: Earth and Environmental Science*. IOP Publishing.
- Chen, S., Ying Chang, L., Sun, S., Kang, S., Cheng, W., & Peng, M. (2020). Vision, requirements, and technology trend of 6G: How to tackle the challenges of system coverage, capacity, user data-rate and movement speed. *IEEE Wireless Communications*, 27(2), 218-228.
- Hood, W., & Wilson, C. (2001). The literature of bibliometrics, scientometrics, and informetrics. *Scientometrics*, 52, 291-314.
- Hsu, C. H., Slagter, K., & Chung, Y. C. (2015). Locality and loading aware virtual machine mapping techniques for optimizing communications in MapReduce applications. *Future Generation Computer Systems*, 53, 43-54.
- Kumas, E. (2023). *Blok zincir tabanlı sanal gerçeklik ve Metaverse'e giden yol* (pp.347-361). Ankara, Turkey: Nobel Bilimsel.
- Maddikunta, P., Pham, Q.V., B., P., Deepa, N., Dev, K., Gadekallu, T., . . . & Liyanage, M. (2022). Industry 5.0: A survey on enabling technologies and potential applications. *Journal of Industrial Information Integration*, 26, 100257.
- Madsen, D., & Berg, T. (2021). An exploratory bibliometric analysis of the birth and emergence of industry 5.0. *Applied System Innovation*, 4(4), 1-15.
- McKinsey. (2017). *What the future of work will mean for jobs, skills and wages: Jobs lost, jobs gained*. McKinsey Global Institute.
- Ok, S., & Kagitçı, S. (2023). Endüstri 5.0'a doğru pazarlama 5.0: İnsan ve teknoloji. T. Oguzhan, & S. Ok (Ed.), *Sanayi yönetiminde gelecek yaklaşımları dijitalleşme ve yetenekler* (1st ed., pp. 59-82). Ankara: Nobel Akademik Yayıncılık.
- Rada, M. (2018). Industry 5.0-from virtual to physical. Retrieved from <https://www.linkedin.com/pulse/industry-50-from-virtual-physical-michael-rada/>

- Rey Marti, A., Ribeiro Soriano, D., & Palacios Marques, D. (2015). A bibliometric analysis of social entrepreneurship. *Journal of Business Research*, 5(69), 1651-1655.
- Tuegel, E., Ingraffea, A., Eason, T., & Spottswood, S. (2011). Reengineering aircraft structural life prediction using a digital twin. *International Journal of Aerospace Engineering*. Article ID 154798. <https://doi.org/10.1155/2011/154798>
- Xu, X., Yuqian, L., Birgit, V.-H., & Lihui, W. (2021). Industry 4.0 and industry 5.0—inception, conception and perception. *Journal of Manufacturing Systems*, 61, 530-535.

Author Information

Beste Alpaslan

OSTIM Technical University

Ankara, Turkey

Contact e-mail: beste.alpaslan@ostimtekniik.edu.tr

Serdar Celik

OSTIM Technical University

Ankara, Turkey

To cite this article:

Alpaslan, B. & Celik, S. (2023). Industry 5.0 and national development plans. *The Eurasia Proceedings of Science, Technology, Engineering & Mathematics (EPSTEM)*, 24, 149-157.

The Eurasia Proceedings of Science, Technology, Engineering & Mathematics (EPSTEM), 2023

Volume 24, Pages 158-164

IConTech 2023: International Conference on Technology

The Effect of HFMI Treatment on Stress Concentration for S355J2C+N Steel with Fillet Weld Joint

Mehmet Can Katmer

HIDROMEK Research and Development Center

Sami Gokberk Bicer

HIDROMEK Research and Development Center

Abstract: In this study, the effect of weld toe improvement application (HFMI) on stress concentration (K_t) was investigated. Welding connection and load type specified in IIW No. 511 / FAT 80 are preferred. The structure was joined with MAG welding and S355J2C+N was used as the main material. After the HFMI application, the geometry (width: 3 mm, 3.75 mm, 4.5 mm, 5.25 mm, 6 mm and depth: 0.2 mm, 0.3 mm, 0.4 mm, 0.5 mm, 0.6 mm) formed at the transition from the welding tip to the base material was determined as a variable and modeled using the Creo Parametric package program. These values are referenced from the IIW recommendations document. The structure was analyzed with the finite element method using the MSC Marc package program. This scope of work; only surface improvement was focused, compressive stresses after HFMI were not modeled. Analyzes were made by changing the transition geometry, and the stress values were read for each. According to the analysis results obtained, it has been observed that the stress concentration in the transition geometry decreases with the increase in width but increases with the increase in depth. In parallel with this result, the lowest stress concentration was seen in the geometry with 6 mm width and 0.2 mm depth dimensions.

Keywords: High frequency mechanical impact (HFMI), Stress concentration, Weld toe

Introduction

As it is known, the welded joining technique has a wide area of use in the machinery manufacturing industry. Because machine parts operate under significantly variable stresses, welded joints always carry the risk of fatigue damage. Carrying out the welded joint under high heat and/or pressure and the temperature created in the weld bead being above the melting temperature of the material, causes thermal stresses in the joint. In addition, the fact that the metallurgical structure of the region under the influence of heat differs from the main material shortens the time for fatigue crack initiation and propagation in the part working under dynamic stress. As a result, the fatigue life of welded joints is always shorter than that of the base metal (Aydodu & Genel, 2002, p. 84). Therefore, various techniques have been developed to increase the fatigue life of welded joints. Weld improvement techniques can be divided into two main groups, depending on how the improvement is done. One of these is local weld geometry editing methods. In this improvement technique, local stress peaks are reduced and the surface quality is improved. The other is residual stress reduction methods. In this improvement technique, the weld is improved by reducing the residual tensile stress in cases where strain hardening or phase change occurs. Burr grinding and TIG remelting methods are generally classified as geometry improvement techniques, and the primary purpose of these techniques is to eliminate weld tip defects and reduce local stress concentration by providing a smooth transition between the plate and the weld surface. Hammer peening and needle peening methods are classified as residual stress modification techniques that eliminate the residual tensile stress in the weld tip area and create residual compressive stress in the weld tip. HFMI methods improve

local weld geometry and surface quality while also introducing high residual compressive stress. Commonly used weld improvement techniques are shared in the Table 1 below (Marquis & Barsoum 2016, p. 4).

Table 1. Example of weld improvement methods and their main effects (Marquis & Barsoum, 2016, p. 4)

Method	Weld geometry improvement		Mechanical effects
	Increasing and smoothing transition	Eliminates defects	Induces compressive residual stresses
Grinding	x	x	-
TIG-remelting	x	x	-
Shot peening (blasting)	-	-	x
Hammer/needle peening	x	x	x
HFMI	x	x	x

Ono et al. (2022) determine the fatigue crack initiation location of high-strength steel welded joints applied with high-frequency mechanical impact (HFMI) exposed to high peak stresses in their study. They discussed the observation results of fracture samples through damage-based evaluation using the Smith-Watson-Topper parameter based on local strain.

Harati et al. (2016) investigated the effects of high-frequency mechanical impact (HFMI) treatment procedure on weld toe geometry and fatigue strength in steel welds with a fatigue strength of 1300 MPa. They are concluded that the three run treatment would be a more economical option than the six run treatment providing a similar or even more favorable geometry modification.

Aldén et al. (2020) founded that no significant influence from the HFMI operator or HFMI equipment on the fatigue life in their study. However, the scatter in fatigue testing results varied with HFMI operator and indicated that different HFMI operators could produce consistent treatment results.

In this study, the effect of weld toe improvement application (HFMI) on stress concentration (K_t) was investigated. This scope of work; only surface improvement was focused, compressive stresses after HFMI were not modeled. According to the analysis results obtained, it has been observed that the stress concentration in the transition geometry decreases with the increase in width but increases with the increase in depth.

Method

Stress Concentration

Weld constitutes a sudden change in the geometry of the joint that causes high-stress concentrations. The stress concentration is defined by the stress concentration factor K_t . The highest concentration occurs at the weld toe, which is therefore the most likely place of fatigue failure. The smaller the notch radius, the higher the stress concentration and, ultimately, the shorter the fatigue life (Fustar et al., 2020, p. 424). The stress concentration factor can be formulated as follows;

$$\sigma_{\max} = \sigma_{\text{nom}} * K_t \quad (1)$$

$$K_t = \frac{\sigma_{\max}}{\sigma_{\text{nom}}} \quad (2)$$

Geometric Model

In this study, modeling was done in the Creo Parametric package program, taking the IIW No. 511 / FAT 80 filled weld connection type as reference. Dimensions of geometric model are shown in Figure 1. Geometry (detail A) after HFMI is defined as variable and 25 models were created. Horizontal dimension of geometric model is defined as width and variable of width are used 3 mm, 3.75 mm, 4.5 mm, 5.25 mm, 6 mm. Vertical dimension of geometric model is defined as depth and variable of depth are used 0.2 mm, 0.3 mm, 0.4 mm, 0.5 mm, 0.6 mm.

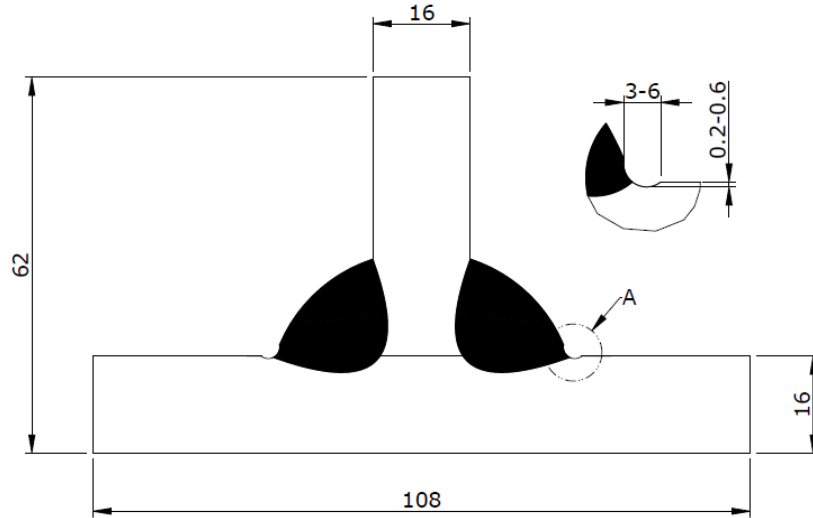


Figure 1. Dimensions of geometric model

In design S355J2C+N steel was chosen as the base material. Parts were joined by gas arc welding method and SG2 welding wire was used in these works. Mechanical properties of S355J2C+N steel and SG2 welding wire are shared in Table 2.

Table 2. Mechanical properties of S355J2C+N (Erdemir, 2020, p. 59) and SG2 (Askaynak, 2022)

	Yield Strength	Tensile Strength	Elongation
S355J2C+N	345 N/mm ²	470-630 N/mm ²	-
SG2	440 N/mm ²	540 N/mm ²	30 %

Structural Analysis

The network structure of the solid models whose designs were completed was created in the MSC Apex program. HEX8 element type was preferred as the network structure. In order to obtain realistic and consistent analysis results, a study was carried out for the most appropriate element size. Analyzes were carried out in the MSC Marc program. Analysis results; The solution time was compared considering the convergence of the obtained stresses and the number of elements used. According to these evaluations, the most appropriate network size was determined. In boundary conditions details; A fixed support is defined on the top surface of model. Tensile forces were applied to the right and left surfaces of the model. Boundary conditions are shown Figure 2.

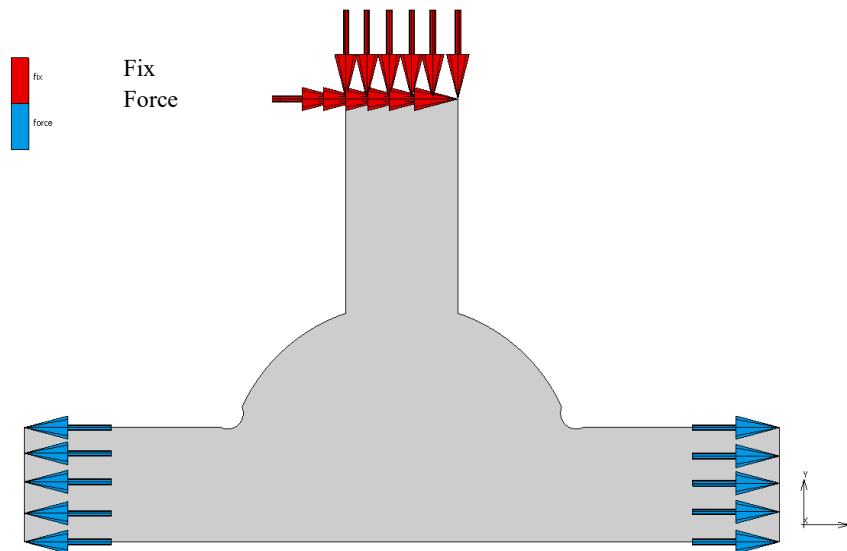


Figure 2. Boundary conditions

Results and Discussion

A total of 25 models were analyzed under the same boundary conditions. According to analysis results; nominal stress was obtained approximately 31 MPa in all models. Then, stress concentration (K_t) was calculated by the ratio of maximum stress to nominal stress for each model. All results are shared in the table 3.

Table 3. Analysis results

Model No	w mm	d mm	σ_{max} MPa	K_t	σ_{nom} MPa
Model 1 6		0.6	59.87	1.93	31
Model 2 6		0.5	57.55	1.86	31
Model 3 6		0.4	55.08	1.78	31
Model 4 6		0.3	52.50	1.69	31
Model 5 6		0.2	49.79	1.61	31
Model 6 5,25		0.6	62.53	2.02	31
Model 7 5,25		0.5	60.21	1.94	31
Model 8 5,25		0.4	57.26	1.85	31
Model 9 5,25		0.3	54.44	1.76	31
Model 10 5,25		0.2	51.70	1.67	31
Model 11 4,5		0.6	66.25	2.14	31
Model 12 4,5		0.5	63.23	2.04	31
Model 13 4,5		0.4	60.39	1.95	31
Model 14 4,5		0.3	57.35	1.85	31
Model 15 4,5		0.2	53.96	1.74	31
Model 16 3,75		0.6	70.17	2.26	31
Model 17 3,75		0.5	67.23	2.17	31
Model 18 3,75		0.4	64.08	2.07	31
Model 19 3,75		0.3	60.58	1.95	31
Model 20 3,75		0.2	56.93	1.84	31
Model 21 3		0.6	77.24	2.49	31
Model 22 3		0.5	73.45	2.37	31
Model 23 3		0.4	69.32	2.24	31
Model 24 3		0.3	65.41	2.11	31
Model 25 3		0.2	60.92	1.97	

The stress distribution graph (Figure 3) of the model with after HFMI and the as-welded model is shared.

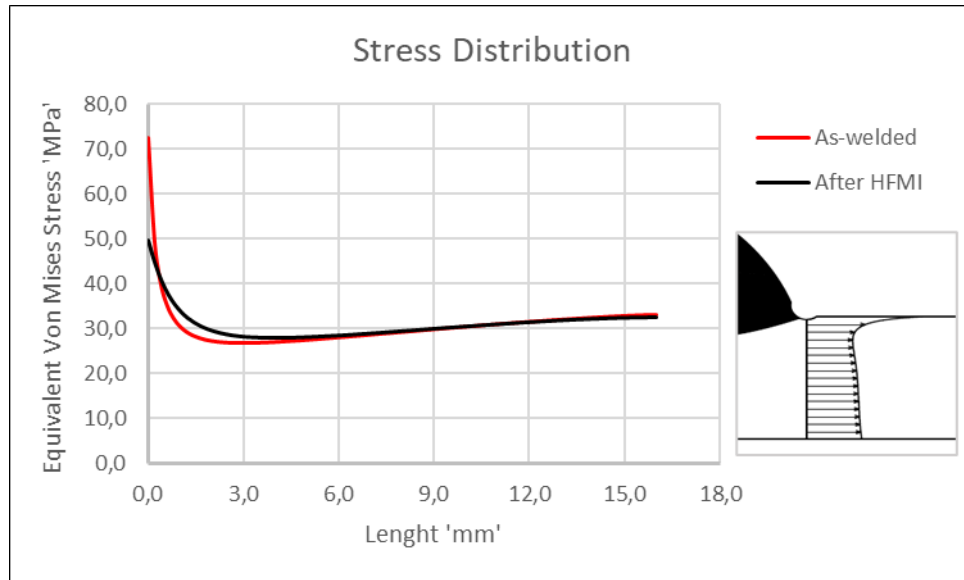


Figure 3. Stress distribution of as-welded and after HFMI

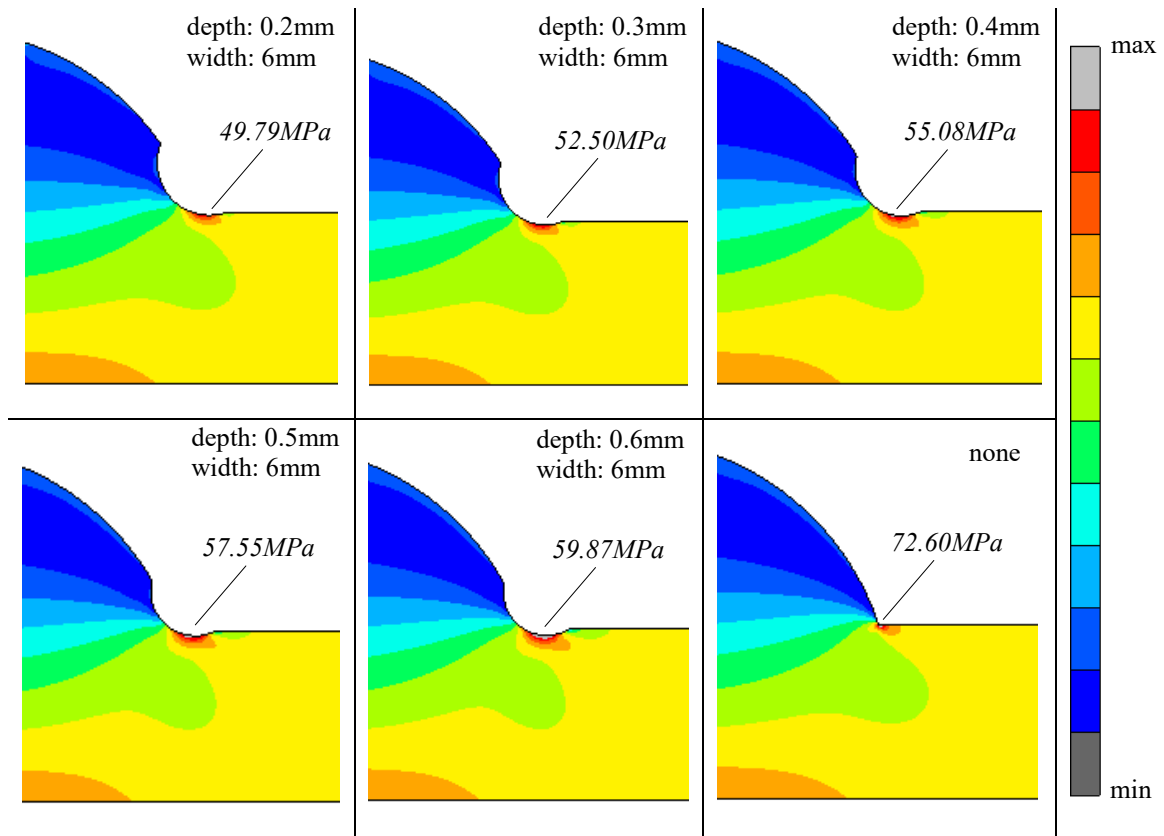


Figure 4. Comparison of as-welded and after HFMI geometries

Lowest maximum stress is 49,79 MPa between all models. Maximum stress of as-welded model is 72,60 MPa. This situation clearly showed that positive effect of HFMI application on stress concentration. When the graph is examined; in the region nearly the stress concentration, lower stresses than the nominal stress were obtained. This result is very important for fatigue life because stress amplitude used in calculation of fatigue life.

In the analysis results; maximum stress was observed as 49.79 MPa in model of depth 0.2 mm and width 6 mm, 52.50 MPa for model of depth 0.3 mm and width 6 mm, 55.08 MPa for model of depth 0.4 mm and width 6 mm, 57.55 MPa for model of depth 0.5 mm and width 6 mm, 59.87 MPa for model of depth 0.6 mm and width

6 mm. When the study is examined, width increase in geometry after HFMI caused stress concentration decreasing. The Figure 4 shows the effect of increasing the depth at a fixed width value (6mm) on the stress concentration. In addition, the stress value in the geometry without HFMI is higher than the highest stress at 6 mm width. On the other hand, there are also geometries that higher stress than the geometry without HFMI application. This situation clearly demonstrates the importance of the application level.

Stress concentration was calculated theoretically according to the stress results obtained from the analyzes (maximum and nominal stresses). According to calculations; K_t was obtained as 1.61 in model of depth 0.2 mm and width 6 mm, 1.69 for model of depth 0.3 mm and width 6 mm, 1.78 for model of depth 0.4 mm and width 6 mm, 1.86 for model of depth 0.5 mm and width 6 mm, 1.93 for model of depth 0.6 mm and width 6 mm. These values are lowest K_t for all width.

According to calculations; K_t was obtained as 1.97 in model of depth 0.2 mm and width 3 mm, 2.11 for model of depth 0.3 mm and width 3 mm, 2.24 for model of depth 0.4 mm and width 3 mm, 2.37 for model of depth 0.5 mm and width 3 mm, 2.49 for model of depth 0.6 mm and width 3 mm. These values are highest K_t for all width.

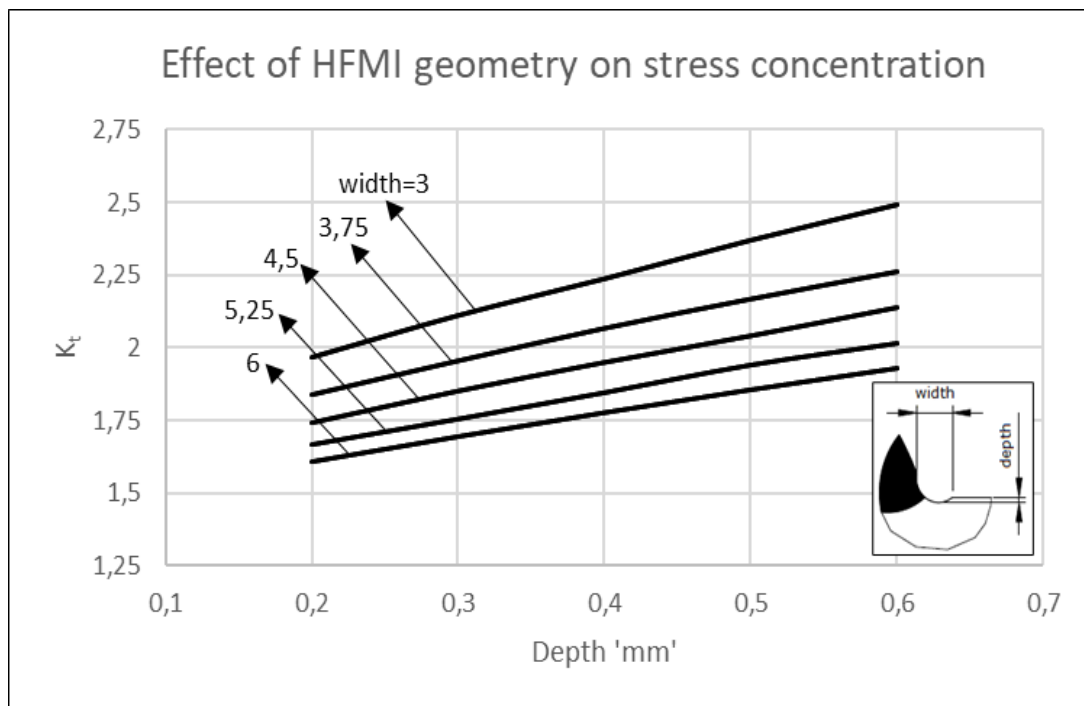


Figure 5. Effect of HFMI geometry on stress concentration

Conclusion

HFMI treatment may vary from operator to operator in practice and these situations may cause differences in the geometry after HFMI. As a result of analyses on geometry after HFMI treatment, the following conclusions were reached;

The stress concentration in as-welded geometry is higher (approximately 1.5 times) than the HFMI geometry (the model that gives the best results).

Increase of depth in geometry after HFMI caused stress concentration increasing. For all width values, the lowest K_t factor value was obtained at 0.2 mm depth value.

Increase of width in geometry after HFMI caused stress concentration decreasing. For all depth values, the lowest K_t factor value was obtained at 6 mm width value.

When all data were evaluated, the lowest K_t value was obtained at 6 mm width and 0.2 mm depth.

Scientific Ethics Declaration

The authors declare that the scientific ethical and legal responsibility of this article published in EPSTEM journal belongs to the authors.

Acknowledgements or Notes

* This article was presented as an oral presentation at the International Conference on Technology (www.icontechno.net) held in Antalya/Turkey on November 16-19, 2023.

* This study has been published with the support of Hidromek company. The authors would like to thank the Hidromek.

References

- Aldén, R., Barsoum, Z., Vouristo, T., Al- Emrani, M. (2020). Robustness of the HFMI techniques and the effect of weld quality on the fatigue life improvement of welded joints. *Welding in the World*, 64, 1947–1956.
- Askaynak. (2022, Jun 14). *AS MIG SG2 performance*. Retrieved from [https://www.askaynak.com.tr/urunler/kaynak-elektrodlari-telleri-ve-tozlari/gazalti-\(mig-mag\)-kaynak-telleri/as-mig-sg2-performance.pdf](https://www.askaynak.com.tr/urunler/kaynak-elektrodlari-telleri-ve-tozlari/gazalti-(mig-mag)-kaynak-telleri/as-mig-sg2-performance.pdf)
- Aydogdu, K., & Genel, K. (2002). Kaynaklı bağlantıların yorulma dayanımını etkileyen faktörler. *Sakarya University Journal of Science*, 6(1), 84-89.
- Erdemir. (2020). *Yassı ürün katalogu 2020*, 59. Retrieved from https://www.erdemir.com.tr/Sites/1/upload/files/yassi_urun_Katalogu_2020_TR-4649.pdf
- Fustar, B., Lukacevic, I., & Dujmović, D. (2020). High-frequency mechanical impact treatment of welded joints. *GRAĐEVINAR*, 72(5), 421-436.
- Harati, E., Svensson, L., Karlsson, L., & Hurtig, K. (2016). Effect of HFMI treatment procedure on weld toe geometry and fatigue properties of high strength steel welds. *Procedia Structural Integrity*, 2, 3483-3490.
- Marquis, G. B., & Barsoum, Z. (2016). *IIW recommendations for the HFMI treatment for improving the fatigue strength of welded joints*. Paris: Springer IIWCollection.
- Ono, Y., Yıldırım, H.C., Kinoshita, K., & Nussbaumer, A. (2022). Damage-based assessment of the fatigue crack initiation site in high-strength steel welded joints treated by HFMI. *Metals*, 12(1), 145.

Author Information

Mehmet Can Katmer

HIDROMEK, Research and Development Center
Ahi Evran OSB mh. Osmanlı cd. No:1
06935 Sincan – Ankara / Turkey
Contact e-mail: mehmet.katmer@hidromek.com

Sami Gokberk Bicer

HIDROMEK, Research and Development Center
Ahi Evran OSB mh. Osmanlı cd. No:1
06935 Sincan – Ankara / Turkey

To cite this article:

Katmer, M.C., & Bicer, S.G. (2023). The effect of HFMI treatment on stress concentration for S355J2C+N steel with fillet weld joint. *The Eurasia Proceedings of Science, Technology, Engineering & Mathematics (EPSTEM)*, 24, 158-164.

The Eurasia Proceedings of Science, Technology, Engineering & Mathematics (EPSTEM), 2023

Volume 24, Pages 165-170

IConTech 2023: International Conference on Technology

The Prototype of Reactor for Carbon Capture in Molten Salts

Stanislaw Pietrzyk

AGH-University of Science and Technology

Piotr Palimaka

AGH-University of Science and Technology

Abstract: Carbon Capture in Molten Salts (CCMS) a new method of capturing CO₂ was developed on a sorption and desorption principle similar to that used in the calcium loop, but proceeding in the molten salt environment (alkali metal chlorides and fluorides): $\text{MeO}_{(\text{s, diss. in molten salts})} + \text{CO}_{2(\text{g})} \leftrightarrow \text{MeCO}_{3(\text{diss. in molten salt})}$. The idea of the CCMS reactor presented in the only patent assumes its operation in a two-chamber system, allowing to separate the stages of CO₂ sorption and desorption. The paper presents the development of a reactor prototype consisting of three basic elements, i.e. a sorption, desorption and intermediate chamber. The transport/pumping of salt between the reactor elements will take place on the principle of a gas lift, i.e. the transport will be forced by the pressure of inert gas. It was necessary to determine what the gas pressure in the gas lift should be to effectively pump molten salts. The reactor chambers will be located inside the heating modules however, some elements for transporting molten salts will protrude above the heating zones and they must be thermally insulated. And here another problem arose, whether the insulation of the pipelines for the transport of molten salts is sufficient to protect them from freezing during contact with colder elements, and if not, then how to prevent it. The scope of the research included performing numerical simulations in order to:

- determination of the gas pressure needed to pump the molten salt between the reactor chambers;
- determination of the temperature distribution as the molten salts flow through the conveying system to anticipate the possibility of loss of pumpability due to salt freezing.

The above-mentioned problems of the CCMS reactor prototype operation were solved by means of thermal-flow analysis, performed using computational fluid mechanics methods (Ansys Fluent and SolidWorks programs).

Keywords: Carbon capture, Molten salts, CCMS reactor

Introduction

Calcium loop (CaL) is a carbonate looping method (MacDowell et al., 2010) in which a metal (Me) undergoes a reversible reaction between its carbonate (MeCO₃) and its oxide form (MeO) to separate carbon dioxide from other exhaust components:



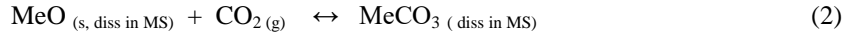
The processes of oxide carbonization/CO₂ sorption and carbonate calcination/CO₂ desorption take place in a fluidized bed in separate reactors. One of the major challenges of this technology is the relatively fast sorbent reactivity decay resulting in a residual activity of 8-10% after about 20, due to sintering during calcination (Blamey et al., 2009). For this reason, it is necessary to periodically remove part of the sorbent from the system and replace it with fresh.

In the 21st century, a new method of capturing carbon dioxide was developed on a sorption and desorption principle similar to that used in the calcium loop, but proceeding in the molten salt environment (CCMS - Carbon Capture in Molten Salts) (Olsen et al., 2013; Tumkote et al., 2013, 2014). In this method, the unreacted

- This is an Open Access article distributed under the terms of the Creative Commons Attribution-Noncommercial 4.0 Unported License, permitting all non-commercial use, distribution, and reproduction in any medium, provided the original work is properly cited.

- Selection and peer-review under responsibility of the Organizing Committee of the Conference

sorbent as CaO and as CaCO₃ after CO₂ sorption are found in solutions of molten salts (alkali metal halides - Ca, Na, Li, mainly chlorides and fluorides):



In this concept, molten salts are used as solvents of the active sorbent in CaL, with the main idea of hindering CaO particles degradation. Exhaust gases containing CO₂ go to the absorber, where CaO is in the form of molten salts. CaCO₃ is formed through reaction (2) and dissolves continuously in the melt, leaving highly reactive surfaces of CaO readily available. Molten salts containing CaCO₃ are directed to the desorber chamber operating at a higher temperature. The calcination reaction takes place, and the pure CO₂ is removed from the desorber (Figure 1).

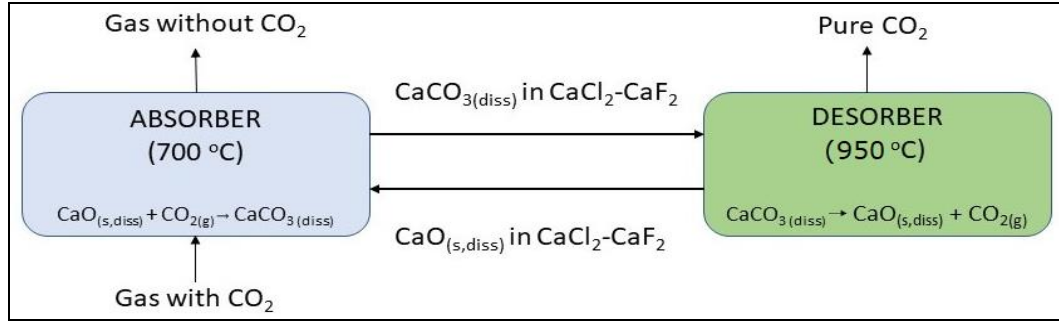


Figure 1. Scheme of CCMS process

So far, the CCMS method is at the stage of advanced research on a laboratory scale (Olsen et al., 2013; Nygård et al., 2017; Nygård et al., 2019). The salt solutions in which the capture was carried out were based on the CaF₂-CaCl₂ solutions with the addition of CaO. The studies of sorption and desorption cycles were carried out only in a single-chamber reactor. The process is carried out cyclically, i.e. after the sorption process is completed (no CO₂ capture), the flow of the exhaust gas mixture is closed and the reactor is heated to a higher temperature at which the thermodynamically justified reaction (2) proceeds to the left towards the decomposition of calcium carbonate and desorption of pure CO₂. After the completion of CO₂ desorption is confirmed, the reactor is cooled again to the temperature at which the reaction (2) proceeds from left to right and the process of CO₂ sorption from the flue gases is carried out.

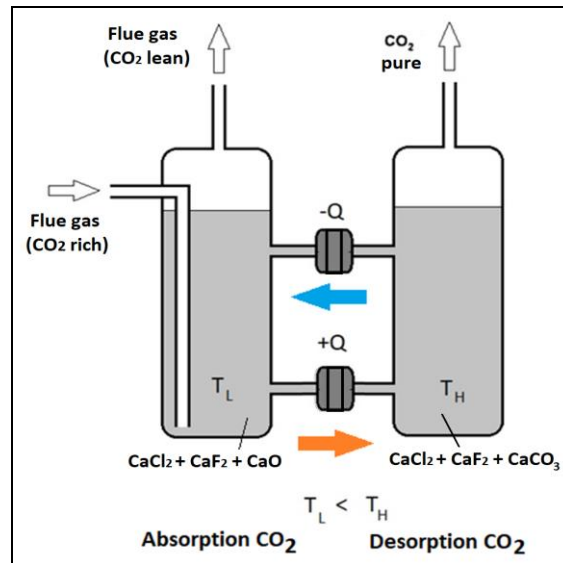


Figure 2. Two chamber reactor CCMS –simplified and adapted (Olsen, 2013)

The idea of the CCMS reactor presented in the only patent (Olsen, 2013) assumes its operation in a two-chamber system, allowing to separate the stages of CO₂ sorption and desorption. However, the reactor presented in the patent solution provides that the exchange of molten salts will take place by convection, through a system of two channels connecting both chambers. One of them will cool the melted salts flowing to the desorption chamber to the temperature of about 700⁰C, while the other one will heat the melted salts flowing to the desorption chamber to the temperature of about 950⁰C (Figure 2). That solution is to enable the reactor to

operate continuously. However, there is a concern that this will make it difficult to complete the sorption and desorption of CO_2 and make it difficult to fully use the sorption capacity of the sorbent. This paper presents the completely new development of the reactor prototype (Pietrzyk, 2023) consisting of three basic elements, i.e. a sorption and desorption chamber and an intermediate one (auxiliary tank) (Figure 3).

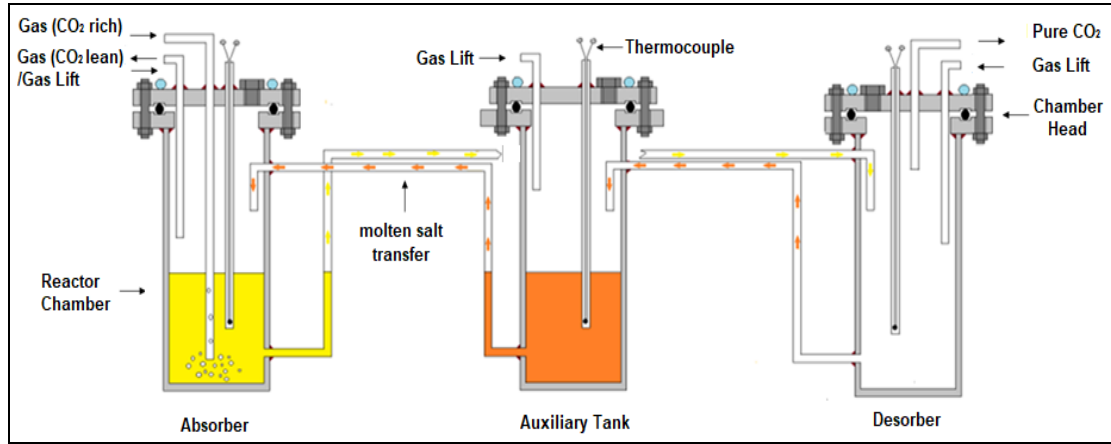


Figure 3. The new design of the CCMS reactor (Pietrzyk, 2023)

This solution will shorten the duration of a single cycle. Waiting for the end of sorption processes (depletion of the ability of CaO to capture CO_2) or the desorption process (no release of CO_2 from the decomposition of CaCO_3) will be eliminated. The reactor will be operated cyclically and each cycle will consist of three stages and a $\text{CaCl}_2\text{-CaF}_2$ solution will be used. In each stage of the cycle, only two of the three reactor elements contain molten salts and one always remains empty, ready to be filled with them in the next stage. Figure 4 shows the reactor chamber design stages.

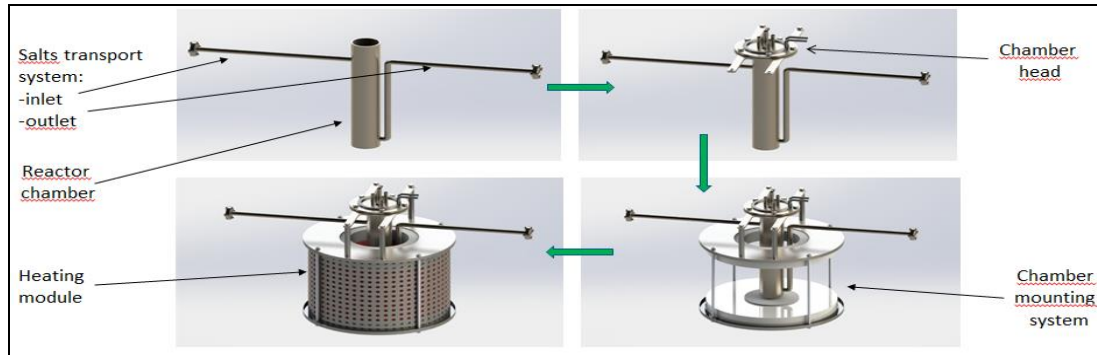


Figure 4. Reactor chamber design stages (made in SolidWorks)

Methods

During the design of the reactor prototype, many design problems were encountered that needed to be resolved by numerical simulations, of which only two are presented in this article. The scope of the research included performing numerical simulations in order to:

- determination of the gas pressure needed to pump the $\text{CaCl}_2\text{-CaF}_2$ molten salt between the reactor chambers;
- determination of the temperature distribution as the molten salts flow through the conveying system to anticipate the possibility of loss of pumpability due to salt freezing and pipelines clogging.

The above problems were solved using simulation methods available in the following programs: AnsysFluent® and SolidWorks®. Ansys Fluent as a computational fluid dynamics (CFD) software was used to model molten salts flow, heat and mass transfer in chambers of reactor. This software was also used to solve problem (a). In turn, SolidWorks is software (CAD) used for parametric three-dimensional modeling. It allowed us to design individual reactor details and assemble them into a whole. This software was also used to solve problem (b).

Results and Discussion

The transport of molten salts between the reactor elements will take place on the principle of a gas lift, i.e. the transport will be forced by the pressure of inert gas (N_2 or Ar) ((Mullen et al., 2017). The gas will be pumped under increased pressure into the chamber, above the level of molten salts, which will cause their pumping to the next element of the reactor. The effectiveness of the "gas lift" method was verified by testing on water, which has a density of approximately 1 g/cm^3 , while the density of liquid $CaCl_2$ is 2.01 g/cm^3 at a temperature of 775°C , which is more than twice as high (Janz, 1988) Therefore, computer simulations were carried out for the medium in the form of molten salts at the operating temperatures of the reactor chambers. It was necessary to determine what the gas pressure in the gas lift should be to effectively pump molten salts. An example of the simulation results of the operation of a gas lift is shown in Figure 5.

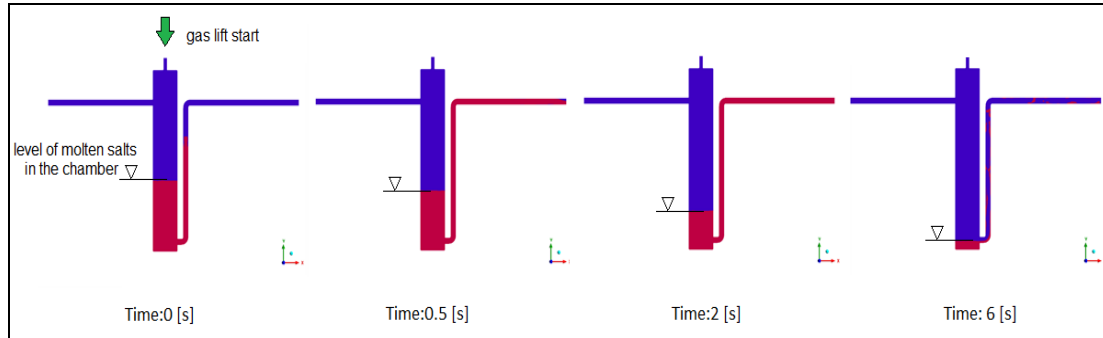


Figure 5. Simulation of the transport of molten salts using a gas lift (made in Ansys Fluent)

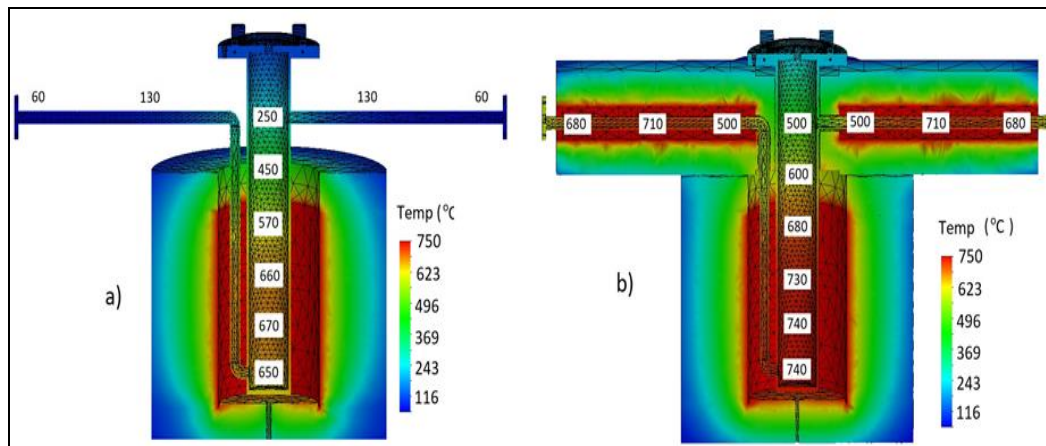


Figure 6. Simulation of the temperature distribution of a low-temperature chamber (made in SolidWorks)

The time needed to pump the molten salts from the chamber is 6 seconds and the gas overpressure at the inlet of the gas lift is 10 kPa. The reactor chambers will be located inside the heating modules, allowing to maintain the temperature of the working medium at an appropriate level, however, some elements for transporting molten salts will protrude above the heating zones and they must be thermally insulated. And here another problem arose that had to be solved during the design of the reactor prototype, namely whether the insulation of the pipelines for the transport of molten salts is sufficient to prevent the salt from freezing, with an excessive drop in their temperature during contact with colder elements, and if not, then how to prevent it.

The simulation results of the temperature distribution in the low-temperature reactor chamber showed the existence of underheated places on the pipelines transporting salts, which could lead to their solidification and clogging. Similar, underheated zones also confirmed the simulation results of temperature distribution in the high-temperature chamber. Fig. 6 shows a comparison of numerical simulations of the temperature distribution in a situation where the horizontal molten salt transport pipelines: (a) were not and (b) were insulated and heated by additional heating elements. The results of the thermal simulations showed the necessity of installing additional thermal insulations and heating modules on the horizontal pipelines transporting molten salts, between the chambers (Figure 7).

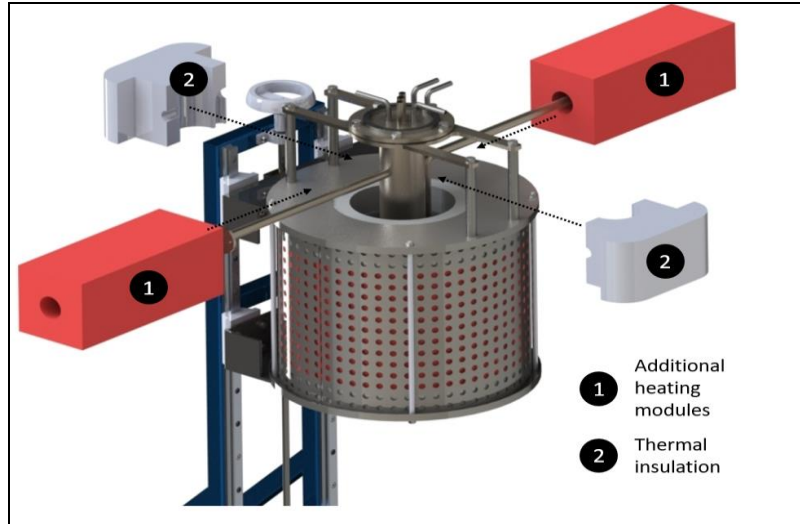


Figure 7. 3-D model of low-temperature chamber with additional thermal insulations and heating modules (made in SolidWorks)

The results of computer simulations were used to design and build a prototype of the CCMS reactor (Figure 8). The constructed prototype is equipped with six independent programmatically controlled heating systems (three for the reactor chambers/tanks and three for the pipelines transporting molten salts between them). The pipeline transporting system has been equipped with high-temperature valves, allowing for the isolation of individual sections and the use of a gas lift to transport molten salts between tanks after the completion of the absorption/desorption processes.



Figure 8. CCMS reactor prototype designed and built at AGH-UST

Conclusions

Based on the obtained results of computer simulations, the following conclusions were reached:

- The designed and constructed prototype of reactor enables cyclic operation of CO₂ capture from the flue gases and release a pure CO₂
- The use of an auxiliary tank allows for the separation of sorption/desorption cycles and maximizes the use of CaO sorption capacity (recently, the first successful tests were carried out on a prototype of a three-chamber reactor, confirming the above-suggested thesis).
- The operating conditions of the gas lift, calculated on the basis of computer simulations, have been checked and confirmed in the operating conditions of the reactor prototype and ensure effective transport of molten salts.

- The use of additional thermal insulation and heating modules allows for the preheating of the transporting system for molten salts, preventing their solidification and clogging of the pipeline.

Scientific Ethics Declaration

The authors declare that the scientific ethical and legal responsibility of this article published in EPSTEM journal belongs to the authors.

Acknowledgements or Notes

* This article was presented as an oral presentation at the International Conference on Technology (www.icontechno.net) held in Antalya/Turkey on November 16-19, 2023.

* The research leading to these results has received funding from the Norway Grants 2014-2021 via the National Centre for Research and Development (NCBiR). The results are part of the Polish–Norwegian project: Carbon Capture in Molten Salts -Prototype, Acronym CCMS-P, registration number NOR/POLNORCCS/CCMS-P/0004/2019-00.

References

- Blamey, J., Anthony, E.J., Wang, J., & Fennell, P.S. (2010). The calcium looping cycle for large-scale CO₂ capture. *Progress in Energy and Combustion Science*, 36(2), 260-279.
- Janz, G. J. (1988). Thermodynamic and transport properties of molten salts: Correlation equations for critically evaluated density, surface tension, electrical conductance, and viscosity data. *J. Phys. Chem. Ref. Data*, 17(2), 126-129
- MacDowell, N., Florin, N., Buchard, A., Hallett, J., Galindo, A., Jackson, G., Adjiman, C.S., Williams, C. K. Shah, N., & Fennell, P. (2010). An overview of CO₂ capture technologies. *Energy and Environmental Science*, 3(11), 1645-1669
- Mullen, E., Harris, R., Graham, D., Rhodes, Ch., & Hodgson, Z. (2017). Transfer characteristics of a lithium chloride-potassium chloride molten salt. *Nuclear Engineering and Technology*, 49(8), 1727-732
- Nygård, H. S., Hansen, M., Alhaj-Saleh, Y., Palimaka, P., Pietrzyk, S., Olsen, E. (2019). Experimental evaluation of chemical systems for CO₂ capture by CaO in eutectic CaF₂-CaCl₂. *AIMS Energy*, 7(5), 619-633.
- Nygård, H.S, Tomkute, V., & Olsen, E. (2017). Kinetics of CO₂ absorption by calcium looping in molten halide salts. *Energy Procedia*, 114, 250–258.
- Olsen, E. (2013). CO₂ - capture in molten salts. U.S. Patent No. 8,540,954. 24 Sep. 2013.
- Olsen, E., & Tomkute, V. (2013). Carbon capture in molten salts. *Energy Science & Engineering*, 1(3), 144–150.
- Pietrzyk, S. (2023). Device for removing CO₂ from exhaust gases.
- Tomkute, V., Solheim, A., & Olsen, E. (2013). Investigation of high-temperature CO₂ capture by CaO in CaCl₂ molten salt. *Energy & Fuels*, 27(9), 5373–5379.
- Tomkute, V., Solheim, A., & Olsen, E. (2014). CO₂ Capture by CaO in molten CaF₂–CaCl₂: Optimization of the process and cyclability of CO₂ capture. *Energy & Fuels*, 8(28), 5345 – 5353.

Author Information

Stanisław Pietrzyk

AGH-University of Science and Technology
Kraków, Poland
Contact e-mail: pietstan@agh.edu.pl

Piotr Palimaka

AGH-University of Science and Technology
Kraków, Poland

To cite this article:

Pietrzyk, S., & Palimaka, P. (2023). The prototype of reactor for carbon capture in molten salts. *The Eurasia Proceedings of Science, Technology, Engineering & Mathematics (EPSTEM)*, 24, 165-170.

The Eurasia Proceedings of Science, Technology, Engineering & Mathematics (EPSTEM), 2023

Volume 24, Pages 171-176

IConTech 2023: International Conference on Technology

Isotopic Geochemistry Applied on Marble Samples of Kythnos Island in Greece

Petros Karalis

National Centre for Scientific Research (N.C.S.R.)

Elissavet Dotsika

National Centre for Scientific Research (N.C.S.R.)

Alexandros Mazarakis -Ainian

University of Thessaly

Evaggelia Kolofotia

University of Thessaly

Iakovos Raptis

Centre for Research and Technology Hellas

Anastasia Electra Poutouki

University of Pavia

Anastasios Drosou

Centre for Research and Technology Hellas

Brunella Raco

Institute of Geoscience and Earth Resources-CNR

Panagiotis Leandros Poutoukis

University of Patras

Dafni Kyropoulou

National Centre for Scientific Research (N.C.S.R.)

Dimitrios Tzovaras

Centre for Research and Technology Hellas

Abstract: The present contribution aims to study the isotopic characteristics of various marbles from the archaeological site of Kythnos Island in the Cyclades, Greece. The database of this research is very important and useful in the conservation and restoration of monuments as these tasks should aim at preserving their material status and their authenticity. The characterization of marble taken from this site contributes significantly to the determination of the origin of the raw materials used in monuments in the wider area of the Aegean Sea. Samples were obtained mainly from the inner layers of the findings, which were not exposed to the weather conditions and without remarkable traces or signs of severe corrosion. The methods that were used required very small quantities of material. The measurements are considered almost non-destructive and based on isotopic geochemistry.

- This is an Open Access article distributed under the terms of the Creative Commons Attribution-Noncommercial 4.0 Unported License, permitting all non-commercial use, distribution, and reproduction in any medium, provided the original work is properly cited.

- Selection and peer-review under responsibility of the Organizing Committee of the Conference

© 2023 Published by ISRES Publishing: www.isres.org

Keywords: Oxygen isotopes, Carbon isotopes, Marbles, Kythnos, Tinos, Raw materials

Introduction

An island with a long history and particular archaeological importance is Kythnos, which is situated between Kea and Serifos. The ancient city of "Vryokastro", on the island's northwest shore, was a fortified polis that was continually inhabited from the first millennium B.C. to the sixth or seventh century A.D (Fig 1). The remains of the ancient city occupy an area of approximately 28,5 hectares, including the small islet of Vryokastraki, which was connected to the shore in antiquity by a narrow isthmus. During the systematic investigations that have been in progress since 1990 (survey and subsequent excavations) numerous finds and several ancient structures, such as temples, public buildings, houses, port facilities, burial monuments, etc., have been brought to light. These discoveries have provided valuable insights into the urban planning of the city and the sociopolitical and economic development of the ancient community.

Regarding the construction of the buildings, the island's ground is composed of various types of crystalline slates (metamorphic rock) with intervening marble horizons. Slate and limestone appear to have been used extensively for the buildings of the ancient city, and the discovery of marble fragments of architectural elements from the sanctuaries of the Upper Town confirms its parallel use. Several samples of marble were chosen in order to identify the marble's provenance (Fig.2).

During the field inspection of the intramural sanctuaries located on the Middle Plateau, a deliberate selection of marble samples was made. These samples encompassed both structural elements derived from the buildings and structural components originating from various artifacts, scattered throughout the archaeological site. More specifically, the chosen specimens were procured from the Upper Town precinct, housing the sanctuaries of Asklepios, Aphrodite, and the Samothracian Gods (Mazarakis Ainian, 2019), as well as from the Archaic sanctuary dedicated to Artemis and Apollo (Mazarakis Ainian 2017, 2019). Furthermore, the catalog of marble samples includes a subset originating from sculptures from the ancient harbor. Among these pieces, one find is a Hermaic stele, dating to the 2nd century A.D., subsequently reused as "spolia" during the Roman era, eventually being incorporated into the now-submerged fortification wall of Mandraki Bay. Additionally, there is a statue featuring a seated male figure, identified as Menander, who is credited as the founder of "New Comedy".



Figure 1. Aerial photograph of Vryokastro

In order to identify the origin of marble artifacts and understand the characteristics of marble, samples from the Kythnos quarries in Greece were analyzed using a variety of techniques. These included stable isotope analysis of carbonates (^{13}C , ^{18}O), SEM-EDXA analysis, and optical microscopy. Through these methods, information regarding the origin and texture of the marble used in the production of the artifacts was obtained (see Fig. 2).

Materials and Methods

We studied marble material from the island of Kythnos and of many islands in Cyclades. Samples were collected from Cyclades islands (Andros, Naxos, Syros, Sifnos, Paros and Tinos). In the current work, analytical results from samples extracted from Tino's quarries were presented. On Tinos, most of the island is a part of the Cycladic blueschist unit, which is represented by a marble-schist sequence. The whole succession can be subdivided by means of three mappable marble horizons, m3, m2 and m1 (Melidonis, 1980). From Tinos, we selected samples that represent the three major marble horizons m3, m2 and m1 (m1 calcite marble and M1 dolomite marble). We report petrographic characteristics and results of C, O isotopes analyses. From Tinos, the samples came from the three marble horizons M3, M2, and M1 and the fossil-bearing lowermost dolomite (Melidonis, 1980). The calcite marbles show all color gradations between white and grey, in alternating layers. The dolomites from the Panormos area on Tinos (> 100 m in thickness) are poorly bedded massive rocks. Their color is less white than the calcite marbles and shows a weak yellowish tint. We also collect samples from archaeological marble pieces (D2-D3-D4) from Kythnos. The samples come from buildings 1 and 2.



Figure 2. Marble samples

Table 1. SEM results identify the mineralogical structure of each material.

Samples	Mg	Al	Si	P	S	K	Ca	Fe	Marble
D2									
Max.	44,99	4,46	8,75	1,62	3,41	2,48	100	11,52	Calcite, with dolomite (Mg)
Min.	0,58	0,38	1,02	1,08	0,01	1,04	49,34	2,8	
D3									
Max.	2,78	28,42	47,88		1,38	16,71	99,04	3,95	Calcite
Min.	-1,13	-0,54	-0,74		-1,1	-0,43	9,23	-0,59	
D4									
Max.	12,32	0,69	1,69		1,55	0,97	0,97	0,99	Calcite, with Mg
Min.	0,75	-0,49	-1,38		-0,59	-0,25	-0,25	-1	

Based on that, the isotopic measurements ($\delta^{13}\text{C}$, $\delta^{18}\text{O}$) were used to determine the origin of the carbonate material. The isotopic analyses took place in the Stable Isotope Unit of the Institute of Materials Science (NCSR Demokritos) on a Thermo Delta V Plus IRMS equipped with GasBenchII. In order to distinguish the material of the tesserae in more detail, the maximum grain size (MGS) of each was determined by optical microscopy.

Results – Discussion

The full range of grain sizes and isotopic signatures that occur in a lot of different quarries has been measured and presented. In a $\delta^{13}\text{C}$ versus $\delta^{18}\text{O}$ diagram, the fields corresponding to all known ancient quarries from Penteli, Cyclades (especially Naxos, Keros, Paros), Thassos and Asia Minor (Ephesos, Proconnesus, Dokimeion, Aphrodisias, Usak) are reported (Moens et al., 1992a, Moens et al., 1992b, Moens, 2003). The plots

representing the analyzed samples are also shown on the same diagram. In the same samples we locate and isotopic values from Tinos island. This diagram indicates the origin of the carbonate material of the artifacts from each of the ancient monuments (Fig.3). In cases where the samples plot on overlapping areas, a further study is applied, using the maximum grain size (MGS) of the material (Polikreti & Maniatis, 2002; De Nuccio et al., 2000; Attanasio, 2003).

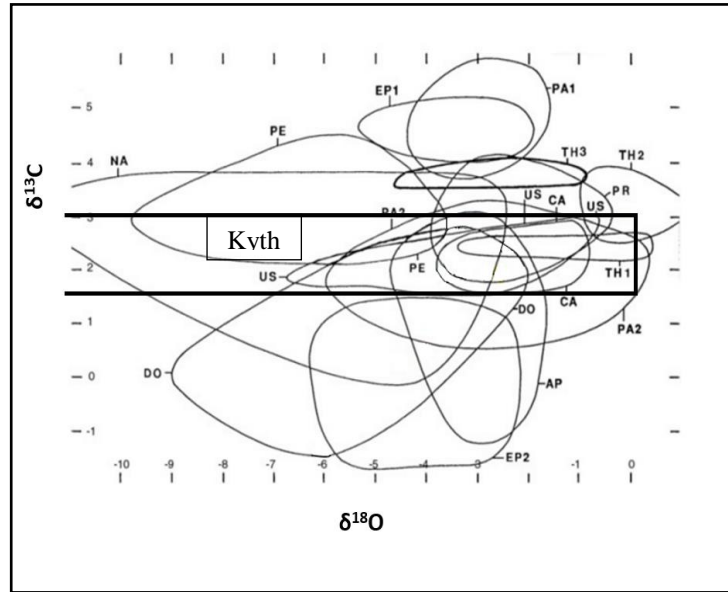


Figure 3. Isotopic signatures (vs PDB, ‰) of the marble pieces plotted against the quarry field parameters of most of the known ancient marble quarries (Moens, 2003). PE = Penteli, NA = Naxos, EP1 = Ephesos-1, EP2 = Ephesos-2, DO = Dokimeion, AP = Aphrodisias, US = Ussak, CA = Carrara, PR = Proconnesus, PA1 = Paros-1, PA2 = Paros-2, TH1 = Thassos-1 (calcitic), TH2 = Thassos-2 (calcitic), TH3 = Thassos-3 (dolomitic).

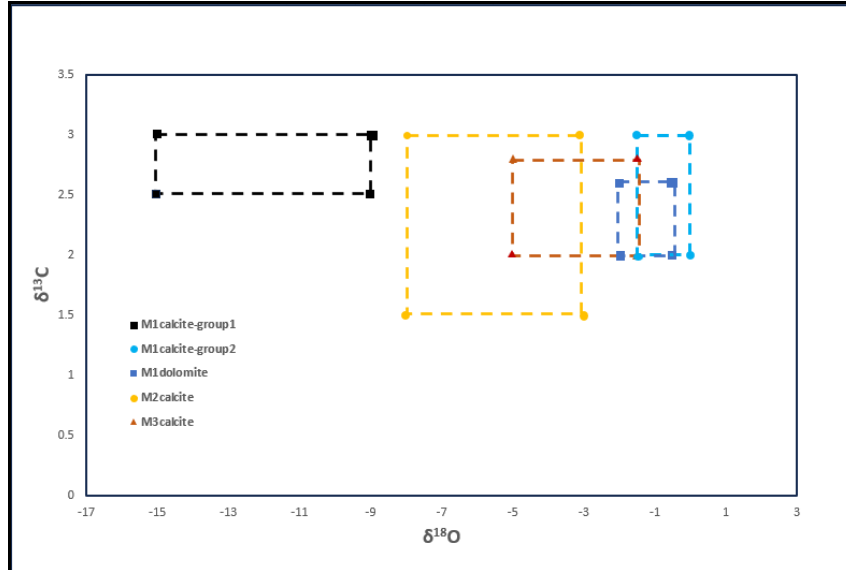


Figure 4. $\delta^{18}\text{O}$ vs $\delta^{13}\text{C}$ for Tinos samples quarries are plotted in the diagram that includes the known ancient marble quarries.

Marbles from the M1 horizon (Calcite marble, Tinos) present variable MgO contents (< 7 wt %; Mg/Ca range between 0 and 0,6), due to different contents of dolomite. Calcite marbles from M1 present Mg/Ca that range between 0 and 0,12, while dolomitic marbles from M1 present Mg/Ca that range between 0,4 and 0,6. Marbles from M2 and M3 horizons have MgO concentrations lower of 1.0 wt % and Mg/Ca range between 0 and 0,013 and 0 with 0,03 respectively. Table 1 demonstrates the chemical analysis of marbles from Kythnos island. SEM analysis of the archaeological samples (from Kythos) indicated that some pieces are not marbles, thus they were not considered suitable for isotopic fingerprinting. The rest samples (D2-D3-D4) were analyzed (Table 1).

Marbles from M3 horizon, present $\delta^{18}\text{O}$ that range between -5‰ and -1.5‰ . Kythnos M2 marbles present $\delta^{18}\text{O}$ values varying between -8‰ and -3.1‰ . Calcite marbles from the M1 horizon, present $\delta^{18}\text{O}$ that range between -1.5‰ and 0‰ , while dolomitic marbles from the M1 horizon, present $\delta^{18}\text{O}$ that range between -2‰ and -0.5‰ , $\delta^{13}\text{C}$ values of most samples from M1, M2, M3 horizons fall within the range of 1.5‰ – 3‰ . Marbles from Kythnos display the highest variability in $\delta^{18}\text{O}$ with values between -15.1‰ and $+0\text{‰}$. While, the $\delta^{13}\text{C}$ of marbles from Kythnos present the same values as the samples from M1, M2, M3 Tinos horizons. So, based on $\delta^{18}\text{O}$ and $\delta^{13}\text{C}$ values, the marbles from Tinos quarries can be separated into four groups, according to the different M1, M2, M3 horizons (Fig. 4). According to the Mg/Ca ratio the archaeological samples probably come from M1 and M2 horizons. The isotopic values ($\delta^{18}\text{O}$ and $\delta^{13}\text{C}$ values) of samples from Kythnos quarries are plotted in the diagram that includes the known ancient marble quarries (Figs 3 and 4).

Conclusion

After analyzing the $\delta^{18}\text{O}$ and $\delta^{13}\text{C}$ values, the marbles from Tinos quarries (M1 and M2 horizons) were categorized into four groups based on the different M1, M2, and M3 horizons. The archaeological samples from Kythnos underwent elemental and microscopic analysis and some pieces were found not to be marbles, therefore they were not suitable for isotopic fingerprinting. The remaining samples (D2-D3-D4) were analyzed showing that the Mg/Ca ratio suggests that the archaeological samples most likely originated from the M1 and M2 horizons. Furthermore, the $\delta^{18}\text{O}$ and $\delta^{13}\text{C}$ values from Tinos marbles were located on a diagram that includes known ancient marble quarries.

Recommendations

In the continuation of this study, the residual stress effect together with the geometry effect can be evaluated. This experiment would be more appropriate because HFMI does not only perform geometry improving. The relationship between residual stress and geometry can be direct or inverse. A test bench for residual stress measurement will make the results more realistic and consistent. In addition, outputs in terms of life can be obtained with a fatigue test bench.

Scientific Ethics Declaration

The authors declare that the scientific ethical and legal responsibility of this article published in EPSTEM journal belongs to the authors.

Acknowledgments

* This article was presented as an oral presentation at the International Conference on Technology (www.icontechno.net) held in Antalya/Turkey on November 16-19, 2023.

* This research has been co-financed by the European Regional Development Fund of the European Union and Greek national funds through the Operational Program Competitiveness, Entrepreneurship and Innovation, under the call RESEARCH – CREATE – INNOVATE (projects code : T1EDK 12500 and T1EDK 12516)

References

- Attanasio, D. (2003) *Ancient white marbles: Analysis and identification with paramagnetic resonance spectroscopy*. Rome: L'erma di Bretschneider.
- De Nuccio, M., Bruno, M., Gorgoni, C., & Pallante, P. (2000). The use of Proconnesian marble in the architectural decoration of the Bellona Temple in Rome. In L. Lazzarini (Ed.), *Interdisciplinary studies of ancient stone. Proceedings of the 6th International Conference ASMOSIA VI* (pp. 293–302). Laboratorio di Analisi dei Materiali Antichi.

- Mazarakis Ainian, A. (2017). Νεότερα για τα ιερά της αρχαίας πόλης της Κύθνου. In V. Vlachou & A. Gadolou (Eds.), *ΤΕΡΨΙΣ. Studies in Mediterranean archaeology in honour of nota Kourou* (pp. 303–315). Brussels.
- Mazarakis Ainian, A. (2019). *The sanctuaries of Ancient Kythnos*. Rennes, France.
- Melidonis, N. G. (1980). The geological structure and mineral deposits of Tinos Island (Cyclades – Greece). In *The geology of Greece IGME,13*, 1–80.
- Moens, L. (2003). *He kindly provided the updated isotope field diagram*. Faculty of Sciences, Ghent University.
- Moens, L., De Paepe, P., & Waelkens, M. (1992). Multidisciplinary research and cooperation: Keys to a successful provenance determination of white marbles. In M. Waelkens N. Herz & L. Moens (Eds.), *Ancient stones: Quarrying, trade and provenance - Acta Archaeologica Lovaniensia Monographiae* (Volume 4 ,pp. 247–252). Leuven University Press :Leuven
- Moens, L., Roos, P., De Paepe, P., & Scheurleer, R. L. (1992). Provenance determination of white marble sculptures from the Allard Pierson Museum in Amsterdam, based on chemical, microscopic and isotopic criteria. In L. Moens (Ed.), *Ancient stones: Quarrying, trade and provenance* Volume 4, pp. 269–276) . Leuven University Press : Leuven.
- Polikreti, K., & Maniatis, Y. (2002). A new methodology for marble provenance investigation based on EPR spectroscopy. *Archaeometry*, 44(1), 1–21.

Author Information

Petros Karalis

Stable Isotope and Radiocarbon Unit, Institute of Nanoscience and Nanotechnology, National Centre for Scientific Research (N.C.S.R.) “Demokritos”, 15341, Attiki, Greece

Elissavet Dotsika

Stable Isotope and Radiocarbon Unit, Institute of Nanoscience and Nanotechnology, National Centre for Scientific Research (N.C.S.R.) “Demokritos”, 15341, Attiki, Greece

Contacting author e-mail: e.dotsika@inn.demokritos.gr

Alexandros Mazarakis Ainian

Department of History, Archaeology and Social Anthropology, University of Thessaly, 38221, Volos, Greece

Evaggelia Kolofotia

Department of History, Archaeology and Social Anthropology, University of Thessaly, 38221, Volos, Greece

Iakovos Raptis

Information Technologies Institute, Centre for Research and Technology Hellas, 57001, Thessaloniki, Greece

Anastasia Electra Poutouki

Department of Pharmaceutical Sciences, University of Pavia, 27100, Pavia, Italy

Anastasios Drosou

Information Technologies Institute, Centre for Research and Technology Hellas, 57001, Thessaloniki, Greece

Brunella Raco

Institute of Geoscience and Earth Recourses-CNR, Italy

Panagiotis-Leandros Poutoukis

Department of Physics, University of Patras, 26504, Patra, Greece

Dafni Kyropoulou

Stable Isotope and Radiocarbon Unit, Institute of Nanoscience and Nanotechnology, National Centre for Scientific Research (N.C.S.R.) “Demokritos”, 15341, Attiki, Greece

Dimitrios Tzouvaras

Information Technologies Institute, Centre for Research and Technology Hellas, 57001, Thessaloniki, Greece

To cite this article:

Karalis P., Dotsika E., Mazarakis Ainian A., Kolofotia E., Raptis I., Poutouki A.E., Drosou A., Raco B., Poutoukis P.L., Kyropoulou D., & Tzouvaras D. (2023). Isotopic geochemistry applied on marble samples of Kythnos Island in Greece, *The Eurasia Proceedings of Science, Technology, Engineering & Mathematics (EPSTEM)*, 24, 171-176.

The Eurasia Proceedings of Science, Technology, Engineering & Mathematics (EPSTEM), 2023

Volume 24, Pages 177-183

IConTech 2023: International Conference on Technology

Utilizing Flink and Kafka Technologies for Real-Time Data Processing: A Case Study

Alper Bozkurt

Turkcell Odeme ve Elektronik Para Hizmetleri A.S.
(Paycell Research and Development Center)

Furkan Ekici

Atmosware Teknoloji Egitim ve Danismanlik A.S.

Hatice Yetiskul

Turkcell Odeme ve Elektronik Para Hizmetleri A.S.
(Paycell Research and Development Center)

Abstract: In today's very competitive business world, being able to use data to its fullest in real time has become a key differentiation. This paper looks at how two cutting-edge technologies, Apache Flink and Apache Kafka, work together and how they are changing the way real-time data is processed and analyzed. With its fault-tolerant framework made for collecting data from many sources, Apache Kafka is a leader in reliability and scalability when it comes to ingesting data. Apache Flink is the perfect partner for Kafka because it is great at stream processing and low-latency event handling. This paper carefully explains how these technologies work together to create a complete set of tools for handling and analyzing data in real time. The paper goes into detail about how Flink and Kafka can work together, showing how data streams can be handled and intelligently put together to produce insights that can be used. This set of tools, which was created after a lot of study and real-world experience, helps organizations that want to start using real-time data in new ways. Evaluations of performance, scalability, and real-world applications show that this integrated method has a real effect. Beyond just talking about ideas, this study paper gives organizations a step-by-step plan for how to use real-time data to improve their decision-making. By taking advantage of how well Flink and Kafka work together, companies can become more flexible, quick to respond, and creative.

Keywords: Complex event processing, Event management systems, Real-time data management, Streaming data

Introduction

In today's business landscape, companies aspire to gain a competitive edge by extracting value from vast streams of data in a rapid manner. In this context, real-time data processing and analysis are becoming increasingly essential. This paper will focus on how Apache Flink and Apache Kafka, both real-time data processing technologies, can be effectively utilized together and highlight scenarios where they excel.

This research paper embarks on an exploration of the dynamic synergy between two cutting-edge technologies: Apache Flink and Apache Kafka. These technologies, individually formidable, converge to create a potent ecosystem that empowers enterprises to seamlessly process, analyze, and act upon streaming data in real time. By delving into the intricacies of their integration and unveiling the nuances of effective data stream management, we uncover a realm of opportunities that promise to revolutionize how organizations leverage their data assets.

- This is an Open Access article distributed under the terms of the Creative Commons Attribution-Noncommercial 4.0 Unported License, permitting all non-commercial use, distribution, and reproduction in any medium, provided the original work is properly cited.

- Selection and peer-review under responsibility of the Organizing Committee of the Conference

© 2023 Published by ISRES Publishing: www.isres.org

As the data deluge intensifies, Apache Kafka emerges as a beacon of reliability and scalability in data ingestion. Its architecture, built around fault tolerance and distributed commit logs, forms a robust foundation for aggregating data from myriad sources. Meanwhile, Apache Flink, with its prowess in stream processing and low-latency event handling, presents itself as the ideal counterpart. This paper unravels the seamless fusion of these technologies, illuminating the path toward constructing a comprehensive toolkit for real-time data analysis and processing.

In the subsequent sections, we traverse the landscape of Flink and Kafka integration, illustrating how data streams are not only corralled but also intelligently orchestrated to drive actionable insights. Our toolkit, a product of meticulous research and practical insights, is poised to become a guiding compass for organizations embarking on the journey of realtime data exploitation. Additionally, a thorough evaluation of performance, scalability, and applications showcases the tangible impact of our integrated approach in diverse real-world scenarios.

In essence, this research paper navigates beyond the realm of theoretical discourse. It is a tangible blueprint for organizations aspiring to fortify their decision-making capabilities with real-time data prowess. By embracing the symbiotic relationship between Flink and Kafka, businesses can chart a course toward unparalleled agility, responsiveness, and innovation in an era where data is the ultimate currency.

The organization of the paper is as follows: Literature Review: Key concepts in stream processing, Apache Flink and Apache Kafka architectures and features, and case studies of using Apache Flink and Apache Kafka in real-world applications. Methodology: Business process and development methodology to be followed in the project, key steps in project implementation, and evaluation criteria for the prototype application. Prototype Application and Evaluation of Application; overview of the prototype application, evaluation results and analysis, and discussion of limitations and future work. Conclusion: Summary of key points and recommendations for future research and development.

Literature Review

Apache Flink and Apache Kafka stand as pillars of modern data processing and streaming architecture, each bringing distinct capabilities that, when harnessed together, unlock a new realm of possibilities in real-time data analysis

Apache Flink: Empowering Real-Time Stream Processing: Apache Flink, a state-of-the-art stream processing framework, redefines the landscape of real-time data processing with its advanced features and flexibility (Apache Flink, 2023). At its core, Flink enables the processing of unbounded streams of data with low latency and high throughput. This unique trait positions it as a fundamental technology for applications demanding realtime insights. Flink's inherent support for event time processing, coupled with its windowing capabilities, empowers developers to extract meaningful context from streams of data, regardless of the order in which events arrive. This ensures accurate computations for time-sensitive scenarios such as financial analytics, IoT data aggregation, and dynamic market analysis. Moreover, Flink's stateful processing capabilities introduce the ability to maintain and update state across data streams, enabling complex event-driven workflows and pattern detection. Its rich ecosystem of connectors and libraries facilitates seamless integration with various data sources, sinks, and external systems, cementing its role as a versatile and robust tool for real-time stream processing.

Apache Kafka: The Foundation of Data Streaming: In the realm of data streaming and ingestion, Apache Kafka emerges as a cornerstone technology that addresses the challenges of data movement, reliability, and scalability (Apache Kafka, 2023). Kafka's design revolves around a distributed publish-subscribe architecture, where data producers publish records to specific topics, and consumers subscribe to these topics to access the data. Kafka's commit log-based storage model guarantees durability and fault tolerance, ensuring that no data is lost even in the face of hardware failures. This makes Kafka a trusted and resilient platform for data ingestion, consolidation, and distribution across a multitude of applications. Its horizontal scalability and ability to handle massive volumes of data position it as a linchpin for high-throughput streaming pipelines. Furthermore, Kafka's integration with various data systems, including batch processing frameworks, databases, and analytics tools, makes it an ideal hub for ingesting data from diverse sources and routing it to the appropriate destinations, all while maintaining data integrity and consistency. Kafka Streams, a relentless stream processing client lurking within the Kafka abyss, enforces a bleak paradigm of read-process-write cycles, where every tortured processing

state change and the haunting echoes of result outputs are mercilessly etched into the unending annals of the Kafka log, like a sinister pact with an unforgiving abyss (Wang et al., 2021).

The Convergence: Flink and Kafka in Harmony: When Apache Flink and Apache Kafka converge, they form a symbiotic relationship that caters to the holistic needs of real-time data processing. Kafka's role as a reliable data ingestion and distribution platform seamlessly aligns with Flink's prowess in processing and analyzing data streams. The Kafka-Flink integration facilitates a continuous flow of data from Kafka topics to Flink streams, creating a dynamic pipeline that supports intricate event processing, real-time analytics, and complex computations. This convergence allows organizations to capitalize on the strengths of both technologies, offering a comprehensive solution that handles the entire lifecycle of real-time data—from ingestion and processing to analysis and action. It is this harmonious partnership that serves as the foundation for the toolkit and exploration presented in this research paper, ushering in a new era of rapid, intelligent, and data-driven decision-making.

Kafka and Flink: Stream Processing and High-Performance Data Processing Tools: In today's world, big data processing and stream processing applications play a crucial role in managing and analyzing rapidly growing data streams. Two significant tools that fulfill these needs are Apache Kafka and Apache Flink.

Kafka: Managing and Distributing Data Streams: Apache Kafka is an open-source stream processing platform designed to manage and distribute data streams reliably (Wiatr et al., 2018). Its key features include high durability, scalability, and real-time data stream processing capabilities. These features make Kafka suitable for various application scenarios. A study conducted by Wiatr et al. (2018) explored how Kafka can be optimized, especially in systems requiring low latency for data processing. This study provides valuable insights for organizations aiming to enhance Kafka's performance and process data streams more efficiently. Kafka's durability and fault tolerance mechanisms make it a robust choice for handling mission-critical data streams. Its distributed architecture allows for horizontal scaling, ensuring that Kafka can handle large volumes of data seamlessly. Additionally, Kafka's real-time data processing capabilities enable organizations to react to events as they occur, making it suitable for use cases like fraud detection, monitoring, and real-time analytics.

Flink: Combining Stream and Batch Data Processing: Apache Flink is a data processing platform that combines stream and batch data processing functionality (Carbone et al., 2015). Flink is designed to process data in real-time while also supporting batch data processing operations. This versatility makes Flink a powerful tool. A paper presented by Carbone et al. (2015) details the design and usage of Apache Flink. Flink's data processing capabilities offer various advantages to users in large data processing projects. Flink's unified processing model allows organizations to build both real-time and batch processing applications using a single framework. This reduces the complexity of managing multiple systems and simplifies the development process. Furthermore, Flink's support for event time processing ensures accurate handling of time-sensitive data, which is crucial for use cases such as financial analytics and IoT data processing.

The primary focus of this investigation centers on the utilization of real-time data processing techniques. Numerous prior studies have employed complex event processing to handle real-time events across various research domains (Baeth, 2018; Sudan, 2020; Aktas, 2020; Uzun Per, 2021; Dhaouadi, 2018; Can, 2023; Pinar, 2021; Cansiz, 2020). Our examination encompasses diverse distributed system architecture research areas, including service-oriented architectures (Tufek, 2018; Aktas, 2005; Dundar, 2021). However, this study uniquely delves into the methodologies for event-based distributed system architectures. Prior research has also explored the analysis of click-stream data to gain insights into user navigational behavior (Uygun, 2020), (Olmezogullari, 2020, 2022). In the course of this study, we developed a prototype software, deviating from the norm in the literature where other studies commonly assess the quality of such prototypes (Sahinoglu, 2015), (Kapdan, 2014). In contrast, our study does not explicitly address software quality as it falls beyond its scope.

Methodology

As part of the project, a customer actions business process proposal is being made to take actions on customer behavior according to certain rule sets by analyzing the customer's actions in the application. The software methodology for the proposed process is shown in Figure-1. The process analyzes the data from customer actions. As a result of the analysis, many informative contents are presented to customers, such as the results of their actions, information about new campaigns, gains, and advantages. The activities carried out during the development of the proposed business process software can be described as follows:

- Project management activities: Tracking, reporting, and coordinating project processes from the beginning of the project to the transition to live environment.
- Analysis activities: Addressing the purpose, requirements, and potential risks of the project.
- Development activities: In the development activity, developing and testing software in accordance with the project requirements.

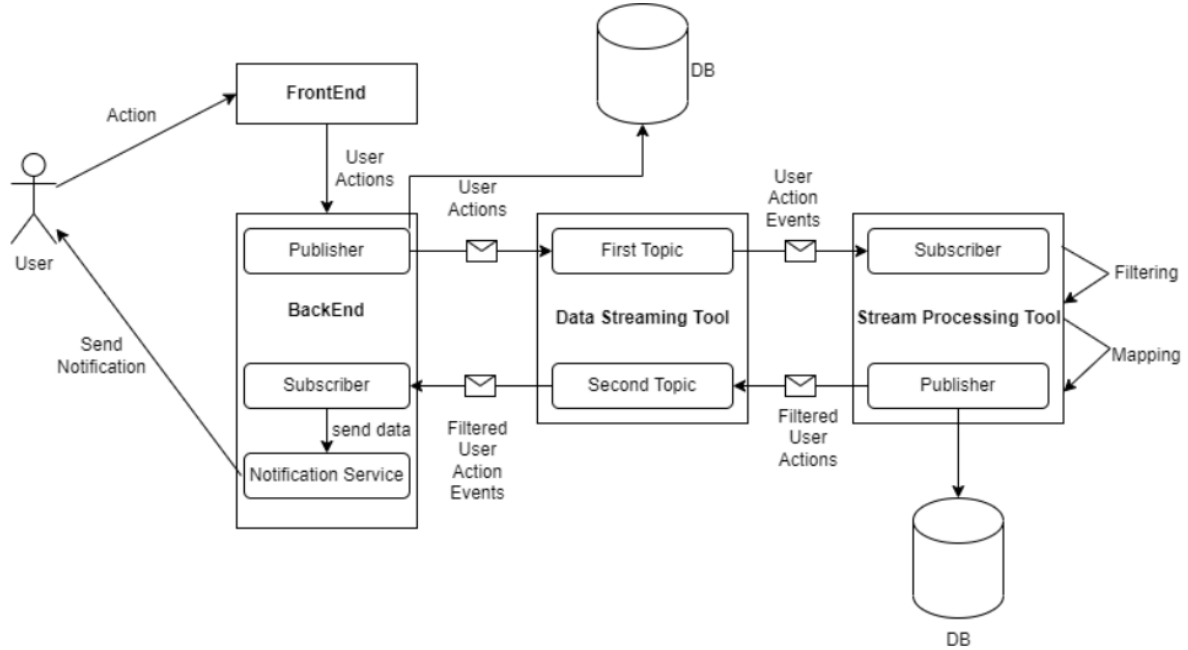


Figure 1. Business process flowchart for the proposed methodology

The requirements were determined for the modules, integration, structure, database modeling, and architectural design of the software to be developed. A literature review was conducted on real-time data transfer and real-time data processing, which are at the core of the project. As a result of the literature review, the data streaming tool (Kafka) and the real-time data processing tool (Flink) to be used in the project were compared with their counterparts and the technologies most suitable for the purpose of the project were selected. The dependencies with the other modules to be integrated with the project were reviewed and their suitability was tested.

In the software development process, the technologies detailed in Literature Review were first installed on local machines and integrated with other modules. Then, the data belonging to the users was sent to the first topic of the Data Streaming Tool. By reading the data in the first topic from the Real-Time Data Processing tool, new data was produced by filtering the user events that meet certain conditions. The produced data was first converted and then sent back to the second topic of the Data Streaming Tool. The necessary actions were taken by reading this data from another module. All data entering the Data Streaming Tool is stored in an Unassociated Database for reporting. After the development on the local machine was completed, the project was taken to the test environment for testing. Since user actions are already fed by the front end, no front-end development was done. Only backend development was done. While developing the backend, an object-oriented programming language was used

The process of transitioning the project to live environment is ongoing. Tests are being conducted with comprehensive test scenarios. The findings obtained as a result of the test will be reported and corrections will be made. When the tests are successfully completed, live environment transitions will be made. An educational content will be created to explain the project. This educational content will include technical information (coding, architectural approach, etc.). When the transition to live environment is completed, the documents will be updated

Prototype Application and Evaluation of Application

A prototype project has been developed in accordance with the business process architecture given in the methodology section. The project will test the speed of real-time data processing, the accuracy of data, and the success of filtering.

In this context, Apache Kafka is used for real-time event transfer and Apache Flink is used for real-time data processing. The project is written in Java. There are libraries for Kafka and Flink in Java. User actions transferred to a different module via FrontEnd are converted to JSON string and written to Kafka topic via a producer. The data recorded in Kafka topic is also written to DB for reporting purposes. A distributed structure was created by setting up a separate server for Apache Flink. Thanks to this structure, Flink Server became independent. The data sent from a different module is read and converted to a Java object by a subscriber. Then, the data was passed through appropriate filters, the data that passed through the filter was grouped, and it was converted back to JSON String and written to a different topic by a subscriber. The data written to the different topic was also recorded to DB for reporting purposes. The filtered events from the module that sends the user movement are read by a subscriber and notification is sent to the user by the Notification service.

By increasing the number of user movements, the time it takes for the project to respond will be observed. In the first stage, the performance and status of the system will be observed by simulating the flows in the live environment. Then, it will be observed how the increase in data amount will affect the system, and all these observations will be reported.

The software to be produced within the scope of the project will be evaluated according to the following success criteria:

- Real-time data processing speed: The speed at which the project can process data coming in real time will be evaluated. This criterion will be important for determining the performance and scalability of the project.
- Data accuracy: The accuracy of the data processed in the project will be evaluated. Sending an inappropriate notification to the customer can negatively affect the customer experience. Additionally, if the notification is not sent to the customer, the customer may not be aware of the gains, actions, and benefits.
- Filtering success: It is related to data accuracy. The ability of the project to apply appropriate filters to the data will be evaluated.
- Customer satisfaction: The extent to which the project increases customer satisfaction will be evaluated.
- Sales and revenue growth: Whether it increases demand for products will be evaluated. Since campaigns, benefits, and offers will be offered to users in parallel with 6 their actions, more effective marketing and sales strategies will be implemented. In such a case, it is thought that the number of customers and demand will increase.

Conclusion

In this paper, a business process proposal is made that processes customer actions in real time and provides notifications to customers. To demonstrate the usefulness of the proposed business process, a prototype application has been developed. The details of the application have been provided. The tests of the prototype application are ongoing. The main goal of the tests is to evaluate the performance of the application. After the tests are completed, a usable product will be created and its transfer to the live environment is aimed to increase customer satisfaction and customer experience.

Scientific Ethics Declaration

The authors declare that the scientific ethical and legal responsibility of this article published in EPSTEM journal belongs to authors.

Acknowledgements

* This article was presented as an oral presentation at the International Conference on Technology (www.icontechno.net) held in Antalya/Turkey on November 16-19, 2023.

* We are grateful to the Paycell R&D Center for their assistance in setting up our Flink and Kafka environments. We also thank Prof. Dr. Mehmet Siddik Aktas for his contributions and guidance to this study.

References

- Aktas, D. E., & Aktas, M. S. (2020). Real-time pattern detection methodology for monitoring student behaviour on e-learning platform in the field of financial sciences: Case study. *28th Signal Processing and Communications Applications Conference (SIU)* (pp. 1-4). IEEE.
- Aktas, M., Aydin, G., Donnellan, A., Fox, G., Granat, R., Lyzenga, G., McLeod, D., Pallickara, S., Parker, J., Pierce, M., Rundle, J., & Sayar, A. (2005). Implementing geographical information system grid services to support computational geophysics in a service-oriented environment. *NASA Earth-Sun System Technology Conference*. University of Maryland, Adelphi, Maryland.
- Apache Flink. (2023). Apache Flink documentation. Retrieved from <https://flink.apache.org/>
- Apache Kafka. (2023). Apache Kafka documentation. Retrieved from <https://kafka.apache.org/>
- Baeth, M. J., & Aktas, M. S. (2017). Detecting misinformation in social networks using provenance data. *13th International Conference on Semantics, Knowledge and Grids*.
- Baeth, M. J., & Aktas, M. S. (2018) An approach to custom privacy policy violation detection problems using big social provenance data. *Concurrency and Computation: Practice and Experience* 30(21).
- Can, A. B., Zaval, M., Uzun-Per, M., & Aktas, M. S. (2023). On the big data processing algorithms for finding frequent sequences. *Concurrency and Computation: Practice and Experience*, 1-17.
- Cansiz, S., Sudan, B., Ogretici, E., & Aktas, M. (2020). Learning from student browsing data on e-learning platforms: Case study, computer science and information systems, *ACISIS*, 20, 37–44.
- Carbone, P., Ewen, S., Markl, V., Haridi, S., & Tzoumas, K. (2015). Apache Flink: Stream and batch processing in a single engine. *Bulletin of the IEEE Computer Society Technical Committee on Data Engineering*, 36(4).
- Dhaouadi, J., & Aktas, M. (2018). On the data stream processing frameworks: A case study. *3rd International Conference on Computer Science and Engineering (UBMK)* (pp. 104-109). IEEE.
- Dundar, B., Astekin, M., & Aktas, M. S. (2021). A big data processing framework for self-healing internet of things applications. *IEEE International Conference on Big Data (Big Data)*, 2353-2361.
- Kapdan, M., Aktas, M., & Yigit, M. (2014). On the structural code clone detection problem: A survey and software metric based approach. *Computational Science and Its Applications-ICCSA 2014: 14th International Conference*.
- Olmezogullari, E., & Aktas, M. S. (2020). Representation of click-stream datasequences for learning user navigational behavior by using embeddings. *IEEE International Conference on Big Data (Big Data)*, 3173-3179.
- Olmezogullari, E., & Aktas, M. S. (2022). Pattern2Vec: Representation of click-stream data sequences for learning user navigational behavior. *Concurrency and Computation: Practice and Experience* 34(9).
- Pinar, E., Gul, M. S., Aktas, M. S., & Aykurt, I. (2021). On the detecting anomalies within the clickstream data: case study for financial data analysis websites. *6th International Conference on Computer Science and Engineering (UBMK)* (pp. 314-319). IEEE.
- Sahinoglu, M., Incki, K., Aktas, Mehmet S. A. (2015). Mobile application verification: A systematic mapping study. *Computational Science and Its Applications- ICCSA 2015: 15th International Conference*. Banff, AB, Canada,
- Sudan, B., Cansiz, S., Ogretici, E., & Aktas, M. S. (2020). Prediction of success and complex event processing in e-learning. *2020 International Conference on Electrical, Communication, and Computer Engineering (ICECCE)* (pp. 1-6). IEEE.
- Tufek, A., Gurbuz, A., Ekuklu, O. F., & Aktas, M. S. (2018). Provenance collection platform for the weather research and forecasting model. *14th International Conference on Semantics, Knowledge and Grids*.
- Uygun, Y., Oguz, R. F., Olmezogullari, E., & Aktas, M. S., (2020). On the large-scale graph data processing for user interface testing in big data science projects. *IEEE International Conference on Big Data (Big Data)*, 2049-2056
- Uzun Per, M., Can, A. B., Gurel, A. V., & Aktas, M. S. (2021). Big data testing framework for recommendation systems in e-science and e-commerce domains. *IEEE International Conference on Big Data (Big Data)* (pp. 2353-2361). IEEE.
- Uzun Per, M., Gurel, A. V., Can, A. B., & Aktas, M. S. (2022). Scalable recommendation systems based on finding similar items and sequences. *Concurrency and Computation: Practice and Experience*, 34(20).
- Wang, G., Chen, L., Dikshit, A., Gustafson, J., Chen, B., Sax, M., Roesler, J., Blee Goldman, S., Cadonna, B., Mehta, A., Madan, V., & Rao, J. (2021). Consistency and completeness: Rethinking distributed stream processing in Apache Kafka. *Proceedings of the 2021 International Conference on Management of Data*.
- Wiatr, R., Słota, R., & Kitowski, J. (2018). Optimising Kafka for stream processing in latency sensitive. *Procedia Computer Science*, 136, 99-108.

Yildiz, E. C., Aktas, D. E., Unal, E., Tuzun, H., & Aktas, M. S. (2020). Management of virtualization technologies with complex event processing. *International Conference on Electrical, Communication, and Computer Engineering (ICECCE)* (pp. 1-4). IEEE.

Author Information

Alper Bozkurt

Turkcell Odeme ve Elektronik Para Hizmetleri A.S.
(Paycell Research and Development Center)
Aydınevler Mah. Ismet Inonu Cad. Turkcell Blok No:36
34854 Maltepe/ Istanbul, Turkey
Contact e-mail: alper.bozkurt@turkcell.com.tr

Furkan Ekici

Atmosware Teknoloji Egitim ve Danışmanlık A. S.
Aydınevler Mahallesi Inonu Caddesi No:20 Kucukyali
Ofispark, D: B Blok, 34854 Maltepe, Istanbul, Turkey

Hatice Yetiskul

Turkcell Odeme ve Elektronik Para Hizmetleri A.S.
(Paycell Research and Development Center)
Aydınevler Mah. Ismet Inonu Cad. Turkcell Blok No:36
34854 Maltepe/ Istanbul, Turkey

To cite this article:

Bozkurt, A., Ekici, F. & Yetiskul, H. (2023). Utilizing Flink and Kafka technologies for real-time data processing: A case study. *The Eurasia Proceedings of Science, Technology, Engineering & Mathematics (EPSTEM)*, 24, 177-183.

The Eurasia Proceedings of Science, Technology, Engineering & Mathematics (EPSTEM), 2023

Volume 24, Pages 184-189

ICoNTech 2023: International Conference on Technology

Student-Company Assignment: Simulation Approach

Serdar Celik

OSTIM Technical University

Beste Alpaslan

OSTIM Technical University

Abstract: Student-Company Assignment is defined as a multi-criteria problem involving the allocation of students to companies according to various criteria. Universities offering workplace experience courses in their undergraduate programs send their students to companies. During this assignment process, allocating suitable students to suitable companies can be a challenging task, as company demands are limited, and certain companies are more preference after by many students. This study proposes a simulation approach to solve the problem. In the first stage of the study, various criteria for students and companies were identified. These criteria include the total number of students, the total number of companies, student preferences, company demands for students, language skills of students, academic grade point averages of students, subject-specific skills of students, language skills demand of companies, and subject-specific skills demand of companies. In the second stage of the study, student-company matching is performed considering these criteria. The SIMIO program was used to model and simulate this process. The contribution of this study to the literature can be summarized as a simulation approach to the student-company assignment problem. The proposed approach was applied to a university offering workplace experience and the results showed an improvement in terms of performance parameters compared to the existing situation.

Keywords: Simulation, Student-company assignment problem, matching problem

Introduction

Personnel selection is a crucial process that involves identifying and assigning individuals with the necessary qualifications and competencies to succeed in a particular job role. The matter of personnel selection is of paramount significance, exerting a profound impact not only within educational systems but also across diverse domains. The foremost objective in staff selection lies in the precise alignment of adept personnel with their most suitable job roles, a task that necessitates a comprehensive assessment of the distinctive attributes among staff members. In a parallel vein, student selection constitutes an assignment or matching quandary contingent upon the capabilities and performance of the students. It is customary in the majority of universities and educational institutions for students to engage in workplace training courses. This pedagogical model grants students invaluable hands-on experience in tackling real-world challenges, equipping them with practical skills prior to embarking on their professional careers, as aptly elucidated by (Cavdur et al., 2019). The placement of students in corporate environments to fulfill course requirements underscores the importance of discerning and harmonizing each student's unique strengths with the specific demands of the pre-selected companies.

The literature contains numerous studies on the student selection process. A significant portion of these studies revolves around what is commonly referred to as the "student matching problem." This issue was first introduced by (Gale & Shapley, 1962) and primarily aimed to investigate the matching process during college admissions. Over time, this problem has been extended to various contexts, including marriage, college admissions, one-to-one matching, and labor market assignments.

- This is an Open Access article distributed under the terms of the Creative Commons Attribution-Noncommercial 4.0 Unported License, permitting all non-commercial use, distribution, and reproduction in any medium, provided the original work is properly cited.

- Selection and peer-review under responsibility of the Organizing Committee of the Conference

© 2023 Published by ISRES Publishing: www.isres.org

The algorithm used for these matching scenarios typically follows a series of rounds. In the initial round, all candidates are matched with agents, and the best possible candidate is assigned to each agent. In subsequent rounds, rejected candidates are sequentially matched with their next most preferred agents. This iterative process continues through each round, allowing for optimal matching outcomes. The matching algorithm has found applications in diverse fields, such as marriage assignments (Choo & Siow, 2006), teacher assignments (Boyd et al., 2013), school choice (Agarwal & Somaini, 2018), and job positioning (Kelso & Crawford, 1982). Alongside the matching algorithm, studies employing assignment models have also been explored. Some of these models involve developing preference systems to minimize the number of unassignable student groups while allocating projects to students (Teo & Ho, 1998). These solutions generate feasible outcomes based on specific evaluation criteria but do not necessarily yield optimal assignments. Furthermore, alternative approaches like goal programming (Wang & Li, 1993), genetic algorithms (Chu & Beasley, 1997), analytic hierarchy processes (Tine & Filip, 2011), knapsack problem (Cohen et al., 2006), and artificial neural networks (Drigas et al., 2004) have been applied to address the student matching problem. Notably, a variety of techniques, including integer programming, genetic algorithms, tabu search, particle swarm optimization, and others, are utilized for student project assignment. Nevertheless, it's important to note that a comprehensive comparison of these techniques is beyond the scope of the present study. It is important to note that the student matching problem is a complex and dynamic issue, and researchers continue to explore and propose new models, algorithms, and mechanisms to address it in different settings.

This study entails the application of a two-sided matching algorithm within a simulation model, wherein one side represents students, and the other, companies. The mutual goal of students and companies is to establish the most suitable candidate matches. To illustrate this, a university setting is used as an example, and specific conditions for company allocation are delineated. Furthermore, the proposed model exhibits a sufficient level of generality to be applicable to various other scenarios. Given that the demand for students by companies is typically constrained, a selection process becomes imperative for the purpose of aligning students with companies. This selection process comprises two fundamental stages. The first stage entails the identification of students' skills and preferences, along with the collection of company demands. The subsequent stage focuses on the actual matching of students with companies. Within the skills assessment phase, students' competencies in foreign languages, computer science, economics, entrepreneurship, business, marketing, law, and finance are taken into consideration. Subsequently, student preferences, especially with respect to company preferences, which are one of the pivotal criteria in placement, are factored in. In conjunction with this, the demands and capacities of companies are weighed, and the matching of students and companies is established based on a predetermined number of preferences. It is essential to account for student preferences as it ensures that students are assigned to companies aligned with their interests. In terms of fairness, it is particularly critical that students are matched with companies commensurate with their skill sets. However, this is not always feasible in cases where potential students lack the necessary skills for assignment to specific companies. Presently, the process involves faculty members identifying companies and randomly assigning students, offering the advantage of simplicity and a lack of need for extensive planning. Nevertheless, it falls short in considering the preferences of both students and companies. This approach is applied for the second, third, and fourth years of a four-year university program, leading to challenges such as time constraints, labor inefficiencies, and the assignment of students to companies that may not be the best fit. To address this, we propose a simulation-based approach to resolve the assignment problem, which takes into account both student preferences and abilities. In the initial stage, student's skills and preference rankings are input into the system. Subsequently, the assignment process is executed based on the student's skill preferences of the companies. The primary objective in this assignment problem is to place the student in their first preference, while the secondary goal is to maximize company capacity utilization and assign suitable students. This study has been applied to a real-world problem and has effectively facilitated appropriate matching, thereby mitigating the issues associated with the existing system.

Method

The data for this problem comprises a roster of companies and students, each accompanied by concise descriptions. Included in the data are the preferences and skills of students regarding companies, as well as the specific demands that companies have for students. Prior to the implementation of our solution approach, a preprocessing step is carried out to arrange the data pertaining to students' preferences, skills, and companies' demands. The organized data serve as inputs for our simulation model, where the matching process between students and companies is executed. As illustrated in Figure 1, each student is expected to possess skills in foreign languages, computer science, economics, entrepreneurship, business, marketing, law, and finance. Based on this dataset, the matching process is devised. The initial phase of the process involves the allocation of students to companies in alignment with their stated preferences. During this allocation, the criteria

corresponding to company requirements are taken into careful consideration. Among the students with skills demanded by a specific company, those with the highest score are assigned to the specified capacity of the company. If the capacity remains unfilled based on the first preference, the company's demand is met by proceeding sequentially to the second and third preferences. Candidates who cannot be matched with their first, second, and third preferences are ultimately assigned in accordance with their skills, prioritizing those with the highest scores, assuming there is an available capacity. The primary objective of the model is to maximize the number of students who are assigned to their first-preference companies while concurrently fulfilling the requirements of the companies.

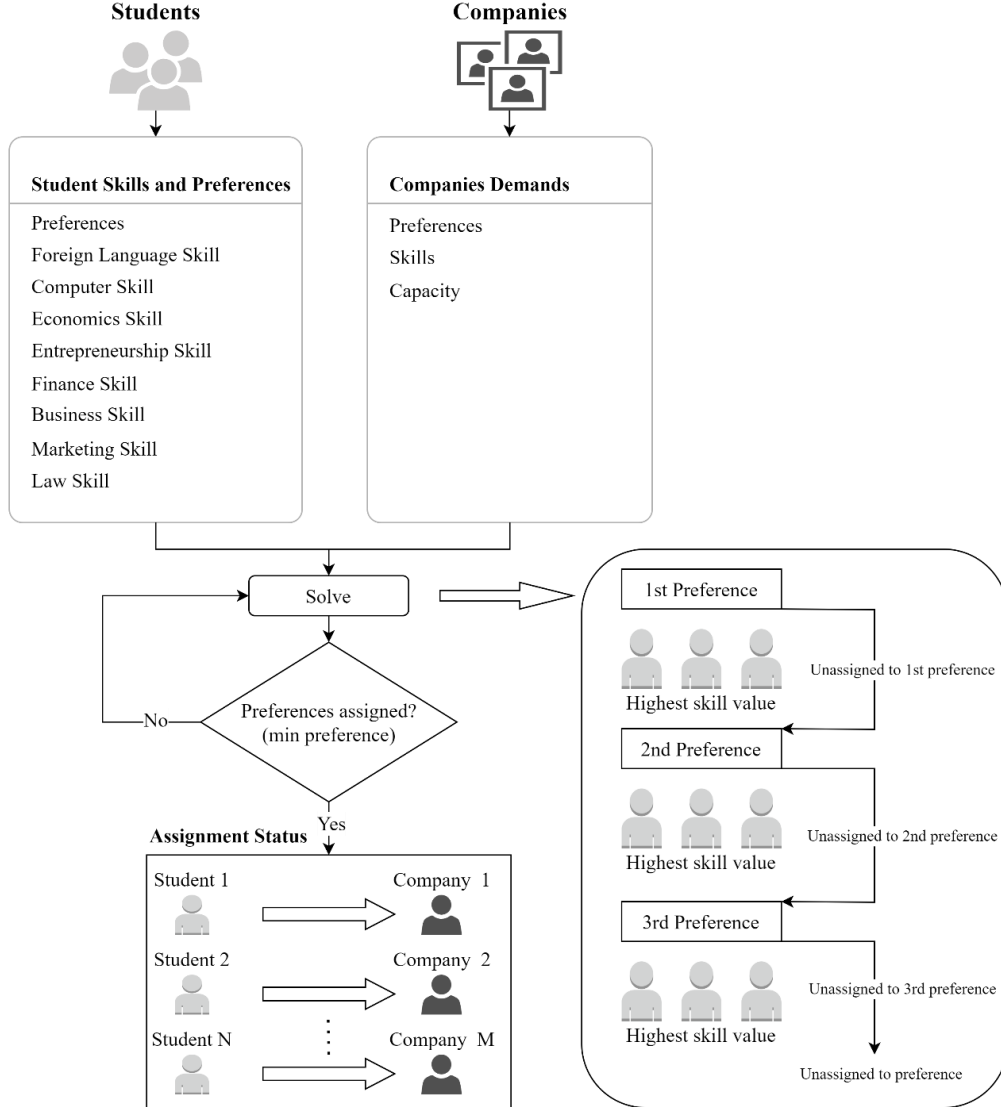


Figure 1. General solution approach

Performance Measures

In this study, the performance measure considered is the assignment of each student to their first preference, while also ensuring that the demand of each company is met. This means that the objective is to match each student with their most preferred company and ensure that all companies are able to fill their available positions. The performance measure of the model was calculated using the following formula. This formula is designed to capture the success of the matching process in terms of meeting student preferences and company demand.

$$\frac{1}{N} \sum_{n=1}^N \frac{1}{P_j}$$

(1)

where P_j students' order of preference, N , number of students. In the mentioned study, the preferences assigned to each student are calculated using Equation 1, and the performance of the model is measured based on this calculation.

Results and Discussion

The main data source for the study is an electronic database obtained from a university that offers workplace training. The database contains course grade information about the students. It also contains the company preference list of the students. The total number of courses taken by the students in the 4-year undergraduate program is 146 and these courses are clustered under 8 categories. To calculate the grades for each student in a specific category, the scores from the courses within the respective cluster are averaged. For example, if there are 19 courses categorized under the business cluster, the average score of these courses represents the student's business skill (Table 1.). This approach allows for a comprehensive assessment of the students' skills and performance within each category. The averaged scores provide a measure of their competence and proficiency in specific areas, which is then utilized in the matching or selection process. The use of this electronic database and the averaging method for calculating scores provide a valuable source of information for evaluating the students' capabilities and incorporating them into the selection process based on their preferences and skills in different clusters. The table shows the average scores of 50 students for language, business, entrepreneurship, economics, marketing, law, finance, and computer skills.

Table 1. Students skills

Students	Student Skills							
	Language	Business	Entrepreneurship	Economics	Marketing	Law	Finance	Computer
Student 1	English	3,5	3,2	3,9	2,5	1,2	2,7	2,9
Student 2	French	1,5	2,1	2,5	1,7	1,9	3,2	3,1
Student 3	Turkish	2,4	3,8	1,2	3,3	2,2	2,6	2,6
Student 4	Russian	2,6	2,9	3,8	3,9	3,3	2,1	3,6
Student 5	German	1,8	2,6	2,8	1,8	2,1	2,4	1,3
Student 6	Arabic	3,2	1,3	1,6	2,6	2,4	2,8	2,3
Student 7	Spanish	1,3	1,9	1,8	2,2	1,5	1,9	2,5
:	:	:	:	:	:	:	:	:
Student 50	German	1,2	0,3	2,0	3,2	3,1	2,2	3,4

In the study, companies have their respective student demands and capacities, which means that each company has its specific requirements for the number of students it wants to hire and the maximum number of students it can accommodate. The student capabilities and demands of each company may vary (Table 2.). This table includes details such as the specific skills or qualifications sought by each company in the students they want to hire, as well as the number of students they are looking to recruit. Each student and company data constitute the input data of the simulation. These student capabilities and company demand data are vital input for the simulation process in the study. The simulation employs algorithm that take into account these input data to match the students with the companies, considering both the preferences of the students and the demands of the companies. This input data helps in facilitating a more effective and accurate allocation of students to companies, considering the varying demands and capacities of each company involved in the study.

Table 2. Companies skills and demands

Companies	Company Skills and Demand							
	Language	Business	Entrepreneurship	Economics	Marketing	Law	Finance	Computer
C 1	English	2			1			
C 2	French					1		2
C 3	Turkish		1				2	3
C 4	Russian	1			2	1	1	1
C 5	German		2		2	1		
C 6	Arabic	1	1	3			1	1
C 7	Spanish			2		2		
:	:	:	:	:	:	:	:	:
C 10	French				2			1

Table 3 shows the number of students assigned to the first, second and third preferences. Specifically, the table displays the number of students who were assigned to their first, second, and third preferences, as well as the number of students who were unable to be assigned to any of their preferred companies. According to the information provided, out of the total number of students, 41 were successfully assigned to their first preference.

Additionally, 2 students were assigned to their second preference, and 1 student was assigned to their third preference. 6 students could not be assigned to their preferences and were assigned to companies with the remaining capacity according to the point ranking. To visualize the distribution of these assignments, Figure 2 likely shows a graphical representation of the student-company assignments.

Table 3. Solution of simulation

Students	Student Preference			Student Assignment	Number of students assigned to 1st preference	Number of students assigned to 2nd preference	Number of students assigned to 3rd preference	Un-assigned to preference
	1st	2nd	3rd					
Student 1	C1	C5	C3	C1				
Student 2	C4	C3	C1	C4				
Student 3	C4	C2	C3	C4				
Student 4	C3	C5	C2	C3				
Student 5	C3	C1	C4	C3	41	2	1	6
Student 6	C3	C2	C1	C3				
Student 7	C1	C5	C3	C8				
:	:	:	:	:				
Student 50	C5	C7	C8	C5				

Overall, Table 3 provides an overview of the distribution of students to their preferred companies, including the number of successful assignments, the number of students assigned as per their second and third preferences, and the number of students who were unable to be assigned to their preferences and instead assigned according to the remaining capacity and point ranking. The performance of the model was calculated using equation 1 and was found to be 84.7%. The model was run with 100 replications. With this result, we can say that our model gives good results.

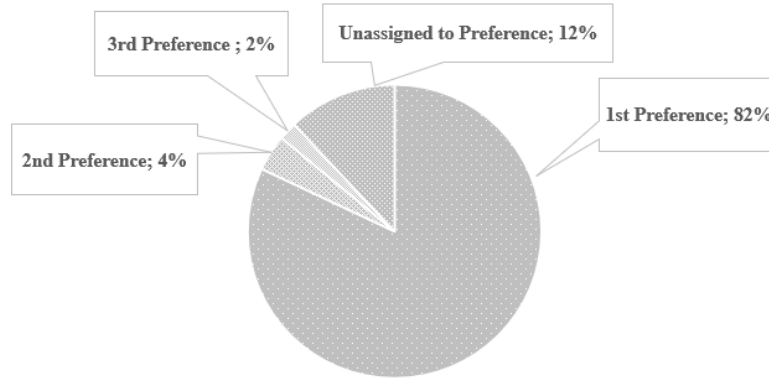


Figure 2. Distribution of assignments

Conclusion

This paper presents a simulation model for the student-company allocation problem where both students and companies have preferences. The main model is summarized as follows: Initially, priority is given to the students' preferences for companies. Each student has three fixed preferences. Once the students are grouped based on their first preference, they are further sorted according to their skills. Considering the companies' demands, the student with the highest aptitude score among those with the desired aptitude is assigned to the company. The primary aim at this stage is to maximize the number of students assigned to their first preference. The algorithm terminates when the companies' demand is fulfilled. For companies whose demand cannot be met in the first preferences, second preferences are taken into account and reassignments are made. Finally, if there are still unmatched students when third preferences are considered and company capacity is available, students are allocated to the company with the highest skill level regardless of their preferences. The results show that an effective solution can be produced by eliminating the matching uncertainty of both students and companies. Considering the performance output of 84.7% achieved through the simulation approach, it can be inferred that the mutual needs in student-company matching are largely addressed.

Recommendations

Research can be conducted on different universities that provide workplace training by taking into account the group ability average of students who go to companies.

Scientific Ethics Declaration

The authors declare that the scientific ethical and legal responsibility of this article published in EPSTEM journal belongs to the authors.

Acknowledgements or Notes

* This article was presented as an oral presentation at the International Conference on Technology (www.icontech.net) held in Antalya/Turkey on November 16-19, 2023.

References

- Agarwal, N., & Somaini, P. (2018). Demand analysis using strategic reports: An application to a school choice mechanism. *Econometrica*, 86(2), 391-444.
- Boyd, D., Lankford, H., Loeb, S., & Wyckoff, J. (2013). Analyzing the determinants of the matching of public school teachers to jobs: Disentangling the preferences of teachers and employers. *Journal of Labor Economics*, 31(1), 83-117.
- Choo, E., & Siow, A. (2006). Who marries whom and why. *Journal of Political Economy*, 114(1), 175-201.
- Chu, P., & Beasley, J. (1997). A genetic algorithm for the generalised assignment problem. *Computers & Operations Research*, 17-23.
- Cohen, R., Katzir, L., & Raz, D. (2006). An efficient approximation for the generalized assignment problem. *Information Processing Letters*, 162-166.
- Cavdur, F., Sebatli, A., & Kose Kucuk, M. (2019). A group-decision making and goal programming-based solution approach for the student-project team formation problem. *Journal of the Faculty of Engineering and Architecture of Gazi University*, 34(1), 505-521.
- Drigas, A., Kouremenos, S., Vrettos, S., Vrettaros, J., & Kouremenos, D. (2004). An expert system for job matching of the unemployed. 26(2), 217-224.
- Gale, D., & Shapley, L. (1962). College admissions and the stability of marriage. *The American Mathematical Monthly*, 69(1), 9-15.
- Kelso, A., & Crawford, V. (1982). Job matching, coalition formation, and gross substitutes. *Econometrica*, 1483-1504.
- Teo, Y., & Ho, D. (1998). A systematic approach to the implementation of final year project in an electrical engineering undergraduate course. *IEEE Transactions on Education*, 25-30.
- Tine, B., & Filip, L. (2011). Situational judgment tests as a new tool for dental student selection. *Journal of Dental Education*, 743-749.
- Wang, Z. J., & Li, K. (1993). Goal programming approaches to deriving interval weights based on interval fuzzy preference relations. *Information Sciences*, 180-198.

Author Information

Serdar Celik

OSTIM Technical University
Ankara, Turkey

Contact e-mail: serdar.celik@ostimteknik.edu.tr

Beste Alpaslan

OSTIM Technical University
Ankara, Turkey

To cite this article:

Celik, S. & Alpaslan, B. (2023). Student-company assignment: Simulation approach. *The Eurasia Proceedings of Science, Technology, Engineering & Mathematics (EPSTEM)*, 24, 184-189.

The Eurasia Proceedings of Science, Technology, Engineering & Mathematics (EPSTEM), 2023

Volume 24, Pages 190-195

IConTech 2023: International Conference on Technology

Smart Cart Application for E-Commerce Websites: A Case Study

Tahir Enes Adak

Casper Research and Development Center

Mehmet S. Aktas

Yıldız Technical University

Abstract: In the past few years, customers' buying habits have changed a lot because of e-commerce. E-commerce systems have a lot of benefits over traditional ways of selling things in stores because they can be changed to fit the wants and tastes of each user. Personalizing these experiences has the ability to make customers happier, which could increase sales and make platforms more successful. In sales of things like computers, users often put together a product based on its parts in a way that suits their personal tastes. To successfully plan inventory management, pricing strategies, and marketing efforts, it is very important to be able to correctly predict which product combinations will be the most popular. This position paper is focusing on how to build a decision support system software that can predict the likelihood of a buy for product baskets that are put together on the fly. The main goal of this decision support system software is to help e-commerce companies better understand what customers want and adjust their tactics to meet those needs. By designing, building and using this software, e-commerce companies can learn more about how their customers behave and increase their sales.

Keywords: E-commerce systems, Intelligent smart cart applications, Decision support system

Introduction

E-commerce sites are becoming more popular because technology is getting better and digitization is making things easier. But one thing that makes these sites successful is how the user experience is personalized and changes over time. When it comes to goods with multiple parts, like computers, offering the right combinations serves a double purpose: it makes customers happier and boosts sales.

E-commerce sites try to stay relevant in a market that is becoming more international and where competition is strong. Those sites that stand out from the crowd do so by giving their users a unique, personalized experience. By highlighting goods and services that match a user's tastes, personalization makes it more likely that they will buy. In particular, the likelihood of a sale goes up by a lot when a customer's wants and needs are taken into account when putting together a product basket. How well these personalized experiences work depends directly on how well the tools and methods used to make them work. When selling products with multiple parts, like computers, offering the right setup and adding it to an automatically created shopping cart has a big impact on customer happiness and sales data.

For e-commerce platforms to be more successful, they need decision support systems that can predict how likely it is that a customer will buy a product basket that is created on the fly. These systems help platforms boost their sales and give customers a more personalized and satisfying shopping experience. But for such a system to work well, it needs to use specific techniques and methods. This position paper is about the design and development of a decision support system for e-commerce platforms that can predict how likely it is that a customer will buy

a product basket that is produced on the fly. Also, a detailed explanation of the methods used, the technical problems that came up, and how they were solved is discussed in this position paper.

Motivation: Due to the changing nature of the business world today, it's important to have strategies and tools that can target specific clients. The lofty goal of this project is to create and build a decision support system that is just right for sellers. The most important job of this system is to guess whether a buyer will buy a product basket that is put together on the fly. We'll talk about what made us want to do this study below.

Complex Product Configurations: In computer goods, it is normal for dozens of different parts to be put together in a complicated way. Because of how complicated it is, it is possible to make thousands of different designs for sellers. So, it's clear and urgent that we need to come up with product sets that include the right combinations. Making the right mix is not just a matter of being able to do it, but also has big effects on sales success and partner happiness.

Highlighting Relevant Options: There are a lot of different ways to set up a computer, so it's important to find and highlight the ones that fit buyer tastes. One possible way to deal with this problem is to keep up with product design trends and carefully think about dealer needs. By taking these ideas into account, product baskets can be made in a moving way. But there is still a lot of uncertainty: after the product baskets are made, it's not clear if the sellers will like them and buy them.

Problems with Current Offerings: In the current way of doing business, it's common to approach sellers with product sets that are less likely to be bought. This way of doing things accidentally lowers the happiness of our dealer clients, which leads to a drop in sales. Such situations are not only missed chances, but they also hurt the brand's image and credibility in the eyes of key partners. In light of these problems, this project isn't just a technological effort; it's also a strategy move to fix structural errors, improve partner happiness, and increase sales potential.

Summary: To sum up, for e-commerce sites to do well in a competitive market, it's important to make the user experience unique and dynamic. This paper goes into great detail about how to build and use a decision support system that was made to meet this need.

Organization structure: This paper is put together in the following way: We start with the "Methodology" section, which explains in detail the methods and techniques used to figure out how likely it is that randomly produced product baskets will be bought. Here, we also discuss how this study is different from other research and what is new about it. The "Literature Review" section overviews the related literature. The "Expected Outputs and Benefits" section goes into detail about how this decision support system could help e-commerce sites and end users. Lastly, the "Conclusion and Future Work" section gives an overview of the study's results and talks about possible directions for future research. This style is meant to make it easy for readers to get around the study and focus on its most important parts.

Literature Survey

Wang et al. (2020) looked into how product recommendations on e-commerce sites change over time. Their study showed how suggestions are changing from being set and based on simple user choices to being dynamic and changing in real time based on how users browse and what they've bought in the past. Loukili et al. (2023) looked at how machine learning algorithms are becoming more and more important in predicting what people will buy. Their research showed how much prediction analytics can improve the customer experience and boost sales. Veres et al. (2023) looked into how clustering methods could be used to divide e-commerce markets into different groups. Their results showed that these kinds of systems are good at putting people into groups based on how they buy things, which lets marketers make more focused plans.

Punia et al. (2022) did a thorough study of how deep learning models, especially LSTM (Long Short-Term Memory) networks, can be used to predict sales. Their study showed that LSTM networks were better at predicting sales than standard time series models, especially in markets with a lot of different products, like computer sales. Almahmood et al. (2022) looked into the problems that e-commerce platforms have with putting together product carts on the fly. This job is hard because of things like real-time product changes, quickly changing customer tastes, and logistics. Chandra et al. (2022) looked into the direct link between personalized product suggestions and customer satisfaction. Their study showed that customers were more likely to buy and come back to platforms that suggested products that fit their needs. This shows how important personalized e-

commerce experiences are for businesses. Different web service-oriented architecture-based systems have been described that are made to solve problems in different fields (Aktas et al., 2005a, Aktas et al., 2005b, Aktas& Aydın, 2005a, Aktas& Aydın, 2005b). For example, Baloglu et al. (2010) looked into how web activity mining data is classified. The present project, on the other hand, finds its own area by focusing on a predictive system that figures out how well certain groups of products will sell. Some study has looked at how to structure datasets more effectively through data representation and embedding (Uygun et al., 2020; Olmezogullari & Aktas, 2022, Olmezogullari & Aktas, 2020). This project, on the other hand, uses transaction data to look at how people buy things. There have been some interesting studies (Sahinoglu et al., 2015; Kapdan et al., 2014) that look at how to judge the quality of software made during a project. However, this part of our project will arrive later. The current study also doesn't look at past user actions like other studies have (Tufek et al., 2018; Dundar et al., 2016; Baeth & Aktas, 2017). Instead, it plans to look at what users did in the past in a later study.

Methodology

The main goal of this study is to discuss how to create and implement a decision support system to meet the needs that have been listed in the introduction. This method is good at figuring out if sellers will buy a constantly put together basket of products. Here are some details about the tasks that will be done as part of the project:

Analysis, review of the literature, and project management tasks: Activities for the preliminary analysis include holding the first talks and making a list of the needs. Activities for Technical Analysis and Design: Figuring out what kind of technical equipment is needed based on the needs. After comparing the project's results to those of competitors, the right methods and techniques are chosen. Activities for the Literature Review: During the analysis and idea confirmation studies, academic advice from the university will be used to do a thorough analysis of the literature. Activities for project management include making project plans, holding weekly project meetings, and giving reports. After figuring out what the project needs, the planning part tries to come up with a plan for meeting these needs. The best method is one that is flexible at every stage of the job.

Software design Determination Activities: Getting ready for the project's software design. Setting up the technical infrastructure and environment: Platform Creation Activities: Tasks linked to software development, server requests, database connections, server connections, and figuring out what the technology and software development infrastructure needs are. Setting up the data architecture for the software that will be made: Putting in place the data infrastructure that is needed. Scripts are made to collect raw data from different sources that will be used to make the project result. Design Activities: Finish the general design and specific design of the program. User interface ideas are done. Activities in software development include making software modules, working on the front end, integrating modules, and checking modules at the unit level.

Activities for the Functional and User Acceptance Tests: Functional tests include making functional test cases, running the tests, reporting errors, fixing the mistakes, and re-testing. User Acceptance Tests include setting up situations, running the tests, reporting mistakes, fixing the problems, and re-testing. Live Transition Activities: Making user papers, getting ready for the transition, planning the return, and finishing the transfer.

Key Points for Project Research: Methodology for Dealer Segmentation: By looking at what Casper's dealer clients have bought in the past, it is possible to find goods that have already been bought. A product profile vector can be made for each product, and the goods a dealer bought can be used to make a dealer profile vector. For example, a dealer's profile vector could be found by averaging the profile vectors of the goods they have bought in the past. Using different grouping analysis methods, this project will focus on putting sellers into groups based on their character vectors. Metrics like the v-measure and the Silhouette Coefficient will be used to judge the results of the segmentation.

Modeling with machine learning and deep learning to predict product basket purchases: Labeled product basket vectors will be used with supervised machine learning algorithms to predict how people will buy things. Different methods will be used, such as Logistic Regression, Winnow Algorithm, and SVM. Deep learning methods that use LSTM will also be looked into.

Data Preprocessing for Product Basket Vectors: As product sales go up over time, the amount of product basket vectors will go up. High-performance data preparation methods for each dealer section will be worked on as part of the project.

Classic machine learning (ML) algorithms and deep learning (DL) algorithms will both be used as binary predictors for purchase behavior. Different measures, like F-Score and Accuracy, will be used to compare the results of the algorithms.

Expected Outputs and Benefits

The main thing that will come out of this study is software for a decision support system. This software is good at figuring out how likely it is that sellers will buy a constantly put together basket of products. Benefits expected: When the project is done, there will be a number of benefits, which can be put under different headings: Gains for the Company: Expertise in research and development: The research and development (R&D) efforts in this project will help our company learn a lot, especially about group analysis and machine learning/deep learning methods. Adding to our product line: As a result of this project, our company will have a decision support system software that can estimate the chance that a product basket will be bought, which will add to our current line of products.

Skill Improvement: The software that comes out of this project will give engineers in our country more information and experience that will help them become more skilled in this area.

Contribution to Global Academic Literature: The research and development work done for this project will be published at international conferences and in international papers. This will make a big contribution to the global academic literature in the field. From this study, a decision support system should be made that will help companies improve their sales tactics and make their customers happier. These improvements are expected to help the company make more money. This project will only work if the following conditions are met:

Probability to Buy Prediction: The system should be able to predict with at least 90% accuracy how likely it is that a product basket will be bought. Success in Dealer Segmentation: The accuracy of dealer segmentation should be at least 90%. Response Time of Software: The response time of the software should never be longer than 5 seconds.

Results and Future Work

With the introduction of dynamic product assembly and its following buy likelihood predictions, e-commerce has changed in a big way, especially in the computer sales market. The results of this study not only show that such a method is possible, but also show how it could change how businesses think about making sales strategies in a market that is becoming more digitalized. Methodological accuracy is one of the most important strengths of this study. By using both grouping techniques and machine learning or deep learning methods, the system has a detailed knowledge of how dealers act and what they like. This method makes sure that the product boxes are not just thrown together, but are carefully put together to meet the wants and preferences of the potential buyer.

Also, the measuring measures set for this project, such as a minimum forecast accuracy of 90% for the chance of buying a product basket and the success of dealer segmentation, along with the strict software response time, show how efficient and strong the system is. When these standards are met, it shows not only that the system is technically sound, but also that it has the ability to bring about real business results. But even though what we know now is hopeful, there is a lot more to find out. In future study projects, more can be done to improve the methods used. For example, more complex neural network designs or real-time data sets can be added to increase the dynamic nature of product basket forecasts. Also, the system's formulas can be updated periodically to keep up with changing market trends. This keeps the system accurate and up-to-date. The system's ability to grow and change is another area where more work could be done. Even though the focus has been on selling computers so far, the system's basic ideas could be used in other areas as well. With some small changes and adjustments, the system could be made to work with different e-commerce sites that sell different kinds of products. This kind of flexibility can help drive sales and improve customer happiness in many different industries.

In the end, this study has made it possible for e-commerce sales to be more data-driven, specialized, and efficient. Combining cutting-edge business methods with real-world business needs has led to a system that claims to have both academic and real-world effects.

Scientific Ethics Declaration

We declare that the ethical and legal scientific responsibility for this article published in the EPSTEM journal lies with the authors.

Acknowledgments or Notes

* This article was presented as an oral presentation at the International Conference on Technology (www.icontechno.net) conference held in Antalya/Turkey, 2023.

* We thank Caper R and D Center for providing the necessary datasets and computation facilities to help with this research.

References

- Aktas, M.S., & Aydın, G. (2005). Implementing geographical information system grid services to support computational geophysics in a service-oriented environment. *NASAEarth-Sun System Technology Conference*. Adelphi, Maryland.
- Aktas, M.S., Fox, G.C., & Pierce, M. (2005). An architecture for supporting information services for dynamically assembled semantic grids. *The First International Conference on Semantics Knowledge and Grid (SKG 2005)*. Beijing, China.
- Aktas, M.S., Fox, G.C., & Pierce, M. (2005). Information services for grid/web service-oriented architecture (soa) based geospatial applications, *The First International Conference on Semantics Knowledge and Grid (SKG 2005)*. Beijing, China.
- Aktas, M.S., Fox, G.C., & Pierce, M. (2005). Managing dynamic metadata as context, *The 2005 Istanbul International Computational Science and Engineering Conference (ICCSE2005)*, Istanbul, Turkey, 2005.
- Almahmood, R. J. K., & Tekerek, A. (2022). Issues and solutions in deep learning-enabled recommendation systems within the e-Commerce field. *Applied Sciences*, 12(21).
- Baeth, M. J., & Aktas, M. (2017). Detecting misinformation in social networks using provenance data. *13th International Conference on Semantics, Knowledge and Grids (SKG)* (pp.85-89). Beijing, China
- Baloglu, A., & Aktas, M. S. (2010). BlogMiner: Web blog mining application for classification of movie reviews. *2010 Fifth International Conference on Internet and Web Applications and Services*.
- Chandra, S., Verma, S., Lim, W. M., Kumar, S., & Donthu, N. (2022). Personalization in personalized marketing: Trends and ways forward. *Psychology & Marketing*, 39(8), 1529-1562.
- Dundar, B., Astekin, M., & Aktas, M. (2016). A big data processing framework for self-healing internet of things Applications. *12th International Conference on Semantics, Knowledge and Grids (SKG)* (pp.62-68). Beijing, China
- Kapdan, M., Aktas, M., & Yigit, M. (2014). On the structural code clone detection problem: A survey and software metric based approach. *Computational Science and Its Applications – ICCSA 2014, LNTCS*. Springer, Cham.
- Loukili, M., Messaoudi, F., & El Ghazi, M. (2023). Machine learning based recommender system for e-commerce. *IAES International Journal of Artificial Intelligence*, 12(4), 1803-1811.
- Olmezogullari, E., & Aktas, M. S. (2020). Representation of click-stream datasequences for learning user navigational behavior by using embeddings (3173-3179). *2020 IEEE International Conference on Big Data*.
- Olmezogullari, E., & Aktas, M. S. (2022). Pattern2vec: Representation of clickstream data sequences for learning user navigational behavior. *Concurrency and Computation: Practice and Experience* 34(9).
- Punia, S., & Shankar, S. (2022). Predictive analytics for demand forecasting: A deep learning-based decision support system. *Knowledge-Based Systems*, 258.
- Sahinoglu, M., Incki, K., & Aktas, M.S. (2015). Mobile application verification: A systematic mapping study. In *Computational Science and Its Applications ICCSA 2015* (p.11). Springer, Cham.
- Tufek, A. Gurbuz, A., Ekuklu, O. F. & Aktas, M. S.(2018). Provenance collection platform for the weather research and forecasting model, *2018 14th International Conference on Semantics, Knowledge and Grids* (pp. 17-24). Guangzhou, China.
- Uygun, Y., Oguz, R. F., Olmezogullari, E., & Aktas, M. S. (2020). On the large-scale graph data processing for user interface testing in Big Data Science projects. *2020 IEEE International Conference on Big Data* (pp. 2049-2056). Atlanta, GA, USA. IEEE

- Veres, O., Yu, M., Batiuk, T., Teslia, S., Shakhno, A., Kopach, T., ... & Pihulechko, I. (2022). Cluster analysis of exclamations and comments on e-commerce products. In *COLINS-2022: 6th International Conference on Computational Linguistics and Intelligent Systems* (pp. 12-13).
- Wang, K., Zhang, T., Xue, T., Lu, Y., & Na, S. G. (2020). E-commerce personalized recommendation analysis by deeply-learned clustering. *Journal of Visual Communication and Image Representation*, 71.

Author Information

Tahir Enes Adak

Casper Research and Development Center,

Istanbul, Turkey

Contact e-mail: tahirenes.adak@casper.com.tr

Mehmet S. Aktas

YTU

Istanbul, Turkey

To cite this article:

Adak, T. E., & Aktas, M. S. (2023). Smart cart application for e-commerce websites: A case study. *The Eurasia Proceedings of Science, Technology, Engineering & Mathematics (EPSTEM)*, 24, 190-195.

The Eurasia Proceedings of Science, Technology, Engineering & Mathematics (EPSTEM), 2023

Volume 24, Pages 196-203

IConTech 2023: International Conference on Technology

Torsional Fatigue and Static Torsion Strength and Test Validations of Composite Tube Hybrid Drive Shafts

Onur Ozbek
Tirsan Kardan A.S.

Serdar Kaan Hortooglu
Tirsan Kardan A.S.

Sedat Tarakci
Tirsan Kardan A.S.

Efe Isik
Tirsan Kardan A.S.

Abstract: Drive shafts are the transmission components which transfer power from power source to required location. The connection may be between steering wheel and rack & pinion mechanism or gearbox to differential. As in gearbox to differential connection, operational conditions are harsh and high loads are generated, steel materials are mainly preferred to be used. Though steels have such advantages in cost, performance and durability, it is heavier compared to other engineering materials. Since international regulations dictate to decrease the carbon emissions rates due to global concerns, weight decrement of automobile components plays an important role in solving such problem. Considering the operational requirements and boundary conditions, weight reduction in steel parts might be tough. For this reason, alternative materials must be deeply investigated and implemented into the traditional technologies. In the scope of this study, fatigue and torsional strength of propeller shaft with composite tube and aluminum subcomponents were investigated.

Keywords: Composite shaft, Drive shaft, Lightweight applications

Introduction

Steel and steel alloys are predominantly used in today's automotive industry since it provides many advantages in terms of its cost, strength, durability and manufacturability. However, in the recent years, lightweight applications gain popularity due to global concerns and electrification trend in automotive industry. Each reduction in the weight designates the efficiency of the vehicle which play an important role in competitive automotive market. Even 1 kg improvement in vehicle's weight leads to 20 kg less emission during the entire service life of vehicle (Hortooglu et al., 2023) so that common objective of manufacturers is to minimize the weight of each component without sacrificing performance, strength or other essential characteristics.

Ecological concerns have prompted the manufacturers to come up with more advanced design solutions. Aluminum, magnesium, titanium and many other materials present advanced characteristics and lighter weight opportunities compared with steel and steel alloys. However, many of them such as titanium is expensive and shows inefficient manufacturability. Magnesium is mainly utilized in unloaded location and some low loaded housing applications due to its low density. However, casting operation of magnesium housings is a challenging

- This is an Open Access article distributed under the terms of the Creative Commons Attribution-Noncommercial 4.0 Unported License, permitting all non-commercial use, distribution, and reproduction in any medium, provided the original work is properly cited.

- Selection and peer-review under responsibility of the Organizing Committee of the Conference

© 2023 Published by ISRES Publishing: www.isres.org

process due to high-flammability characteristics. Therefore, aluminum and composite have been leading the lightweight studies recently.

Literature

Comprehensive studies have been conducted for many years for the sake of lightweight constructions in automobile industry. Ozgen et al. (2019) studied on static torque transmission capability, torsional buckling and natural bending frequency optimization of propeller shafts composed of carbon epoxy and glass epoxy composite tube. Finite element analyses of composite tube were performed and validated by tests. Sun et al. (2019) conducted different analyses for embedded-in-flanges composite and glued tube for different ply angles. They revealed that bonding type does not affect the natural frequency. Ply angle and damper utilization played a neglectable role in natural frequency. Elanchezhian et al. (2018) compared the advantages and disadvantages of composite and steel tubes. Kim et al. (2004) studied the effects of foreign object impacts and damage characteristics of hybrid drive shaft. It was concluded that $\pm 10^\circ$ stacking angle with glass fabric insulation layer significantly decreased the damage area of the composite shaft. Bert and Kim (1994) investigated the buckling characteristics of hollow laminated composite drive shaft and offered a close form solution for buckling calculations. Qi et al. (2021) researched the effect of reinforced fibers on vibration characteristics of composite tubes. It is unveiled that increasing the elasticity modulus of the fibers enhanced the natural frequency of fiber-reinforced composite shafts.

In the scope of our study, static torsion and fatigue analysis of hybrid drive shafts were performed. Criteria and close form solutions for composite tubes were investigated and results were compared with each other. It is revealed that composite tubes are safe to be used for drive shaft applications.

Drive Shafts

Traditional drive shafts have been used for many years in automotive industry. All components of drive shaft subjected to torque are made of steel materials due to low cost and high-performance characteristic. With a different viewpoint to traditional driveshafts, a hybrid driveshaft which consists of aluminum (Al), steel (St) and composite components were utilized in. The weight of the drive shaft by means of lighter component utilization is achieved as %39 percent. A representative model of hybrid drive shaft is given in **Figure 1**.

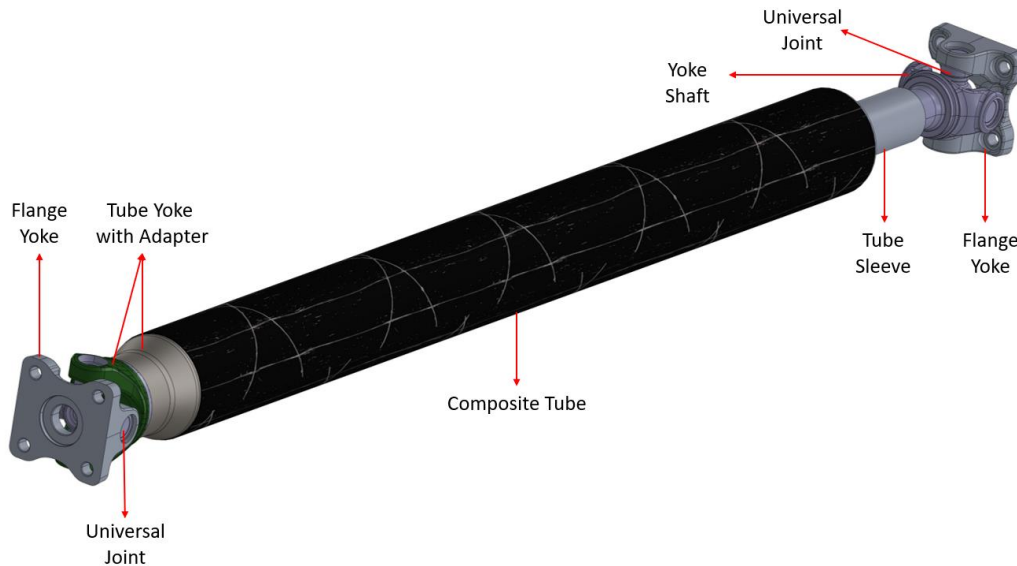


Figure 1. Hybrid drive shaft representative model

Method

Tube yoke-tube and tube sleeve-tube connection is performed by adhesive special to composite bonding application. Adhesive selection criteria, thickness, length, analysis and test result are given by Hortooglu et al.

(2023). Bonded components were designed and manufactured regarding aforementioned selection parameters for the required torque levels. Part designs were validated by FE analysis which can be seen in Figure 2.

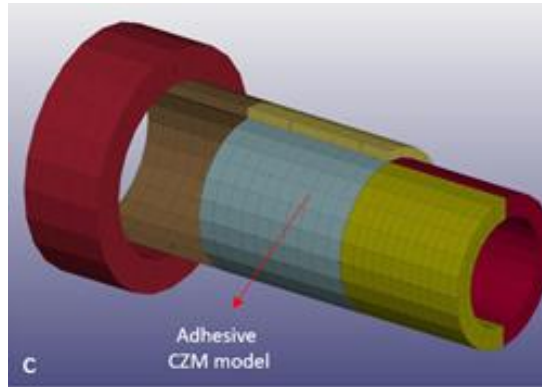


Figure 2. FE analysis of bonded components

Ozbek et al. (2022) develops a FE method in order to find out stress levels of aluminium flange yoke (Ozbek et al., 2022). Results of the study were validated by static torsional tests. Figure 3 shows the FE analysis of aluminum flange yoke.

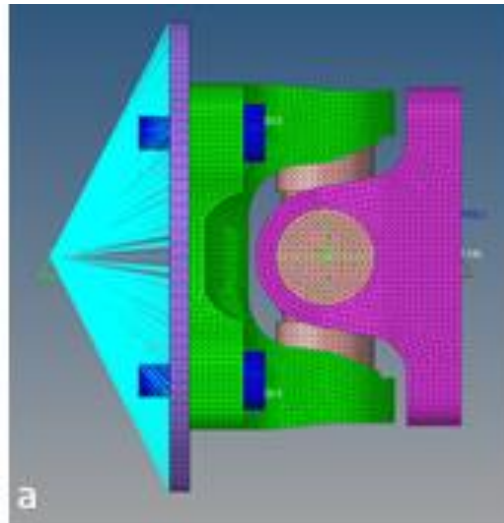


Figure 3. FE analysis of aluminum flange yoke

Composite tube dimensioning, stacking angle and stacking order are essential for the performance of the driveshaft. Parameters, formulas and test results were presented by Tarakcı et al. (2022) Composite tubes were procured and some tests were performed in order to validate composite tube design criteria which can be seen in Figure 4.

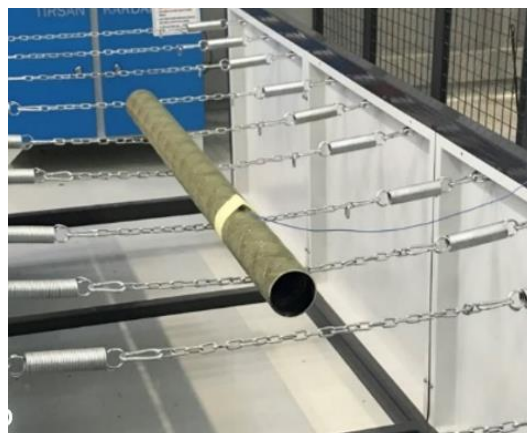


Figure 4. Natural frequency test of composite tube

Universal joint, tube yoke and yoke shaft were chosen steel materials depending on various reasons. Tube yoke is manufactured by forging to increase compressive stresses thus, to increase material strength. However, it is hard to manufacture tube yoke with a long sleeve extension where composite tube and tube yoke are bonded. Therefore, forged tube yoke and a sleeve were welded together. Yoke shaft possesses a small diameter with a relatively sharp transition section by the end of the spline through yoke. To satisfy the high torque requirements, steel material was selected. Universal joint is the lightest component among others and therefore, it is a must to use a strong material. Considering its negligible effect in the total weight of driveshaft, steel material was preferred to be used. Comprehensive studies can be conducted for each component for the sake of decreasing the total weight of driveshaft. Only the composite tube fatigue and torsional strength were focused on that study.

Fatigue and Torsional Tests

Assembly of hybrid drive shafts is given in Figure 2. In order to comprehend the operational behavior of composite tube drive shaft, it must be subjected to various test conditions regarding to requirements of equivalent drive shafts. The requirements of drive shafts are given in Table 1.



Figure 2. Hybrid drive shaft

Table 1. Drive shaft requirements		
Test Condition	Torque Requirement (N.m)	Cycle Requirements
Torsional Fatigue Test	1200	400.000
Static Torsion Test	3500	1

Dimensions of composite tubes were investigated by considering the requirements as given in Table 1. 100mm inner diameter with 4mm thickness was selected accordingly. After assembly of subcomponents, 3 static and 3 fatigue tests were performed for hybrid drive shafts in Tirsan Kardan R&D center. Static torsion and torsional fatigue tests were conducted by fixing the fixed side of the propeller shafts and applying the torque on the opposite side. Sinusoidal torque in 2 Hz was applied for torsional fatigue tests.

Results and Discussion

Static torsional test results and failure points are presented between Figure 3 and Figure 5.

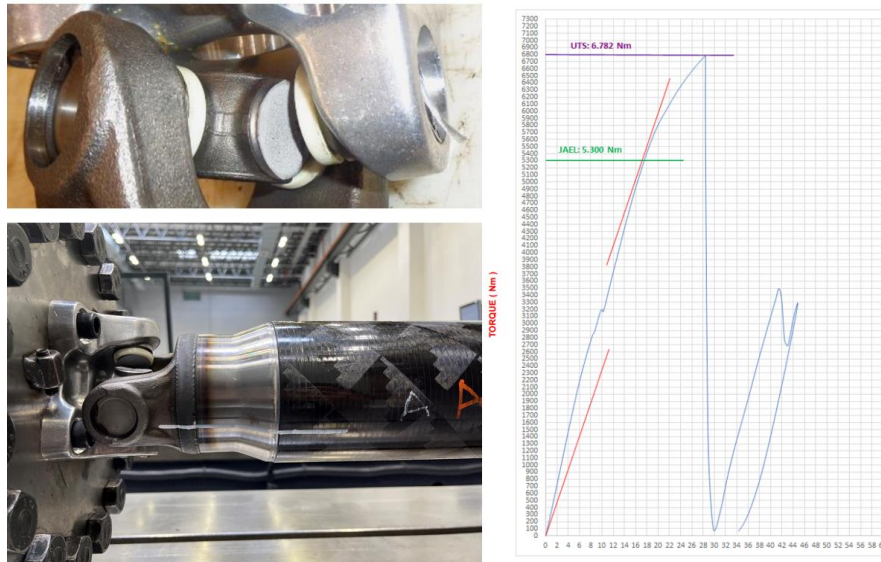


Figure 3. 1st Hybrit drive shaft static torsion test

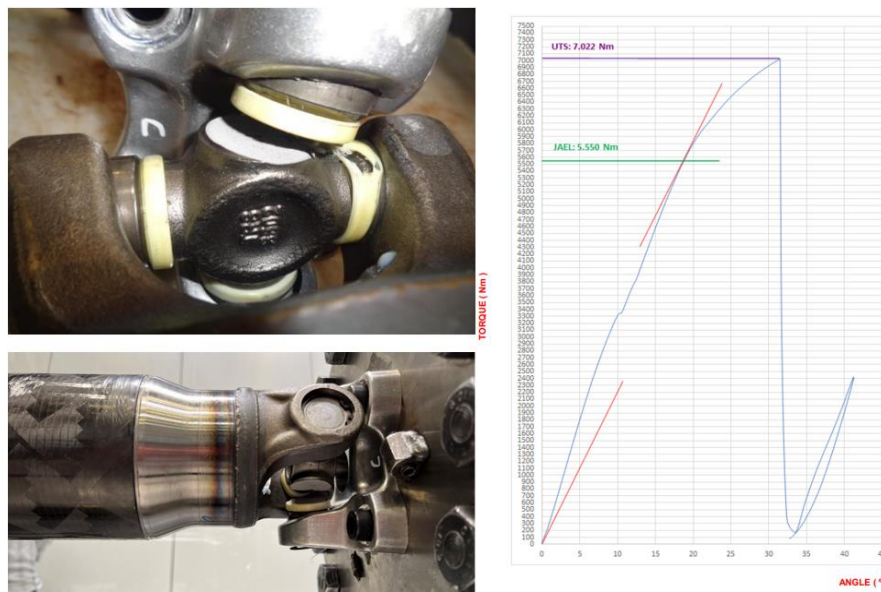


Figure 4. 2nd Hybrit drive shaft static torsion test

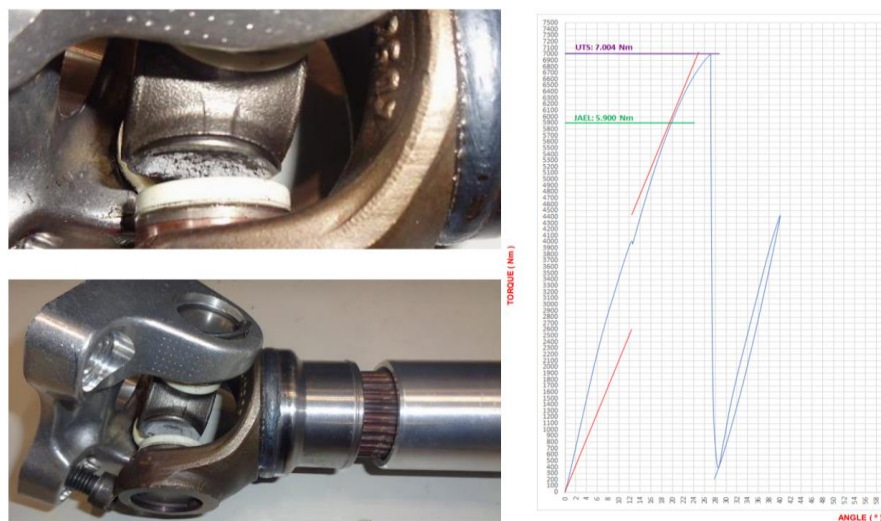


Figure 5. 3rd Hybrit drive shaft static torsion test

Johnson apparent elastic limit (JAEL) and ultimate tensile strength (UTS) for each hybrid drive shaft with respect to test results are given in Table 2.

Table 2. JAEL and UTS values		
Drive Shaft	JAEL	UTS
1 st Drive Shaft	5300	6782
2 nd Drive Shaft	5550	7022
3 rd Drive Shaft	5900	7004

All the failures were occurred on universal joints as expected. Composite tubes were cut and any fiber rupture was not observed in the internal media. Static torsional tests fulfilled the requirements. 3 torsional fatigue tests were performed after satisfactory results in static torsion tests. Test results are shown between Figure 6 and Figure 8.

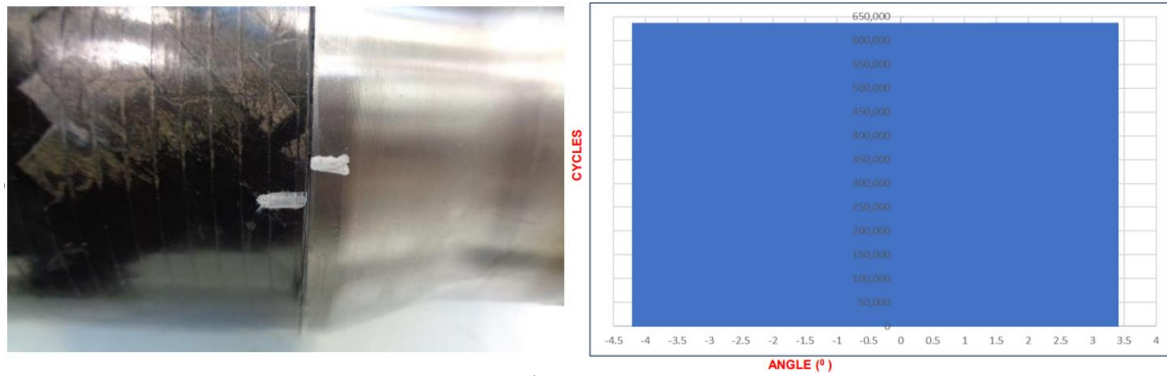


Figure 6 1st Torsional fatigue test

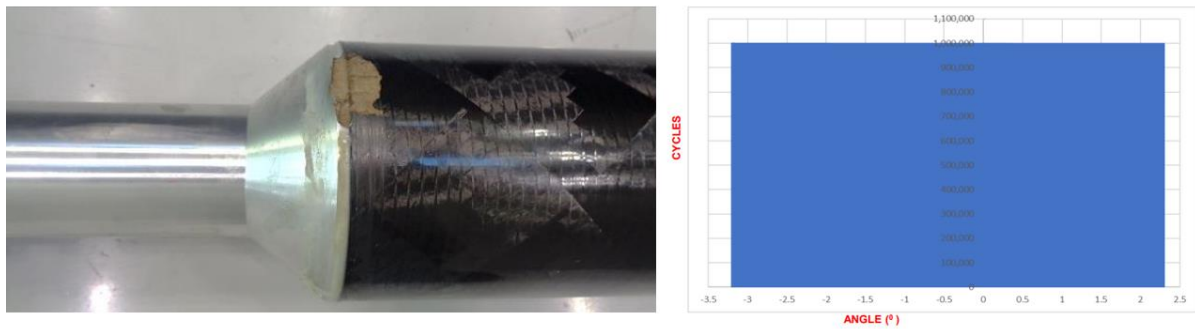


Figure 7 2nd Torsional fatigue test



Figure 8 3rd Torsional fatigue test

Table 3 Torsional fatigue test results		
Drive Shaft	Cycle	Failure Location
1 st Drive Shaft	635.441	Adhesive
2 nd Drive Shaft	1.000.000	Not failed
3 rd Drive Shaft	1.036.237	Aluminum TS

Hybrid drive shafts were not failed in composite tube, however shown different failure characteristics in various locations. The adhesive failure of drive shaft was observed in the first test. The test of second drive shaft was stopped after 1.000.000 cycle. Third drive shaft failed in the neck of aluminum tube sleeve. Both composite tubes and the entire drive shafts satisfied the criteria given in Table 1.

Conclusion

Hybrid drive shafts were subjected to torsional fatigue tests and static tests. All the driveshafts shown reliable results and satisfied the requirements of their equivalents. It is revealed that composite tubes can safely be utilized in transmission applications.

Recommendations

Although it is not presented in the scope of this study, the selection of composite tube must be carried out carefully. The stacking angle, natural frequency, number of carbon and fiber glass layers and order of carbon and fiber glass layers should be conducted with regard to intended application and requirements of the operation. All parameters mentioned play essential role in the characteristics and properties of composite tube.

Scientific Ethics Declaration

The authors declare that the scientific ethical and legal responsibility of this article published in EPSTEM journal belongs to the authors.

Acknowledgements or Notes

* This article was presented as an oral presentation at the International Conference on Technology (www.icontechno.net) held in Antalya/Turkey on November 16-19, 2023.

* We would like to thank to Tirsan Kardan R&D Center and Test Center for their support in conducting this study.

References

- Bert, C. W., & Kim, C. (1994). Analysis of buckling of hollow laminated composite drive shaft, composite science and technology. *Composite Science and Technology*, 53, 343-351.
- Elanchezhian, C., Ramnath, V. B., Raghavendra, K.N., Muralidharan, M., & Rekha, G. (2018). Design and comparison of the strength and efficiency of drive shaft made of steel and composite materials. *Materials Today*, 5(1), 1000-1007.
- Hortooglu, S. K., Ozbek, O., Tarakcı, S., & Isık, E. (2023). Verification of adhesive application in composite driveshafts by using finite element method. *CMES-2023*.
- Isık, E., Ozbek, O., & Tarakcı, S. (2022). A new aluminum design solution for traditionally forged steel flange yoke Used in drive shafts. *DEU International Symposium Series on Graduate Researches*.
- Kim, H. S., Kim, B. C., Lim, T. S., & Lee, D. G. (2004). Foreign objects impact damage characteristics of aluminum/composite hybrid drive shaft. *Composite Structures*, 66(1-4), 377-389.
- Ozgen, G. A., Yuceturk, K., Tanoglu, M., & Aktas, E. (2019). An investigation on hybrid composite drive shaft for automotive industry. *International Journal of Mechanical and Materials Engineering*, 13(4), 258-263.
- Qi, L., Li, C., Yu, X., Min, W., Shi, H., Tao, L., Wang, H., Yu, M., & Ni, Lei., & Sun, Z. (2021). Effect of reinforced fibers on the vibration characteristics of fibers reinforced composite shaft tubes with metal flanges. *Composite Structures*, 275(1).
- Sun, Z., Xiao, J., Yu, X., Tusiime, R., Gao, H., Min, W., Tao, L., Qi, L., & Zhang, H., Yu, M. (2019). Vibration characteristics of carbon-fiber reinforced composite drive shafts fabricated using filament winding technology. *Composite Structures*, 241, 111725.

Tarakcı, S., Hortooglu, S. K., & Isik. E. (2022), Kompozit Kardan mili borusu tasarım kriterlerinin belirlenmesi üzerine bir çalışma. *International Mediterranean Science and Engineering Congress*.

Author Information

Onur Ozbek

Tirsan Kardan A.S.
Kecilikoy O.S.B. Mah. Ahmet Nazif Zorlu Bulvari 4. Kisim
No:31, Manisa Organize Sanayi Bolgesi, 45300, Keçilikoy
Osbyunusemre/Manisa, Turkey
Contact e-mail: o.ozbek@tirsankardan.com.tr

Serdar Kaan Hortooglu

Tirsan Kardan A.S.
Kecilikoy O.S.B. Mah. Ahmet Nazif Zorlu Bulvari 4. Kisim
No:31, Manisa Organize Sanayi Bolgesi, 45300, Keçilikoy
Osbyunusemre/Manisa, Turkey

Sedat Tarakcı

Tirsan Kardan A.S.
Kecilikoy O.S.B. Mah. Ahmet Nazif Zorlu Bulvari 4. Kisim
No:31, Manisa Organize Sanayi Bolgesi, 45300, Kecilikoy
Osbyunusemre/Manisa, Turkey

Efe Isik

Tirsan Kardan A.S.
Kecilikoy O.S.B. Mah. Ahmet Nazif Zorlu Bulvari 4. Kisim
No:31, Manisa Organize Sanayi Bolgesi, 45300, Kecilikoy
Osbyunusemre/Manisa, Turkey

To cite this article:

Ozbek, O., Hortooglu, S. K. Tarakcı, S., & Isik, E. (2023). Torsional fatigue and static torsion strength and test validations of composite tube hybrid drive shafts. *The Eurasia Proceedings of Science, Technology, Engineering & Mathematics (EPSTEM)*, 24, 196-203.

The Eurasia Proceedings of Science, Technology, Engineering & Mathematics (EPSTEM), 2023

Volume 24, Pages 204-210

IConTech 2023: International Conference on Technology

Experimental Investigation on Thermal Properties of Al2024 Alloy by Friction Stir Welding

Lingaraju Dumpala

University College of Engineering Kakinada (A)
Jawaharlal Nehru Technological University Kakinada

Shaik Ghouse Mohiddin

Addl. CCE, DRDO

P. Vamsi Krishna

National Institute of Technology Warangal

U. Rajyalakshmi

Aditya Engineering College (A)

Abstract: Friction stir welding (FSW) connects the parts without melting the metal and produces a plasticized zone of metal. The main objective of this paper is to examine the temperature distribution that results from friction stir-lap welding of Al2024 alloy at varying rotating speeds and feed rates. Temperature distribution, heat flow, directional heat flux, thermal stresses, and strain energy are analyzed at different speeds of 700, 1000rpm, and at feed rate of 20 mm/min and 40 mm/min. Comparing the experimental temperatures with the simulated temperatures an error of 0.6% has been observed which is negligible. By comparing the numerical values of heat flux to the simulated values, the maximum error found to be 5.8% for the similar lap Al 2024-T3 joint. Temperature and heat flux values are gradually decreased from nugget zone to thermo-mechanical zone. But when compared to the nugget zone with the thermo-mechanical zone, the values of thermal stress and strain energy were abnormally altered.

Keywords: Friction stir welding, AL2024 alloy, Temperature distribution, Heat flux, Thermal stress and strain energy

Introduction

Friction stir welding (FSW) is a solid state joining process that uses a third body tool to joining two facing surfaces. Heat is to be generated between the tool and material which leads to a very soft region near the FSW tool. It then mechanically inter mixes the two pieces of metal at the place of the joint, and then the softened metal can be joined using mechanical pressure, much like joining clay or dough. It is primarily used on aluminium and most often on extruded aluminium, and on structures which need superior weld strength without a post weld heat treatment.

For dissimilar lap joints, the temperature changes from low to high and vice versa at the 1000 rpm rotational speed which is lower than the melting point of the materials. This is mainly due to the two kinds of materials with different specific heat capacity, viscosity and thermal conductivity, and the mutual influence between temperature and material properties (Teng & Shen, 2016; Meng et al., 2021). High heat generation and low thermal gradient were obtained at an increased value of tool rotational speed which produced coarser microstructure in the HAZ (Song et al., 2014; Mahto et al., 2021). The lap shear strength generally increases

- This is an Open Access article distributed under the terms of the Creative Commons Attribution-Noncommercial 4.0 Unported License, permitting all non-commercial use, distribution, and reproduction in any medium, provided the original work is properly cited.

- Selection and peer-review under responsibility of the Organizing Committee of the Conference

© 2023 Published by ISRES Publishing: www.isres.org

with increasing welding speed (Dumpala et al., 2017; Paidar et al., 2020). These parameters can change the mechanical properties at the heat affected zone to thermo mechanically zone is to be studied.

Experimental Procedure

Experimental Analysis



Figure 1. Friction stir welding machine

Figure 1 shows the Friction Stir Welding (FSW) machine holding two Al2024-T3 alloy work pieces of size 125mm x 60mm x 6mm are used to be welded, by placing one over another and are clamped on a rigid back plate. The fixture prevents the work pieces from spreading apart or lifting during welding process. The welding tool, consisting of a shank, shoulder and pin is then rotated to a specified speed and oriented normal with respect to the work piece. During horizontal movement of spindle i.e., along Z- axis, welding was carried out with feeds of 20 & 40 mm/min for 125 mm length. The welding was done for two different speeds 700 and 1000 rpm. The temperature measured on tool, at welding and some distance from welding with infrared thermometer during welding process.

Numerical Analysis

The 3-D conduction equation is taken into consideration to determine the overall heat transfer during the welding process of comparable plates because heat transfer occurs between the rotating tool and the workpieces. The 3-D conduction equation is given by:

$$Q = -KA \left(\frac{dt}{dx} + \frac{dt}{dy} + \frac{dt}{dz} \right) \quad \text{--- (1)}$$

Here,

Q = Heat Transfer in watts

K = Material's thermal conductivity = 121 W/m-K

A = Cross-sectional area = $15 \times 10^{-3} \text{ m}^2$

t = Temperature distribution along X, Y & Z coordinates

$$dt = T_i - T_f$$

T_i = Initial temperature; T_f = Final temperature

dx = Change in length along X-axis = $45 \times 10^{-3} \text{ m}$

Total heat flux,

$$q = \frac{Q}{A} \quad \text{--- (2)}$$

From the equations (1) and (2) we obtained the values as $Q = 24259.92 \text{ W}$ and $q = 2.156 \times 10^7 \text{ W/m}^2$ at a rotational speed of 700 rpm and feed of 70mm/min.

Modeling and Simulation Process

Transient thermal analysis was performed in the following two ways:

Geometry and Material Properties

Figure 2 shows the modeling of workpiece and tool geometry, which was done by selecting X-Y plane. A rectangle of size 45mm x 6mm was drawn by using sketching operation on drawing area and extruded to generate the rectangular plate to 125 mm length. Similarly, another rectangular plate is generated with the same dimensions. After modelling the workpieces and tool, Aluminium 2024-T3 alloy is assigned for workpiece (two plates) and H13 tool steel is assigned for tool.

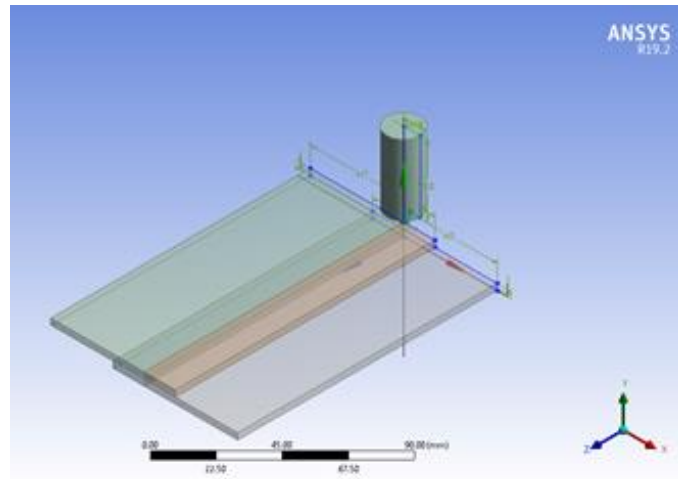


Figure 2. Creation of workpiece and tool geometry

Modeling and Solution

To update it, choose the mesh option and then choose fine size. Next, apply the generated temperature and initial temperature by clicking on Transient Thermal, and then click on Convection to apply the Film Coefficient to the surface.

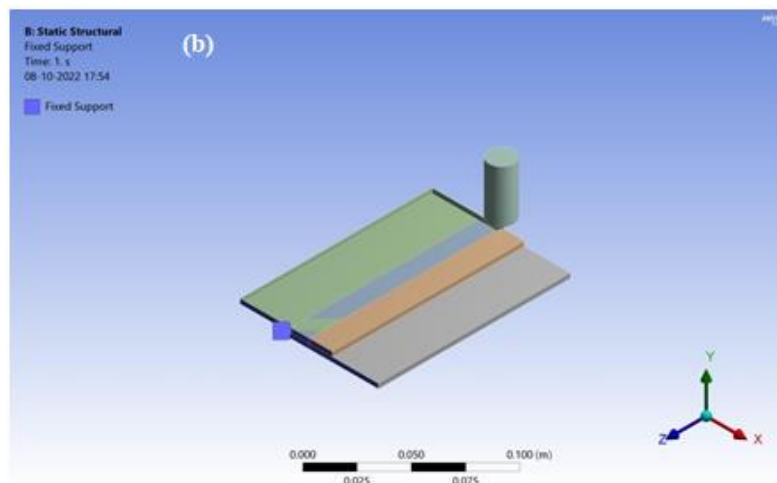


Figure 3. Boundary conditions applied to the developed model

Select temperature, heat flux, and directional heat flux in the solution phase before solving it. Select Static Structural once Transient Thermal is complete to connect the Model and Setup in Static Structural to the Geometry and Solution in Transient Thermal. To perform the static analysis, the rotational velocity of the tool was assigned and the boundary conditions were setup as shown in the Figure 3.

Results and Discussion

Experimentation Results

Table 1. Heat transfer at different spindle speeds for 2024-T3 similar lap joints

Spindle speed (rpm)	Feed Rate (mm/min)	Temp. ($^{\circ}\text{C}$)	Heat transfer (Watt)	Total Heat flux (W/m^2)
700	20	385	11524.62	1.283e7
700	40	396	14438.32	1.538e7
1000	20	408	15891.3	1.712e7
1000	40	436	16738.33	1.987e7

Similar plates made of Al2024-T3 are welded at spindle speeds of 700 and 1000 rpm with feed rates of 20 and 40 mm per minute. As stated in table 1, the maximum and minimum temperatures were determined. The temperatures and heat transmission through the material rise for similar joints as the rotating speed and feed rates increase. Additionally, as shown in table 1, the material's overall heat-flux increased.

Simulation Results

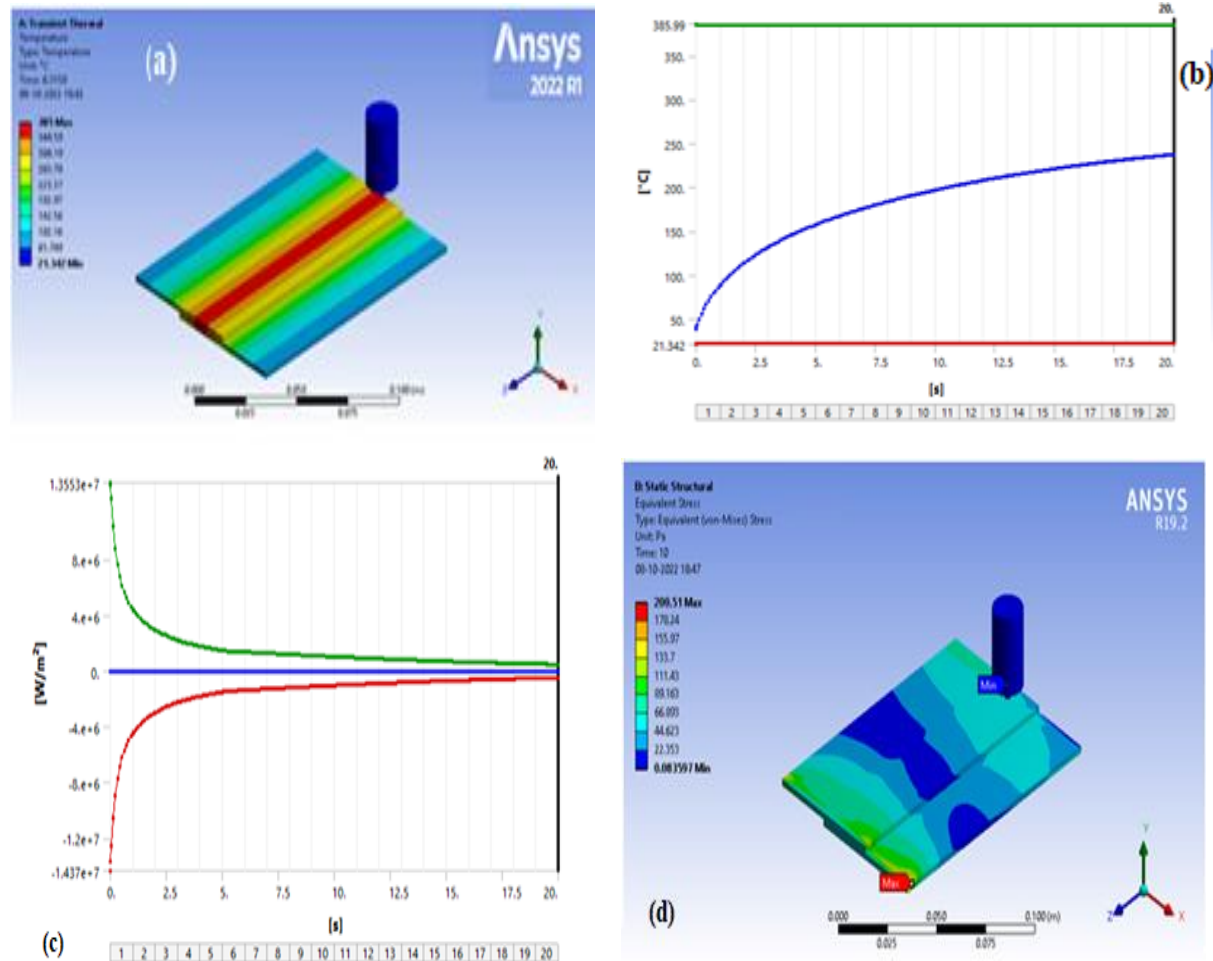


Figure 4. (a) Temperature distribution, (b) Graphical representation of maximum and minimum temperatures, (c) Graphical representation of directional heat flux, and (d) Thermal stress distributions.

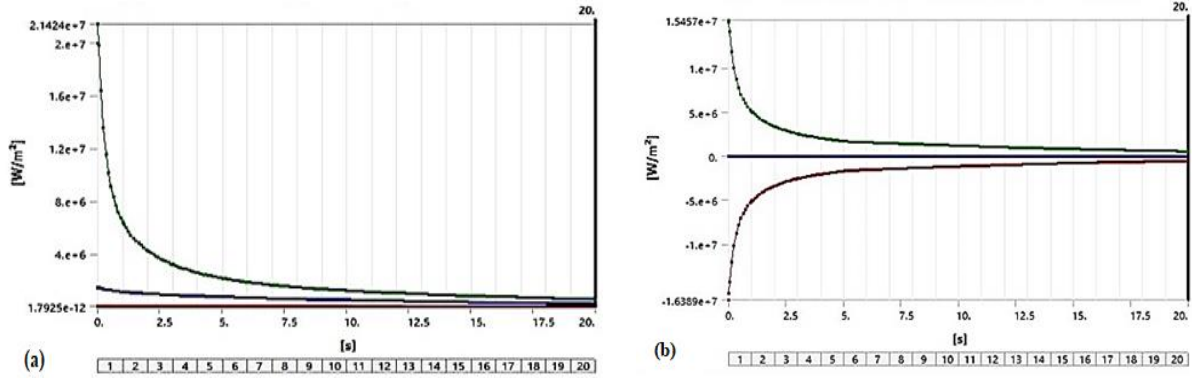


Figure 5. (a) Graphical representation of total heat flux, (b) Graphical representation of directional heat flux.

Figure 4 shows the results obtained for AA2024-T3 similar lap joint at spindle speed of 700 rpm and feed rate of 40 mm/min. The maximum temperature is 397.02°C and minimum temperature is 21.32°C whereas maximum directional heat flux is 1396.475 kW/m² and minimum directional heat flux is -1480.60 kW/m². Furthermore, maximum thermal stress is 577.34Pa and minimum thermal stress is 7.01 x 10⁻² Pa. It was observed that the temperature, heat flux, thermal stress and strain energy are found maximum in the nugget zone and are minimum at thermo-mechanical zone. Temperature and heat flux values are gradually decreased from nugget zone to thermo - mechanical zone. When compared to temperature and heat flux, the thermal stress and strain energy values are changing abnormally from the thermo-mechanical zone to the nugget zone.

Figure 5 shows the simulation results of AA2024-T3 similar lap joints at 1000 rpm rotational speed and feed rate of 40 mm/min. At spindle speed of 1000 rpm and feed rate of 40 mm/min, the maximum total heat flux of 2142.43kW/m² and minimum total heat flux of 1.79 x 10⁻¹² W/m², maximum directional heat flux of 1545.75kW/m² and minimum directional heat flux -1638.90 kW/m² are obtained. It was found that maximum heat flux is obtained at the nugget zone and minimum value is obtained at the thermo-mechanical zone. These values are gradually decreased from nugget zone to thermo- mechanical zone. Temperature and heat flux values are gradually decreased from nugget zone to thermo-mechanical zone.

Comparison of Temperatures between Experimentation and Simulation

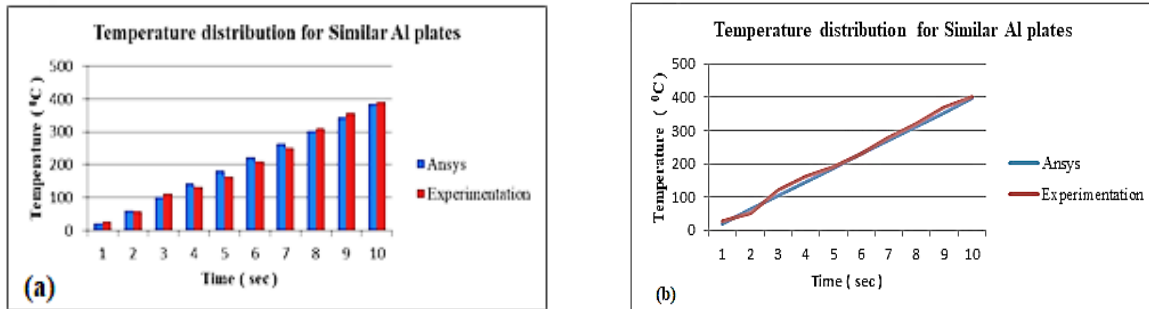


Figure 6: Comparison between the experimental and analytical values of temperature distribution (a) For spindle speed of 700 rpm with feed rate 20 mm/min, (b) For spindle speed of 700 rpm with feed rate 40 mm/min

From the figure 6, the error in temperature distribution between the experimental and analytical values is obtained as 0.25% for 2024-T3 similar lap joints. These results are well agreed with each other. From the above comparison graph it shows that the initial temperatures of all the weld joints are same but during the process the temperature will be increased.

Table 2. Percentage of error between the analytical and experimental values of heat flux

Heatflux (W/m ²)			
S.No	Analytical	Experimental	% Error
1.	1.87 x 10 ⁷	1.26 x 10 ⁷	5.5
2.	1.93 x 10 ⁷	1.58 x 10 ⁷	3.8
3.	1.99 x 10 ⁷	1.75 x 10 ⁷	2.6
4.	2.14 x 10 ⁷	1.93 x 10 ⁷	1.9

From the table 2, it shows that the maximum error found for the similar 2024-T3 series is 5.5% at a rotational speed of 700rpm with a feed rate of 20mm/min. At a rotational speed of 1000 rpm with feed rate 40mm/min, the minimum error for 2024-T3 is 1.9%.

Summary and Conclusions

The major goal of this work to investigate the temperature distribution, heat flow direction, thermal stress, and strain energy at the weld bead of similar AA2024-T3 plates welded by Friction Stir Welding technique. This material is particularly used in the fields of transportation, military, marine, and aerospace.

- With spindle speed of 700 rpm and feed rate of 20 mm/min and 40 mm/min, it was found that maximum temperatures are 385.9⁰C and 397.02⁰C respectively. Total heat flux is 18785 kW/m² and 19354 kW/m², directional heat flux is 13553 KW/m² and 13964 KW/m², thermal stress 200.51 Pa and 577.34 Pa, and strain energy 8.972 x 10⁻¹³J and 7.44 x 10⁻¹² J.
- With spindle speed of 1000 rpm and feed rate of 20 mm/min and 40 mm/min, it was found that maximum temperatures are 409.05⁰C and 436⁰C respectively, Total heat flux is 19970 kW/m² and 21424 kW/m², directional heat flux is 14412 kW/m² and 15450 kW/m², thermal stress is 200.51 Pa and 577.34 Pa, and Strain energy is 8.979 x 10⁻¹³J and 7.44x 10⁻¹² J.
- By comparing the numerical heatflux data to the simulated values, it can be seen that the maximum error for comparable lap 2024-T3 joints was 5.5%, while the smallest error was 1.9%. This demonstrates that the materials' high thermal conductivity is highly heat dissipated that provides superior weldability.

Scientific Ethics Declaration

The authors declare that the scientific ethical and legal responsibility of this article published in EPSTEM journal belongs to the authors.

Acknowledgements or Notes

* This article was presented as an oral presentation at the International Conference on Technology (www.icontechno.net) held in Antalya/Turkey on November 16-19, 2023.

* The authors gratefully acknowledge DST – INDIA, his assistance in the machining process. Additionally, the two of the authors are thankful to the DRDO for the support and encouragement.

References

- Dong, Z. Yang, K., Ren, R., Wang, G., Wang, L., & Lv, Z. (2019). Friction stir lap welding 0.8-mm-thick 2024 aluminum alloy with the assistance of stationary shoulder. *Journal of Materials Engineering and Performance*, 28(5-8).
- Dumpala, L., Chintada, L. M. K., Deepu, D., & Kumar Yadav, P. (2017). Study of mechanical properties of aluminium alloys on normal friction stir welding and underwater friction stir welding for structural applications. *International Journal of Mechanical and Mechatronics Engineering*, 11(7), 1344-1348.
- Mahto, R., Kumar, R., Pal, S. K., & Panda, S. (2018). A comprehensive study on force, temperature, mechanical properties and micro-structural characterizations in friction stir lap welding of dissimilar materials (AA6061-T6 & AISI304). *Journal of Manufacturing Processes*, 31, 624-639.
- Meng, X., Cao, B., Qiu, Y., Chen, H., Xie, Y., Wan, L., & Huang, Y. (2021). Equal-load-bearing joining of alclad AA2024-T4 alloy stringers and skins in aviation via friction stir lap welding. *Journal of Manufacturing Processes*, 68, 1295-1302.
- Paidar, M., Tahani, K., Ramalingam, V. V., Ojo, O. O., Ezatpour, H., & Moharami, A. (2020). Modified friction stir clinching of 2024-T3 to 6061-T6 aluminium alloy: Effect of dwell time and precipitation-hardening heat treatment. *Materials Science and Engineering A*, 791(3), 139734.
- Song, Y., Yang, X., Cui, L., Hou, X., Shen, Z., & Xu, Y. (2014). Defect features and mechanical properties of friction stir lap welded dissimilar AA2024-AA7075 aluminum alloy sheets. *Materials & Design*, 55(4), 9-18.

Tang, J., & Shen, Y. (2016). Numerical simulation and experimental investigation of friction stir lap welding between aluminium alloys AA2024 and AA7075. *Journal of Alloys and Compounds*, 666, 493-500.

Author Information

Lingaraju Dumpala

Department of Mechanical Engineering
University College of Engineering Kakinada (A)
Jawaharlal Nehru Technological University Kakinada
Kakinada, Andhra Pradesh, India

Shaik Ghouse Mohiddin

Addl. CCE, DRDO
Hyderabad, Telangana, India

P. Vamsi Krishna

Department of Mechanical Engineering
National Institute of Technology Warangal
Warangal, Telangana, India
Contact e-mail: vamsikrishna18@gmail.com

U. Rajyalakshmi

Aditya Engineering College (A)
Surampalem, India

To cite this article:

Dumpala, L., Mohiddin, S. G. Krishna, P. V., & Rajyalakshmi, U. (2023). Experimental investigation on thermal properties of Al2024 alloy by friction stir welding. *The Eurasia Proceedings of Science, Technology, Engineering & Mathematics (EPSTEM)*, 25, 204-210.

The Eurasia Proceedings of Science, Technology, Engineering & Mathematics (EPSTEM), 2023

Volume 24, Pages 211-218

IconTech 2023: International Conference on Technology

Quenching: An Improvement Factor of HSS Twist Drill Tool-Life When Machining C22 Steel

Nacer Mokas

Badji Mokhtar Annaba University

Sabiha Tekili

Badji Mokhtar Annaba University

Youcef Khadri

Badji Mokhtar Annaba University

Abstract: The present work is a contribution in understanding the effect of quenching and tempering of C22 steel on the tool life of twist high speed steel (HSS) grade drill bits. Experimental investigation has been conducted on annealed and tempered steel according to the planning methodology (L8). The input parameters are cutting regime elements (cutting speed, feed rate and drill diameter) and the output parameter is the tool wear related to tool life. Beyond, the common behavior that suggests that when the feed rate on tool life increases the tool life increases, the most interesting phenomenon is the controversial effect of the cutting speed when drilling the steel in tempered condition. The objective of this contribution then to in make in evidence the benefit effect of quench hardening on drill tool life through exploratory chip microstructure observations.

Keywords: HSS drill beet, Cutting speed, Machinability, Toole live, Hardening.

Introduction

In the machining industry, a great interest is given to tool life despite the high technological efforts that have been spent in developing the cutting systems. For instance, drilling which remains a complex operation represents almost 30% of the machining processes that needs much attention in order to increase the drill bit life and improve the surface quality of the produced hole.

During the last decade, there have been a large number of investigations in understanding the drilling machinability and the behavior of drilling tools and hole surface (Biermann et al., 2011; Desargues et al., 2013; Lin, 2002; Khashaba et al., 2010; Bryukhanova, 1978) according to factors controlling the drilling cutting conditions such as the cutting drill material, the geometry of the drill, the workpiece material, the cutting speed, the feed rate, the depth of cut, the lubricating conditions, the rise of temperature in the cutting zone and so on. Most of the investigations relied on tool wear behavior and surface roughness through experimental studies including different design experiment methods. Results are usually expressed in terms of wear behavior and surface roughness as a function of the cutting conditions. The interpretation of these results are difficult to follow and usually complex to adapt in real industrial applications. Moreover, some very interesting results such as the benefit effect of increasing the cutting speed on drilling machinability and on wear behavior of drill bits have been reported without convincing evidences.

In soft or annealed materials, the common observations reveal that when increasing the cutting speed, the drill bit tool life decreases (Okay et al., 2013; Kayhan & Budak, 2009). This is supported by the recent contribution of Kaplan et al. (2016) on the effects of process parameters on acceleration amplitude in the drilling of cold

- This is an Open Access article distributed under the terms of the Creative Commons Attribution-Noncommercial 4.0 Unported License, permitting all non-commercial use, distribution, and reproduction in any medium, provided the original work is properly cited.

- Selection and peer-review under responsibility of the Organizing Committee of the Conference

© 2023 Published by ISRES Publishing: www.isres.org

work tool steels. They have reported that when drilling annealed AISI D2 and AISI D3 steels with respective hardness of 20HRC and 28 HRC, increasing the cutting speed from 5 m/min to 15 m/min resulted in a decrease of tool life of 50% to 80% because tool wear increases up to cause the increase of the cutting forces, chatter, and vibration. SEM images of tool wear patterns when drilling AISI D3 steel at different cutting speeds and at a feed rate of 0.06 mm/rev, showed flank wear, chisel edge wear, outer corner wear, and BUE in the cutting tool that result excessive wear progression.

In hard-to-machine materials, there is a great deal in comprehending the effect of cutting speed on the drill bit life. Xu et al. (2016), have shown in hard-to-cut materials as 1Cr18Ni9Ti stainless steel and ZGMn13 high-manganese steel that the flank wear can be reduced by appropriately increasing the cutting speed from 9.4 m/min to 23.5 m/min. Balaji et al. (2016) have contributed in optimizing the cutting parameters, cutting speed, feed rate, and helix angle when drilling AISI304 steel with carbide drill bits using design experiments according to L8 Taguchi orthogonal array with two levels. However, they should have pointed out that when increasing the cutting speed from 600 rpm to 800 rpm, the values of roughness decreased slightly resulting in a slight improvement of the tool life. Meena and El Mansori (2013) have proposed to assess the dry drilling machining of austempered ductile iron for different cutting parameters using physical vapour deposition-coated carbide tools in terms of specific cutting forces, tool wear mechanisms, chip morphology and machined surface roughness. They reported that there is a tendency towards the reduction in roughness values when the cutting speed increased from 30 to 60 m/min. Meanwhile the chip analysis revealed the segmentation of chips at higher cutting speed and the back surface analysis revealed the chip sticking and fold-type patterns at higher cutting speed suggesting that this can be explained by the increase of temperature in the cutting zone during drilling operation. Abouridouane et al. (2017) have conducted experimental and simulative investigations on the machinability of ferritic-pearlitic steels with different microstructures using twist drilling to predict four aspects of machinability thermomechanical, feed force, cutting torque and chip forming. Three graded steels 27MnCr5, C45 and C60 have shown different machinability and the best machinability is observed for the C45 grade steel. Adem et al. (2012) have evaluated the performance of cryogenically treated M35 high speed steel (HSS) twist drills in drilling of two stainless steels AISI 304 and 316 with respectively a hardness of 70 and 79 HRB, in terms of thrust force, surface roughness, tool wear, tool life, and chip formation. They have shown that treated drills expressed better tool life than untreated ones. Meanwhile it is important to note that regarding to the applied cutting speed, in both conditions of untreated and treated drill, the drill bit tool life was better when the cutting speed was 16 m/min, than that obtained at a cutting speed of 10m/min, suggesting that increasing the cutting speed resulted in increasing the drill bit life. Wang et al. (2013) have investigated the influence of the geometric structure of coated cemented carbide twist drills and various cutting parameters on the drill tool life when drilling ultrahigh-strength hardened steel 42CrMo steel. When increasing the cutting speed from 80 m/s to 120 m/s, tool life decreased significantly in most drill bit geometry particularly at a feed rate of 0.14 mm/r; meanwhile when the feed rate increases to 0.18 mm/r the effect of cutting speed is greatly dependant on drill bit geometry. Zeilmann et al. (2012) have studied the Implications of the reduction of cutting fluid in drilling with carbide tools, AISI P20 steel hardened by heat treatment to obtain a final hardness of 36 to 39 HRC. They have reported that dry drilling presented better results comparing to those obtained by emulsion drilling tests. They have explained that the worst results for emulsion tests is attributed first to the presence of the cutting fluid that removed the positive effect of heat in the cutting zone, which facilitate the material shear and also to a high adhesion of material on the flank of the tools which led to microchipping and tool failure.

During the drilling process, a rapid plastic deformation of the workpiece and a friction along the drill-chip interface generates localized heat where temperature increases until sometimes reaching at the tool nose the fusion temperature at an instant time. The cutting temperature at the tool-chip interface is an important factor which directly affects workpiece surface integrity, tool wear, and hole diameter and cylindricity in the drilling process. However, the complex access to the cutting zone does not permit measurements of temperature. Meanwhile, temperature can be measured in regions close to the cutting zone. Bagci and Ozcelik (2006) have investigated the effects of sequential dry drilling operations on temperature changes in twist drill bit using two different workpiece materials, AISI 1040 steel and Al 7075-T651. Drill temperatures were measured by inserting standard thermocouples into the coolant and (oil) hole of TiN/TiAlN-coated carbide drills. They have reported that tool temperature increased with the number of drilled holes. Le Coz et al. (2017) have analyzed the local cutting edge geometry on temperature distribution and surface integrity when dry drilling of difficult to machine aeronautical alloys such as AA 7075 aluminum and Ti-6Al-4V titanium alloys. This has been achieved through experimental exploration of cutting temperature using a technique of dynamic thermocouple. They observed that the Temperature variation along the cutting edge depends on cutting speed, work material and local geometry and reported that temperature is much higher when drilling titanium Ti-6Al-4V than when drilling aluminum AA7075. Moreover, microstructural observations revealed that surface and subsurface are affected with grains elongation in cutting direction.

The present work is a contribution in improving steel drilling machinability and the drill bit lifetime through quench hardening of the workpiece. Drilling tests have been conducted on C 22 steel in annealed and tempered conditions using drill bits made of high speed steel (HSS). The input parameters are cutting regime elements (cutting speed, feed rate and drill diameter) and the output parameter is the tool wear related to tool life. Therefore, the objective of this contribution is to make in evidence of the benefit effect of quench hardening on drill tool life through exploratory chip microstructure observations.

Experimental Procedure

Workpiece Material and Preparation

C18 low carbon steel produced by the Algerian steel company of under the standard NF EN 10027-1 has been used. The chemical composition and mechanical properties are respectively given in Table 1 and Table 2.

Table 1. Chemical composition of C18 steel (NF EN 10027-1 standard) in weight %

Elements	C	Mn	Si	P	S	Cr	Mo	Ni	V	Cu
Composition	0.22	0.492	0.307	0.09	0.033	0.032	0.021	0.078	-	0.195

Table 2. Mechanical properties of C22 steel (NF EN 10027-1 standard)

Property	Hardness	Yield Strength	Tensile Strength	Strain
Unit	HRB	MPa	MPa	%
Mean value	67.8	210	590	10

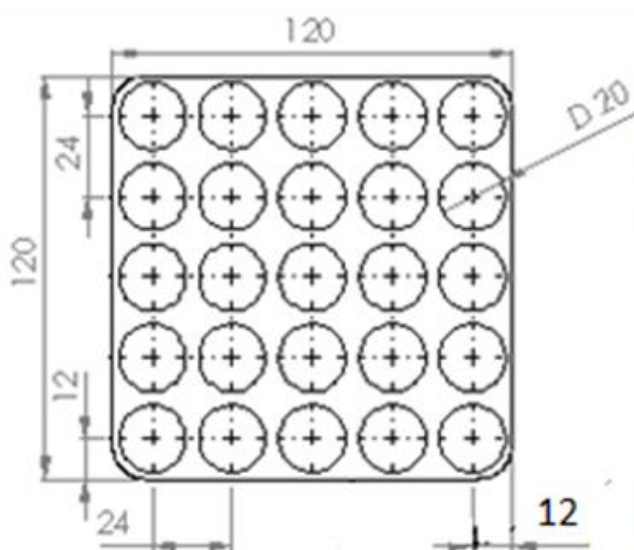


Figure 1. Specimen preparation hole repartition (25 holes for 20 mm diameter drill and 50 holes for 10 mm diameter drill) and photography of 20 mm hole blind drilling operation

Workpieces have been prepared from a square cross section parent bar of 120 x 120 mm² by cutting 60 mm length blanks on which intensive drilling operations will be carried out throughout the whole length. Figure 6 shows the cutting of the blanks and the repartition of the holes to be drilled on each blank.

Heat Treatment of the Blanks

Tool wear investigation has been conducted in two conditions: annealed and quenched states. The heat treatment has been achieved in a Nabertherm N 100 - N 2200/H furnace. Annealing has been conducted by heating the blanks at 900 °C for 1 hour and cooled them in the furnace. Austenisation of the blanks has been done at 850 °C for 35 min and water quench. Tempering at 240°C for 2 hours has followed the water quench. In addition, hardness tests have been carried out on a universal LEICA Wetzlar Vikers Indenter for both heat treatment conditions.

Results and Discussions

As expected the main observation is that when drilling annealed drill bits is generated rather than when drilling quenched and tempered workpiece. Regarding the cutting parameters, the best performance of wear resistance of twist drill bits giving a tool life T_{maxann} of 456 min, corresponded to the combination of $V_c = 11.15$ m/min, $f = 0.1$ mm/rev and $D = 20$ mm when the workpiece is annealed. In the quenched and tempered condition of the workpiece, the performance dropped to a tool life $T_{maxquen}$ of 331 for a cutting speed of 22.30 mm/min, a feed rate of 0.1 mm/rev and a drill diameter of 20 mm. The respective rate of the beneficial heat treatment effect and cutting conditions is 1.38. The wear curves followed the conventional trend showing an initial wear zone, a steady wear zone and accelerated wear zone. The worst performance is observed for $V_c = 22.30$ m/min; $f = 0.2$ mm/rev and $D = 10$ mm, where the trend of the wear curve accelerated drastically and fast from the beginning of the curve. Table 3 illustrates the effect of the cutting parameters and workpiece heat treatment on the twist drill bit lifetime. The rate of heat treatment effect suggests that for lower value of the cutting speed ($V_c = 11.15$ m/min) the rate between the values of tool lifetime according to the allowable value of wear VB equals to 0.5 mm is less than 100% and in the case of higher value of cutting speed ($V_c = 22.3$ m/min) the rate is higher than 100%.

Table 3. Effect of cutting parameters and blank heat treatment on twist drill bit lifetime

N° essais	C22 Steel Heat Treatment					
	Cutting parameters			Annealing	Quench & Temper	Heat treatment effect rate
	V_c m/min	f mm/rev	D mm	T_{05a} (mm)	T_{05Q} (mm)	T_{05a} / T_{05Q} (%)
1	11.15	0.10	10	420	168	40,0
2	22.30	0.10		218	272	124,8
3	11.15	0.20		160	43	26,9
4	22.30	0.20	20	18	118	655,6
5	11.15	0.10		456	185	40,6
6	22.30	0.10		235	331	140,9
7	11.15	0.20		178	63	35,4
8	22.30	0.20		46	153	332,6

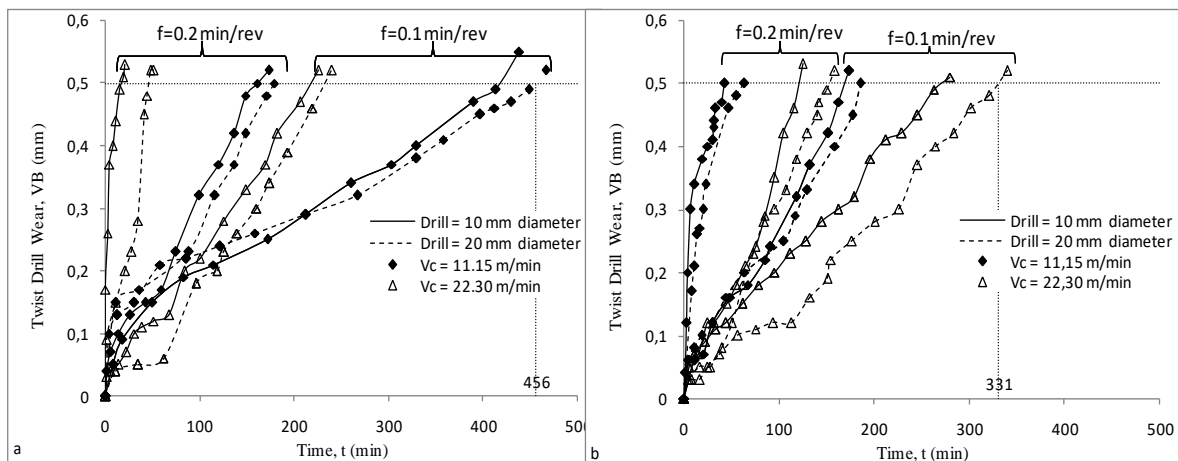
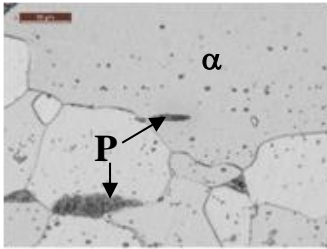
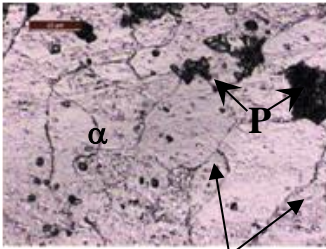
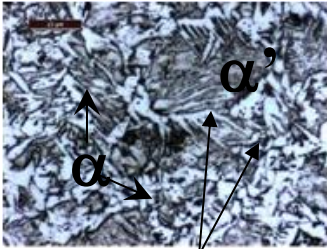
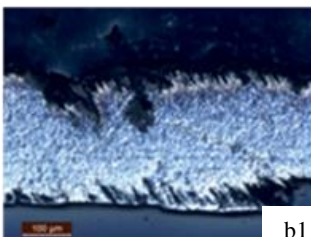
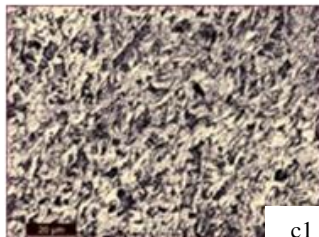
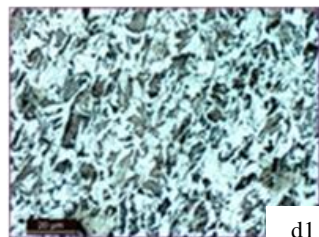

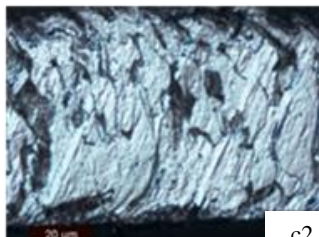
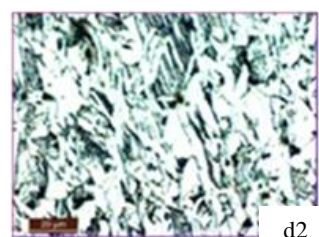
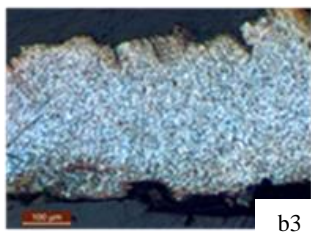
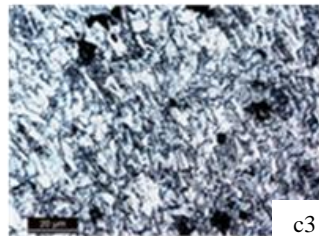
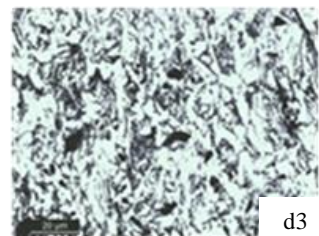
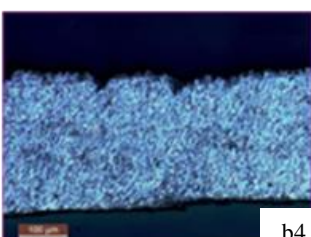
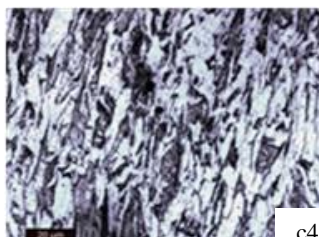
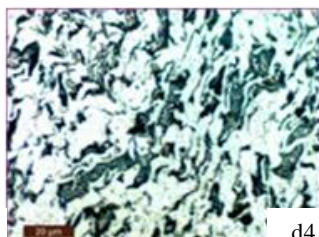


Figure 2. Evolution of flank wear in twist drill bits when drilling C22 steel:
a) annealed steel; b) quenched and tempered steel.

The most effective cutting parameter influencing flank wear is the feed rate. Effectively, in both heat treatment conditions, at lower value of feed rate of 0.1 mm/rev the tool lifetime is longer than that of 0.2 mm/rev. Then unexpected phenomena occurred when the heat treatment revealed that there has been a controversial effect of the cutting speed on twist drill resistance to flank wear between drilling annealed steel and drilling quenched and tempered steel. In fact, when drilling annealed steel, the common effect of cutting speed on tool wear is observed, Figure 2a: the lower the cutter speed the longer the lifetime of the twist drill bit. When drilling the quenched and tempered steel the effect of cutting speed is inversed, figure 2b: the higher the cutting speed, the longer the lifetime of the twist drill bit. The phenomena is observed for the 2 drill diameters as shown in Figure 4 suggesting the controversial effect of the cutting speed on flank wear in twist drill with respected to heat treatment condition of the workpiece.

Table 4. Effect of heat treatment of C22 steel blanks and twist drill cutting speed on chip microstructure

Heat Treatment					As Received	Annealed	Quenched & Tempered
a) Blank Microstructure (X600)							
					a ₁	a ₂	a ₃
Cutting Regime					b) Shape and Thickness of the chip (X120)	c) Chip Profile Microstructure (X600)	d) Chip Surface Microstructure (X600)
D							
f							
Vc							
Tool life							
Twist Drill Diameter, D=20 mm							
0.1 mm/rev							
11.15 mm/min							
					b1	c1	d1
22.30 mm/min							
					b2	c2	d2
11.15 mm/min							
					b3	c3	d3
22.30 mm/min							
					b4	c4	d4

Meanwhile, there should be stated that drilling with a twist drill bit of 20 mm has contributed slightly in improving the tool lifetime than drilling with a drill of 10 mm. In drilling operations, the diameter of the drill represents the cut of depth, so unlike the other machining processes where tool life decreases when depth of cut

increases, the effect of depth of cut is inversed. This is due to the rapid dissipation of heat from the cutting zone as larger diameters have more space to ensure good lubrication and chip evacuation.

As reported in the above literature review and in the present investigation, when machining hardened materials using high-speed steel twist drills, the increase of cutting speed could bring beneficial effect as the tool life increases, Figure 4b. Therefore, in order to explain the physical significance of this unusual behavior additional investigation throughout microstructure observations of the formed chips according to cutting speed has been conducted. table 4 shows exploratory microstructure observations on blank material and formed chips according to heat treatment condition of the blanks and the cutting parameters.

Optical microstructure observations of the blank in the conditions as received, annealed and then quenched and tempered, revealed the usual transformation of a carbon steel when ferrite and perlite (P) of soft C22 steel by annealing (tab 4.a2) changes into martensite and rediffusion of ferrite when C22 steel is hardened by austenising process at 850 °C during 30 min and water quenched, then tempered for 2 hours at 240°C. So the final structure is martensitic with well-defined grain boundaries (tab 4.a3). During twist drilling with HSS drill bit, the material removal causes changes in the original martensitic structure because of large amount of heat generated at the surface contact between the cutting tool and the workpiece. The removed chips have been subjected to microscopic observations that are discussed below.

The first apparent feature is that the thickness of the chip is affected by the feed rate and the cutting speed. Effectively, when drilling with the same drill bit diameter of 20 mm, as the feed rate increases from 0.1 mm/rev to 0.2 mm/rev, the chip thickness increased from a range 1.73 to 2.90 times depending on the cutting speed. Lower cutting speed ($V_c = 11.15$ m/min) resulted in higher irregular chip thickness for a given feed rate such as at 0.1 mm/rev, the chip thickness is 0.22 (Table 4.b1) and at 0.2 mm/rev the chip thickness is 0.38 mm (table 4.b3) (1.73 times higher). Higher cutting speed ($V_c = 22.30$) resulted in lower regular chip thickness of 0.11 mm (table 4.b2) when f is 0.1 mm/rev and 0.32 mm (table 4.b4) when f is 0.2 mm/rev.

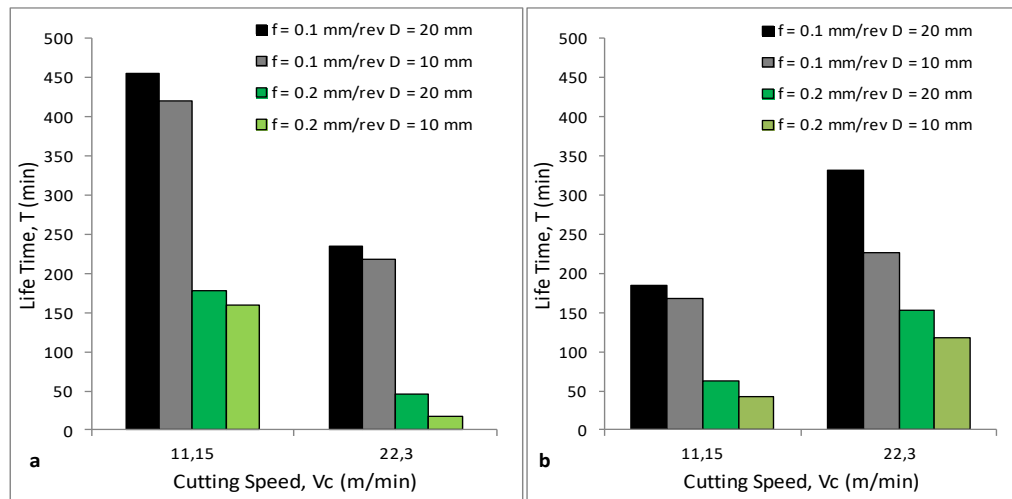


Figure 3. Effect of cutting speed on twist drill lifetime. a) When drilling annealed C18 steel. b) When drilling hardened C22 steel

The second feature is the change of microstructure due material removal as the drilling operation is complex. The original grain boundaries observed the microstructure of C22 steel after austenizing and quenched then tempering, table 4. a3 are no more apparent in the microstructure of the chips. table 4. c and d because, heat generated by the friction between the drill cutting nose and the surface blank is so high and could even reach the melting point instantly as the material is removed in the form of chip. Therefore, the initial repartition of grains the structural microstructure in the initially quenched and tempered, changes. However, at higher cutting speed $V_c = 22.30$ m/min, the grains elongate, revealing a tendency toward a return to a structure of an annealed material which means that the material softens. The phenomenon is well observed on the microstructure of the chip profile (table 4. c2 and c4). At lower cutting speed $V_c = 11.15$, the phenomenon is much more less important (table 4. c1 and c3) suggesting that the material still hard. Observing the chip surface, the microstructures obtained at $V_c = 11.15$ m/min (table 4. d1 and d3) are similar and approach the initial structure (table 4. a3) and at $V_c = 22.30$ m/min, the microstructures (table 4.d2 and d4) are also similar but move away from the initial microstructure suggesting that the steel microstructure is recrystallising. Hence, the increase of the tool life as the cutting speed increases is justified through microstructure observations.

Conclusion

The present work is a contribution in understanding the effect of quench hardening on machinability of C22 steel when executing drilling operations using twist HSS drill bit. Beyond, the common behavior suggesting that when the feed rate on tool life increases the tool life increases, the most interesting phenomenon is the controversial effect of the cutting speed when drilling the steel in tempered condition. Effectively, high cutting speeds generate large increase of temperature in the cutting zone permitting changes in microstructure. Chip microstructure observation revealed that the material is recrystallized as to get a consequent improvement in material machinability from 1.14 to 3.70. Moreover, more the thickness of the chip is small more the recrystallization is important. An engineering correlation between the thickness and tool life has been given in the form of third degree polynomial equation. At lower cutting speed, the phenomenon is not observed.

Scientific Ethics Declaration

The authors declare that the scientific ethical and legal responsibility of this article published in EPSTEM journal belongs to the authors.

Acknowledgements

* This article was presented as an oral presentation at the International Conference on Technology (www.icontechno.net) held in Antalya/Turkey on November 16-19, 2023.

*This work is achieved in the LRTAPM, Laboratory of advanced technology in mechanical engineering of badji Mokhtar-Annaba University, in collaboration with the LEM3, material mechanics and microstructure studies of the University of Lorraine, Metz, France. Financial support are due to the delegated ministry of scientific research (MDRS) of the Algerian ministry of higher education and scientific research (MESRS) under the CNEPRU research projet-LRTAPM: A11N01UN230120140056 (Annaba).

References

- Abouridouane, M., Klocke, F., & Dobbeler, B. (2017). Characterisation and modelling of the machinability of ferritic-pearlitic steels in drilling operations. *16th CIRP Conference on Modelling of Machining Operations*, 58, 79 – 84.
- Bagci, E., & Ozcelik, B. (2006). Analysis of temperature changes on the twist drill under different drilling conditions based on Taguchi method during dry drilling of Al 7075-T651. *International Journal of Advanced Manufacturing Technology*, 29, 629–636.
- Balajia, M., Murthy, B. S. N., & Mohan Rao, N. (2016). Optimization of cutting parameters in drilling of AISI 304 stainless steel using Taguchi and ANOVA. *Procedia Technology*, 25, 106 – 113.
- Biermann, D., Heilmann, M., & Kirschner, M. (2011). An analysis of the influence of tool geometry on surface integrity in single-lip deep hole drilling with small diameters. *First CIRP Conference on Surface Integrity (CSI)*, 19, 16 – 21.
- Bryukhanova, L. S., Miroshniehenko, U. M., Polukarova, Z. M., & Shehukin, E. D. (1978). Optimum conditions for using molten metals in cutting solids. Effect of molten-metal chemical composition and cutting tool material on drilling of steel 45. *Fiziko-Khimicheskaya Mekhanika Materialov*, 14(6), 14-18.
- Cicek, A., Kivak, T., Uygur, I., Ekici, E., & Turgut, Y. (2012). Performance of cryogenically treated M35 HSS drills in drilling of austenitic stainless steels. *International Journal of Advanced Manufacturing Technology*, 60(1-4), 65–73.
- Desargues, J. E., Lescallier, C., Bomont Arzur, A., & Bomont, O. (2013). High strength steel solutions for automotive parts: State of the art of machinability enhancement and further developments steel. *Proceedings of the Tenth International Conference on High Speed Machining - Progress in Productivity and Quality*. Germany.
- Kaplan, Y., Motorcu, A. R., Nalbant, M., & Okay, S. (2016). The effects of process parameters on acceleration amplitude in the drilling of cold work tool steels. *International Journal of Advanced Manufacturing Technology*, 80, 1387–1401.
- Kayhan, M., & Budak, E. (2009). An experimental investigation of chatter effects on tool life. *P I Mech Eng B- Journal of Engineering Manufacture*, 223(111), 1455–1463.

- Khashaba, U. A., El-Sonbaty, I. A., Selmy, A. I., & Megahed, A.A. (2010). Machinability analysis in drilling woven GFR/epoxy composites: Part II – effect of drill wear. *Composites: Part A, Applied Science and Manufacturing*, 41(9), 1130–1137.
- Le Coz, G., Jrad, M., Laheurte, P., & Dudzinski, D. (2017). Analysis of local cutting edge geometry on temperature distribution and surface integrity when dry drilling of aeronautical alloys. *International Journal of Advanced Manufacturing Technology*, 93, 2037-2044.
- Lin, T. R. (2002). Experimental design and performance analysis of TiN-coated carbide tool in face milling stainless steel. *Journal of Materials Processing Technology*, 127(1), 1-7.
- Meena, A., & El Mansori, M. (2013). Specific cutting force, tool wear and chip morphology characteristics during dry drilling of austempered ductile iron (ADI). *International Journal of Advanced Manufacturing Technology*, 69, 2833–2841.
- Okay, S., Kaplan, Y., Motorcu, A. R., & Nalbant, M. (2013). Evaluation of cutting tool wear characteristics and removed chip volumes in drilling of AISI D2 and AISI D3 cold work tool steels. *7th International Advanced Technologies Symposium (IATS'13)*, 7. Istanbul, Turkey.
- Wang, X., Huang, C., Bin Zou, B., Liu, H., & Wang, J. (2013). Effects of geometric structure of twist drill bits and cutting condition on tool life in drilling 42CrMo ultrahigh-strength steel. *International Journal of Advanced Manufacturing Technology*, 64, 41–47.
- Xu, L., Wu, Q., Qin, M., & Yong Tang, Y. (2016). Flank wear of twist drills and surface quality of holes in hard-to-cut materials by electric hot drilling. *The International Journal of Advanced Manufacturing Technology*, 84, 513–522.
- Zeilmann, R. P., Nicola, G. L., Vacaro, T., Teixeira, C. R., & Heiler, R. (2012). Implications of the reduction of cutting fluid in drilling AISI P20 steel with carbide tools. *International Journal of Advanced Manufacturing Technology*, 58, 431–441.

Author Information

Nacer Mokas

Badji Mokhtar Annaba University,
P.O. Box. 12, 23000, Algeria
Contact e-mail: nacer.mokas60@gmail.com

Sabiha Tekili

Badji Mokhtar Annaba University,
P.O. Box. 12, 23000, Algeria.

Youcef Khadri

Badji Mokhtar Annaba University,
P.O. Box. 12, 23000, Algeria

To cite this article:

Mokas, N., Tekili, S., & Khadri, Y. (2023). Quenching: An improvement factor of HSS twist drill tool-life when machining C22 steel. *The Eurasia Proceedings of Science, Technology, Engineering & Mathematics (EPSTEM)*, 24, 211-218.

The Eurasia Proceedings of Science, Technology, Engineering & Mathematics (EPSTEM), 2023

Volume 24, Pages 219-224

IConTech 2023: International Conference on Technology

The Effects of the Use of DRx Antenna Structure on the Rx Performance of Smartphones

Emirhan Aydin

Samsung Electronics Turkey

Ramiz Erdem Aykac

Samsung Electronics Turkey

Tekin Akpolat

Samsung Electronics Turkey

Abstract: Receiving the power emitted from the base station by smart phones and providing effective signaling is seen as a very critical problem. In order to eliminate this situation, some antenna technologies have been developed and started to be used in smart devices. The smart phones, which were developed by adhering to the DRx (Diversity Receive) design scheme, best perceived the signals emitted from the base station, thus increasing the Rx performance of the developed products. Typical integrated (total) surface metrics include Total Radiated Power (TRP) and Total Isotropic Sensitivity (TIS). TIS and TRP metrics have become increasingly important for carriers, because a TRP measurements used to verify your transmitter or transmitter antenna design. A TIS measurement used to verify how your receiver or receiver antenna design performs. In this study, we aimed to determine the Rx performance of the DRx scheme used in smartphones by using 3D radiation test setup (TIS - Total Isotropic Sensitivity).

Keywords: DRx (Diversity Receive) module, EIRP measurement, OTA test, Radiation efficiency for mobile phones, 3D TIS test for mobile.

Introduction

The radio performance of the mobile phone depends on its antenna and it needs to be tested both during the design and the production phases. Active antenna measurements are very meaningful for wireless devices/applications. A single point metrics include Effective Isotropic Radiated Power (EIRP) and Effective Isotropic Sensitivity (EIS). Based on this, Over The Air (OTA) measurements attempt to test system components closer to the environment in which they will be used. Typical integrated (total) surface metrics include Total Radiated Power (TRP) and Total Isotropic Sensitivity (TIS). TIS and TRP metrics have become increasingly important for carriers, because a TRP measurements lets you to verify your transmitter or transmitter antenna design. A TIS measurement lets you to verify how your receiver or receiver antenna design performs.

Diversity Receive (DRx) module combines switch, RF Filter and LNA (Low Noise Amplifier) in a single module in the RF Receiver. By amplifying received signal, DRx (Diversity Receive) module improves receiver sensitivity and data throughput while reducing receiver noise figure. Diversity receive modules were used for various applications such as antenna cable loss compensation circuit for LTE data antenna, 3G/4G/5G multimode cellular handsets and tablets etc. Specifically, diversity schemes enhance reliability by minimizing

- This is an Open Access article distributed under the terms of the Creative Commons Attribution-Noncommercial 4.0 Unported License, permitting all non-commercial use, distribution, and reproduction in any medium, provided the original work is properly cited.

- Selection and peer-review under responsibility of the Organizing Committee of the Conference

© 2023 Published by ISRES Publishing: www.isres.org

the channel fluctuations due to fading. To define TIS, the receiver sensitivity meaning should be defined, as it is a function of sensitivity (W. Xue, F. Li and X. Chen, 2021).

Sensitivity measurements in wireless communications seek to determine the cell phone's ability to receive low signals. The lowest power level that can be received by the handset while maintaining connection with the base station, the lower the TIS measurements, means the better sensitivity of the handset. Making these measurements is an iterative process which varies the base station (BS) output power at the phone while measuring the Bit-Error-Rate (BER) or the Frame Erasure Rate (FER), depending on the system (target is 2.0%). When a target BER/FER is achieved, the iteration is stopped and the output power at the phone is recorded as the sensitivity (i.e., the minimum power required to maintain a specified BER/FER).

Sensitivity can also have measured by lowering the BS Traffic Channel (TCH) power level until the specified digital error limit is exceeded (2.0%). The TCH power that was required to obtain the error limit is the sensitivity value. To do this, the BS is placed in loop-back mode. The BS transmits a bit pattern to the phone and the phone transmits it back. The returned bit pattern is then compared and the BER/FER is determined. As the output power from the BS to the phone is reduced, the BER/FER increases (>2.0%). Therefore, TIS is a figure of merit of overall radiated sensitivity of a wireless terminal. It is calculated as the integral of the measured Effective Isotropic Sensitivity (EIS) at every point at the intersection of a spherical grid.

Method

Coordinate System

The definition of TRP and TIS measurements are based on a spherical coordinate system. The spherical coordinate system describes any point in 3D space relative to the coordinate system origin with three spherical coordinates (r, θ, ϕ). A point on a sphere with radius r around the origin is described with (θ, ϕ) , with elevation $\theta \in (0^\circ, 180^\circ)$ and azimuth $\phi \in (0^\circ, 360^\circ)$. The equator is located at $\theta = 90^\circ$ elevation. For measurements, the DUT is located in the coordinate system origin and the measurement antenna is located in direction (θ, ϕ) relative to the DUT. As the path loss caused by the distance between DUT and measurement antenna must be calibrated for the test system, the radius r is not required (ITU-T, 2019).

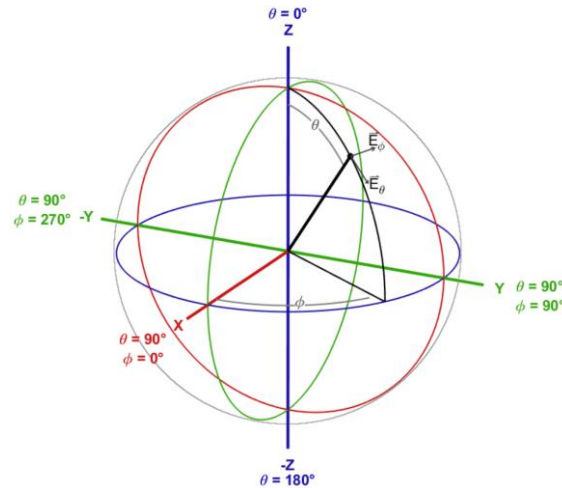


Figure 1. Spherical coordinate system

At each measurement point, two orthogonal components of the field are measured, defined as the theta polarization E_θ and phi polarization E_ϕ , pointing along the corresponding rotation vectors θ and ϕ , respectively. The theta polarization vector points along the positive direction of increasing theta values, and the phi polarization vector points along the positive direction of increasing phi values.

Transmitter Performance

The signal power as received by the measurement receiver test instrument is corrected by the corresponding signal path correction of the currently active signal path as determined during calibration. The resulting value is

the EIRP of the current polarization in the current measurement direction. To access the total radiated power of the DUT, the EIRP in all direction is spatially averaged:

$$TRP = \frac{1}{4\pi} \int_0^{2\pi} \int_0^{2\pi} EIRP(\theta, \phi) \cdot \sin(\theta) d\theta d\phi \quad (1)$$

As the EIRP is measured as vertical and horizontal component with a dual polarized probe antenna at sampled measurement locations, the TRP is approximated with:

$$TRP \approx \frac{\pi}{2NM} \sum_{n=0}^{N-1} \sum_{m=0}^{M-1} \left(EIRP_{\theta}(\theta_n, \phi_m) + EIRP_{\phi}(\theta_n, \phi_m) \right) \sin(\theta_n) \quad (2)$$

The measurement locations (θ_n, ϕ_m) are defined in a grid on a sphere around the DUT. The angular spacing of measurement points is chosen as a trade-off between measurement time and accuracy, while for low directivity antennas as used in typical UE for 2G, 3G, and 4G a low sampling of 15° is sufficient.

Receiver Performance

The measurement site is expected to be validated and calibrated. The signal received by the DUT shall be transmitted with a calibrated test instrument. To access the EIS of the receiver in a given direction, the transmitted signal is reduced in power until the error criteria (e.g., bit error ratio (BER) or frame error rate (FER) is above a defined threshold. The lowest signal power that still enables the receiver to be within the error criteria limits, corrected by the corresponding signal path correction of the currently active signal path, is the EIS of the receiver for the given direction and polarization (K. A. Remley, C. J. Wang, D. F. Williams, 2016). The total isotropic sensitivity (TIS) is the EIS spatially averaged over the whole sphere around the DUT:

$$TIS = \frac{4\pi}{\int_0^{2\pi} \int_0^{\pi} \left(\frac{1}{EIS_{\theta}(\theta, \phi)} + \frac{1}{EIS_{\phi}(\theta, \phi)} \right) \sin\theta d\theta d\phi} \quad (3)$$

For TIS determination, it is not sufficient to rely on the conducted sensitivity of the receiver combined with the radiation pattern of the used antenna, as signal strength and noise received by the antenna will vary and is influenced by the DUT itself. To determine the TIS from sampled measurement points, the TIS is approximated with:

$$TIS \approx \frac{2NM}{\pi \sum_{i=1}^{N-1} \sum_{j=0}^{M-1} \left(\frac{1}{EIS_{\theta}(\theta_i, \phi_j)} + \frac{1}{EIS_{\phi}(\theta_i, \phi_j)} \right) \sin(\theta_i)} \quad (4)$$

$EIS_{\theta}(\theta_i, \phi_j)$ and $EIS_{\phi}(\theta_i, \phi_j)$ are the determined effective isotropic sensitivity in the direction (θ_i, ϕ_j) in the theta and phi polarization. The measurement locations (θ_n, ϕ_m) are defined in a grid on a sphere around the DUT. The angular spacing of measurement points is chosen as a trade-off between measurement time and accuracy, while for low directivity antennas as used in typical UE for 2G, 3G, and 4G a low sampling of 15° is sufficient.

Measurement Frequencies

The radiation patterns of handset antennas can be expected to be frequency dependent. Achieved TRP and TRS values can vary over frequency and shall be measured in three channels in a frequency band (low, mid and high channel). The specified bands will be chosen to cover national or regional aspects. For any DUT, frequencies are selected based on the supported frequency bands of all supported wireless communication standards of the device and the admitted frequencies in the region the DUT is to be operated (W. Xue, F. Li and X. Chen, 2021).

OTA Testing with RTS65 Chamber

The RTS65 from Bluetest is a Reverberation Test Chamber for Bluetooth, WLAN, 2G, 3G, 4G LTE, mm-Wave, and the latest 5G NR standards. The chamber can be used for applications from 500 MHz to 40 GHz. It can be configured to support up to 16 antenna configurations up to 6 GHz and two mm-Wave antenna configurations at 40 GHz and 43 GHz. The 16 antennas configuration can for example support four LTE carriers with 4x4 MIMO in four different frequency bands. With its 40/43 GHz capability, the chamber is also usable for 5G NR and the combination of sub-6 GHz LTE carriers and sub-6 GHz or mmWave 5G NR carriers (Non-Standalone).



Figure 2. RTS65 3D chamber overview

As shown in Figure 2., RTS65 chamber consists of a shielded reverberation chamber with reflecting walls. The device to be tested is placed on a turntable. The reflective walls in combination with moving reflectors (mode stirrers), and the turntable, create a Rayleigh faded rich isotropic multipath environment (RIMP) inside the chamber. This environment is very well suited for antenna and radio performance evaluation of modern multi-antenna (MIMO) devices.

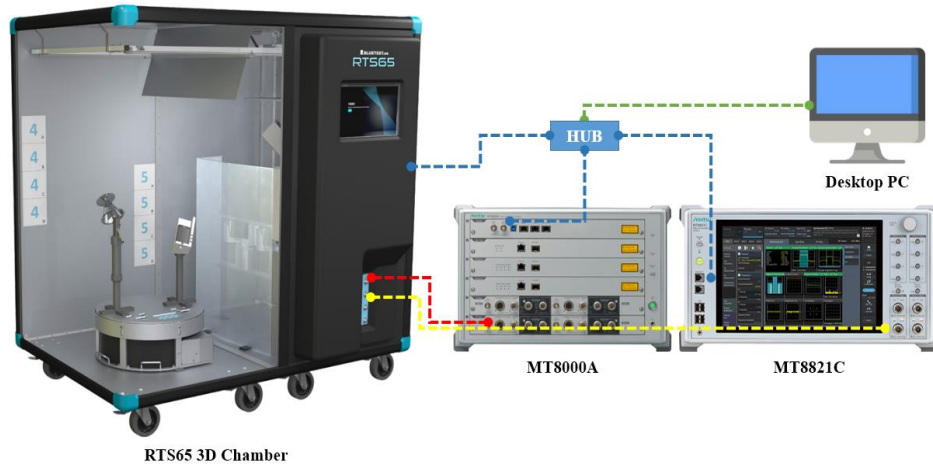


Figure 3. RTS65 3D chamber setup overview

The device is typically used for measuring Antenna Efficiency and MIMO/Diversity gain, Total Radiated Power (TRP), Total Isotropic Sensitivity (TIS) and Data Throughput vs received power. These measurements are done using a vector network analyzer or radio communication tester connected to one or several of the chamber measurement antennas. In our setup, we are using MT8821C and MT8000A equipment. A basic structure explained in (Figure 3). The connection between the equipment, chamber and Desktop PC provided over HUB.

TIS Test Method and Procedure

The DUT is placed in a free-space holder on a rotation table within the anechoic RF chamber and the communication between the DUT and the command module is established via over-the-air inside the chamber. The command module converts the commands of Test PC to control the DUT to the required test channel. To

determine the TIS the reference antenna in the RF chamber transmits at the DUT, and the TX power is lowered until the radiated sensitivity BER or PER limit reaches a given threshold. The DUT then rotates in increments of 30 degrees along the vertical axis. At each vertical position, the horizontal axis steps in increments of 30 degrees. The horizontal and vertical polarization are measured at each position. After all measurements are completed, the sensitivity is calculated at each measurement point and the TIS is automatically calculated. This process repeated for all test channels (Y. Feng and W.L. Schroeder, 2009). The test procedure as follows:

- DUT shall receive TX packets from a Signal Generator's output.
- Signal Generator transmits a standard conforming signal and packet.
- Measure free space effective isotropic sensitivity (EIS) pattern. Adjust the TX downlink signal level until the BER=0.04% threshold is reached. The downlink step size shall be no more than 0.5 dB when the downlink power is near sensitivity.
- Calculate using EIS pattern. For a complete sphere measured with N Theta intervals and M Phi intervals, both with even angular spacing, the Total Isotropic Sensitivity will be calculated an automated calculation tool.

Results and Discussion

We completed TIS test process for A54 5G model in our lab for LTE bands. In the scope of this test process, we tested B1, B5, B12, B20, B28 for FDD bands and B38, B40, B41 for TDD bands. Our test cases planned as standart set measurement and PRx antenna measurement. Standart SET means that all the antenna functions are activated (DRx & PRx antennas are enabled). Only PRx means that DRx antennas bloked for test purposes. Please note that before to check the Table.1.

Table 1 - TIS Measurement Results for both FDD/TDD Bands

Bands	B1	B5	B12	B20	B28	B38	B40	B41
Test Channel	300ch	252ch	5095ch	6300ch	9410ch	3800ch	39150ch	40620ch
Standart SetTIS(dBm)	99.39	93.03	95.78	93.25	92.29	93.03	94.19	94.08
Only PRx Set TIS(dBm)	95.81	88.00	89.74	88.92	86.40	89.44	90.90	90.22
Delta	3.58	5.03	6.04	4.33	5.89	3.59	3.29	3.86

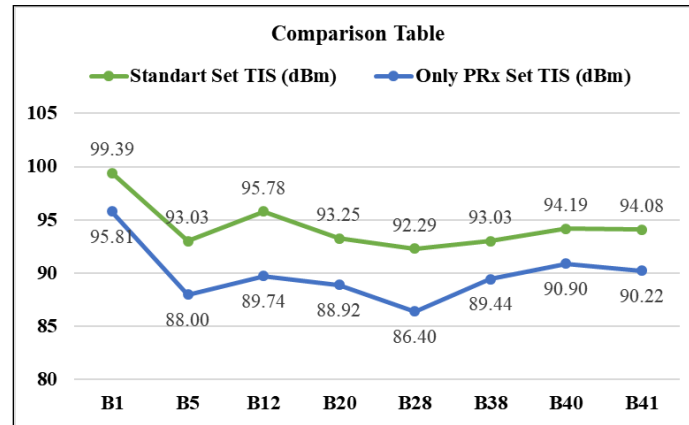


Figure 4. Comparison table for both FDD/TDD Bands

In Table-1, we can see the test bands, test channels, and test results. Please also note that especially there are 3 channels (low, mid and high channel) for each band, although we measured all the channels, only shared mid channel results to summarize the table. According to test results we measure in our Lab, there is 3.29 ~ 6.04 dBm difference between the standart set and only PRx set as shown in (Table.1). We also figured Delta for quick review as shown in (Figure 4). As we can see, standart set results better than only PRx set.

Conclusion

The use of the DRx antenna scheme in next-generation smartphones is a necessity, especially for 5G technology. When high frequencies are used in communication areas such as 4G and 5G technologies, the signals emitted from the base station radiate effectively over shorter distances. In addition to this, due to

environmental and geographical factors, there is a significant attenuation in the signals, which prevents effective communication between the base station and the users, and causes a significant decrease in data rates and signal strength. Therefore, we have to use next-generation antenna combinations to improve Rx performance in smartphones. As a result of this study, it has been observed that the use of the DRx antenna scheme in smartphones has a direct impact on the Rx performance of the smartphone.

Scientific Ethics Declaration

The authors declare that the scientific ethical and legal responsibility of this article published in EPSTEM journal belongs to the authors.

Acknowledgements or Notes

* This article was presented as an oral presentation at the International Conference on Technology (www.icontechno.net) held in Antalya/Turkey on November 16-19, 2023.

References

- Crawford, M. L., & Koepke, G. H. (1986). *Design, evaluation, and use of a reverberation chamber for performing electromagnetic susceptibility/vulnerability measurements*. NBS technical note 1092. NBS Publication. Retrieved from <https://nvlpubs.nist.gov/nistpubs/Legacy/TN/nbstechnicalnote1092.pdf>
- Feng, Y., & Schroeder, W. L. (2009). Extending the definition of TIS and TRP for application to MIMO OTA testing. *COST 2100 TD*, 866(9). Valencia, Spain.
- International Telecommunication Union. (2019). *Guideline for general test procedure and specification for measurements of the LTE, 3G/2G user equipment/mobile stations (UE/MS) for over-the-air performance testing*. TP-TEST-UE-MS.
- Remley, K. A., Wang, C. J., Williams, D. F., & Toorn, J. J. (2016). A significance test for reverberation-chamber measurement uncertainty in total radiated power of wireless devices. *IEEE Trans. Electromagnetic Compatibility*, 58(1), 207-219.
- Sanchez Heredia, J. D., Beltran-Alfageme, D., Valenzuela Valdes, J. F., Garcia-Fernandez, M. A., & Martinez Gonzalez, M. A. (2011). MIMO TIS/TRP active testing with second-generation mode-stirred chambers. *Espacio-Telecon*.
- Xu, Q., & Huang, Y. (2019). *Anechoic and reverberation chambers: Theory design and measurements*. UK: Wiley-IEEE.
- Xue, W., Li, F., & Chen, X. (2021). Effects of signal bandwidth on total isotropic sensitivity measurements in reverberation chamber. *IEEE Transactions on Instrum. Measurement*, 70, 1-8.

Author Information

Emirhan Aydın

Samsung Electronics Turkey
Cerkezkoy, Tekirdag
Contact e-mail: e.aydin@samsung.com

Ramiz Erdem Aykac

Samsung Electronics Turkey
Cerkezkoy, Tekirdag

Tekin Akpolat

Samsung Electronics Turkey
Cerkezkoy, Tekirdag

To cite this article:

Aydın, E., Aykac, R. E. & Akpolat, T. (2023). The effects of the use of DRx antenna structure on the Rx performance of smartphones. *The Eurasia Proceedings of Science, Technology, Engineering & Mathematics (EPSTEM)*, 24, 219-224.

The Eurasia Proceedings of Science, Technology, Engineering & Mathematics (EPSTEM), 2023

Volume 24, Pages 225-234

IconTech 2023: International Conference on Technology

Reduction of Shipping Greenhouse Emission by Alternative Fuels Used

Yordan Denev

Technical University of Varna

Abstract: The article examines, assesses, and analyses various types of fuels used in shipping, between the ports of Varna and Rotterdam. In order to determine the fuel that generates the least amount of carbon dioxide and is cost-effective, various types of traditional marine fuels and those that are yet to be introduced into operation have been considered. The advantages and disadvantages of bunkering, transporting, and storing various types of alternative marine fuels have been defined. The analysis shows that the lowest carbon dioxide emissions are generated when using alternative biofuels such as methanol and methane. Furthermore, if HVO fuel, which has not yet gained widespread use in shipping, is employed, emissions will be reduced by approximately 90%. From an economic perspective, methane and methanol have the lowest cost per ton of fuel compared to HVO, which is about four times higher in comparison to methane and methanol. Considering the IMO regulations for reducing harmful emissions into the atmosphere, HVO appears to be the future fuel that will normalize its prices.

Keywords: Greenhouse emission, Shipping, Alternative fuels, HVO

Introduction

According to the latest research and analyses as of 2021, greenhouse gases amount to approximately 55 billion tons on a global scale. The largest share is carbon dioxide, followed by methane and nitrous oxides (Hannah, 2020). The generation of greenhouse gases is associated with various industries and manufacturing sectors in countries worldwide. For example, in 2020, shipping generated around 700 million tons of carbon emissions. Considering the recommendations and requirements of the International Maritime Organization, measures must be taken to reduce greenhouse gas emissions from shipping by up to 40% by 2030 and up to 70% by 2050 (UNCTAD, 2022). Furthermore, the EU aims to establish a system for assessing and analysing CO₂ emissions from shipping in EU ports, which is set to come into effect in January 2024 (European Commission, 2018). This goal can be achieved through various measures aimed at improving the energy efficiency of existing ships, such as modernizing their hulls, retrofitting main engines, and utilizing alternative fuels, among others.

In recent years, the use of liquefied natural gas (LNG) as a fuel has become increasingly prevalent in shipping. Currently, it is predominantly used on existing vessels, accounting for around 40% of the global fleet as of January 2023. An analysis of the operational efficiency of LNG-powered ships was conducted in (Gonzales Gutierrez et al., 2023) with the aim of providing a clear assessment of the energy efficiency of these vessels and their compliance with modern environmental requirements.

Measures such as reducing ship speed, using liquefied natural gas, and retrofitting container carriers are presented in (Ammar, 2020). An assessment of the energy efficiency index after implementing these measures has been conducted, and it was found that the speed should be reduced by approximately 22% to significantly improve the energy efficiency index, resulting in annual fuel savings of around 23 million dollars.

The use of methanol as an additional ship fuel to comply with IMO regulations was conducted in Ammar (2019), meaning the ship operates with dual fuel systems. The analysis was performed on a container ship. To

- This is an Open Access article distributed under the terms of the Creative Commons Attribution-Noncommercial 4.0 Unported License, permitting all non-commercial use, distribution, and reproduction in any medium, provided the original work is properly cited.

- Selection and peer-review under responsibility of the Organizing Committee of the Conference

© 2023 Published by ISRES Publishing: www.isres.org

achieve significant reductions in generated gases, the ship's speed was also reduced. As a result, CO₂ emissions decreased by approximately 18%, leading to fuel cost savings. The cost-effectiveness of dual fuel for reducing NO_x, CO, and CO₂ emissions is \$385.2/ton, \$6548/ton, and \$39.9/ton, respectively.

A similar analysis with a reduction in the speed of a RO-RO ship was conducted in Ammar (2018). The results show that with a reduction in speed of approximately 40%, CO₂ emissions decrease by about 73%. Although the energy efficiency index improves after reducing the speed, in accordance with IMO requirements, it must be further reduced to meet those set to take effect in 2025.

The authors, Acomi & Cristian Acomib (2014), focus on the environmental protection within the maritime transportation sector. Their study revolves around the Energy Efficiency Operational Index (EEOI), designed to assist ship-owners in assessing and reducing emissions from ships in operation. The EEOI serves as a monitoring tool, measuring the mass of CO₂ emitted per unit of transport work. Using software developed by them, they analysed how the EEOI value varies for a specific vessel when different types of fuel are used during laden and ballast voyages over a three-month period, as recorded on board on ship. Their analyses aims to highlight the cost-effectiveness of the methods studied for minimizing air emissions.

With the aim of energy savings and consequently lower levels of generated gases, an attempt was made in OECD (2023) to implement a clean propulsion system for a 5000 t DWT bulk carrier. The authors have based this on a shaft generator using a dual-fuel engine, combining diesel and liquefied natural gas (LNG). By developing a simulation of the engine's RPM, it was determined that this system ensures satisfactory engine power and reduces CO₂ emissions.

Greenhouse Emissions Generated by Shipping

The greenhouse gases generated by shipping are primarily CO₂, nitrogen oxides, and sulphur oxides in different percentages, Figure.1. They are measured in tons of generated gas per ton of sea mile. The percentage share of CO₂ is the largest, which has an adverse impact on the environment and climate change. This provides a basis for seeking measures to reduce its proportion. Distribution of percentages from transport industries is shown on Figure 2.

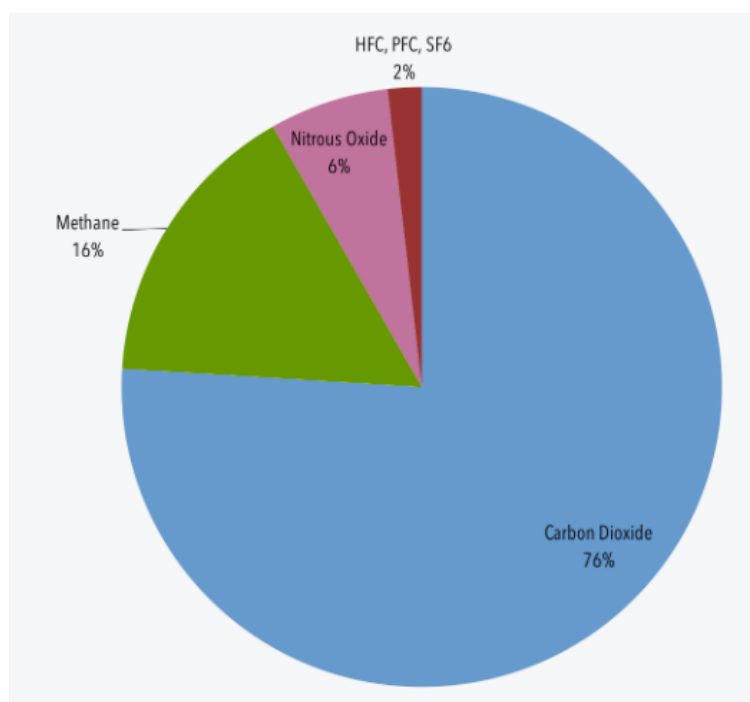


Figure 1. Percentage of GHG(CCES, 2023)

From the figure, it can be seen that the share of emissions generated by shipping, according to (EEA, 2019) is approximately 13%. This is comparable to aviation, where there are not as drastic measures to reduce harmful emissions

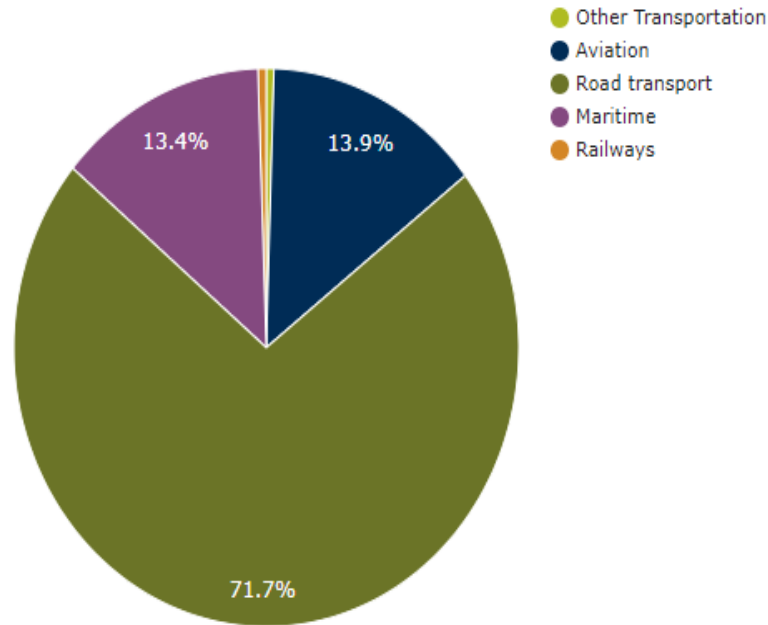


Figure 2. Distribution of emissions form transport industries (EEA, 2019)

In 2022, the generated CO2 emissions into the atmosphere amounted to approximately 860 million tons. When distributed by types of ships, the CO2 emissions are illustrated in Figure 3.

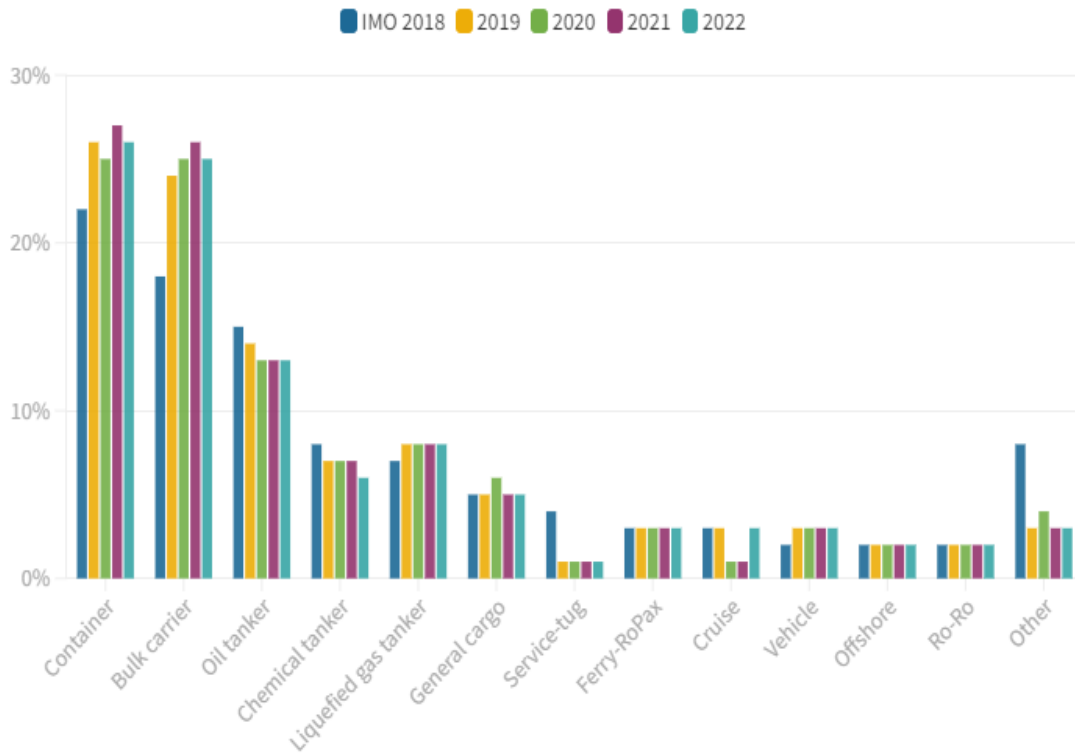


Figure 3. Distribution of CO2 emissions generated by ships (OECD, 2023)

Figure 3 presents the results of generated CO2 emissions from different types of ships for the period from 2018 to 2022. Container ships stand out prominently, ranking first in terms of the highest emissions generated. This is primarily due to their high speed compared to tankers or general cargo ships. During the period from 2020 to 2021, emissions generated by passenger ships were the lowest due to the COVID-19 pandemic. For ferries and RO-PAX ships, the emissions generated for the entire analysed period remained the same because these types of ships operate on the same route with a limited speed range.

Alternative Shipping Fuels

After IMO adopted the strategy for reducing greenhouse gases from shipping, many shipping companies have shifted their focus toward using alternative power sources (fuels) for their fleet of ships. In general, alternative power sources can be divided into two groups: renewable, fuels and combined, Figure 4.

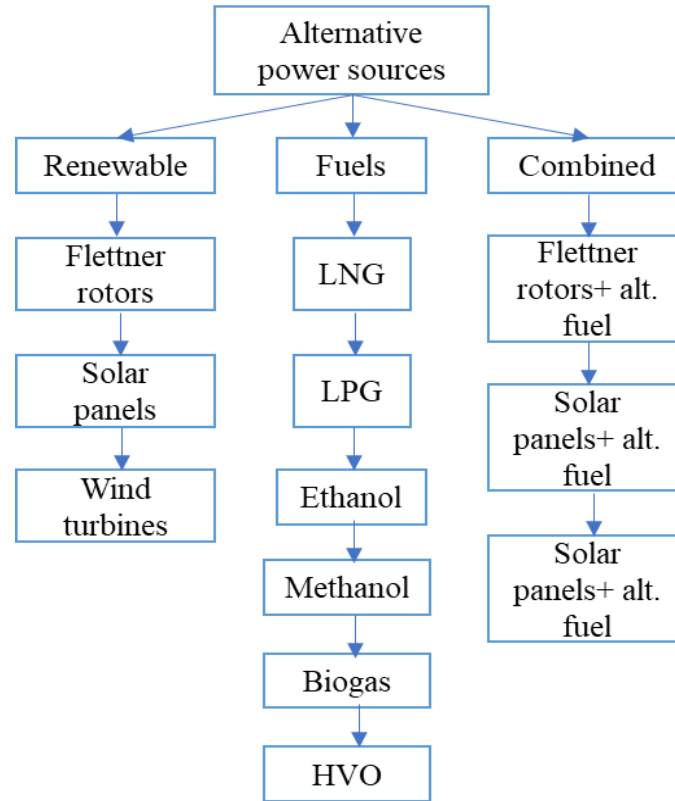


Figure 4. Classification of alternative power sources

Such alternative fuels include liquefied natural gas, liquefied biogas, hydrogen, methanol, ammonia, hydro-treated vegetable oil, renewable sources, and others. When using alternative fuels, some of them come with operational risks. For example, methane is stored at temperatures as low as -162 degrees Celsius, which can be harmful to the crew and impact the mechanical characteristics of the ship's structure. The use of liquefied gases significantly increases the risk of leaks and explosions on board the ship, which can lead to loss of human lives, cargo, and the entire vessel. In such cases, environmental pollution, especially in the sea, can be much more significant than emissions generated into the atmosphere. Properties of some alternative fuels are shown in Table 1 (Cheliotis, 2021).

Table 1. Properties of some alternative fuels

Type of fuel	Storage Pressure, bar	Liquified Storage Temperature , °C	Energy Density, MJ/kg	Volumetric Energy Density, GJ/m ³
Compressed hydrogen	700	20	120	4.7
Liquid ammonia	1 or 10	-34 or 20	18.6	12.7
Liquid hydrogen	1	-253	120	8.5
Ethanol	1	20	26.7	21.1
Methanol	1	20	19.9	15.8
Liquid methane	1	20	50	23.4

The easiest to store are ethane, methanol, and liquefied methane. This is one of the main reasons for their rapid adoption in practice. The applicability of various alternative fuels for different sailing zones varies. In (ETIP, 2023), such an analysis is presented, which to date has a different format, as shown in Table.2. The red colour means that the fuels are not so appropriate, while the blue one means that they are very appropriate.

Table 2. Applicability of alternative fuels in sailing area

Fuel	Inland	Short sea	Maritime
LPG			
LNG			
Biofuels			
CNG			
Hydrogen			
Electricity			

Liquefied natural gas and LPG are suitable for all sailing zones, whereas biofuels and hydrogen are not. CNG is also not suitable for all sailing zones, as there may not be storage opportunities everywhere. Another option is the use of biofuels. Their use can achieve a 100% reduction in CO₂ emissions. Unlike other alternative fuels, biofuels are easily transported and stored, and working with them does not require special skills.

They are three generations. First-generation biofuels are produced from food crops grown on arable soil. The sugar, starch, or oil contained is converted into biodiesel or ethanol. This is currently 99% of today's biofuels. Second-generation biofuels are made on the basis of lignocelluloses, wood biomass, agricultural residues, waste vegetable oil, and public waste. Third-generation biofuels are derived from microalgae cultivation; however, most efforts to produce fuel from algae have been abandoned (MAN, 2023).

Methodology Selection

The effect of using alternative fuels is studied by calculating the EEOI (Energy Efficiency Operational Indicator) for multi-purpose ships with a deadweight of 7,000 tons. A sailing route between the port of Varna, located in the Black Sea, and the port of Rotterdam, situated on the northwest coast of Europe, has been selected, Figure.5. Traveling along this route, the ship passes through the ecological zones of four regions: the Black Sea, the Mediterranean Sea, the Aegean Sea, and the Atlantic Ocean, Figure.6.



Figure 5. Ship route map between port of Varna and Port of Rotterdam

In addition, it is important to determine the quantity of harmful emissions generated by various alternative fuels as the ship passes through these regions. Considering that the ship's speed is not constant at every moment of the voyage, it is advisable to establish the energy efficiency index for different operational periods.

Alternative biofuels also require energy, which releases CO₂ emissions, and in some cases, such as biodiesel production via the Fischer-Tropsch method, the overall emissions are only slightly lower than conventional diesel.

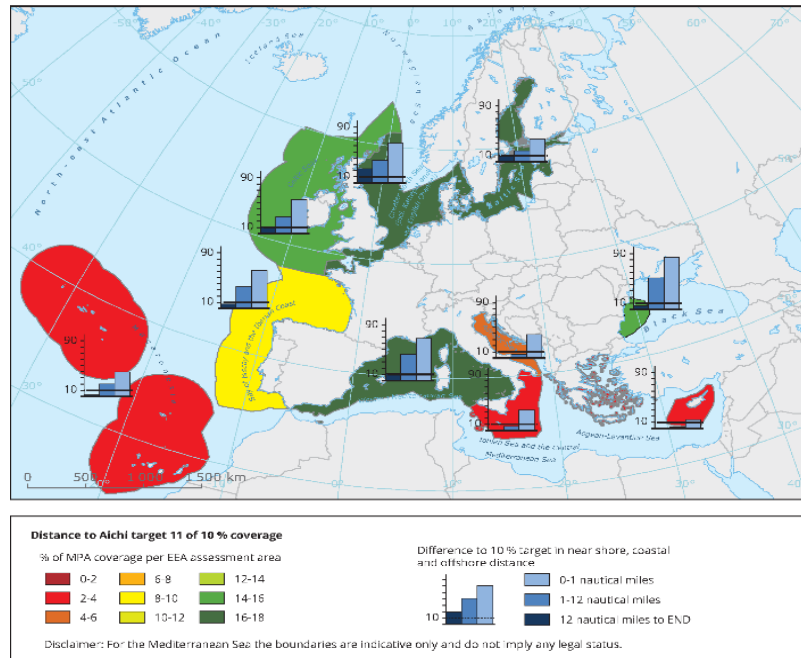


Figure 6. Marine protected areas in Mediterranean and Atlantic Ocean (EEA, 2021)

The calculation of the amount of CO₂ gases per burned ton of fuel is determined by the following formulae [Engineering Toolbox, 2023] and values are shown in Table.3:

$$q_{CO_2} = \frac{c_f * M_m}{h_f * M_{CO_2}} \quad (1)$$

Where: qCO₂- specific CO₂ emission, kgCO₂/kWh; c_f - specific carbon content in the fuel, kgC/kgfuel; h_f- specific energy content in the fuel, kWh/kgfuel; M_m- Molecular weight Carbon kg/kmol Carbon; MCO₂ - Molecular weight Carbon Dioxide, kg/kmol CO₂;

Table 3. Carbon content in different fuels (Engineering Toolbox, 2023)

Fuel Type	Carbon content, tCO ₂ /t fuel
LFO	3.15
Butane	3.03
Propane	3.00
Methan	2.75
Ethanol	1.91
Methanol	1.37

The generated CO₂ emissions from HVO (Hydrogenated Vegetable Oil) are 0.192 tons per 1000 liters of fuel, which is practically negligible when compared to the other fuels. Based on the ship's speed of 15 knots, under normal conditions, it would cover the distance between the two ports in approximately 11 days. Using the formula... the results are presented in Table.4.

$$s = V_s * T, \text{ nm} \quad (2)$$

Where: s- sailing distance, nm, V_s- ship speed, kn; T- time for sailing, days, weeks, months, year;

Table 4. Sailing nautical miles

Sailing times	Nm
Distance, nm	3940
Distance nm/day	358
Distance, nm/week	2507
Distance, nm/m	7880
Distance, nm/y	86680

By using the results from the table, an assessment of the generated CO₂ emissions into the atmosphere when using alternative and biofuels has been made.

Results

The assessment of the energy efficiency index is an important characteristic of existing ships, as it provides information about the suitable type of alternative fuel based on the operational characteristics of the ship. Using the data on sailing time in Table.4., an assessment of the EEOI (Energy Efficiency Operational Indicator) was made for potential use of alternative fuels. The results are presented in Figure 7.

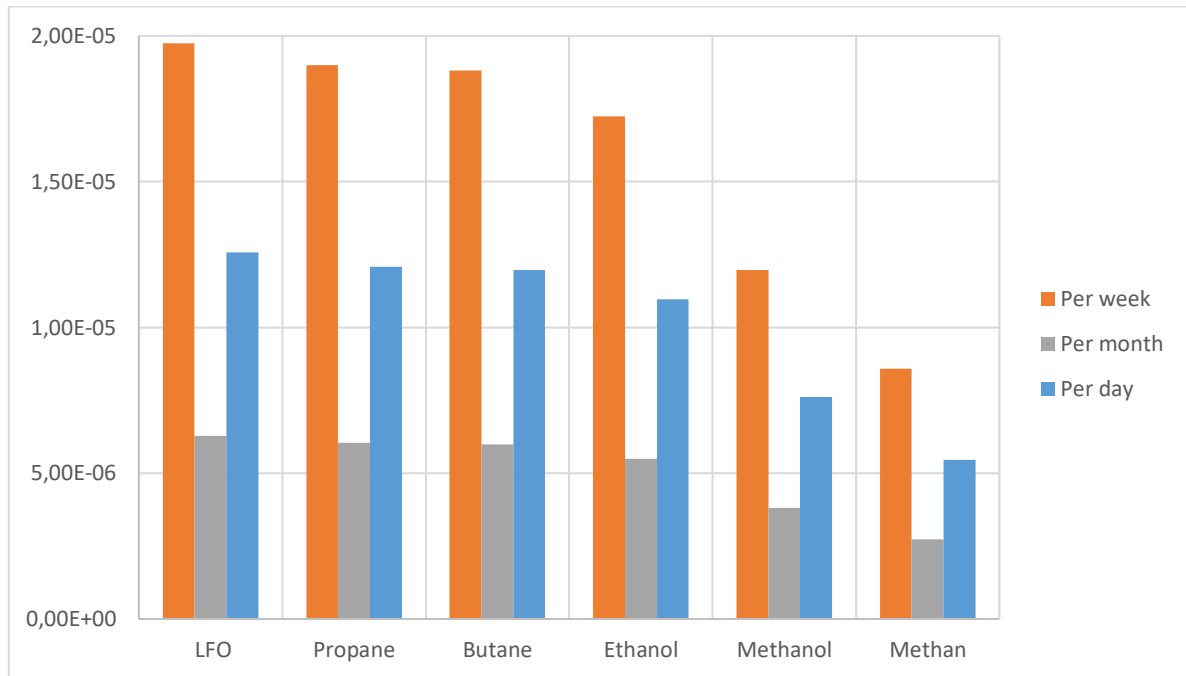


Figure 7. EEOI of different fuels

From the results in Figure 7. it can be seen that when using alternative fuels, the generated emissions are lower during different assessment periods. For example, if methane is used, CO₂ emissions decrease by over 50% for all stages of operation compared to the use of traditional marine diesel fuel. There is a significant reduction in CO₂ emissions with methanol as well, while for the other fuels, the effect is not very significant. Similar are the percentage reductions in the generated CO₂ emissions on an annual basis. There, once again, it can be seen and becomes clear that methane has the lowest values.

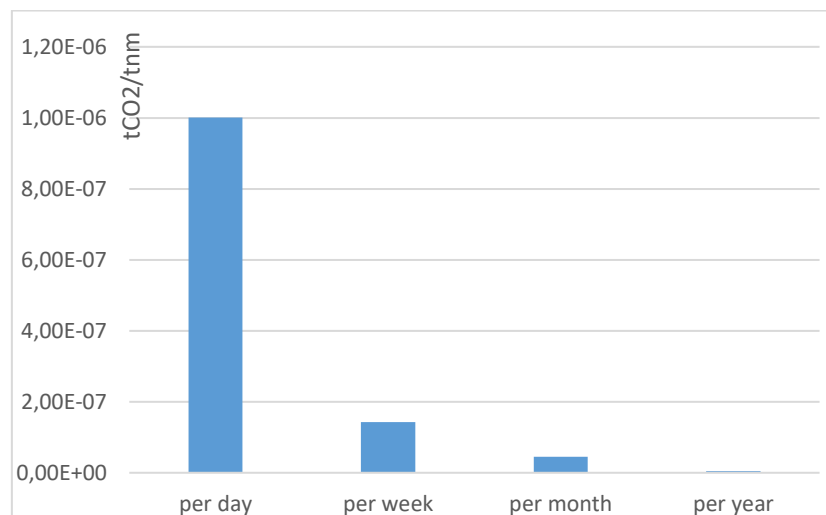


Figure 8. CO₂ emission by HVO

However, the situation is not the same when it comes to the use of HVO (Hydrotreated Vegetable Oil). With this type of fuel, the generated CO₂ emissions into the atmosphere are almost 80% reduced compared to those from light fuel oil and 100%, reduced compared to those from methane Figure.8.

The relationships of the generated emissions between HVO (Hydrotreated Vegetable Oil) and LFO (Light Fuel Oil) are presented in Figure 9. It becomes clear that in the ratio between HVO/Methane, the values are smaller than those in HVO/LFO. This provides information that a combination can be made when using both fuels, with the main engine running on HVO and the diesel generators using methane, or vice versa.

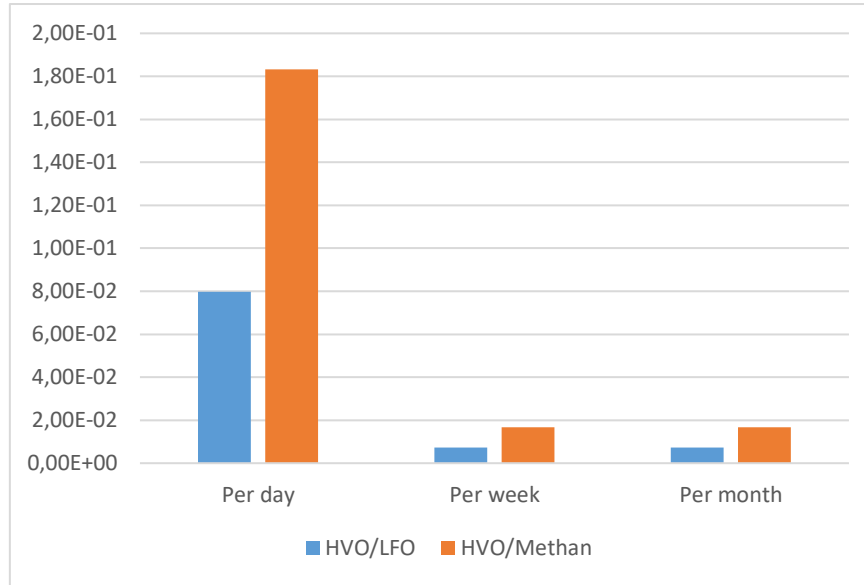


Figure 9. Relations of CO₂ emissions for HVO/LFO and HVO/Methan

The production of HVO in Europe is available in nine European countries, including Belgium, Denmark, Finland, Estonia, Lithuania, Latvia, the Netherlands, Sweden, and Norway. The largest producer is the Netherlands, and the largest consumer is France. The presence of HVO in Europe provides a strong basis for its use as a fuel, especially considering that the Netherlands is the largest producer, and it is home to one of Europe's major ports, Rotterdam. When using HVO (Hydrotreated Vegetable Oil), the generated CO₂ emissions are reduced to 0%, which fully complies with the emissions reduction requirements set by IMO (International Maritime Organization). However, not everything can be in the right direction, as a drawback of HVO is its excessively high market price as of today. It is approximately twice as high as that of LFO (Light Fuel Oil) and about 3.5 times higher than that of methane and methanol, figure 10.

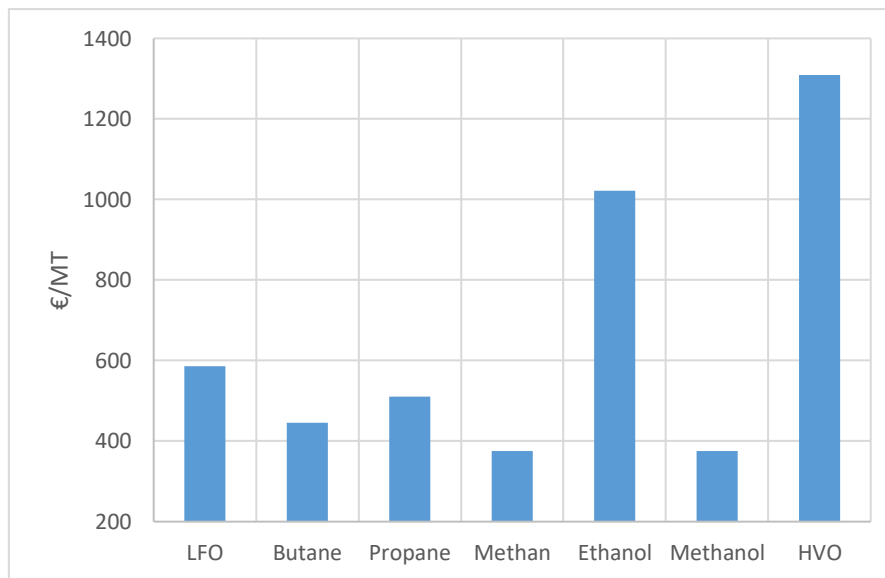


Figure 10. The price of fuels

It's precisely due to its higher price that its adoption in shipping is not as pronounced. Over time and as environmental requirements become stricter, its price is expected to normalize, providing opportunities for its use as a marine fuel. Once the environment is damaged, it's difficult to restore it compared to the money spent on its preservation.

Conclusions

The article explores the possibilities of using alternative fuels in shipping as a measure to reduce the emissions generated in the environment, specifically CO₂ emissions, which have the highest percentage contribution to the atmosphere. Data on the generated CO₂ emissions in the atmosphere from various modes of transportation are presented, with the finding that shipping accounts for approximately 13% of all emissions. The largest share is attributed to land transportation, approximately 80%. Referring to data on CO₂ emissions generated by shipping, it becomes clear that container ships contribute the most emissions. This is largely due to their relatively high sailing speeds compared to other types of vessels, such as tankers.

A classification of alternative fuels is presented, divided into three groups with typical representatives for each group. The last group, the combined group, presents various combinations of renewable sources and fuels. Information is also provided regarding the applicability of various alternative fuels in different sailing regions. It has been determined that LNG (Liquified Natural Gas) and LPG (Liquified Petroleum Gas) have the widest range of applications.

Calculations of the EEOI (Energy Efficiency Operational Indicator) have been conducted for a multi-purpose cargo ship with 7000 DWT following the accepted sailing route between the port of Varna and the port of Rotterdam. These calculations were performed for various alternative fuels as well as for LFO (Light Fuel Oil). When using methane as the primary fuel, the generated CO₂ emissions are approximately 50% lower than those with LFO. The calculations were done for harmful emissions generated per day, week, and month, depending on the ship's speed and the nautical miles sailed.

For the same ship, the same sailing speed, and the same route, when using HVO (Hydrotreated Vegetable Oil) as the primary ship fuel, the reduction in harmful emissions is approximately 90%, even compared to LFO (Light Fuel Oil), it's about 100%. This suggests that this type of fuel is environmentally clean and alternative. Its drawback, however, is its high cost, which is approximately 2 times higher than that of LFO and about 3.5 times higher than that of methane. Nonetheless, in the future, its price is expected to normalize, and it will find its place in shipping.

Future work in this direction will involve the stages of ship operation and the use of alternative fuels that still generate some degree of CO₂ emissions. The gases from these emissions, which have applications in the industry (such as CO₂), will need to be captured, separated, and utilized for the ship's needs.

Scientific Ethics Declaration

The author declares that the scientific ethical and legal responsibility of this article published in EPSTEM journal belongs to the author.

Acknowledgements or Notes

* This article was presented as an oral presentation at the International Conference on Technology (www.icontech.net) held in Antalya/Turkey on November 16-19, 2023.

References

- Acomi, N., & Cristian Acomib, O. (2014). The influence of different types of marine fuel over the energy efficiency operational index, *Energy Procedia*, 59, 243-248.
- Ammar, N.R. (2018). Energy- and cost-efficiency analysis of greenhouse gas emission reduction using slow steaming of ships: case study RO-RO cargo vessel. *Ships and Offshore Structures*, 13 (8), 868-876.

- Ammar, N.R., & Seddiek, I.S. (2020). An environmental and economic analysis of emission reduction strategies for container ships with emphasis on the improved energy efficiency indexes. *Environmental Science and Pollution Research*, 27 (18), 23342-23355.
- Ammar, N.R., 2019, An environmental and economic analysis of methanol fuel for a cellular container ship. *Transportation Research Part D: Transport and Environment*, 69, 66-76.
- Center of Climate and Energy Solutions. (2023). Global emissions. Retrieved from <https://www.c2es.org/content/international-emissions/>
- Cheliotis, M., Boulougouris, E., Trivyza, N.L., Theotokatos, G., Livanos, G., Mantalos, G., Stubos, A., Stamatakis, E., & Venetsanos, A. (2021). Review on the safe use of ammonia fuel cells in the maritime industry. *Energies*, 14, 3023.
- Engineering Toolbox. (2009). Combustion of fuels-carbon di. Retrieved from https://www.engineeringtoolbox.com/co2-emission-fuels-d_1085.html
- European Commission. (2018). Reducing emissions from the shipping sector. Retrieved from https://climate.ec.europa.eu/eu-action/transport/reducing-emissions-shipping-sector_en
- European Environment Agency. (2019). Share of transport greenhouse gas emissions. Retrieved from <https://www.eea.europa.eu/data-and-maps/daviz/share-of-transport-ghg-emissions-2>
- European Environment Agency. (n.d.). Marine protected area coverage. Retrieved from https://www.eea.europa.eu/data-and-maps/figures/distance-to-aichi-target/24383_percentage-cover-of-marine-protected-areas.eps
- European Technology and Innovation Platform (ETIP). (2023). Use of biofuels in shipping, available online at <https://www.etipbioenergy.eu>
- Gonzales Gutierrez, C., Diaz-Ruiz-Navamuel, E., A. Herrero, A., & Ortega-Piris, A. (2023). Assessing energy efficiency and regulatory complexity in steam-powered LNG carriers, *Ocean Engineering*, 286, 115671.
- MAN Energy Solutions. (2023). Biofuels. Retrieved from <https://www.man-es.com/marine/strategic-expertise/future-fuels/biofuel>
- OECD. (2023). New estimates provide insights on CO2 emissions from global shipping. Retrieved from <https://oecdstatistics.blog/2023/06/15/new-estimates-provide-insights-on-co2-emissions-from-global-shipping/>
- Ritchie, H., Rosado, P., & Roser, M. (2020). Greenhouse gas emissions. Retrieved from: <https://ourworldindata.org/greenhouse-gas-emissions>
- UNCTAD. (2022). Roadmap to decarbonize the shipping sector: Technology development, consistent policies and investment in research, development and innovation. Retrieved from <https://unctad.org/news/transport-newsletter-article-no-99-fourth-quarter-2022>

Author Information

Yordan Denev

Technical University of Varna
Studentska 1 str., Varna, Bulgaria
Contact e-mail: y.denev@tu-varna.bg

To cite this article:

Denev, Y. (2023). Reduction of shipping greenhouse emission by alternative fuels used. *The Eurasia Proceedings of Science, Technology, Engineering & Mathematics (EPSTEM)*, 24, 225-234.

The Eurasia Proceedings of Science, Technology, Engineering & Mathematics (EPSTEM), 2023

Volume 24, Pages 235-242

IConTech 2023: International Conference on Technology

Indeterminate Continuously Inhomogeneous Beam under End Rotation: A Longitudinal Fracture Study

Victor Rizov

University of Architecture

Abstract: The present paper describes a theoretical analysis of the effect of the end rotation of a statically indeterminate beam structure on the behaviour of a longitudinal crack. The beam is made of a material that is continuously inhomogeneous along the beam thickness. Besides, the material has non-linear elastic behaviour. The left end of the beam is supported with an axial double rod, while the right end is rigidly fixed. There is no external mechanical loading on the beam. Thus, the only influence on the beam is the rotation of the beam left end. Equations for determination the curvatures and the coordinates of the neutral axes are worked out and solved together with equations for resolving the static indeterminacy. The response of the longitudinal crack to the rotation of the beam left end is studied by deriving the strain energy release rate. For this purpose the balance of the energy in the beam is analyzed. The strain energy release rate is verified by applying the integral, J . A parametric analysis is performed to evaluate the influence of the beam end rotation and other factors on the longitudinal fracture.

Keywords: Continuously inhomogeneous structure, Longitudinal fracture, Statically indeterminate beam, End rotation, Non-linear elastic behaviour

Introduction

The increased interest for continuously inhomogeneous structural materials shown by the research community around the globe in recent decades is due in a large measure to the intensive application of functionally graded materials in different areas of engineering (Gandra et al., 2011; Toudehdehghan et al., 2017). In fact, the functionally graded materials are continuously inhomogeneous composites with a controlled continuous distribution of material properties along one or more directions (Nikbakht et al., 2019; Nagara et al., 2019; Radhika et al., 2020; Riov, 2018). Thus, the material properties are smooth functions of one or more coordinates (Gururaja Udupa et al., 2014; Fanani et al., 2021).

In order to meet the constantly increasing requirements of up-to-date engineering towards the quality and properties of continuously inhomogeneous (functionally graded materials), different technologies for manufacturing of that sort of materials have been developed. One of the widely used technologies consists in building-up layer-by-layer (Mahamood & Akinlabi, 2017). However, the functionally graded materials manufactured by this technology have layered structure that makes them rather vulnerable to appearance of longitudinal cracks between the layers. As a result of this, one of the factors which have significant influence on the deformability, load-carrying capacity and safety of engineering structures made of such materials is the longitudinal fracture. Thus, various analyses of longitudinal fracture in continuously inhomogeneous (functionally graded) structural members have been performed recently (Carpinteri & Pugno, 2006; Rizov, 2019; Rizov & Altenbach, 2020; Tilbrook et al., 2005). These analyses usually are concerned with structures subjected to external mechanical loading. However, displacements and/or rotations of supports in statically indeterminate structures influence the longitudinal fracture behaviour even if external mechanical loading (forces, moments, etc.) is not applied on structures. This influence is subject of a theoretical analysis in the present paper.

- This is an Open Access article distributed under the terms of the Creative Commons Attribution-Noncommercial 4.0 Unported License, permitting all non-commercial use, distribution, and reproduction in any medium, provided the original work is properly cited.

- Selection and peer-review under responsibility of the Organizing Committee of the Conference

© 2023 Published by ISRES Publishing: www.isres.org

In particular, the present paper deals with longitudinal fracture behaviour of a statically indeterminate beam structure under rotation of its left end (the beam is supported with an axial double rod in the left end, while the right end is rigidly fixed). No external mechanical loading is applied on the beam under consideration. Thus, the beam is only under the rotation of its left end. The beam is continuously inhomogeneous along the beam thickness. Besides, the beam has non-linear elastic behaviour. The strain energy release rate for the longitudinal crack under the beam left end rotation is derived. The integral, J , is used for verification. The influence of the beam end rotation on the longitudinal fracture is evaluated.

Theoretical Model

This paper addresses the problem of longitudinal fracture in the continuously inhomogeneous non-linear elastic beam structure, S_1S_4 , depicted in Fig. 1.

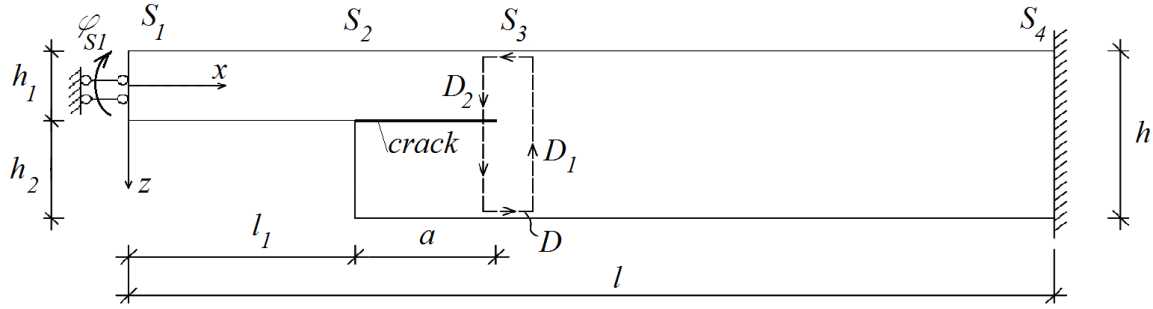


Figure1. Scheme of the beam structure.

The beam is supported with an axial double rod at its left end. The right end of the beam is rigidly fixed. Thus, the beam represents a statically indeterminate structure. The beam has three portions, S_1S_2 , S_2S_3 and S_3S_4 . The beam thickness in portion, S_1S_2 , is h_1 , while in portions, S_2S_3 and S_3S_4 , the thickness is h (Fig. 1). There is a longitudinal crack in portion, S_2S_3 , of the beam (the thicknesses of the upper and lower crack arms are h_1 and h_2 , respectively). The left end of the beam undergoes a rotation at angle, φ_{S1} , as shown in Fig. 1. We analyze the crack response to the rotation of the beam left end. For this purpose, we derive the strain energy release rate, G , for the crack by analyzing the energy balance. This analysis yields the following expression for the strain energy release rate:

$$G = \frac{M_{S1}}{b} \frac{\partial \varphi_{S1}}{\partial a} - \frac{1}{b} \frac{\partial U}{\partial a}, \quad (1)$$

where

$$U = U_{S1S3} + U_{S3S4}. \quad (2)$$

In the above formulas, M_{S1} is the bending moment in the axial double rod at the left end of the beam, b is the beam width, a is the crack length, U is the strain energy in the beam, U_{S1S3} and U_{S3S4} are the strain energies in portions, S_1S_3 and S_3S_4 , of the beam, respectively.

U_{S1S3} is determined by formula (3).

$$U_{S1S3} = (l_1 + a) \iint_{(A)} u_0 dA, \quad (3)$$

where l_1 is the length of portion, S_1S_2 , of the beam, A is the area of the cross-section, u_0 is the strain energy density. The latter is defined by

$$u_0 = \int_0^{\varepsilon} \sigma d\varepsilon, \quad (4)$$

where σ is the stress, ε is the strain. The stress is expressed as a function of ε by the following non-linear stress-strain relation (Lukash, 1997):

$$\sigma = B \left[1 - \left(1 - \frac{\varepsilon}{\beta} \right)^n \right], \quad (5)$$

where B , n and β are material properties. The beam exhibits continuous material inhomogeneity along the thickness. The change of the material properties along the beam thickness is given by

$$B = B_{gr} + \frac{B_{dm} - B_{gr}}{h_1^{\lambda_1}} \left(\frac{h_1}{2} + z \right)^{\lambda_1}, \quad (6)$$

$$n = n_{gr} + \frac{n_{dm} - n_{gr}}{h_1^{\lambda_2}} \left(\frac{h_1}{2} + z \right)^{\lambda_2}, \quad (7)$$

$$\beta = \beta_{gr} + \frac{\beta_{dm} - \beta_{gr}}{h_1^{\lambda_3}} \left(\frac{h_1}{2} + z \right)^{\lambda_3}, \quad (8)$$

where

$$-\frac{h_1}{2} \leq z \leq \frac{h_1}{2}. \quad (9)$$

In formulas (6) – (9), the subscripts, gr and dm , refer to the upper and lower surface of the beam, z is the vertical centric axis of the beam, λ_1 , λ_2 and λ_3 are parameters. The distribution of ε along the beam thickness is given by

$$\varepsilon = \kappa(z - z_{nn}), \quad (10)$$

where κ is the beam curvature, z_{nn} is the neutral axis coordinate.

First, we have to resolve the static indeterminacy in order to obtain the curvatures and the neutral axis coordinates in the beam portions. For this purpose, we work out the following equations:

$$\varphi_{S1} = \kappa(l_1 + a) + \kappa_1(l - l_1 - a), \quad (11)$$

$$\delta_{S1} = -\kappa z_{nn} + \kappa_1 \left(\frac{h_1}{2} - \frac{h}{2} - z_{1nn} \right), \quad (12)$$

$$\iint_{(A)} \sigma dA = \iint_{(A_1)} \sigma_{S2S4} dA, \quad (13)$$

$$\iint_{(A)} \sigma_z dA = \iint_{(A_1)} \sigma_{S_3 S_4} z_1 dA, \quad (14)$$

where

$$\delta_{S_1} = 0, \quad (15)$$

$$\sigma_{S_3 S_4} = B \left[1 - \left(1 - \frac{\varepsilon_{S_3 S_4}}{\beta} \right)^n \right], \quad (16)$$

$$\varepsilon_{S_3 S_4} = \kappa_1 (z_1 - z_{1nn}), \quad (17)$$

$$-\frac{h}{2} \leq z_1 \leq \frac{h}{2}. \quad (18)$$

In formulas (11) – (17), κ_1 and z_{1nn} are the curvature and the neutral axis coordinate in portion, $S_3 S_4$, of the beam, $\sigma_{S_3 S_4}$ is the stress, $\varepsilon_{S_3 S_4}$ is the strain, δ_{S_1} is the horizontal displacement of the left end of the beam (δ_{S_1} is zero due to the fact that the left end of the beam is constrained with an axial double rod as shown in Fig. 1), z_1 and A_1 are the vertical centric axis and the area of the cross-section of the beam in portion, $S_3 S_4$. The curvatures and the neutral axis coordinates are determined from equations (11) – (14) by using the MatLab. ,

$U_{S_3 S_4}$ is determined by formula (19).

$$U_{S_3 S_4} = (l - l_1 - a) \iint_{(A_1)} u_{01} dA, \quad (19)$$

where

$$u_{01} = \int_0^{\varepsilon_{S_3 S_4}} \sigma_{S_3 S_4} d\varepsilon. \quad (20)$$

The bending moment, M_{S_1} , is found-out by formula (21), i.e.

$$M_{S_1} = \iint_{(A)} \sigma_z dA. \quad (21)$$

Then the strain energy release rate is obtained by using formula (1).

The strain energy release rate is verified by applying the integral, J , (Broek, 1986). The integration is performed along the contour, D , that has two sectors, D_1 and D_2 , as shown in Fig. 1. We derive

$$J = J_{D_1} + J_{D_2}, \quad (22)$$

where

$$J_{D_1} = \int_{D_1} \left[u_{01} \cos \alpha_{D_1} - \left(p_{x_{D_1}} \frac{\partial u}{\partial x} + p_{y_{D_1}} \frac{\partial v}{\partial x} \right) \right] ds_{D_1}, \quad (23)$$

$$J_{D2} = \int_{D_2} \left[u_0 \cos \alpha_{D_2} - \left(p_{x_{D_2}} \frac{\partial u}{\partial x} + p_{y_{D_2}} \frac{\partial v}{\partial x} \right) \right] ds_{D_2}. \quad (24)$$

The MatLab is used to perform the integration in (23) and (24). The values of the integral, J , match the strain energy release rates which is a verification of the current analysis.

Numerical Results

We apply the solution of the strain energy release rate to obtain numerical results which illustrate the influence of the beam end rotation and other factors on the longitudinal fracture behaviour of the beam under consideration.

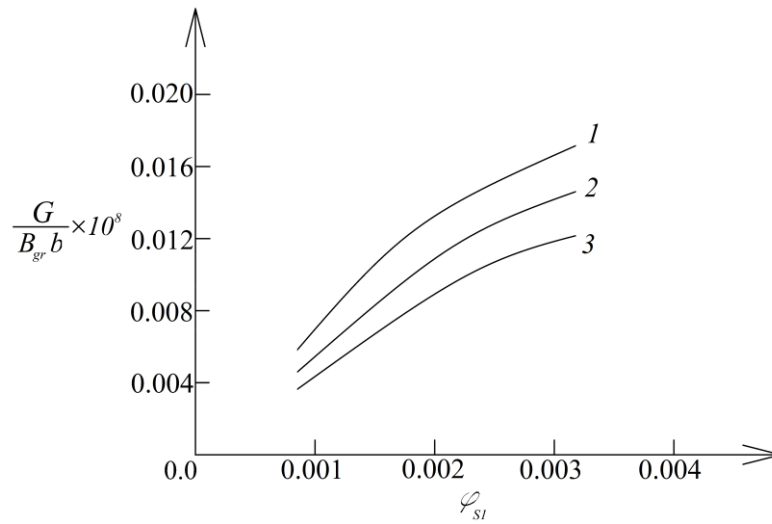


Figure 2. The strain energy release rate versus φ_{S1} (curve 1 – at $B_{dm} / B_{gr} = 0.5$, curve 2 – at $B_{dm} / B_{gr} = 1.0$ and curve 3 – at $B_{dm} / B_{gr} = 2.0$).

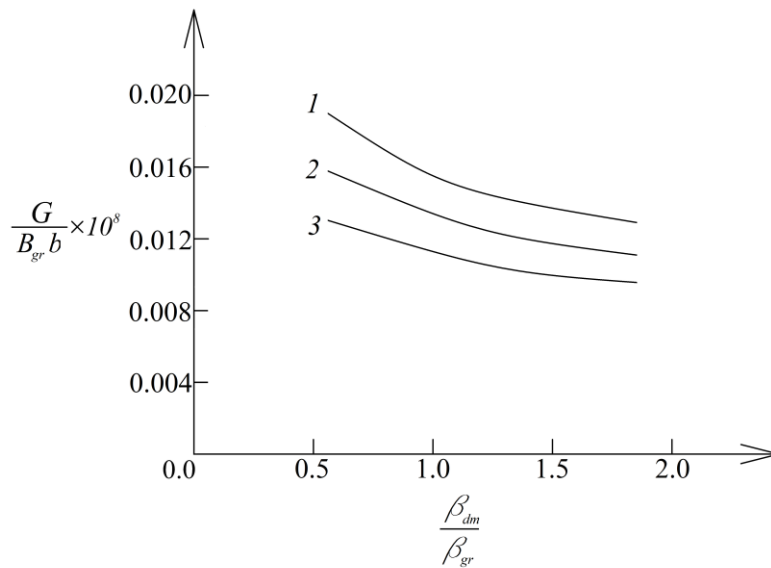


Figure 3. The strain energy release rate versus β_{dm} / β_{gr} ratio (curve 1 – at $a/l = 0.25$, curve 2 – at $a/l = 0.50$ and curve 3 – at $a/l = 0.75$).

These influences are visualized in the next four figures. The following data are used: $b = 0.010$ m, $h = 0.015$ m, $h_1 = 0.012$ m, $l = 0.400$ m, $\lambda_1 = 0.8$, $\lambda_2 = 0.8$, $\lambda_3 = 0.8$ and $\varphi_{s1} = 0.005$ rad.

Figure 2 illustrates the variation of the strain energy release rate with increasing of the magnitude of the angle of rotation, φ_{s1} , at three B_{dm} / B_{gr} ratios. The curves in Fig. 2 indicate that the strain energy release rate grows at increase of φ_{s1} which is an expected behaviour.

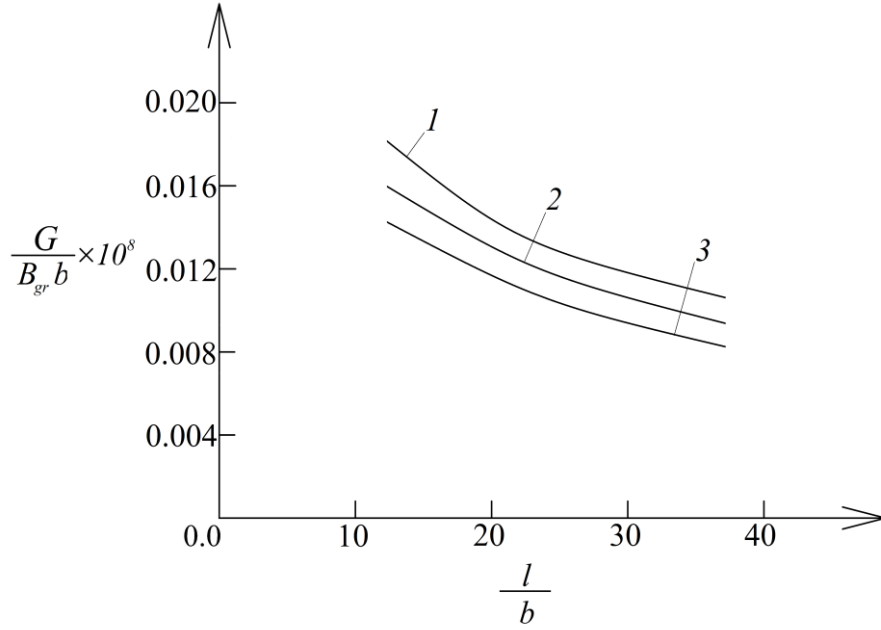


Figure 4. The strain energy release rate versus l/b ratio (curve 1 – at $n_{dm} / n_{gr} = 0.2$, curve 2 – at $n_{dm} / n_{gr} = 0.4$ and curve 3 – at $n_{dm} / n_{gr} = 0.6$).

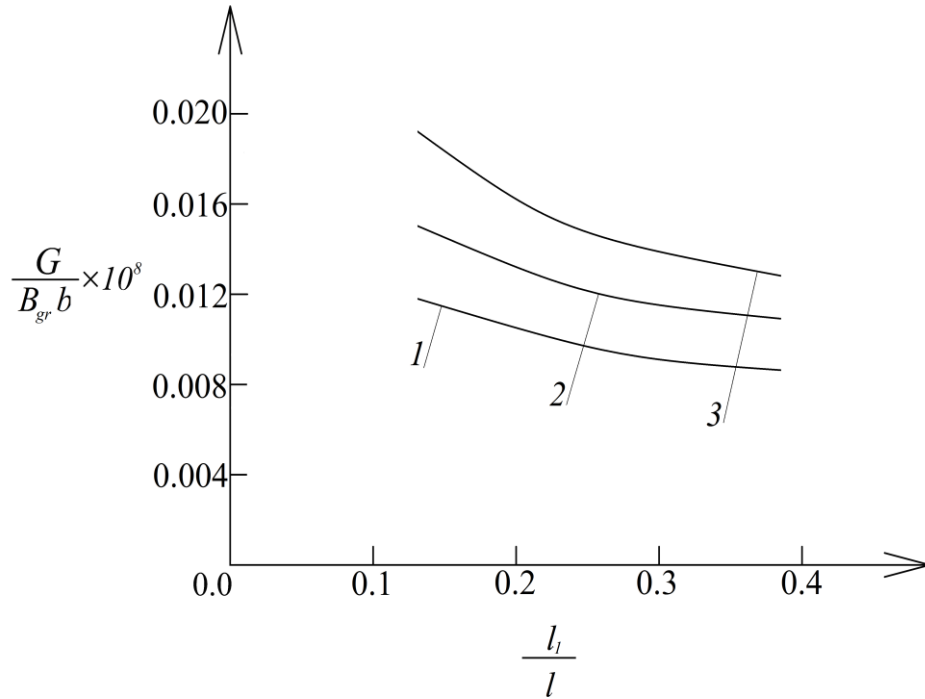


Figure 5. The strain energy release rate versus l_l/l ratio (curve 1 – at $h/b = 1.2$, curve 2 – at $h/b = 1.2$ and curve 3 – at $h/b = 1.2$).

However, the strain energy release rate reduces when B_{dm}/B_{gr} ratio increases as one can observe in Fig. 2. The influence of β_{dm}/β_{gr} and a/l ratios on the strain energy release rate is visualized by the curves presented in Fig. 3. It can be seen in Fig. 3 that increase of β_{dm}/β_{gr} ratio causes a gradual reduction of the strain energy release rate. The strain energy release rate reduces also with increase of a/l ratio (this finding is attributed to the fact that the beam becomes more deformable).

Figure 4 shows the effect of the variation of l/b ratio on the strain energy release rate at three n_{dm}/n_{gr} ratios. The reduction of the strain energy release rate when l/b ratio grows is due again the fact that the beam deformability increases. The increase of n_{dm}/n_{gr} ratio generates a decrease of the strain energy release rate (Fig. 4). The dependence of the strain energy release rate on l/l_1 and h/b ratios is visualized by three curves in Fig. 5. The inspection of these curves reveals that increase of l/l_1 ratio generates a continuous reduction of the strain energy release rate. Increase of h/b ratios leads to growth of the strain energy release rate (Fig. 5).

Conclusion

Longitudinal fracture in a statically indeterminate beam structure under end rotation is studied theoretically. It is found that:

- the strain energy release rate grows at increase of φ_{S1} ;
- the strain energy release rate reduces when B_{dm}/B_{gr} ratio increases;
- increase of β_{dm}/β_{gr} ratio causes a gradual reduction of the strain energy release rate;
- the strain energy release rate reduces also with increase of a/l , l/b and l/l_1 ratio;
- increase of h/b ratio leads to growth of the strain energy release rate.

Recommendations

It is recommendable to refine the present fracture analysis by considering the viscoelastic behaviour of the statically indeterminate beam structure under end rotation.

Scientific Ethics Declaration

The author declares that the scientific ethical and legal responsibility of this article published in EPSTEM journal belongs to the author.

Acknowledgements or Notes

* This article was presented as an oral presentation at the International Conference on Technology (www.icontech.net) held in Antalya/Turkey on November 16-19, 2023.

References

- Broek, D. (1986). *Elementary engineering fracture mechanics*. Springer.
- Carpinteri, A., & Pugno, N. (2006). Cracks in re-entrant corners in functionally graded materials. *Engineering Fracture Mechanics*, 73(10), 1279-1291.
- Fanani, E. W. A., Surojo, E., Prabowo, A. R., & Akbar, H. I. (2021). Recent progress in hybrid aluminum composite: Manufacturing and application. *Metals*, 11(12), 1919-1929.

- Gandra, J., Miranda, R., Vilaca, P., Velinho, A., & Teixeira, J.P. (2011). Functionally graded materials produced by friction stir processing. *Journal of Materials Processing Technology*, 211(11), 1659-1668.
- Udupa, G., Shrikantha Rao, S., & Rao Gangadharan, K. (2014). Functionally graded composite materials: An overview. *Procedia Materials Science*, 5, 1291-1299.
- Lukash, P. (1997). *Fundamentals of non-linear structural mechanics*. Science.
- Mahamood, R. C., & Akinlabi, E. T. (2017). *Functionally graded materials*. Springer.
- Nagaral, M., Nayak, P. H., Srinivas, H. K., & Auradi V. (2019). Characterization and tensile fractography of Nano ZrO₂ reinforced copper-zinc alloy composites. *Frattura ed Integrità Strutturale*, 13(48), 370-376.
- Radhika, N., Sasikumar, J., Sylesh, J. L., & Kishore, R. (2020). Dry reciprocating wear and frictional behaviour of B4C reinforced functionally graded and homogenous aluminium matrix composites. *Journal of Materials Research and Technology*, 9(2), 1578-1592.
- Rizov, V. I. (2019). Non-linear elastic analysis of delamination in two-dimensional functionally graded multilayered beam. *International Journal of Structural Integrity*, 11(4), 1-17.
- Rizov, V.I. (2019). Influence of material inhomogeneity and non-linear mechanical behaviour of the material on delamination in multilayered beams. *Frattura ed Integrità Strutturale*, 13(47), 468-481.
- Rizov, V. I & Altenbach, H. (2020). Longitudinal fracture analysis of inhomogeneous beams with continuously varying sizes of the cross-section along the beam length. *Frattura ed Integrità Strutturale*, 14(53), 38-50.
- Tilbrook, M. T., Moon, R. J., & Hoffman, M. (2005). Crack propagation in graded composites. *Composite Science and Technology*, 65(2), 201-220.
- Toudehdeghghan, J., Lim, W., Foo1, K. E., Ma'arof, M. I. N., & Mathews, J. (2017). A brief review of functionally graded materials. *MATEC Web of Conferences*, 131.

Author Information

Victor Rizov

University of Architecture

Sofia, Bulgaria

Contact e-mail: v_rizov_fhe@uacg.bg

To cite this article:

Rizov, V. (2023). Indeterminate continuously inhomogeneous beam under end rotation: A longitudinal fracture study. *The Eurasia Proceedings of Science, Technology, Engineering & Mathematics (EPSTEM)*, 24, 235-242.

The Eurasia Proceedings of Science, Technology, Engineering & Mathematics (EPSTEM), 2023

Volume 24, Pages 243-256

IConTech 2023: International Conference on Technology

A Numerical Study of the Efficiency of the Sono Galvano-Fenton Process as a Tertiary Treatment Technique for the Wastewater Reuse in Agriculture

Kaouthar Kerboua

National Higher School of Technology and Engineering

Abstract: In the present study, the Sono-Galvano-Fenton process is studied numerically as a tertiary treatment process for treated wastewater reuse in irrigation, with in situ generation of the Fenton's reagent and catalyst, i.e., H_2O_2 and Fe^{2+} . The sonochemical pathway is examined as a source of hydrogen peroxide under the pre-optimized condition of acoustic frequency, 200 kHz. The macroscopic model accounting for the performance of the single acoustic cavitation bubble and the bubble population density is combined with the Fe/Cu galvanic cell operating in acidic conditions (pH 3), following a cumulative and instantaneous production approach in terms of Fenton's reagent. The combination is optimized based on the rate of hydroxyl radicals generated by the Galvano-Fenton process, as a non-selective powerful oxidant against recalcitrant pollutants, then considering the synergetic effect of the hybrid process in terms of HO^\bullet pumped sonochemically and via the Fenton based pathway, treated using simulations of the isolated processes then their combined configuration following both aforementioned approaches.

Keywords: Numerical model, Synergy, Hydroxyl radical, Ultrasounds, Galvano Fenton, Simulation.

Introduction

Ultrasounds as a carrier of mechanical power is used in chemistry in the so-called sonochemical processes (Mason, 1999). Sonochemistry is defined as the chemistry induced by ultrasounds indirectly, through the microscopic process of acoustic cavitation bubble (Leighton, 1994). Acoustic cavitation bubble is formed by heterogeneous nucleation as small pockets of gas are present in the sonicated liquid, it then oscillates under the pace of the ultrasonic wave, it accumulates energy so that a chemical mechanism is activated starting with the decomposition of water molecules. Under oxygen atmosphere, the hydrogen, hydroxyl and oxygen radicals that appear in the liquid medium interact to form new molecules, including hydrogen peroxide (Dalodiere et al., 2016; Ziembowicz et al., 2017). Hydrogen peroxide is a powerful oxidant used as a precursor for hydroxyl radicals (He et al., 1988) in advanced oxidation processes (Palit, 2012). It is also the well-known reagent of the Fenton reaction (Barbusinski, 2009). The combination of ultrasounds with Fenton based processes may be an efficient option for the in-situ production of hydrogen peroxide, especially if the integration considers a method for the in-situ production of the Fenton's catalyst, namely ferrous ions. In the present paper, direct continuous sonication is integrated to the Galvano-Fenton process studied in our previous papers (Kerboua, 2022; Kerboua et al., 2021) in order to investigate numerically the possibility of producing autonomously hydrogen peroxide. The proposed model considers the microscopic and macroscopic effect of sonication in terms of the sonochemical production of H_2O_2 , and the simultaneous performance of the Sono-Galvano-Fenton process. A preliminary study for the optimization of acoustic frequency condition is carried out using modeling and simulation.

Method

- This is an Open Access article distributed under the terms of the Creative Commons Attribution-Noncommercial 4.0 Unported License, permitting all non-commercial use, distribution, and reproduction in any medium, provided the original work is properly cited.

- Selection and peer-review under responsibility of the Organizing Committee of the Conference

© 2023 Published by ISRES Publishing: www.isres.org

Configuration of the Modelled Process

The integrated process accounts for direct continuous sonication using a transducer placed at the bottom of the reactor, and delivering an acoustic amplitude of 1.5 atm. The studied frequencies are supposed to vary from 20 to 800 kHz, including 200, 300, 360, 443, 500 and 600 kHz. The adopted acoustic frequency is selected based on the optimal reactor scale production of hydrogen peroxide.

The Galvano-Fenton process is designed by immersing a galvanic cell of iron anode (sacrificial anode) and copper cathode within an acidified electrolyte, at the pH condition allowing the formation of ferrous ions according to the Pourbaix diagram, i.e., pH 3. Hydrogen peroxide is produced sonochemically while the spontaneous corrosion of iron occurs, inducing the Fenton reaction. The process is simulated considering a corrosion current of 300 μA , determined experimentally during the preliminary test described in our previous works (Kerboua, 2022). The Galvano-Fenton system is modeled by combining electrochemical reactions taking place at the anode and the cathode with chemical reactions related to the Fenton mechanism occurring in the bulk liquid volume. The Fenton based mechanism has been validated experimentally in our previous studies using blank tests (Gasmi et al. 2020; Gasmi et al., 2020). The specifications of the parameters corresponding to the aforementioned described configuration are all reported in Table. 1. A schema of the integrated process is presented in Fig.1.

Table 1. Specifications of the Sono-Galvano-Fenton cell

Parameter	Specification
Type of sonication	Direct
Mode of sonication	Continuous
Acoustic frequency to be tested	20, 200, 360, 443, 600, 800 kHz
Acoustic amplitude	1.5 atm
Electrodes form	rectangular smooth plates
Immersed electrodes surface	12 cm^2
Electrolyte volume	100 mL
Electrodes disposition	In parallel
Electrolyte nature	Acidified water (H_2SO_4)
pH	3
Electrical connection	External wire
Ionic displacement	Aided by a magnetic stirring
Initial concentration of hydrogen peroxide	0 mM

Numerical Modelling

The Microscopic Effect Of Sonication

The single bubble dynamics is governed by the modified Keller-Miksis equation accounting for the non-equilibrium of evaporation and condensation of water molecules at the gas-liquid interface (Kerboua & Hamdaoui, 2019; Yasui, 1997), as expressed in Eq. 1. The present numerical model is based on combining both sonochemical activity of single acoustic cavitation bubble and kinetic evolution of number density of bubbles within a control volume of a sonochemical reactor filled of water saturated with oxygen.

$$\begin{aligned}
 \ddot{R} - \frac{(c + \dot{R})}{\rho_L \left(cR - \dot{R}R + \frac{\dot{m}R}{\rho_L} \right) + 4\mu} & \left(P_g - \frac{26}{R} - 4\mu \frac{\dot{R}}{R} - P_\infty + P_a \sin \left(2\pi f \left(t + \frac{R}{c} \right) - kx \right) \right) \\
 = \frac{R}{\rho_L \left(cR - \dot{R}R + \frac{\dot{m}R}{\rho_L} \right) + 4\mu} & \left(\frac{dP_g}{dt} + \frac{26\dot{R}}{R^2} + 4\mu \frac{\dot{R}^2}{R^2} \right) - \frac{\rho_L \left((3c - \dot{R}) + \frac{2\dot{m}}{\rho_L} \right) \dot{R}^2}{2 \left(\rho_L \left(cR - \dot{R}R + \frac{\dot{m}R}{\rho_L} \right) + 4\mu \right)} \\
 + \frac{\dot{m} \left(cR - \dot{R}R + \frac{\dot{m}R}{\rho_L} \right)}{\rho_L \left(cR - \dot{R}R + \frac{\dot{m}R}{\rho_L} \right) + 4\mu} & + \frac{\dot{m} \left(c\dot{R} + \frac{\dot{m}}{2\rho_L} (c + \dot{R}) \right)}{\rho_L \left(cR - \dot{R}R + \frac{\dot{m}R}{\rho_L} \right) + 4\mu}
 \end{aligned} \quad (1)$$

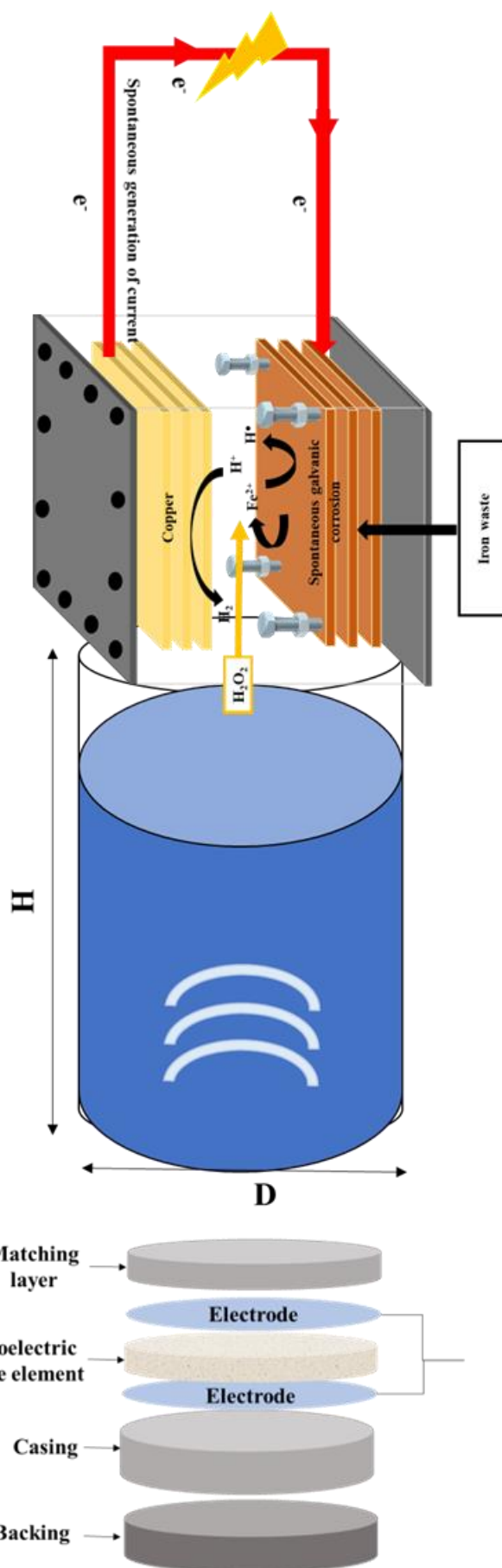


Figure 1. Schema of the integrated Sono-Galvano-Fenton process

The active bubble population is supposed to be composed of bubbles having similar equilibrium radius R_0 . The value of R_0 is frequency dependent, ambient radii were selected in respect to the theoretical intervals defined by Yasui (2002) and reported by Brothie et al. (2009). These values are limited by Blake (Atchley, 1989) and Minnaert et al. (1933) thresholds under the frequencies i.e. 20, 200, 300, 360, 443, 500, 600 and 800 kHz. The assumed acoustic amplitude is equivalent to an acoustic intensity 0.77 W/cm^2 according to Eq. 2 (Authier et al., 2018), and a power density is also expressed according to Eq. 3.

$$P_a = \sqrt{2\rho_L c I} \quad (2)$$

$$P = \frac{P_a^2 A}{2\rho_L c V_R} \quad (3)$$

Each single bubble constitutes a microreactor of spherical form and varying volume, the volume variation is then expressed by Eq. 4.

$$\frac{dV}{dt} = 4\pi R^2 \frac{dR}{dt} \quad (4)$$

While the volume of each microreactor varies in function of time, temperature and pressure within it evolves according to Eq. 5 and 6, respectively

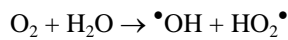
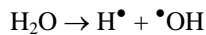
$$-P_g 4\pi R^2 \dot{R} - \frac{1}{3} \sum_{j=1}^{45} \Delta H_j r_j 4\pi R^3 + 4\pi R^2 \frac{m}{M_{H_2O}} C_{V_{H_2O}} T = \frac{\lambda}{\xi} 4\pi R^2 (T - T_\infty) + \sum_{k=1}^9 n_k C_V \dot{T} \quad (5)$$

$$\left(P_g + \frac{n^2 a}{V^2} \right) (V - nb) = n R_g T \quad (6)$$

Eq. 5 represents the heat balance applied to the single bubble volume. This heat balance considers the single acoustic cavitation bubble as opened to heat exchange through thermal diffusion across the thin heat transfer layer at the bubble interface, and evaporation and condensation processes carrying water molecules enthalpy toward and outward the bubble volume as illustrated in Fig. 1. Each microreactor is also considered open to mass transfer through physical phenomenon of simultaneous evaporation and condensation of water molecules at bubble interface as shown in Fig. 1, whose kinetics is governed by Hertz-Knudsen equation shown in Eq. 7 (Yasui, 1996).

$$\dot{m} = M_{H_2O} \frac{dn_{H_2O}}{dt} = \frac{\sqrt{M_{H_2O}}}{\sqrt{2\pi R_g}} \alpha \frac{1}{\sqrt{T}} (P_v - P_i) \quad (7)$$

The oscillation of active acoustic cavitation bubbles is particularly characterized by spectacular elevations of pressures and temperatures attaining 1000 bar and 6000 K, respectively, under 1.5 atm of acoustic amplitude (Kerboua & Hamdaoui, 2017, 2018) and occurring when the bubble contracts to its minimal size and collapses. The harsh conditions then attained activate a considerable number of elementary reactions initiated by the thermal decomposition of H_2O into hydroxyl and hydrogen radicals, and the reaction of H_2O and O_2 as shown below.



In the present model, 45 elementary reactions are expected to occur according to the schema reported in Table 2 and initially suggested by Yasui (1997) and inspired from Baulch et al. (1972, 1974, 1976) and Kamath et al. (1993). The molar rate related to i^{th} reaction is expressed in Eq. 8. Hence, the molar rate due to chemical reactions and related to the k^{th} species among the nine involved in the model is represented by Eq. 9.

$$r_i = A_i e^{\left(\frac{-E_i}{R_g T}\right)} \prod_{k=1}^9 (c_k)^{\vartheta_{ki}} \quad i = \overline{1,45} \quad (8)$$

$$\frac{dn_k}{dt} = \frac{4}{3} \pi R^3 \sum_{i=1}^{45} (\vartheta'_{ki} - \vartheta_{ki}) A_i e^{\left(\frac{-E_i}{R_g T}\right)} \prod_{k=1}^9 (c_k)^{\vartheta_{ki}} \quad k = \overline{1,9} \quad (9)$$

According to Eqs. 7, 8 and 9, the molar yields of the HO^\bullet and H_2O_2 involved in the chemical schema can be expressed in terms of molar concentration as shown in Eqs. 10 and 11.

$$\frac{dc_{HO^\bullet}}{dt} = \sum_{i=1}^{45} (\vartheta'_{HO^\bullet i} - \vartheta_{HO^\bullet i}) A_i e^{\left(\frac{-E_i}{R_g T}\right)} \prod_{k=1}^9 (c_k)^{\vartheta_{ki}} - 3c_{HO^\bullet} \frac{\dot{R}}{R} \quad (10)$$

$$\frac{dc_{H_2O_2}}{dt} = \sum_{i=1}^{45} (\vartheta'_{H_2O_2 i} - \vartheta_{H_2O_2 i}) A_i e^{\left(\frac{-E_i}{R_g T}\right)} \prod_{k=1}^9 (c_k)^{\vartheta_{ki}} - 3c_{H_2O_2} \frac{\dot{R}}{R} \quad (11)$$

At the macroscopic scale, the sonochemical activity of bubble population is observed within a cylindrical control volume. The energy balance applied to the control volume leads to Eq. 12, already demonstrated in a previous work of our research group (Kerboua & Hamdaoui, 2019).

$$\begin{aligned} - \sum_{j=1}^{45} \frac{4}{3} \pi \Delta H_j r_j R^3 N - \frac{4}{3} \pi (P_g - P_\infty - P) (3\dot{R}R^2N + R^3\dot{N}) - \sigma 4\pi (2\dot{R}RN + R^2\dot{N}) \\ - 2\pi \rho_L (3R^2\dot{R}^3N + 2R^3\dot{R}\ddot{R}N + R^3\dot{R}^2\dot{N}) \\ - \left(N \sum_{i=1}^9 \dot{n}_i u_i + N \sum_{i=1}^9 n_i \dot{u}_i + \dot{N} \sum_{i=1}^9 n_i u_i \right) = \frac{d}{dt} \left(\frac{P^2}{2\rho_L c^2} + \frac{\rho_L U^2}{2} \right) \end{aligned} \quad (12)$$

In this equation, N represents the number density of bubbles at instant t . Hence, the molar rates related to the sonochemical products (HO^\bullet , HO_2^\bullet , H^\bullet , H_2O_2 , O , O_3 , H_2), emerging from the reactions reported in Table 2, are expressed at reactor scale according to Eq. 13.

$$\frac{dC_k}{dt} = N \frac{4}{3} \pi R^3 \sum_{i=1}^{45} (\vartheta'_{ki} - \vartheta_{ki}) A_i e^{\left(\frac{-E_i}{R_g T}\right)} \prod_{k=1}^K (C_k)^{\vartheta_{ki}} + \dot{N} n_k \quad (13)$$

C_k represents the molar concentration of the k^{th} species (among HO^\bullet , HO_2^\bullet , H^\bullet , H_2O_2 , O , O_3 , H_2) within the control volume, while ϑ_{ki} , ϑ'_{ki} , $\frac{E_i}{R_g}$ and A_i are the parameters relative to the chemical kinetics, explained and

explicated in Table 2.

In order to model the integrated Sono-Galvano-Fenton process, the macroscopic sonochemical production of hydrogen peroxide retrieved previously will be expressed based on zero order kinetics model, considering a constant production rate as shown in Eq. 14.

$$\frac{dC_{H_2O_2}}{dt} = k_0 \quad (14)$$

Iron constitutes the sacrificial electrode, Fe oxidizes to Fe^{2+} ($E^0 = -0.44$ V vs. SHE) according to Equation 1, in Table.3. At the cathode, the most probable reaction concerns the reduction of H^+ to form H_2 ($E^0 = 0$ V vs. SHE) according to Eq.2 in Table.3, owing to the acidity of the medium. This has been proven in a previous work conducted by our research group (Intissar Gasmi, Kerboua, Haddour, Hamdaoui, et al. 2020). The kinetics related to all of the electrochemical reactions are governed by Faraday's law (Ahmad, 2006), given in Eq. 15, and describe the evolution of the C_k concentration of the species involved in the electrochemical reactions in a function of time.

$$\frac{dC_k}{dt} = \pm \frac{i_{corr}}{nFV} \quad (15)$$

n represents the valence number; it equals 2 for reaction 1 and 1 for reaction 2. F is Faraday's number, which equals 96,490 C/mol. i_{corr} represents the corrosion current, while V constitutes the volume of the electrolyte.

Table 2. Adopted scheme of the possible reactions occurring inside an O_2/H_2O collapsing bubble (Yasui, 1997).

M is the third body. A_i is expressed in ($m^3/mol.s$) for two body reaction ($m^6/mol^2.s$) for a three-body reaction.

i	Reaction i	A_i	b_i	E_i/R_g (K)	ΔH_i (kJ/mol)
1	$H + O_2 \Rightarrow O + \bullet OH$	1.92×10^8	0	8270	69,17
2	$O + H_2 \Rightarrow H\bullet + \bullet OH$	5.08×10^{-2}	2.67	3166	8,23
3	$\bullet OH + H_2 \Rightarrow H\bullet + H_2O$	2.18×10^2	1.51	1726	-64,35
4	$\bullet OH + \bullet OH \Rightarrow H_2O + O$	2.1×10^2	1.4	200	-72,59
5	$H_2 + M \Rightarrow H\bullet + H\bullet + M$; Coef. H_2 : 2.5, H_2O : 16.0	4.58×10^{13}	-1.4	52500	444,47
6	$O + O + M \Rightarrow O_2 + M$; Coef. H_2 : 2.5, H_2O : 16.0	6.17×10^3	-0.5	0	-505,4
7	$O + H\bullet + M \Rightarrow \bullet OH + M$; Coef. H_2O : 5.0	4.72×10^5	-1.0	0	-436,23
8	$H\bullet + \bullet OH + M \Rightarrow H_2O + M$; Coef. H_2 : 2.5, H_2O : 16.0	2.25×10^{10}	-2.0	0	-508,82
9	$H\bullet + O_2 + M \Rightarrow HO_2\bullet + M$; Coef. H_2 : 2.5, H_2O : 16.0	2.00×10^3	0	-500	-204,8
10	$H\bullet + HO_2\bullet \Rightarrow O_2 + H_2$	6.63×10^7	0	1070	-239,67
11	$H\bullet + HO_2\bullet \Rightarrow \bullet OH + \bullet OH$	1.69×10^8	0	440	-162,26
12	$O + HO_2\bullet \Rightarrow O_2 + \bullet OH$	1.81×10^7	0	-200	-231,85
13	$\bullet OH + HO_2\bullet \Rightarrow O_2 + H_2O$	1.45×10^{10}	-1.0	0	-304,44
14	$HO_2\bullet + HO_2\bullet \Rightarrow O_2 + H_2O_2$	3.0×10^6	0	700	-175,35
15	$H_2O_2 + M \Rightarrow \bullet OH + \bullet OH + M$; Coef. H_2 : 2.5, H_2O : 16.0	1.2×10^{11}	0	22900	217,89
16	$H_2O_2 + H\bullet \Rightarrow H_2O + \bullet OH$	3.2×10^8	0	4510	-290,93
17	$H_2O_2 + H\bullet \Rightarrow H_2 + HO_2\bullet$	4.82×10^7	0	4000	-64,32
18	$H_2O_2 + O \Rightarrow \bullet OH + HO_2\bullet$	9.55	2	2000	-56,08
19	$H_2O_2 + \bullet OH \Rightarrow H_2O + HO_2\bullet$	1.00×10^7	0	900	-128,67
20	$O_3 + M \Rightarrow O_2 + O + M$; Coef. O_2 : 1.64; Coef. O_2 : 1.63, H_2O : 15	2.48×10^8	0	11430	109,27
21	$O_3 + O \Rightarrow O_2 + O_2$	5.2×10^6	0	2090	-396,14
22	$O_3 + \bullet OH \Rightarrow O_2 + HO_2\bullet$	7.8×10^5	0	960	-164,92
23	$O_3 + HO_2\bullet \Rightarrow O_2 + O_2 + \bullet OH$	1×10^5	0	1410	-121,92
24	$O_3 + H\bullet \Rightarrow HO_2\bullet + O$	9×10^6	0.5	2010	-135,65
25	$O_3 + H\bullet \Rightarrow O_2 + \bullet OH$	1.6×10^7	0	0	-96,2
26	$O + \bullet OH \Rightarrow H + O_2$	7.18×10^5	0.36	-342	-69,17
27	$H\bullet + \bullet OH \Rightarrow O + H_2$	2.64×10^{-2}	2.65	2245	-8,23
28	$H\bullet + H_2O \Rightarrow \bullet OH + H_2$	1.02×10^3	1.51	9370	64,35
29	$H_2O + O \Rightarrow \bullet OH + \bullet OH$	2.21×10^3	1.4	8368	72,59
30	$H\bullet + H\bullet + M \Rightarrow H_2 + M$; Coef. H_2 : 2.5, H_2O : 16.0	2.45×10^8	-1.78	480	-444,47
31	$O_2 + M \Rightarrow O + O + M$; Coef. H_2 : 2.5, H_2O : 16.0	1.58×10^{11}	-0.5	59472	505,4
32	$\bullet OH + M \Rightarrow O + H\bullet + M$; Coef. H_2O : 5.0	4.66×10^{11}	-0.65	51200	436,23
33	$H_2O + M \Rightarrow H\bullet + \bullet OH + M$; Coef. H_2 : 2.5, H_2O : 16.0	1.96×10^{16}	-1.62	59700	508,82
34	$HO_2\bullet + M \Rightarrow H\bullet + O_2 + M$; Coef. H_2 : 2.5, H_2O : 16.0	2.46×10^9	0	24300	204,8
35	$O_2 + H_2 \Rightarrow H\bullet + HO_2\bullet$	2.19×10^7	0.28	28390	239,67
36	$\bullet OH + \bullet OH \Rightarrow H\bullet + HO_2\bullet$	1.08×10^5	0.61	18230	162,26
37	$O_2 + \bullet OH \Rightarrow O + HO_2\bullet$	3.1×10^6	0.26	26083	231,85
38	$O_2 + H_2O \Rightarrow \bullet OH + HO_2\bullet$	2.18×10^{10}	-0.72	34813	304,44
39	$O_2 + H_2O_2 \Rightarrow HO_2\bullet + HO_2\bullet$	4.53×10^8	-0.39	19700	175,35
40	$\bullet OH + \bullet OH + M \Rightarrow H_2O_2 + M$; Coef. H_2 : 2.5, H_2O : 16.0	9.0×10^{-1}	0.90	-3050	-217,89
41	$H_2O + \bullet OH \Rightarrow H_2O_2 + H\bullet$	1.14×10^3	1.36	38180	290,93
42	$H_2 + HO_2\bullet \Rightarrow H_2O_2 + H\bullet$	1.41×10^5	0.66	12320	64,32
43	$\bullet OH + HO_2\bullet \Rightarrow H_2O_2 + O$	4.62×10^{-3}	2.75	9277	56,08
44	$H_2O + HO_2\bullet \Rightarrow H_2O_2 + \bullet OH$	2.8×10^7	0	16500	128,67
45	$O_2 + O + M \Rightarrow O_3 + M$; Coef. O_2 : 1.64; Coef. O_2 : 1.63, H_2O : 15	4.1	0	-1057	-109,27

Table 3. Electrochemical and chemical scheme of the possible reactions occurring at the electrodes and in the electrolyte by the Sono-Galvano Fenton-based processes. k_i is the absolute reaction constant of the i^{th} reaction. Adapted from Bray (1931) and Koprivanac & Lonč (2006) and De Laat & Le 2006 and Machulek et al. (2009).

	i	i^{th} Reaction	k_i	Unit of k_i
Anode	1	$\text{Fe} \rightarrow \text{Fe}^{2+} + 2\text{e}^-$	-	-
Cathode	2	$2\text{H}^+ + 2\text{e}^- \rightarrow \text{H}_2$	-	-
	3	$\text{Fe}^{2+} + \text{H}_2\text{O}_2 \rightarrow \text{Fe}^{3+} + \text{OH}^- + \text{HO}^\bullet$	6.3×10^{-2}	$\text{mol}^{-1} \cdot \text{m}^3 \cdot \text{s}^{-1}$
	4	$\text{Fe}^{3+} + \text{H}_2\text{O}_2 \rightarrow \text{Fe}(\text{HO}_2)^{2+} + \text{H}^+$	3.1×10^4	$\text{mol}^{-1} \cdot \text{m}^3 \cdot \text{s}^{-1}$
	5	$\text{Fe}(\text{HO}_2)^{2+} + \text{H}^+ \rightarrow \text{Fe}^{3+} + \text{H}_2\text{O}_2$	1.0×10^7	$\text{mol}^{-1} \cdot \text{m}^3 \cdot \text{s}^{-1}$
	6	$\text{Fe}(\text{HO}_2)^{2+} \rightarrow \text{Fe}^{2+} + \text{HO}_2^\bullet$	2.3×10^{-3}	s^{-1}
	7	$\text{H}_2\text{O}_2 + \text{HO}^\bullet \rightarrow \text{HO}_2^\bullet + \text{H}_2\text{O}$	3.3×10^4	$\text{mol}^{-1} \cdot \text{m}^3 \cdot \text{s}^{-1}$
	8	$\text{HO}_2^\bullet \rightarrow \text{O}_2^{\bullet-} + \text{H}^+$	1.58×10^5	s^{-1}
	9	$\text{O}_2^{\bullet-} + \text{H}^+ \rightarrow \text{HO}_2^\bullet$	1.0×10^7	$\text{mol}^{-1} \cdot \text{m}^3 \cdot \text{s}^{-1}$
	10	$\text{Fe}^{2+} + \text{HO}^\bullet \rightarrow \text{Fe}^{3+} + \text{OH}^-$	3.2×10^5	$\text{mol}^{-1} \cdot \text{m}^3 \cdot \text{s}^{-1}$
	11	$\text{HO}_2^\bullet + \text{Fe}^{2+} + \text{H}_2\text{O} \rightarrow \text{Fe}^{3+} + \text{H}_2\text{O}_2 + \text{OH}^-$	1.2×10^3	$\text{mol}^{-1} \cdot \text{m}^3 \cdot \text{s}^{-1}$
	12	$\text{HO}_2^\bullet + \text{Fe}^{3+} \rightarrow \text{Fe}^{2+} + \text{H}^+ + \text{O}_2$	3.6×10^2	$\text{mol}^{-1} \cdot \text{m}^3 \cdot \text{s}^{-1}$
	13	$\text{O}_2^{\bullet-} + \text{Fe}^{2+} + 2\text{H}_2\text{O} \rightarrow \text{Fe}^{3+} + \text{H}_2\text{O}_2 + 2\text{OH}^-$	1.0×10^4	$\text{mol}^{-1} \cdot \text{m}^3 \cdot \text{s}^{-1}$
	14	$\text{O}_2^{\bullet-} + \text{Fe}^{3+} \rightarrow \text{Fe}^{2+} + \text{O}_2$	5.0×10^4	$\text{mol}^{-1} \cdot \text{m}^3 \cdot \text{s}^{-1}$
	15	$\text{HO}^\bullet + \text{HO}^\bullet \rightarrow \text{H}_2\text{O}_2$	5.2×10^6	$\text{mol}^{-1} \cdot \text{m}^3 \cdot \text{s}^{-1}$
	16	$\text{HO}_2^\bullet + \text{HO}_2^\bullet \rightarrow \text{H}_2\text{O}_2 + \text{O}_2$	8.3×10^2	$\text{mol}^{-1} \cdot \text{m}^3 \cdot \text{s}^{-1}$
	17	$\text{O}_2^{\bullet-} + \text{H}^+ \rightarrow \text{HO}_2^\bullet$	1.0×10^7	$\text{mol}^{-1} \cdot \text{m}^3 \cdot \text{s}^{-1}$
	18	$\text{HO}^\bullet + \text{HO}_2^\bullet \rightarrow \text{O}_2 + \text{H}_2\text{O}$	7.1×10^6	$\text{mol}^{-1} \cdot \text{m}^3 \cdot \text{s}^{-1}$
	19	$\text{HO}^\bullet + \text{O}_2^{\bullet-} \rightarrow \text{O}_2 + \text{OH}^-$	1.01×10^7	$\text{mol}^{-1} \cdot \text{m}^3 \cdot \text{s}^{-1}$
Electrolyte	20	$\text{HO}_2^\bullet + \text{O}_2^{\bullet-} + \text{H}_2\text{O} \rightarrow \text{H}_2\text{O}_2 + \text{O}_2 + \text{OH}^-$	9.7×10^4	$\text{mol}^{-1} \cdot \text{m}^3 \cdot \text{s}^{-1}$
	21	$\text{HO}_2^\bullet + \text{H}_2\text{O}_2 \rightarrow \text{O}_2 + \text{HO}^\bullet + \text{H}_2\text{O}$	5.0×10^{-4}	$\text{mol}^{-1} \cdot \text{m}^3 \cdot \text{s}^{-1}$
	22	$\text{O}_2^{\bullet-} + \text{H}_2\text{O}_2 \rightarrow \text{O}_2 + \text{HO}^\bullet + \text{OH}^-$	1.3×10^{-4}	$\text{mol}^{-1} \cdot \text{m}^3 \cdot \text{s}^{-1}$
	23	$\text{Fe}^{2+} + \text{SO}_4^{2-} \rightarrow \text{FeSO}_4$	2.29×10^8	$\text{mol}^{-1} \cdot \text{m}^3 \cdot \text{s}^{-1}$
	24	$\text{SO}_4^{2-} + \text{HO}^\bullet \rightarrow \text{SO}_4^{\bullet-} + \text{OH}^-$	1.4×10^4	$\text{mol}^{-1} \cdot \text{m}^3 \cdot \text{s}^{-1}$
	25	$\text{HSO}_4^- + \text{HO}^\bullet \rightarrow \text{SO}_4^{\bullet-} + \text{H}_2\text{O}$	3.5×10^2	$\text{mol}^{-1} \cdot \text{m}^3 \cdot \text{s}^{-1}$
	26	$\text{SO}_4^{\bullet-} + \text{H}_2\text{O} \rightarrow \text{H}^+ + \text{SO}_4^{2-} + \text{HO}^\bullet$	3.0×10^5	s^{-1}
	27	$\text{SO}_4^{\bullet-} + \text{OH}^- \rightarrow \text{SO}_4^{2-} + \text{HO}^\bullet$	1.4×10^4	$\text{mol}^{-1} \cdot \text{m}^3 \cdot \text{s}^{-1}$
	28	$\text{SO}_4^{\bullet-} + \text{H}_2\text{O}_2 \rightarrow \text{SO}_4^{2-} + \text{H}^+ + \text{HO}_2^\bullet$	1.2×10^4	$\text{mol}^{-1} \cdot \text{m}^3 \cdot \text{s}^{-1}$
	29	$\text{SO}_4^{\bullet-} + \text{HO}_2^\bullet \rightarrow \text{SO}_4^{2-} + \text{H}^+ + \text{O}_2$	3.5×10^6	$\text{mol}^{-1} \cdot \text{m}^3 \cdot \text{s}^{-1}$
	30	$\text{SO}_4^{\bullet-} + \text{Fe}^{2+} \rightarrow \text{Fe}^{3+} + \text{SO}_4^{2-}$	3.0×10^5	$\text{mol}^{-1} \cdot \text{m}^3 \cdot \text{s}^{-1}$
	31	$\text{FeSO}_4 \rightarrow \text{Fe}^{2+} + \text{SO}_4^{2-}$	1.0×10^{10}	s^{-1}
	32	$\text{Fe}^{3+} + \text{H}_2\text{O} \rightarrow \text{FeOH}^{2+} + \text{H}^+$	2.9×10^7	s^{-1}
	33	$\text{FeOH}^{2+} + \text{H}^+ \rightarrow \text{Fe}^{3+} + \text{H}_2\text{O}$	1.0×10^7	$\text{mol}^{-1} \cdot \text{m}^3 \cdot \text{s}^{-1}$
	34	$\text{FeOH}^{2+} + \text{H}_2\text{O}_2 \rightarrow \text{Fe}(\text{OH})\text{HO}_2^+ + \text{H}^+$	2.0×10^3	$\text{mol}^{-1} \cdot \text{m}^3 \cdot \text{s}^{-1}$
	35	$\text{Fe}(\text{OH})\text{HO}_2^+ + \text{H}^+ \rightarrow \text{FeOH}^{2+} + \text{H}_2\text{O}_2$	1.0×10^7	$\text{mol}^{-1} \cdot \text{m}^3 \cdot \text{s}^{-1}$
	36	$\text{Fe}(\text{OH})\text{HO}_2^+ \rightarrow \text{Fe}^{2+} + \text{HO}_2^\bullet + \text{OH}^-$	2.3×10^{-3}	s^{-1}

Each reaction from the previous Table can be schematized according to Eq.16.

$$\sum_{k=1}^K v'_{ki} X_k \rightarrow \sum_{k=1}^K v''_{ki} X_k \quad (16)$$

v'_{ki} is the stoichiometric coefficient related to the k^{th} species X_k within the i^{th} chemical reaction. The kinetics rate related to the i^{th} reaction is expressed as reported in Eq.17.

$$r_i = k_i \prod_{k=1}^K [\text{C}_k]^{\theta'_{ki}} \quad (171)$$

k_i is the kinetic constant related to the i^{th} reaction occurring in the electrolyte among the 36 reactions reported in Table 3 and is determined at the operating temperature of 25 °C in the present study.

The kinetics of apparition and the disappearance of a species X_k in the electrolyte is governed by Eq.18 for species involved in the electrochemical reactions:

$$\frac{d[X_k]}{dt} = \pm \frac{1}{nV} \frac{i_{corr}}{F} + \sum_{i=1}^N (v''_{ki} - v'_{ki}) k_i \prod_{j=1}^K [X_j]^{\theta'_{ji}} \quad (18)$$

Eq.19 is applicable to species that are only implicated in the electrolytic reactions (Davis & Davis, 2003).

$$\frac{d[X_k]}{dt} = \sum_{i=1}^N (v''_{ki} - v'_{ki}) k_i \prod_{j=1}^K [X_j]^{\theta'_{ji}} \quad (19)$$

Eq.18 is particularly expressed for hydrogen peroxide as follows, considering the kinetics of production through sonochemistry:

$$\frac{d[H_2O_2]}{dt} = k_0 + \sum_{i=1}^N (v''_{ki} - v'_{ki}) k_i \prod_{j=1}^K [X_j]^{\theta'_{ji}} \quad (20)$$

The system of non-linear differential equations related to sonochemistry, on one hand, and Sono-Galvano-Fenton, on the other hand, is resolved using the fourth-order Runge–Kutta algorithm on Matlab with a fixed step of 1 s. The simulation is performed over 1200 s.

Results and Discussion

Hydrogen Peroxide Production at Single Bubble Scale

The performed simulations of the sonochemical process under oxygen atmosphere considering the configuration described earlier result in the molar yields of hydrogen peroxide produced at the single bubble scale as shown in Fig.2. The figure demonstrates that the lower the frequency, the higher the yield of sonochemical hydrogen peroxide. This is in good agreement with the fact that harsher conditions of temperature and pressure are retrieved when lower acoustic frequencies are used in sonication within the ultrasonic range. Higher temperature and pressure are probably responsible of the activation of the sonochemical mechanism inside the bubble. Nonetheless, the sonochemical production at the reactor scale should consider the number density of bubbles, which is a parameter that is highly influenced by the acoustic frequency. This will be verified in the following figure.

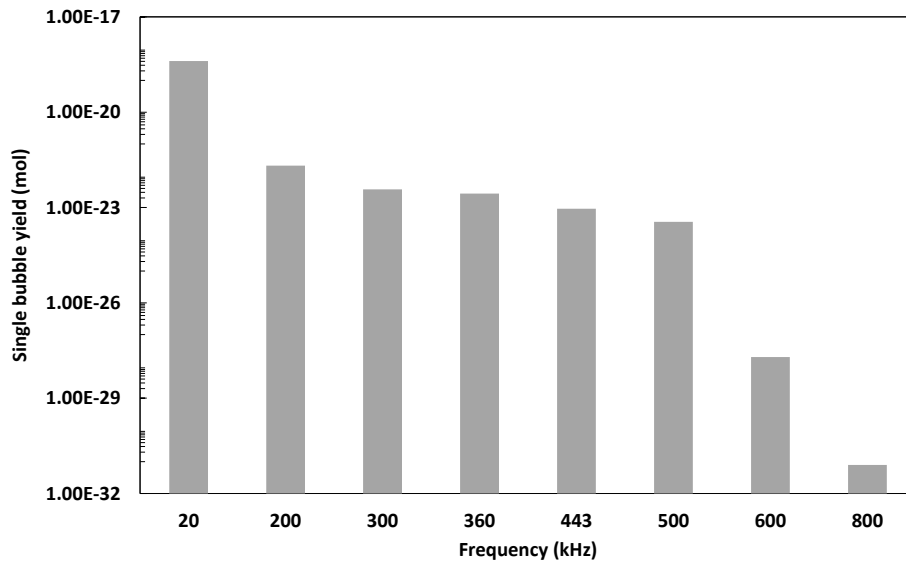


Figure 2. Evolution of H_2O_2 molar yield at single bubble scale as a function of the acoustic frequency under oxygen atmosphere, 1.5 atm of amplitude and within 50 μ s of sonication.

Hydrogen Peroxide Production at Reactor Scale

Fig. 3 shows the molar yields of hydrogen peroxide produced sonochemically within a reactional volume of 1 dm^3 . The introduction of the number density of bubbles according to Eq.13 completely changes the trend shown previously in Fig. 3. The production at the reactor scale demonstrates a quite stable value for frequencies comprised between 200 and 500 kHz, with a maximum achieved at 200 kHz, of $1.59 \times 10^{-15} \text{ mol/dm}^3$ attained in $50 \mu\text{s}$. This leads to a production rate of $0.0318 \mu\text{mol/s.m}^3$ in the electrolyte. This value will be used in the zero-order kinetics adopted for the macroscopic sonochemical production of hydrogen peroxide. It is worthy to mention that 200 kHz has been selected as the optimal frequency for sonication not only as it leads to maximum production of hydrogen peroxide, but also to take benefit of the relatively low frequency role in physical effects, contributing to mixing and transport phenomena.

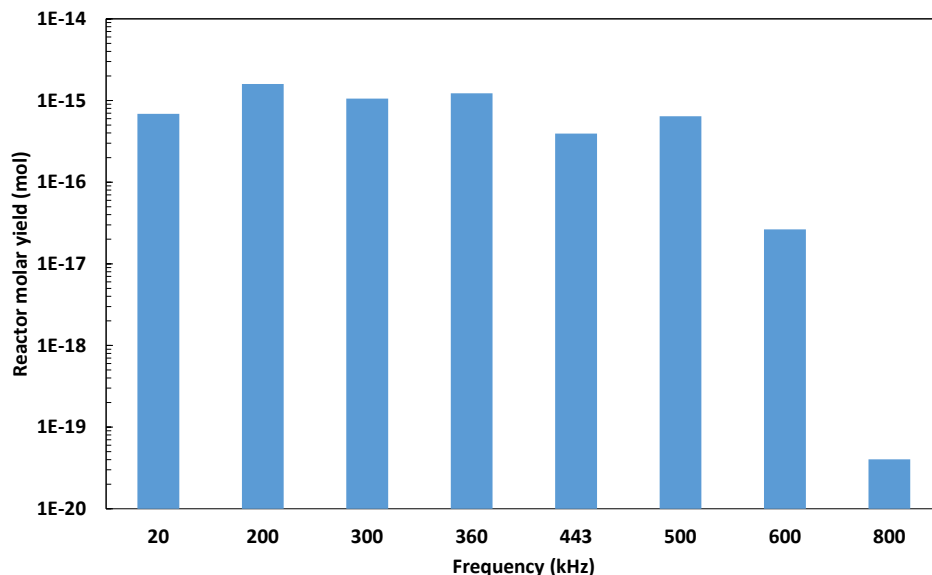


Figure 3. Evolution of H_2O_2 molar yield at reactor scale of a volume of 1 dm^3 as a function of the acoustic frequency under oxygen atmosphere, 1.5 atm of amplitude and within $50 \mu\text{s}$ of sonication.

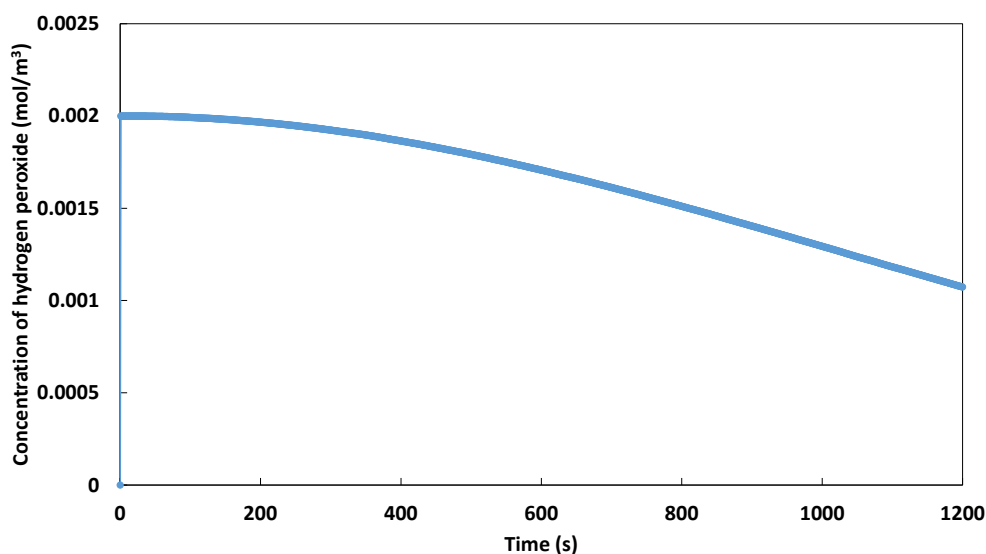


Figure 4. Evolution of the concentration of hydrogen peroxide in the electrolyte

Integrated Sono-Galvano-Fenton Process

The kinetics of hydrogen peroxide in the integrated process is investigated considering the sonochemical production rate mentioned in the previous paragraph. Fig.4 reports the evolution of the concentration of

hydrogen peroxide taking into account all the reactions that involve it, i.e., the sonochemical reactions mentioned in Table.2 and the electrolytic reactions mentioned in Table.3. Within 1200 s of operation, the concentration of hydrogen peroxide passes from 0.002 mol/m³ to 0.0011 mol/m³, with a negative exponential trend.

Hydrogen peroxide is implicated in the main Fenton reaction, where it decomposes to hydroxyl radicals in the presence of ferrous ions provided by the Galvano-Fenton process. The evolution of the concentration of hydroxyl radical coming from the integrated Sono-Galvano-Fenton process is reported in Fig.5, the evolution of the concentration of the same radical induced by the sonochemical process is also reported in the same figure.

Surprisingly, the sonochemical process is able to provide 10⁵ folds higher yield of hydroxyl radical, while producing the Fenton reagent to the Sono-Galvano-Fenton process. This makes evidence for an upscaled configuration of the Sono-Galvano-Fenton process based on the multiplication of the number of galvanic cells to put in the process (scaling out), while maintaining the configuration of the sonochemical process integrated to the parallel galvanic cells.

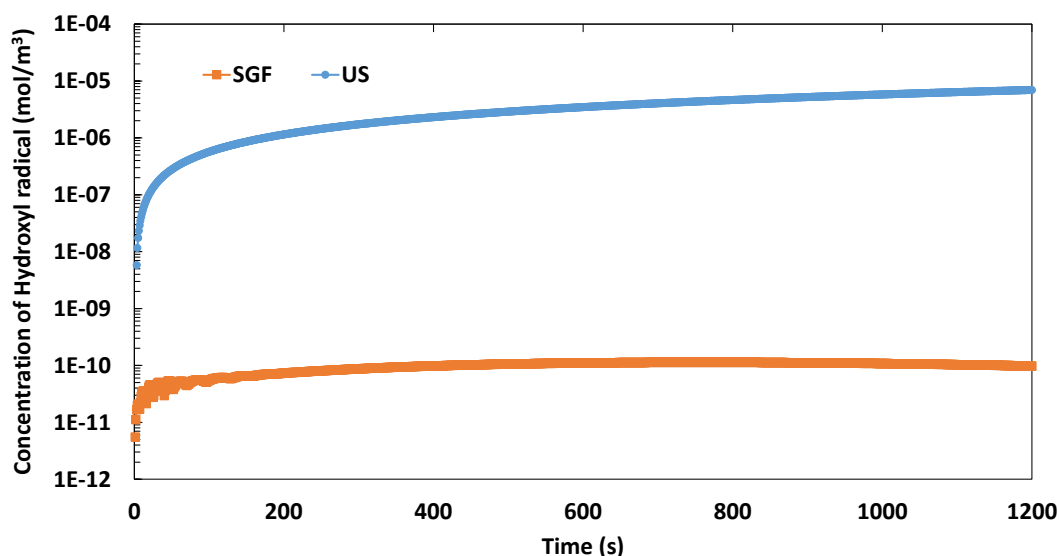


Figure 5. Evolution of the concentration of hydroxyl radical within the integrated Sono-Galvano-Fenton reactor

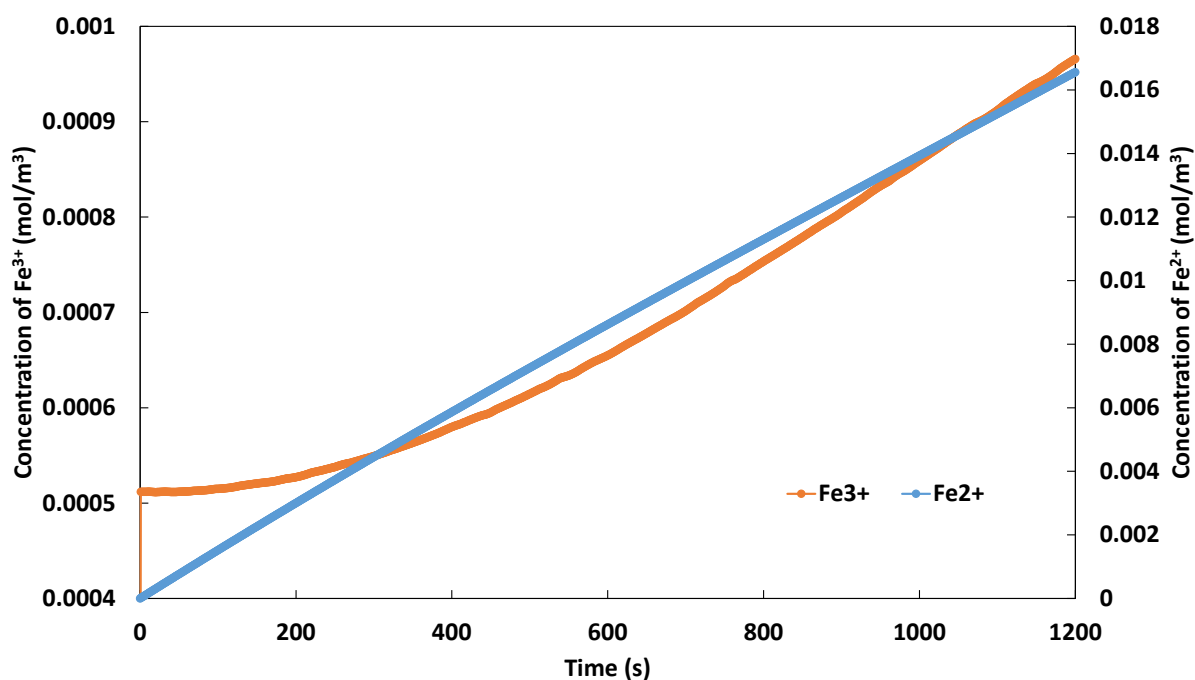


Figure 6. Evolution of the concentration of ferric and ferrous ions during the Sono-Galvano-Fenton operation

We suggest in the following to evaluate the kinetics of ferrous and ferric ions in the electrolyte during the operation of the Sono-Galvano-Fenton process. Fig.6 shows the evolution of the concentrations of both ions as function of time. We notice that the evolution of ferrous ions is quasi-linear, starting from zero at the initial time, since no catalyst is added to the electrolyte.

The linear trend is well justified by the Faraday's law, governing the spontaneous corrosion of iron waste under the potential induced by the copper cathode. Simultaneously, ferric ions produced by the reaction of hydrogen peroxide and ferrous ions, but also responsible of the regeneration of ferrous ions (the catalyst) through reactions 4, 5 and 6 reported in Table. 3, show a quite different curve of evolution in function of time. Ferric ions are produced rapidly at the initial time, then evolve exponentially due to the simultaneous production and consumption in the regeneration reaction, with the upper hand to the production reaction. The regeneration reactions are indeed known to be slow (I. Gasmi et al. 2020; Intissar Gasmi et al. 2021), and consequently, the source of ferrous ions should provide continuously sufficient yield of catalyst to maintain a high reactional rate of Fenton mechanism.

Secondary Physical Effects of Ultrasounds

In this last section, we propose to investigate the secondary role of ultrasounds in the integrated process, namely the possible physical effects inducing the enhancement of the mixing and transport phenomena in the electrolyte, particularly through shockwaves and microjets. The microscopic powers associated to the microjet and shockwave emitted by the bubble around the collapse have been assessed and their evolution during this time slot is reported in Fig.7.

The figure shows that the time intervals preceding and following immediately the instant of harsh collapse are characterized by a high power related to microjet, while the instant of harsh collapse exhibits a maximum power related to shockwave, both of them are in the order of magnitude of 1 W. Hence, the sonication at 200 kHz has obviously a chemical role demonstrated through the production of hydroxyl radicals and hydrogen peroxide as a feedstock for Fenton reaction, but may also play a physical role by improving the transport phenomena and mixing of the electrolyte and consequently enhancing the corrosion current. This track will be the subject of upcoming studies of our research group.

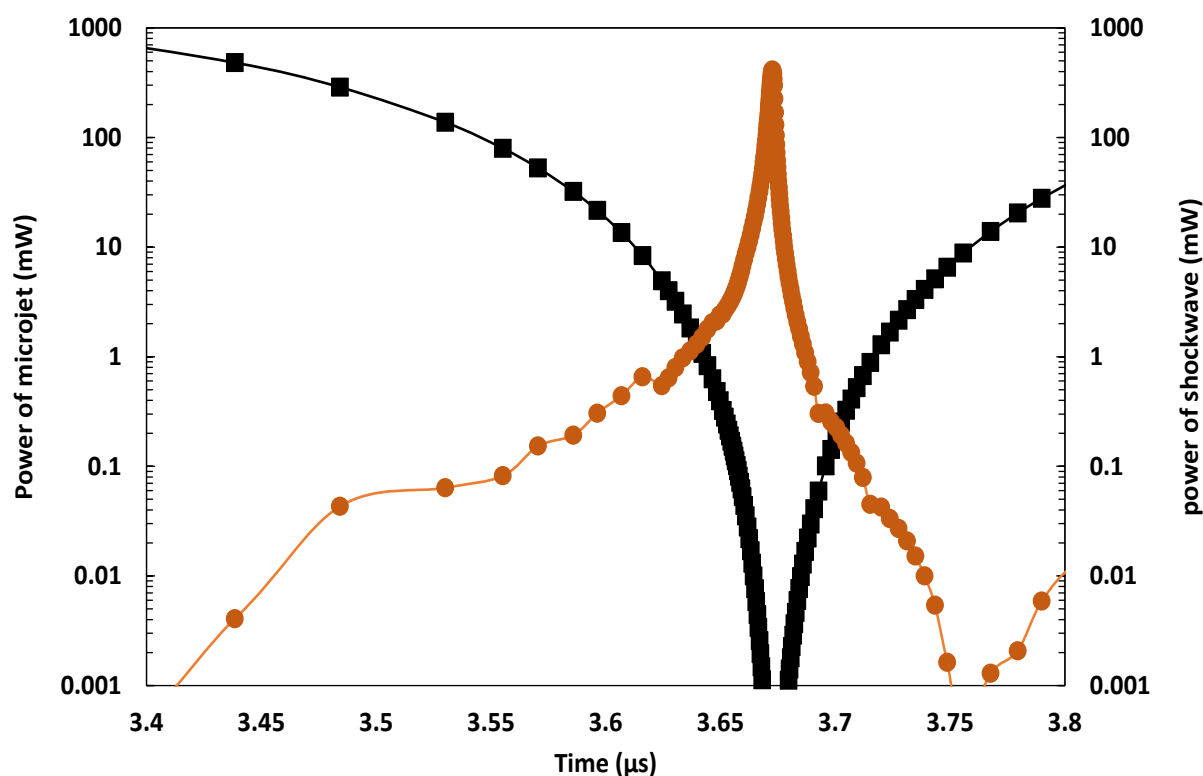


Figure 7. Powers associated with the secondary physical effects of the acoustic cavitation bubble around its collapse (microjet in black and shockwave in orange)

Conclusion

The investigation of the isolated sonochemical effect at single bubble scale demonstrated that the lower the frequency, the higher the yield of sonochemical hydrogen peroxide. However, at the reactor scale, 200 kHz has been selected as the optimal frequency for sonication not only as it leads to maximum production of hydrogen peroxide, but also to take benefit of the relatively low frequency role in physical effects, contributing to mixing and transport phenomena.

In the integrated Sono-Galvano-Fenton process, within 1200 s of operation, the concentration of hydrogen peroxide passes from 0.002 mol/m³ to 0.0011 mol/m³, with a negative exponential trend. The investigation of the production of hydroxyl radicals in the integrated process has shown that the sonochemical process is able to provide 10⁵ folds higher yield of hydroxyl radical, while producing the Fenton reagent to the Sono-Galvano-Fenton process. This makes evidence for an upscaled configuration of the Sono-Galvano-Fenton process based on the multiplication of the number of galvanic cells to put in the process (scaling out), while maintaining the configuration of the sonochemical process integrated to the parallel galvanic cells. In terms of ferrous and ferric ions kinetics in the integrated process, the regeneration reactions proved to be slow as demonstrated in several previous studies, and consequently, the source of ferrous ions should provide continuously sufficient yield of catalyst to maintain a high reactional rate of Fenton mechanism.

In terms of the physical effects of mechanical nature, the study at the single bubble scale proved that microjet achieve the highest power values around the collapse instant, while shockwave does at the instant of the harsh collapse with a value of 1 W. The sonication at 200 kHz has obviously a chemical role demonstrated through the production of hydroxyl radicals and hydrogen peroxide as a feedstock for Fenton reaction, but may also play a physical role by improving the transport phenomena and mixing of the electrolyte and consequently enhancing the corrosion current. This track will be the subject of upcoming studies of our research group.

Scientific Ethics Declaration

The author declares that the scientific ethical and legal responsibility of this article published in EPSTEM journal belongs to the author.

Acknowledgements or Notes

* This article was presented as an oral presentation at the International Conference on Technology (www.icontechno.net) held in Antalya/Turkey on November 16-19, 2023.

*This work was financially supported by the National Direction for Research and Technological Development DGRSDT, Algeria, in the frame of the “PISE” project entitled “GreEnAREA”, supported by the mixed team of research “PVA” and affiliated to the National Higher School of Technology and Engineering.

References

- Ahmad, Z.(2006). Corrosion kinetics. In B. T. Zaki (Ed.), *Principles of Corrosion Engineering and Corrosion Control Ahmad* (pp.57-119). Oxford: Butterworth-Heinemann.
- Atchley, A. A. (1989). The Blake threshold of a cavitation nucleus having a radius-dependent surface tension.” *The Journal of the Acoustical Society of America*, 85(1), 152–57.
- Authier, O., Ouhabaz, H., & Bedogni, S.(2018). Modeling of sonochemistry in water in the presence of dissolved carbon dioxide. *Ultrasonics Sonochemistry*, 45,17–28.
- Barbusinski, K. (2009). Fenton reaction - controversy concerning the chemistry. *Ecological Chemistry and Engineering*, 16(3), 347–358.
- Baulch, D. L., Drysdale, D. D. D., Duxbury, J., & Grant, S. (1972). *Evaluated kinetic data for high temperature reactions* (Vol. 1): *Homogeneous gas phase reactions of the O2–O3 systems, the CO–O2– H2 system, and of sulphur-containing species*.
- Baulch, D. L., Drysdale, D. D. D., Duxbury, J., & Grant, S. (1974). *Evaluated kinetic data for high temperature reactions* (Vol. 2): *Homogeneous gas phase reactions of the O2–O3 systems, the CO–O2– H2 system, and of sulphur-containing species*.

- Baulch, D. L., Drysdale, D. D. D., Duxbury, J., & Grant, S. (1976). *Evaluated kinetic data for high temperature reactions* (Vol. 3): *Homogeneous gas phase reactions of the O₂—O₃ systems, the CO—O₂—H₂ system, and of sulphur-containing species*.
- Bray, W.C. (1931). The mechanism of reactions in aqueous solution examples involving equilibria and steady states. *Chemical Reviews*, 10(1), 161–177.
- Brotchie, A., Grieser, F., & Ashokkumar, M. (2009). Effect of power and frequency on bubble-size distributions in acoustic cavitation. *Physical Review Letters*, 102(8), 1–4.
- Dalodiere, E., Matthieu, V., Philippe, M., & Sergey I. N. (2016). Effect of ultrasonic frequency on H₂O₂ sonochemical formation rate in aqueous nitric acid Solutions in the Presence of Oxygen.” *Ultrasonics Sonochemistry*, 29(2), 198–204.
- Davis, M. E., & Robert, J., & Davis, R. J. (2003). *The basics of reaction kinetics for chemical reaction engineering fundamentals of chemical reaction engineering* (pp.1-52). New York, NY: McGraw Hill. Retrieved from <http://resolver.caltech.edu>.
- De Laat, J., & Le, T.G. (2006). Effects of chloride ions on the iron(III)-catalyzed decomposition of hydrogen peroxide and on the efficiency of the fenton-like oxidation process. *Applied Catalysis B: Environmental*, 66(1–2), 137–146.
- Gasmi, I., Kerboua, K., Haddour, N., & Hamdoui, O. (2020). Kinetic pathways of iron electrode transformations in galvano-fenton process: A mechanistic investigation of in-situ catalyst formation and regeneration. *Journal of the Taiwan Institute of Chemical Engineers*, 116(2020), 1–11.
- Gasmi, I., Kerboua, K., Haddour, N., Hamdoui, O., Alghyamah, A., & Buret, F. (2021). The Galvano-Fenton process: Experimental insights and numerical mechanistic investigation applied to the degradation of acid orange 7. *Electrochimica Acta*, 373.
- He, Y. Z., Mallard, W. G., & Tsang, W. (1988). Kinetics of hydrogen and hydroxyl radical attack. *Journal of Physical Chemistry*, 92(8), 2196–2201.
- Kamath, V., Prosperetti, A., & Egolfopoulos, F. N. (1993). A theoretical study of sonoluminescence. *Journal of the Acoustical Society of America*, 94(1), 248–260.
- Kerboua, K. (2022). Water remediation from recalcitrant pollution using the Galvano-Fenton process: A modeling approach of the hydroxyl radical generation and the energy efficiency. *The Eurasia Proceedings of Science, Technology, Engineering & Mathematics*, 21, 506–516.
- Kerboua, K., & Hamdaoui, O. (2017). Computational study of state equation effect on single acoustic cavitation bubble's phenomenon. *Ultrasonics Sonochemistry*, 38, 174–188.
- Kerboua, K., & Hamdaoui, O. (2018). Ultrasonic waveform upshot on mass variation within single cavitation bubble: Investigation of physical and chemical transformations. *Ultrasonics Sonochemistry*, 42, 508–516.
- Kerboua, K., & Hamdaoui, O. (2019). Void fraction, number density of acoustic cavitation bubbles and acoustic frequency: A numerical investigation. *The Journal of the Acoustical Society of America*, 146(4), 2240–2252.
- Kerboua, K., Hamdaoui, O., Haddour, N., & Alghyamah, A. (2021). Simultaneous Galvanic generation of Fe²⁺ catalyst and spontaneous energy release in the Galvano-Fenton technique: A numerical investigation of Phenol's oxidation and energy production and saving. *Catalysts*, 11(943).
- Koprivanac, N., & Lon, A. (2006). Photo-assisted fenton type processes for the degradation of phenol: A kinetic study. *Journal of Hazardous Materials*, 136, 632–644.
- Langlois, T. R., Changxi, Z., & Doug L. J. (2016). Toward animating water with complex acoustic bubbles. *ACM Transactions on Graphics*, 35(4), 1–13.
- Leighton, T. G. (1994). The acoustic bubble. *The Journal of the Acoustical Society of America*, 96(4).
- Machulek, A., de Moraes, J. E. F., Okano, L.T., & Silverio, C. A. (2009). Photolysis of ferric ions in the presence of sulfate or chloride ions: Implications for the photo-fenton process. *Photochemical & Photobiological Sciences*, 8(7), 985–991.
- Mason, T. J. (1999). Sonochemistry: Current uses and future prospects in the chemical. *Philosophical Transactions of the Royal Society*, 357(1751), 355–369.
- Mason, T. J. (1999). Sonochemistry: Current uses and future prospects in the chemical. *Philosophical Transactions of the Royal Society*, 357(1751), 355–369.
- Minnaert, M. (1933). XVI on musical air-bubbles and the sounds of running water. *The London, Edinburgh, and Dublin Philosophical Magazine and Journal of Science*, 16(104), 235–248.
- Palit, S. (2012). An overview of advanced oxidation process as an effective and visionary environmental engineering procedure to treat dye effluents from textile industries. *IEEE International Conference on Engineering Education: AICERA*, 1–1.
- Yasui, K. (1996). Variation of liquid temperature at bubble wall near the sonoluminescence threshold. *Journal of the Physical Society of Japan*, 65(9), 2830–40.
- Yasui, K. (1997). Alternative model of single bubble sonoluminescence. *Physical review E*, 56(6), 6750–6760.

- Yasui, K. (2002). Influence of ultrasonic frequency on multibubble sonoluminescence. *The Journal of the Acoustical Society of America*, 112(4), 1405–1413.
- Ziembowicz, S., Małgorzata, K., & Koszelnik, P. (2017). Sonochemical formation of hydrogen peroxide. *Proceedings*, 2(5), 188.

Author Information

Kaouthar Kerboua

Department of Process and Energy Engineering,
National Higher School of Technology and Engineering,
23005, Annaba, Algeria
Contact e-mail: k.kerboua@ensti-annaba.dz

To cite this article:

Kerboua, K. (2023). A numerical study of the efficiency of the sono Galvano Fenton process as a tertiary treatment technique for the wastewater reuse in agriculture. *The Eurasia Proceedings of Science, Technology, Engineering & Mathematics (EPSTEM)*, 24, 243-256.

The Eurasia Proceedings of Science, Technology, Engineering & Mathematics (EPSTEM), 2023

Volume 24, Pages 257-262

IConTech 2023: International Conference on Technology

User-Selected Sets of Algorithmic Implementation of Fuzzy Processing Subsystem for Embedded Intelligent Control Systems

Alexei Evgenievich Vassiliev

Saint-Petersburg State Marine Technical University

Htut Shine

Saint-Petersburg State Marine Technical University

Ye Min Htet

Saint-Petersburg State Marine Technical University

Viktoriia Alexeevna Karpenko

Saint-Petersburg State Marine Technical University

Abstract: Embedded intelligent control systems (EICS) have been used in a wide range of tasks involving the adaptive control of technical objects and processes. For the hardware implementation of EICS, developers actively use function-oriented microcontrollers, that aimed to be the effective implementation of control algorithms, including adaptive and intelligent control. Embedded control systems based on the concept of fuzzy set theory have recently been developed for specific individual control operations, allowing more efficient implementation of complex object control algorithms. This paper approaches the study of the different implementation of control algorithms in embedded microcontrollers based on fuzzy sets theory to result in reduced hardware area and complexity, high operating speed, and adaptability to various applicable domains. It shows that the performance of fuzzy computing specialized in embedded systems has significantly increased and makes possible a huge scope for further improvement of the implementation of fuzzy control algorithms at the hardware level.

Keywords: Embedded control system, MCS-51, Control algorithms, Fuzzy sets, Fuzzy computation

Introduction

The embedded control systems based on the methods of fuzzy logic have been extensively used in control engineering, consumer electronics, house hold appliances, data processing, decision making systems, expert and signal processing systems including in the tasks of managing objects of marine engineering (Juuso, 2004). A biggest advantage of the fuzzy logic is the easy modelling of human behaviour; it directly maps the human inference system to the fuzzy *if – then* rules, which are easily understood by the human beings. Just as fuzzy logic can be described simply as “computing with words rather than numbers”, fuzzy control can be described simply “control with sentences rather than equations” (Togai & Watanabe, 1986). The first hardware realization of a fuzzy logic processor was done by Togai and Watanabe. Nowadays the intelligent control systems built on the basic concept of the theory of fuzzy sets, have recently become more popular, allowing more efficiently to implement complex object control algorithms (Fons et al., 2006). It should be noted that current using fuzzy control systems are built for general-purpose computing machines and programmable fuzzy processors designed to store and process fuzzy rules (Evmorfopoulos & Avaritsiotis, 2002). Since the mathematical apparatus of the fuzzy sets is quite varied from the view of different theories, the algorithmic implementations for fuzzy computation processes are much diverse to achieve the user’s desires.

In this paper, we concentrate an analyze in different algorithmic implementations of fuzzy processing subsystem based on a function-oriented microcontroller with bit manipulation through low level language aimed to be the effective implementation of control algorithms, including adaptive and intelligent control. It is possible to increase the productivity of fuzzy information processing processes, which are specialized on MCS-51 that support the integrated implementation of fuzzy control algorithms for embedded intelligent control systems.

Analysis of Structural and Algorithmic Operation in Fuzzy Computation System

The fuzzy computing subsystem solves the problems of adaptive and intelligent control based on the theory of fuzzy sets, forming the values of the ultrasonic setpoints parameters for the control subsystem by generalized information about the state of the control object (Niu et al., 2019). As shown in (Fig.1) the number of input and output variables used triggered terms corresponding to each linguistic variable from the table of fuzzy transformation rules (Fons et al., 2006). Since there is a number of stages in fuzzy computation based on microcontroller, that uses the resources of the main controller processor, which leads to automatic suspension for algorithmic calculations running in the fuzzy subsystem. It should also be noted that, the current existing technical solutions do not provide the possibility of specifying arbitrary membership functions, allowing only their piecewise linear form, which negatively affects the achievable accuracy of calculations. Thus, the problem of improving the performance of embedded intelligent control systems is approached by developing an embedded mathematical apparatus for describing membership terms and rule base, and ensure efficient (in the typical sense of intelligent control) calculation of fuzzy processing subsystem with bit manipulation based on MCS-51. This approach manages to describe the arbitrary form of various membership terms with the higher possible accuracy. The inevitable task for the algorithmic and schematic implementation of fuzzy computing subsystem using in this subjected area of embedded control system will be considered in this paper.

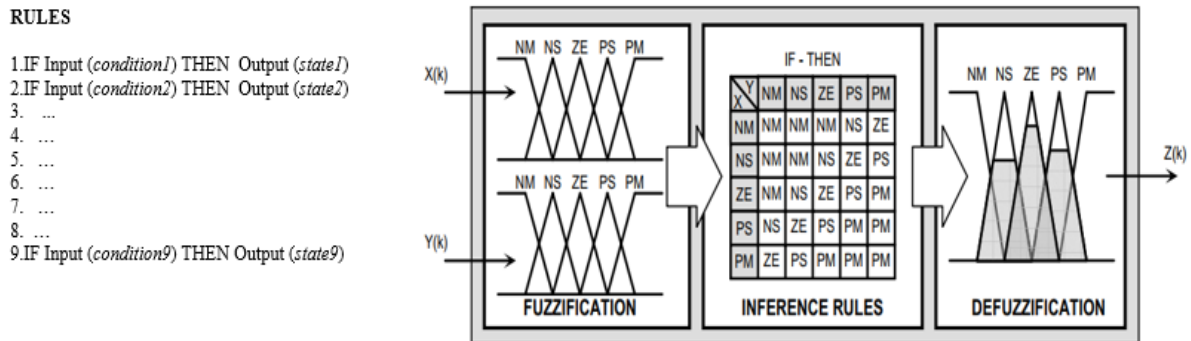


Figure1. General fuzzy computation system (Niu et al., 2019)

Algorithmic Implementation for Improving Fuzzy Computation Performance

According to the improving task mentioned above, we have considered to effectively organize algorithmic structure and memory organization in single chip microcontroller that support efficient fuzzy computation. There are many priorities in developing a new structural organization of fuzzy computing subsystems and the principles of their functioning :1) effective implementation of the proposed high-speed fuzzy data processing algorithm, 2) significant expansion of the variety of hardware-implemented control systems with fuzzy information processing, 3) ensuring a high rate of fuzzy data processing, which is performed in parallel with the execution of the program of the control processor(Vassiliev et al., 2017). Thus, a vital need in developing new algorithms for the functioning fuzzy computation is to develop effective methods to support the execution of fuzzy operations in the sense of minimizing computing time and memory demands. The most common using algorithms for fuzzy information processing include Sugeno, Larsen and Mamdani algorithms (Togai & Watanabe, 1986). The last one has the highest accuracy but it is most demanding on the amount of allocated computing resources (Mamdani, 1974). To implement the most high-speed algorithm proposed in this paper (Fig. 2(a)) uses the method of “look-up tables”, which operates with graphs specified by a set of vector arrays and a rule base specified by a table. In order to assemble compact memory organization, suggest to assign memory locations as in (Fig. 2(b)). The terms are stored as an array of membership degree values, ordered in ascending order by a clear variable. In this case, the range of membership degree values [0...1] is equivalent to the range [0...255]; for example, the value 0.5 will be equivalent to code 128, the value 1 will be 255 (Fig. 3(a)).

When fuzzification and defuzzification performing, the corresponding term array is addressed by the value of the input variable, and return the linguistic value to the term belonging of this variable.

The rule base is set by the table in which number of rows corresponds to the number of rules. Each row consists of “input” and “output” columns (Fig.3(b)). The input columns describe the term numbers of the input variables involved in the formation of the conditions of the rule, and the output columns describe the numbers of outputs calculated if the conditions of this rule are triggered. The input and output cells do not depend each others, and the example rule structure R_5 is presented as follow:

$$\text{IF } (X_2 \in T_{x2r5}) \text{ and } (X_5 \in T_{x5r5}), \text{ THEN } (Y_1 \in T_{y1r5}), \text{ as well } (Y_4 \in T_{y4r5}) \quad (1)$$

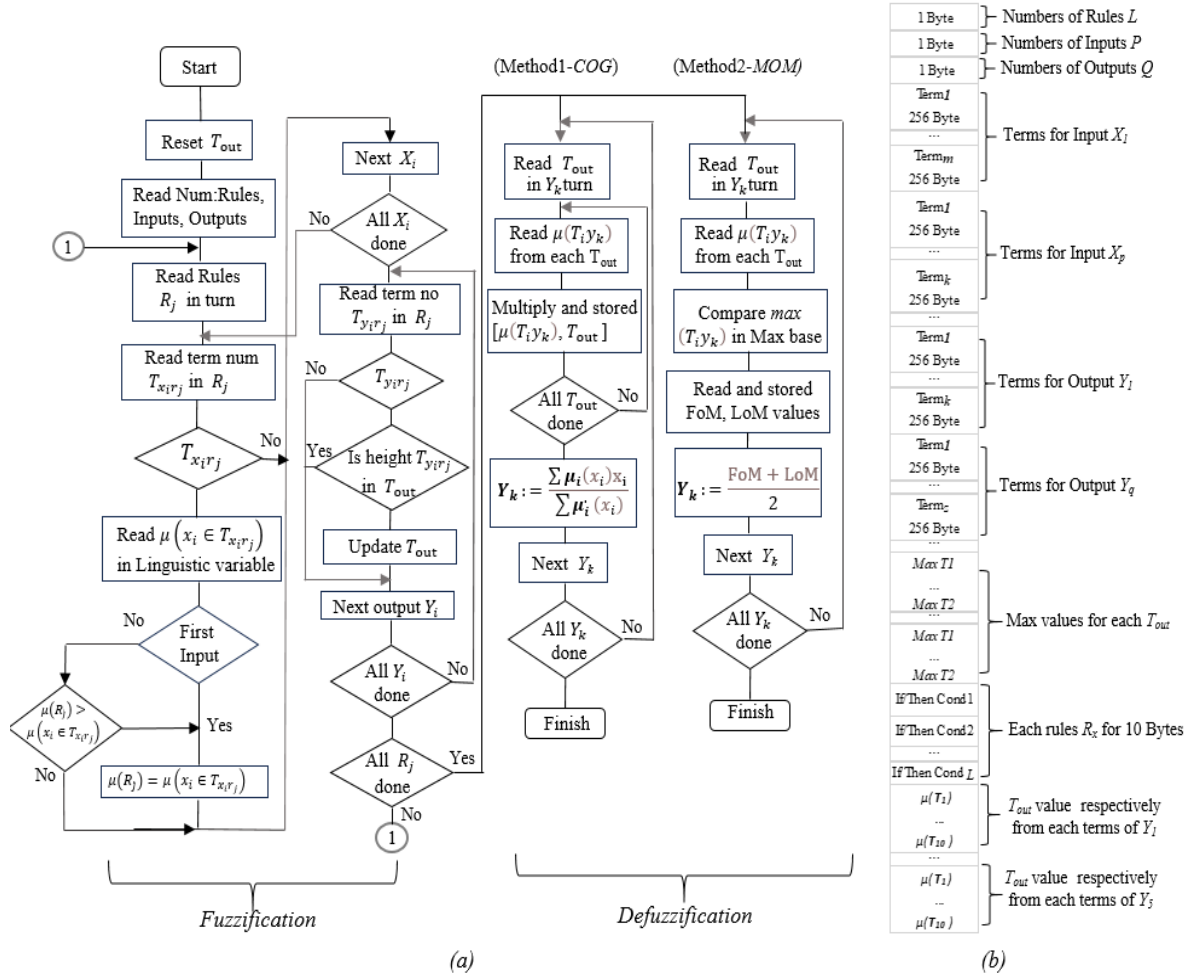


Figure 2. (a) Algorithmic structure of fuzzy computation subsystem, (b) Memory organization for fuzzy computation

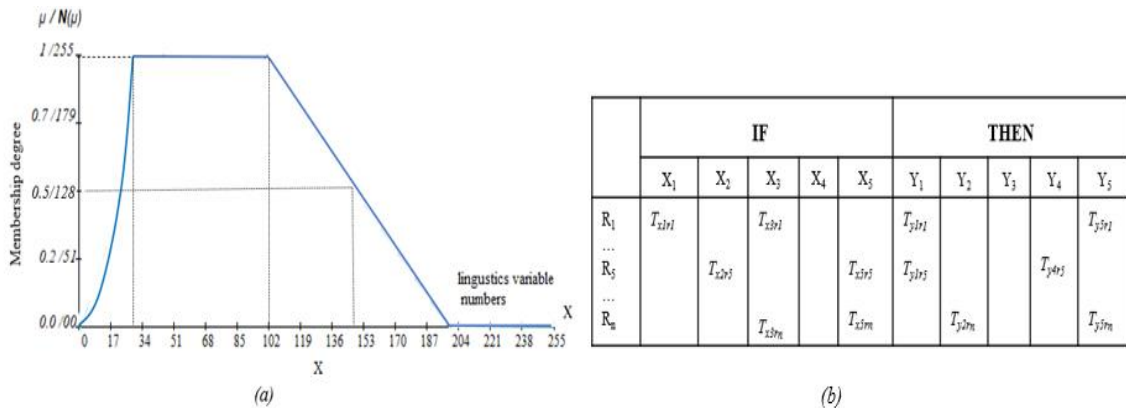


Figure 3. (a) General membership term, (b) Rule base organization

Such a structural organization of the fuzzy knowledge base provides a significant increase in accuracy and productivity compared to previous known solutions, since it allows you to operate with membership functions of an arbitrary type. At the same time, the fuzzification speed does not depend on the type of membership function and is the maximum achievable (since the procedure for calculating the value of the membership function is reduced by indexing a given cell of a one-dimensional array). The absolute values of the performance gain are obviously determined by the use of the algorithmic implementation with selected defuzzification methods. In the proposed implementation, the calculation methods are used the widely used methods “Center of Gravity” and “Middle of Maxima” presented in equations (2) and (3):

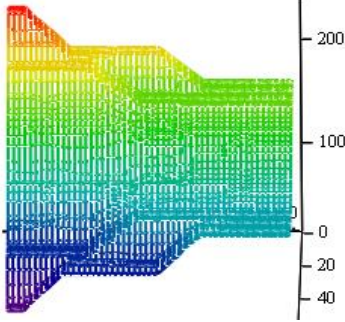
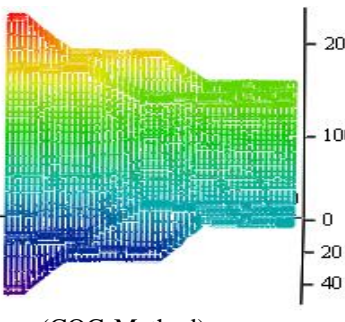
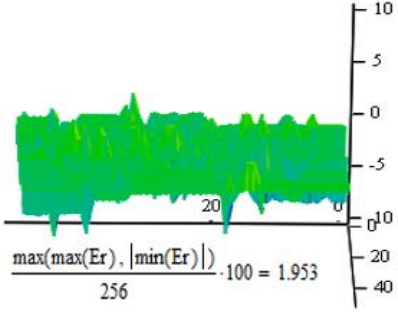
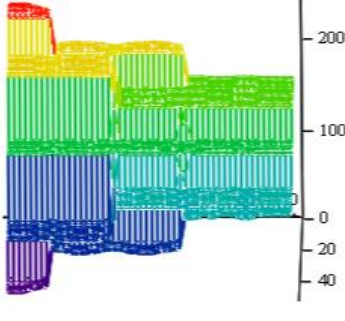
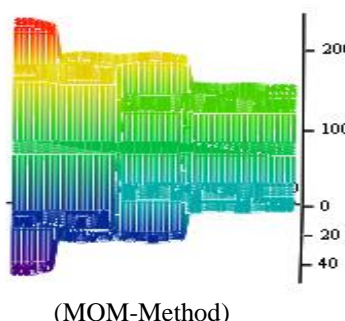
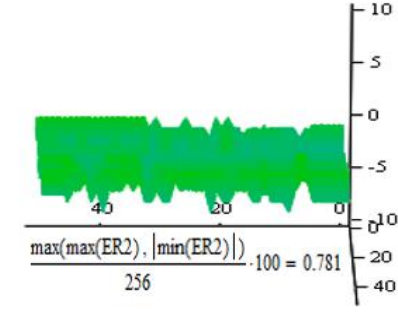
$$Y_k := \frac{\sum \mu_i(x_i)x_i}{\sum \mu_i(x_i)}, i \in 1,2,3,...,k \quad (2)$$

$$Y_k = \frac{\sum_{x \in M} (x_i)}{|M|}, i \in 1,2,3, ..., k \quad (3)$$

Experimental Analysis of Algorithmic Implementation

As Vassiliev et al. (2017) explained, the fuzzy information processing subsystem can be described and calculated in the low-level programming language to approach a simple structure and high speed general-purpose fuzzy logic microcontroller. It is intended to communicate directly with specific hardware/software resources on the MCS-51 device. In this proposed implementation, MCS-51 is set with 12 MHz internal bus frequency for processing up to 25rule base through 2 inputs and 1 outputs properly. The data collections of the statistical results and visual experiments are carried out by means of Mamdani Inference System and Shell51 developed by the author (Vassiliev,2017) of this paper. To analyze the accuracy of the developed fuzzy computation,we represent different algorithmic implementations and compare to corresponding simulation results.

Table 1. Analyze developed fuzzy computation system

Data surface from MATLAB	Results from MCS-51	Differentiation (%)
		 $\frac{\max(\max(ER), \min(ER))}{256} \cdot 100 = 1.953$
(COG-Method)		
		 $\frac{\max(\max(ER2), \min(ER2))}{256} \cdot 100 = 0.781$
(MOM-Method)		

It can be seen from the table that the different implementation results are quite uniform compared to MATLAB data surface simulation. It indicates that the developed information subsystem strategy can be achieved by using

function-oriented microcontroller with bit manipulation through look-up table algorithm based on MCS-51 device. Additionally this analyze shows that developed fuzzy subsystem with low level language harmonically engaged with commercial simulation results without losing the generality of actual processing characteristics. It makes advantage of increasing productivity in certain control system that needs high operating speed and reduced complexity to a compact design.

Conclusion

This paper presents a methodological principals of developing fuzzy computing subsystem that taking into account a clear tradeoff in the development phases of fuzzy coprocessor and the calculation accuracy supported for the low cost and compact implementation design. The developed subsystem with bit manipulation makes possible to meet high speed real time requirements, reducing the intense resource of fuzzy information converters. It has shown that there is a huge scope for further improvement in these fuzzy systems at hardware level to reduce the complexity of analysis and synthesis in co-processor and their performance can be improved further by designing optimized architectures.

Scientific Ethics Declaration

The authors declare that the scientific ethical and legal responsibility of this article published in EPSTEM journal belongs to the authors.

Acknowledgements or Notes

* This article was presented as an oral presentation at the International Conference on Technology (www.icontechno.net) held in Antalya/Turkey on November 16-19, 2023.

References

- Ascia, G., Catania, V., & Russo, M. (1999). VLSI hardware architecture for complex fuzzy systems. *IEEE Transactions on Fuzzy Systems*, 7(5), 553–570.
- Barrett, S. F., & Magleby, D. B. (2004). Embedded systems: Design and applications with the 68HC12 and HCS12. Retrieved from <https://www.amazon.com/Embedded-Systems-Design-Applications>
- Evmorfopoulos, N., & Avaritsiotis, J. (2002). An adaptive digital fuzzy architecture for application-specific integrated circuits. *Active and Passive Electronic Components*, 25(4), 289-306.
- Fons, F., Fons, M., & Cantó, E. (2006). System-on-chip design of a fuzzy logic controller based on dynamically reconfigurable hardware. *International Transactions on Systems Science and Applications*, 2, 191–196. Retirved from <https://dblp.uni-trier.de/db/journals/itssa/itssa2.html>
- Juuso, E. (2004). Integration of intelligent systems in development of smart adaptive systems. *International Journal of Approximate Reasoning*, 35(3), 307–337.
- Gabrielli, A., & Gandolfi, E. (1999). A fast digital fuzzy processor. *IEEE Micro*, 19(1), 68–79.
- Johnson, J., Madhumitha, G., Yousuf, N., & Harikrishnan, S. (2016). Design, development and fuzzy logic based control of a remotely operated underwater vehicle. *International Conference on Robotics and Automation for Humanitarian Applications (RAHA)*.
- Kandel, A., & Langholz, G. (1997). *Fuzzy hardware: Architectures and applications*. In Kluwer Academic Publishers eBooks. Retrieved from <http://ci.nii.ac.jp/ncid>
- Lee, C. (1990). Fuzzy logic in control systems: fuzzy logic controller. I. *IEEE Transactions on Systems, Man, and Cybernetics*, 20(2), 404–418.
- Mamdani, E. (1974). Application of fuzzy algorithms for control of simple dynamic plant. *Proceedings of the Institution of Electrical Engineers*, 121(12), 1585.
- Minghui, W., Yongquan, Y., & Bi, Z. (2005). Ship steering system based on fuzzy control using real-time tuning algorithm. *ICITA 2005*, 1.
- Niu, J., Wang, Z., Zhang, P., Zhang, B., & Xu, C. (2019). Research on implementation method of fuzzy logic control based on MCU. *Journal of Physics: Conference Series*, 1345.
- Ross, T. J. (1994). Fuzzy logic with engineering applications. Retrieved from <http://202.159.8.148:8001/~digilib/index.php?>

- Togai, M., & Watanabe, H. (1986). Expert system on a chip: an engine for real-time approximate reasoning. *IEEE Expert*, 1(3), 55–62.
- Tran, T. A., & Haidara, G. (2019). A research on marine diesel engine speed controller by fuzzy logic control theory based on experimental investigation. *Journal of Mechanical Engineering Research and Developments*. 42(2), 18-26.
- Vassilev, A., Ivanova, T. Y., Cabezas, T. D. F., & Sadin, Y. D. (2015). Design of function-oriented microcontrollers on equipment of programmable logic integrated circuits for embedded systems. *Automatic Control and Computer Sciences*. 49, 404-411.
- Vassiliev, A. E. (2011a, June 17). RU2477525C2 - Microcontroller with hardware fuzzy variable structure calculator - *Google Patents*. Retrieved from <https://patents.google.com/patent/RU2477525C2/ru>
- Vassiliev, A., & Giganova, V. I. (2014). Networks of elementary fuzzy solvers for synthesizing and analyzing fuzzy data processing and control Systems. *Proceedings of the Russian Academy of Sciences*. 2014(6), 34–44.
- Vassiliev, A.E., Vasilyanov, G. S., Cabezas, T. D. F., Pereverzev, A. E., & Nguyen, B. H. (2017). Hardware implementation of high-performance fuzzy computing on programmable logic integrated circuits, *Радиотехника и электроника Радиотехника и Электроника*, 12, 1243–1256.
- Watanabe, H., Dettloff, W., & Yount, K. M. (1990). A VLSI fuzzy logic controller with reconfigurable, cascable architecture. *IEEE Journal of Solid-State Circuits*, 25(2), 376–382.

Author Information

Alexei Evgenievich Vassiliev

Saint-Petersburg State Maritime Technological University
Saint Petersburg, Russia

Htet Shine

Saint-Petersburg State Maritime Technological University
Saint Petersburg, Russia

Ye Min Htet

Saint-Petersburg State Maritime Technological University
Saint Petersburg, Russia
Contact e-mail: ye.min.htet.5127@gmail.com

Viktoriia Alexeevna Karpenko

Saint-Petersburg State Maritime Technological University
Saint Petersburg, Russia

To cite this article:

Vassiliev, A. E., Shine, H., Htet, Y.M. & Karpenko, V. A. (2023). User-selected sets of algorithmic implementation of fuzzy processing subsystem for embedded intelligent control systems: *The Eurasia Proceedings of Science, Technology, Engineering & Mathematics (EPSTEM)*, 24, 257-262.

The Eurasia Proceedings of Science, Technology, Engineering & Mathematics (EPSTEM), 2023

Volume 24, Pages 263-270

IConTech 2023: International Conference on Technology

Using Oxygen and Carbon Isotopic Signatures in order to Infer Dietary Information in Bones from Kythnos Island, Greece

Giorgos Diamantopoulos

International School of Athens

Petros Karalis

National Centre for Scientific Research Demokritos

Elissavet Dotsika

National Centre for Scientific Research Demokritos

Alexandros Mazarakis-Ainian

University of Thessaly

Evaggelia Kolofotia

University of Thessaly

Stavroula Samartzidou-Orkopoulou

Ministry of Culture, Athens, Greece

Katerina Trantalidou

Ephorate of Palaeoanthropology-Speleology

Eleanna Prevedorou

Ephorate of Palaeoanthropology-Speleology

Panagiotis Leandros Poutoukis

University of Patras

Vasileios Mpletsos

Centre for Research and Technology Hellas

Anastasios Drosou

Centre for Research and Technology Hellas

Anastasia Electra Poutouki

University of Pavia

Dimitrios Tzovaras

Centre for Research and Technology Hellas

Abstract. Isotopic studies have been conducted on skeletal remains of ancient populations from Kythnos, an island of the Cyclades in Greece, for the purpose of dietary reconstruction; mostly through carbon and nitrogen isotopic signals of bone collagen, and apatite signatures (oxygen and carbon) as dietary and palaeoenvironmental tools. The basic aims of the present study are to reconstruct the diet of this population and

- This is an Open Access article distributed under the terms of the Creative Commons Attribution-Noncommercial 4.0 Unported License, permitting all non-commercial use, distribution, and reproduction in any medium, provided the original work is properly cited.

- Selection and peer-review under responsibility of the Organizing Committee of the Conference

© 2023 Published by ISRES Publishing: www.isres.org

to detect possible differentiations between the adult and the childhood/juvenile diet. The results of this study revealed that residents of Kythnos probably consumed C3 and C4 products as their primary protein source. In addition, the collagen results along with the collagen-apatite spacing possibly indicated a detectable consumption of freshwater sources. The isotopic analyses have been conducted at the Stable Isotope and Radiocarbon Unit of INN, NCSR “Demokritos”.

Keywords: Skeletal remains, Bone collagen, Dietary, Reconstruction, Isotopic signals

Introduction

Kythnos belongs to the complex of northwestern Cyclades, located between Kea and Serifos. It is an island with a long history and special archaeological interest. The most important site of historical era was Vryokastro, the ancient capital of Kythnos. The fortified polis is situated on the northwest coast of the island and has been continuously inhabited from the beginning of the first millennium B.C. until the 6th – 7th century A.D (Figure 1). The remains of the ancient city occupy an area of approximately 28,5 hectares, including the small islet of Vryokastraki, which was connected to the shore in antiquity by a narrow isthmus. During the systematic investigations which have been in progress since 1990 (survey and subsequent excavations) numerous finds and several ancient structures, such as temples, altars, public buildings, underground cisterns, houses, port facilities, burial monuments, etc., have been brought to light. These discoveries have provided valuable insights into the urban planning of the city and the sociopolitical and economic development of the ancient community.

Important information about the city can be obtained also from the study of the deceased. The ancient city had two cemeteries (Mazarakis Ainian 1980,1994, 2019). The main necropolis occupies a large area outside the southern part of the fortification wall, where several tombs from Classical and Hellenistic periods have been excavated by the Archaeological Service (Samartzidou Orkopoulou 1997; Samartzidou, 2004). From the rescue excavations, sixty-eight graves were uncovered in an area of about 400 square meters. The graves were cut into the bedrock and arranged densely. Among them, only one incrustation in an amphora and a jar burial in a beehive have been found. Unfortunately, the majority of the graves are looted. Out of the total number of burial 41 have been certainly attributed to adults, only 8 to children, and an additional 2 to infants. Due to the various disturbances, only a limited number of skeletons has been well preserved, rendering the identification of the gender and age of the deceased a challenging task. The aim of the ongoing study is to investigate the diet using stable isotopes from bone samples of ancient skeletal material. Bone consists of two parts, the organic phase (collagen) and the inorganic phase (hydroxyapatite carbonate). Both phases are directly intertwined with nutrition. Specifically, the food consumed by the man during his lifetime contains various elements such as carbon and nitrogen which are assimilated in the various tissues of the body such as bones and teeth. These particular tissues are characterized by a very low rate of reorganization and therefore reflect the diet consumed by the individual, on average, during the last ten years of his life. The stable isotope method is used to study the diet of the skeletal finds that have been found in the archaeological site of Kythnos.

Reconstructing the diet of ancient populations using stable carbon and nitrogen isotopes is a well-established method in bioarchaeology. $\delta^{13}\text{C}_{\text{coll}}$ values can indicate the type of consumed plants. According to the photosynthetic pathway that they follow, plants are distinguished into three categories: C3 plants, C4 plants, and CAM. C3 plants display carbon values ranging from -24‰ to -36‰ (closed canopy) (Smith & Epstein, 1971; O’Leary, 1981; Heaton 1999). In contrast, C4 plants have $\delta^{13}\text{C}_{\text{coll}}$ values ranging from -9‰ to -14‰ (Smith & Epstein, 1971), (global mean -12.5‰ (Lee-Thorp, 2008).

CAM plants (cactus) display intermediate values between C3 and C4 plants. Nitrogen-stable isotopes can be used in order to determine the trophic level of the foods consumed and distinguish between marine vs. terrestrial intake. Higher trophic level marine carnivores tend to display elevated nitrogen values (above 10‰ – 12‰) (Schoeninger et al., 1983a; Schoeninger et al., 1983b). In addition, $\delta^{15}\text{N}$ values of marine plants are approximately 4‰ higher than the ones of terrestrial plants (Yoder, 2012). Feeding experiments and anthropological studies have demonstrated that the $\delta^{15}\text{N}$ offset between dietary protein and human bone collagen is approximately 5.5‰ (Minagawa et al., 1986; Schoeller et al., 1986; Minagawa, 1992; Yoshinaga et al., 1996; Hedges et al., 2009; Huelsemann et al., 2009; O’Connell & Hedges, 1999; O’Connell et al., 2001; Richards, 2001). Hence, the objectives of the present study are to elucidate the dietary habits of Kythnos population.



Figure 1. Aerial photograph of Vryokastro.

Materials and Methods

With just a 5-gram bone sample, a comprehensive range of isotope analyses can be performed, including $\delta^{13}\text{C}$, $\delta^{15}\text{N}$, $\delta^{18}\text{O}$, $\delta^{34}\text{S}$, ^{14}C , and Sr, providing detailed information about an individual's origin, immigration history, and nutritional profile. Van der Merwe et al. (1982) developed a methodology that distinguishes between different photosynthetic pathways used by plants. These pathways result in different isotopic signatures. There are three main photosynthetic cycles: C3, C4, and CAM. C3 plants, which include trees, rice, cereals, citrus fruits, and legumes, typically have $\delta^{13}\text{C}$ isotopic values of around -27 ± 2 ‰. C4 plants, which include tropical grasses, corn, sugarcane, alder, and millet, have an average $\delta^{13}\text{C}$ isotopic value of -13 ± 1.2 ‰. The third photosynthetic cycle is used by plants such as cacti and prickly pears that alternate between the two types of photosynthesis, resulting in intermediate values.

Animals that move up the food chain consume plants, which affects the isotopic concentration of the plant that gets incorporated into their bones and teeth. This is also true for humans. If an animal feeds exclusively on C3 plants, it will have a lower $\delta^{13}\text{C}$ value compared to one that feeds only on C4. In the former case, the value is around -21 ‰, while in the latter, it is about -7 ‰. Animals that have a mixed diet of C3 and C4 plants should have values that are intermediate. Greece, like most of Europe and North America, has predominantly C3 plants, except for corn and cane sugar, which are crops or imports from the last century. Millet is the only C4 plant that seems to have been cultivated in ancient Greece since the Bronze Age, according to excavations. In order to approach the problem of the geographical origin of the individuals who have been found in Kythnos, as well as the specific diet of the population of ancient Kythnos, the isotopic analysis of a series of archaeological and

environmental samples is required, both from Kythnos itself and from neighboring areas. The samples, human remains and animal tissues, have been analyzed for stable isotopes ($\delta^{13}\text{C}$, $\delta^{15}\text{N}$, $\delta^{18}\text{O}$, $\delta^{34}\text{S}$).

Analysis

The isotopic analyses were conducted at the Stable Isotope and Radiocarbon Unit of the Institute of Nanoscience and Nanotechnology, of N.C.S.R Demokritos, in Athens, Greece. Collagen was extracted from the bone samples following Longin (1971) and Bocherens et al. (1991). Approximately 250 mg of each bone sample, after being ultrasonically cleaned, was crushed into small pieces using a mortar and a pestle. The small chunks of bone were soaked in 0.5 M hydrochloric acid (HCl) until all the minerals were dissolved. The remaining samples were then soaked in 0.5 M sodium hydroxide (NaOH) for 20 h, in order to remove any humic contaminants. The samples were afterwards soaked in aqueous solution reaching a temperature of 100 °C, until the collagen could be isolated. Finally, the collagen was subjected to the lyophilization process (freeze-dried). The atomic C:N ratio along with the collagen yields were used in order to determine the quality of collagen preservation. Collagen yields over 1wt% are considered acceptable for carbon and nitrogen values, while the C:N ratio should range between 2.9 and 3.6 (DeNiro, 1985).

Bone collagen samples were analyzed using an Elemental Analyzer (EA1112). The separated CO_2 and N_2 are carried in a helium stream to the mass spectrometer (ThermoScientific Delta V Plus Isotope Ratio Mass Spectrometer) via a ConFlo III coupling. The isotopic ratios expressed for carbon as $\delta^{13}\text{C}$ versus PDB (a marine carbonate), and for nitrogen as $\delta^{15}\text{N}$ versus atmospheric N_2 (AIR):

$$X = [(R_{\text{sample}} - R_{\text{standard}})/R_{\text{standard}}] \cdot 1000 \quad (1)$$

where X is the $\delta^{13}\text{C}$ or $\delta^{15}\text{N}$ value and $R = {}^{13}\text{C}/{}^{12}\text{C}$ and ${}^{15}\text{N}/{}^{14}\text{N}$ respectively. Analytical precision was 0.1‰ for both $\delta^{13}\text{C}$ and $\delta^{15}\text{N}$ values.

Results

The results of the isotopic values of $\delta^{13}\text{C}$, $\delta^{15}\text{N}$ and $\delta^{34}\text{S}$ collagen of animal bone, 15 samples, from building 3 located in the archaeological site of Kythnos (7th-5th century BC) and 14 samples of human bone from the classical period and 22 animal specimens and 3 (bones found in a deposit) found mainly in the deposit are given in Figs. 2 and 3. Bone sampling consists of taking a small piece of bone of the order of a few centimeters. This is a great advantage of the technique because it allows the analysis of a large number of bones without destroying the find, especially in cases where the findings are important and of small quantity. The determination of the relative ratios between the stable isotopes of carbon and nitrogen (${}^{13}\text{C}/{}^{12}\text{C}$, ${}^{15}\text{N}/{}^{14}\text{N}$, ${}^{34}\text{S}/{}^{32}\text{S}$) is done in collagen extracted from ancient bones.

Regarding the stable isotopes, the values from the analyzes were placed on a $\delta^{13}\text{C}$ - $\delta^{15}\text{N}$ diagram together with other isotopic values of the Greek area (Panagiotopoulou & Papathanasiou, 2015; Lagia, 2015; Borstad McConnan et al., 2018). The results of the samples, animal tissues, from the same area are placed in the same diagram (Fig.2). If one considers (Richards et al., 1999) that:

- 1) the value of $\delta^{13}\text{C}$ in human bone collagen, when its diet is based exclusively on a terrestrial C3 food chain, is about -20 ‰,
- 2) the value of $\delta^{13}\text{C}$ in human bone collagen, when fed an exclusively marine diet, is approximately $-12 \pm 1\text{‰}$, and
- 3) values for ${}^{15}\text{N}$ in human bone collagen range from 4 to 10‰ and 10 to 22‰ when fed exclusively terrestrial and marine diets respectively;

One sees that the prices for the samples fall between these two nutritional extremes. Compared to the literature data, the values of Kythnos are more positive in both nitrogen and carbon, showing that their diet, while based mainly on terrestrial plants and animals, also contained a small percentage of marine protein. Furthermore, the enriched isotopic values suggest a greater exploitation of the marine ecosystem for nutrition during the Classic period.

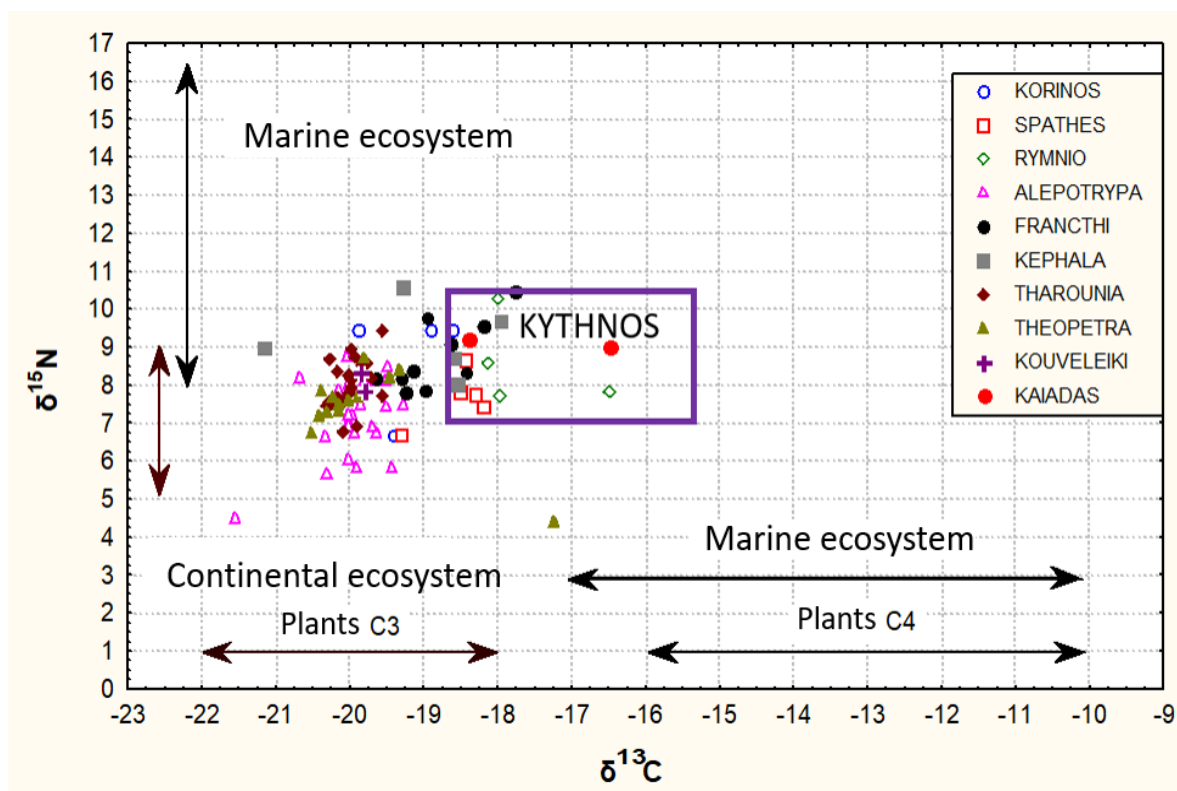


Figure 2. Diagram of the results of isotopic analysis of the Kythnos samples in comparison with isotopic values of human bones from various archaeological sites in Greece. Arrows indicate ranges of values occurring in flora and fauna samples worldwide.

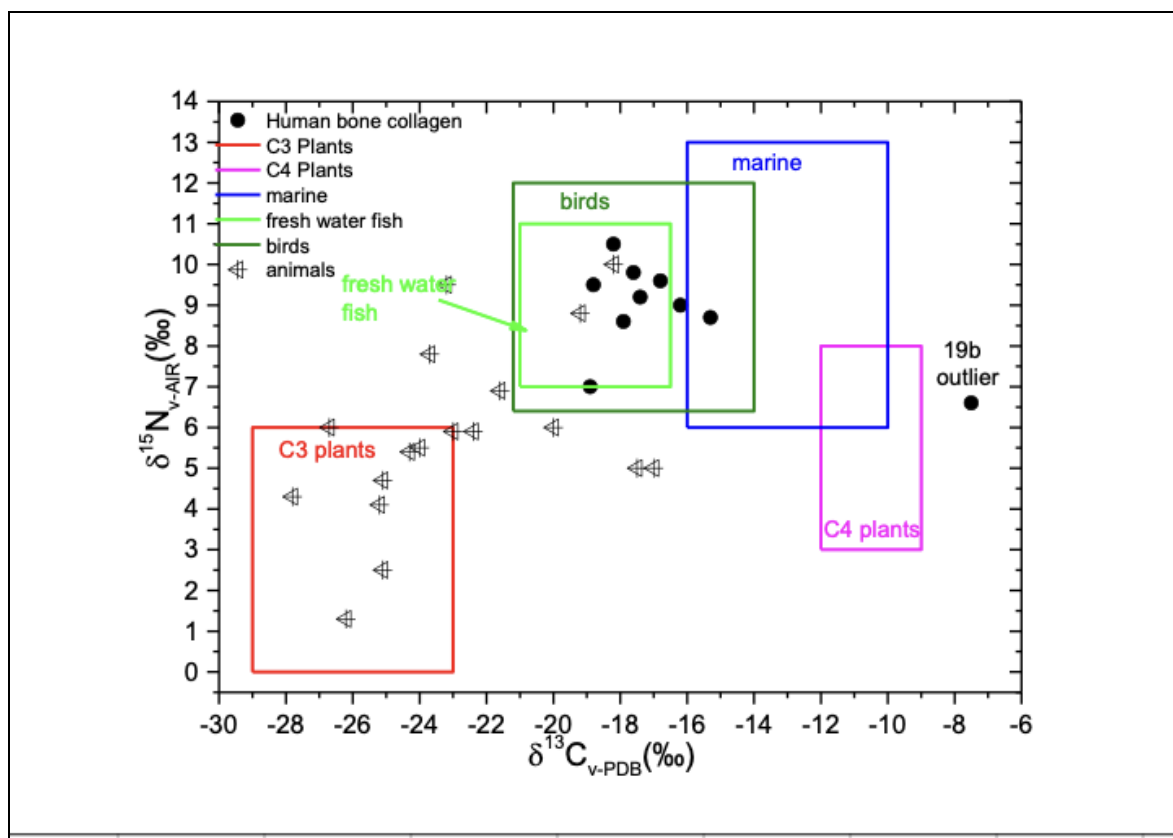


Figure 3. Mean values and error bars ($\delta^{13}\text{C}_{\text{CO}}$ vs. $\delta^{15}\text{N}$) of Kythnos in relation to reconstructed values for floral and faunal items of Greek territory. The isotopic ranges of C3 and C4 plants; C3 animals; Large fish and small fish derive from (Dotsika et al., 2018).

Compared to the literature data, the values of Kythnos are more positive in both nitrogen and carbon, showing that their diet, while based mainly on terrestrial plants and animals, also contained a small percentage of marine protein. Furthermore, the enriched isotopic values suggest a greater exploitation of the marine ecosystem for nutrition during the Classic period.

The isotopic values for all samples range between -15.3 to -18.9‰ and 7 to 10.5‰ , for $\delta^{13}\text{C}_{\text{coll}}$ and $\delta^{15}\text{N}$ respectively. The mean carbon collagen value is at $-17.5 \pm 3.3\text{‰}$ and the $\delta^{15}\text{N}$ at $9.1 \pm 1.2\text{‰}$. According to Tykot (2004) a diet completely reliant on C3 terrestrial sources would lead to a collagen carbon value at -21.5‰ , thus pointing out to significant inclusion of more ^{13}C enriched food sources.

As presented in Fig. 3., there is a significant diversity among the inhabitants of Kythnos. In general, the individuals are placed above/within the C3 animal range, the animals are placed in the range of small fish and birds, and one sample is placed near the C4 plant range. It seems possible that these individuals consumed small fish, such as sardine or anchovy, which display rather low nitrogen values; $7.1 \pm 0.8\text{‰}$ and $6.7 \pm 0.8\text{‰}$ respectively. Another possibility could be that C4 sources, i.e. millet/corn constituted an important source for the individuals along with C3 items, leading them to elevated carbon values. In addition, unexpectedly elevated nitrogen values could also be attributed to the high consumption of birds, of garum, or to the extensive use of manure (Dotsika & Michael, 2018). It has been observed that a single individual is consuming C4 sources that constitute up to 70% of their total diet. Possibly is an immigrant.

Conclusions

Therefore, these isotopic patterns, $\delta^{13}\text{C}$ and $\delta^{15}\text{N}$, probably indicate a general diet in which most dietary protein came from resident fauna and flora and partly from marine resources. In a C3 diet type, $\delta^{13}\text{C}$ values would mainly reflect a terrestrial diet, while consumption of marine resources would contribute to elevated levels of C and N isotopes. The isotopic reconstruction has provided important information regarding the diet of the Kythnos population. As revealed by the isotopic values, low trophic position freshwater input has possibly been detected in the human diet. However, another possibility could be that C4 sources, i.e. millet/corn constituted an important source for the individuals along with C3 items. According to the data, the island's inhabitants had a varied diet including both C3 and C4 terrestrial food sources, and possibly freshwater items.

Scientific Ethics Declaration

The authors declare that the scientific ethical and legal responsibility of this article published in EPSTEM journal belongs to the authors.

Acknowledgments

* This article was presented as an oral presentation at the International Conference on Technology (www.icontechno.net) held in Antalya/Turkey on November 16-19, 2023.

* This research has been co-financed by the European Regional Development Fund of the European Union and Greek national funds through the Operational Program Competitiveness, Entrepreneurship and Innovation, under the call RESEARCH – CREATE – INNOVATE (project code: T1EDK-12500)

References

- Bocherens, H., Fizet, M., Mariotti, A., Lange-Badre, B., Vandermeersch, B., Borel, J. P., & Bellon, G. (1991). Isotopic biogeochemistry (^{13}C , ^{15}N) of fossil vertebrate collagen: application to the study of a past food web including Neandertal man. *Journal of Human Evolution* 20, 481–492.
- DeNiro, M. J. (1985). Post-mortem preservation and alteration of in vivo bone collagen isotope ratios in relation to paleodietary reconstruction. *Nature*, 317(6040), 806–809.
- Dotsika, E., & Michael, D. E. (2018). Using stable isotope technique in order to assess the dietary habits of a Roman population in Greece. (2018). *Journal of Archaeological Science: Reports*, 22, 470–481.

- Dotsika, E., Michael, D. E., Iliadis, E., Karalis, P., & Diamantopoulos, G. (2018). Isotopic reconstruction of diet in Medieval Thebes (Greece). *Journal of Archaeological Science: Reports*, 22, 482–491.
- Heaton, T. H. E. (1999). Spatial, species, and temporal variations in the $^{13}\text{C}/^{12}\text{C}$ ratios of C3 plants: Implications for palaeodiet studies. *Journal of Archaeological Science*, 26(6), 637–649.
- Hedges, R., Rush, E., & Aalbersberg, W. (2009). Correspondence between human diet, body composition and stable isotopic composition of hair and breath in Fijian villagers. *Isotopes in Environmental Health Studies*, 45(1), 1–17.
- Huelsemann, F., Flenker, U., Koehler, K., & Schaenzer, W. (2009). Effect of a controlled dietary change on carbon and nitrogen stable isotope ratios of human hair. *Rapid Communications in Mass Spectrometry*, 23(16), 2448–2454.
- Lagia, A. (2015). *The potential and limitations of bioarchaeological investigations in classical contexts in Greece* An example from the polis of Athens. In D. Haggis & C. Antonaccio (Eds.), *Classical archaeology in context* (pp. 149–173). De Gruyter: Berlin.
- Lee Thorp, J. A. (2008). On isotopes and old bones. *Archaeometry*, 50(6), 925–950.
- Longin, R. (1971). New method of collagen extraction for radiocarbon dating. *Nature*, 230(5291), 241–242.
- Mazarakis Ainian, A. (1980). *The Kythnos survey project: A preliminary report*. In L. G. Mendoni & A. Mazarakis (Eds.), *Kea-Kythnos: History and Archaeology*, 363–379.
- Mazarakis Ainian, A. (2019). *The sanctuaries of Ancient Kythnos*. Rennes, France.
- Mazarakis Ainian, K. (1994). Kythnos. In *History and archaeology. Proceedings of the an International Symposium (MELETHMATA 27)*. Athens.
- McConnan Borstad, C., Garvie Lok, S., & Katsonopoulou, D. (2018). Diet at ancient Helike, Achaea, Greece based on stable isotope analysis: from the Hellenistic to the Roman and Byzantine periods. *Journal of Archaeological Science: Reports*, 18, 1–10.
- Minagawa, M. (1992). Reconstruction of human diet from $\delta^{13}\text{C}$ and $\delta^{15}\text{N}$ in contemporary Japanese hair: A stochastic method for estimating multi-source contribution by double isotopic tracers. *Applied Geochemistry*, 7(2), 145–158.
- Minagawa, M., Karasawa, K., & Kabaya, Y. (1986). Carbon and nitrogen isotope abundances in human feeding ecosystem. *Chikyu-Kagaku*, 20(2), 79–88.
- O'Connell, T. C., & Hedges, R. E. M. (1999). Isotopic comparison of hair and bone: Archaeological analyses. *Journal of Archaeological Science*, 26(6), 661–665.
- O'Connell, T. C., Hedges, R. E. M., Healey, M. A., & Simpson, A. H. R.W. (2001). Isotopic comparison of hair, nail and bone: Modern analyses. *Journal of Archaeological Sciences*, 28(11), 1247–1255.
- O'Leary, M. H. (1981). Carbon isotope fractionation in plants. *Phytochemistry*, 20(4), 553–567.
- Pangaiotopoulou, E., & Papathanasiou, A. (2015). Stable carbon and nitrogen isotope analysis for diet reconstruction of a population from the geometric-period burial site of Agios Dimitrios in central Greece. In A. Papathanasiou, M. Richards & C. Fox (Eds.), *Stable isotope dietary studies of Prehistoric and Historic Greek populations, Occasional Wiener Laboratory Series 2* (49). Princeton University Press.
- Richards, M. P. (2001). Paleodietary reconstruction. In M. Brickley & S. Buteux (Eds.), *St Martin's uncovered: Investigations in the churchyard of St Martin's-in-the-bull ring* (pp.147–151). Oxbow Books.
- Samartzidou, & Orkopoulou, S. (1997). Κύθνος. *ArchDelt*, 52, 917–918.
- Samartzidou, S. (2004). *Cycladic, funerary and burial monuments*. (Doctoral dissertation). University of Crete.
- Schoeller, D. A., Minagawa, M., Slater, R., & Kaplan, I. R. (1986). Stable isotopes of carbon, nitrogen, and hydrogen in the contemporary North American human food web. *Ecology of Food and Nutrition*, 18(3), 159–170.
- Schoeninger, M. J., Deniro, M. J., & Tauber, H. (1983). N-15/N-14 ratios of bone-collagen reflect marine and terrestrial components of prehistoric human diet. *American Journal of Physical Anthropology*, 60, 252.
- Schoeninger, M. J., Deniro, M. J., & Tauber, H. (1983). Stable nitrogen isotope ratios of bone-collagen reflect marine and terrestrial components of the prehistoric human diet. *Science*, 220(4604), 1381–1383.
- Smith, B. N., & Epstein, S. (1971). Two categories of $^{13}\text{C}/^{12}\text{C}$ ratios for higher plants. *Plant Physiology*, 47(3), 380–384.
- Tykot, R. H. (2004). Stable isotopes and diet: You are what to eat. In M. Martini, M. Milazzo & M. Piacentini (Eds.), *Proceedings of the International School of Physics Enrico Fermi*. CLIV Course, IOS Press.
- Van der Merwe, N. J. (1982). Carbon isotopes, photosynthesis, and archaeology: Different pathways of photosynthetic changes in carbon ratios that make possible the study of prehistoric human diets. *American Scientist*, 70(6), 596–606.
- Yoder, M. C. (2012). Human endothelial progenitor cells. *Cold Spring Harbor Perspectives in Medicine*, 2(7), a006692.

Yoshinaga, J., Minagawa, M., Suzuki, T., Ohtsuka, R., Kawabe, T., Inaoka, T., & Akimichi, T. (1996). Stable carbon and nitrogen isotopic composition of diet and hair of Gidra- speaking Papuans. *American Journal of Physical Anthropology*, 100(1), 23–34.

Author Information

Giorgos Diamantopoulos

Stable Isotope and Radiocarbon Unit, Institute of Nanoscience and Nanotechnology, National Centre for Scientific Research (N.C.S.R.) “Demokritos”, 15341, Attiki, Greece

Elissavet Dotsika

Stable Isotope and Radiocarbon Unit, Institute of Nanoscience and Nanotechnology, National Centre for Scientific Research (N.C.S.R.) “Demokritos”, 15341, Attiki, Greece

Contact Email: e.dotsika@inn.demokritos.gr

Evaggelia Kolofotia

Department of History, Archaeology and Social Anthropology, University of Thessaly, 38221, Volos, Greece

Katerina Trantalidou

Ephorate of Palaeoanthropology-Speleology Ministry of Culture, 10682, Athens, Greece

Panagiotis Leandros Poutoukis

Department of Physics, University of Patras, 26504, Patra, Greece

Anastasios Drosou

Information Technologies Institute, Centre for Research and Technology Hellas, 57001, Thessaloniki, Greece

Dimitrios Tzouvaras

Information Technologies Institute, Centre for Research and Technology Hellas, 57001, Thessaloniki, Greece
Contact email: Dimitrios.tzouvaras@iti.gr

Petros Karalis

Stable Isotope and Radiocarbon Unit, Institute of Nanoscience and Nanotechnology, National Centre for Scientific Research (N.C.S.R.) “Demokritos”, 15341, Attiki, Greece

Alexandros Mazarakis -Ainian

Department of History, Archaeology and Social Anthropology, University of Thessaly, 38221, Volos, Greece

Stavroula Samartzidou-Orkopoulou

Ministry of Culture, 10682, Athens, Greece

Eleanna Prevedorou

Center for Bioarchaeological Research, School of Human Evolution and Social Change, Arizona State University, Tempe, AZ, 85281, United States

Vasileios Mpletsos

Information Technologies Institute, Centre for Research and Technology Hellas, 57001, Thessaloniki, Greece

Anastasia Electra Poutouki

Department of Pharmaceutical Sciences, University of Pavia, 27100, Pavia, Italy

To cite this article:

Diamantopoulos, G., Karalis, P., Dotsika, E., Mazarakis-Ainian, A., Kolofotia, E., Samartzidou-Orkopoulou, S., Trantalidou, K., Prevedorou, E., Poutoukis, P.L., Mpletsos, V., Drosou, A., Poutouki, A.E., & Tzouvaras, D. (2023). Using oxygen and carbon isotopic signatures in order to infer dietary information in bones from Kythnos Island, Greece. *The Eurasia Proceedings of Science, Technology, Engineering & Mathematics (EPSTEM)*, 24, 263-270.

The Eurasia Proceedings of Science, Technology, Engineering & Mathematics (EPSTEM), 2023

Volume 24, Pages 271-278

IConTech 2023: International Conference on Technology

Design and Development of Mobile Payment Platform Software Supported by Analytical Capabilities for Payment Systems

Pinar Celdirme-Kaygusuz

Turkcell Ödeme ve Elektronik Para Hizmetleri A.Ş. (Paycell Research and Development Center)

Unal Asil

Turkcell Ödeme ve Elektronik Para Hizmetleri A.Ş. (Paycell Research and Development Center)

Semih Kokcu

Turkcell Ödeme ve Elektronik Para Hizmetleri A.Ş. (Paycell Research and Development Center)

Abstract: The Paycell Mobile Payment application serves as a platform where users can benefit from various payment and shopping services. Each user explores services within the application based on their own interests and needs, and this process generates a significant amount of data. The data created has become an important resource for improving user experience and enhancing the services offered. The primary goal of our project is to enrich the user experience and offer personalized recommendations based on real transactions to meet financial needs more effectively. This approach represents a significant step in the mobile payment systems industry in terms of data analytics and personalization. Simultaneously, this approach aims to position the Paycell application as a 'super app' where users can personalize their financial transactions. Our project captures user-initiated transactions with the aim of providing personalized recommendations tailored to users' interests and needs. These data are analyzed using data processing methods to obtain meaningful results. The results are then used to offer personalized recommendations to users. This approach contributes to users having more tailored experiences and meeting their financial needs more effectively.

Keywords: Super app, Data processing, Mobile payment

Introduction

Mobile payment systems represent a rapidly growing and evolving field in the financial technology world. These systems enable users to perform their financial transactions quickly and securely in their daily lives and are increasingly adopted by more people every day. Gaining a competitive advantage in this dynamic sector and enhancing the user experience are the cornerstones of a successful mobile payment application. The main objective of the project is to improve the Paycell application, increase customer satisfaction, and employ innovative approaches and technologies for new Paycell customers. By analyzing the transactions users perform in the application using complex data processing methods, it is possible to enhance the ease of use and effectiveness of the application. This enables users to use the application more actively with an innovative approach and highlights the gains obtained, with the aim of achieving more gains. Paycell Mobile Payment aims to provide personalized services to every user by focusing on their unique interests and needs. This application is a platform that uses data based on real transactions to enrich the user experience and meet financial requirements more effectively.

In conclusion, the Paycell Mobile Payment application aims to transform financial needs into a personalized experience, providing users with more benefits on a reliable and user-friendly platform. This project represents a significant step in the mobile payment sector and elevates user expectations to a new level.

- This is an Open Access article distributed under the terms of the Creative Commons Attribution-Noncommercial 4.0 Unported License, permitting all non-commercial use, distribution, and reproduction in any medium, provided the original work is properly cited.

- Selection and peer-review under responsibility of the Organizing Committee of the Conference

© 2023 Published by ISRES Publishing: www.isres.org

Throughout this paper, the project's main objectives, features, and advantages will be discussed in more detail. Additionally, the paper will emphasize the project's significance in the industry and how it can impact future financial transactions.

Recommended Project Architecture

The proposed software architecture we recommend processes data using the Apache Flink library, handling complex data by considering a series of events the user performs, and extracting personalized recommendations (García-Gil et al., 2017). Our project is designed to work on the existing Paycell microservices architecture. The Paycell Mobile Payment Platform is composed of a series of microservices. Requests are routed through the gateway. Figure 1 illustrates the communication between the client, gateway, and Flink.

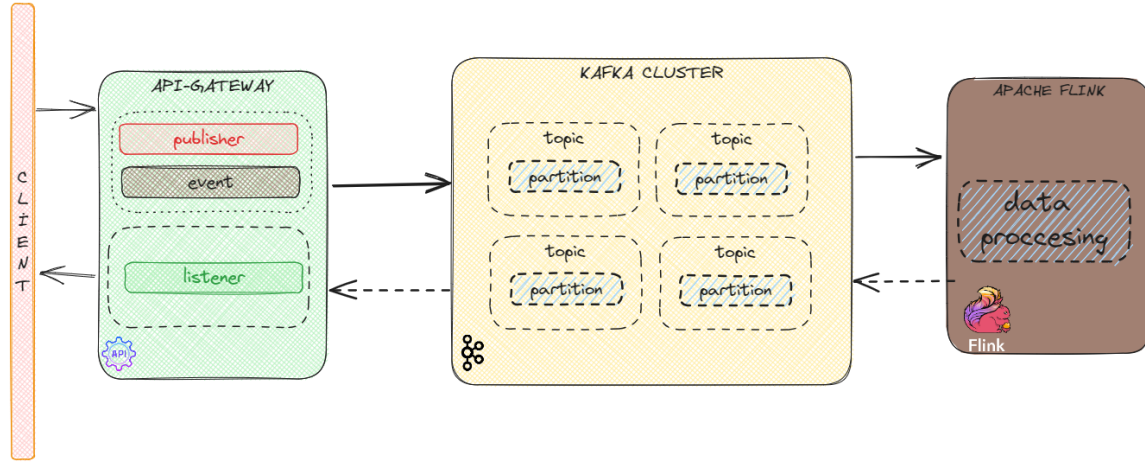


Figure 1. Communication between the client, gateway, and flink

On the API Gateway side, events are generated as a result of user interactions. The Kafka Cluster, which is an important component, comes into play. User events are sent to the Kafka Cluster and stored there (Sharvari T et al., 2019). Subsequently, Apache Flink processes this data in a complex manner. Apache Flink uses this data to generate personalized recommendations based on the user's actions.

Data Modelling: In the project, the data obtained for processing is referred to as events. Event data obtained from the Paycell application can include various activities that occur, such as visit activities and purchase activities. In this context, an event can be defined as follows:

Event: It represents interactions that occur as a result of users of the Paycell Mobile Application using its features. Each event data includes the date and time of the event, user information who performed the event, object information related to the feature, and other relevant data.

Data Flow: Let's assume a digital product purchase request is generated by the client. In this case, the API Gateway point will create an ORDER_CREATED event in the Kafka Cluster to initiate the order. The Payment Service, listening to this event, will attempt to process the payment with the relevant user's information and update the payment status, creating an event like PAYMENT_SUCCESS or PAYMENT_FAILED. Simultaneously, the developed Flink application will listen to these created events, track the user's transactions, and prepare a recommendation tailored to the user, feeding the Kafka Cluster with an event like ADVICE_CREATED. This event can be listened to on the API Gateway, allowing the relevant client to access recommendations through notifications, messages, emails, and other channels.

Data Processing: Apache Flink is a powerful open-source data stream processing framework designed for real-time data processing and analysis, especially suitable for event processing scenarios. In our project, it processes the data obtained, generating meaningful insights based on the designed architecture. For example, it can perform data filtering, grouping, merging, or transformation steps. (Alaasam et al., 2019).

MongoDB Data Storage Environment: Within the scope of our developed module, event data collected is stored for reporting purposes after complex event processing analyses using Flink. MongoDB is used as the storage tool because it allows flexible data models, fast access, indexing, and querying capabilities. MongoDB

accommodates complex and hierarchical data structures, providing an environment for organizing and querying various analysis results (Patil et al., 2017).

Data Protection: One of the key features of the proposed software architecture is ensuring that created events are transmitted without loss or corruption. Data transfer from the data source to the data processing module is done through a topic-based data subscription communication method. With this method, it is possible to collect, store, and process data in real-time without any data loss. The Kafka Cluster structure enables this capability, ensuring data is processed without loss (Apache Kafka, 2023).

Implementation

In the implementation of the proposed project architecture, Java technologies have been utilized. Apache Kafka serves as the data subscription message delivery channel, and the Apache Flink library is used for complex data analysis. As depicted in Figure 2, the implemented system's architecture is based on the proposed project architecture illustrated in Figure 1.

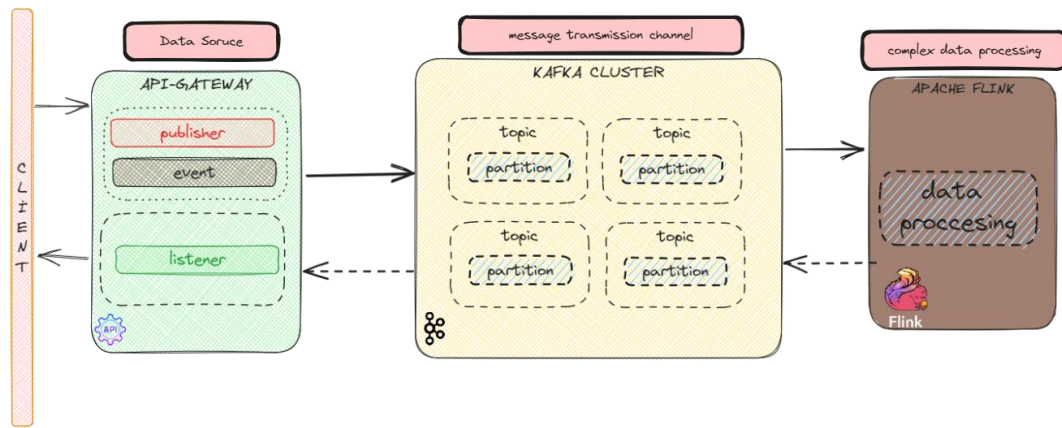


Figure 2. The implemented system's proposed architecture

Data Modeling in the Prototype: Complex event analysis will be performed on the collected event data, and events will be processed based on their adherence to predefined rules and the ranking of events. In this context, event data has been appropriately modeled to enable fast reading (runtime analysis), writing (for reporting), and querying (filtering events at runtime according to rules).

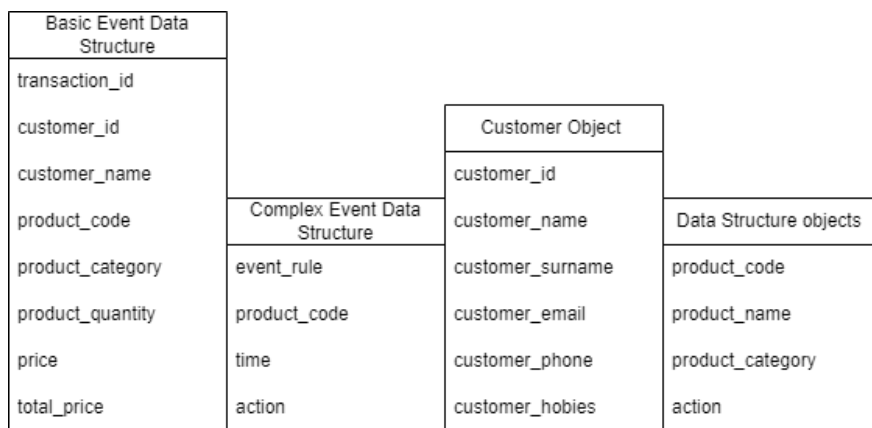


Figure 3. Event data structure

The data model used in the prototype is designed for conducting activities such as real-time campaigns and personal recommendations in the Paycell Mobile Application. The model is based on the user's example of purchasing digital game pins. The customer and product data structure is shown in Figure 3. In the proposed system, the customer's transactions in this area are considered events. The fundamental event data structure contains information related to the pins the customer purchases and their expenses within the Paycell Mobile Application. Data elements found in the event structure are depicted in Figure 3. As can be seen from the figure,

the event data structure includes data elements such as transaction_id, customer_id, customer_name, product_code, product_quantity, price, total_price, and more.

When a complex event chain adhering to the defined rules is established, a complex event chain is created. Complex event data contains the actions the system desires. When designing the complex event data structure, activities like campaigns and similar product recommendations that can be performed as transactions in the Paycell application were considered. The information related to the Customer Object and Product Data Structure objects is as shown in the figure.

Rule Design: The rules triggering complex event formation have been implemented in Apache Flink. The design follows a specific sequence of events and generates recommendations as events that meet the appropriate conditions follow one another. The structure that satisfies consecutive rules is shown in the schema in Figure 4. In the inclusive example shown in Figure 4, when an event providing the starting parameter in the event chain is encountered, the chain of rules advances. When the desired event is satisfied, the next node is visited, and the result is achieved. Event sequences can be defined based on project requirements and decisions to be made (Carbone et al., 2015).

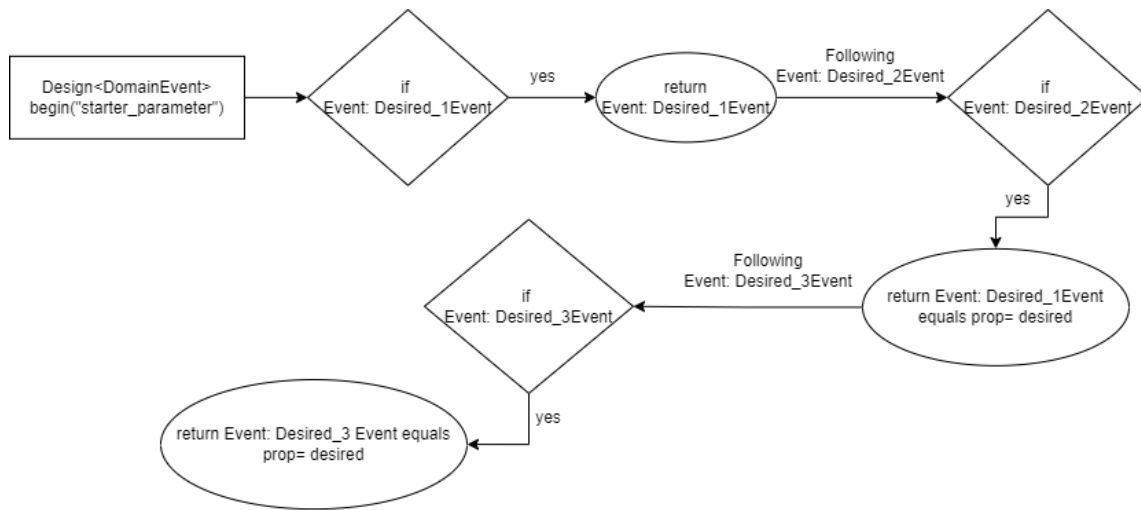


Figure 4. Sequence of rules

The occurrence of desired events leads to a conclusion as shown in Figure 5. In this scenario, a user who purchases in-game content in the Paycell mobile app satisfies the first rule, which is the "game content purchase" event. Subsequently, in the second step following this event, it is checked whether the content the user has purchased falls under the relevant category. If it falls under the "pubg_pin" category, the process advances to the final rule. When the subsequent event related to the vendor code has occurred and the code specified in the rule is satisfied, the user is provided with similar recommendations through in-app notifications, SMS, email, or other channels defined within the application.

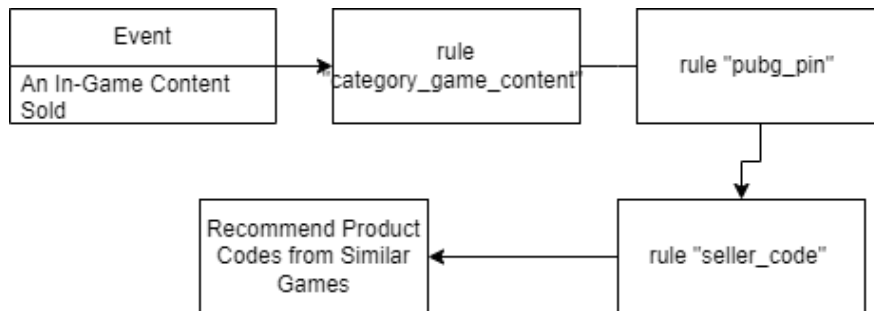


Figure 5. Example event loop

Working Scenario of the Prototype System: The primary objective of the prototype application we have developed is to track and analyze users' actions in real-time based on the transactions they perform and provide recommendations. These recommendations can be delivered through various communication channels (SMS, Bip, email, in-app notifications, etc.). The developed system is expected to be a high-performance management system. Figure 6 primarily illustrates the working scenario of the system.

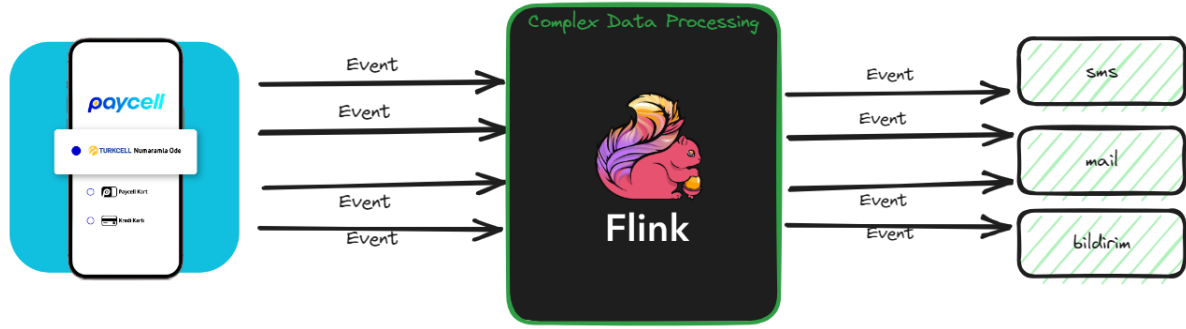


Figure 6. System work

The events generated as a result of these activities are sent to the Complex Event Processing Module. The Complex Event Processing Module generates complex events based on rule-based rules. Instant discounts, campaigns, bonuses, and other recommendations are made to the customers who cause these complex events. While implementing our system, we used the Apache Flink library. Flink is fed with data coming in real-time via a data subscription message delivery channel. For this purpose, Apache Kafka, which is the most suitable data subscription system for our system in terms of performance, has been chosen and used in the realization of the proposed system architecture. Apache Kafka is a high-throughput, fault-tolerant, distributed data streaming platform that records data like a log and can be used for transmission among different applications. It is designed to process large data streams reliably and fault-tolerantly. Additionally, it is scalable as your workload grows, and it can work in a distributed architecture.

For the simple and complex event data generated by customers through different sources, it is necessary to store and make it queryable in a big data infrastructure. After the events generated by customer actions in the Paycell mobile application are collected via Apache Kafka, these events are processed for complex data analysis using Flink. Flink is a powerful tool for big data processing and smart analytics. The collected event data is sent to Flink in real-time, and complex analyses are performed there.

Flink supports various data analysis scenarios, including understanding customer behaviors, providing personalized recommendations, and more. This allows for a better understanding of customer actions and providing valuable insights into the Paycell mobile application.

Possible Scenarios: It designs a highly functional data analytics system based on the concept of real-time data analysis and recommendations. Additionally, this structure can effectively work in terms of performance and scalability using powerful tools like Apache Flink and Apache Kafka. However, various other scenarios and benefits of this system can be considered.

It is possible to offer personalized offers, recommendations, and customizations for user interactions on other functionalities in the Paycell mobile application. At the same time, with this structure, a different perspective can be used to quickly prevent potential security threats or fraud by examining the events created by the user along with Flink. The analysis of user interactions can be used as a tool to monitor and improve operational processes within the system. This aims to efficiently manage resources and increase operational excellence within the Paycell application.

Discussion on the Proposed Methodology

Paycell Mobile Application provides a platform for fast and secure financial transactions. The primary goal of this project has been to personalize the user experience and effectively meet financial needs. Within the project scope, user transactions have been recorded and analyzed using complex data analysis methods. These analyses have made it possible to provide personalized recommendations tailored to users' interests and needs. This approach has encouraged users to use the application more effectively and achieve their financial goals.

The personalized recommendations provided to users are based on real-time transactions, leading to increased app usage. This is a result of focusing on meeting the needs of users to enhance their experience. Additionally, by analyzing shopping habits and expenses, financial improvements have been made, and users have been provided with recommendations to make better decisions.

Paycell Mobile Application is moving towards becoming more than just a payment tool; it aims to become a "super app" and provide more benefits to users. Finally, real-time data processing capabilities have been enhanced using powerful tools. This plays a critical role in processing large data streams and providing quick responses. This successful project encourages opportunities to enhance the application's functionality in the future. For example, new use cases can be explored, such as monitoring security threats or optimizing operational processes.

In conclusion, Paycell Mobile Application not only meets financial needs but also provides a personalized experience. This success can inspire similar applications in the future to offer more personalization and user-friendly services.

Literature Review

This study focuses on big data processing techniques for real-time data. There exist a number of studies utilizing complex event processing for real-time event processing in different studies (Baeth et al., 2018; Sudan et al., 2020; Yildiz et al., 2020; Aktas et al., 2020; Uzun-Per et al., 2021; Dhaouadi et al., 2018; Uzun-Per et al., 2022; Can et al., 2022; Baeth et al., 2017; Pinar et al., 2021, Yildiz et al, 2020; Cansiz et al., 2020). We observe studies in different distributed system architecture research fields such as service-oriented architectures (Tufek et al., 2018; Aktas et al, 2005; AsTekin et al., 2021). However, this study is investigating methodologies for event-based distributed system architectures. There exist studies focusing on analyzing analyzing click-stream data to understand the user navigational behavior (Uygun et al., 2020; Olmezogullari et al., 2022; Olmezogullari et al., 2020). This study produced a prototype software. Different studies are seen in the literature to measure the quality of the prototype software implemented within the research studies (Sahinoglu et al., 2015; Kapdan et al., 2014). However, in this study, software quality is considered as out-of-scope.

Results and Future Work

Paycell Mobile Application is a platform developed with the goal of providing more than just speed and reliability in financial transactions. It aims to personalize the user experience and effectively address financial needs. In this academic paper, we share the design details and software development approaches we have identified for this application. By utilizing complex data analyses, it offers users personalized recommendations tailored to their interests and needs, encouraging users to use the application more effectively. Real-time personalized recommendations based on actual transactions have led to increased app usage, and by analyzing shopping habits and expenses, financial improvements have been achieved. Paycell Mobile Application goes beyond being a mere financial payment tool, striving to become a "super app" with strong data processing capabilities to handle large data streams and provide quick responses.

The system implemented in the Paycell Mobile application, when considered within a broader context, could serve as an inspiration for other payment system tools and e-commerce platforms in the market. With its advanced data analysis feature, it has the potential to contribute to the more efficient development of systems. This project also inspires opportunities to enhance the application's functionality in the future, such as monitoring security threats or optimizing operational processes. In conclusion, Paycell Mobile Application not only meets financial needs but also serves as a source of inspiration for similar applications in the future by offering a personalized experience.

Scientific Ethics Declaration

The authors declare that the scientific ethical and legal responsibility of this article published in EPSTEM journal belongs to the authors.

Acknowledgement

* This article was presented as an oral presentation at the International Conference on Technology (www.icontechno.net) held in Antalya/Turkey on November 16-19, 2023.

* This research is supported by the PayCell R&D Center. The authors would like to express their gratitude for the contributions from the Paycell R&D Center. We express our deepest gratitude to our esteemed mentor, Professor Dr. Mehmet Aktas, for providing us with invaluable guidance and support at every step of this study.

References

- Aktas, D. E., & Aktas, M. S. (2020). Real-time pattern detection methodology for monitoring student behaviour on e-learning platform in the field of financial sciences: Case study. In *2020 28th Signal Processing and Communications Applications Conference (SIU)* (pp. 1-4). IEEE.
- Aktas, M., Aydin, G., Donnellan, A., Fox, G., Granat, R., Lyzenga, G., ... & Sayar, A. (2005). Implementing geographical information system grid services to support computational geophysics in a service-oriented environment. *NASA Earth-Sun System Technology Conference*. University of Maryland, Adelphi, Maryland.
- Alaasam, A. B. A., Radchenko, G., & Tchernykh, A. (2019). Stateful stream processing for digital twins: Microservice-based Kafka stream DSL. In *2019 International Multi-Conference on Engineering, Computer and Information Sciences (SIBIRCON)* (pp. 804-0809). Novosibirsk, Russia.
- Apache Kafka. (2023). *Kafka cluster encryption and authentication*. Retrieved from <https://kafka.apache.org/35/documentation/streams/developer-guide/security.html>
- Astekin, M., & Aktas, M. S. (2021). A big data processing framework for self-healing internet of things applications. *IEEE International*
- Baeth, M. J., & Aktas, M. S. (2017). Detecting misinformation in social networks using provenance data. *13th International Conference on Semantics, Knowledge and Grids*.
- Baeth, M. J., & Aktas, M. S. (2018). An approach to custom privacy policy violation detection problems using big social provenance data. *Concurrency and Computation: Practice and Experience*, 30(21).
- Can, A. B., Zaval, M., Uzun-Per, M., & Aktas, M. S. (2023). On the big data processing algorithms for finding frequent sequences. *Concurrency and Computation: Practice and Experience*, 35(4), 1-17.
- Cansiz, S., Sudan, B., Ogretici, E., & Aktas, M. (2020). Learning from student browsing data on e-learning platforms: Case study. *Computer Science and Information Systems*, 22, 37-44.
- Carbone, P., Ewen, S., Haridi, S., Katsifodimos, A., Markl, V., & Tzoumas, K. (2015). Apache flink: Stream and batch processing in a single engine. *The Bulletin of the Technical Committee on Data Engineering*, 38(4), 1-6.
- Dhaouadi, J., & Aktas, M. (2018). On the data stream processing frameworks: A case study. In *2018 3rd International Conference on Computer Science and Engineering (UBMK)* (pp. 104-109). IEEE.
- García-Gil, D., Ramírez-Gallego, S., García, S., & Herrera, F. (2017). A comparison on scalability for batch big data processing on Apache Spark and Apache Flink. *Big Data Anal*, 2(1), 1.
- Kapdan, M., Aktas, M., & Yigit, M. (2014). On the structural code clone detection problem: A survey and software metric based approach. *Computational Science and Its Applications-ICCSA 2014: 14th International Conference* Guimarães, Portugal.
- Olmezogullari, E., & Aktas, M. S. (2022). Pattern2Vec: Representation of click-stream data sequences for learning user navigational behavior. *Concurrency and Computation: Practice and Experience*, 34(9).
- Olmezogullari, E., & Aktas, M. S. (2020). Representation of click-stream data sequences for learning user navigational behavior by using embeddings. *2020 IEEE International Conference on Big Data (Big Data)*, 3173-3179.
- Patil, M. M., Hanni, A., Tejeshwar, C. H., & Patil, P. (2017). A qualitative analysis of the performance of MongoDB vs MySQL database based on insertion and retrieval operations using a web/android application to explore load balancing — Sharding in MongoDB and its advantages. In *2017 International Conference on I-SMAC (IoT in Social, Mobile, Analytics and Cloud)* (pp. 325-330). Palladam, India.
- Pinar, E., Gul, M. S., Aktas, M., & Aykurt, I. (2021). On the detecting anomalies within the clickstream data: Case study for financial data analysis websites. In *2021 6th International Conference on Computer Science and Engineering (UBMK)* (pp. 314-319). IEEE.
- Sahinoglu, M., Incki, K., & Aktas, M. S. (2015). Mobile application verification: A systematic mapping study. *Computational Science and Its Applications- ICCSA 2015: 15th International Conference*. Banff, AB, Canada.
- Sharvari T, & Sowmya Nag, K. (2019). *A study on modern messaging systems- Kafka, RabbitMQ and NATS Streaming*. Retrieved from <https://arxiv.org/abs/1912.03715>
- Sudan, B., Cansiz, S., Ogretici, E., & Aktas, M. S. (2020). Prediction of success and complex event processing in E-learning. In *2020 International Conference on Electrical, Communication, and Computer Engineering (ICECCE)* (pp. 1-6). IEEE.

- Tufek, A., Gurbuz, A., Ekuklu, O. F., & Aktas, M. S. (2018). Provenance collection platform for the weather research and forecasting model. In *2018 14th International Conference on Semantics, Knowledge and Grids. Conference on Big Data (Big Data)*, 2353-2361.
- Uygun, Y., Oguz, R. F., Olmezogullari, E., & Aktas, M. S. (2020). On the large-scale graph data processing for user interface testing in big data science projects. In *2020 IEEE International Conference on Big Data (Big Data)*, 2049-2056.
- Uzun-Per, M., Can, A. B., Gurel, A. V., & Aktas, M. S. (2021). Big data testing framework for recommendation systems in e-science and e-commerce domains. In *2021 IEEE International Conference on Big Data (Big Data)* (pp. 2353-2361). IEEE.
- Uzun-Per, M., Gurel, A. V., Can, A. B., & Aktas, M. S. (2022). Scalable recommendation systems based on finding similar items and sequences. *Concurrency and Computation: Practice and Experience*, 34(20).
- Yildiz, E. C., Aktas, D. E., Unal, E., Tuzun, H., & Aktas, M. S. (2020). Management of virtualization technologies with complex event processing. In *2020 International Conference on Electrical, Communication, and Computer Engineering (ICECCE)* (pp. 1-4). IEEE.

Author Information

Pınar Celdirme-Kaygusuz

Turkcell Ödeme ve Elektronik Para Hizmetleri A.Ş.
(Paycell Research and Development Center)
Contact e-mail: pinar.kaygusuz@turkcell.com.tr

Unal Asil

Turkcell Ödeme ve Elektronik Para Hizmetleri A.Ş.
(Paycell Research and Development Center)

Semih Kokcu

Turkcell Ödeme ve Elektronik Para Hizmetleri A.Ş.
(Paycell Research and Development Center)

To cite this article:

Celdirme-Kaygusuz, P., Asil, U. & Kokcu, S. (2023). Design and development of mobile payment platform software supported by analytical capabilities for payment systems. *The Eurasia Proceedings of Science, Technology, Engineering & Mathematics (EPSTEM)*, 24, 271-278.

The Eurasia Proceedings of Science, Technology, Engineering & Mathematics (EPSTEM), 2023

Volume 24, Pages 279-286

IConTech 2023: International Conference on Technology

Integration of STM32 Microcontroller with Arm Cortex Architecture into the 8-Bit Measurement Circuit Customized for Real-Time Data Acquisition on Propeller Shaft to Increase Data Speed and Accuracy

Oguzhan Aldemir
Tirsan Kardan A.S.

Sedat Tarakci
Tirsan Kardan A.S.

Serhan Ozdemir
İzmir Institute of Technology

Efe Isik
Tirsan Kardan A.S.

Abstract: Propeller shafts transmit torque and high-speed rotational movement from the engine to related equipment. Expected propeller shaft functions are calculated and designed by using an analytical and numerical approaches. The verification tests are significant in that they provide feedback to the design and development processes. Therefore, acquiring accurate data from power transmission equipment is becoming even more important. This paper focuses on the study of circuit boards customized for use in the validation tests of the propeller shafts. It should be noted that these measurement circuits were integrated on the propeller shafts. These measurement circuits were used to acquire data such as torque, temperature, etc. in real time. Especially with instantaneous signals such as torque, data loss can occur due to low microcontroller resolution. Therefore, it was aimed to develop to the microcontroller to 32-bit resolution from 8-bit resolution to increase data speed and accuracy. As the first step, an INA125P operational amplifier was installed to amplify the low voltage values gathered from the gages and the sensors. The gain value of the amplifier was calculated in order to provide the highest data resolution and sensitivity. And then, ADS1115 analog to digital converter circuit with a rate of 860 samples per second and 16-bit resolution was used to interpret the analog data. A low pass filter was installed to remove noise from the output signal. Embedded code was also locally developed for the hardware installed. The system was calibrated on a validated test rig. Real-time torque and temperature data were acquired from the propeller shaft. It is observed that compared to the previous 8-bit system, the data accuracy and integrity from the new 32-bit board has increased by a factor of 5 to 100 Hz. The collected data was found to be 99.4% compatible with the validated test rig data.

Keywords: STM32, 32-Bit, Propeller shaft, Microcontroller, Measurement

Introduction

In global markets, the balance between cost and profit per product has great importance, especially in mass produced industries such as automotive. Under mass production conditions, the profit or loss per product increases cumulatively and its effects can not be ignored. Therefore, the optimum product and production process are designed with precision. There are development studies for these products and production processes. Verification tests are one of the main features of the development studies (Aldemir et al., 2021).

- This is an Open Access article distributed under the terms of the Creative Commons Attribution-Noncommercial 4.0 Unported License, permitting all non-commercial use, distribution, and reproduction in any medium, provided the original work is properly cited.

- Selection and peer-review under responsibility of the Organizing Committee of the Conference

© 2023 Published by ISRES Publishing: www.isres.org

Propeller shafts are the mechanical components which transmit power produced by the engine through transmission organs. Besides two main functions, propeller shafts are responsible for compensating angular and axial displacement caused by rear suspension. Propeller shafts have complex kinematic structure. It contains many different components. As a result, there are many different types of failure appear on this shaft working under a vehicle. For this reason, numerical calculations and analytical approaches are used during design studies (Isik, 2009).

Many verification tests are applied to propeller shafts for failure detection or development studies. Road conditions are simulated and the effects on the propeller shaft are observed in these tests. This health monitoring studies help to understand the failure modes and provide feedback for design studies. For example, torque is applied to the propeller shaft up to failure and stress values are measured instantaneously. According to the test results, critical regions can be strengthened by making design changes.

This paper focused on examination of circuit boards that customized for using on propeller shafts verification tests. These boards are used to acquire torque and temperature data in real-time. It has to be noticed that the aforementioned circuit board is designed for propeller shafts. With instantaneous signals such as torque, data loss can occur due to low microcontroller resolution. Especially in commercial applications where measurement precision is critical, the speed and accuracy of the data acquisition influences the quality of the data. Therefore, the microcontroller is replaced with 32-bit resolution from 8-bit resolution to increase data speed and accuracy. The difference in data resolution between 32-bit and 8-bit microcontrollers was shown in Figure 1 below.

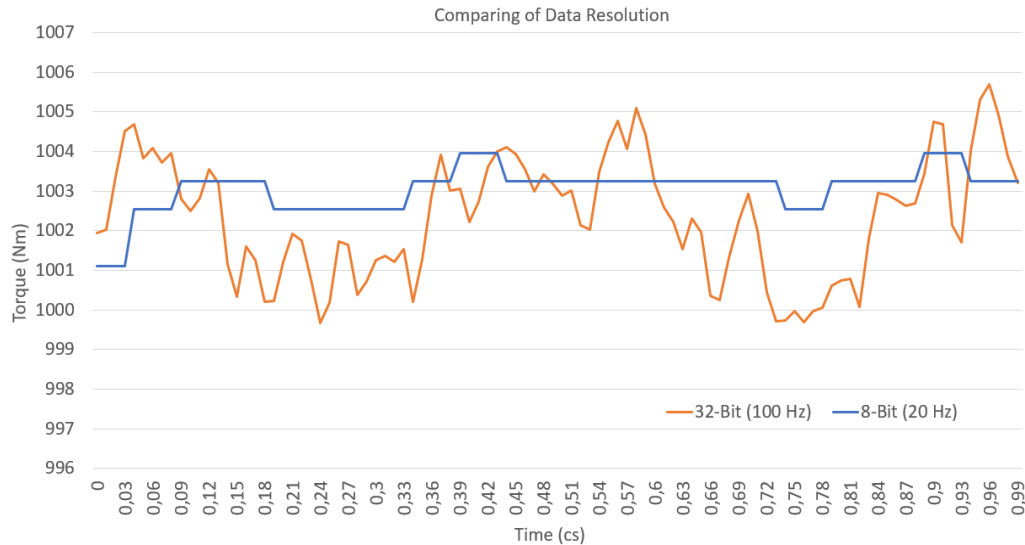


Figure 1. The difference between data resolution

Literature

Hui-fu Zhang and Wei Kang were studied on “Design of the data acquisition system based on STM32”. On the study, an embedded signal acquisition system for real-time was explained. The system was involved in a three-axis acceleration sensor which has high sensitivity. It was possible to detect the mechanical failure of the rotating machines with measuring high frequency vibration. The measurement system was designed based on STM32 (Zhang & Kang, 2013).

Also, Xie et al. (2017). studied on named as “STM32-based vehicle data acquisition system for internet-of-vehicles” that includes the feasibility and effectiveness of a data acquisitions system based on STM32. The system works with the vehicle complex sensors and communications network, and it was provided cybersecurity with IoT (Xie et al., 2017).

In addition to STM32 studies, Alp İmer worked on “Smart irrigation system”. The system controls an autonomous irrigation system using STM32 microcontroller. The system has different communication protocol and peripheral units. A sensor with limiter switch was used as input and a DC motor was used to drive the pulse width modulation unit on STM32. The microcontroller user interface Cube MX was mentioned on the paper (İmer, n.d.).

Hardware Method

As the first step of the study, a fundamental test setup was built for improving current circuit board. Here, it was started with applying a strain gauge on a simple steel bar and a quarter wheat stone bridge was built. Analogue signals were generated on the strain gauge by applying force to the steel bar. This is a simulation of the torque loaded propeller shaft. Then, a typical low-pass filter was used in order to prevent the noise of the analogue signals of the output.

Operational Amplifier

Strain gauges generate voltages difference at millivolt levels. These low-level voltages is needed to amplify before reading by an electronic device. The amplifying process has to be performed instantaneously. According to the research, INA125P operational amplifier is explored to be enable 0-10,000 of range a high gain. Also, this operational amplifier provides a reference voltage on high precision for mentioned bridge applications. (Burr-Brown Corporation, 1998). Traditional INA125P operational amplifier application was shared on Figure 2.

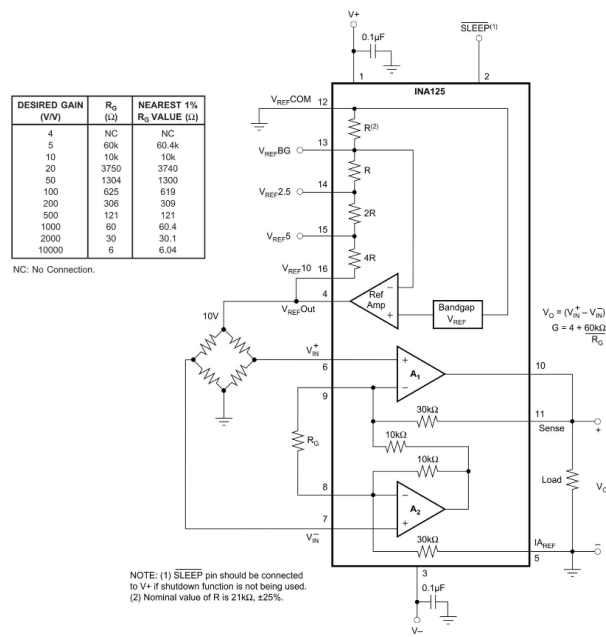


Figure 2. INA125P operational amplifier application [6]

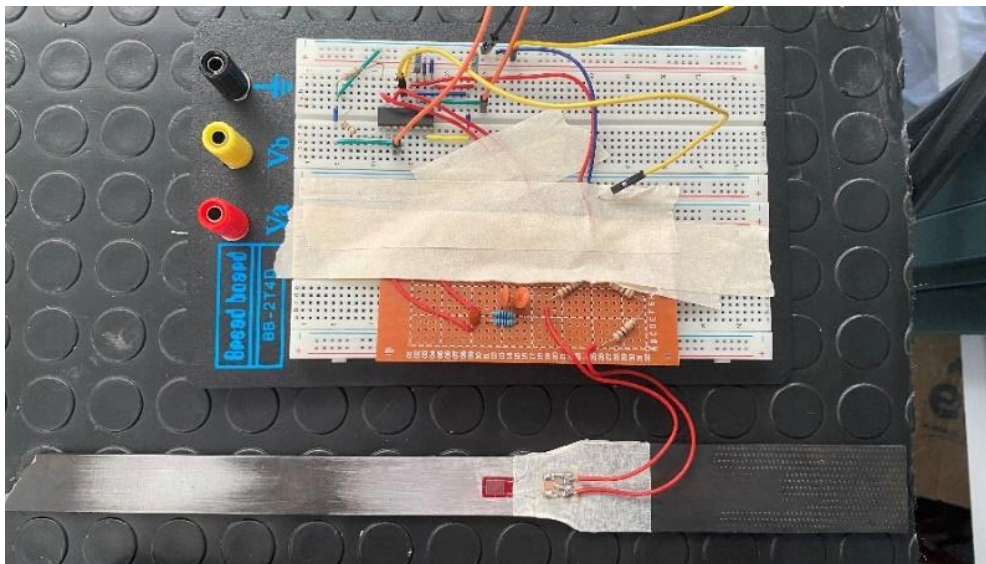


Figure 3. The picture of the test setup

The analogue signals were amplified from ± 0.5 V to ± 4.5 V thanks to INA125P operational amplifier. It was placed at the output of the analogue signal generator test setup. Furthermore, the INA125 gain ratio can be easily adjusted by changing the value of the gain resistor R_g . The picture of the real test setup with the steel bar, the bridge, the low pass filter and the amplifier was shown in Figure 3.

Analog Digital Converter

The mentioned analogue signals were generated on the steel bar. Electronic devices communicate using binary language. This language is explained by the digital signals such as logic 0 and 1 with a resolution of 2^n . [7] This part of the study explained the conversation of the analogue signals to digital ones. Thus, the microcontroller can able to process these digital signals. Analog digital converters that have high sampling rates were researched. The data resolution and speed were determined. Then, ADS1115 analog to digital converter with 860 SPS data sampling speed and 16-bit resolution was chosen. Thanks to ADS1115, ± 4.5 V analogue torque signal range are divided into 65,536 parts and matched with digital signals. This conversion of the signals improved the data speed and accuracy.

ADS1115 footprint was printed for preparing prototype. ADS1115 and its printed footprint output were shown in Figure 4 below.

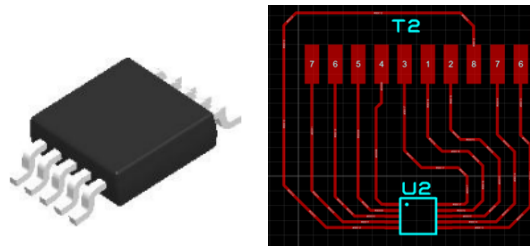


Figure 4. ADS1115 and its footprint [8]

ADS1115 prototype was placed beyond the INA125P operational amplifier. After the signal amplification, amplified analog signals was converted to digital signals.

STM32 Microcontroller

Generally, microcontrollers have a central processing unit, type of memories, input and output ports, etc. It can be considered as a computer with its serial communication, analog-to-digital conversion or signal processing features (Hariz et al., 2015).

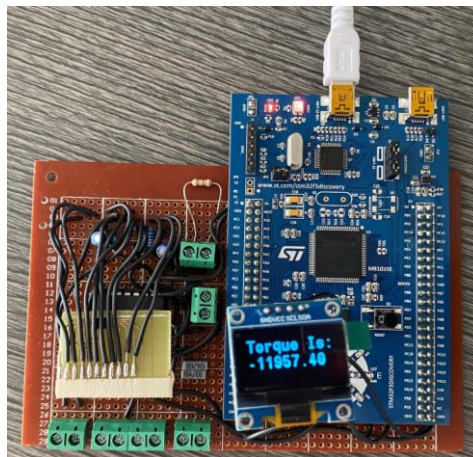


Figure 5. The first assembled prototype of the hardware

STM32 microcontrollers are signal processors with their high core speed and resolution. These controllers have different interfaces for instruction and data storage. This architecture is enabled to synchronized access to memories. This allows the microcontroller to achieve high communication speeds (Brown, 2012).

STM32F3 microcontroller has M4 core running at 72 MHz and it is customized for signal processing. It was chosen to use on this study. The DMA (Direct Memory Access) function is a bus manager in STM32F3. It has a special peripheral unit and enables to reach the limits of the data speed (ST. life augmented, n.d.). Finally, STM32F3 controller was integrated into the system. The first assembled prototype of the system was shown in Figure 5.

Software Method

In order to acquire torque data, the strain gauge electrical power without any fluctuation. This need was supplied by INA125P with its reference voltage output. Respectively, the resistance on the strain gauge was changed caused by mechanical stresses. Low level analogue torque signals were generated. These weak signals were amplified in INA125P, then they were converted into digital signals in ADS1115. These digital signals were ready to be processed on STM32F3.

CubeMX

The embedded software needs to include instructions and features for signal processing by the STM32F3 microcontroller. The instructions of input, output and function ports were assigned on Cube MX. This is a free software provided by STM32 manufacturer.

The project was started by selecting the microcontroller on the Cube MX interface. The digital input pins were defined for connecting the torque digital signals. The microcontroller serial wire programming type and core speed were defined. I²C communication protocol and features for the monitoring system were assigned to the specified ports. An example of the Cube MX interface is shown in Figure 6.

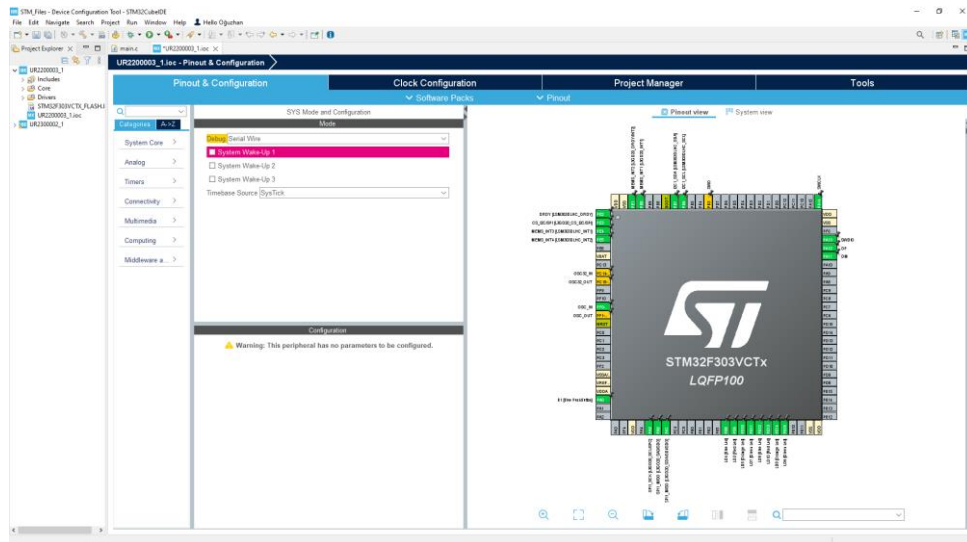


Figure 6. Cube MX user interface

After the definitions were completed, the project file was generated. Cube MX software constituted the basic version of the embedded code to be loaded into the microcontroller.

CubeIDE

C based code prepared for assigning instructions to the microcontroller. It included related libraries, variables and Cube IDE monitoring descriptions. The libraries contained typical code sets for the monitoring instructions and the input and output functions of the controller. The variables are used to assign the digital voltage levels to numerical data. UART and I²C communication protocols were automatically implemented to the code by the Cube IDE. In addition, a sequential print loop was defined due to a variable can be written to the SWV (serial wire viewer) monitoring tab in the Cube IDE interface. These code sets are given as an example in Figure 7.


```

24 #include "LCD.h"
25 #include <stdio.h>
26 #include "ssd1306.h"
27 #include "fonts.h"
28
107 MX_GPIO_Init();
108 MX_I2C1_Init();
109 MX_USART2_UART_Init();
110 MX_I2C2_Init();
111 /* USER CODE BEGIN 2 */
112
113 float data;
114 char yazi[16] = "";
115
29 float Read_ADS1115(void);
30 float voltage;
31
32 int _write(int file, char *ptr, int len)
33 {
34     int i=0;
35     for(i=0 ; i<len ; i++)
36         ITM_SendChar((*ptr++));
37     return len;
38 }

```

Figure 7. Code sets of the libraries, variables and SWV

A function was written to define and address the rules of the I2C communication protocol. In this function, the data are called by means of these addresses. Simple mathematical operations, offset values, experimentally determined calibration coefficients and printing instructions were created. Figure 8 shows the content of these functions. The prepared code was uploaded to the microprocessor via UART protocol.

```

131 while (1)
132 {
133     /* USER CODE END WHILE */
134
135     /* USER CODE BEGIN 3 */
136     voltage = Read_ADS1115();
137     HAL_Delay(10);
138
139     data = voltage;
140     printf("Torque is: %-.2f Nm\n", (data-10501.00)*1.3951);
141     /*lcd_print(1,1, "Torque Is:");
142     sprintf(yazi, "%-.2f", (data-7237.00)*1.3951);
143     lcd_print(2,1, yazi);
144     HAL_Delay(50);*/
145     /* USER CODE BEGIN 3 */
146
147     SSD1306_GotoXY(10,10);
148     SSD1306_Puts ("Torque Is:", &Font_11x18, 1);
149     SSD1306_GotoXY(10,30);
150     sprintf(yazi, "%-.2f Nm", (data-10501.00)*1.3951);
151     SSD1306_Puts(yazi, &Font_11x18, 1);
152     SSD1306_UpdateScreen();
153     HAL_Delay(1);
154 }
155
399 /* USER CODE BEGIN 4 */
400 float Read_ADS1115(void)
401 {
402     unsigned char buffer[3];
403     unsigned char i2c_addr = 0x90;
404     unsigned short data=0;
405
406     buffer[0] = 0x01;
407     buffer[1] = 0xC2;
408     buffer[2] = 0x85;
409     HAL_I2C_Master_Transmit(&hi2c1, i2c_addr, (uint8_t*)buffer, 3, 100);
410
411     buffer[0] = 0x00;
412     HAL_I2C_Master_Transmit(&hi2c1, i2c_addr, (uint8_t*)buffer, 1, 100);
413     HAL_I2C_Master_Receive(&hi2c1, i2c_addr+1, buffer, 2, 100);
414     data = (buffer[0]<<8) + buffer[1];
415     if(data==0xFFFF) data = 0;
416
417     return (float)(0.5 * ((float)data));
418
419 }
420 }

```

Figure 8. Code sets of functions and transitions

Results and Discussion

Scope of the study, the aimed torque measurement system was created. The measurement system as prototype was thought to use during a static torsion test of the propeller shaft. The propeller shaft was connected to the static torsion test rig with full bridge strain gauge application on its tube. Torque was loaded on the propeller shaft. The data was acquired successfully by STM32 data acquisition system. The picture of the static torsion test was shared in Figure 9.

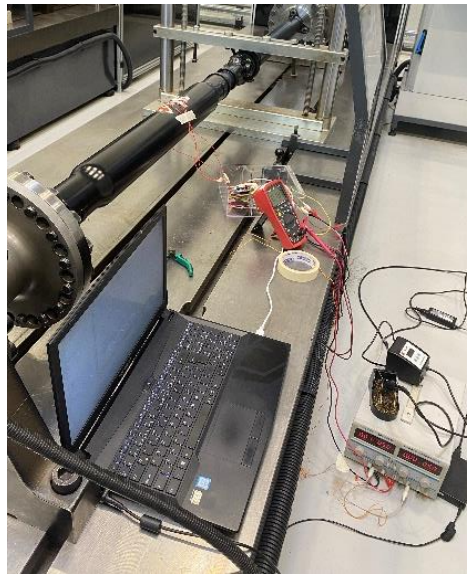


Figure 9. Data acquisition on propeller shaft

Acquired data was compared with previous data acquired with 8-bit system. It was seemed the data acquisition speed was increased 5 times to 100 Hz. This ability was contributed to prevent data loss of instantaneous torque signals. The torque that loaded to the propeller shaft was applied by accredited test rig. Accuracy of these applied torque values were compared with the data acquired by STM32. High-precision torque data were found be 99.4% consistent. The propeller shaft was gradually torque loaded in steps of 500 Nm by the test rig. The graph of the data acquired by STM32 was shown in Figure 10.

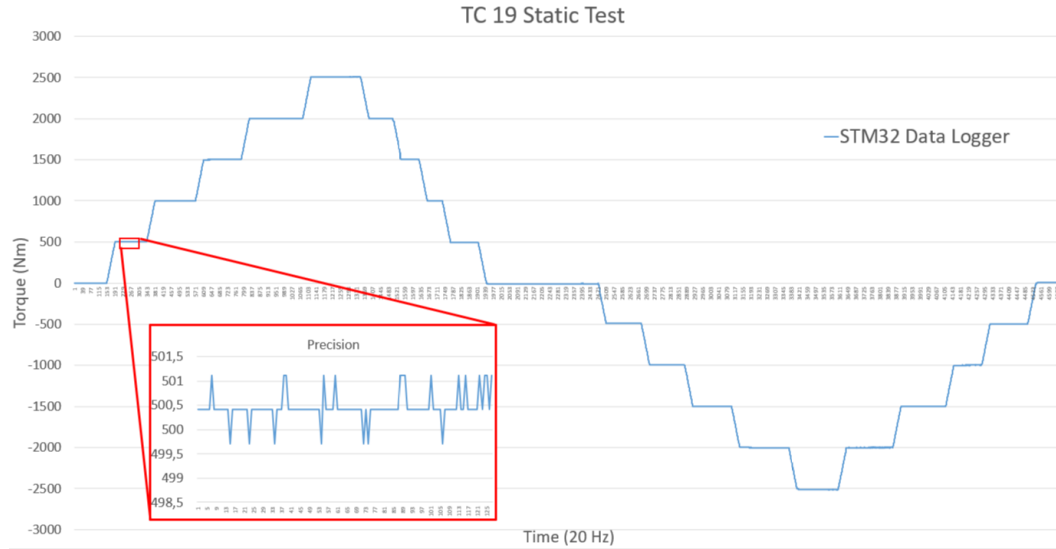


Figure 10. The graph of the data acquired by STM32

A housing was designed to protect the hardware as a mechanical and seem like a fundamentally data logger. Input/output ports and OLED display were added on the housing. Completed data logger was shared in Figure 11.



Figure 11. Data logger

Scientific Ethics Declaration

The authors declare that the scientific ethical and legal responsibility of this article published in EPSTEM journal belongs to the authors.

Acknowledgements or Notes

* This article was presented as an oral presentation at the International Conference on Technology (www.icontechno.net) held in Antalya/Turkey on November 16-19, 2023.

*We would like to thank to Tirsan Kardan R&D Center and Test Center for their support in conducting this study.

References

- Aldemir, O., Tarakcı, S., Solmaz, T., & Isık, E. (2020). External system design for real time monitoring of temperature and torque data on the driveshaft. *10 th International Automotive Technologies Congress Book* (pp.769-776).
- Antoniu, A. (2006). *Digital signal processing*. University of Victoria British Columbia, Canada: McGraw-Hill Education.
- Brown, G. (2012). *Discovering the STM32 microcontroller*. Indiana University Publishing.
- Burr-Brown Corporation. (1998). Instrumentation amplifier with precision voltage reference, *INA125 datasheet*.
- Hariz, M B., Bouani, F., & Ksouri, M. (2015). *Design of a controller with time response specifications on STM32 microcontroller*. IGI Global Publishing.
- Imer, A.(n.d.). *Smart irrigation system*. Ege University, Turkey.
- Isık, E. (2009). *Topoloji optimizasyonu catallı flans uygulaması*. (Master's thesis). Dokuz Eylul University, Turkey.
- ST Life. Augmented (n.d.). Microcontrollers & microprocessors STM32F3 series. Retrieved from <https://www.st.com/en/microcontrollers-microprocessors/stm32f3-series.html>
- Texas Instruments. (2009). *ADS111X ultra-small, low-oper, I2C-compatible, 860-SPS, 16-bit ADCs with internal reference, oscillator, and programmable comparator, ADS115 datasheet*. Retrieved from <https://www.ti.com/lit/ds/symlink/ads1114.pdf>
- Xie, Y., Su, X., He, Y., Chen, X., Cai, G., Xu, B., & Ye, W. (2017), STM32-based vehicle data acquisition system for internet-of-vehicles. *16 th International Conference on Computer and Information Science*. IEEE.
- Zhang, H., & Kang, W. (2013). Design of the data acquisition system basen on STM32. *Information Technology and Quantitative Management (ITQM)*, 17, 222-228.

Author Information

Oguzhan Aldemir

Tirsan Kardan A.S.
Kecilikoy O.S.B. Mah. Ahmet Nazif Zorlu Bulvari 4. Kisim
No:31, Manisa Organize Sanayi Bolgesi, 45300, Kecilikoy
Osmaniyemre/Manisa, Turkey
Contact e-mail: o.aldemir@tirsankardan.com.tr

Sedat Tarakcı

Tirsan Kardan A.S.
Kecilikoy O.S.B. Mah. Ahmet Nazif Zorlu Bulvari 4. Kisim
No:31, Manisa Organize Sanayi Bolgesi, 45300, Kecilikoy
Osmaniyemre/Manisa, Turkey

Serhan Ozdemir

Izmir Institute of Technology
Izmir Yuksek Teknoloji Enstitusu Muhendislik Fakultesi
Dekanligi Gulbahce Mah. 35430, Urla/Izmir, Turkey

Efe Isık

Tirsan Kardan A.S.
Kecilikoy O.S.B. Mah. Ahmet Nazif Zorlu Bulvari 4. Kisim
No:31, Manisa Organize Sanayi Bolgesi, 45300, Kecilikoy
Osmaniyemre/Manisa, Turkey

To cite this article:

Aldemir, O., Tarakcı, S., Ozdemir, S., & Isık, E. (2023). Integration of STM32 microcontroller with arm cortex architecture into the 8-bit measurement circuit customized for real-time data acquisition on propeller shaft to increase data speed and accuracy. *The Eurasia Proceedings of Science, Technology, Engineering & Mathematics (EPSTEM)*, 24, 279-286.

The Eurasia Proceedings of Science, Technology, Engineering & Mathematics (EPSTEM), 2023

Volume 24, Pages 287-300

IConTech 2023: International Conference on Technology

Numerical Simulation on Microwave Melting of Hastelloy C-276

Kadapa Vijaya Bhaskar Reddy

National Institute of Technology Warangal

K.V. Hari Shankar

National Institute of Technology Warangal

Venkatesh Gudipadu

National Institute of Technology Warangal

Abstract: Melting of metals is of utmost importance in the manufacturing industry as it is the primary manufacturing process to obtain the desired shape and size. microwave melting is a novel technique that uses electromagnetic wave radiation to heat materials. In the present work, the melting of Hastelloy C-276 inside a multimode microwave applicator operating at 2.45 GHz and 900 W input power, is explored in numerical and experimental. This results in a significant reduction in processing time and leads to lesser material wastage. The distribution of temperature, electric field, and resistive losses was analysed to understand the microwave melting of the Hastelloy C-276 sample. The study revealed that the melting time taken was ~440 seconds for microwave melting of Hastelloy C-276.

Keywords: Microwave melting, Hastelloy C-276, Susceptor, Skin depth.

Introduction

Microwave processing is a material processing technique that uses electromagnetic waves at a frequency of 2.45 GHz. This technique has emerged in the last decade and is widely used in various industries, including food processing, chemical synthesis, melting of metals, etc(Mishra & Sharma, 2016b). Microwave processing has several advantages over traditional processing methods, fast and efficient method that can reduce processing time and energy consumption(Gupta& Sharma,2014). However, microwave processing also has some limitations, such as the need for specialized equipment and the potential for uneven heating furnaces. Metals do not couple with microwave (MW) radiations, however, they require initial heating to reach critical temperature (until then they act as reflectors to MW). Initial heating is enabled by using susceptor material which couples with microwaves and heats the bulk metal or alloy. Once the bulk metal reaches its critical temperature direct coupling of microwaves takes place and then gets heated.(Mishra & Sharma, 2016a).

Various studies were carried out on microwave melting of different metals. in-situ microwave casting of AA 7039 was examined using an industrial multimode microwave applicator running at 1400 W power and 2.45 GHz frequency(Mishra & Sharma, 2016c). The results show that 920 seconds of microwave irradiation was sufficient to produce a thick cast. It was seen that the oxide layer was forming; this layer serves as a susceptor and aids further in the casting process. It was determined that by adjusting the microwave irradiation period during its processing, it could be possible to develop a material with the necessary amount of hardness. The results of the study showed that the use of microwave energy resulted in faster melting times and reduced energy consumption compared to conventional melting methods. The authors attributed this to the selective heating of the material due to the interaction of microwaves with the alloy. This method also produced a finer microstructure, which improved the mechanical properties of the aluminum alloy. The study concludes that in-

- This is an Open Access article distributed under the terms of the Creative Commons Attribution-Noncommercial 4.0 Unported License, permitting all non-commercial use, distribution, and reproduction in any medium, provided the original work is properly cited.

- Selection and peer-review under responsibility of the Organizing Committee of the Conference

© 2023 Published by ISRES Publishing: www.isres.org

situ microwave casting of aluminum alloys is a promising technique that can provide significant benefits in terms of energy efficiency, cost-effectiveness, and improved material properties. It has the potential to revolutionize the casting industry and reduce the environmental impact of traditional casting methods. Copper casting was analyzed inside the applicator cavity using MHH at 2.45 GHz and 1400 W. There was an improvement in the properties of the microwave cast. A study was carried out to know the microwave interaction with the charge during exposure and how the oxide layer affected on melting of the copper (Mishra & Sharma, 2018b). There has been an improvement in the microwave cast's mechanical characteristics. The uniform and dense structure demonstrates the potential of the process. However, the porosity was reported to be 2–5% and the castings were found to have an average micro indentation hardness of 93 ± 20 HV. Similarly, using microwave radiation, the Al-Zn-Mg alloy (Al 7039) was cast (Mishra & Sharma, 2018a). The alloy charge was subjected to microwave hybrid heating using SiC and CC susceptors. It was discovered that the susceptor material's qualities have a substantial impact on how hot the charge becomes. The temperature of the mold has a major impact on the size of the grain in alloy castings. This effect results from the interaction of microwaves with the mold materials throughout various exposure intervals, which leads to a range of temperatures reached by the mold during preheating, exposure, and post-exposure.

The study by Fujiwara et al. investigated the microwave heating behavior of fine stainless steel powders in an H-field at 2.45 GHz (Fujiwara et al., 2020). The authors utilized a resonant cavity to measure the temperature rise of the samples. Results showed that the temperature of the samples increased rapidly within the first few minutes of microwave irradiation. The heating behavior was found to be strongly dependent on the particle size, with smaller particles exhibiting a more rapid temperature increase. Additionally, the heating behavior was found to be influenced by the packing density of the samples and the presence of air gaps. The study suggested that microwave heating can be a promising method for the sintering of fine stainless steel powders, with potential applications in the production of various metallic components.

The energy consumption of melting bulk non-ferrous metallic materials utilizing microwave hybrid heating (MHH) and conventional heating was examined in the study by Lingappa et al. The authors used a specially designed microwave cavity to heat the samples and measured the energy consumption during melting. Results showed that the energy consumption during MHH was significantly lower than that during conventional heating. Additionally, the study found that MHH was able to achieve complete melting of the samples in a shorter time compared to conventional heating. It is attributed to the lower energy consumption during MHH due to the selective heating of the metallic materials, which reduces heat loss to the surrounding environment. The study suggested that MHH can be an effective and energy-efficient method for the melting of non-ferrous metallic materials, with potential applications in various industries (Lingappa et al., 2018). Microstructural investigation revealed that the samples melted using microwave processing had a finer grain structure and uniform distribution of intermetallics than the conventional processing. The study conducted by Gouthama et al. (2016) compared the melting behavior of tin using a muffle furnace and microwave energy. It was found from the study that microwave energy was more efficient and had a shorter melting time than the conventional method. It was observed that the microwave-melted tin had a finer grain size and higher hardness compared to the conventionally melted tin.

From the literature, it was observed that most of the studies focused on microwave casting or melting of non-ferrous, ferrous materials. Melting of super alloys was seldom found. Hence, this study focused on the melting of Hastelloy C-276 inside a multimode microwave applicator operating at 2.45 GHz, and 900 W input power. From the simulation study, temperature distribution, electric field, and resistive losses were analyzed to understand the microwave melting of the Hastelloy C-276 sample. The model has been validated by experimentally melted Hastelloy C-276 samples.

Materials and Methodology

Modelling

The microwave melting model was developed similarly to the experimental setup using the COMSOL Multiphysics 5.5a software package as shown in Figure 1. The parameters used for modeling are listed in Table 1. The time taken for computation was approximately 180 minutes. The material properties used in the simulation are listed in Table 2. The COMSOL Multiphysics software tool to analyze the thermal characteristics of Hastelloy C-276. The oven walls and the waveguide in the model are made of copper. Although it is anticipated that resistive losses would be minimal, the impedance boundary condition on these walls makes sure that they are taken into consideration. Alumina was used for the cascade because it is a good electrical

conductor. An ACER workstation with Ryzen 5, 32 GB RAM, and RADEON graphics card-4GB was used for modelling and simulation studies. Hastelloy C-276 bulk metal having $10 \times 10 \times 5$ mm. Graphite is a good susceptor and has good irradiating properties at ambient as well as elevated temperatures with electromagnetic radiation. the susceptor and crucible were considered graphite.

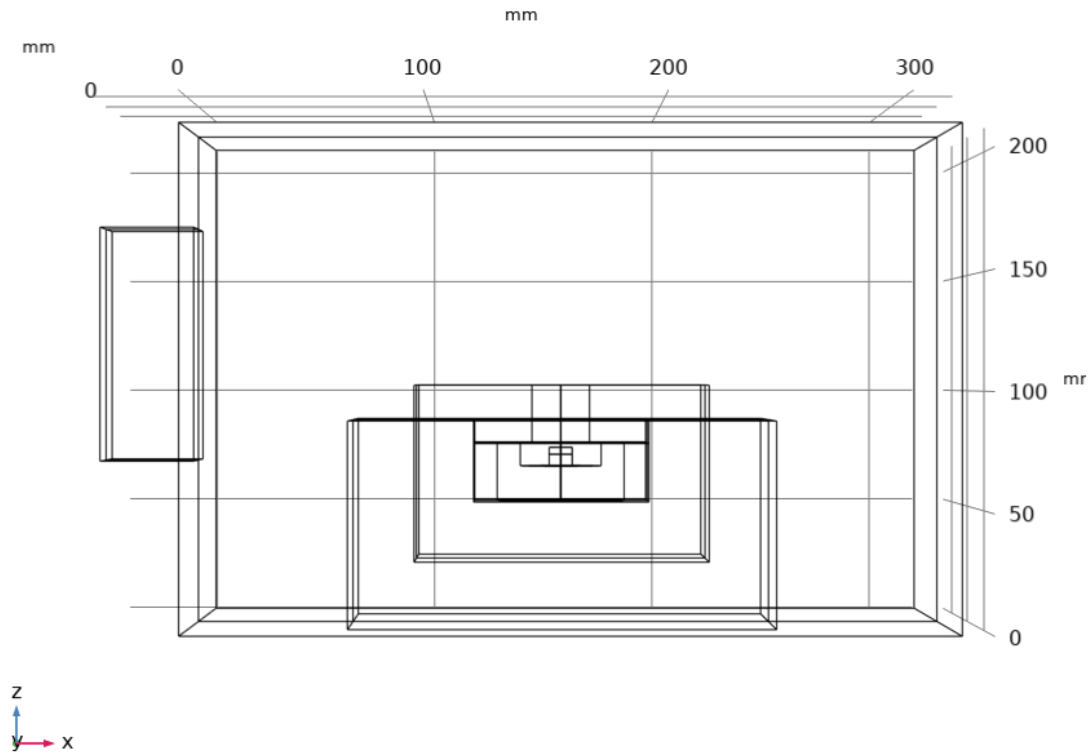


Figure 1. The 3D geometry model in Comsol

Table 1. Model parameters used for simulation

Serial No	Label	Dimension (mm)
1	Microwave cavity	320 x 320 x 210
2	Waveguide	40 x 80 x 100
3	Bottom cascade	185 x 185 x 140
4	Top cascade	125 x 125 x 110
5	Through-hole diameter	25
6	Graphite susceptor	10 x 10 x 5
7	Graphite Cylinder outer	55 x 25
8	Graphite Cylinder inner	55x10
9	Hastelloy C-276 plates	10x10x5

Table 2. Material properties

Property	Unit	Air(Tama ng & Aravindan, 2022)	Copper(Ta mang & Aravindan, 2019)	Alumina (Reddy et al., 2023)	Graphite(Redd y et al., 2023)	Hastelloy C-276 (Haynes Hastelloy® C-276 Alloy & Solution Heat Treated Flat Products, n.d.)
Relative Permeability	1	1	1	1	1	1
Relative Permittivity	1	1	1	4.2	23.5	1
Electrical Conductivity	S/m	0	5.99e7	1e-14	1.667	1/(1.26e-6)
Heat Capacity at constant pressure	J/(kg-K)	-	385	900	707.7	427
Density	Kg/m ³	-	8960	3900	2490	8890
Thermal Conductivity	W/(m-K)	-	400	27	24	18.3

Governing Equations

Permittivity is the property of a material to get polarized under the influence of an external electric field. It is also called the dielectric constant. The absolute permittivity of a material is given by Eq.1 (Mishra&Sharma, 2017)

$$\varepsilon' = \varepsilon_0 \varepsilon'_r \quad (1)$$

Where $\varepsilon_0 = 8.854 \times 10^{-12}$ F/m is the permittivity of free space and ε'_r is the relative permittivity. The complex permittivity of a material accounts for the absorption and storage of the electrical energy inside the material. It is given by Eq.2 (Gupta & Eugene, 2011)

$$\varepsilon^* = \varepsilon' - j\varepsilon'' \quad (2)$$

where ε'' is the dielectric loss factor. The extent of penetration and absorption of microwaves inside a material is represented by its permittivity, ε' , and the ability to store energy is represented by the dielectric loss factor, ε'' . The dielectric loss factor accounts for the various losses occurring due to the resistance offered to the translational and rotational motions of electrons, ions, and dipoles, which in turn are induced due to the electric field generation inside the material.

The effect of the magnetic field on the absorption of microwaves and heating is generally ignored since it is dominated by the electric field. However, a magnetic property called permeability (μ') has a significant influence on the skin depth of the material. For better penetration of microwaves, more skin depth is required, and this is possible only when the permeability is low. Permeability (μ'), accounts for the effect of the magnetic field on the material and is given by Eq.3 (Reddy et al., 2023).

$$\mu' = \mu_0 \mu'_r \quad (3)$$

Where $\mu_0 = 8.854 \times 10^{-12}$ F/m is the permeability of free space and μ'_r is relative permeability. The complex permeability, μ^* , is given by Eq.4 (Gupta & Eugene, 2011).

$$\mu^* = \mu' - j\mu'' \quad (4)$$

Where μ'' is magnetic loss factor. The magnetic loss factor accounts for relaxation and resonance occurring due to the magnetic field.

Boundary Conditions

To approach the real experimental conditions, certain selected boundary conditions have been applied by heat transfer in solids and electromagnetic wave frequency domain modules in the developed model. The boundary conditions shall be set out as follows:

Port boundary condition: It was applied on the entrance to the rectangular waveguide as shown in Fig. 2(a) and transverse electric (TE₁₀) mode was considered with 2.45 GHz frequency using Eq.5 (Tamang & Aravindan, 2019).

$$\text{Cut-off frequency } (f_c)_{mn} = \frac{c}{2} \sqrt{\frac{m^2}{a^2} - \frac{n^2}{b^2}} \quad (5)$$

Impedance boundary condition: it is applied on the walls of the microwave cavity and the waveguide as shown in Fig. 2(b) to account for minute losses (skin effect) due to skin depth using Eq.6 (Tamang & Aravindan, 2022)

$$\sqrt{\frac{\mu_r \mu_0}{\varepsilon_r \varepsilon_0 - j \frac{\sigma}{\omega}}} n \times H + E - (n \cdot E) n = (n \cdot E_s) n - E_s \quad (6)$$

Perfect Magnetic Conductor: It is applied on the central plane of symmetry of the microwave applicator so that the magnetic field and current density along the symmetry plane are zero, which is represented by the following equation: (Mishra & Sharma,2017).

$$\mathbf{n} \times \mathbf{H} = 0$$

(7)

Heat transfer boundary condition: It is applied to the Hastelloy C-276 charge and susceptor using Eq. 8 (Redy et al., 2023) as shown in Fig. 2(d).

$$\rho C_p \frac{\partial T}{\partial t} = \nabla \cdot (K \nabla T) + Q_{rms}$$

(8)

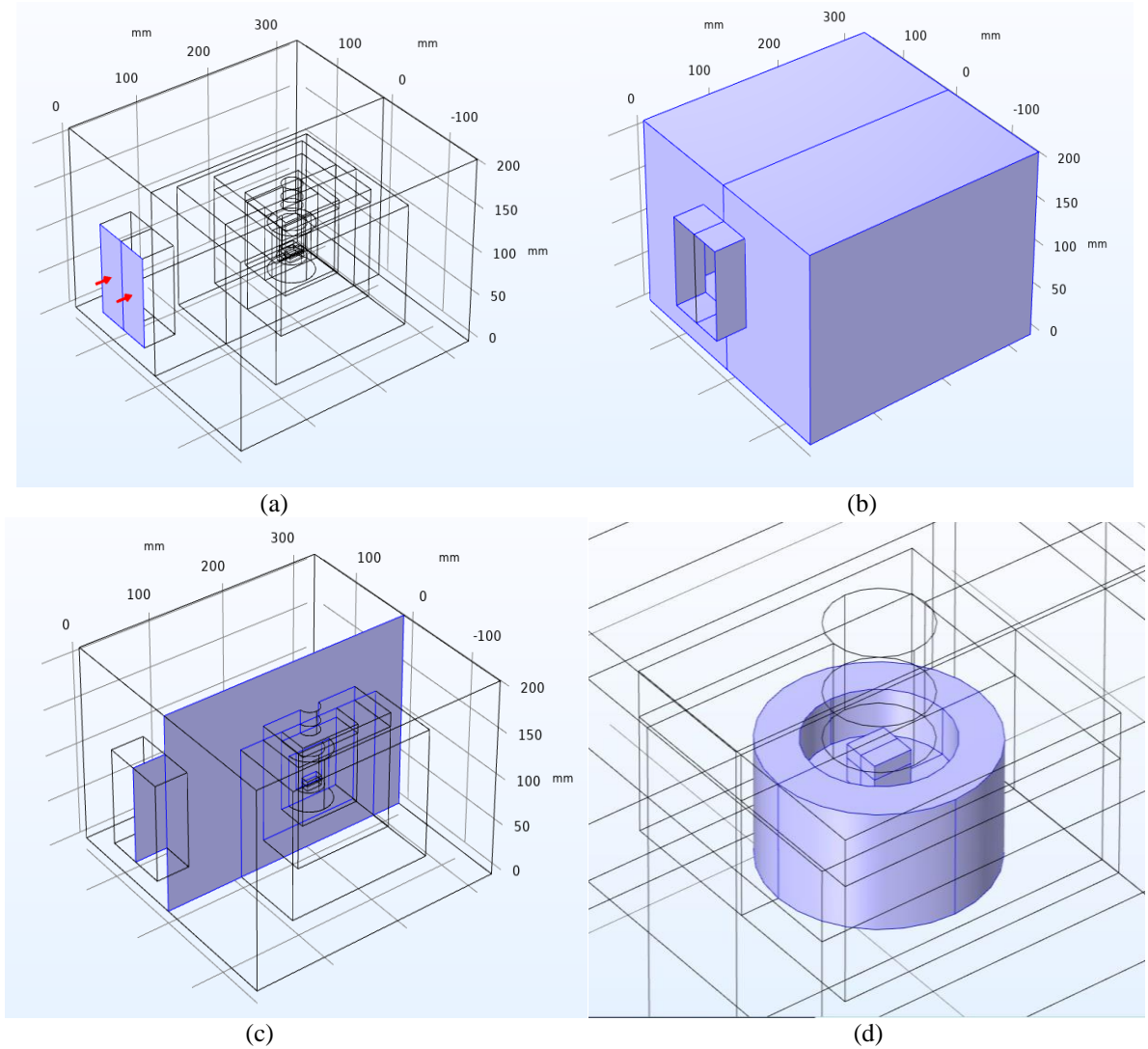


Figure 2. Boundary conditions used (a) Port boundary condition (b) Impedance boundary condition (c) Perfect magnetic conductor (d) Heat transfer in solid

Certain assumptions were considered for simplifying the model. They are as follows:

- Copper has high electrical conductivity, so the walls of the waveguide and the micro-oven are considered to be copper material.
- The surrounding temperature of the system is considered 27 °C.
- Turn table rotation and speed were not considered
- For simulation the phase change is not considered.

Mesh Quality

Using a model solver tool to facilitate meshing, the 3D model was composed of physics-controlled meshes and tetrahedral elements. The suitable element size was chosen by examining the element quality for ‘fine’ (Fig. 3(a)), ‘finer’ (Fig. 3(b)), ‘extra fine’ (Fig. 3(c)), and ‘extremely fine’ (Fig. 3(d)) element sizes in terms of average element quality, minimum element quality, and maximum growth rate. 0.0 is a degenerated element while 1.0 is a completely symmetrical element in the element quality. By contrast, the highest element growth rate determines whether or not an element size may increase in a region of smaller elements and grow in a region with greater elements. The mesh generated (Fig. 4(a)) with ‘extremely fine’ elements (total number: 107724) was found more effective with optimum characteristics (average element quality 0.663, maximum growth rate 1.30) than ‘fine’, ‘finer’, and ‘extra fine’ elements. Fig. 4(b) shows an evaluation of the mesh quality to indicate that it is more than 0.7 for mold assembly and charge.

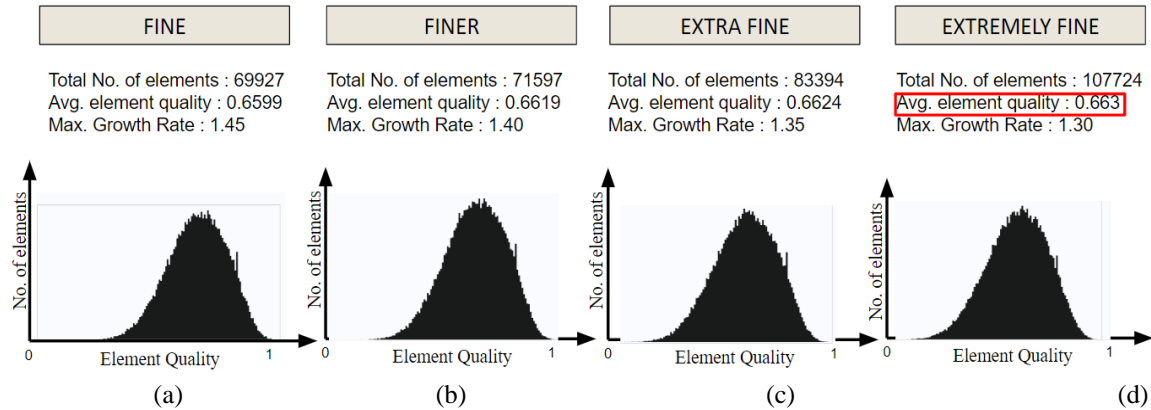


Figure 3. Comparison of element quality in (a) fine, (b) finer, (c) extra fine, and (c) extremely fine element size.

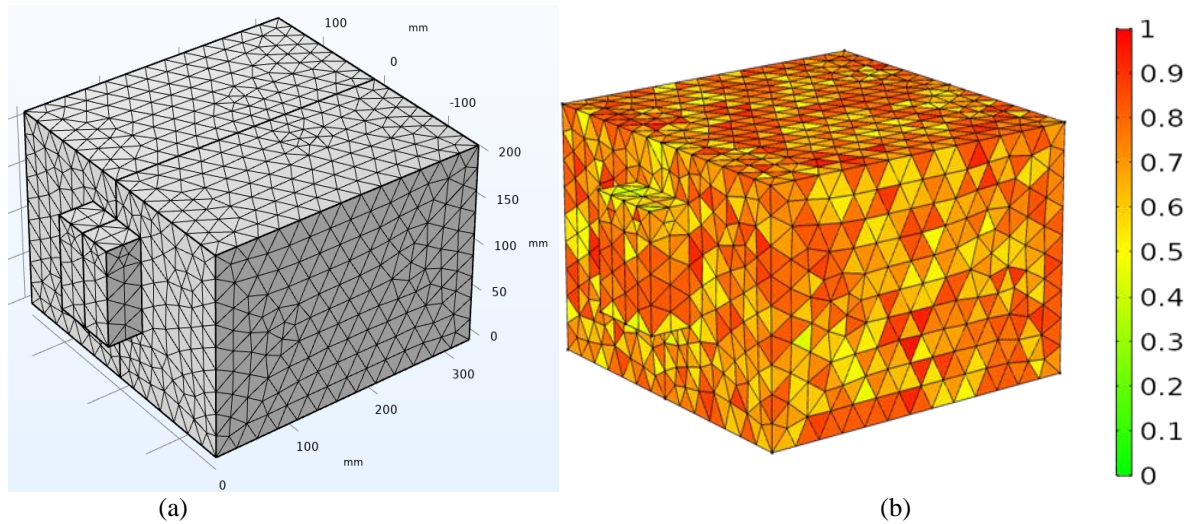


Figure 4. (a) Meshed model (b) Mesh quality

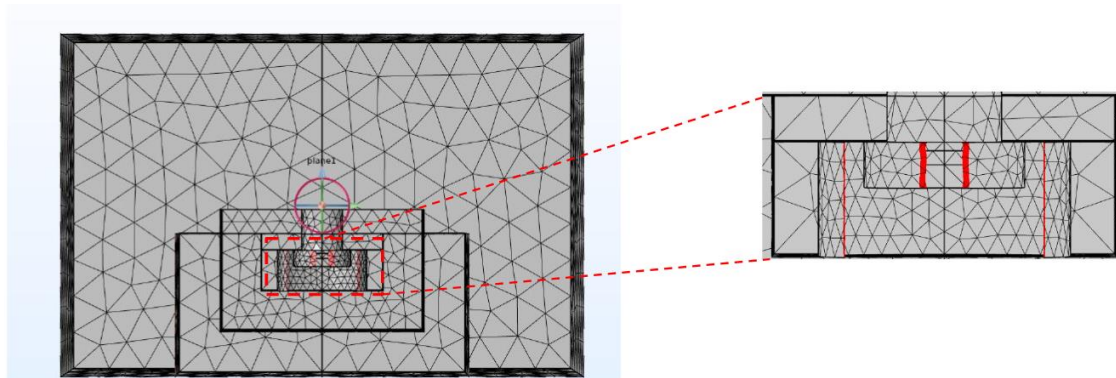


Figure 5. Mesh distribution of microwave setup with an enlarged view of the interlayer.

Physics-controlled mesh of size “extremely fine” containing 107724 elements was used for the simulation as depicted in Fig. 5, the enlarged view of the figure shows that the interlayer has very fine elements compared to the substrate, which is necessary for accurate results.

Results and Discussion

The results in the form of resistive losses due to electric field distribution, magnetic field distribution, variation of electric field distribution, magnetic field distribution, and temperature distribution of Hastelloy were studied.

Effect of Power

With the following stages of unit power: 1500 W, 2000 W, 2500 W, 3000 W, and 3500 W, the impact of power fluctuation on the melting of the charge was examined. Figure 6(a) illustrates how power affects the distribution of the electric field inside the microwave cavity and the related temperature distribution in the charge at the moment of melting. The distribution patterns of the electric fields in all of the situations are clearly shown in the figure. The intensity of the electric field, however, rises as the power increases. The pattern of temperature distribution shows the impact of increasing electric field intensity. The temperature distribution reveals that as power increases, both the distribution pattern and temperature change. Although heating is caused by dielectric losses in the Hastelloy, the conduction loss and eddy current loss dominate heating in the metallic charge. An increase in power increases the heat generation inside the charge and materials. An increase in power increases the field intensity inside the cavity, making more energy available for heat generation and heat dissipation inside the metallic charge.

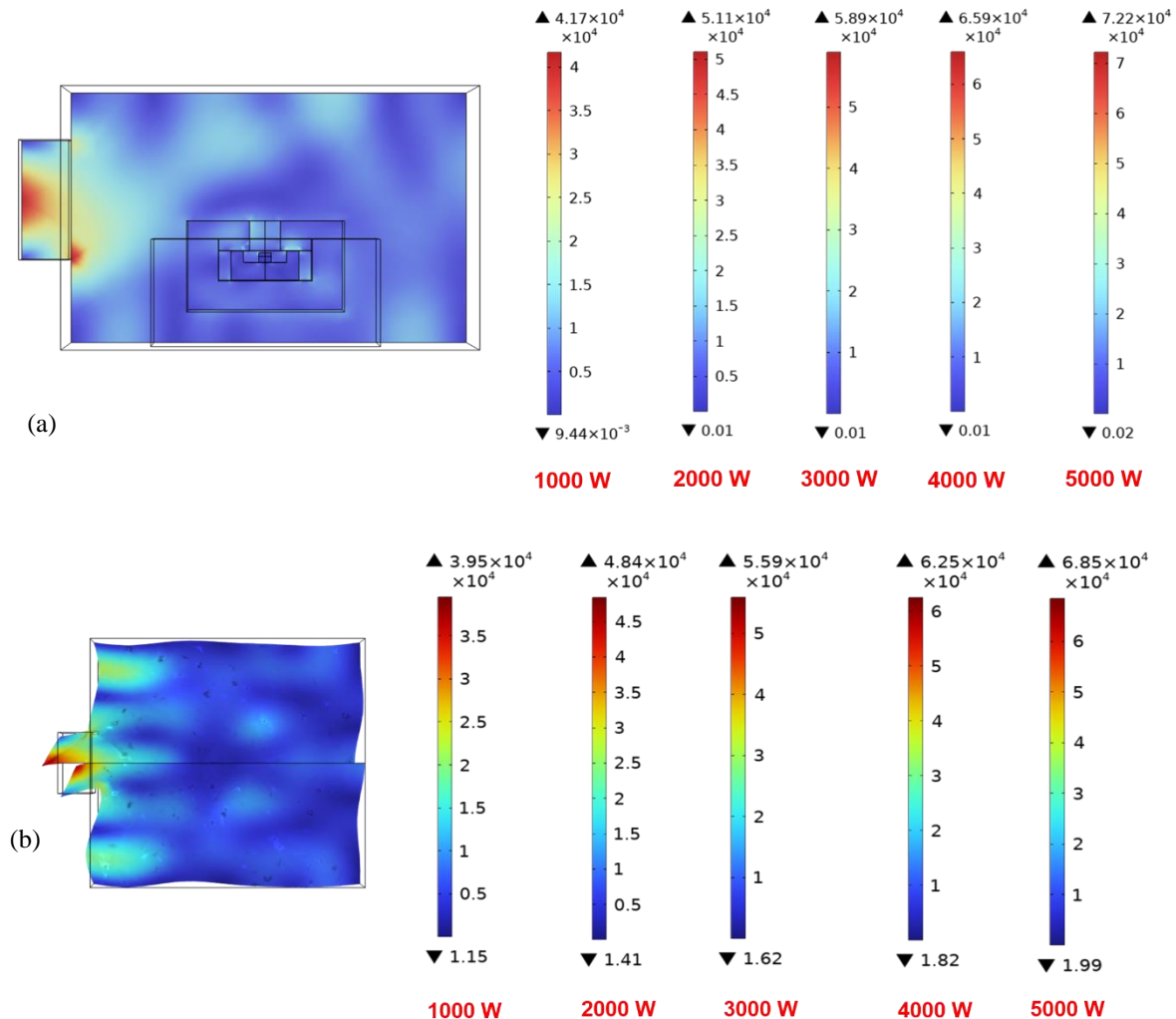


Figure 6. Electric field distribution (a) in Enorm direction with different powers. (b) in Ez with different Powers

The distribution of temperature inside the charge is substantially impacted by power change. Heat dissipation inside the assembly and the susceptor rises as power levels rise. The charge is quickly carried into the microwave absorption domain by heat transfer from these components (assembly and susceptor) into it. More heat is released inside it at a higher strength as the charge interacts with the microwaves. Due to the conduction of heat dissipated within the charge, temperature distribution will be less uniform at lower power steps. Due to a decreased mean free path of free electrons, a metallic charge's thermal conductivity and energy conduction reduce as temperature rises. At increased power, heat transmission will be slower because of improved heat dissipation across the charge volume, which will outweigh heat conduction. As seen by the predicted temperature distribution at the moment of charge melting, increased power thus delivers a more uniform temperature distribution inside the charge. The temperature will drop as we approach the charge's outer surfaces. Convective and radiative heat losses from the charge into the cavity environment are responsible for this. This is yet another distinctive feature of microwave heating, commonly known as inside-out heating

It is important to determine the electric field distribution inside the microwave applicator as it assists in the appropriate location of the sample to ensure less processing time. The positions having higher field intensity enable better microwave coupling of materials. Electric field distribution in the XY plane (E_z) is shown in Fig. 6(b). The distortion in the electric field represents the conversion of microwave energy to heat energy. The locations of maximum and minimum electric field intensity represent the nodes and anti-nodes in the propagation of microwaves. It is observed that the electric field distribution ranges from 4.17×10^4 (V/m) to 7.22×10^4 (V/m).

Figure 7. depicts the impact of power on the charge's melting time. The amount of time needed for the charge to melt is reduced when input power is increased. The data are mathematically correlated, and the relation between melting time and input power is as follows:

$$t = -187.4 \ln(P) + 441.44 \quad (9)$$

The model displays a hyperbolic trend and a correlation of almost 99% ($R^2 = 0.994$). Additionally, it is clear from the equation that melting time (t) decreases as power provided (P) increases and follows a hyperbolic trend. As a result, the mathematical model depicted in the aforementioned equation is comparable to the model based on simulation data.

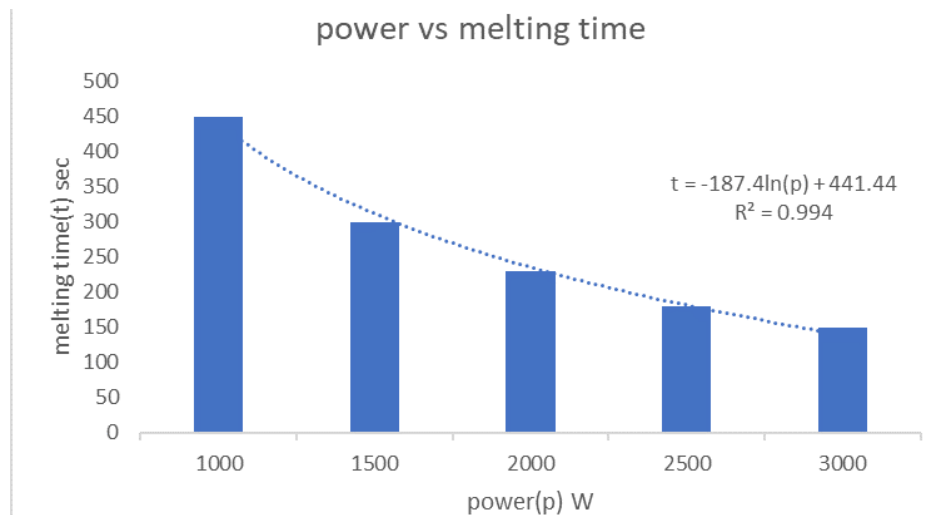


Figure 7. Influence of input power (P) on melting time (t).

Figure 8 depicts the impact of power on the charge's average heating rate. In compared to 1500 W, the charge heats up more quickly on average at 3500 W (200.285%). By accelerating the rate at which heat escapes from the charge, the rate of heat generation is improved and the time needed to heat the charge to its melting point is shortened, due to increase in input power. When power inside the microwave applicator increases, so does the average heating rate of the charge. Figure 4 depicts how power affects the amount of energy needed to melt the charge.2. Immense generation of energy and the resulting increased dissipation of microwave energy inside the metallic charge due to improved electric and magnetic fields at higher powers are responsible for the greatest energy reduction.

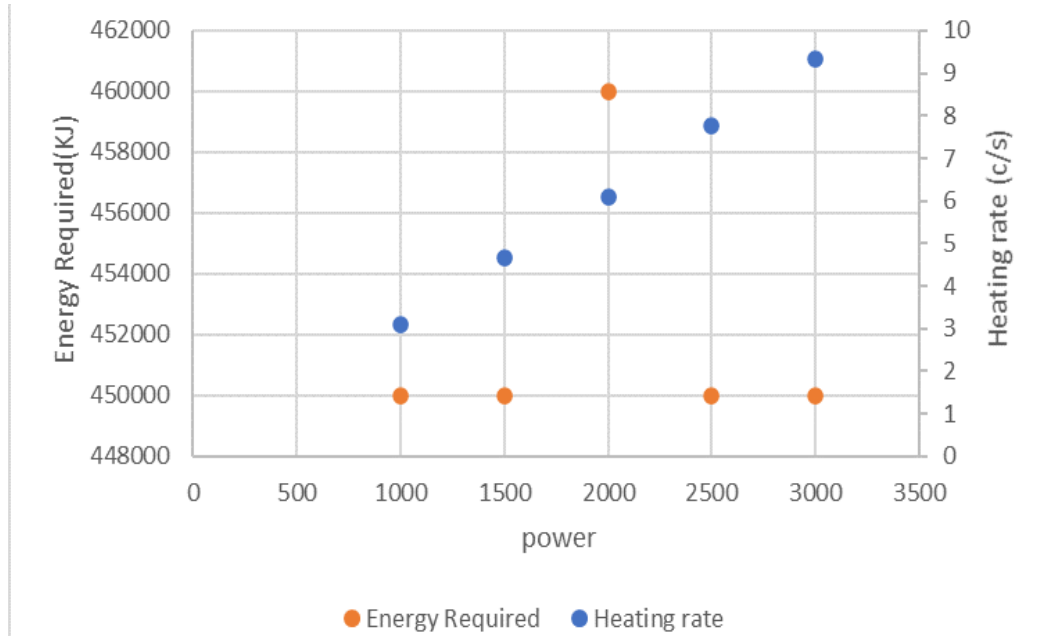
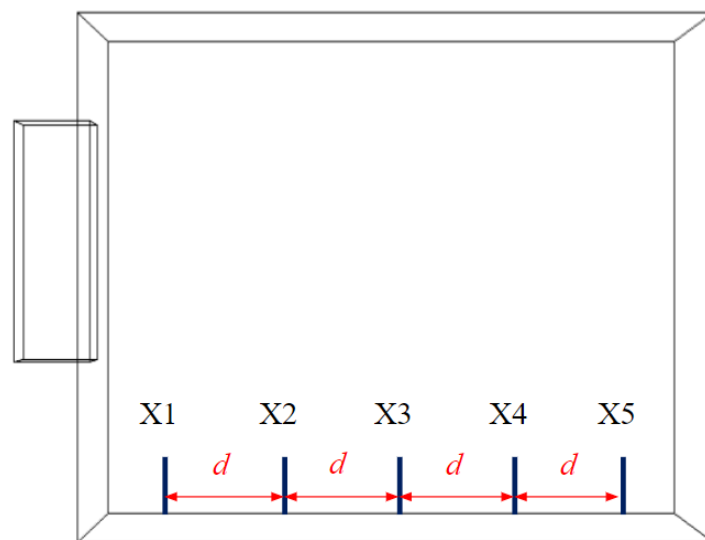


Figure 8. Influence of input power on heating rate and energy requirement for melting of the charge.

Effect of Assembly Location

According to a report, the electric and magnetic field strengths are distributed in a high-low pattern inside the microwave applicator cavity. When a material is present in the cavity during processing, this pattern reorients itself. A method for locating the setup at ideal coordinates within the cavity can be found by simulating the operation.

Figure 9. depicts the equivalent impact of mold assembly position (at X1, X2, X3, X4, and X5) on the cavity's electric field distribution and the charge's temperature distribution. According to location, the distribution shows the pattern and value of field intensity. In addition, due to potential disruption in the absorbed and reflected microwaves, the distance (L) between the source and the location of the load influences the interference pattern and placements of nodes ($L=n\lambda$, where n is a positive integer). The decline in field strength near the charge when it is transported in the x-direction is another finding in the simulated electric field distribution (Fig. 9). On the other hand, the temperature gradually drops away from the charge's outer surface in a more consistent manner. This is explained by the heat that is lost by convection and radiation from the charged surface into the hollow environment.



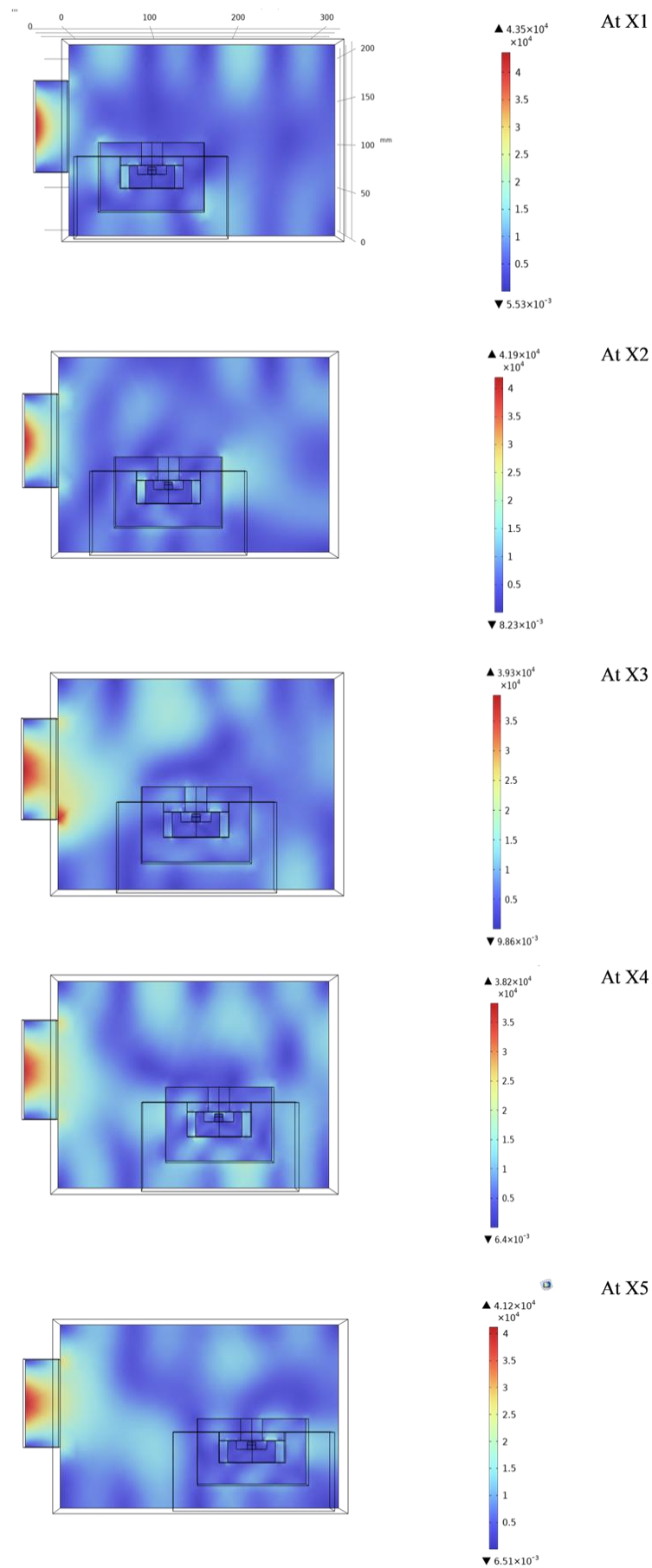


Figure 9. Effect of location on electric field distribution inside microwave applicator

Figure 10 illustrates the impact of mold assembly position on melting time during charge heating. The charge's heating properties are impacted by the fluctuation in electric field strength as the mold assembly and charge are placed in various places. When compared to places with low electric fields, higher electric fields improve the polarization of molecules in the Hastelloy and the susceptor, which also improves the mobility of the free electrons in the charge. The typical heating period of the charge to reach the critical temperature is shortened by the rapid heating of the Hastelloy and the susceptor. The charge is heated over the critical temperature by coupling with microwaves. The charge heats up quickly, which shortens the whole melting time.

The melting time is influenced by the node distribution and the strength of their fields. The charge has the quickest melting time and the least amount of non-uniformity when it is heated quickly at site X4. As a result of the charge heating more uniformly at site X4, there is less heat transfer through conduction mode within the charge. As a result, the charge melts faster when the degree of non-uniformity is lower (Figure 10). When compared to site X2, the melting time of the charge decreased by 51.61% and 40.3%, respectively, at locations X4 and X5. To guarantee that the charge is melted in less time with a lower amount of microwave energy, the mold assembly and the charge should be placed in an appropriate area.

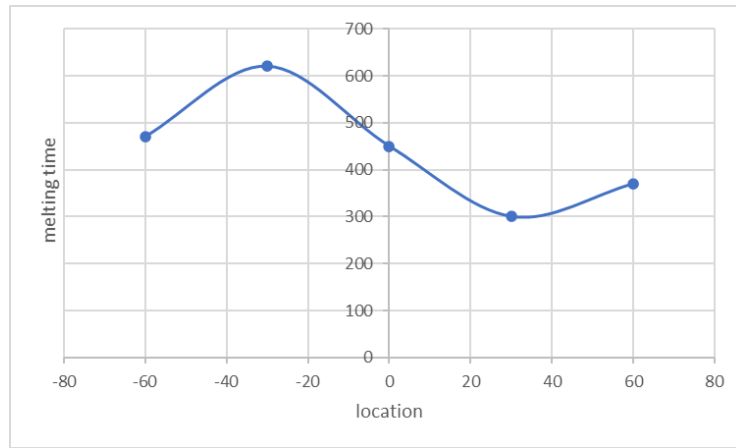
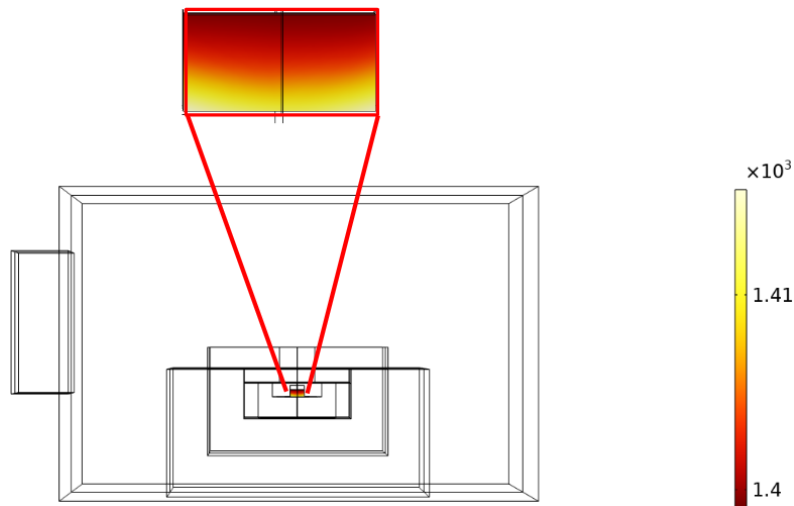


Figure 10. Influence of setup location on melting time.

Temperature Distribution

The temperature distribution in Hastelloy is shown in Figure 11. It is consistent with the fact that the heat is transferred from the graphite susceptor to the joining region. The temperature change across the Hastelloy is achieved by measuring the temperature along a line from the bottom of the assembly to the top of the assembly (Figure 11). The temperature of the bottom layer, i.e. Graphite is higher at each time interval, whereas the temperature of the top layer is lower compared to graphite plate and almost uniform. Temperature value depends on the permeability, permittivity, and electrical conductivity for simulation, and various thermal properties are also required for the study.



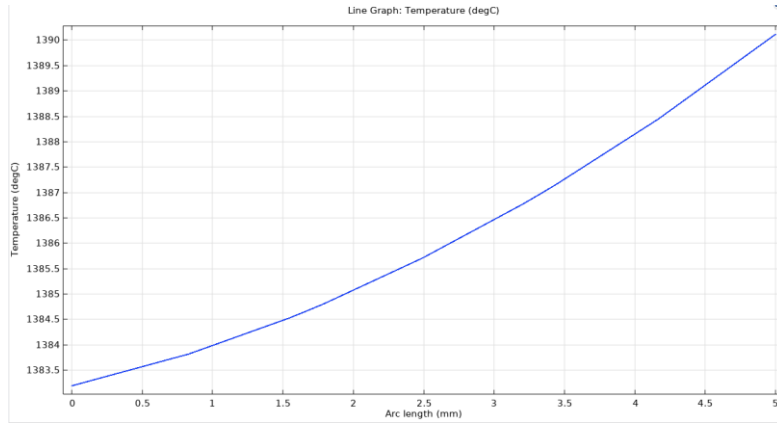


Figure 11. Temperature distribution and Temperature v/s distance plot

Resistive Losses

It is observed from Fig. 12 The resistive losses are not uniform throughout the assembly. Mostly it is concentrated at the corners of the graphite cylinder and graphite plate, this may be due to the effect of conduction of heat by the interface layer or it might be microwave energy absorption.

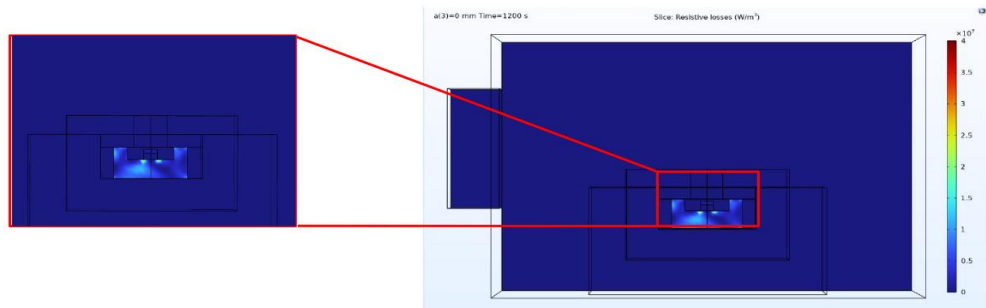


Figure 12. Resistive losses

Experimental Validation

The experiment was done using a LG microwave with a frequency of 2.45GHz and 900W power. The assembly was made similar to the geometry used for simulation. An aluminum cascade was placed inside a microwave oven and glasswool was coated around that material. Inside the cascade, a graphite cylinder was placed in the middle and a Hastelloy was placed inside the cylinder, susceptor was also placed on the Hastelloy and then the Hastelloy and susceptor were covered with charcoal powder. This whole setup was placed inside the microwave oven and the experiment was done for 470 seconds. The melting characteristic for different melting times is depicted in Fig. 13.

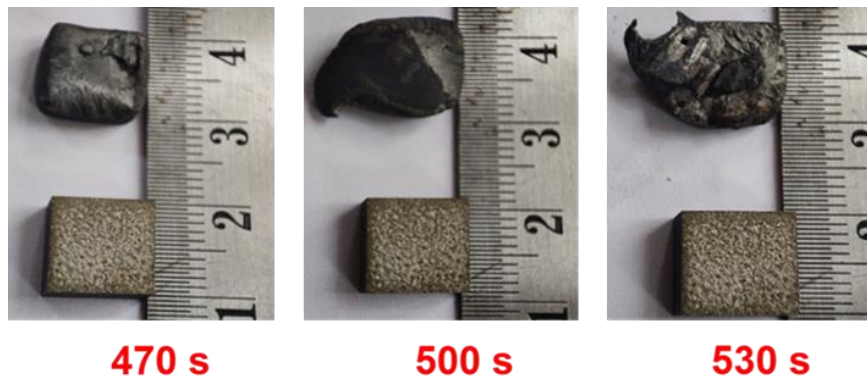


Figure 13. Microwave melting of Hastelloy C-276 with time.

Conclusions

The simulation of Microwave processing in a domestic oven was successfully performed and the following conclusions were drawn:

Melting of Hastelloy C-276 using microwave casting in a multimode microwave applicator was investigated experimentally and its numerical simulation was also performed using COMSOL Multiphysics. It was found that the temperature profile obtained from the experiment was in good agreement with the results obtained from the simulation as the error was within 5%.

The power input and setup location has significant effects on melting time, heating rate, energy requirement, etc. during the microwave casting process. Electric field distribution influences the temperature distribution inside the charge. At higher power input and favorable setup locations, heating rates are higher which results in uniform heating of the charge and also leads to reduction in melting time and energy.

Melting of the Hastelloy C-276 workpiece took place in 450 seconds in simulation whereas melting took place at 470 seconds while experimenting.

When power input increases, melting time decreases. To get the lowest melting time, x4 is the suitable location and x2 is the least suitable. Maximum Enorm is concentrated for x1 setup location and is least for x4 location. It is observed that the electric field distribution ranges from 4.17×10^4 (V/m) to 7.22×10^4 (V/m) when power varies from 1000W to 3000W.

Scientific Ethics Declaration

The authors declare that the scientific ethical and legal responsibility of this article published in EPSTEM journal belongs to the authors.

Acknowledgements or Notes

* This article was presented as an oral presentation at the International Conference on Technology (www.icontechno.net) held in Antalya/Turkey on November 16-19, 2023.

References

- Fujiwara, H., Toyota, S., Anggraini, L., Ameyama, K., & Agrawal, D. (2010). Microwave heating behavior of fine stainless steel powders in. *International Microwave Power Institute's 44th Annual Symposium*, 44, 79–82.
- Gouthama, T. R., Harisha, G., Manjunatha, Y. R., Kumara, S. M. M., Srinath, S., & Lingappa, M. S.(2016). Melting of tin using muffle furnace and microwave energy and its characterization. *IOP Conf Ser Mater Sci Eng*, 149(1).
- Gupta, D., & Sharma, A. K. (2014). Microwave cladding: A new approach in surface engineering. *Journal of Manuf Process*, 16(2), 176–182.
- Gupta, M., & Eugene, W. W. L. (2011). *Microwaves—theory. Microwaves and Metals*. John Wiley & Sons (Asia) Pte Ltd.: Singapore, 25-41.
- Lingappa, S. M., Srinath, M. S., & Amarendra, H. J. (2018). Melting of bulk non-ferrous metallic materials by microwave hybrid heating (MHH) and conventional heating: A comparative study on energy consumption. *Journal of the Brazilian Society of Mechanical Sciences and Engineering*, 40(1), 1–11.
- Matweb. (2022). Haynes Hastelloy® C-276 alloy, solution heat treated flat products,” matweb material property data. Retrieved from <https://www.matweb.com>
- Mishra, R. R., & Sharma, A. K. (2016). A review of research trends in microwave processing of metal-based materials and opportunities in microwave metal casting. *Critical Reviews in Solid State and Materials Sciences*, 41(3), 217–255.
- Mishra, R. R., & Sharma, A. K. (2016). Experimental investigation on in-situ microwave casting of copper. *IOP Conf Ser Mater Sci Eng*, 346(1).

- Mishra, R. R., & Sharma, A. K. (2016). Microwave-material interaction phenomena: Heating mechanisms, challenges and opportunities in material processing. *Compos Part A Appl Sci Manuf*, 81, 78–97.
- Mishra, R. R., & Sharma, A. K. (2016). On mechanism of in-situ microwave casting of aluminium alloy 7039 and cast microstructure. *Materials & Design*, 112, 97–106.
- Mishra, R. R., & Sharma, A. K. (2017). On melting characteristics of bulk Al-7039 alloy during in-situ microwave casting *Appl Therm Eng*, 111, 660–675.
- Mishra, R. R., & Sharma, A. K. (2018). Effect of solidification environment on microstructure and indentation hardness of Al–Zn–Mg alloy casts developed using microwave heating. *International Journal of Metalcasting*, 12(2), 370–382.
- Reddy, K. V. B., Venkatesh, G., & Mishra, R. R. (2023). Microwave joining of SS-316 plates: A multi-physics simulation study. *Journal of Manuf Process*, 98, 29–41.
- Tamang, S., & Aravindan, S. (2022). Joining of dissimilar metals by microwave hybrid heating: 3D numerical simulation and experiment. *International Journal of Thermal Sciences*, 172.
- Tamang, S., & Aravindan, S. (2019). 3D numerical modelling of microwave heating of SiC susceptor,” *Appl Therm Eng*, 162, 114250

Author Information

Kadapa Vijaya Bhaskar Reddy

National Institute of Technology
Warangal, Telangana, 506004
India.
Contact e- mail: bhaskarsave.61@gmail.com

K.V. Hari Shankar

National Institute of Technology
Warangal, Telangana, 506004
India.

Venkatesh Gudipadu

National Institute of Technology
Warangal, Telangana, 506004
India.

To cite this article:

Reddy, K. V. B., Shankar, K.V. H. & Gudipadu, V (2023). Numerical simulation on microwave melting of Hastelloy C-276. *The Eurasia Proceedings of Science, Technology, Engineering & Mathematics (EPSTEM)*, 24, 287-300